MANEUVERING CHARACTERISTICS IN CALM WATER AND REGULAR WAVES FOR ONR TUMBLEHOME

by

Haitham Abdalla. Elshiekh

A thesis submitted in partial fulfillment
of the requirements for the Master of
Science degree in Mechanical Engineering
in the Graduate College of
The University of Iowa

May 2014

Thesis Supervisors: Professor Frederick Stern
Associate Research Scientist Yugo Sanada

ProQuest LLC.
789 East Eisenhower Parkway
P.O. Box 1346
Ann Arbor, MI 48106 - 1346

Graduate College
The University of Iowa
Iowa City, Iowa

CERTIFICATE OF APPROVAL

MASTER'S THESIS

This is to certify that the M.S. thesis of

Haitham Abdalla. Elshiekh

has been approved by the Examining Committee
for the thesis requirement for the Master of Science
degree in Mechanical Engineering at the May 2014 graduation.

Thesis Committee: _____
Frederick Stern, Thesis Supervisor

_____
Yugo Sanada, Thesis Supervisor

_____
H.S. Udaykumar

_____
Albert Ratner

To the memories of my father, my aunt Zubieda, and my best friend Abdelwahid and to my eldest brother Elhaj, nothing can be said or done to thank you.

ACKNOWLEDGMENTS

The Office of Naval Research sponsored this research under the grants N00014-01-1-0073 and NICOP N00014-06-1-064 administered by Dr. Ki-Han Kim. The author expresses thanks for the ONR continual support and contributions to the ship hydrodynamics program at IIHR. IIHR, College of engineering and the University of Iowa also contributed to this research fund. JSPS KAKENHI provided the fund for the development of 6DOF-VMCS and RLD system under the grant number 23760783.

The guidance of thesis supervisors Dr. Fred Stern and Dr. Yugo Sanada contributed to a profound learning experience. The author is honored for the opportunity to serve under the guidance of two iconic figures in ship hydrodynamics world. The incomparable vision and supervision of Dr. Yugo Sanada is greatly appreciated. Dr. Sanada provided considerable mentoring and training during the phases of the data collection and analysis. Dr. Sanada's insights within the vast complex ship hydrodynamics and experimental fields are greatly appreciated. The author is extremely grateful for Dr. Sanada's patience and willingness to help with the development of the data processing software. Under no other person could an experiment with such overwhelming properties be undertaken with such smoothness. The author is grateful to the individuals who contributed to efficient and quality execution of research support. These include undergraduate mechanical engineering students who co-endured tedious rounds of data acquisition and IIHR mechanical and electrical shop personal who committed time to help with technical support.

Greatest thanks must be expressed to great friend and mentor Dr. Hyunse Yoon who graciously provided new levels of understanding within the vast and complex world of experimental engineering and data analysis.

ABSTRACT

Standard maneuvering tests were executed at the IIHR wave basin using free-running model. Experiments in calm water as well as wave were performed for a surface combatant with primary focus on establishing a validation benchmark dataset for an unsteady Reynolds-averaged Navier-Stokes (RANS)-based computational fluid dynamics (CFD) code used for computing both air and water flow around a ship. Experimental data from this study will also be used in developing a mathematical model for computing the external forces exerted on the ship model during maneuvering. The geometry is 1/49 scale fully appended ONR Tumblehome model 5613, with a length of 3.147 m. Tests are performed in 20 x 40 x 4.5 m wave basin which is equipped with six plunger-type wave makers, free-running system, as well as carriage tracking system. The maneuvering tests included course keeping, zigzag, and turning tests in head and following waves as well as calm water. Course keeping and zigzag tests were performed at Froude number 0.2 while turning tests were performed at Froude numbers 0.1, 0.2, and 0.3. While the wave height to wavelength ratio was held constant at 0.02 for all the test cases, experiments were performed at three different wavelengths for each Froude number case at different wave encounter angles. Maneuvering trajectories for each test as well as results such as roll, pitch, yaw and yaw rate results were analyzed for all tests. Drift angle, drifting distance, tactical diameter, advance and transfer results from turning tests were obtained and tactical diameter and advance are compared to other facilities data. 1st and 2nd overshoot angles results from zigzag tests and counter rudder angle and speed loss in course keeping were obtained and documented along with the turning test results to help in developing a mathematical model for calculating the forces and moments acting on the ship model and to establish a benchmark data for the CFD validation use.

TABLE OF CONTENTS

LIST OF TABLES

Table

LIST OF FIGURES

Figure

CHAPTER 1

INTRODUCTION

The rapidly growing capability of computing power has led the computational fluid dynamics (CFD) to revolutionize the ship hydrodynamics research. Over the last few decades, CFD has opened new horizons in the research field of ship hydrodynamics. The simulation based design (SBD) approach is replacing the now old fashion build and test approach enabling innovative designs and cost saving to meet the challenges of the 21st century, especially with regard to safety, energy and economy (Sanada et al., 2013). Even though, model testing is only required at the final stages of the design in the SBD approach; there is still need of experimental fluid dynamics (EFD) tests for further model development and CFD validation. This development of CFD and SBD necessitates even more advanced measurement systems for both global and local flow variables to produce validating data for these approaches. More stringent requirements are also placed on experimental uncertainty analysis as it plays an important role in the validation procedures (Sanada et al., 2013).

Initially, researchers and scientists have relied on the use of wind tunnel and towing tank data for validation. The ship hydrodynamics CFD Workshops over the past three decades have shown the struggle of experimental measurement capability for providing validation data to match with the rapid development of CFD capability. Local flow measurement capability has evolved from 5-hole pitot tubes, capacitance wires and point gauges (Toda et al., 1992) to 2D Particle Image Velocimetry (PIV) and servo mechanism wave gauges (Longo et al., 2007; Irvine et al., 2004) to stereoscopic PIV (Yoon, 2009) and Tomographic PIV (Yoon, et al., 2014a). Global flow measurements have evolved from load cells and camera/LED motion tracking in towing tanks (Irvine et al., 2008) to detailed trajectory and appendage force/moment measurements for free running models in wave basins (Toxopeus et al., 2011). In recent years, wave basin tests

have expanded from seakeeping in oblique headings and calm water to cover course keeping (Toxopeus et al., 2011), maneuvering (Ueno et al., 2003; Yasukawa and Nakayama, 2006) and capsize (Furukawa et al., 2012) in waves as well as high-speed multi-hull ships in deep and shallow water (Milanov et al., 2011).The need for free running model tests in wave basins including local flow measurements is of paramount importance as CFD has achieved free running capability including calm water maneuvering (Carrica et al., 2010), course keeping in waves (Stern et al., 2011), and capsize (Sadat-Hosseni et al., 2011a).

To keep pace with CFD, EFD research have developed from captive testing in calm water in towing tanks to captive model testing in waves to free-running model testing in waves. Pioneered by (Eda et al., 1962), ship maneuverability in wave research has excelled to study ship stability and capsizing in violent flow as recommended by International Towing Tank Conference (ITTC) (2002), estimation of ship performance in actual sea as well as the development of mathematical models with the capability of predicting the forces/moments acting on a ship. These mathematical models have relied on the fluid potential theory when studying ship turning trajectory in regular waves (Hirano et al., 1980a) , effects of ship motion on ship maneuvering in waves (Seo et al., 2011), and in the study of the 6DOF simulations of a turning ship in regular/irregular waves (Yasukawa et al., 2006). In attempt to improve the prediction capability of the mathematical model, (Hirano et al., 1980b) took the coupling effect due to heel into consideration. With the new International Maritime Organization (IMO) adopted mandatory Energy Efficiency Design Index (EEDI) with regard to ship greenhouse gas (GHG) emission, these mathematical models accuracy in predicting ship performance and the forces/moments acting on the ship are limited due to the fact that potential theory does not consider the viscous effects of the flow around the ship hull nor the interaction between the wave and flow around the ship. To better investigate the wave drift forces and its effects on ship maneuverability, new approaches must be developed. This led to a

rising demand for new type of wave basin with the capabilities of executing local flow measurements to study the viscous effects and wave-flow interaction around the ship model for better evaluation of the ship resistance and propulsion performance to enhance hydrodynamic performance which can lead to energy efficient ship design that comply with the IMO regulation and satisfy the need of the marine industry for energy-efficient ship technologies because of the continually rising fuel price. The IIHR ship hydrodynamics program is combining the CFD analysis with EFD model testing to provide a basis for designing energy-saving ships as well as performing an integral evaluation of wave drift force and ship hydrodynamic performance. IIHR towing tank experiments are used for CFD validation (Yoon et al., 2014b); however, there is a need for new facilities with free-running experiments capability since CFD is simulating free-running ships.

To accomplish these ship hydrodynamics program goals, a new IIHR wave basin facility was specifically designed for local flow measurements around free running models including six plunger-type wave makers, x carriage, and y, θ sub-carriage/turntable with model tracking system, model release system, and semi-captive mount and traverse for ensemble-averaged local flow PIV and wave elevation measurements (Sanada et al., 2013). The local flow measurements along with the free-running model tests will provide better means to study and evaluate ship hydrodynamic performance as well as benchmark data for the validation of the IIHR CFD codes. As a part of this project, the present study objective is to ensure the data quality of the measurement system and its repeatability for the use of local flow PIV measurements. Another objective of this study is to provide wide range of maneuvering tests data in different wave encounter angles to investigate the wave drift forces which will help establish ONR Tumblehome (ONRT) maneuvering benchmark data for CFD validation. Data obtained in this experiment will also be used to improve the system-based (SB) method and the development of a mathematical model to evaluate the forces/moments

exerted on the ship. The present study describes the IIHR wave basin facility, the free running measurement systems, and calm water and wave trajectories and maneuvering characteristics in head and following wave for the ONRT.

CHAPTER 2

EXPERIMENTAL METHODS

2.1 IIHR Wave Basin Facility

The IIHR- Hydroscience & Engineering wave basin dimensions are 40-m, 20-m, and 4.3-m for length, width and depth respectively and the basin is filled with 3-m deep water. Along with the capability of executing local flow measurement, the wave basin is designed for conducting semi-captive or radio-controlled free-running ship model tests in calm water or under a wide range of wave's conditions induced by six plunger-type wave makers. As shown in Figures 2.1 and 2.2, the wave makers are located on the east side of the wave basin and a 7.8x20-m^2 wave beach is at the west end with 11.3° tilt angle to reduce reflected waves. The wave basin is also equipped with two dampers along the north and south side walls. These side wall dampers help minimizing the waiting periods to be calm down between testing when downward between tests and moved upward during tests. A dock and a work platform are set above the wave beach for test setup. A trimming tank is attached to the wave basin the south-west corner. The 4.0x0.9x1.5 m^3 trimming tank is for the purpose of placing the ship model into and out of the water. It is also used for completing ship model ballasting process. A carriage system is placed over the wave basin that is consisted of a main carriage, sub carriage, and a turntable. The main carriage is designed to move on the railway in the x-direction (east-west). The sub carriage is designed to move on a rack-gear in the y-direction (north-south). The turntable that is attached to the sub carriage and is designed to move on a ring-gear in the turning direction in the XY-plane. Two operating control panels are available at the wave basin to control the movement of the carriage system and the wave makers. The combination of the three movements of the carriage provides a system that can be used in semi-captive tests and track a ship model when running freely on the horizontal surface of the wave basin.

The wave makers can generate regular waves when all six plungers are operating in the same amplitude, frequency and initial phase. The wave makers can also generate irregular waves when the time-series of the analog voltage control signal are input into each plunger. The wave makers were calibrated to produce regular waves with four different wave heights for each one of three wavelengths that meet the standard maneuvering tests conditions regulated by the International Maritime Organization (IMO 2002). The details of the wave calibration conditions are outlined in Table 2.1. As shown in Figure 2.3, each wave plunger is 1.2 m, 3.3 m, and 0.8 m in height, width, and depth respectively and has a curvature radius of 100 mm. Figure 2.3 also shows the relationship between the plunger stroke and frequency. The maximal plunger stroke is 250 mm with frequency less than 0.62 Hz.

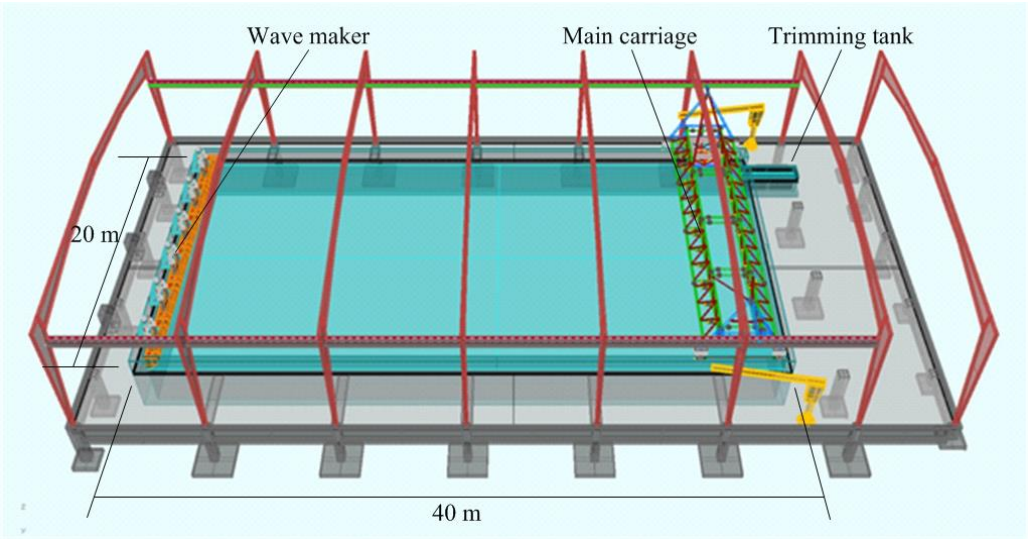

Figure 2.1 A schematic drawing of the IIHR wave basin

Source: (Sanada et al., 2013)

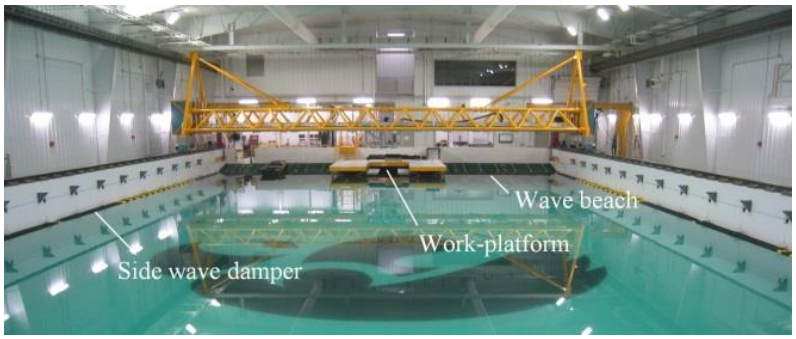

Figure 2.2 A full view picture of the wave basin from the wave makers' side

Source: (Sanada et al., 2013)

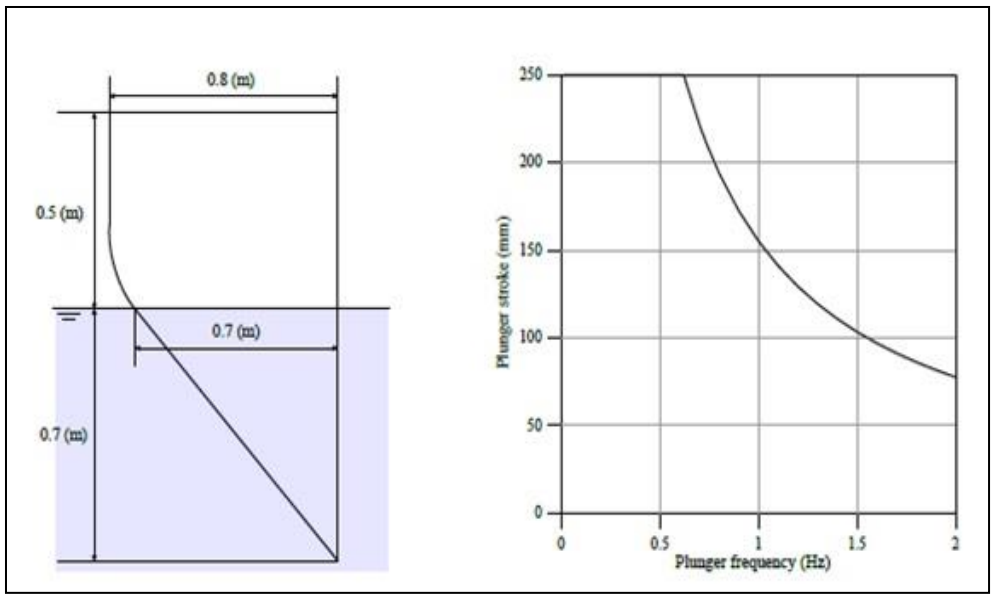

Figure 2.3 A plunger cross sectional (left) and a plunger frequency to plunger stroke relation (right)

Source: (Sanada et al., 2013)

In table 2.1, λ, L, H, T_P, F_P, and Sp are wavelength, ship model length, wave height, plunger period, plunger frequency, and plunger-stroke respectively. The ratios λ/L and H/λ are then the wavelength to ship length ratio and wave steepness respectively.

Table 2.1 Condition of the wave calibration

λ/L	H/λ	λ [m]	H [m]	T_P [s]	F_P [Hz]	Sp [mm] (Before calibration)	Sp [mm] (After calibration)
0.50	0.01	1.57	0.02	1.00	1.00	8.46	10.67
	0.02		0.03			16.94	15.93
	0.03		0.05			25.40	26.98
	0.05		0.08			42.34	43.39
1.00	0.01	3.15	0.03	1.43	0.70	25.22	24.32
	0.02		0.06			50.44	49.05
	0.03		0.10			75.66	82.24
	0.05		0.16			126.10	134.49
1.20	0.01	3.78	0.04	1.56	0.64	33.62	36.17
	0.02		0.08			67.26	72.76
	0.03		0.11			100.88	100.75
	0.05		0.19			168.14	176.35

Source: (Sanada et al., 2013)

2.2 ONR Tumblehome Model

The present study focuses on the ONRT surface combatant, which is publically accessible for fundamental research. The ONRT is a preliminary design of a modern surface combatant with a full scale length of 154 m. Used for this study, the 1/49 scaled ship model is appended with skeg and bilge keels. The model also had two rudders, shafts and two propellers with propeller shaft brackets. For this study, the model superstructure was not attached. Table 2.1 lists the main particulars of the ONRT ship model. The metacentric height above vertical center of gravity (VCG), i.e. GM, natural roll period and radius of gyration in pitch were decided in reference to Sadat-Hosseini et al.,

(2011b). They were adjusted by inclining test, free roll decay test and swing test respectively (Sanada et al., 2013).

Table 2. 2 Principle Particulars of ONR Tumblehome Vessel

	Model Scale
Length (L)	3.147 [m]
Breadth	0.384 [m]
Depth	0.266 [m]
Draft	0.112 [m]
Displacement	72.6 [kg]
Metacentric height	0.0422 [m]
Natural roll period	1.665 [s]
Rudder area	0.012 [m^2] x 2
Block coefficient	0.535
Radius of gyration in pitch	0.246 x L
Maximum rudder Angle	±35°

Figure 2.4 The ONR Tumblehome

Source: (Cook, S.S. 2011)

2.3 Data Acquisition System

The IIHR wave basin is equipped with three major measurement systems that are used to acquire free-running ship model maneuvering data. These three systems are consisted of the free-running measurement system, the carriage tracking system, and the 6DOF visual motion capture system (6DOF-VMCS). The free-running system measures the roll, pitch, and yaw angles of the ship model. The carriage tracking system allows the measurement of the ship model position in x, y, and the yaw angle in a global coordinate system. The 6DOF-VMCS allows the measurement of the ship position as well as the roll angle, pitch angle, yaw angle, and the heave motion of the ship model.

In free-running tests, the propeller starts to rotate once the test is initiated using the graphical user interface (GUI) based software on a laptop computer after all the test conditions are entered. Then the ship model is towed to the test starting initial position by the motion the main carriage using the model release system and the semi-captive mounts. Once the measurement is initiated, the ship model is accelerated with the carriage motion to reach the desired initial speed in a short distance, and then released for free-running. After launching, the ship advances straight without any rudder deflection and starts maneuvering after the elapse of a specified period of time. Propeller number of revolution was kept constant to satisfy required Froude number in free running. When tests were conducted in waves, the ship model was launched after the wave traveled over the half way of the wave basin.

2.3.1 Free-running system

The free-running system allows for radio-controlled ship model tests. The free-running system is composed of four major parts, which are a control unit, a drive unit, a power unit and a communication unit. An on-board computer, a Fiber optic gyro (FOG), and two radio-control RCs are the components of the control unit. The FOG is used to measure the roll, pitch, and yaw angles with an accuracy of ±0.5° for the roll and pitch

angles and ±1.0º for the yaw angle without considering the error caused by the internal signal drift effect. The amount of signal drift of yaw angle can be kept ±1.0º within 5 minutes on the average if the accumulative amount of drift is reset at regular time intervals of about 10 minutes (Sanada et al., 2013). The propulsion and rudder units compose the drive unit of the free-running system. A motor speed controller, a reverse gear, a gear motor, a two-axle allotter, and two shafts and propellers makes the components of the propulsion system of the drive unit while two rudders, step motor and a motors driver for each rudder. The means of measuring the propeller revolutions and the rudder angles were described by (Sanada et al., 2013) as a photo micro sensor to count the number of propeller revolutions while the rudder angle is indirectly estimated from the number of pulse signals transmitted to the stepping motor. A 24-V battery and a 12-V battery equipped with an on/off switching box for power control are the components of the free-running system power unit and are used to power the drive unit and the control unit respectively. Activated by the laptop computer, the GUI based software is used for specifying the test condition and parameters such as test type, timing between test steps, propeller revolution, rudder angle, offset rudder angle, speed/timing of rudder deflection and Proportional-Integral-Derivative (PID) gain. The system and the communication of the devices through Wi-Fi are illustrated in Figure 2.5 and the types of tests, data management and steps LED indicator are described as:

> Three test types are available: one of the test types is for course keeping tests, i.e. the ship model keeps the specified course with auto-pilot control; and the other two are for standard maneuvering tests, i.e. turning tests, and zigzag tests. After the test is over, the recorded measurement data is downloaded from the on-board PC to on-land PC and saved. Wi-Fi is used for data communication, with which a user can check data by drawing a graph on the spot. In addition, the LED flash light is used for announcing the process stage. The way of blinking is changed according to the operation stage such as mooring, data communication, and running w/ and w/o recording. FOG data, rpm, rudder angle are recorded by 20 Hz. Data acquisition of the free-running system, the carriage tracking system and 6DOF visual motion capture system etc. can be synchronized by receiving a start signal of the radio control (Sanada et al., 2013).

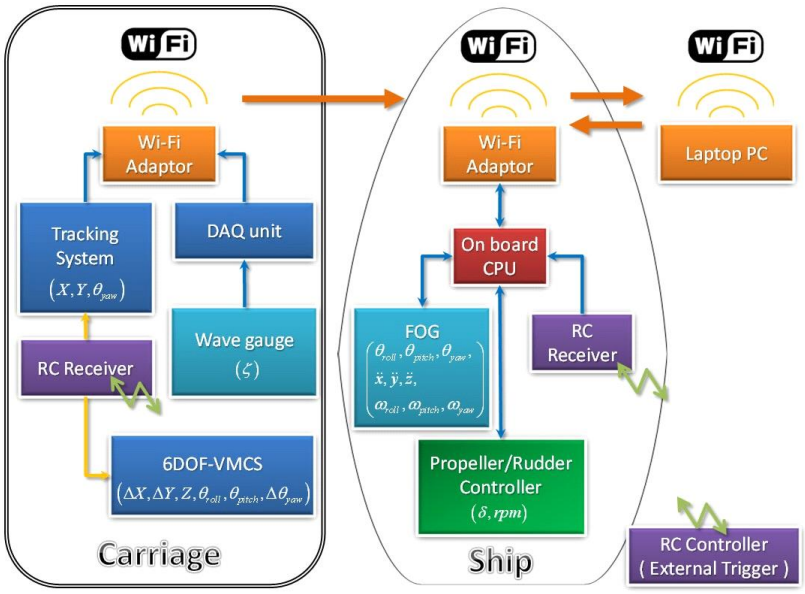

Figure 2.5 Diagram of the free-running system

Source: (Sanada et al., 2013)

2.3.2 Carriage tracking system

The carriage tracking system allows for the measurement of the ship position and the yaw angle in free-running tests. The system is consisted of a 12-ton main carriage that travels on rails in the X direction, a 2-ton sub-carriage that travels in the Y direction, and a turntable attached to the sub-carriage and rotates in the XY plane allowing for the measurement of the ship model yaw angle. The components of the carriage tracking system are illustrated in Figure 2.6 and are described as:

> The carriage tracking system consists of a 12-ton main carriage, 2-ton sub-carriage and a turntable attached to the sub-carriage to enable a 3DOF motion tracking of the ship model position and yaw angle in free-running tests and conducting local flow measurement in semi-captive tests. Two tracking CCD cameras are installed on the turntable of the sub carriage to recognize the brightness of two LED lights placed on the bow and stern of the ship model. The carriage system automatically adjusts the XY-position and the turning angle to keep the two LED dots at the centers of the two camera views. The mid-point

between the two LED dots corresponds to the longitudinal center of gravity LCG of the ship model. The ship model position is defined at the center of gravity and carriage position is defined at the center of the sub-carriage. When the ship model is still at the initial position and attached to the sub-carriage with the semi-captive mount, the center of the sub-carriage comes just above the LCG of the ship model. Therefore we can determine the initial position of the ship model directly by the carriage position. When the ship model is in motion, the ship model position can be determined by the carriage position and positional vector from the center of the sub-carriage to the LCG of the ship model. The positional vector can be calculated by the two LED dots position. The sampling rate of the carriage tracking system for determining the (x, y) position and tuning angle is 20 Hz.

Proportional and integral controls with respect to range error are incorporated into the tracking system. Each gain was adjusted by many trials. Considering the carriage load, the maximum tracking speed in the x and y direction is 2.5 m/s, and the maximal rotational speed is 20deg/s. As for the tracking acceleration, 0.75 m/s^2 and 10deg/s^2 are the maxima for XY-motion and turning, respectively. The effective tracking area in the wave basin is about 29.7 x 15 m^2 or less due to the presence of the work-platform. The system suspends tracking when the carriage comes close to the boundary of the tracking area. Mechanical limit switches are also set up at the end of the tracking area for insurance of not over-running. The number of turns of the turning Table is restricted by 720º due to the cable length (Sanada et al., 2013).

The carriage tracking system errors and their possible sources are also discussed by Sanada as follows:

The possible errors should be assessed for tracking accuracy and they are theoretically from two sources. The first source is mechanical, i.e. the main carriage moving on the railway might have slippage. Since there is no way to recognize the occurrence of slipping, the system would misidentify the current position. This error, however, could be considered to be small unless a sudden and hard acceleration or deceleration occurs. Meanwhile, because the sub carriage moves in the y direction and turntable in the turning direction using a rack and ring gears respectively, it can be expected that no slipping but only the amount of backlash of the gears may result in very small errors. As the second source, the error of image processing should be taken into account. The image processing error depends on the digital resolution of the CCD cameras. The cameras used in the carriage model tracking system have 1/3-inch (3.6 x 4.8 mm^2) CCD sensors with 480 x 640 pixels, and the lens focus length is 8 mm. Assuming the distance from the camera lens to LEDs on the deck as 1.2 m, the resolution is 1.125 mm/pixel, so that the output error of image processing can be estimated as ±0.5625 mm for x and y, and ±0.027º for turning. Note that the output resolution of the carriage model tracking system is 1 mm for the XY-position and 0.1º for the turning angle, such that the image processing errors are not significant. Besides the two main error sources, other factors may also result in errors, such as delay of data communication and alignment accuracy of the x rail, y rack gear and ring-gear(Sanada et al., 2013).

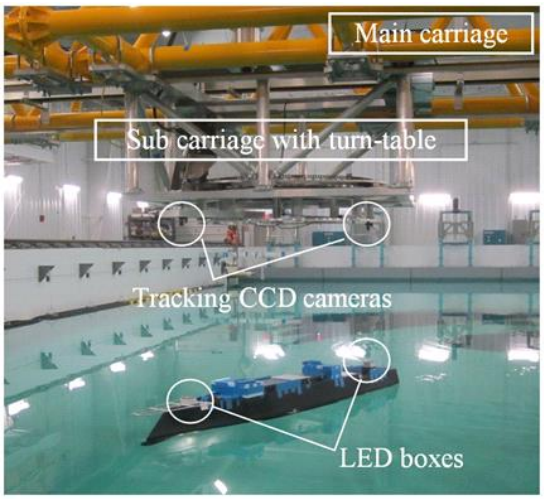

Figure 2.6 Carriage tracking system

Source: (Sanada et al., 2013)

2.3.3 Mirror system

Large roll motion such as tests in waves may results in large position error and high frequency motion of the carriage. This could occur due to the positioning of the LED tracking markers away from the center of gravity of the ship model. To reduce the error and the high frequency, a mirror system is being used. The position error that could result from large roll motion and the mirror system used to reduce it are shown in Figure 2.8. The method is described as:

> The LED maker on the deck of the ship model is displaced from the camera lens axis, and a mirror is inserted at the original position of the LED marker, so that an image of the LED marker is created at the level of ship model gravity center. When the two cameras track the two mirror images of the LED markers, the position error and large high frequency motion of the carriage can be reduced (Sanada et al., 2013).

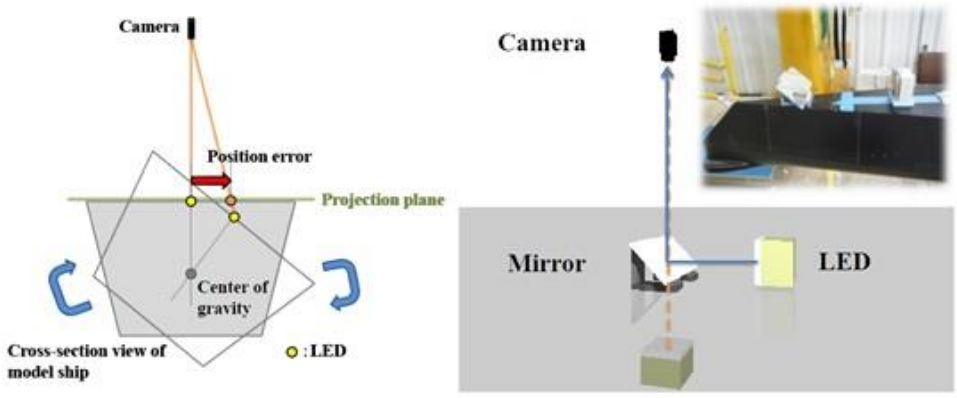

Figure 2.7 Mirror system used to reduce position error of the carriage tracking system. Left: position error resulting from roll motion of the ship hull. Right: a mirror used to lower the image of the LED marker to the center of gravity of the ship model

Source: (Sanada et al., 2013)

2.3.4 6DOF visual motion capture system

The FOG and the carriage tracking system allow for 5DOF measurement in free-running tests when combined. A 6DOF visual motion capture system (6DOF-VMCS) is implemented for the purpose of adding an extra degree of freedom and improving the free-running measurement accuracy of the 5DOF measurement system. The 6DOF-VMCS components are illustrated in Figure 2.8 and are described as:

> A high-resolution CCD camera was installed on the turntable of the sub-carriage that focused on a calibration target plate attached on the deck of the free-running ship model. The target has a regular pattern that consists of black and white squares. Distorted image pattern is obtained when the view angle and distance between the CCD camera and the target plate are changed. The camera position with respect to the target plate can be determined by using a digital image pattern analysis method (Zhang, 2000); so that the target plate motion can be measured (Sanada et al., 2013).

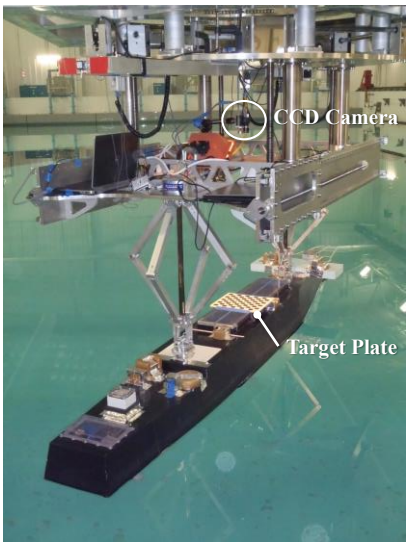

Figure 2.8 6DOF visual motion tracking system

Source: Sanada et al., (2013)

2.3.5 Reflected light distribution method

The concept of the Reflected Light Distribution (RLD) method used in the IIHR wave basin which is illustrated in Figure 2.9a and 2.9b was developed by (Sanada et al., 2008) and is described as:

> A reflected light distribution (RLD) method (Sanada et al., 2008) is used to measure the wave elevation around the test model. The concept of the RLD method is illustrated in Fig. 9a. A diffused light source provides a color coded pattern in a plane that is parallel to the still water surface so that a reference image pattern is captured with a camera. During tests with a wavy surface, a distorted image patterns is obtained at a certain time. The wave elevation distribution is determined with correlation of the distorted image pattern and the reference image pattern. The RLD system enables a non-intrusive and full-field wave elevation measurement (Sanada et al., 2013).

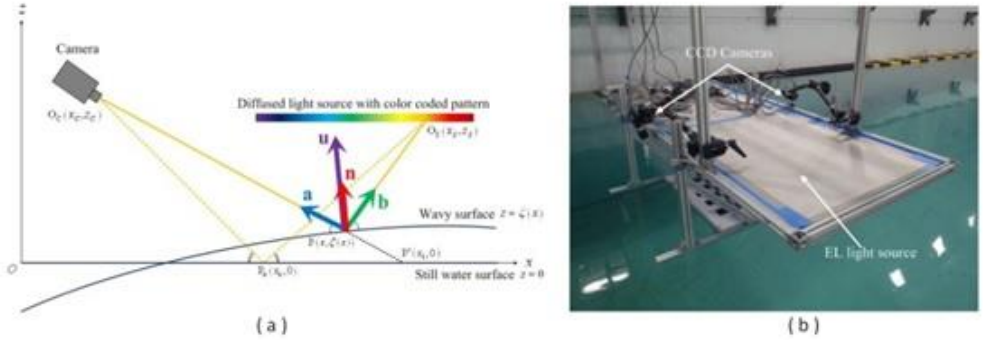

Figure 2.9 Measurement system for RLD method (a) RLD method concept. (b) RLD measurement system

Source: (Sanada et al., 2013)

2.3.6 Model release system and semi-captive mount

Equipped with electromagnetic parts, two mechanical arms are attached to the turntable of the carriage system form the model release system as illustrated in Figure 2.10a. As shown in Figures 2.10b, 2.10c and 2.10d, the electromagnetic parts at the ends of the mechanical arms allows for the ship model roll, heave and pitch motion in a semi-captive mode when these ends are attached to the ship model.

The semi-captive mode and released ship model are illustrated in Figures 2.10e and 2.10f. The semi-captive mounts are used to conduct captive tests to determine the optimum release time when conducting free-running tests. These captive tests are course keeping tests with the same test conditions of which the release time to be determined. When conducting free-running tests, the ship model towed to the initial position if needed. Once the free-running test is initiated, the model is kept attached to the carriage for the specified time to reach the desired initial speed and then released as shown in Figure 2.11

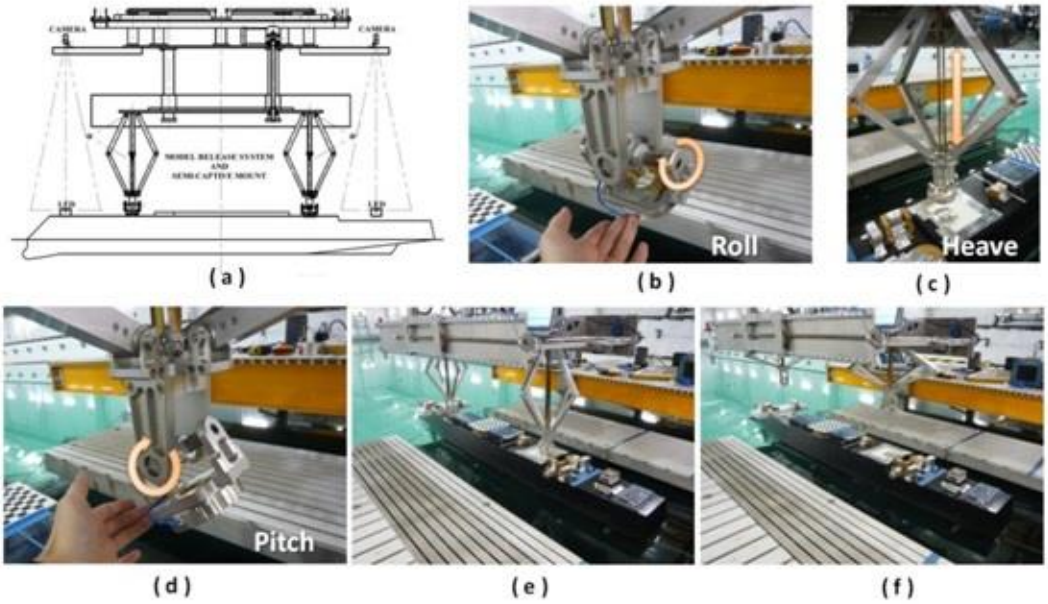

Figure 2.10 Model release system and semi-captive mount: (a) sketch of model release system, (b) roll motion of semi-captive mount, (c) heave motion of semi-captive mount, (d) pitch motion of semi-captive mount, (e) model in semi-captive, and (f) model released

Source: (Sanada et al., 2013)

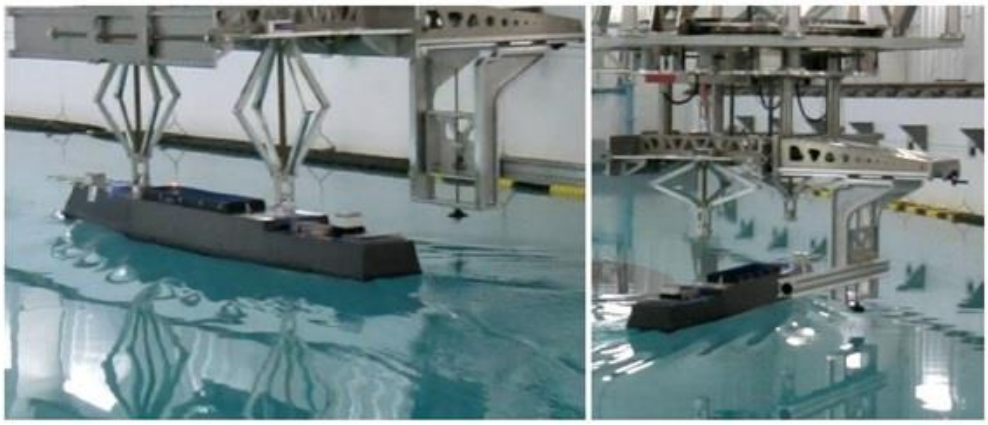

Figure 2.11 Test model in acceleration (left) and released at desired speed (right). Traverse for local flow measurements on the right of the ship model

Source: (Sanada et al., 2013)

2.4 Test Conditions

The global and ship model fixed coordinate systems are defined in Figure 2.12, where X_0 and Y_0 are in the global coordinate and x and y are in the ship coordinate system. The yaw angle Ψ is the same in both coordinate systems r, δ, and β are the roll angle, rudder angle, and drift angle with respect to the ship coordinate system. Figure 2.13 shows the definition of the wave encounter angle χ while Figure 2.14 shows the ship heading and χ relationship. Table 2.3 outlines the details of all the test conditions. The study followed the ship maneuvering tests standards and criteria defined by the American Bureau of Shipping (ABS). Those standards and criteria comply with the IMO standards (ABS 2006a). The IMO maneuvering criteria are outlined in Table H-1 in Appendix H.

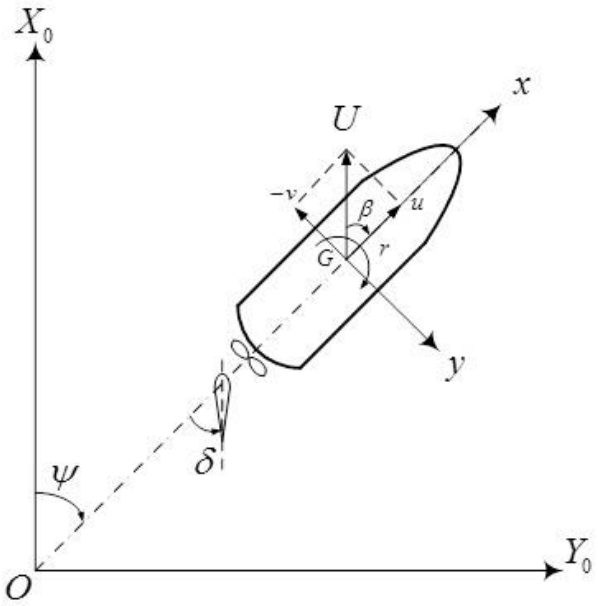

Figure 2.12 Global coordinate system and ship model fixed coordinate systems

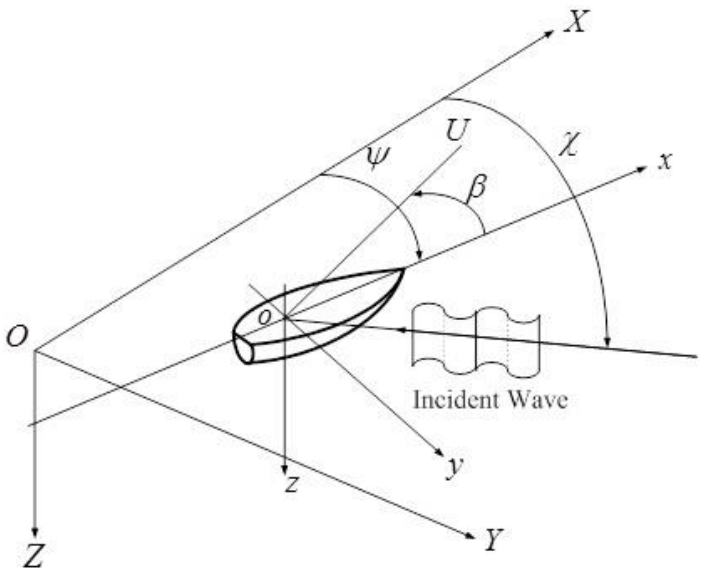

Figure 2.13 Wave encounter angle definition

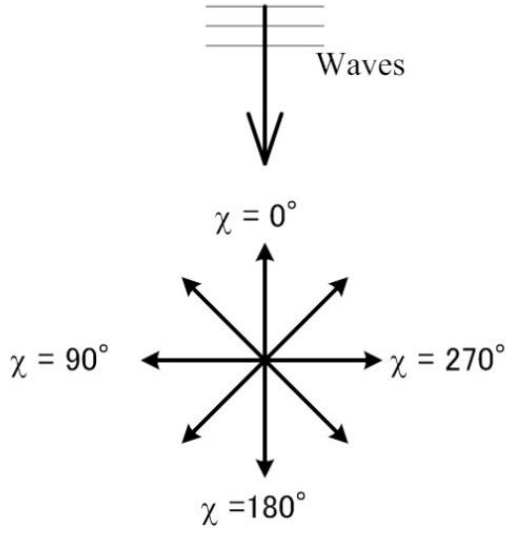

Figure 2.14 Relationship between ship heading direction and wave angle

2.4.1 Course keeping tests in calm water

Course keeping maneuvering tests in calm water were performed at Froude number (Fr) 0.2. These test cases included head, following, beam, quartering, and oblique headings trajectories. To achieve these headings, a suitable initial ship position is chosen to produce the desired trajectory for each test condition case. The course keeping calm water tests are used as a reference for the matching conditions wave tests.

2.4.2 Course keeping tests in waves

Course keeping maneuvering tests in wave conditions were performed at Fr = 0.2. These cases include head, following, beam, quartering waves as well as oblique heading. The ship speed to satisfy Fr = 0.2 was used in combination with several wave encounter angle (χ) to achieve these headings. Three wavelengths to ship length ratio (λ/L) of 0.5, 1.0, and 1.2 were used for each wave encounter case while the wave steepness (H/λ) was held constant at 0.02 for all the course keeping test cases. This allows tests to be performed in head, following, beam, and quartering waves as well as oblique heading tests.

2.4.3 Zigzag tests in calm water

Zigzag maneuvering tests in calm water were performed at Fr = 0.2 for 10°/10°, 20°/20°, and 35°/35° rudder angles (δ). These cases were to simulate the head and following wave zigzag cases. To achieve these headings, a suitable initial ship position is chosen to produce the desired trajectory such as (0, 0, 0) and (29.8, 0, 180) for x, y, and θ. Calm water zigzag tests will also serve as references to their counterpart wave cases.

2.4.4 Zigzag tests in waves

Zigzag maneuvering tests in head and following waves were performed at Fr = 0.2 with three λ/L values of 0.5, 1.0, and 1.2 for each one of the three different rudder angles setup. Two values of 0.02 and 0.03 of the wave steepness were used in the zigzag

tests. For H/λ = 0.02, zigzag tests were performed at three different rudder angles setup of 10°/10°, 20°/20°, and 35°/35° in regular head and following waves. For H/λ= 0.03, only 35°/35° rudder angle setup was used in following waves test cases.

2.4.5 Turning tests in calm water

Turning maneuvering tests in calm water were performed at Froude number 0.1, 0.2, and 0.3 with rudder angle of ±35°. The experimental setup for these cases was chosen to match the turning tests in wave conditions.in order to use these calm water tests as references for the wave cases To achieve these headings, a suitable initial ship position is chosen to produce the desired trajectory for each turning in calm water as well as their matching wave cases. Four different θ values were chosen for the initial heading of the ship model. These values are 0°, ±90°, and 180°.

2.4.6 Turning tests in waves

The turning maneuvering tests were performed at Froude number values of 0.1, 0.2, and 0.3 with rudder angles setup values of ±35°. For all the turning test cases, a constant value of H/λ = 0.02 was used in combination with three λ/L values of 0.5, 1.0, and 1.2. Four different χ values of -90°, 0°, 90°, and 180° were used for Froude number 0.2. For Froude numbers of 0.1 and 0.3, tests were performed at χ value of 0° only.

Table 2. 3 Maneuvering tests conditions in calm water and waves

	Test	Fr*	δ [deg]	Ψ^{**} [deg]	H/L	λ/L	χ [deg]	Numbers of runs
Calm water	Course keeping	0.2	N/A	0, 180	0.02		0, 180	6
				±45, ±135			±45, ±135	12
				±90			±90	6
	Zigzag	0.2	10	10	0.02		0,180	6
			20	20				6
			35	35,90	0.02,0.03			6
	Turning circle	0.1	±35	N/A	0.02		0	10
		0.2					0,±90, 180	31
		0.3					0	10
Head Wave	Course keeping	0.2	N/A	0	0.02	0.5	0	3
						1.0		3
						1.2		3
	Zigzag	0.2	10	10	0.02	0.5,1.0, 1.2	0	9
			20	20		0.5,1.0,1.2		9
			35	35		0.5,1.0, 1.2		9
	Turning circle	0.1	±35	N/A	0.02	0.5,1.0,1.2	0	30
		0.2				0.5,1.0, 1.2	0,±90 ,180	99
		0.3				0.5, 1.0	0	20
Following waves	Course keeping	0.2	N/A	180	0.02	0.5	180	3
						1.0		3
						1.2		3
	Zigzag	0.2	10	10	0.02	0.5,1.0, 1.2	180	9
			20	20		0.5,1.0, 1.2		9
			35	35	0.02,0.03	0.5,1.0,1.2		18
Beam waves	Course keeping	0.2	N/A	±90	0.02	0.5	±90	3
						1.0		3
						1.2		3
Quartering waves*	Course keeping	0.2	N/A	±45, ±135	0.02	0.5	±45, ±135	12
						1.0		12
						1.2		12

Fr*: the nominal Froude number.
Ψ^*: the target yaw angle.
Quartering waves*: are called quartering waves when χ = ±135° and oblique heading when χ = ±45°

2.5 Data Reduction and Analysis Methods

A large amount of data is acquired by the three measurement systems once the test is conducted. The free-running and the carriage tracking systems data sampling rate is 20 Hz while the 6DOF-VMCS sampling rate is 30 Hz. To accommodate the difference in the sampling rates and transform measured parameters from global coordinate system to ship coordinate system, synchronizing software is used to synchronize all data from the three measurement systems into one file for each run. Before synchronizing all the data, filters are needed to be applied to the 6DOF-VMCS data to reduce its signal noise. C++ codes are used to convert these synchronized files to compatible Tec plot ascii format files. A Tecplot layout file is prepared to draw time series of the trajectory, propeller revolution, rudder angle, ship speed, velocity components, drift angle, yaw, yaw rate, heave motion, roll, and pitch for all the runs of the same test case.

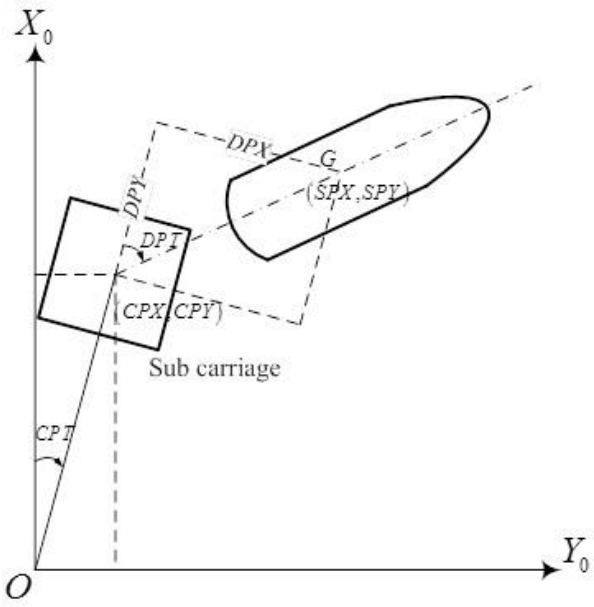

Figure 2.15 Position relationship between carriage and model in global coordinate system

Figure 2.15 describes the relationship of the carriage and model position in global coordinate system where CPX, CPY, and CPT indicate the carriage x, y, and θ position respectively. Similarly, SPX, SPY, and SPT indicate the ship x and y position and ship yaw angle. DPX and DPY are the x and y component of the positional vector from the center of sub-carriage to the longitudinal center of gravity (LCG) of the ship model. DPT is the difference between ship yaw angle and sub-carriage/turntable angle. CPX, CPY, and CPT are obtained by the data from rotary encoders of main and sub-carriage. DPX, DPY, and DPT are obtained by the LED marker tracking system and the 6DOF-VMCS separately.

For the main carriage to track the ship model while test is running, real-time ship position data must be inputted to the Proportional Integral (PI) control. The ship position data is obtained from the LED marker tracking system to PI control and hence the carriage system tracks and calculates the ship model position. This process is done iteratively during the test period. Once the test is completed, the ship position DPX, DPY, and DPT obtained by the 6DOF-VMCS are used in the data reduction because of the fact that 6DOF-VMCS is more accurate than the LED marker tracking system.

To calculate the ship position in the global coordinate system, equation 2.1 and 2.2 are used,

$$\begin{pmatrix} SPX \\ SPY \end{pmatrix} = \begin{pmatrix} CPX \\ CPY \end{pmatrix} + \begin{pmatrix} \cos(CPT) & -\sin(CPT) \\ \sin(CPT) & \cos(CPT) \end{pmatrix} \begin{pmatrix} DPX \\ DPY \end{pmatrix} \tag{2.1}$$

$$SPT = CPT + DPT \tag{2.2}$$

for the ship velocity conversion from ship coordinate to global coordinate, equations 2.3, 2.4, 2.5, and 2.6 are used.

$$\frac{dX_0}{dt} = u\cos\Psi - v\sin\Psi \tag{2.3}$$

$$\frac{dY_0}{dt} = u\sin\Psi + v\cos\Psi \tag{2.4}$$

$$\begin{pmatrix} \frac{dX_0}{dt} \\ \frac{dY_0}{dt} \end{pmatrix} = \begin{pmatrix} \cos\Psi & -\sin\Psi \\ \sin\Psi & \cos\Psi \end{pmatrix} \begin{pmatrix} u \\ v \end{pmatrix} \tag{2.5}$$

$$\begin{pmatrix} u \\ v \end{pmatrix} = \begin{pmatrix} \cos\Psi & -\sin\Psi \\ \sin\Psi & \cos\Psi \end{pmatrix}^{-1} \begin{pmatrix} \frac{dX_0}{dt} \\ \frac{dY_0}{dt} \end{pmatrix} \tag{2.6}$$

where X_0 and Y_0 are the ship position in the global coordinate system, u and v are the ship velocity components in the ship coordinate system, and ψ is ship yaw angle.

Equations 2.7a, 2.7b, 2.8, 2.9, and 2.10 are used to calculate the velocity and drift angle.

$$u = U\cos\beta \tag{2.7a}$$

$$v = -U\sin\beta \tag{2.7b}$$

$$U = \sqrt{u^2 + v^2} \tag{2.8}$$

$$\frac{v}{u} = \frac{-U\sin\beta}{U\cos\beta} = -\tan\beta \tag{2.9}$$

$$\beta = \arctan\left(-\frac{v}{u}\right) \tag{2.10}$$

where U is the ship velocity and β is the drift angle.

CHAPTER 3

UNCERTAINTY ASSESSMENT

3.1 Error Sources

A measurement error is the difference between the measured value and the true value and it is consisted of two components: random error and systematic error. While the random error accounts for the repeatability of the measurements, the systematic error accounts for the consistent deviation from the true value. The measurement uncertainty is then the combination of the random standard uncertainty due to the random error, and systematic standard uncertainty, due to the systematic error.

There are many sources of errors that contribute to the free-running measurement uncertainty. Some of the sources are shown in Table 3.1 are considered as measurement system errors while errors such as rail sinkage, rail alignment, and seiche (standing wave) are considered facility error. Main rail (x- axis rail) sinkage is caused by land sinkage and sub-carriage sinkage is caused by deformation of yellow structure (see Figure 2.2). Heave and wave measurement at sub-carriage are affected by the combination of those two sinkage. The main carriage slippage error is minimal unless sudden and hard acceleration/deceleration occurred during the testing. The LED marker tracking error depends on the resolution of the two CCD cameras. Of the error factors that contribute to the 6DOF-VMCS measurement are camera resolution, lens characteristics, and camera calibration. Another factor is the error of the wave quality incorporated from the wave maker's calibration. The results of these errors shown in Table 3.1 are estimations of the systematic error of each factor. The high accuracy of the 6DOF-VMCS is shown in Table 3.2, where the estimated errors of the 6DOF-VMCS are compared to other instruments.

Table 3.1 The free-running measurement error sources

Item	Error Source	Systematic error
Facility	Rail sinkage	±1.0 [mm]
	Rail alignment	-0.762 [mm]
	Carriage slippage on x- axis rail	Maximum of ±5 [mm]*
	Wave quality	< 5% (Satisfy IMO criteria)**
	Standing wave period	14.7 [s]
Carriage tracking system	Carriage position (CPX, CPY, CPT)	±1.0 [mm] for x and y, ±0.01° for yaw
	Ship position with respect to the sub-carriage obtained by LED marker tracking system (DPX, DPY, DPT)	±0.5625 [mm] for x and y, ±0.027° for yaw
	SPX,SPY,CPX,CPY,DPX,DPY	1.0 [mm]*
	SPT,CPT,DPT	0.1°*
6DOF-VMCS	Ship position with respect to the sub-carriage (DPX, DPY, DPT)	±0.3 [mm] for DPX, DPY and 0.002 rad for DPT***
	Roll, Pitch, Yaw, and Heave***	± 0.1 rad for Roll and Pitch and 2.1 [mm] for Heave***
Free-running system	FOG (Roll, Pitch, and Yaw)	±0.5º for roll and pitch, ±1.0º for yaw

* (Takagi, 2012)
** (Sanada et al., 2013)
*** (Tanimoto, 2012)

Table 3.2 6DOF-VMCS systematic error compared to other instruments

	Estimated error from specification	Maximum difference between 6DOF-VMCS and other instruments
DPX	0.03 mm	0.9 mm (Traversor)
DPY	0.03 mm	0.3 mm (Traversor)
DPT	0.002 rad	0.08 deg (Tracking system)
Heave	2.1 mm	1 mm (Traversor)
Roll	0.1 rad	0.4 deg (FOG)
Pitch	0.1 rad	0.2 deg (Laser sensor)

Source: (Tanimoto, 2012)

3.2 Statistical Analysis

Repeated tests of selected cases of zigzag and turning tests are performed to obtain the converged mean trajectories for the PIV measurements where each repeated test is performed for 21 runs. The statistical convergence error E_{SC} (%) is defined as:

$$E_{SC}(\%) = \frac{c}{\sqrt{N}} \cdot \frac{S_x}{\bar{x}} \times 100 \tag{3.1}$$

where N,$\bar{x}$ and S_x are the sample size, sample mean and standard deviation respectively. For test sample size that is greater than 10, c can be set to equal 2. The mean, standard deviation (STD) and the coefficient of variance are shown in Tables 3.3 through 3.12 for the 1st and 2nd overshoot angles (OSA) in zigzag tests and for the tactical diameter (T_D), advance (A_D) and transfer (T_R) in turning tests. The coefficient of variance is defined as

$$\mathrm{CV}(\%) = \frac{S_x}{\bar{x}} \times 100 \tag{3.2}$$

Table 3.3 Statistical analysis of zigzag 10°/10° in calm water and head and following waves at Fr = 0.2, H/λ= 0.02

Zigzag 10°/10°								
Test conditions		Number of Runs	1st OSA			2nd OSA		
χ	λ/L		Mean	STD	CV (%)	Mean	STD	CV (%)
0°	calm water	3	2.3135	0.0985	4.2593	-2.1029	0.0371	1.7638
180°		3	2.1751	0.1847	8.4904	-2.1430	0.1199	5.5936
0°	0.5	3	2.2005	0.0443	2.0110	-2.2136	0.2175	9.8256
180°		3	1.8218	0.0605	3.3195	-2.3427	0.0426	1.8199
0°	1	3	2.0810	0.0713	3.4272	-2.5454	0.4495	17.6592
180°		3	2.3781	0.0514	2.1634	-2.6321	0.1591	6.0447
0°	1.2	3	2.1256	0.1175	5.5262	-2.1382	0.2532	11.8405
180°		3	2.8364	0.0831	2.9290	-2.9073	0.0417	1.4357

Table 3.4 Statistical analysis of zigzag 20°/20° in calm water and head and following waves at Fr = 0.2, H/λ= 0.02

Zigzag 20°/20° , H/λ =0.02								
Test conditions		Number of Runs	1st OSA			2nd OSA		
χ	λ/L		Mean	STD	CV (%)	Mean	STD	CV (%)
0°	calm water	3	5.7300	0.1709	2.9823	-5.3552	0.1298	2.4244
180°		3	5.7718	0.2391	4.1430	-5.2292	0.2007	3.8380
0°	0.5	3	5.6284	0.0445	0.7915	-5.2566	0.0234	0.4448
180°		3	5.1006	0.2010	3.9401	-5.3470	0.1604	3.0007
0°	1	3	6.2770	0.1043	1.6608	-5.7289	0.4914	8.5775
180°		3	4.4521	0.1533	3.4426	-6.0786	0.2236	3.6777
0°	1.2	3	5.0619	0.3115	6.1529	-5.0529	0.3346	6.6227
180°		3	6.3481	0.2849	4.4882	-5.4694	0.1154	2.1094

Table 3.5 Statistical analysis of zigzag 20°/20° in following waves at Fr = 0.2, H/λ= 0.03

Zigzag 20°/20° , H/λ =0.03								
Test conditions		Number of Runs	1st OSA			2nd OSA		
χ	λ/L		Mean	STD	CV (%)	Mean	STD	CV (%)
180°	0.5	3	4.9805	0.1575	3.1619	-5.8409	0.0423	0.7234
180°	1	3	3.3410	0.0989	2.9597	-6.2633	0.1403	2.2394
180°	1.2	3	6.7691	0.1836	2.7116	-5.1444	0.522763	10.1618

Table 3.6 Statistical analysis of zigzag 35°/35° in calm water and head and following waves at Fr = 0.2, H/λ= 0.02

Zigzag 35°/35°								
Test conditions		Number of Runs	1st OSA			2nd OSA		
χ	λ/L		Mean	STD	CV (%)	Mean	STD	CV (%)
0°	calm water	3	10.6440	0.0855	0.8031	-9.2538	0.0856	0.9253
180°		3	10.4253	0.2108	2.0222	-9.0186	0.0246	0.2731
0°	0.5	3	11.0420	0.2646	2.3963	-9.7129	0.3283	3.3804
180°		3	9.9964	0.3392	3.3928	-8.8714	0.3037	3.4238
0°	1	3	10.5362	0.1975	1.8743	-9.3574	0.3708	3.9630
180°		3	11.3678	0.0222	0.1954	-9.9244	0.0867	0.8735
0°	1.2	3	11.2010	0.1296	1.1573	-10.5249	0.3310	3.1453
180°		3	11.1023	0.1093	0.9849	-10.5715	0.4769	4.5114

Table 3.7 Statistical analysis of turning tests in calm water and waves at Fr = 0.1, $\chi = 0°$

Fr = 0.1, $\chi = 0°$, $\delta = -35°$										
λ/L	Number of Runs	A_D [m]			T_R [m]			T_D [m]		
		Mean	STD	CV (%)	Mean	STD	CV (%)	Mean	STD	CV (%)
Calm water	5	7.0328	0.0857	1.2181	4.0206	0.0514	1.2775	10.0788	0.0585	0.5800
0.5	5	6.4477	0.0434	0.6736	3.8689	0.0665	1.7200	9.1780	0.1007	1.0968
1.0	5	6.0837	0.0485	0.7971	3.6003	0.0336	0.9336	8.9516	0.0237	0.2643
1.2	5	6.1645	0.0492	0.7986	3.4925	0.0420	1.2019	8.9126	0.0692	0.7767
Fr = 0.1, $\chi = 0°$, $\delta = 35°$										
λ/L	Number of Runs	A_D [m]			T_R [m]			T_D [m]		
		Mean	STD	CV (%)	Mean	STD	CV (%)	Mean	STD	CV (%)
Calm water	5	7.1152	0.0945	1.3282	4.1080	0.0790	1.9226	10.1729	0.1060	1.0420
0.5	5	6.6015	0.0822	1.2447	4.0248	0.0577	1.4342	9.4648	0.0861	0.9101
1.0	5	5.9932	0.0333	0.5552	3.7245	0.0658	1.7661	9.1272	0.0907	0.9938
1.2	5	6.1549	0.0977	1.5870	3.7881	0.0993	2.6206	9.2194	0.0675	0.7316

Table 3.8 Statistical analysis of turning tests in calm water and waves at Fr = 0.2, χ = -90°

Fr = 0.2, χ = -90°, δ = -35°										
λ/L	Number of Runs	A_D [m]			T_R [m]			T_D [m]		
		Mean	STD	CV (%)	Mean	STD	CV (%)	Mean	STD	CV (%)
Calm water	3	7.4293	0.0590	0.7938	4.0822	0.0431	1.0554	10.1721	0.0152	0.1490
0.5	3	7.5393	0.0279	0.3697	4.0272	0.0631	1.5678	9.8652	0.0883	0.8952
1.0	3	7.8430	0.0407	0.5188	4.3103	0.0345	0.8009	10.0725	0.0180	0.1789
1.2	3	7.7718	0.0090	0.1162	4.2360	0.0188	0.4436	10.0525	0.0274	0.2730
Fr = 0.2, χ = -90°, δ = 35°										
λ/L	Number of Runs	A_D [m]			T_R [m]			T_D [m]		
		Mean	STD	CV (%)	Mean	STD	CV (%)	Mean	STD	CV (%)
Calm water	3	7.4806	0.0401	0.5359	4.1486	0.0192	0.4638	10.3365	0.0312	0.3017
0.5	3	7.1864	0.0096	0.1335	4.1493	0.0334	0.8059	10.1896	0.0267	0.2620
1.0	3	7.1905	0.0250	0.3477	4.0919	0.0972	2.3745	10.2928	0.1093	1.0622
1.2	3	7.1401	0.0623	0.8731	4.0111	0.0287	0.7150	10.1938	0.0526	0.5159

Table 3.9 Statistical analysis of turning tests in calm water and waves at Fr = 0.2, $\chi = 0°$

Fr = 0.2, $\chi = 0°$, $\delta = -35°$										
λ/L	Number of Runs	A_D [m]			T_R [m]			T_D [m]		
		Mean	STD	CV (%)	Mean	STD	CV (%)	Mean	STD	CV (%)
Calm water	20	7.4789	0.0533	0.7129	4.0382	0.0503	1.2454	10.0208	0.0410	0.4088
0.5	5	7.3010	0.0519	0.7103	3.9608	0.0253	0.6391	9.7092	0.0341	0.3512
1.0	5	6.9965	0.0380	0.5432	3.7817	0.0223	0.5884	9.4334	0.0379	0.4023
1.2	5	7.1016	0.0475	0.6687	3.7792	0.0301	0.7958	9.4436	0.0361	0.3818
Fr = 0.2, $\chi = 0°$, $\delta = 35°$										
λ/L	Number of Runs	A_D [m]			T_R [m]			T_D [m]		
		Mean	STD	CV (%)	Mean	STD	CV (%)	Mean	STD	CV (%)
Calm water	5	7.4806	0.0371	0.4955	4.0539	0.0326	0.8050	10.0068	0.0603	0.6022
0.5	5	7.2614	0.0360	0.4957	3.9066	0.0212	0.5436	9.6486	0.0274	0.2837
1.0	5	6.9978	0.0460	0.6569	3.8797	0.0858	2.2125	9.5848	0.0737	0.7688
1.2	5	7.1875	0.0347	0.4822	3.9397	0.0691	1.7550	9.6464	0.0555	0.5758

Table 3.10 Statistical analysis of turning tests in calm water and waves at Fr = 0.2, $\chi = 90°$

Fr = 0.2, $\chi = 90°$, $\delta = -35°$										
λ/L	Number of Runs	A_D [m]			T_R [m]			T_D [m]		
		Mean	STD	CV (%)	Mean	STD	CV (%)	Mean	STD	CV (%)
Calm water	3	7.4301	0.0241	0.3248	4.0007	0.0453	1.1320	10.1117	0.0247	0.2447
0.5	3	7.3350	0.0354	0.4825	4.1250	0.0362	0.8769	10.3559	0.0274	0.2642
1.0	3	7.1621	0.1095	1.5282	4.0334	0.0203	0.5032	10.1544	0.0820	0.8077
1.2	3	7.1988	0.1033	1.4351	3.8768	0.0383	0.9872	10.0762	0.1513	1.5018
Fr = 0.2, $\chi = 90°$, $\delta = 35°$										
λ/L	Number of Runs	A_D [m]			T_R [m]			T_D [m]		
		Mean	STD	CV (%)	Mean	STD	CV (%)	Mean	STD	CV (%)
Calm water	3	7.3969	0.0536	0.7249	4.2110	0.0464	1.1030	10.2815	0.0316	0.3075
0.5	3	7.5370	0.0526	0.6979	4.1282	0.0310	0.7521	9.9090	0.0302	0.3043
1.0	3	7.7655	0.0543	0.6987	4.3372	0.0328	0.7554	10.1347	0.0493	0.4867
1.2	3	7.6952	0.0650	0.8453	4.2963	0.0812	1.8895	10.1195	0.0944	0.9324

Table 3.11 Statistical analysis of turning tests in calm water and waves at Fr = 0.2, $\chi = 180°$

Fr = 0.2, $\chi = 180°$, $\delta = -35°$										
λ/L	Number of Runs	A_D [m]			T_R [m]			T_D [m]		
		Mean	STD	CV (%)	Mean	STD	CV (%)	Mean	STD	CV (%)
Calm water	3	7.4301	0.0217	0.2927	3.9527	0.0510	1.2914	9.9533	0.0325	0.3267
0.5	3	7.6003	0.0590	0.7766	4.1330	0.0403	0.9758	10.3164	0.0301	0.2916
1.0	3	7.6891	0.0203	0.2644	4.0705	0.0598	1.4694	10.2595	0.0512	0.4993
1.2	3	7.6279	0.0619	0.8119	3.9470	0.0391	0.9910	9.8654	0.0485	0.4915
Fr = 0.2, $\chi = 180°$, $\delta = 35°$										
λ/L	Number of Runs	A_D [m]			T_R [m]			T_D [m]		
		Mean	STD	CV (%)	Mean	STD	CV (%)	Mean	STD	CV (%)
Calm water	3	7.4723	0.0393	0.5254	4.1152	0.0290	0.7042	10.0979	0.0283	0.2798
0.5	3	7.5949	0.0299	0.3932	4.2698	0.0178	0.4161	10.5633	0.0325	0.3081
1.0	3	7.7526	0.0543	0.7009	4.1252	0.0718	1.7406	10.3656	0.0365	0.3519
1.2	3	7.6839	0.0343	0.4459	4.1318	0.0234	0.5660	10.2595	0.0311	0.3034

Table 3.12 Statistical analysis of turning tests in calm water and waves at Fr = 0.3, $\chi = 0°$

Fr = 0.3, $\chi = 0°$, $\delta = -35°$										
λ/L	Number of Runs	A_D [m]			T_R [m]			T_D [m]		
		Mean	STD	CV (%)	Mean	STD	CV (%)	Mean	STD	CV (%)
Calm water	5	8.0548	0.0182	0.2259	4.2139	0.0417	0.9885	10.3467	0.0362	0.3503
0.5	5	7.8599	0.0489	0.6217	4.0752	0.0390	0.9566	10.1084	0.0241	0.2389
1.0	5	7.6211	0.0630	0.8265	3.9384	0.0169	0.4302	10.0946	0.0440	0.4355
Fr = 0.3, $\chi = 0°$, $\delta = 35°$										
λ/L	Number of Runs	A_D [m]			T_R [m]			T_D [m]		
		Mean	STD	CV (%)	Mean	STD	CV (%)	Mean	STD	CV (%)
Calm water	5	7.9861	0.0154	0.1927	4.3328	0.0331	0.7631	10.4940	0.0347	0.3304
0.5	5	7.8779	0.0460	0.5840	4.2292	0.0207	0.4895	10.4132	0.0335	0.3219
1.0	5	7.6078	0.0579	0.7608	4.0608	0.0140	0.3444	10.2018	0.0147	0.1438

CHAPTER 4

MANEUVERING TEST RESULTS AND DISCUSSION

4.1 Course Keeping Tests

4.1.1 Course keeping in calm water conditions

Course keeping tests were performed in calm water condition at Fr = 0.2. Results of the ship trajectories and time histories of the maneuvering parameters such as propeller revolution, rudder angle (δ), ship speed (U), surge speed (u), sway speed (v), drift angle (β), heave motion, roll angle, pitch angle, yaw angle (Ψ), and yaw rate were obtained. These trajectories and time histories as well as their Fast Fourier Transform analysis (FFT) are shown in Appendix B, Figures B-1through B-16. A number of three runs were performed for each test and the trajectories results show good agreement between the three cases. The mean values of these results are shown in Table 4.1. The results were plotted in comparison with the course keeping in wave conditions and are shown in Figures 4.1 through 4.6. Calm water tests are essential to assess the carriage rail sinkage error. They also help predicting the trajectories in waves to help assess the safety of the experiment.

4.1.2 Course keeping in wave conditions

Course keeping tests in waves were conducted at Fr = 0.2 under the conditions of λ/L =0.5, 1.0, and 1.2 and H/λ = 0.02. The wave cases include head, beam, following, and quartering waves as well as oblique heading tests. Results of the ship trajectories and time histories of the maneuvering parameters such as propeller revolution, rudder angle, ship speed, surge speed, sway speed, drift angle, heave motion, roll angle, pitch angle, yaw angle, and yaw rate were obtained. These trajectories and time histories as well as their FFT analysis are shown in Figures C-1 through C-48 in Appendix C. Three runs

were also performed for each test and the trajectories results show good repeatability with in each case.

With a nominal Froude number of 0.2, the speed loss due to wave in course keeping tests is highest in head waves where $\chi = 0°$ in longer wave length cases. This is shown in Figure 4.1 and. The target yaw angle was set to be 0° for all the course keeping cases. The counter rudder angle (δ_c) values of calm water case and all the wave cases are shown in Figure 4.2 with a maximum value at $\chi = \pm 45°$ and $\lambda/L = 1.0$. In Figure 4.3, mean values of drift angle (β) are plotted against the wave encounter angles for all the course keeping cases. The drift angle β has higher values in oblique heading cases where χ is ±45° when compared to the other χ cases with the highest value of occurred with $\chi = \pm 45°$ and $\lambda/L = 1.0$ The minimum and maximum pitch angles recorded in course keeping tests are -0.176° and 0.0175° as shown in Figure 4.4. The roll angle and the yaw angle are shown in Figure 4.5 and 4.6 respectively. Table 4 .2 through 4 .4 show the mean results of these course keeping maneuvering tests in waves.

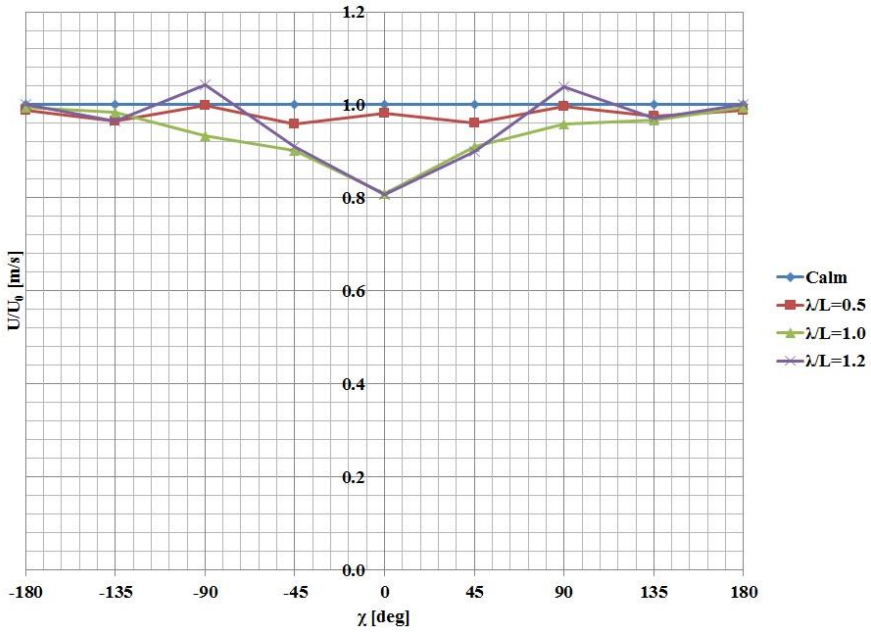

Figure 4.1 Comparison of normalized ship speed of course keeping tests in calm water and waves at Fr = 0.2

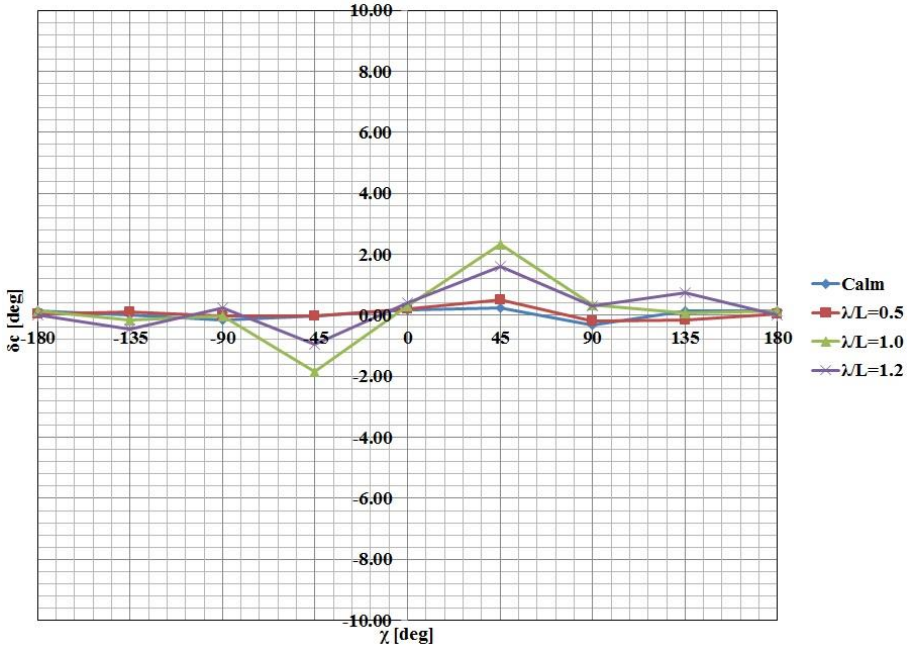

Figure 4.2 Comparison of counter rudder angle of course keeping tests in calm water and waves at Fr = 0.2

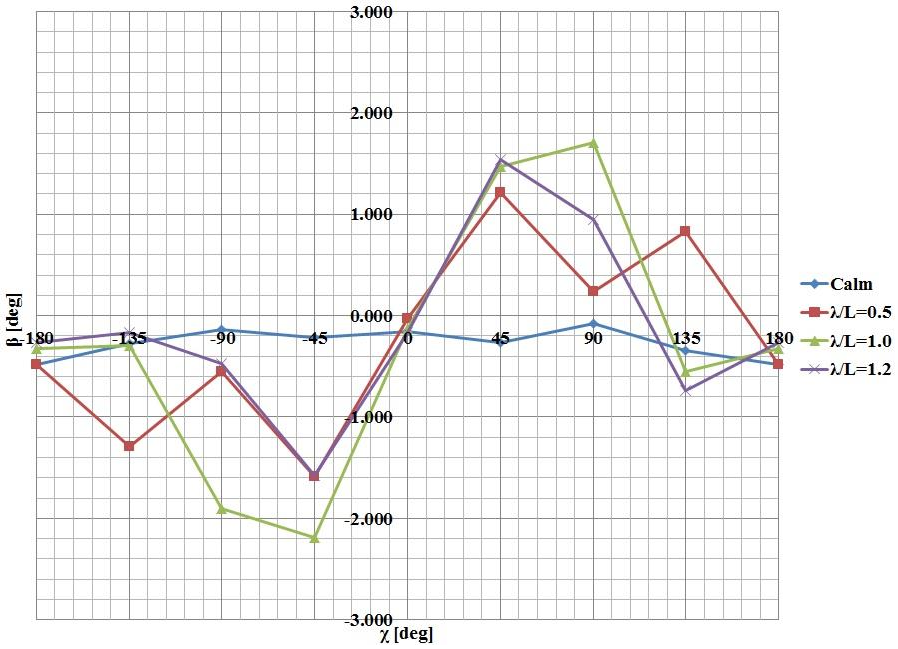

Figure 4.3 Comparison of drift angle of course keeping tests in calm water and waves at Fr = 0.2

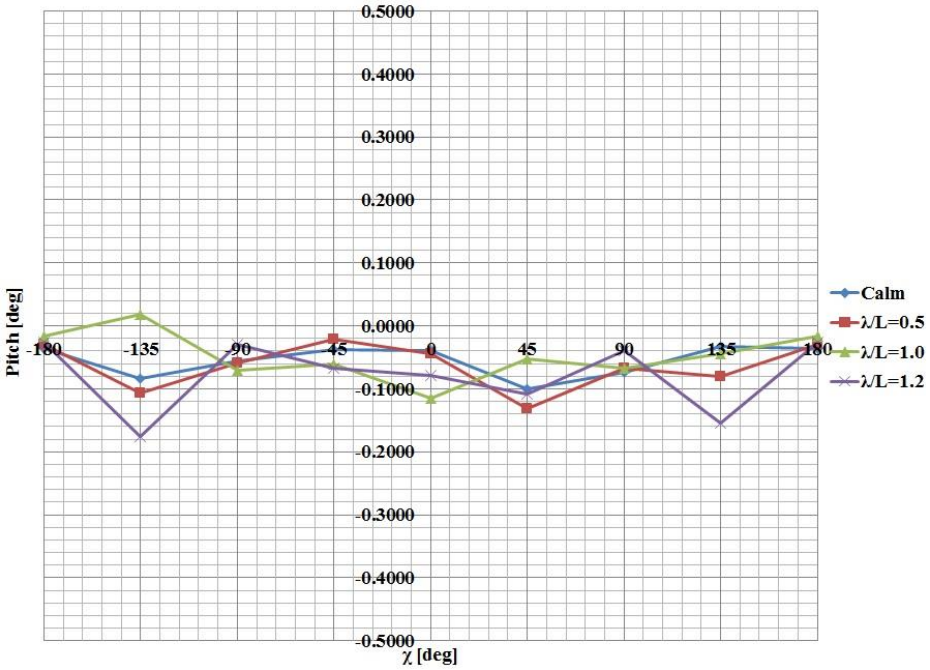

Figure 4.4 Pitch angle of course keeping in calm water and waves at Fr = 0.2

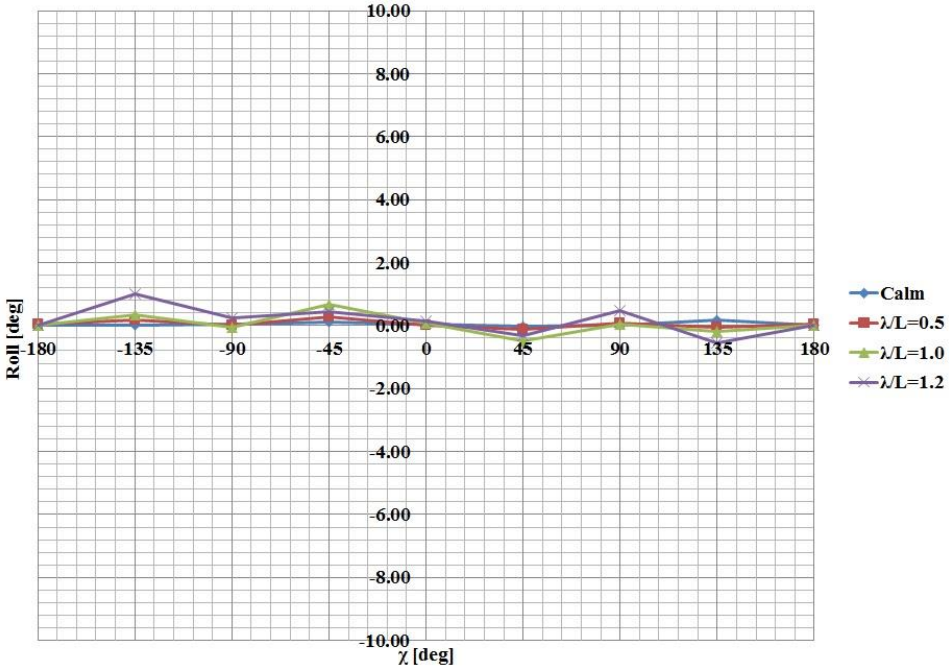

Figure 4.5 Roll angle of course keeping in calm water and waves at Fr = 0.2

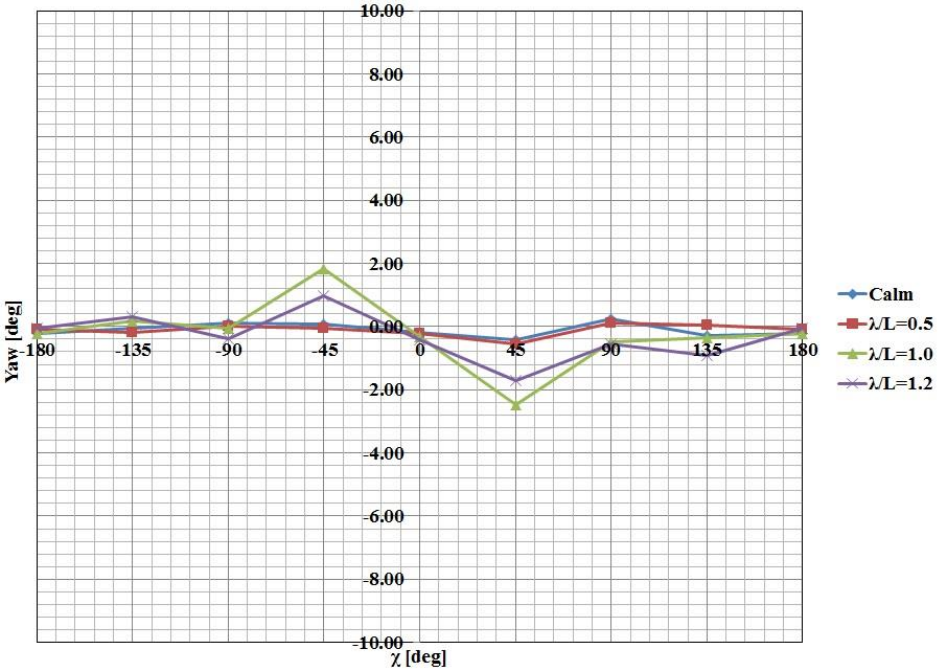

Figure 4.6 Yaw angle of course keeping in calm water and waves at Fr = 0.2

The heave motion results from course keeping tests in wave are shown in Figure A-1 of Appendix A. Figures A-2 and A-3 show the rail sinkage measurement that was done to assess the sinkage error. The heave motion measurement is slightly affected by the small amount of sinkage error. In Tables 4.1 through 4.4, RudFBL and RudFBR are the left rudder fin blade and the right rudder fin blade. U is the averaged velocity of three repeated runs for each case and U_0 is the averaged velocity of the three calm water runs corresponding to the same case.

Table4. 1 Comparison of maneuvering parameters of course keeping in calm water with several heading angles at Fr = 0.2

Calm										
χ	Mean (RudFBL)	Mean (RudFBR)	Mean (Roll)	Mean (Pitch)	Mean (Yaw)	Mean (Heave)	Mean (Yaw Rate)	Mean (U)	Mean (U/U_0)	Mean (β)
-135	0.0101	0.0101	0.0174	-0.0836	-0.0603	-0.0042	-0.0180	1.1225	1.0000	-0.2718
-90	-0.1559	-0.1559	0.0564	-0.0564	0.1186	-0.0043	0.0175	1.0939	1.0000	-0.1321
-45	-0.0309	-0.0309	0.1082	-0.0380	0.0621	-0.0039	0.0265	1.1287	1.0000	-0.2168
0	0.1766	0.1766	0.0345	-0.0393	-0.1871	0.0020	0.0011	1.1310	1.0000	-0.1582
45	0.2282	0.2282	-0.0207	-0.1008	-0.4078	0.0010	-0.0055	1.1273	1.0000	-0.2694
90	-0.3074	-0.3074	0.0088	-0.0744	0.2523	0.0005	-0.0345	1.0920	1.0000	-0.0749
135	0.1349	0.1349	0.1663	-0.0328	-0.2720	0.0001	-0.0673	1.1296	1.0000	-0.3484
180	0.1345	0.1345	0.0102	-0.0359	-0.2076	0.0030	-0.0250	1.1237	1.0000	-0.4795

Table4. 2 Comparison of maneuvering parameters of course keeping in waves with several wave encounter angles at Fr =0.2, λ/L =0.5

λ/L=0.5										
χ	Mean (RudFBL)	Mean (RudFBR)	Mean (Roll)	Mean (Pitch)	Mean (Yaw)	Mean (Heave)	Mean (Yaw Rate)	Mean (U)	Mean (U/U_0)	Mean (β)
-135	0.1253	0.1253	0.1738	-0.1060	-0.1731	-0.0037	-0.0592	1.0843	0.9660	-1.2872
-90	-0.0248	-0.0248	0.0263	-0.0594	-0.0015	-0.0039	-0.0116	1.0930	0.9992	-0.5482
-45	-0.0234	-0.0234	0.2635	-0.0206	-0.0664	-0.0037	-0.0666	1.0816	0.9583	-1.5884
0	0.1970	0.1970	-0.0025	-0.0434	-0.2100	0.0020	0.0228	1.1100	0.9814	-0.0302
45	0.5184	0.5184	-0.1348	-0.1309	-0.5662	0.0015	0.0553	1.0832	0.9609	1.2110
90	-0.1783	-0.1783	0.0855	-0.0671	0.1232	0.0002	-0.0222	1.0886	0.9969	0.2352
135	-0.1491	-0.1491	-0.0551	-0.0801	0.0459	0.0015	-0.0047	1.1017	0.9753	0.8264
180	0.0573	0.0573	0.0285	-0.0296	-0.0874	0.0028	-0.0593	1.1101	0.9879	-0.4823

Table4. 3 Comparison of maneuvering parameters of course keeping in waves with several wave encounter angles at Fr =0.2, λ/L =1.0

λ/L=1.0										
χ	Mean (RudFBL)	Mean (RudFBR)	Mean (Roll)	Mean (Pitch)	Mean (Yaw)	Mean (Heave)	Mean (Yaw Rate)	Mean (U)	Mean (U/U_0)	Mean (β)
-135	-0.1673	-0.1673	0.3451	0.0175	0.1899	-0.0044	0.3451	1.1038	0.9834	-0.2953
-90	-0.0293	-0.0293	-0.0425	-0.0698	-0.0450	-0.0052	0.0202	1.0208	0.9332	-1.9075
-45	-1.8454	-1.8454	0.6809	-0.0613	1.8234	-0.0040	-0.0739	1.0176	0.9015	-2.1888
0	0.3092	0.3092	0.0823	-0.1145	-0.3237	0.0019	0.0093	0.9156	0.8095	-0.1313
45	2.3227	2.3227	-0.4863	-0.0526	-2.4873	-0.0002	-0.0896	1.0267	0.9107	1.4684
90	0.3372	0.3372	0.0596	-0.0669	-0.4832	-0.0013	-0.0309	1.0460	0.9579	1.7098
135	0.0822	0.0822	-0.1876	-0.0443	-0.3530	0.0006	-0.4882	1.0934	0.9679	-0.5469
180	0.1448	0.1448	0.0105	-0.0162	-0.2138	0.0026	-0.0458	1.1188	0.9956	-0.3259

Table4. 4 Comparison of maneuvering parameters of course keeping in waves with several wave encounter angles at Fr =0.2, λ/L =1.2

λ/L=1.2										
χ	Mean (RudFBL)	Mean (RudFBR)	Mean (Roll)	Mean (Pitch)	Mean (Yaw)	Mean (Heave)	Mean (Yaw Rate)	Mean (U)	Mean (U/U_0)	Mean (β)
-135	-0.4619	-0.4619	1.0051	-0.1762	0.3132	-0.0048	-0.3053	1.0843	0.9660	-0.1637
-90	0.2580	0.2580	0.2499	-0.0297	-0.3772	-0.0073	-0.0645	1.1404	1.0426	-0.4686
-45	-0.9494	-0.9494	0.4504	-0.0665	0.9638	-0.0029	0.0172	1.0278	0.9106	-1.5802
0	0.3924	0.3924	0.1472	-0.0791	-0.4280	0.0015	0.0006	0.9138	0.8080	-0.1702
45	1.6140	1.6140	-0.3112	-0.1079	-1.7210	0.0005	0.0819	1.0154	0.9007	1.5414
90	0.3178	0.3178	0.4636	-0.0386	-0.5370	-0.0018	-0.0059	1.1339	1.0384	0.9516
135	0.7552	0.7552	-0.5490	-0.1550	-0.9183	-0.0001	-0.0652	1.0976	0.9717	-0.7414
180	0.0180	0.0180	0.0109	-0.0268	-0.0609	0.0029	0.0050	1.1245	1.0007	-0.2696

4.2 Zigzag Tests

4.2.1 Zigzag tests in calm water

Standard zigzag maneuvering tests in calm water were also conducted at Fr = 0.2 that include 10°/10°, 20°/20°, and 35°/35° rudder angle. Results of the ship trajectories in these cases as well as propeller revolution, rudder angle, ship speed, ship velocity components, drift angle, and yaw rate are shown in Figures D-1through D-6 in Appendix D. 1st and 2nd overshoot angles for calm water cases as well as wave cases were obtained and plotted as shown in Figures 4.7 through 4.12. Tables 4.5 through 4.7 show the mean values of the overshoot angles along with the time and position during the experiment. Three runs were performed for each test condition and the results show a strong agreement within the three repeated runs.

4.2.2 Zigzag tests in waves

Standard zigzag maneuvering tests in wave conditions of λ/L= 0.5, 1.0, and 1.2 and H/λ= 0.02 were also conducted at Fr = 0.2. These tests include 10°/10°, 20°/20°, and 35°/35° rudder angle. Results of the ship trajectories in these cases as well as propeller revolution, rudder angle, ship speed, ship velocity components, drift angle, and yaw rate are shown in Figures E-1through E-21 in Appendix E. 1st and 2nd overshoot angles for calm water cases as well as wave cases were obtained and plotted as shown in Figures 4.7 through 4.12. Tables 4.5 through 4.7 show the mean values of the overshoot angles along with the time and position during the experiment. Three runs were performed for each test condition and the results show a good agreement within the three repeated runs.

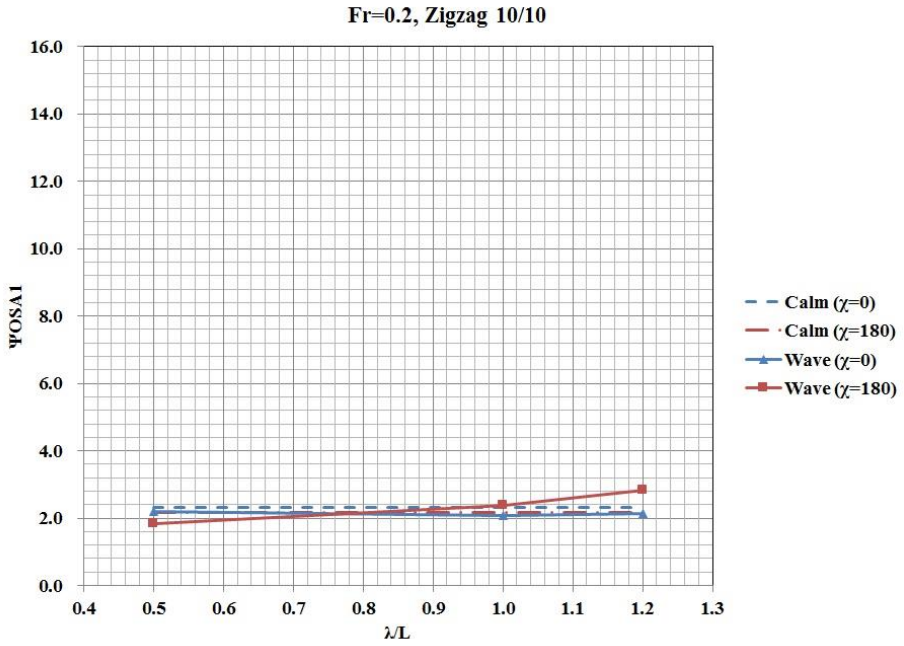

Figure 4.7 Comparison of 1st overshoot angle of zigzag 10°/10° in head and following waves at Fr= 0.2

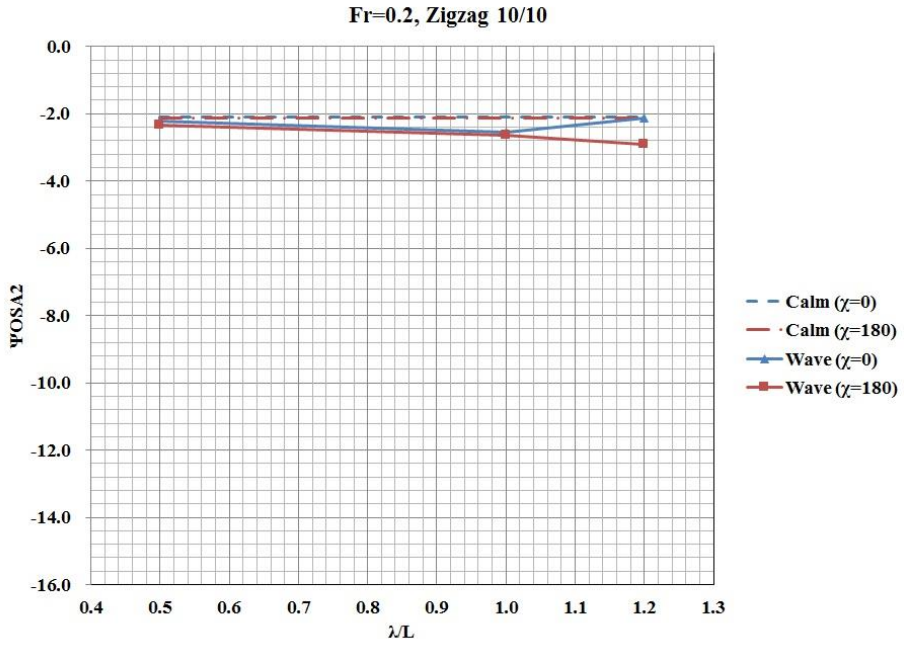

Figure 4.8 Comparison of 2nd overshoot angle of zigzag 10°/10° in head and following waves at Fr= 0.2

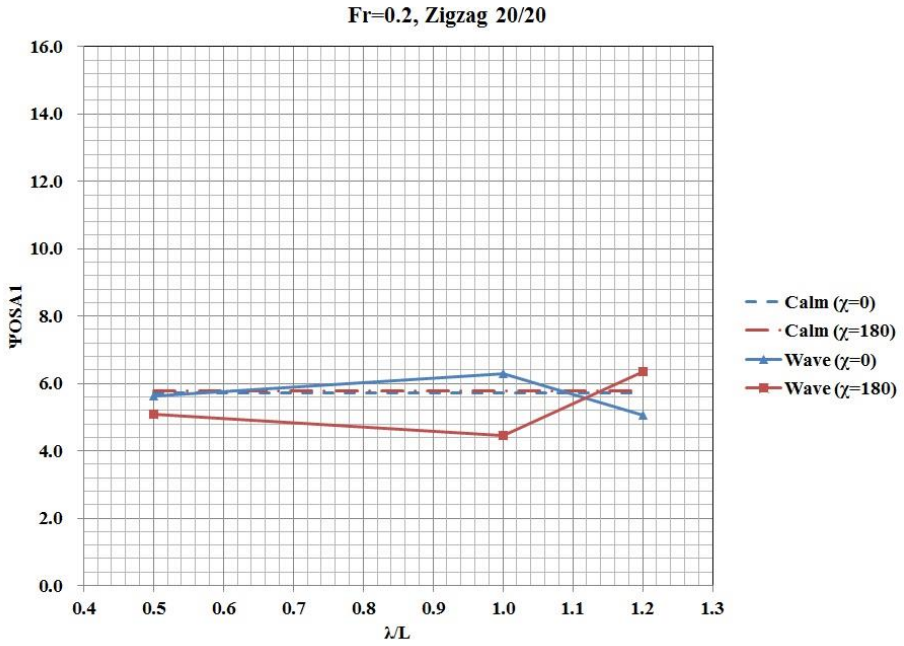

Figure4. 9 Comparison of 1st overshoot angle of zigzag 20°/20° in head and following waves at Fr= 0.2

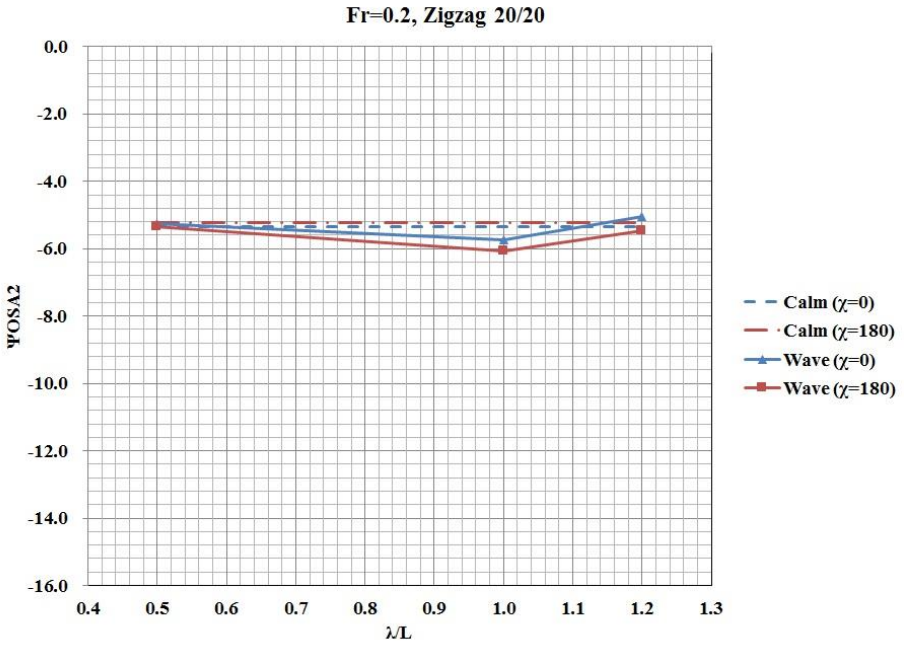

Figure 4.10 Comparison of 2nd overshoot angle of zigzag 20°/20° in head and following waves at Fr= 0.2

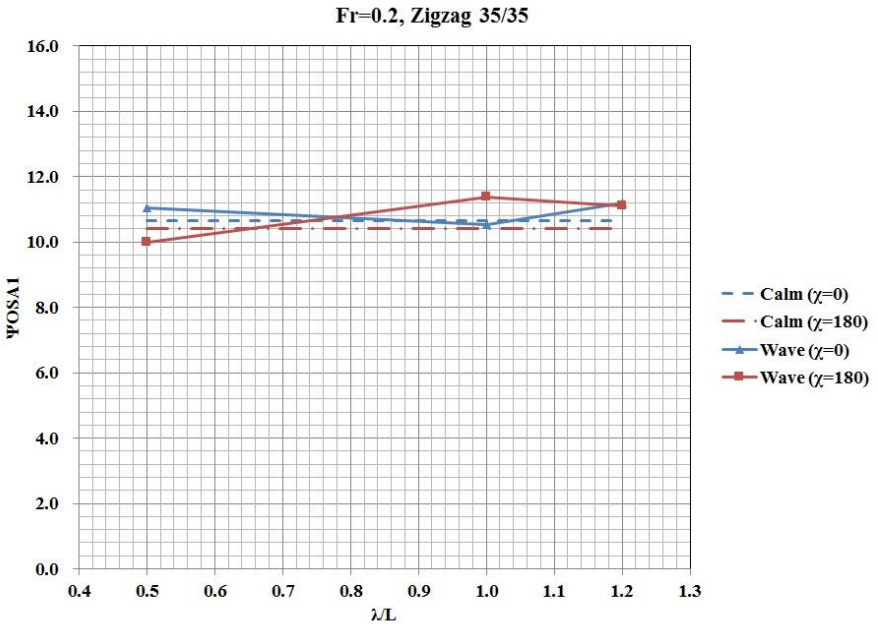

Figure 4.11 Comparison of 1st overshoot angle of zigzag 35°/35° in head and following waves at Fr= 0.2

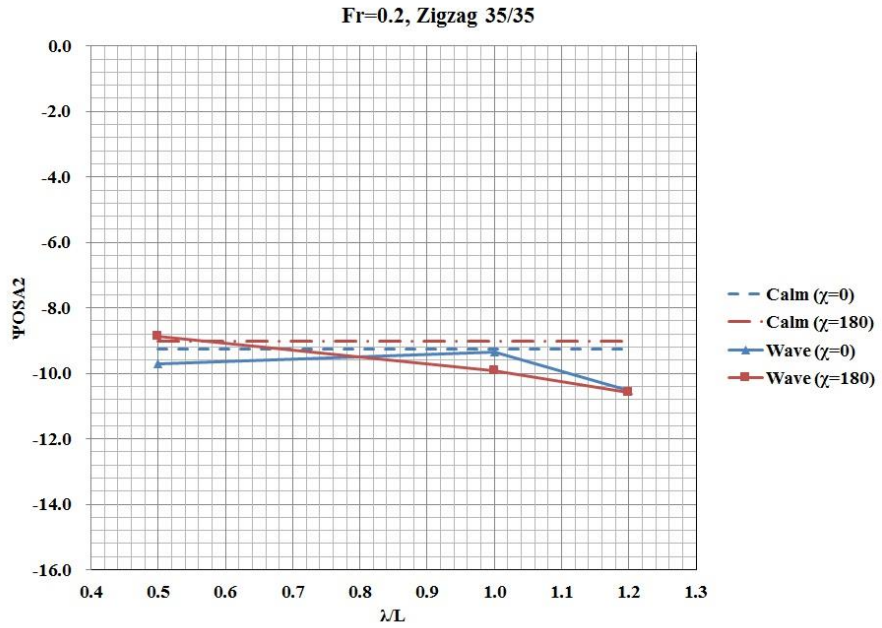

Figure 4.12 Comparison of 2nd overshoot angle of zigzag 35°/35° in head and following waves at Fr= 0.2

Table4. 5 Comparison of 1st and 2nd overshoot angles of zigzag tests in calm water and waves at Fr = 0.2, $\chi = 0°$

Z10/10								
λ/L	t (1st OSA)	SPT_6DOF (1st OSA)	1st OSA	t(2nd OSA)	SPT_6DOF (2nd OSA)	2nd OSA	1st OSA(calm)	2nd OSA(calm)
calm	6.8333	12.3135	2.3135	14.8500	-12.1029	-2.1029	2.3135	-2.1029
0.5	51.7667	12.2005	2.2005	59.3833	-12.2136	-2.2136	2.3135	-2.1029
1.0	41.9333	12.0810	2.0810	51.9167	-12.5454	-2.5454	2.3135	-2.1029
1.2	37.0167	12.1256	2.1256	46.1167	-12.1382	-2.1382	2.3135	-2.1029
Z20/20								
λ/L	t(1st OSA)	SPT_6DOF (1st OSA)	1st OSA	t(2nd OSA)	SPT_6DOF (2nd OSA)	2nd OSA	1st OSA(calm)	2nd OSA(calm)
calm	7.4833	25.7300	5.7300	16.5167	-25.3552	-5.3552	5.7300	-5.3552
0.5	52.2667	25.6284	5.6284	61.1000	-25.2566	-5.2566	5.7300	-5.3552
1.0	42.8167	26.2770	6.2770	53.4500	-25.7289	-5.7289	5.7300	-5.3552
1.2	37.8500	25.0619	5.0619	47.6833	-25.0529	-5.0529	5.7300	-5.3552
Z35/35								
λ/L	t(1st OSA)	SPT_6DOF (1st OSA)	1st OSA	t(2nd OSA)	SPT_6DOF (2nd OSA)	2nd OSA	1st OSA(calm)	2nd OSA(calm)
calm	8.6333	45.6440	10.6440	20.5333	-44.2538	-9.2538	10.6440	-9.2538
0.5	53.5667	46.0420	11.0420	65.6667	-44.7129	-9.7129	10.6440	-9.2538
1.0	44.1500	45.5362	10.5362	57.7667	-44.3574	-9.3574	10.6440	-9.2538
1.2	38.5667	46.2010	11.2010	52.3333	-45.5249	-10.5249	10.6440	-9.2538

Table4. 6 Comparison of 1st and 2nd overshoot angles of zigzag tests in calm water and waves at Fr = 0.2, $\chi = 180°$

Z10/10								
λ/L	t(1st OSA)	SPT_6DOF (1st OSA)	1st OSA	t(2nd OSA)	SPT_6DOF (2nd OSA)	2nd OSA	1st OSA(calm)	2nd OSA(calm)
calm	8.4667	12.1751	2.1751	16.6500	-12.1430	-2.1430	2.1751	-2.1430
0.5	38.5000	11.8218	1.8218	46.2500	-12.3427	-2.3427	2.1751	-2.1430
1.0	27.9167	12.3781	2.3781	35.7000	-12.6321	-2.6321	2.1751	-2.1430
1.2	27.9333	12.8364	2.8364	35.9000	-12.9073	-2.9073	2.1751	-2.1430
Z20/20								
λ/L	t(1st OSA)	SPT_6DOF (1st OSA)	1st OSA	t(2nd OSA)	SPT_6DOF (2nd OSA)	2nd OSA	1st OSA(calm)	2nd OSA(calm)
calm	9.0500	25.7718	5.7718	18.1000	-25.2292	-5.2292	5.7718	-5.2292
0.5	38.9667	25.1006	5.1006	48.0167	-25.3470	-5.3470	5.7718	-5.2292
1.0	28.2833	24.4521	4.4521	37.4333	-26.0786	-6.0786	5.7718	-5.2292
1.2	28.1333	26.3481	6.3481	37.7333	-25.4694	-5.4694	5.7718	-5.2292
Z35/35								
λ/L	t(1st OSA)	SPT_6DOF (1st OSA)	1st OSA	t(2nd OSA)	SPT_6DOF (2nd OSA)	2nd OSA	1st OSA(calm)	2nd OSA(calm)
calm	10.2333	45.4253	10.4253	22.1500	-44.0186	-9.0186	10.4253	-9.0186
0.5	40.2500	44.9964	9.9964	51.9833	-43.8714	-8.8714	10.4253	-9.0186
1.0	29.6833	46.3678	11.3678	41.7833	-44.9244	-9.9244	10.4253	-9.0186
1.2	29.8167	46.1023	11.1023	41.0333	-45.5715	-10.5715	10.4253	-9.0186

4.3 Turning Tests

4.3.1 Turning tests in calm water

Standard turning tests with ±35° rudder angles were conducted in calm water at Fr = 0.1, 0.2, and 0.3. Results of the ship trajectories in these cases as well as propeller revolution, rudder angle, ship speed, ship velocity components, drift angle, and yaw rate as well as their Fast Fourier Transform (FFT) analysis are shown in Figures F-1through F-24 in Appendix F while their mean values are shown in Tables 4.7 through 4.18. Five runs were performed for each test condition and the results show a good agreement within the five repeated runs. The averages values of the normalized ship velocity, yaw rate, and drifting angle were obtained for calm water cases as well as wave cases were obtained and plotted as shown in Figures 4.13 through 4.30.

4.3.2 Turning tests in waves

Standard turning tests were also conducted in wave conditions of λ/L = 0.5, 1.0, and 1.2 and H/λ= 0.02. These cases include turning tests with ±35° rudder angles at Fr = 0.1, 0.2, and 0.3 in four different wave encounter angles. Results of the ship trajectories in these cases as well as propeller revolution, rudder angle, ship speed, ship velocity components, drift angle, and yaw rate as well as their FFT analysis are shown in Figures G-1through G-68 in Appendix G while their mean values are shown in Tables 4.7 through 4.18. Five runs were performed for each test condition and the results show a good agreement within the five repeated runs. The averages values of the normalized ship velocity, yaw rate, and drifting angle were obtained for calm water cases as well as wave cases were obtained and plotted as shown in Figures 4.13 through 4.30. In these figures, U_{ave} is the averaged velocity from the repeated runs of each case and U_0 is the averaged velocity of the repeated corresponding calm water runs. *B*ave and rave are the averaged drift angle and averaged yaw rate for each case while n35 and p35 are negative and

positive 35 rudder angle setup in turning tests. In Tables 4.7 through 4.18, RuddFBL and RuddFBR are the left and right rudder fin blades

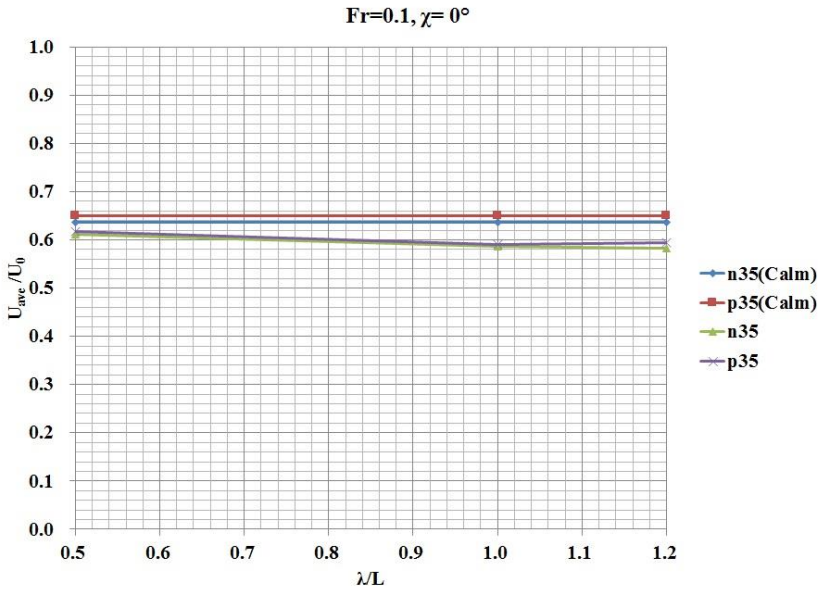

Figure 4.13 Normalized ship speed in turning tests at Fr = 0.1, H/λ = 0.02, and χ = 0°

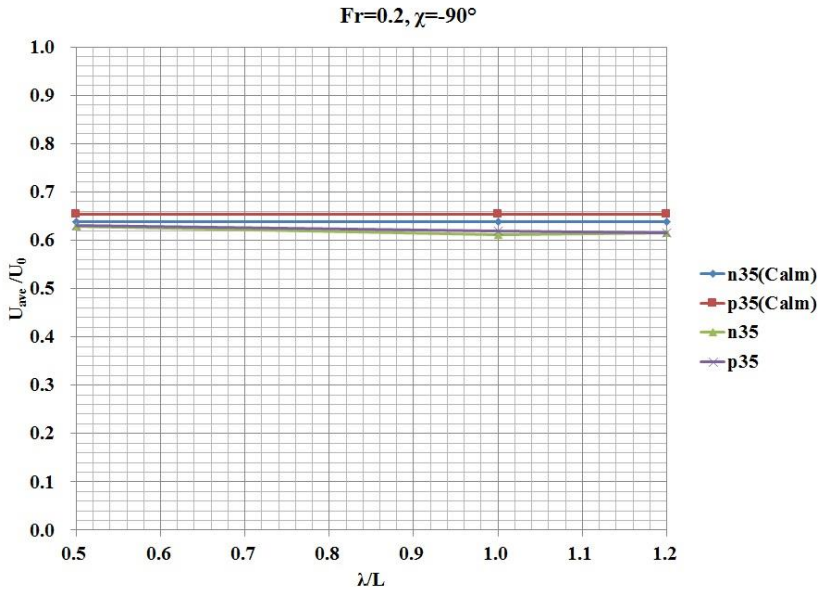

Figure 4.14 Normalized ship speed in turning tests at Fr = 0.2, H/λ = 0.02, and χ = -90°

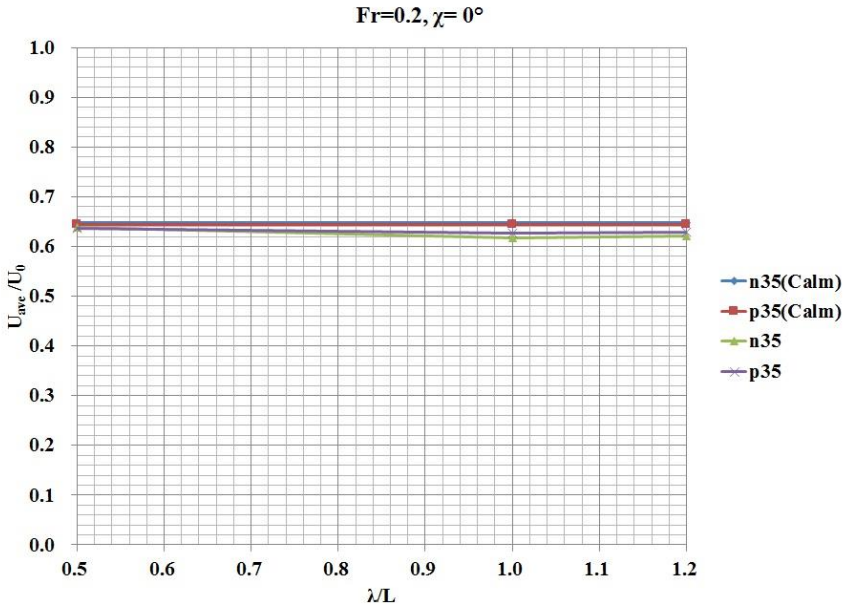

Figure 4.15 Normalized ship speed in turning tests at Fr = 0.2, H/λ = 0.02, and χ = 0°

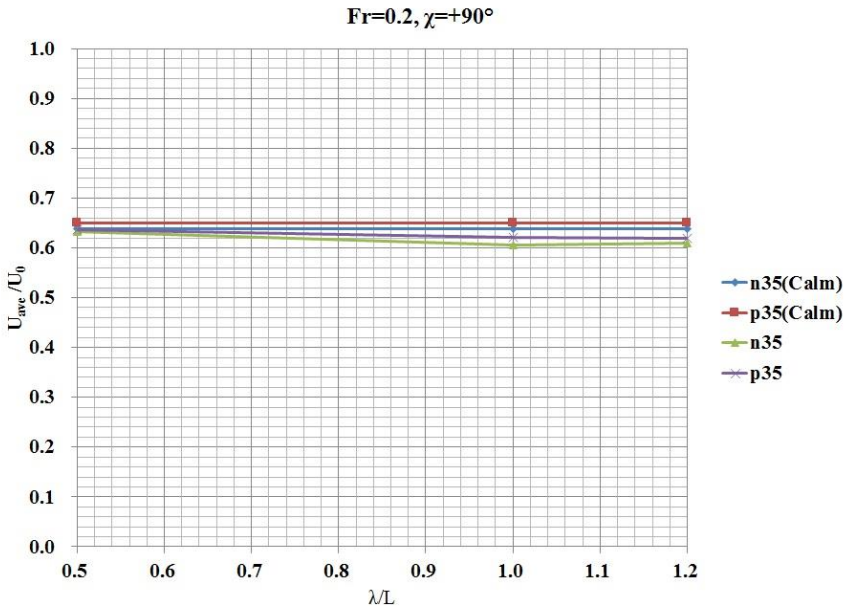

Figure 4.16 Normalized ship speed in turning tests at Fr = 0.2, H/λ = 0.02, and χ = 90°

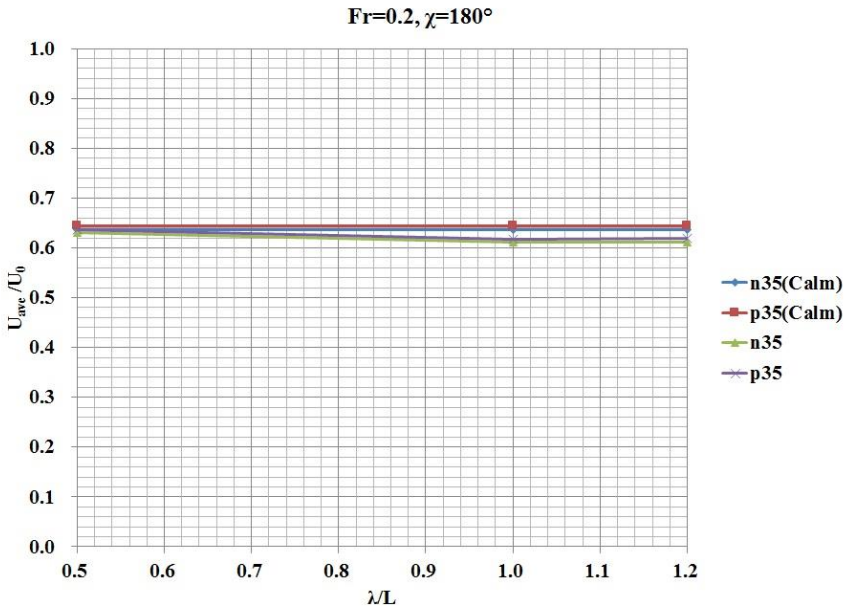

Figure 4.17 Normalized ship speed in turning tests at Fr = 0.2, H/λ = 0.02, and χ = 180°

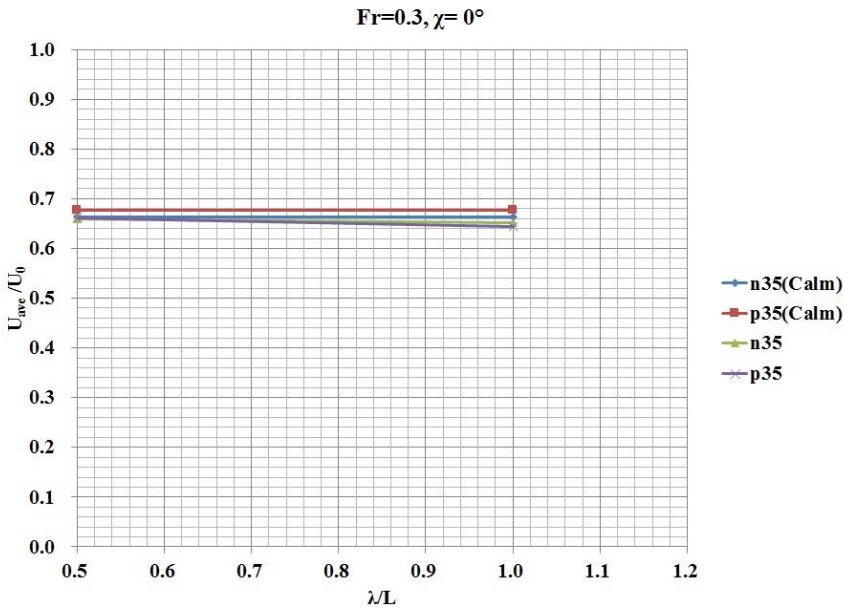

Figure 4.18 Normalized ship speed in turning tests at Fr = 0.3, H/λ = 0.02, and χ = 0°

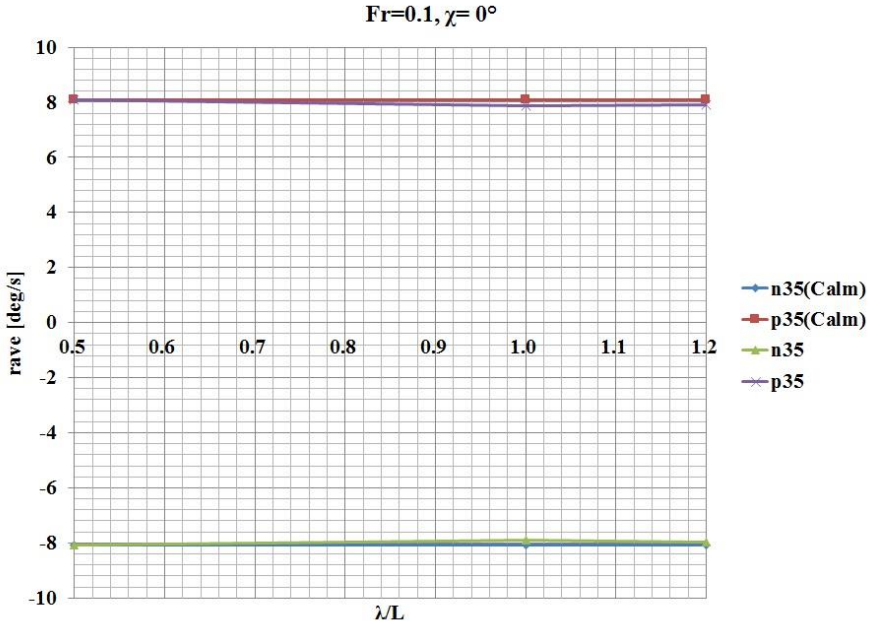

Figure 4.19 Yaw rate in turning tests at Fr = 0.1, H/λ = 0.02, and χ = 0°

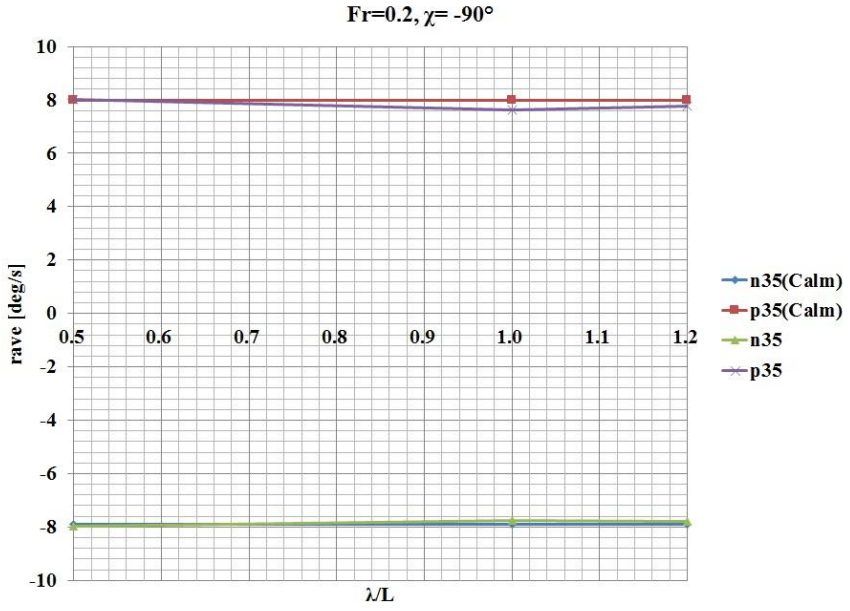

Figure 4.20 Yaw rate in turning tests at Fr = 0.2, H/λ = 0.02, and χ = -90°

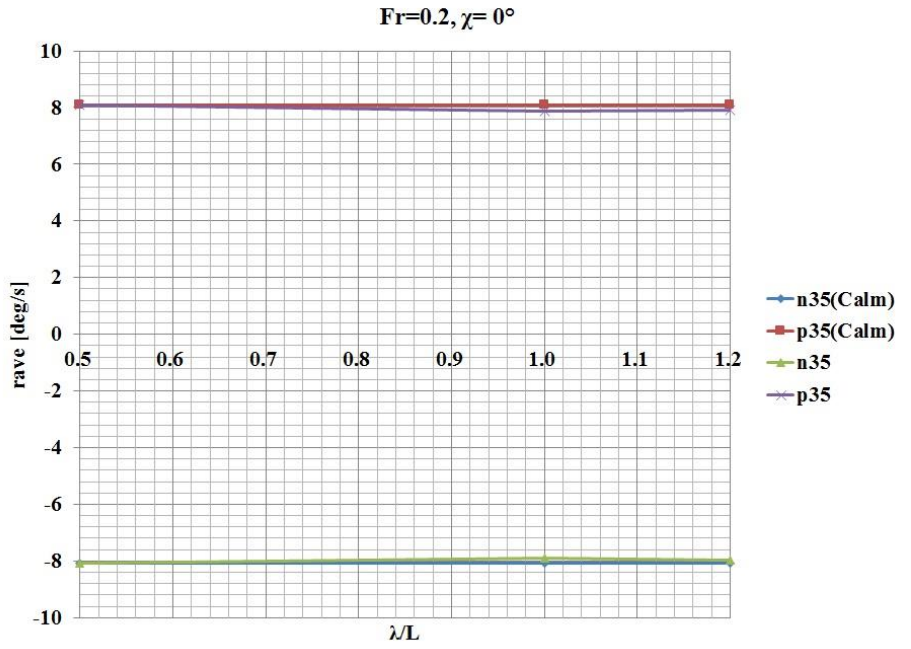

Figure 4.21 Yaw rate in turning tests at Fr = 0.2, H/λ = 0.02, and χ = 0°

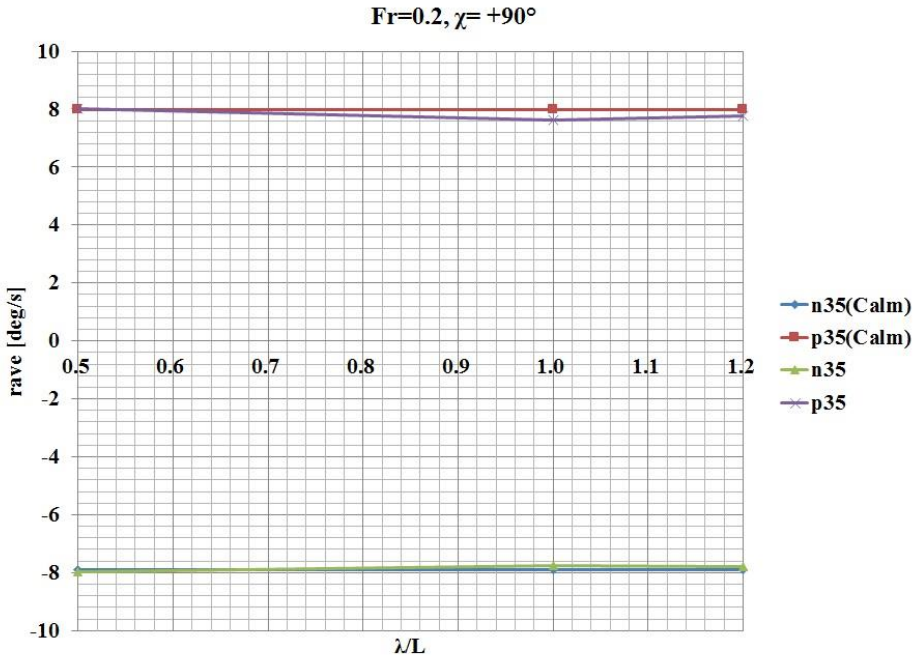

Figure 4.22 Yaw rate in turning tests at Fr = 0.2, H/λ = 0.02, and χ = 90°

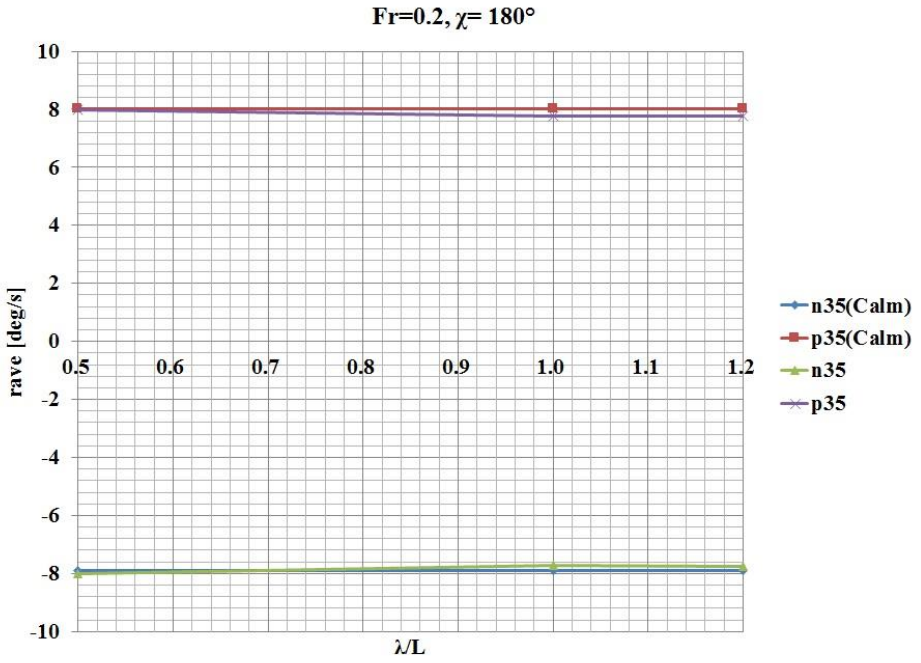

Figure 4.23 Yaw rate in turning tests at Fr = 0.2, H/λ = 0.02, and χ = 180°

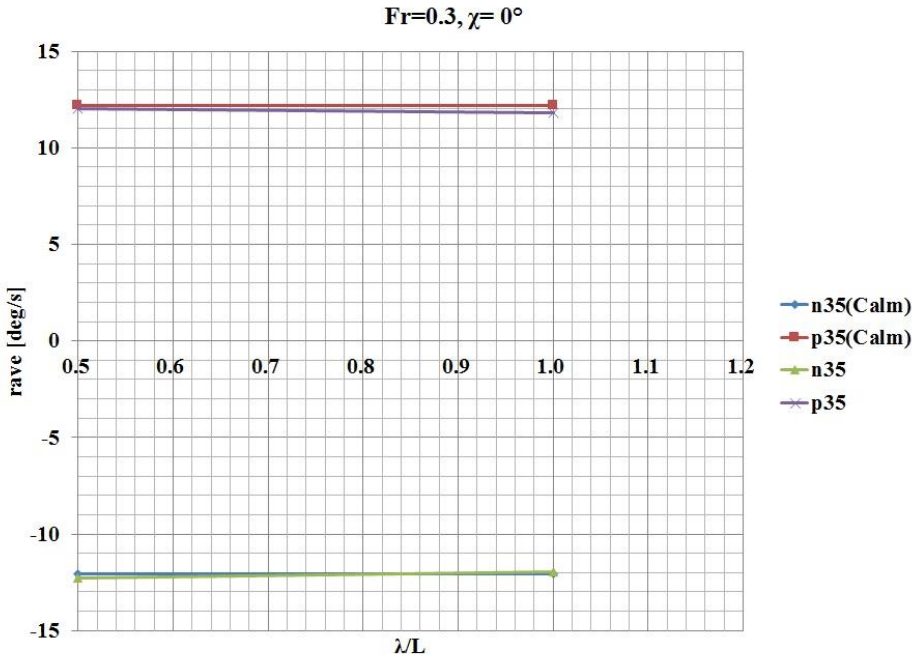

Figure 4.24 Yaw rate in turning tests at Fr = 0.3, H/λ = 0.02, and χ = 0°

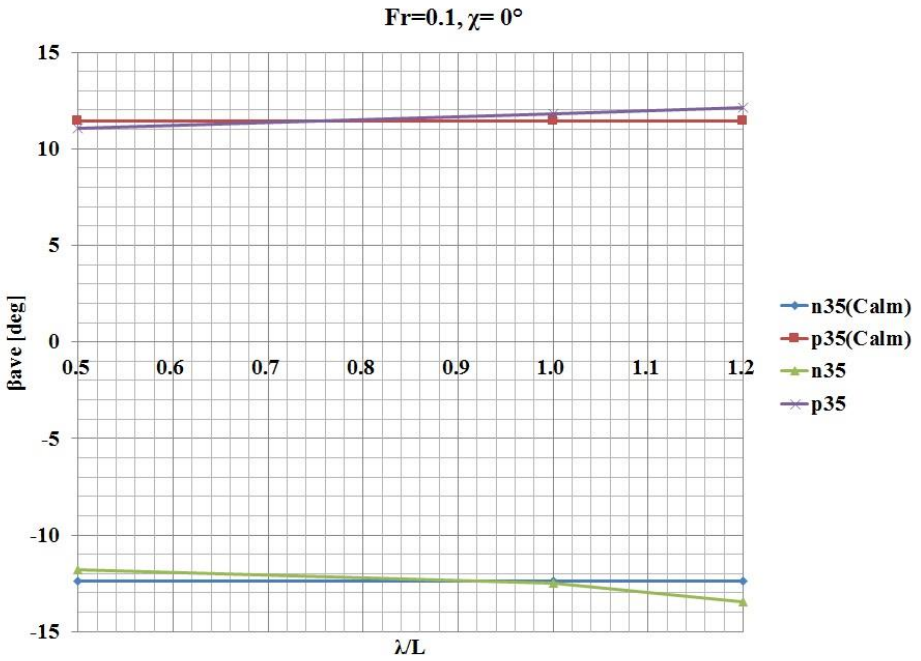

Figure 4.25 Drift angle in turning tests at Fr = 0.1, H/λ = 0.02, and χ = 0°

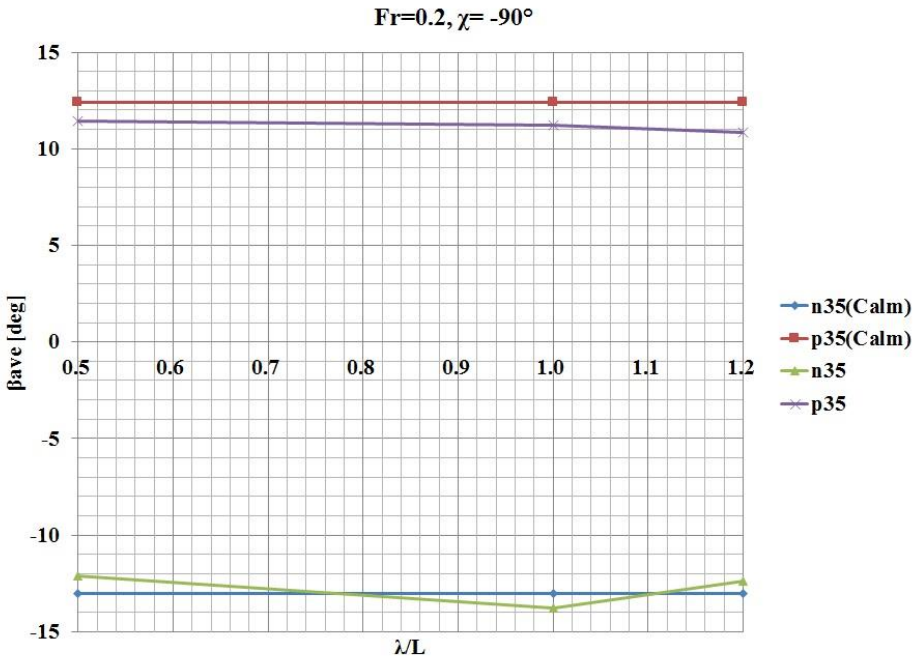

Figure 4.26 Drift angle in turning tests at Fr = 0.2, H/λ = 0.02, and χ = -90°

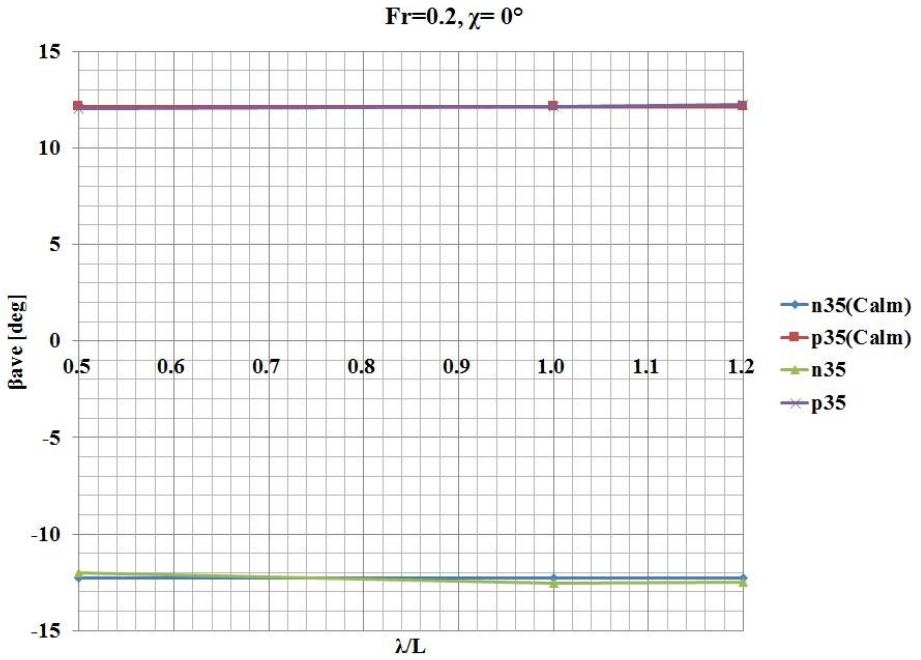

Figure 4.27 Drift angle in turning tests at Fr = 0.2, H/λ = 0.02, and χ = 0°

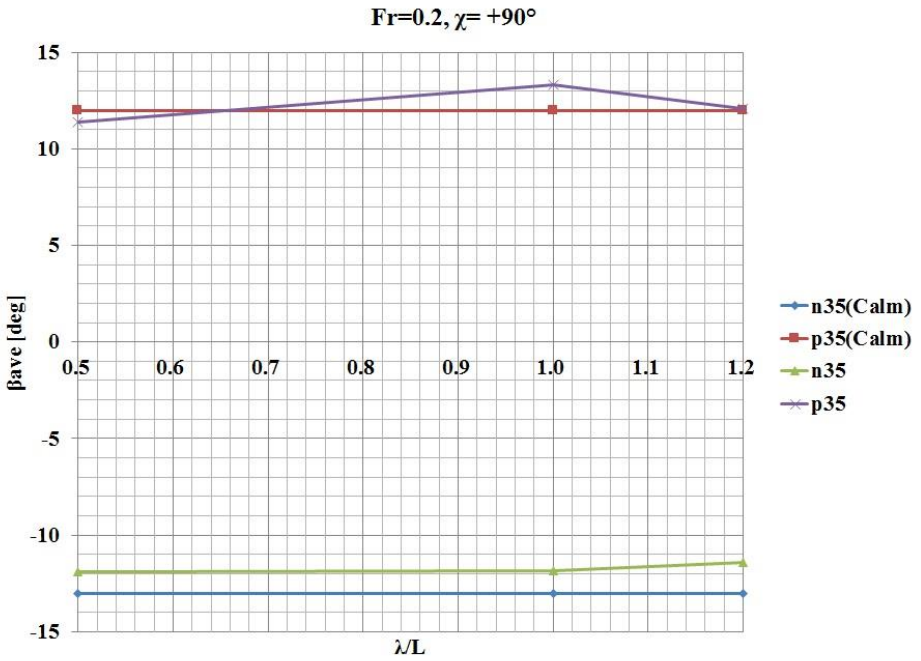

Figure 4.28 Drift angle in turning tests at Fr = 0.2, H/λ = 0.02, and χ = 90°

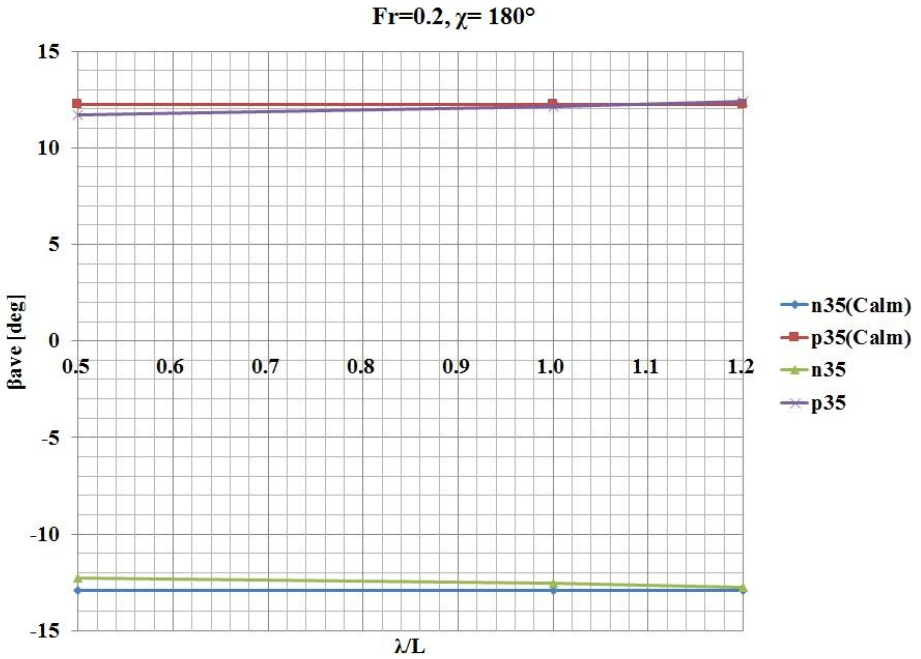

Figure 4.29 Drift angle in turning tests at Fr = 0.2, H/λ = 0.02, and χ = 180°

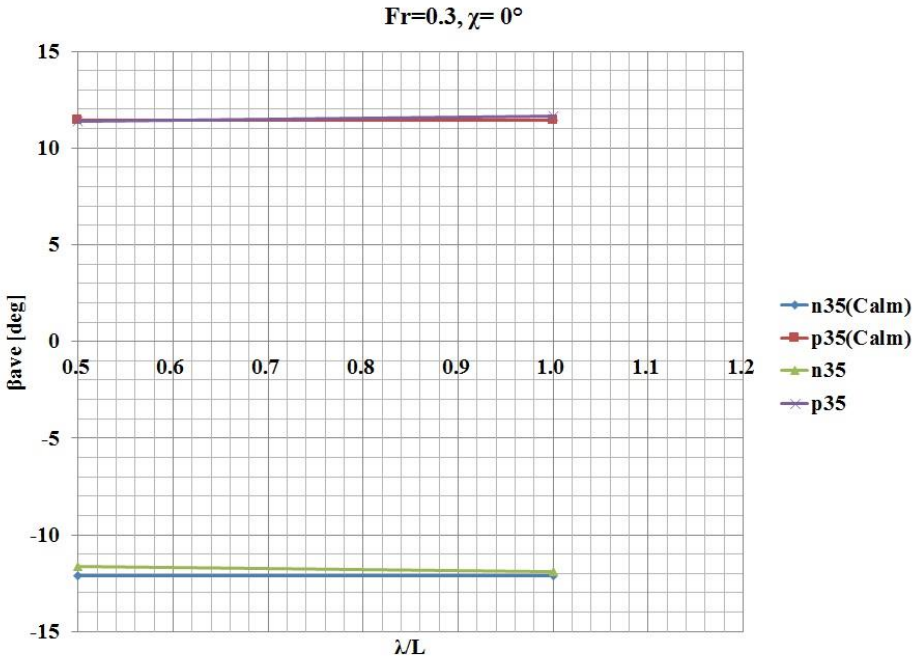

Figure 4.30 Drift angle in turning tests at Fr = 0.3, H/λ = 0.02, and χ = 0°

Table4. 7 Characteristics of turning tests in calm water and waves at Fr = 0.1, $\chi = 0°$, $\delta = -35°$

χ =0 δ = -35	Wave									
λ/L	Mean (RudFBL)	Mean (RudFBR)	Mean (Roll)	Mean (Pitch)	Mean (Yaw)	Mean (Heave)	Mean (Yaw Rate)	Mean (U)	U_{ave}/U_0	Mean (β)
0.5	-34.9920	-34.9920	0.6113	0.0232	4.5866	0.0023	-4.0130	0.3427	0.6119	-11.7914
1.0	-34.9920	-34.9920	0.7495	0.0617	2.2154	0.0014	-3.9095	0.3281	0.5859	-12.4720
1.2	-34.9920	-34.9920	0.8663	0.1067	3.4185	0.0008	-3.9425	0.3263	0.5826	-13.4312
χ =0 δ = -35	Calm									
λ/L	Mean (RudFBL)	Mean (RudFBR)	Mean (Roll)	Mean (Pitch)	Mean (Yaw)	Mean (Heave)	Mean (Yaw Rate)	Mean (U)	U_{ave}/U_0	Mean (β)
0.5	-34.9920	-34.9920	0.5199	0.0944	0.7466	0.0031	-3.9795	0.3565	0.6367	-12.4028
1.0	-34.9920	-34.9920	0.5199	0.0944	0.7466	0.0031	-3.9795	0.3565	0.6367	-12.4028
1.2	-34.9920	-34.9920	0.5199	0.0944	0.7466	0.0031	-3.9795	0.3565	0.6367	-12.4028

Table4. 8 Characteristics of turning tests in calm water and waves at Fr = 0.1, $\chi = 0°$, $\delta = 35°$

χ =0 δ = 35	Wave									
λ/L	Mean (RudFBL)	Mean (RudFBR)	Mean (Roll)	Mean (Pitch)	Mean (Yaw)	Mean (Heave)	Mean (Yaw Rate)	Mean (U)	U_{ave}/U_0	Mean (β)
0.5	34.9920	34.9920	-0.6623	0.0450	-3.4614	-0.0004	3.9397	0.3461	0.6180	11.0772
1.0	34.9920	34.9920	-0.6459	0.0461	-1.8287	-0.0008	3.8967	0.3305	0.5902	11.8133
1.2	34.9920	34.9920	-0.6223	0.0930	-2.8671	-0.0013	3.9223	0.3322	0.5933	12.1246
χ =0 δ = 35	Calm									
λ/L	Mean (RudFBL)	Mean (RudFBR)	Mean (Roll)	Mean (Pitch)	Mean (Yaw)	Mean (Heave)	Mean (Yaw Rate)	Mean (U)	U_{ave}/U_0	Mean (β)
0.5	34.9920	34.9920	-0.4608	0.0480	-1.3137	-0.0007	4.0249	0.3641	0.6503	11.4176
1.0	34.9920	34.9920	-0.4608	0.0480	-1.3137	-0.0007	4.0249	0.3641	0.6503	11.4176
1.2	34.9920	34.9920	-0.4608	0.0480	-1.3137	-0.0007	4.0249	0.3641	0.6503	11.4176

Table4. 9 Characteristics of turning tests in calm water and waves at Fr = 0.2, $\chi = 0°$, $\delta = -35°$

χ =0 δ = -35	Wave									
λ/L	Mean (RudFBL)	Mean (RudFBR)	Mean (Roll)	Mean (Pitch)	Mean (Yaw)	Mean (Heave)	Mean (Yaw Rate)	Mean (U)	U_{ave}/U_0	Mean(β)
0.5	-34.9920	-34.9920	2.2917	0.1546	2.8757	0.0046	-8.0836	0.7085	0.6383	-11.9895
1.0	-34.9920	-34.9920	2.2052	0.1534	1.4646	0.0036	-7.9028	0.6850	0.6171	-12.5392
1.2	-34.9920	-34.9920	2.2793	0.2001	1.9204	0.0033	-7.9881	0.6884	0.6202	-12.4830
χ =0 δ = -35	Calm									
λ/L	Mean (RudFBL)	Mean (RudFBR)	Mean (Roll)	Mean (Pitch)	Mean (Yaw)	Mean (Heave)	Mean (Yaw Rate)	Mean (U)	U_{ave}/U_0	Mean(β)
0.5	-34.9920	-34.9920	2.2382	0.1764	3.7771	0.0052	-8.0725	0.7188	0.6476	-12.3026
1.0	-34.9920	-34.9920	2.2382	0.1764	3.7771	0.0052	-8.0725	0.7188	0.6476	-12.3026
1.2	-34.9920	-34.9920	2.2382	0.1764	3.7771	0.0052	-8.0725	0.7188	0.6476	-12.3026

Table4. 10 Characteristics of turning tests in calm water and waves at Fr = 0.2, $\chi = 0°$, $\delta = 35°$

χ =0 δ = 35	Wave									
λ/L	Mean (RudFBL)	Mean (RudFBR)	Mean (Roll)	Mean (Pitch)	Mean (Yaw)	Mean (Heave)	Mean (Yaw Rate)	Mean (U)	U_{ave}/U_0	Mean (β)
0.5	34.9920	34.9920	-2.2937	-0.0104	-2.6011	0.0017	8.0833	0.7062	0.6362	12.0278
1.0	34.9920	34.9920	-2.1465	0.0267	-1.0549	0.0004	7.8850	0.6948	0.6259	12.1254
1.2	34.9920	34.9920	-2.0981	0.0539	-1.3635	0.0003	7.9102	0.6975	0.6283	12.2197
χ =0 δ = 35	Calm									
λ/L	Mean (RudFBL)	Mean (RudFBR)	Mean (Roll)	Mean (Pitch)	Mean (Yaw)	Mean (Heave)	Mean (Yaw Rate)	Mean (U)	U_{ave}/U_0	Mean (β)
0.5	34.9920	34.9920	-1.9220	-0.4692	-4.2044	0.0044	8.0907	0.7149	0.6441	12.1438
1.0	34.9920	34.9920	-1.9220	-0.4692	-4.2044	0.0044	8.0907	0.7149	0.6441	12.1438
1.2	34.9920	34.9920	-1.9220	-0.4692	-4.2044	0.0044	8.0907	0.7149	0.6441	12.1438

Table4. 11 Characteristics of turning tests in calm water and waves at Fr = 0.2, χ = -90°, δ = -35°

χ =-90 δ = -35	Wave									
λ/L	Mean (RudFBL)	Mean (RudFBR)	Mean (Roll)	Mean (Pitch)	Mean (Yaw)	Mean (Heave)	Mean (Yaw Rate)	Mean (U)	U_{ave}/U_0	Mean(β)
0.5	-34.9920	-34.9920	2.5693	0.2181	1.6316	0.0031	-7.9648	0.6980	0.6288	-12.1066
1.0	-34.9920	-34.9920	2.6451	0.1878	3.0750	0.0024	-7.7624	0.6783	0.6111	-13.7605
1.2	-34.9920	-34.9920	2.7573	0.1723	2.9584	0.0023	-7.7947	0.6832	0.6155	-12.4043
χ =-90 δ = -35	Calm									
λ/L	Mean (RudFBL)	Mean (RudFBR)	Mean (Roll)	Mean (Pitch)	Mean (Yaw)	Mean (Heave)	Mean (Yaw Rate)	Mean (U)	U_{ave}/U_0	Mean (β)
0.5	-34.9920	-34.9920	2.4072	0.2042	8.8019	0.0036	-7.8986	0.7081	0.6379	-13.0304
1.0	-34.9920	-34.9920	2.4072	0.2042	8.8019	0.0036	-7.8986	0.7081	0.6379	-13.0304
1.2	-34.9920	-34.9920	2.4072	0.2042	8.8019	0.0036	-7.8986	0.7081	0.6379	-13.0304

Table4. 12 Characteristics of turning tests in calm water and waves at Fr = 0.2, χ = -90°, δ = 35°

χ =-90 δ = 35	Wave									
λ/L	Mean (RudFBL)	Mean (RudFBR)	Mean (Roll)	Mean (Pitch)	Mean (Yaw)	Mean (Heave)	Mean (Yaw Rate)	Mean (U)	U_{ave}/U_0	Mean(β)
0.5	34.9920	34.9920	-2.3687	-0.1450	-4.3201	0.0031	8.0278	0.7002	0.6308	11.4302
1.0	34.9920	34.9920	-2.4097	-0.2378	-10.8260	0.0020	7.6392	0.6874	0.6193	11.2112
1.2	34.9920	34.9920	-2.2802	-0.1733	-8.8985	0.0016	7.7749	0.6839	0.6161	10.8328
χ =-90 δ = 35	Calm									
λ/L	Mean (RudFBL)	Mean (RudFBR)	Mean (Roll)	Mean (Pitch)	Mean (Yaw)	Mean (Heave)	Mean (Yaw Rate)	Mean (U)	U_{ave}/U_0	Mean(β)
0.5	34.9920	34.9920	-2.2967	-0.1711	-8.2817	0.0027	7.9779	0.7264	0.6544	12.4022
1.0	34.9920	34.9920	-2.2967	-0.1711	-8.2817	0.0027	7.9779	0.7264	0.6544	12.4022
1.2	34.9920	34.9920	-2.2967	-0.1711	-8.2817	0.0027	7.9779	0.7264	0.6544	12.4022

Table4. 13 Characteristics of turning tests in calm water and waves at Fr = 0.2, $\chi = 90°$, $\delta = -35°$

χ =90 δ = -35	Wave									
λ/L	Mean (RudFBL)	Mean (RudFBR)	Mean (Roll)	Mean (Pitch)	Mean (Yaw)	Mean (Heave)	Mean (Yaw Rate)	Mean (U)	U_{ave}/U_0	Mean (β)
0.5	-34.9920	-34.9920	2.4527	0.1710	5.3238	0.0057	-7.8660	0.7017	0.6322	-11.9272
1.0	-34.9920	-34.9920	2.7224	0.1198	11.0156	0.0046	-7.6718	0.6732	0.6065	-11.8404
1.2	-34.9920	-34.9920	2.5578	0.2071	9.7655	0.0043	-7.7089	0.6765	0.6094	-11.4008
χ =90 δ = -35	Calm									
λ/L	Mean (RudFBL)	Mean (RudFBR)	Mean (Roll)	Mean (Pitch)	Mean (Yaw)	Mean (Heave)	Mean (Yaw Rate)	Mean (U)	U_{ave}/U_0	Mean (β)
0.5	-34.9920	-34.9920	2.4072	0.2042	8.8019	0.0036	-7.8986	0.7081	0.6379	-13.0304
1.0	-34.9920	-34.9920	2.4072	0.2042	8.8019	0.0036	-7.8986	0.7081	0.6379	-13.0304
1.2	-34.9920	-34.9920	2.4072	0.2042	8.8019	0.0036	-7.8986	0.7081	0.6379	-13.0304

Table4. 14 Characteristics of turning tests in calm water and waves at Fr = 0.2, $\chi = 90°$, $\delta = 35°$

χ =90 δ = 35	Wave									
λ/L	Mean (RudFBL)	Mean (RudFBR)	Mean (Roll)	Mean (Pitch)	Mean (Yaw)	Mean (Heave)	Mean (Yaw Rate)	Mean (U)	U_{ave}/U_0	Mean (β)
0.5	34.9920	34.9920	-2.5378	-0.1536	-2.1069	0.0067	7.9471	0.7072	0.6371	11.3560
1.0	34.9920	34.9920	-2.3994	-0.1508	-3.0617	0.0055	7.7334	0.6895	0.6212	13.3334
1.2	34.9920	34.9920	-2.4796	-0.1190	-2.4253	0.0050	7.7585	0.6879	0.6198	12.0541
χ =90 δ = 35	Calm									
λ/L	Mean (RudFBL)	Mean (RudFBR)	Mean (Roll)	Mean (Pitch)	Mean (Yaw)	Mean (Heave)	Mean (Yaw Rate)	Mean (U)	U_{ave}/U_0	Mean (β)
0.5	34.9920	34.9920	-2.4044	-0.1250	-8.4401	0.0066	7.9466	0.7203	0.6489	11.9849
1.0	34.9920	34.9920	-2.4044	-0.1250	-8.4401	0.0066	7.9466	0.7203	0.6489	11.9849
1.2	34.9920	34.9920	-2.4044	-0.1250	-8.4401	0.0066	7.9466	0.7203	0.6489	11.9849

Table4. 15 Characteristics of turning tests in calm water and waves at Fr = 0.2, $\chi = 180°$, $\delta = -35°$

χ =180 δ = -35	Wave									
λ/L	Mean (RudFBL)	Mean (RudFBR)	Mean (Roll)	Mean (Pitch)	Mean (Yaw)	Mean (Heave)	Mean (Yaw Rate)	Mean (U)	U_{ave}/U_0	Mean (β)
0.5	-34.9920	-34.9920	2.4936	0.1320	-5.0723	0.0025	-7.9927	0.7006	0.6312	-12.2647
1.0	-34.9920	-34.9920	2.5182	0.1347	-1.5802	0.0014	-7.7248	0.6781	0.6109	-12.5620
1.2	-34.9920	-34.9920	2.5622	0.1422	-1.8654	0.0017	-7.7683	0.6790	0.6117	-12.7352
χ =180 δ = -35	Calm									
λ/L	Mean (RudFBL)	Mean (RudFBR)	Mean (Roll)	Mean (Pitch)	Mean (Yaw)	Mean (Heave)	Mean (Yaw Rate)	Mean (U)	U_{ave}/U_0	Mean (β)
0.5	-34.9920	-34.9920	2.3487	0.1083	5.0426	0.0028	-7.9034	0.7055	0.6356	-12.9457
1.0	-34.9920	-34.9920	2.3487	0.1083	5.0426	0.0028	-7.9034	0.7055	0.6356	-12.9457
1.2	-34.9920	-34.9920	2.3487	0.1083	5.0426	0.0028	-7.9034	0.7055	0.6356	-12.9457

Table4. 16 Characteristics of turning tests in calm water and waves at Fr = 0.2, χ = 1800°, δ = 35°

χ =180 δ = 35	Wave									
λ/L	Mean (RudFBL)	Mean (RudFBR)	Mean (Roll)	Mean (Pitch)	Mean (Yaw)	Mean (Heave)	Mean (Yaw Rate)	Mean (U)	U_{ave}/U_0	Mean (β)
0.5	34.9920	34.9920	-2.5057	-0.1468	4.7223	0.0060	7.9783	0.7072	0.6371	11.6881
1.0	34.9920	34.9920	-2.3419	-0.1423	2.3160	0.0052	7.7586	0.6841	0.6163	12.1565
1.2	34.9920	34.9920	-2.3270	-0.1472	1.5063	0.0049	7.7553	0.6863	0.6183	12.3808
χ =180 δ = 35	Calm									
λ/L	Mean (RudFBL)	Mean (RudFBR)	Mean (Roll)	Mean (Pitch)	Mean (Yaw)	Mean (Heave)	Mean (Yaw Rate)	Mean (U)	U_{ave}/U_0	Mean (β)
0.5	34.9920	34.9920	-2.3342	-0.1110	-3.9271	0.0053	8.0088	0.7159	0.6450	12.2357
1.0	34.9920	34.9920	-2.3342	-0.1110	-3.9271	0.0053	8.0088	0.7159	0.6450	12.2357
1.2	34.9920	34.9920	-2.3342	-0.1110	-3.9271	0.0053	8.0088	0.7159	0.6450	12.2357

Table4. 17 Characteristics of turning tests in calm water and waves at Fr = 0.3, $\chi = 0°$, $\delta = -35°$

χ =0	Wave									
δ = -35										
λ/L	Mean (RudFBL)	Mean (RudFBR)	Mean (Roll)	Mean (Pitch)	Mean (Yaw)	Mean (Heave)	Mean (Yaw Rate)	Mean (U)	U_{ave}/U_0	Mean (β)
0.5	-34.9920	-34.9920	6.1095	0.2966	2.2254	0.0187	-12.2890	1.1017	0.6597	-11.6510
1.0	-34.9920	-34.9920	5.9863	0.3650	2.0283	0.0160	-11.9295	1.0871	0.6510	-11.9198
χ =0	Calm									
δ = -35										
λ/L	Mean (RudFBL)	Mean (RudFBR)	Mean (Roll)	Mean (Pitch)	Mean (Yaw)	Mean (Heave)	Mean (Yaw Rate)	Mean (U)	U_{ave}/U_0	Mean (β)
0.5	-34.9920	-34.9920	6.6916	0.5819	2.0302	0.0196	-12.0884	1.1069	0.6628	-12.1033
1.0	-34.9920	-34.9920	6.6916	0.5819	2.0302	0.0196	-12.0884	1.1069	0.6628	-12.1033

Table4. 18 Characteristics of turning tests in calm water and waves at Fr = 0.3, $\chi = 0°$, $\delta = 35°$

χ =0 δ = 35	Wave									
λ/L	Mean (RudFBL)	Mean (RudFBR)	Mean (Roll)	Mean (Pitch)	Mean (Yaw)	Mean (Heave)	Mean (Yaw Rate)	Mean (U)	U_{ave}/U_0	Mean (β)
0.5	34.9920	34.9920	-6.7331	-0.0900	-0.7345	0.0140	12.0352	1.1053	0.6619	11.3571
1.0	34.9920	34.9920	-6.5128	-0.0443	1.3104	0.0121	11.8260	1.0762	0.6445	11.6737
χ =0 δ = 35	Calm									
λ/L	Mean (RudFBL)	Mean (RudFBR)	Mean (Roll)	Mean (Pitch)	Mean (Yaw)	Mean (Heave)	Mean (Yaw Rate)	Mean (U)	U_{ave}/U_0	Mean (β)
0.5	34.9920	34.9920	-6.5976	-0.0352	-2.1442	0.0143	12.1855	1.1288	0.6759	11.4127
1.0	34.9920	34.9920	-6.5976	-0.0352	-2.1442	0.0143	12.1855	1.1288	0.6759	11.4127

4.4 Conclusion

The wave induced motion is dependent on the ship heading direction to the wave encounter angle. These wave forces have great impacts on both ship stability and maneuverability. The International Maritime Organization (IMO) maneuvering standards are specifically designed to evaluate vessels maneuvering characteristics in calm water and wave conditions in order to assess vessels stability and to establish safer maneuvering criteria. Among the most important aspects in ship designing is the ship stability. A vessel is straight-line stable on straight course if, after small disturbance, it will soon settle on a new straight course without any corrective rudder. The course keeping quality is the measure of the ability of the steered vessel to maintain a straight path in a predetermined course direction without excessive oscillation of rudder or heading (ABS, 2006b). As shown in Figures B-1 through B-16 of Appendix B and C-1 through C-48 of Appendix C, the ONRT has maintained its predetermined straight path in both calm water and wave conditions with a very small counter rudder angle. This indicates that the ONRT is considered to be highly straight-line stable ship.

IMO maneuvering standards requires obtaining the 1st and 2nd overshoot angle and in zigzag maneuvering tests and the advance, transfer, and tactical diameter in turning maneuvering tests (IMO, 2002). As seen in Figures G-1 through G-68 in Appendix G, in turning tests, the ship drifted diagonally to the direction of the wave propagation and the second and third turning circles deviated from the first one. Advance, transfer, and tactical diameter as well as drifting distance and direction between the consecutive turning circles are discussed in chapter 5. Overshoot angle is defined as the difference between the predetermined value of the rudder angle in a zigzag maneuvering and the maximal heading angle reached before the course is reversed. The ONRT have relatively small values of 1st and 2nd overshoot angles in calm water and waves; thus, one can conclude that the ONRT is a highly maneuverable ship that can safely perform zigzag maneuvering motion when entering or leaving harbors.

CHAPTER 5

COMPARISON OF TURNING CHARACTERISTICS

Required by the IMO, assessment of turning maneuvering characteristics such as advance, transfer, and tactical diameter are important for ship safety when maneuvering in or out of harbors and turning is required. Figure 5.1 shows definition of these parameters. Of the other important turning characteristics to safety and ship stability are the drifting distance and drifting direction. Depending on the heading direction to the incident waves, ships have the tendency to drift due to the wave induced-motion. In ±35° turning test in waves, the ONRT drifted and the second and third turning trajectories deviated from the first one. This can be seen in Figures G-1 through G-68 of Appendix G. Figure 5.2 shows the definition of the drifting distance and drifting direction where H_D and μ_D are the drifting distance and the drifting direction between two consecutive turning trajectories. The subscripts 0 and 1 represent drifting distance and drifting direction between the 1st and 2nd turns and 2nd and 3rd turns respectively.

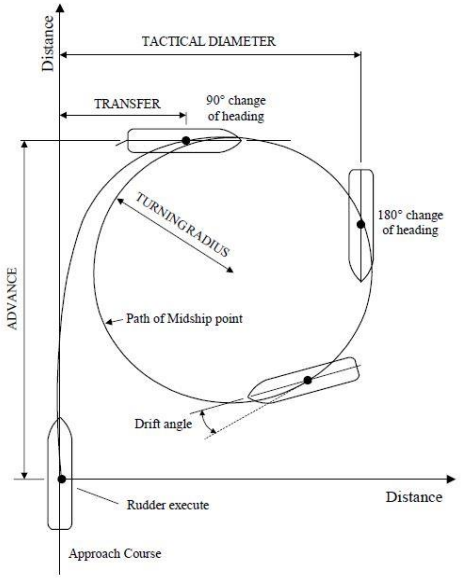

Figure 5.1 Definition of advance, transfer, and tactical diameters

Source: The American Bureau of Shipping (ABS) maneuvering guide (2006)

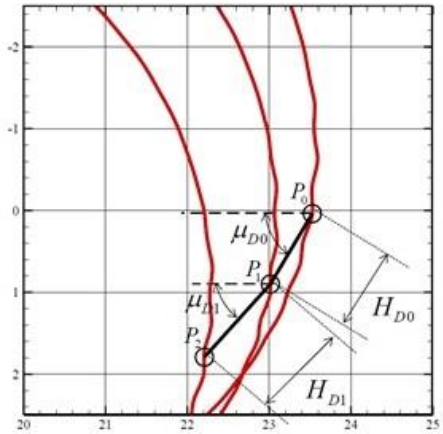

Figure 5.2 Definition of drifting distance and drifting direction

Source: (Sanada et al., 2013)

Of the ONRT turning characteristics, advance, transfer, and tactical diameters were obtained and the results are shown in Tables 5.1 through 5.6. The advances and tactical diameters are compared to those of SR108 (S-175) container ship model obtained at The Seakeeping and Maneuvering Basin, Mitsubishi Heavy Industries (MHI) with different Froude numbers and different wave encounter angles (Yasukawa et al., 2006). As can be seen in Figures 5.3 through 5.9, the ONRT results from 35° turning tests are similar to the ones of -35 turning tests. This indicates that the wave field is equally distributed over the IIHR basin area. There is a small difference between positive and negative rudder angle turning in short waves. This can be due to the interaction of the waves and the flow field around the ship model.

The drifting distance (H_D) and drifting direction (μ_D) are calculated using the method proposed by Ueno et al., (2003). The results were compared to the very large crude carrier (VLCC) results obtained at the National Maritime Research Institute (NMRI). These results are shown in Figures 5.10 and 5.11 where λ/L indicates the wavelength to ship length. When compared to the VLCC, the ONRT has smaller drifting

distance and larger drifting direction which indicates that the ONRT is more stable than the VLCC. The differences in the hull design between the ONRT and the VLCC is the reason that ONRT is more stable since its hull is more slandered. Ship speed difference between the ONRT and the VLCC experiments also plays a key role in the results variation. Another factor is the fact that while the VLCC is one rudder one propeller ship, the ONRT is a twin rudder twin screw propeller ship. This makes the ONRT a faster and more maneuverable than the VLCC. Results of the drifting distance and drifting direction for the ONRT and the VLCC are shown in Tables 5.7 and 5.8.

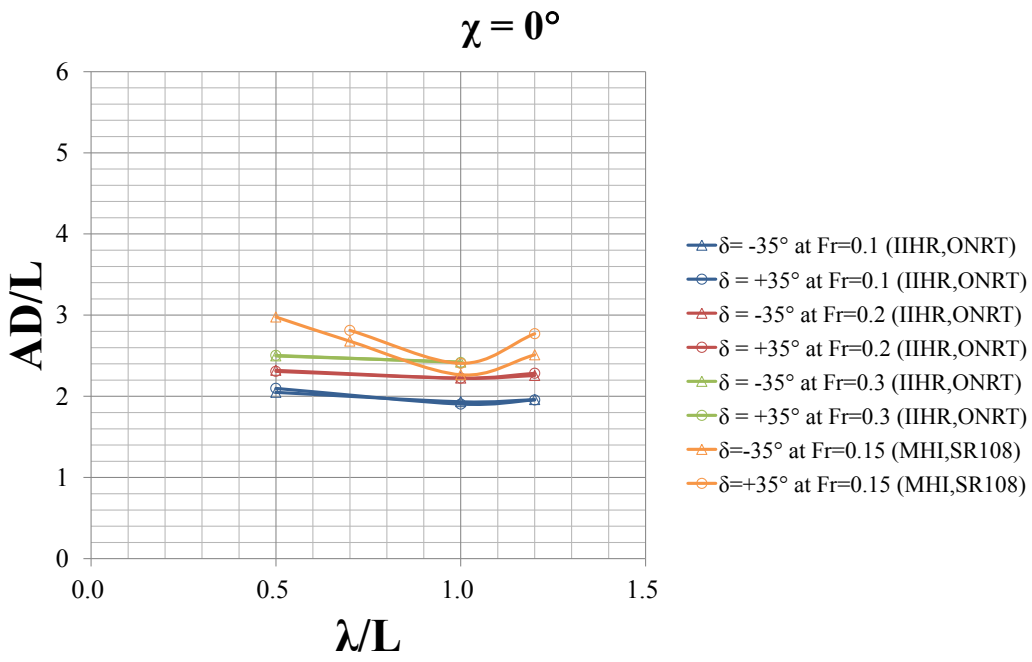

Figure 5.3 Comparison of ONRT and SR-108 advance at $\chi = 0°$

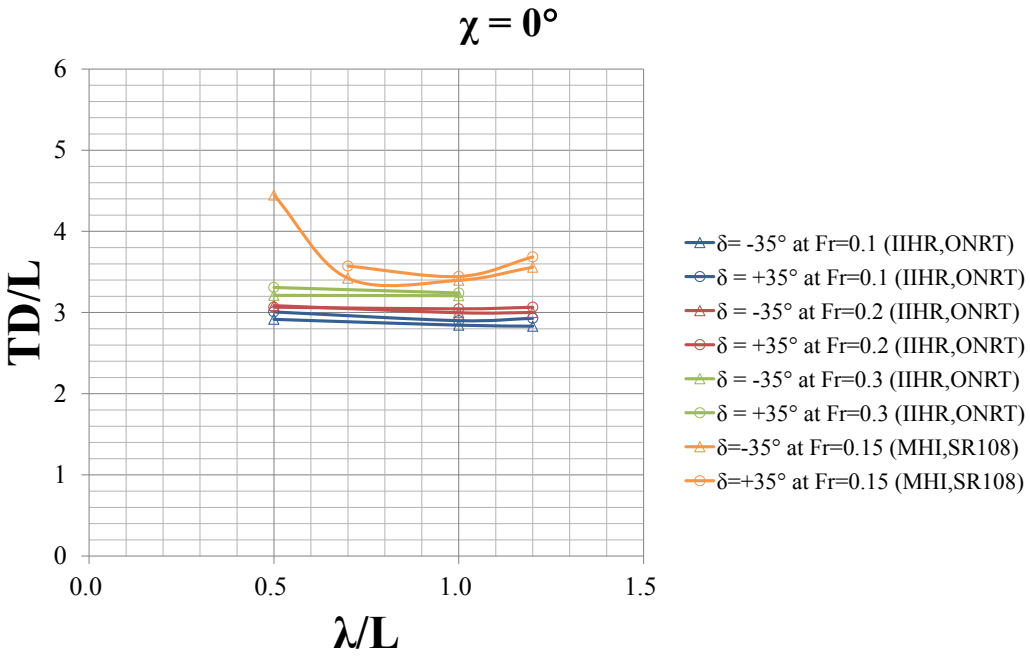

Figure 5.4 Comparison of ONRT and SR-108 tactical diameter at χ = 0°

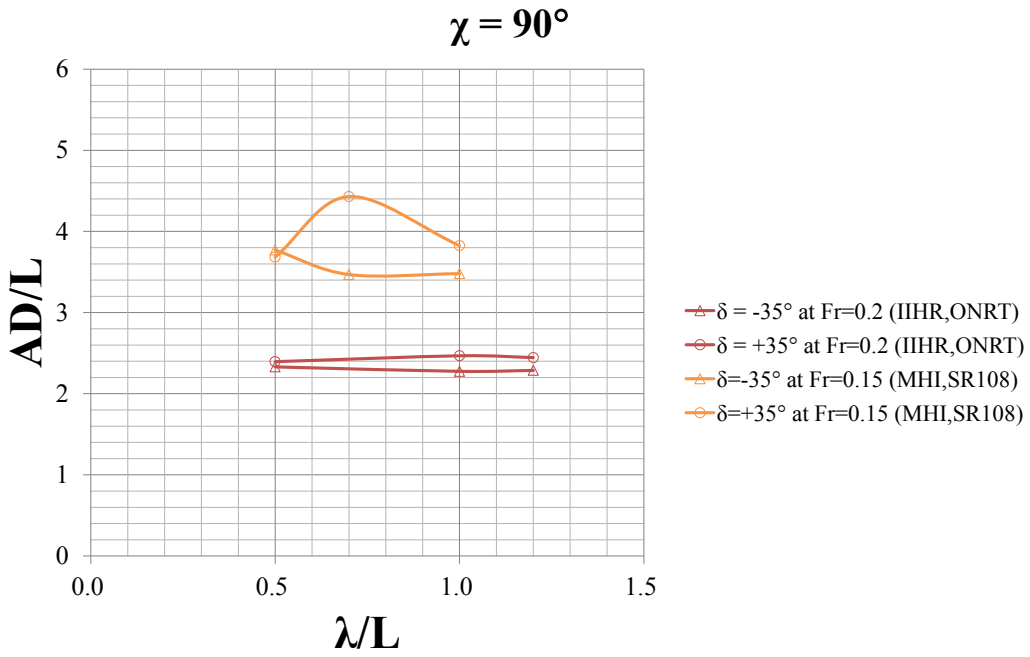

Figure 5.5 Comparison of ONRT and SR-108 advance at χ = 90°

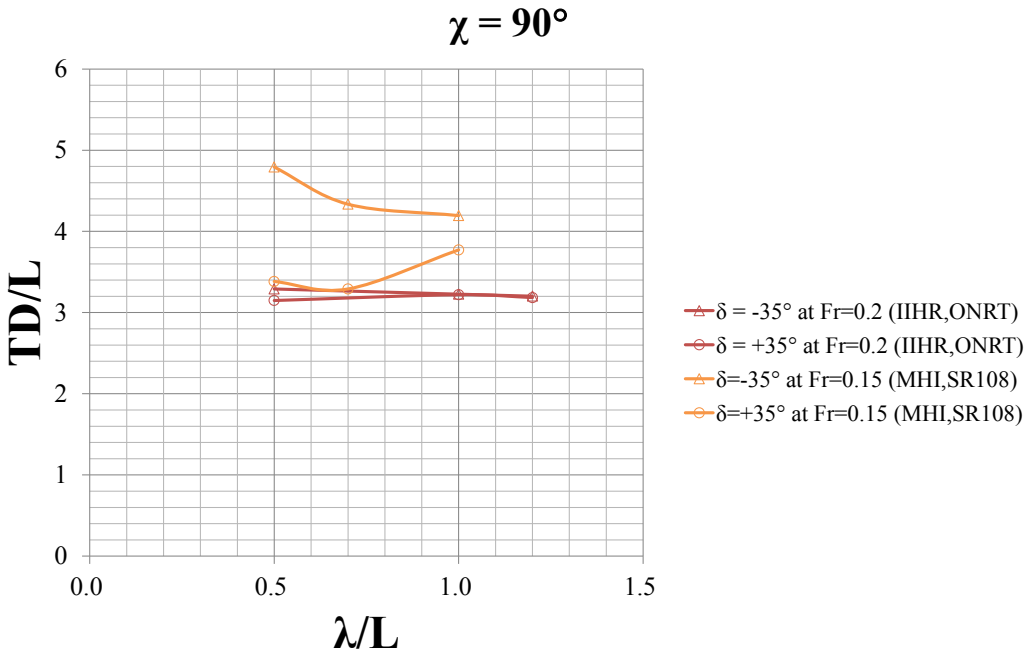

Figure 5.6 Comparison of ONRT and SR-108 tactical diameter at $\chi = 90°$

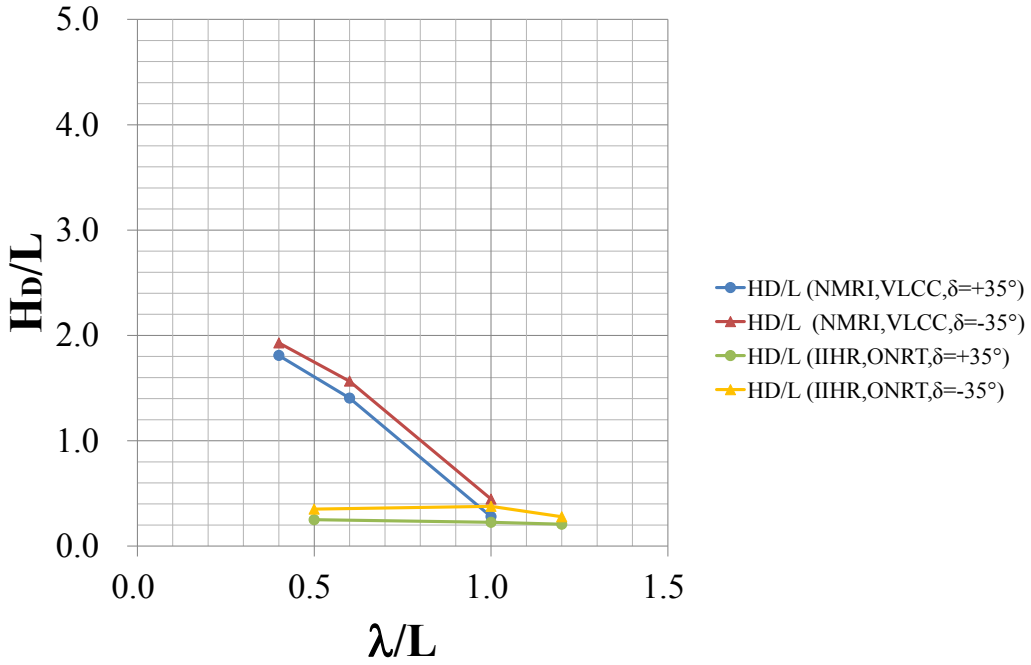

Figure 5.7 Comparison of the drifting distance of ONRT and VLCC

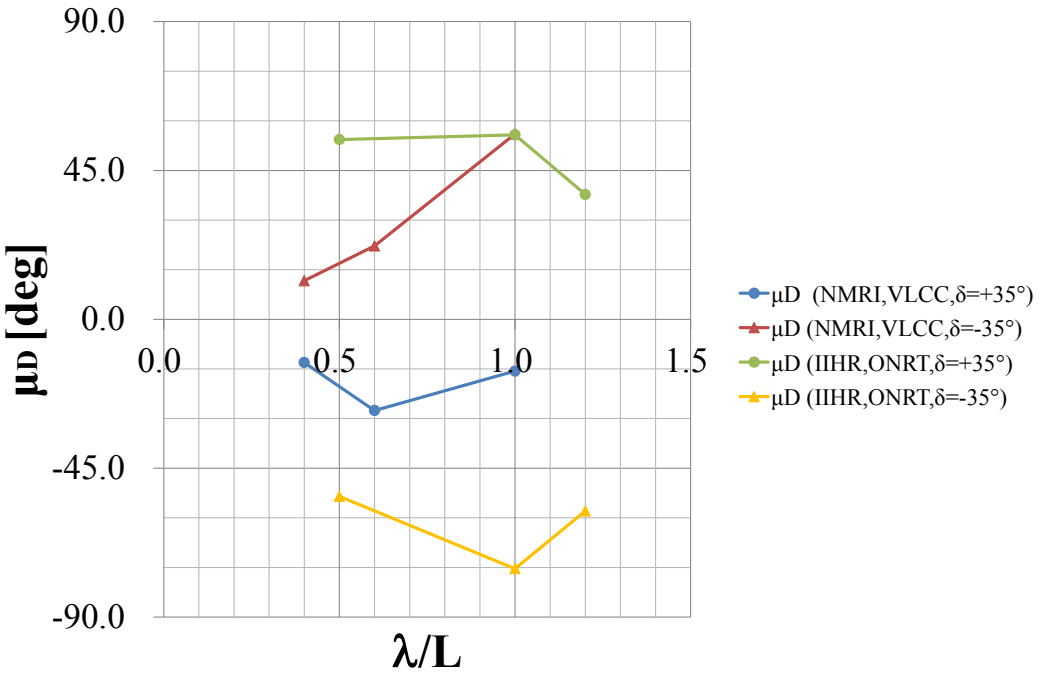

Figure 5.8 Comparison of the drifting direction of ONRT and VLCC

Table 5.1 ONRT turning characteristics in calm water and waves at Fr = 0.1, H/λ = 0.02 and χ = 0°

Fr = 0.1, χ =0°						
δ = -35°						
λ/L	$t(A_D)$	A_D	$t(T_R)$	T_R	$t(T_D)$	T_D
0.5	69.85	6.4477	69.8500	3.8689	90.6500	9.1780
1.0	56.90	6.0837	56.9000	3.6003	77.9300	8.9516
1.2	56.65	6.1645	56.6500	3.4925	77.5800	8.9126
Calm	25.05	7.0328	25.0500	4.0206	47.3100	10.0788
δ = 35°						
λ/L	$t(A_D)$	A_D	$t(T_R)$	T_R	$t(T_D)$	T_D
0.5	70.12	6.6015	70.1200	4.0248	91.3400	9.4648
1.0	56.63	5.9932	56.6300	3.7245	77.7600	9.1272
1.2	57.04	6.1549	57.0400	3.7881	77.9600	9.2194
Calm	25.13	7.1152	25.1300	4.1080	47.2400	10.1729

Table 5. 2 ONRT turning characteristics in calm water and waves at Fr = 0.2, H/λ = 0.02 and χ = -90°

Fr = 0.2, χ = -90°						
δ = -35°						
λ/L	$t(A_D)$	A_D	$t(T_R)$	T_R	$t(T_D)$	T_D
0.5	60.12	7.5393	60.1167	4.0272	71.1500	9.8652
1.0	45.65	7.8430	45.6500	4.3103	57.5333	10.0725
1.2	44.95	7.7718	44.9500	4.2360	56.8667	10.0525
Calm	15.30	7.4293	15.3000	4.0822	26.4333	10.1721
δ = 35°						
λ/L	$t(A_D)$	A_D	$t(T_R)$	T_R	$t(T_D)$	T_D
0.5	58.92	7.1864	58.9167	4.1493	69.9167	10.1896
1.0	43.88	7.1905	43.8833	4.0919	55.1167	10.2928
1.2	44.42	7.1401	44.4167	4.0111	55.6833	10.1938
Calm	15.32	7.4806	15.3167	4.1486	26.4000	10.3365

Table 5. 3 ONRT turning characteristics in calm water and waves at Fr = 0.2, H/λ = 0.02 and χ = 0°

Fr = 0.2, χ =0°						
δ = -35°						
λ/L	$t(A_D)$	A_D	$t(T_R)$	T_R	$t(T_D)$	T_D
0.5	60.00	7.3010	60.0000	3.9608	70.7800	9.7092
1.0	45.52	6.9965	45.5200	3.7817	56.3700	9.4334
1.2	45.53	7.1016	45.5300	3.7792	56.1900	9.4436
Calm	15.14	7.4668	15.1400	4.0825	26.0800	10.0453
δ = 35°						
λ/L	$t(A_D)$	A_D	$t(T_R)$	T_R	$t(T_D)$	T_D
0.5	59.98	7.2614	59.9800	3.9066	70.7400	9.6486
1.0	45.57	6.9978	45.5700	3.8797	56.4100	9.5848
1.2	45.56	7.1875	45.5600	3.9397	56.2700	9.6464
Calm	15.14	7.4806	15.1400	4.0539	26.0700	10.0068

Table 5. 4 ONRT turning characteristics in calm water and waves at Fr = 0.2, H/λ = 0.02 and χ = 90°

Fr = 0.2, χ = 90°						
δ = -35°						
λ/L	$t(A_D)$	A_D	$t(T_R)$	T_R	$t(T_D)$	T_D
0.5	58.98	7.3350	58.9833	4.1250	70.2833	10.3559
1.0	43.77	7.1621	43.7667	4.0334	54.9667	10.1544
1.2	44.47	7.1988	44.4667	3.8768	55.7833	10.0762
Calm	15.33	7.4301	15.3333	4.0007	26.4833	10.1117
δ = 35°						
λ/L	$t(A_D)$	A_D	$t(T_R)$	T_R	$t(T_D)$	T_D
0.5	60.17	7.5370	60.1667	4.1282	71.0333	9.9090
1.0	45.55	7.7655	45.5500	4.3372	57.4000	10.1347
1.2	44.93	7.6952	44.9333	4.2963	56.7833	10.1195
Calm	15.22	7.3969	15.2167	4.2110	26.2333	10.2815

Table 5. 5 ONRT turning characteristics in calm water and waves at Fr = 0.2, H/λ = 0.02 and χ = 180°

Fr = 0.2, χ = 180°						
δ = -35°						
λ/L	$t(A_D)$	A_D	$t(T_R)$	T_R	$t(T_D)$	T_D
0.5	62.68	7.6003	62.6833	4.1330	74.3000	10.3164
1.0	46.75	7.6891	46.7500	4.0705	58.7500	10.2595
1.2	43.68	7.6279	43.6833	3.9470	55.2167	9.8654
Calm	15.20	7.4301	15.2000	3.9527	26.3167	9.9533
δ = 35°						
λ/L	$t(A_D)$	A_D	$t(T_R)$	T_R	$t(T_D)$	T_D
0.5	62.77	7.5949	62.7667	4.2698	74.4833	10.5633
1.0	46.87	7.7526	46.8667	4.1252	58.9833	10.3656
1.2	43.82	7.6839	43.8167	4.1318	55.5333	10.2595
Calm	15.23	7.4723	15.2333	4.1152	26.3000	10.0979

Table 5. 6 ONRT turning characteristics in calm water and waves at Fr = 0.3, H/λ = 0.02 and χ = 0°

Fr = 0.3, χ =0°						
δ = -35°						
λ/L	$t(A_D)$	A_D	$t(T_R)$	T_R	$t(T_D)$	T_D
0.5	56.37	7.8599	56.3700	4.0752	63.6000	10.1084
1.0	41.47	7.6211	41.4700	3.9384	48.9400	10.0946
Calm	11.44	8.0548	11.4400	4.2139	18.7800	10.3467
δ = 35°						
λ/L	$t(A_D)$	A_D	$t(T_R)$	T_R	$t(T_D)$	T_D
0.5	56.49	7.8779	56.4900	4.2292	63.9500	10.4132
1.0	41.45	7.6078	41.4500	4.0608	48.8700	10.2018
Calm	11.39	7.9861	11.3900	4.3328	18.7200	10.4940

Table 5.7 VLCC drifting distance and direction results (NMRI)

λ/L	H_D/L (+35deg)	H_D/L (-35deg)	$[H_D/L(+35deg)]/[H_D/L(-35deg)]$
0.4	1.80952	1.92857	0.93827
0.5	1.60714	1.74702	0.91993
0.6	1.40476	1.56548	0.89734
1.0	0.27976	0.44643	0.62667
λ/L	μ_D/L (+35deg)	μ_D/L (-35deg)	$\lvert[\mu_D/L(+35deg)]\rvert/[\ \mu_D/L(-35deg)]$
0.4	-13.08057	11.65877	1.12195
0.5	-20.33176	16.91944	1.20168
0.6	-27.58294	22.18010	1.24359
1.0	-15.63981	56.01896	0.27919

Highlighted results are interpolated
Source: (Ueno et al., 2003)

Table 5. 8 ONRT drifting distance and direction (IIHR)

$\lambda/L=0.5$	+35 deg	-35 deg	$[H_D/L(+35deg)]/[H_D/L(-35deg)]$	Average
H_{D0}/L	0.24057	0.31823	0.75596	0.71780
H_{D1}/L	0.26020	0.38284	0.67965	
$\lambda/L=0.5$	+35 deg	-35 deg	$[\mu_D/L(+35deg)]/[\mu_D/L(-35deg)]$	Average
μ_{D0}	59.41861	-59.26825	1.00254	1.01687
μ_{D1}	49.28257	-47.79092	1.03121	
$\lambda/L=1.0$	+35 deg	-35 deg	$[H_D/L(+35deg)]/[H_D/L(-35deg)]$	Average
H_{D0}/L	0.21576	0.34553	0.62444	0.60045
H_{D1}/L	0.23579	0.40903	0.57646	
$\lambda/L=1.0$	+35 deg	-35 deg	$[\mu_D/L(+35deg)]/[\mu_D/L(-35deg)]$	Average
μ_{D0}	67.97066	-59.26825	1.14683	0.84149
μ_{D1}	43.56296	-81.25283	0.53614	

CHAPTER 6

CONCLUSION AND FUTURE WORK

Equipped with six plunger-type wave makers, the IIHR wave basin is a uniquely designed for local flow measurements around free running models. A main x carriage, y sub-carriage, and θ turntable is equipped with a model release system, a semi-captive mounts, and model tracking system. A free running measurement system onboard of the model is included and a 6DOF visual motion capture system is added for more measurement accuracy. In this study, the IIHR wave basin is utilized to conduct ONRT maneuvering tests in calm water and wave conditions to assess the data quality of the measurement system and ensure its repeatability. Repeated runs for each case were conducted and the results are satisfying. Another objective of this study is to provide a wide range of data in different heading angles to help investigate the wave drift forces and provide means to improve the System Base (SB) method. The obtained ONRT maneuvering data will also serve as a benchmark data for the IIHR CFD validation.

Standard maneuvering tests were conducted in calm water condition that include course keeping in different heading angles and zigzag tests with 10°/10°, 20°/20°, and 35°/35° rudder angles Fr = 0.2 as well as turning tests with ±35° rudder angles at Fr = 0.1, 0.2, and 0.3. For each test case, several trials were conducted and the repeated trajectories and time histories have good agreement in each.

Standard maneuvering tests were conducted in wave conditions of $\lambda/L = 0.5$, 1.0, and 1.2 and $H/\lambda = 0.02$. These tests include course keeping tests with several headings and zigzag tests with rudder angles 10°/10°, 20°/20°, and 35°/35° in head and following waves. Three runs were executed for each test case and the trajectories and results show good agreement within each case. The maneuvering characteristics of the ONRT were obtained for establishing benchmark data for CFD validation.

Standard maneuvering tests were also conducted in head wave conditions of $\lambda/L=0.5$, 1.0, and 1.2 and $H/\lambda=0.02$ in different wave encounter angles. These tests

include turning tests with ±35° rudder angles at Fr 0.1 and 0.3 for the wave encounter angle $\chi = 0°$ and turning tests with ±35° rudder angles at Fr = 0.2 for $\chi = 0°$, ±90°, and 180°. For each test case, several trials were conducted and the repeated trajectories and time histories have a good agreement in each. Turning characteristics of the ONRT such as drifting distance, drifting direction, advance, tactical diameter, and transfer were obtained. Using Ueno et al. (2003) proposed method, drifting distance and direction were calculated. ONRT has smaller drifting distance and larger drifting direction than that of VLCC (Ueno et al, 2003).

The ONRT trajectories and maneuvering characteristics results show that the ONRT is straight-line stable vessel. The results also show that the ONRT is a highly maneuverable ship when performing course keeping, zigzag, or turning maneuvers. When turning results such as drifting distance and drifting direction of ONRT are compared to those of the VLCC, the ONRT has shown higher stability and easier maneuverability than the VLCC. These comparison observations are attributed to the differences in ship hull design and ship speed in addition to the fact that the ONRT is a twin rudder twin screw propeller while the VLCC is a one rudder one propeller ship.

To investigate the wave drift force, future research will focus on in depth analysis of the ONRT maneuvering data set in order to help improve the predictability of SB method to ship trajectories specially in short waves. In addition, stereoscopic PIV (SPIV) for local flow measurement around the ONRT is of interest. Local flow measurement is needed to investigate the viscous effects and the interaction between free surface and flow field around the ship model. Carriage speed in multiple directions will be utilized to validate the SPIV uniform flow measurement. Future research will also focus on free surface measurements, regular wave measurements and generated waves around ONRT using the RLD system. For better results to help understand the wave drift force, local flow and free surface measurements will be done simultaneously. The development of a

mathematical model for the evaluation and assessment of the forces/moments the ONRT experiences during maneuvering is also one of the future research focuses.

REFERENCES

American Bureau of Shipping, 2006, Guide for Vessel Maneuverability Houston, TX, 2006a, pp. 9.

American Bureau of Shipping, 2006, Guide for Vessel Maneuverability Houston, TX, 2006b, pp. 17.

Carrica, P., Ismail, F., Hyman, H., Bhushan, S., and Stern, F., 2010, Turn and Zigzag Maneuvers of a Surface Combatant using URANS Approach and Dynamic Overset Grids, Journal of Marine Science and Technology, online.

Cook, S. S., 2011 Effects of headwinds on towing tank resistance and PMM tests for ONR Tumblehome, thesis, University of Iowa.

Eda, H., and Shiba, H., 1962, On the Turning Experiments by the Free-Running Models, Monthly Reports of Transportation Technical Research Institute, Vol. 11, No 12.

Furukawa, T., Umeda, N., Hashimoto, H., Matsuda, A., Stern, F., Araki, M., and Sadat-Hosseini, H., 2012, Effect of above water hull forms on extreme ship motions in stern quartering waves 29th Symposium on Naval Hydrodynamics Gothenburg.

Hirano, M., Takashina, J., Takeshi, K., and Saruta, T., 1980a, Ship Turning Trajectory in Regular Waves, West-Japan Society of Naval Architects No 60, pp17-31.

Hirano, M., and Takashina, J., 1980b, A Calculation of Ship Turning Motion Taking Coupling Effect Due to Heel into Consideration, The Japan Society of Naval Architects and Ocean Engineering, No 59.

International Maritime Organization, 2002, Standards for Ship Maneuverability, MSC.137 (76).

International Maritime Organization, 2006, Interim Guidelines for Alternative Assessment of the Weather Criterion, MSC.1/Circ.1200

Irvine, M., Longo, J., and Stern, F., (2004), Towing Tank Tests for Surface Combatant for Free Roll Decay and Coupled Pitch and Heave Motions, 25th ONR Symposium on Naval Hydrodynamics, St Johns, Canada.

Irvine, M., Longo, J., and Stern, F., 2008, Pitch and Heave Tests and Uncertainty Assessment for a Surface Combatant in Regular Head Waves, Journal of Ship Research, Vol. 52, No. 2, pp. 146-163.

ITTC, 2005, Testing and Extrapolation Methods, Loads and responses, Sea Keeping, Sea Keeping Experiments, ITTC–Recommended Procedures and Guide- lines, 7.5-02-07-02.1, pp.1-18

Longo, J., Shao, J., Irvine, M., and Stern, F., 2007, Phase- Averaged PIV for the Nominal Wake of a Surface Ship in Regular Head Waves, ASME J. Fluids Eng., Vol. 129, Issue 3.

Milanov, E., Chotukova, V., and Stern, F., 2011, Experimental and simulation studies on fast Delft 372 catamaran maneuvering and course stability in deep and shallow water, Proc. 11th International Conference Fast Sea Transportation, Hawaii, USA.

Sadat-Hosseini, H., Carrica, P.M., Stern, F., Umeda, N., Hashimoto, H., Yamamura, S. and Mastuda, A., 2011a, CFD, system-based and EFD study of ship dynamic instability events: surf-riding, periodic motion, and broaching", Journal of Ocean Engineering, Vol. 38, Issue 1, pp.88- 110.

Sadat-Hosseini, H., Araki, M., Umeda, N., Sano, M., Yeo, D., Toda, Y. and Stern, F., 2011b, CFD, System-Based, and EFD preliminary investigation of ONR Tumblehome instability and capsize with evaluation of the mathematical model, Proc. The 12th International Ship Stability Workshop, Washington D.C., USA.

Sanada Y., Toda Y. and Hamachi S., 2008, Free Surface Measurement by Reflected Light Image - Introduction and Examples -, Proceedings of 25th ITTC Volume III, pp.814-820.

Sanada Y., Tanimoto, K., Takagi, K., Gui, L., Toda, Y., and Stern, F., 2013, Trajectories for ONR Tumblehome Maneuvering in Calm Water and Waves, Ocean Engineering Vol. 72, pp. 45-65.

Seo, M., and Kim, Y., 2011, Effects of Ship Motion on Ship Maneuvering in Waves, 26th International Workshop on Water Waves and Floating Bodies, Athens, Greece.

Stern, F., Toxopeus, S., Visonneau, M., Lin, W-M, and Grigoropoulos, G., 2011, CFD, potential flow and systems based simulations of course keeping in calm water and seakeeping in regular waves for 5415M, NATO AVT- 189 Specialists Meeting on Assessment of Stability and Control Prediction Methods for NATO Air & Sea Vehicles, Portsdown West UK.

Tanimoto, K., 2012, Development of 6DOF Visual Motion Capture System for Free Running Model Test in Waves, Master thesis, Osaka University.

Takagi, K., 2012, Development of New Tracking System for Free Running Model Test in Waves, Bachelor thesis, Osaka University.

Toda, Y., Stern, F., and Longo, J., 1992, Mean-Flow Measurements in the Boundary Layer and Wake and Wave Field of a Series 60 CB = .6 Model ship - Part 1: Froude Numbers .16 and .316, Journal of Ship Research, Vol. 36, No. 4, pp. 360-377.

Toxopeus, S.L., Walree F. van, and Hallmann R., 2011, Maneuvering and Seakeeping Tests for 5415M. AVT-189 Specialists' Meeting, Portsdown West, UK.

Ueno, M., Nimura, T. and Miyazaki, H., 2003, Experimental Study on Maneuvering Motion of a Ship in Waves, International Conference on Marine Simulation and Ship Maneuverability, MARSIM'03, Kanazawa, Japan.

Yasukawa, H., and Nakayama, Y., 2006, 6-DOF Motion Simulations of a Turning Ship in Regular Waves, Proceedings of the International Conference on Marine Simulation and Ship Maneuverability (MARSIM'09), Panama City.

Yoon, H.S., 2009, Force/Moment and Phase- Averaged Stereo PIV Flow Measurements for Surface Combatant in PMM Maneuvers," Ph.D. Thesis, University of Iowa.

Yoon, H., Gui, L., and Stern, F., 2014a, "Benchmark CFD Validation Tomographic PIV for Surface Combatant 5415 at Zero, Ten, and Twenty Degree Static Drift," 30th Symposium on Naval Hydrodynamics, Hobart, Australia.

Yoon, H., Simonsen, C., Bouscasse, B., Longo, J., Toda, Y., and Stern, F., 2014b, "Benchmark CFD Validation Data for Surface Combatant 5415 in PMM Maneuvers - Part I: Force/Moment/Motion Measurements," in preparation.

APPENDIX A RAIL SINKAGE MEASUREMENT

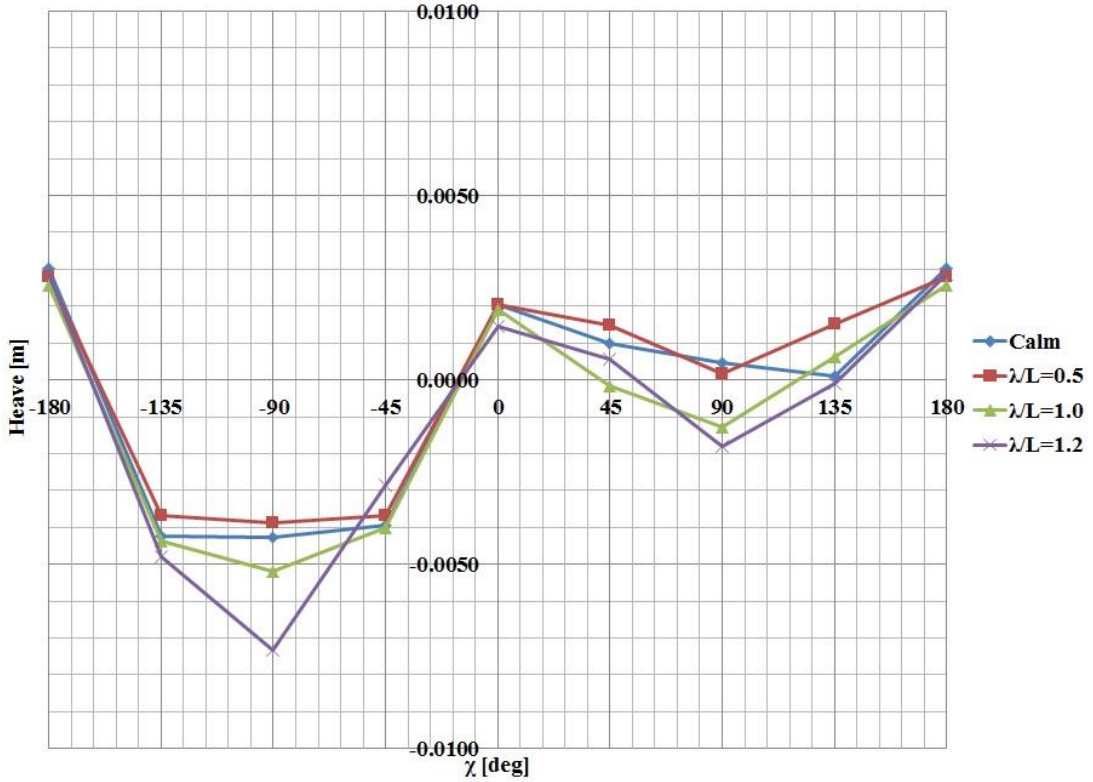

Figure A-1 Heave measurement of course keeping in calm water and waves at Fr = 0.2

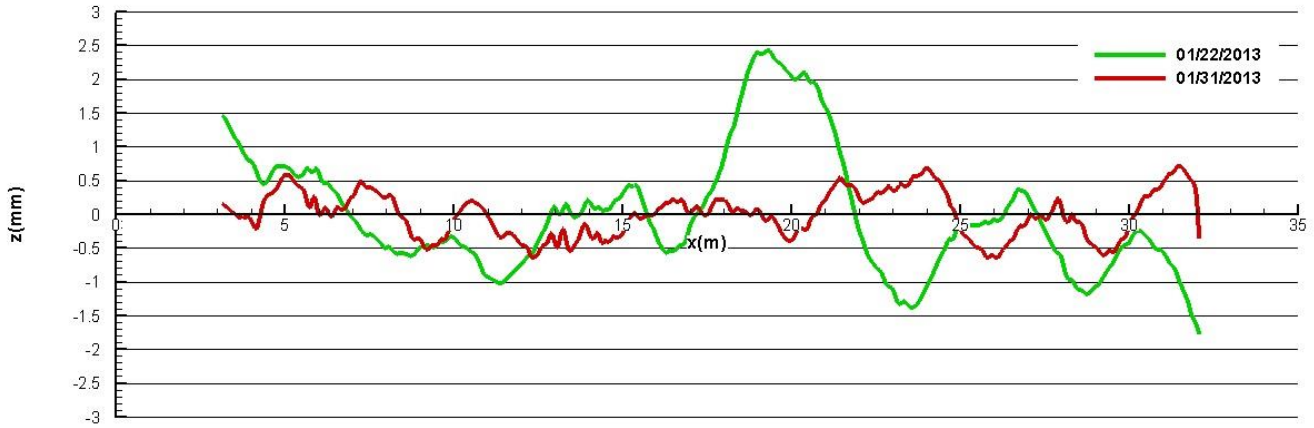

Figure A-2 Rail sinkage measurement-North side (Green: Before adjustment, Red: After adjustment)

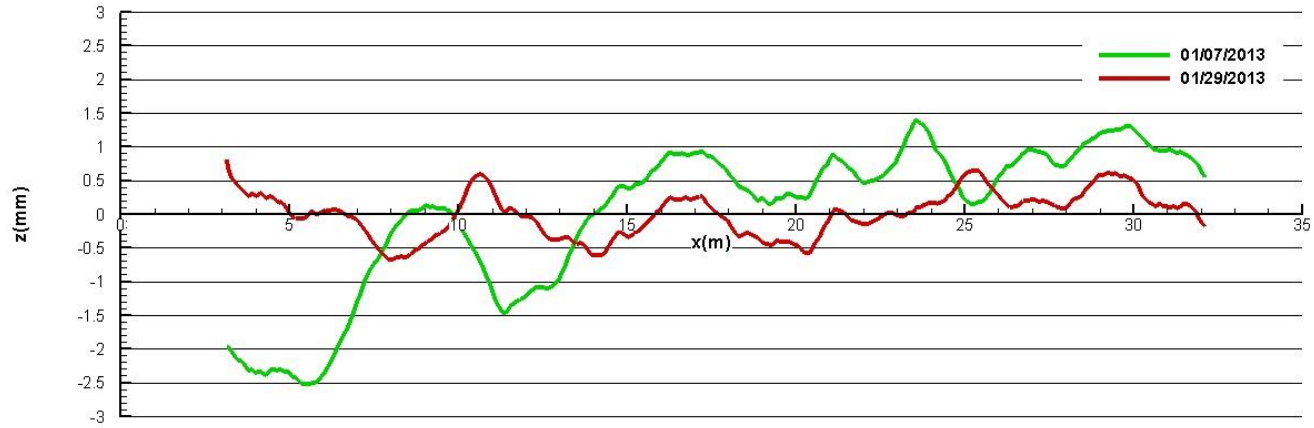

Figure A-3 Rail sinkage measurement-South side (Green: Before adjustment, Red: After adjustment)

APPENDIX B TRAJECTORIES AND TIME HISTORIES RESULTS OF COURSE KEEPING TESTS IN CALM WATER

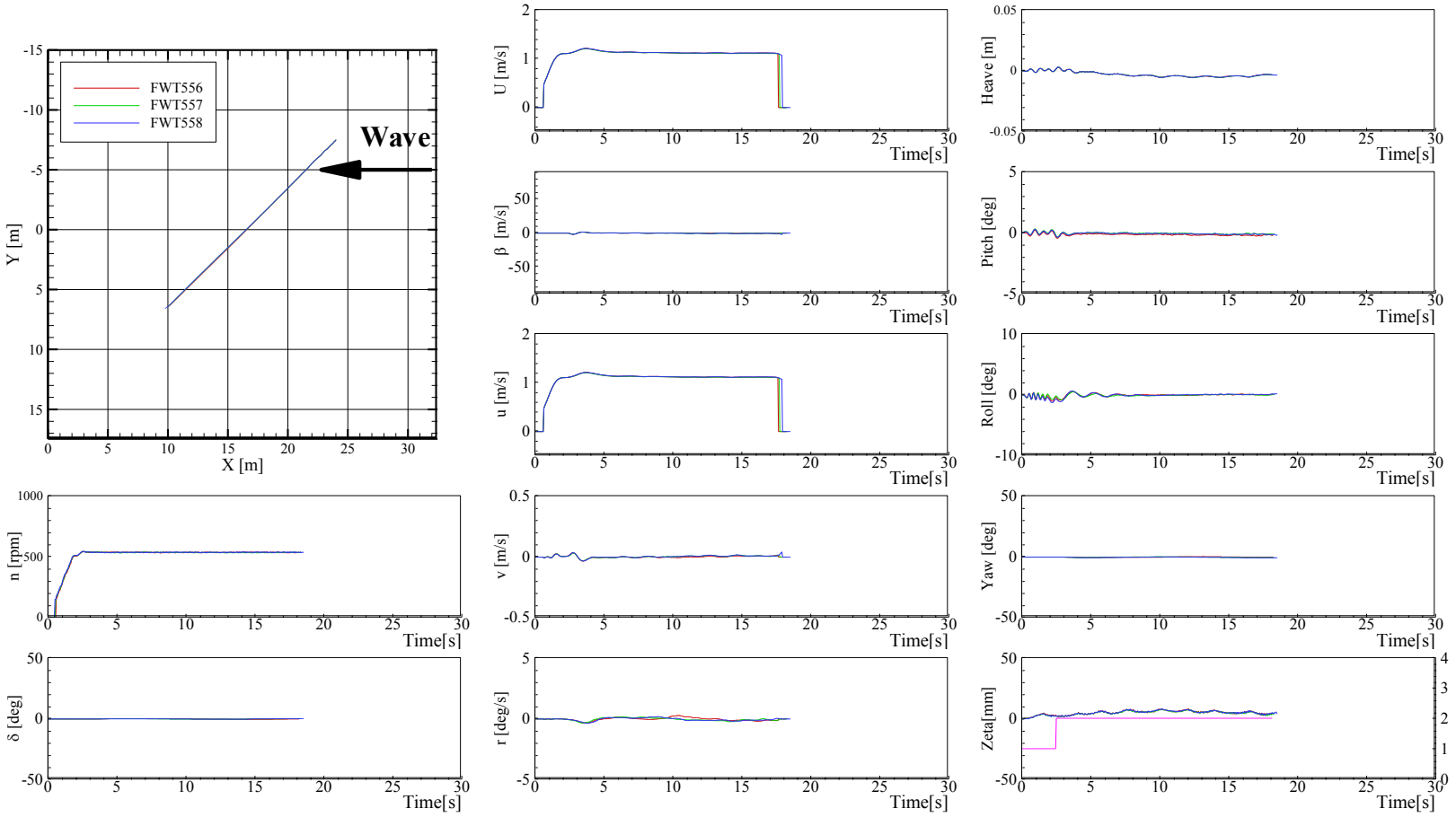

Figure B-1 Trajectories and time histories of course keeping in calm water at Fr = 0.2 and heading angle = -135°

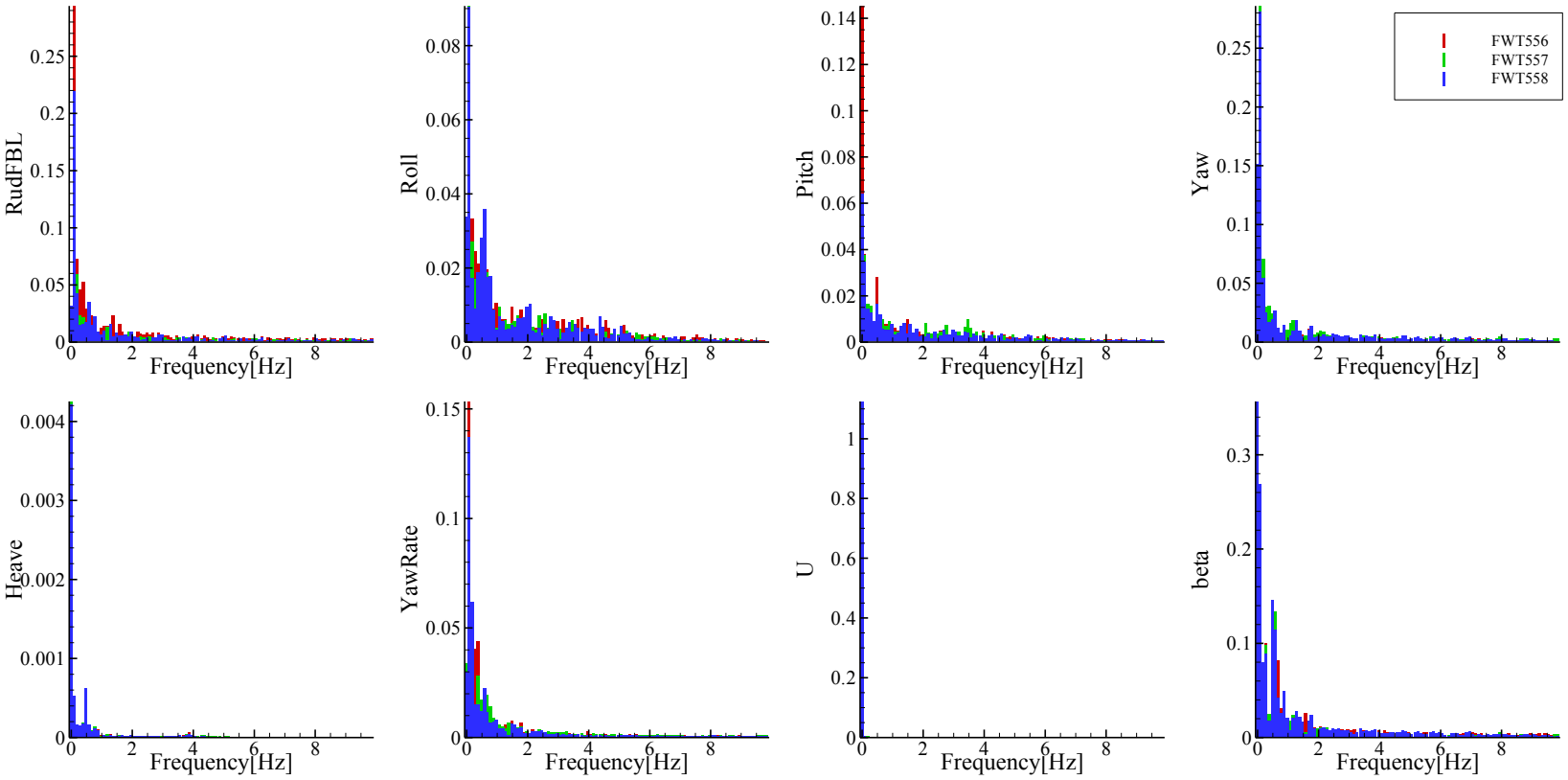

Figure B-2 FFT analysis of time histories of course keeping in calm water at Fr = 0.2 and heading angle = -135°

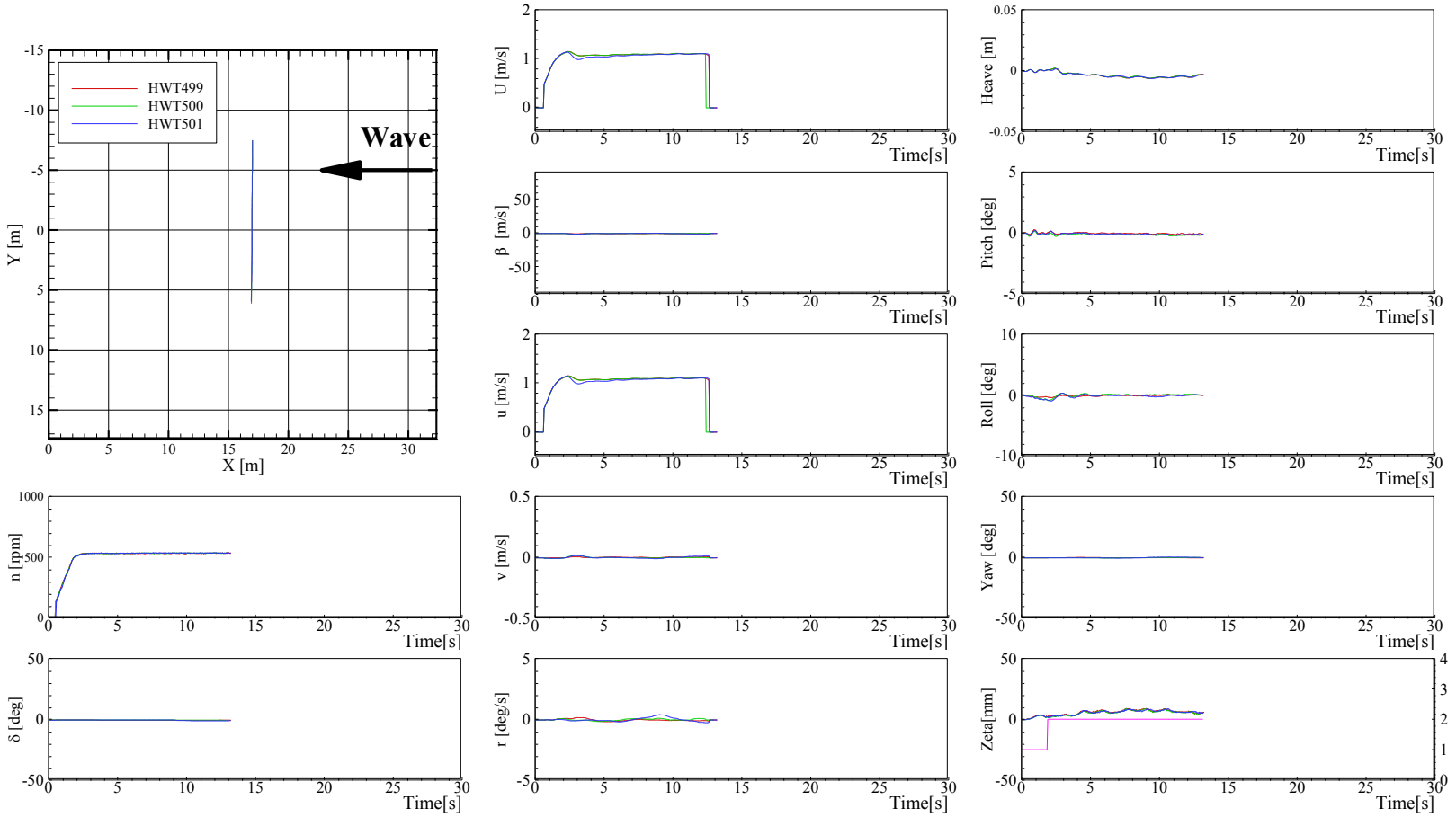

Figure B-3 Trajectories and time histories of course keeping in calm water at Fr = 0.2 and heading angle = -90°

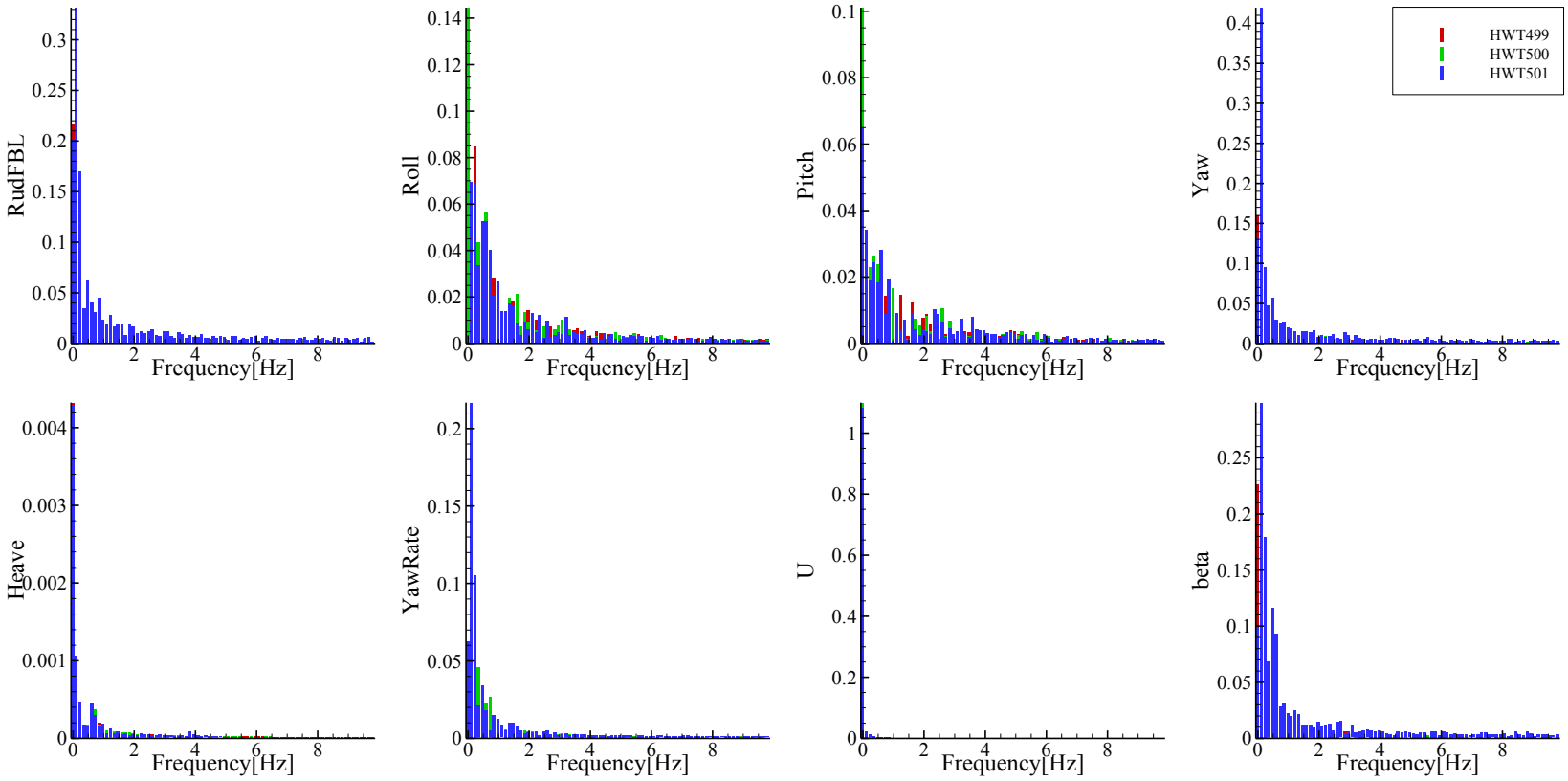

Figure B-4 FFT analysis of time histories of course keeping in calm water at Fr = 0.2 and heading angle = -90°

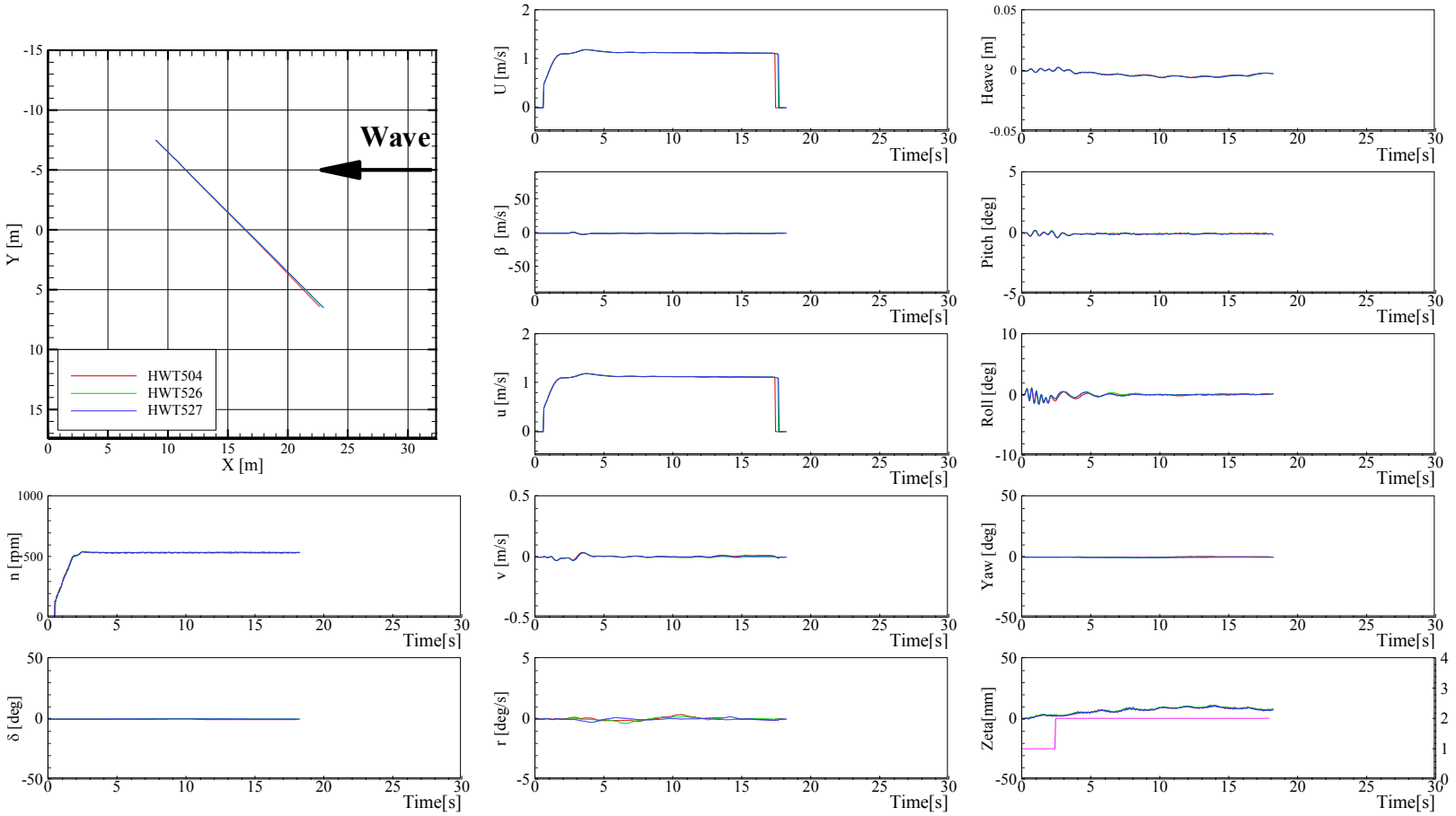

Figure B-5 Trajectories and time histories of course keeping in calm water at Fr = 0.2 and heading angle = -45°

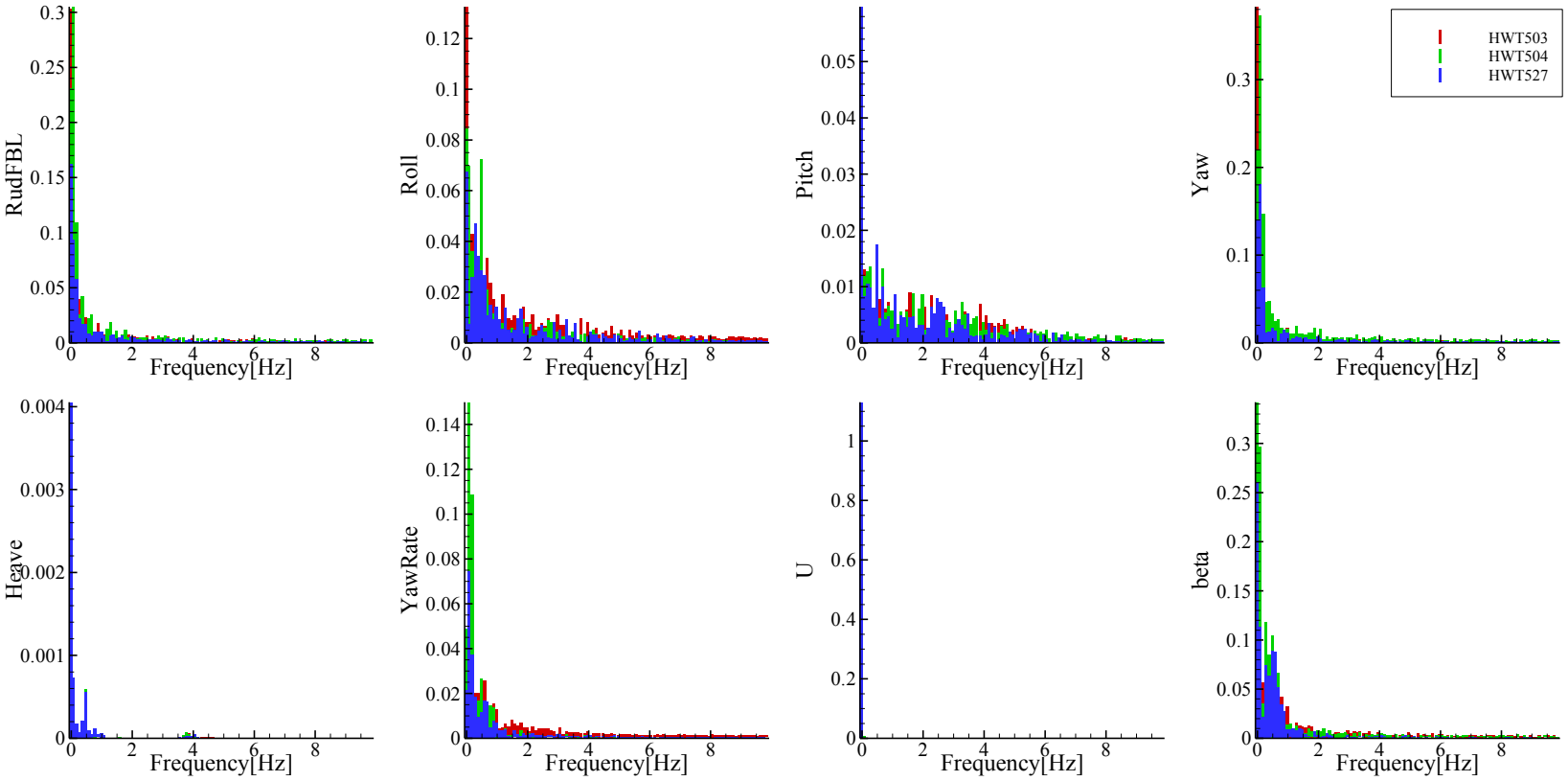

Figure B-6 FFT analysis of time histories of course keeping in calm water at Fr = 0.2 and heading angle = -45°

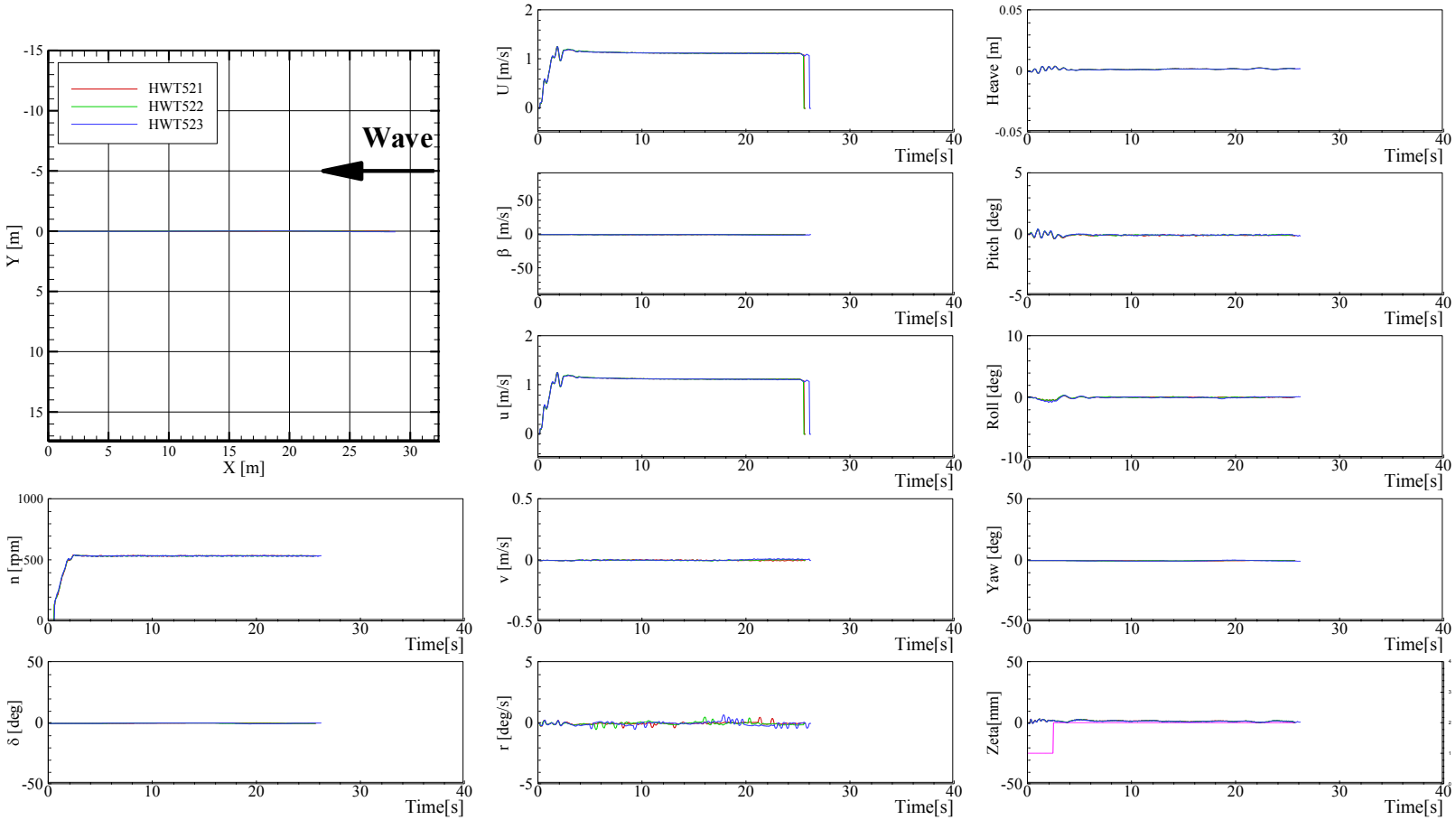

Figure B-7 Trajectories and time histories of course keeping in calm water at Fr = 0.2 and heading angle = 0°

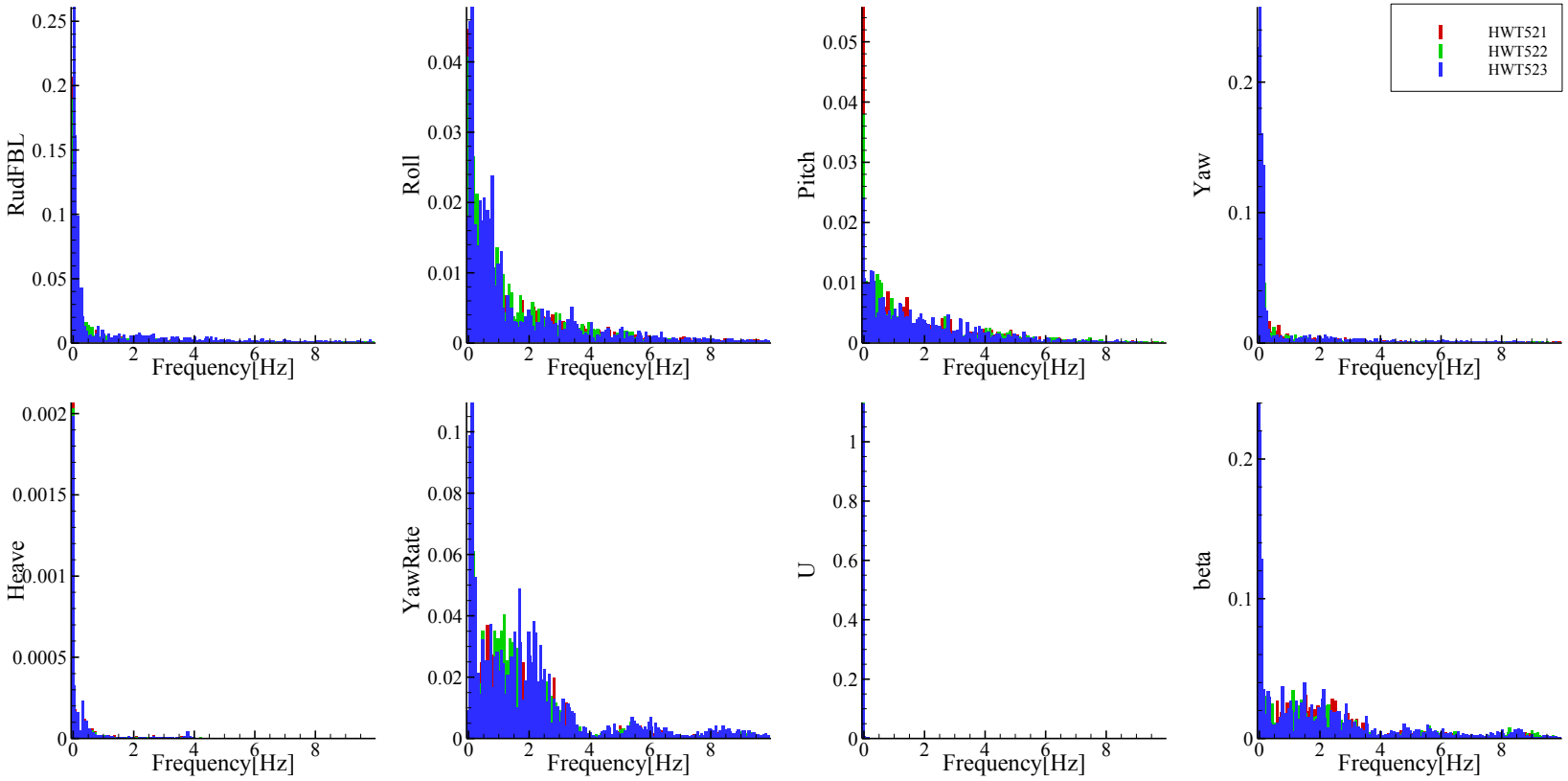

Figure B-8 FFT analysis of time histories of course keeping in calm water at Fr = 0.2 and heading angle = 0°

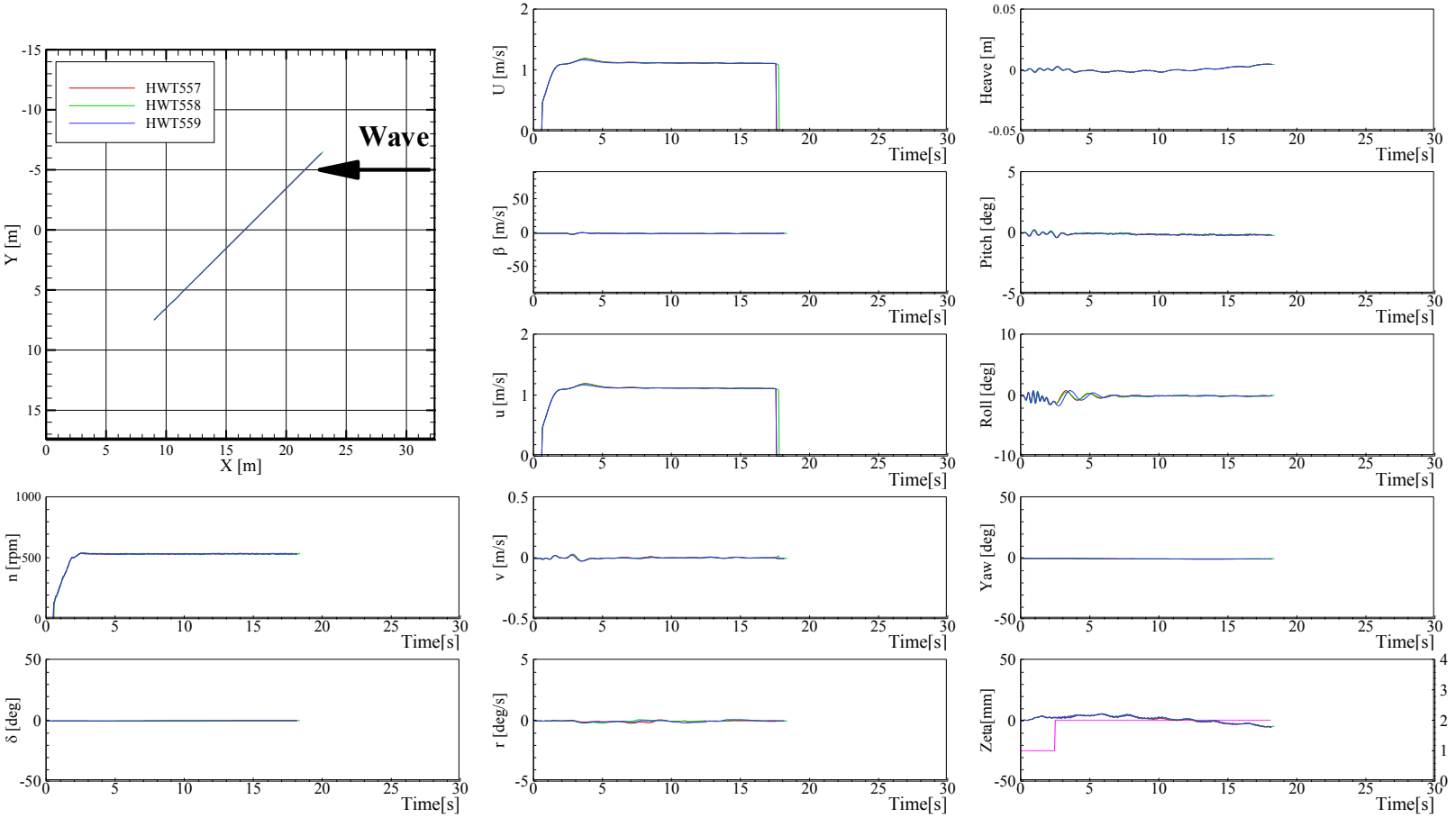

Figure B-9 Trajectories and time histories of course keeping in calm water at Fr = 0.2 and heading angle = 45°

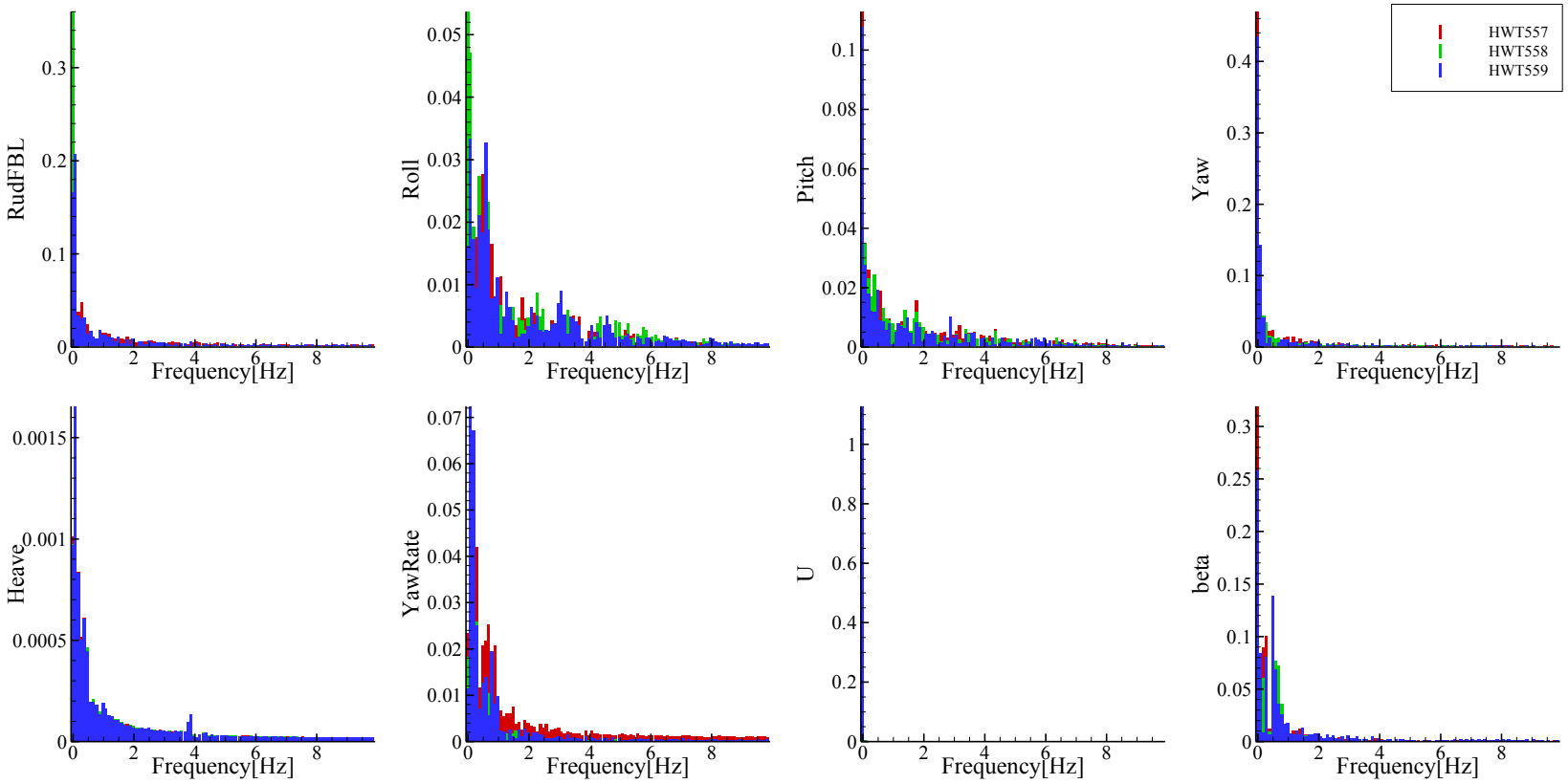

Figure B-10 FFT analysis of time histories of course keeping in calm water at Fr = 0.2 and heading angle = 45°

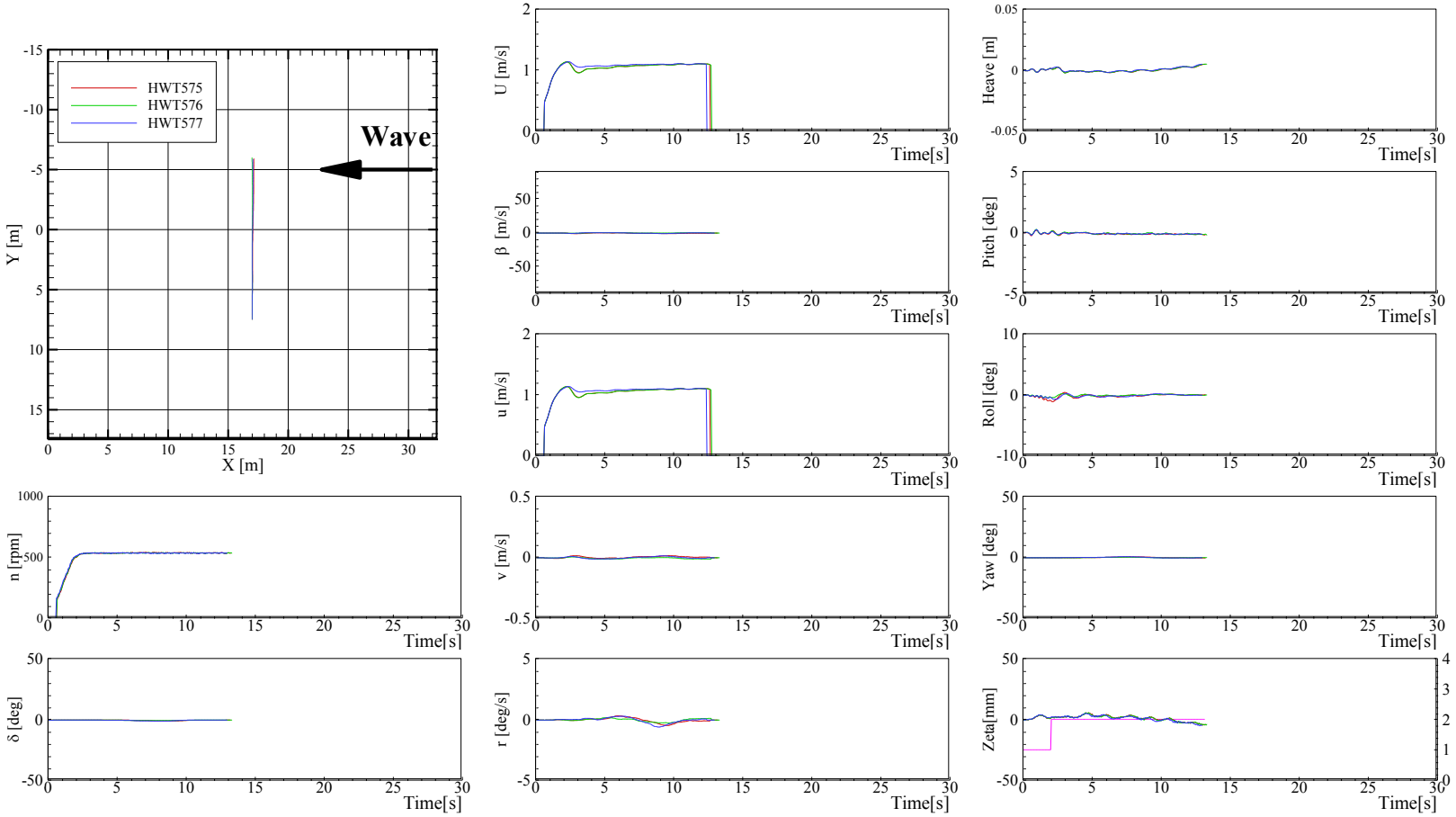

Figure B-11 Trajectories and time histories of course keeping in calm water at Fr = 0.2 and heading angle = 90°

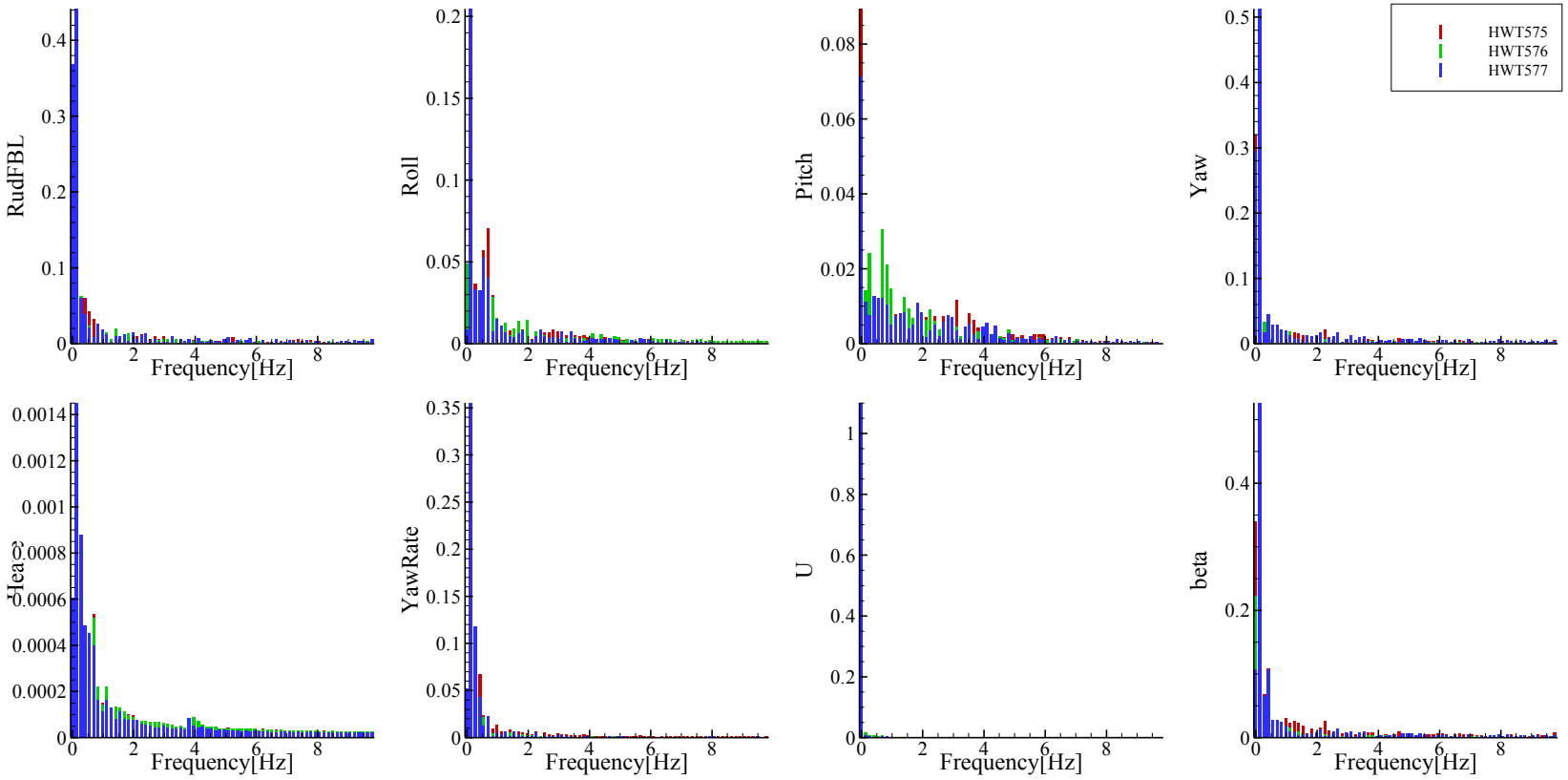

Figure B-12 FFT analysis of time histories of course keeping in calm water at Fr = 0.2 and heading angle = 90°

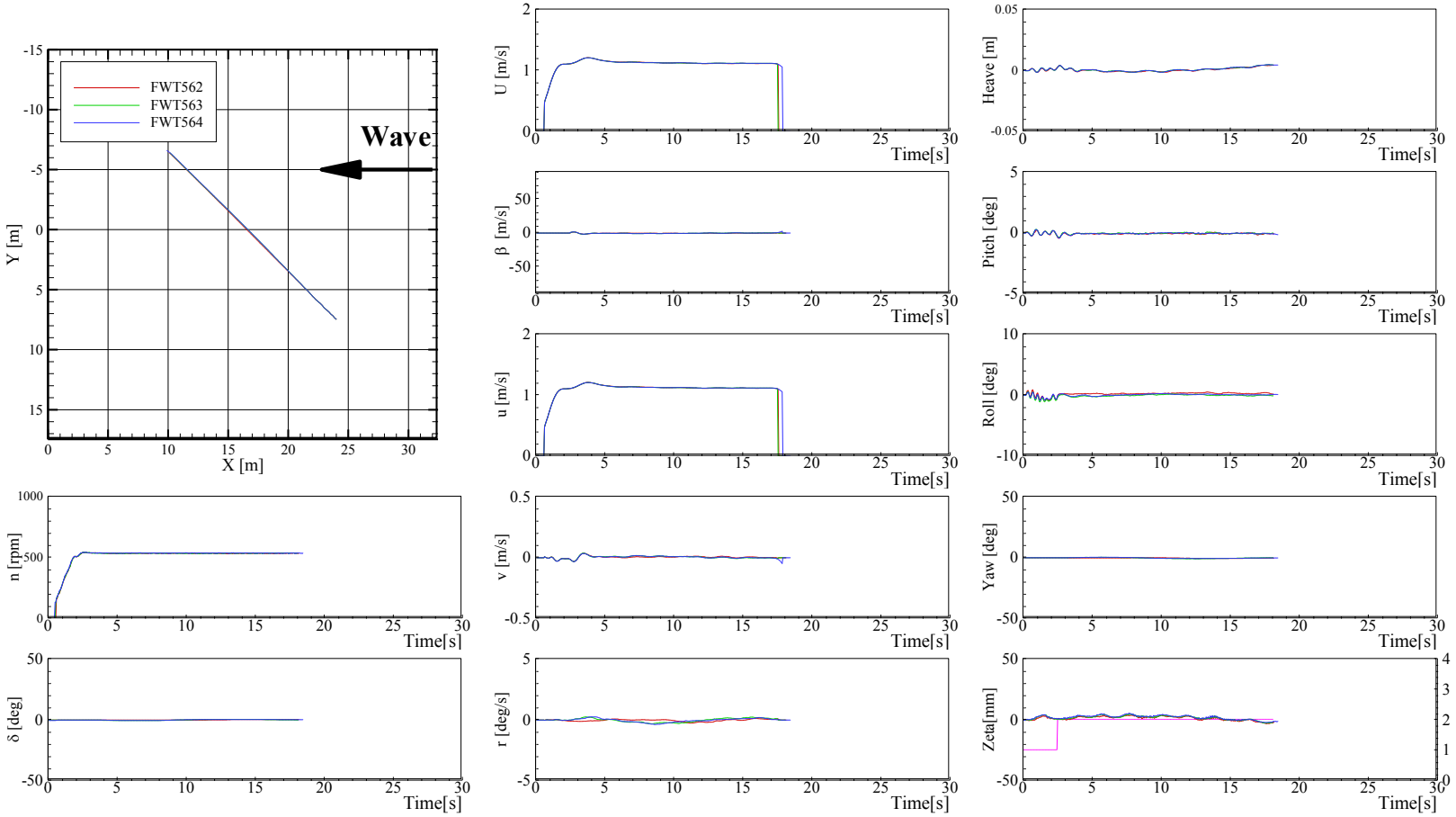

Figure B-13 Trajectories and time histories of course keeping in calm water at Fr = 0.2 and heading angle = 135°

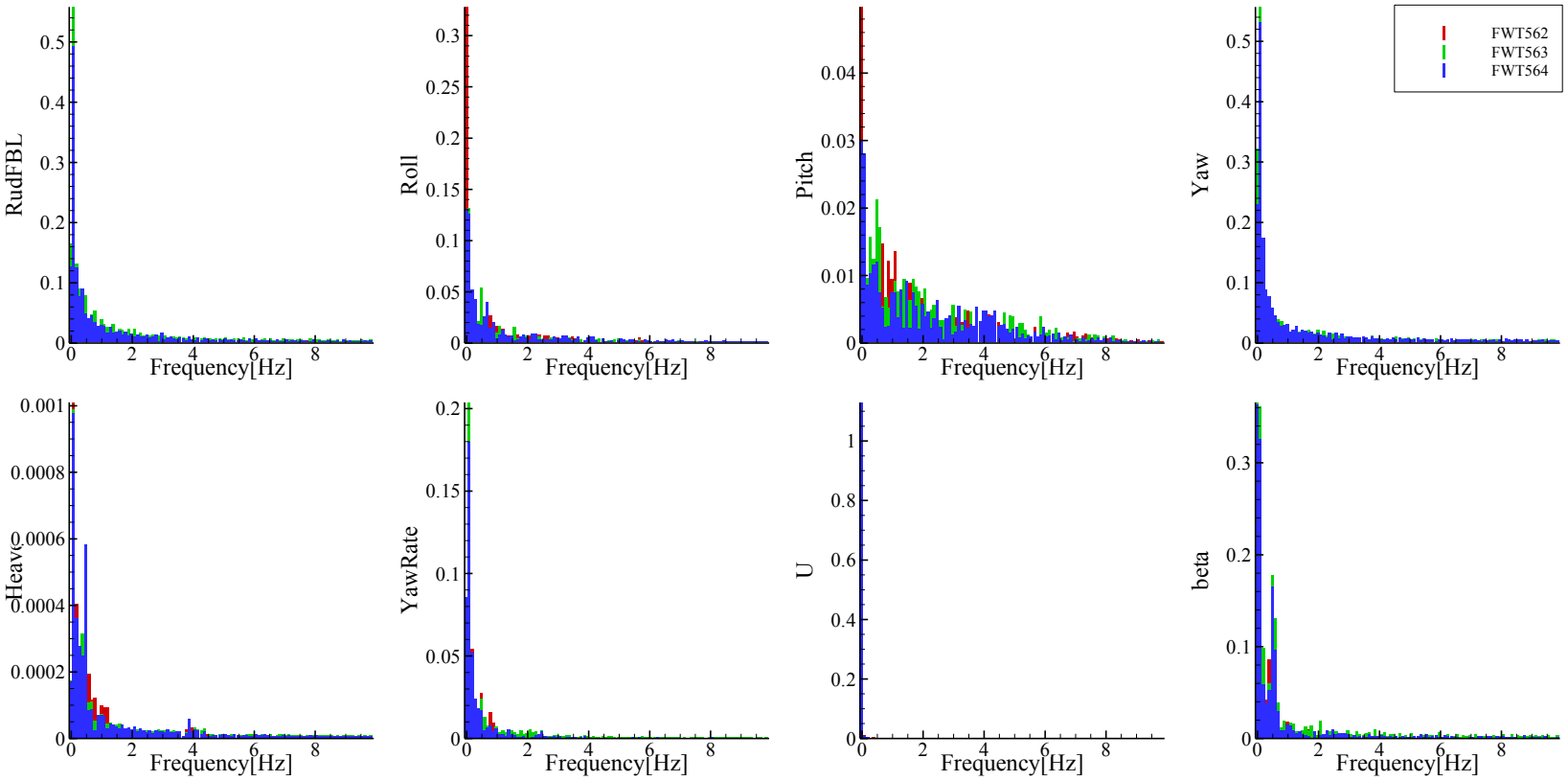

Figure B-14 FFT analysis of time histories of course keeping in calm water at Fr = 0.2 and heading angle = 135°

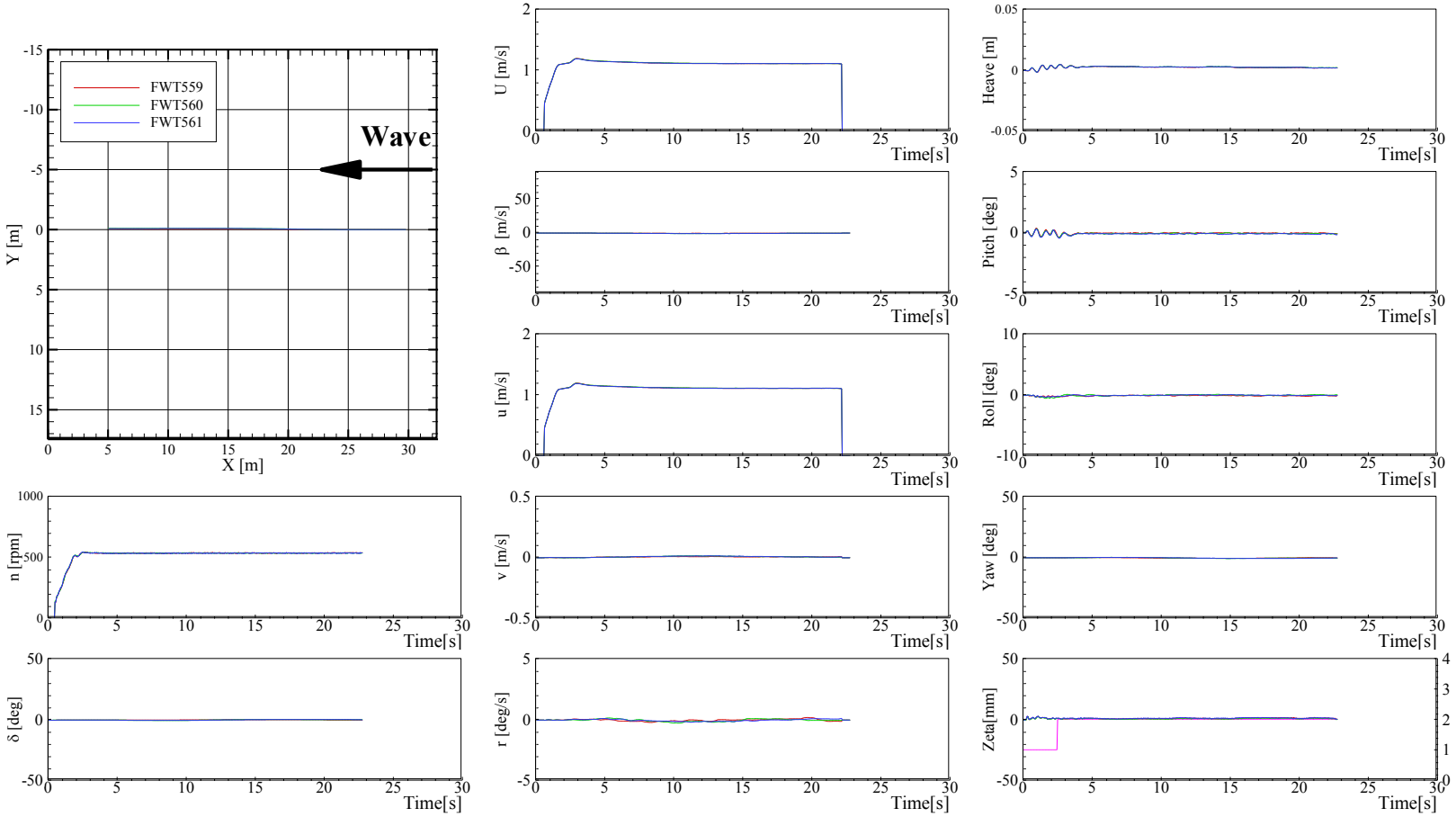

Figure B-15 Trajectories and time histories of course keeping in calm water at Fr = 0.2 and heading angle = 180°

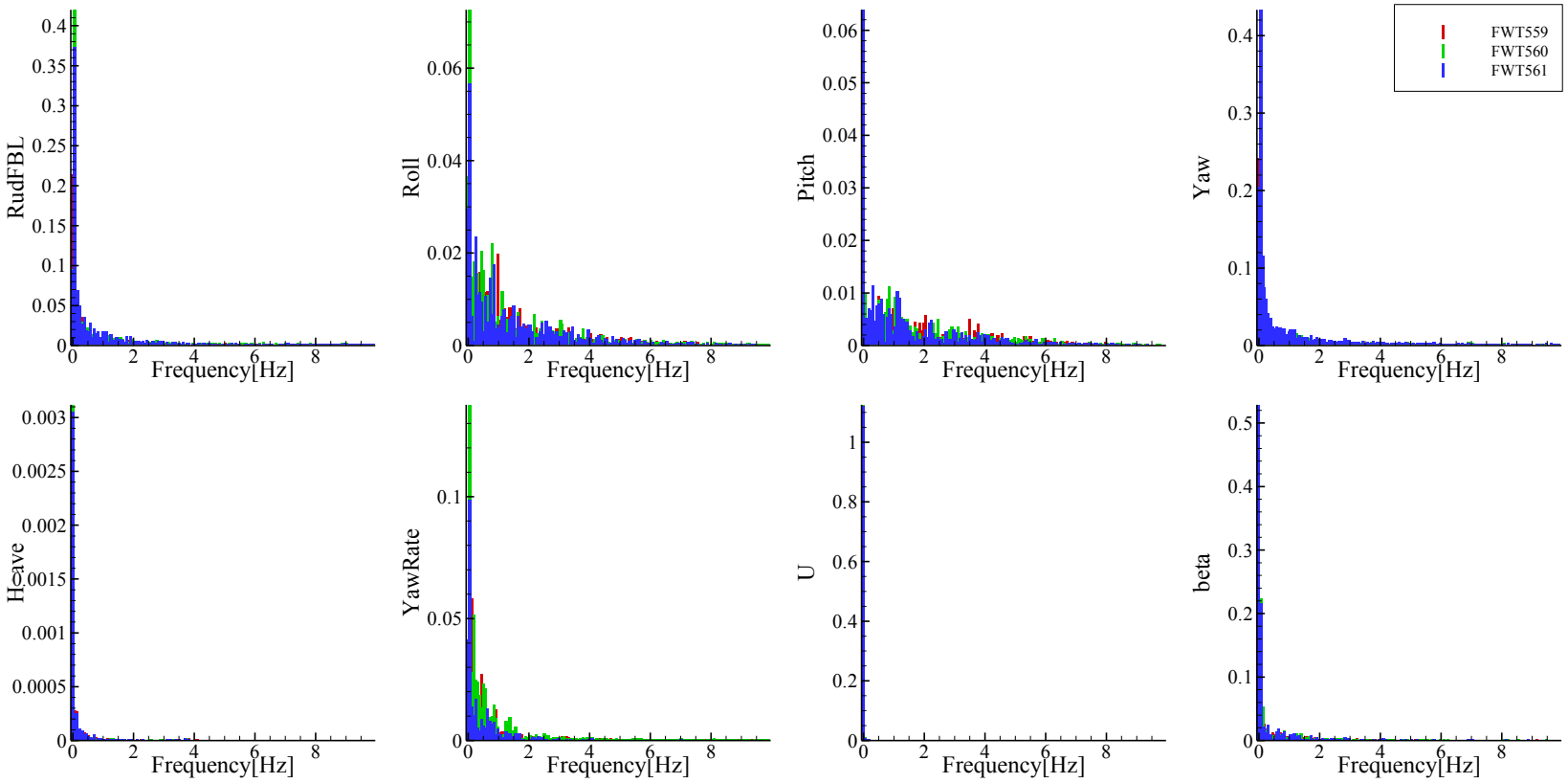

Figure B-16 FFT analysis of time histories of course keeping in calm water at Fr = 0.2 and heading angle = 180°

APPENDIX C TRAJECTORIES AND TIME HISTORIES RESULTS OF COURSE KEEPING TESTS IN WAVES

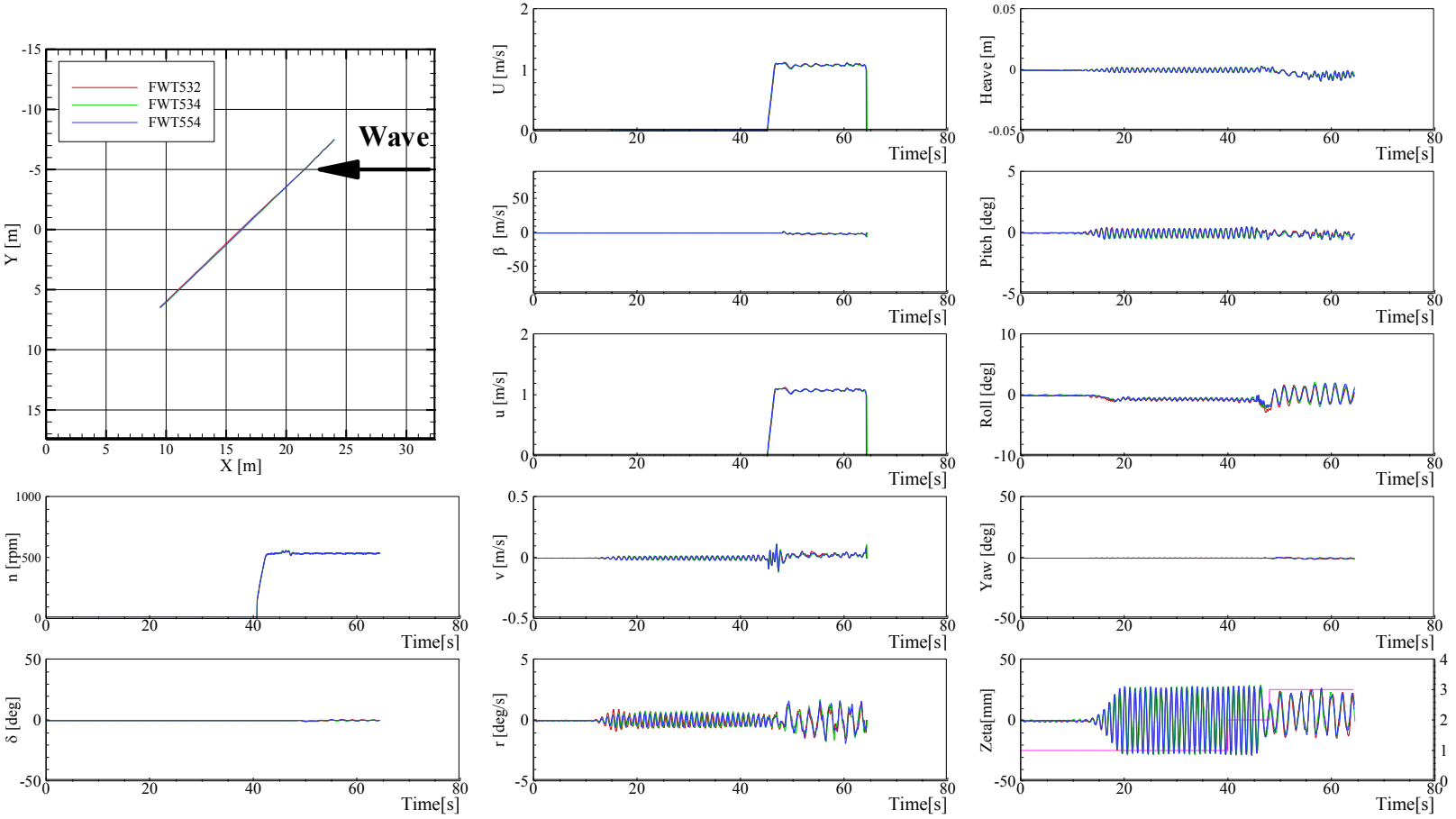

Figure C-1 Trajectories and time histories of course keeping at Fr = 0.2, λ/L = 0.5, H/λ = 0.02, and heading angle = -135°

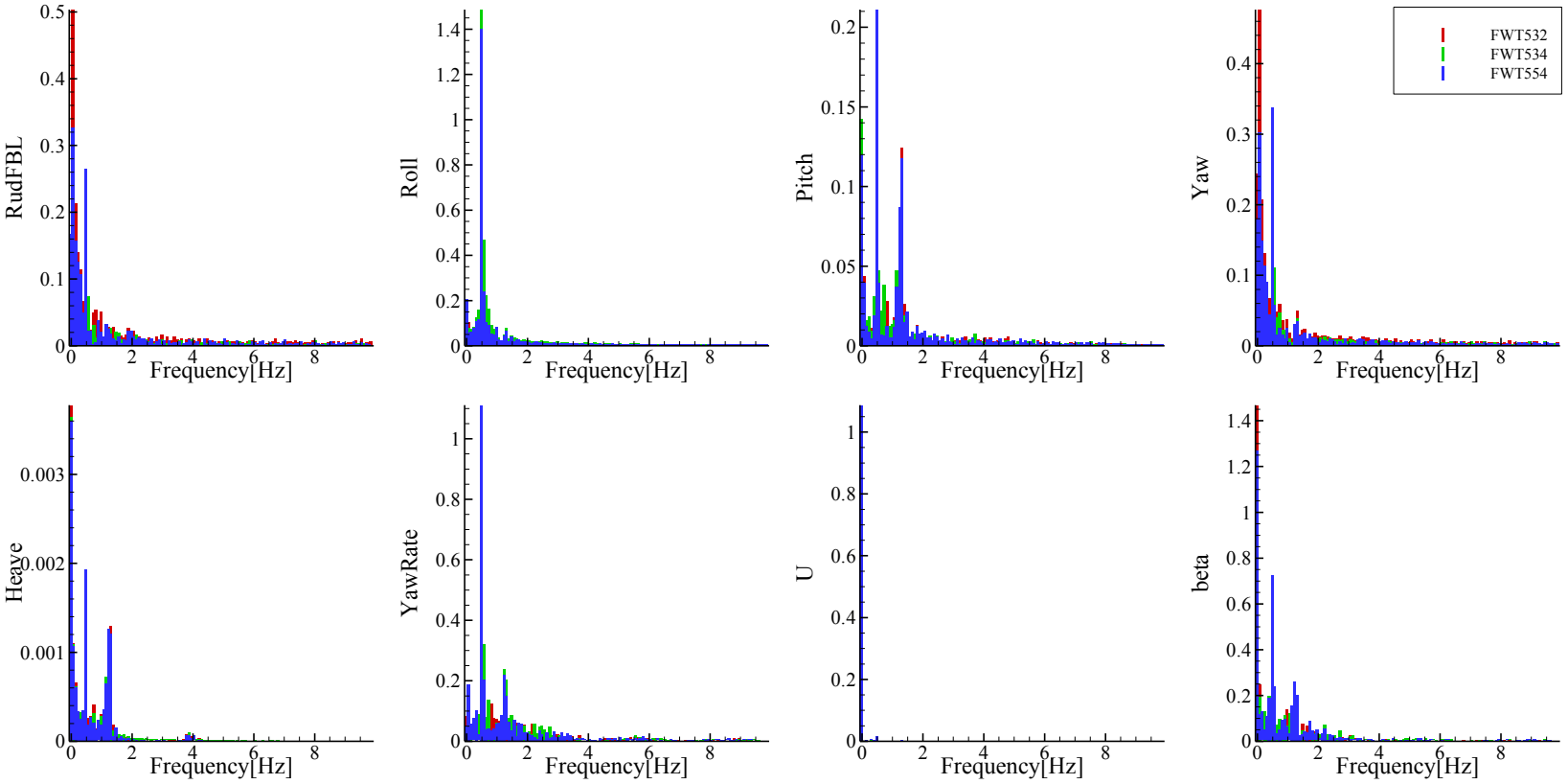

Figure C-2 FFT analysis of time histories of course keeping at Fr = 0.2, λ/L = 0.5, H/λ = 0.02, and heading angle = -135°

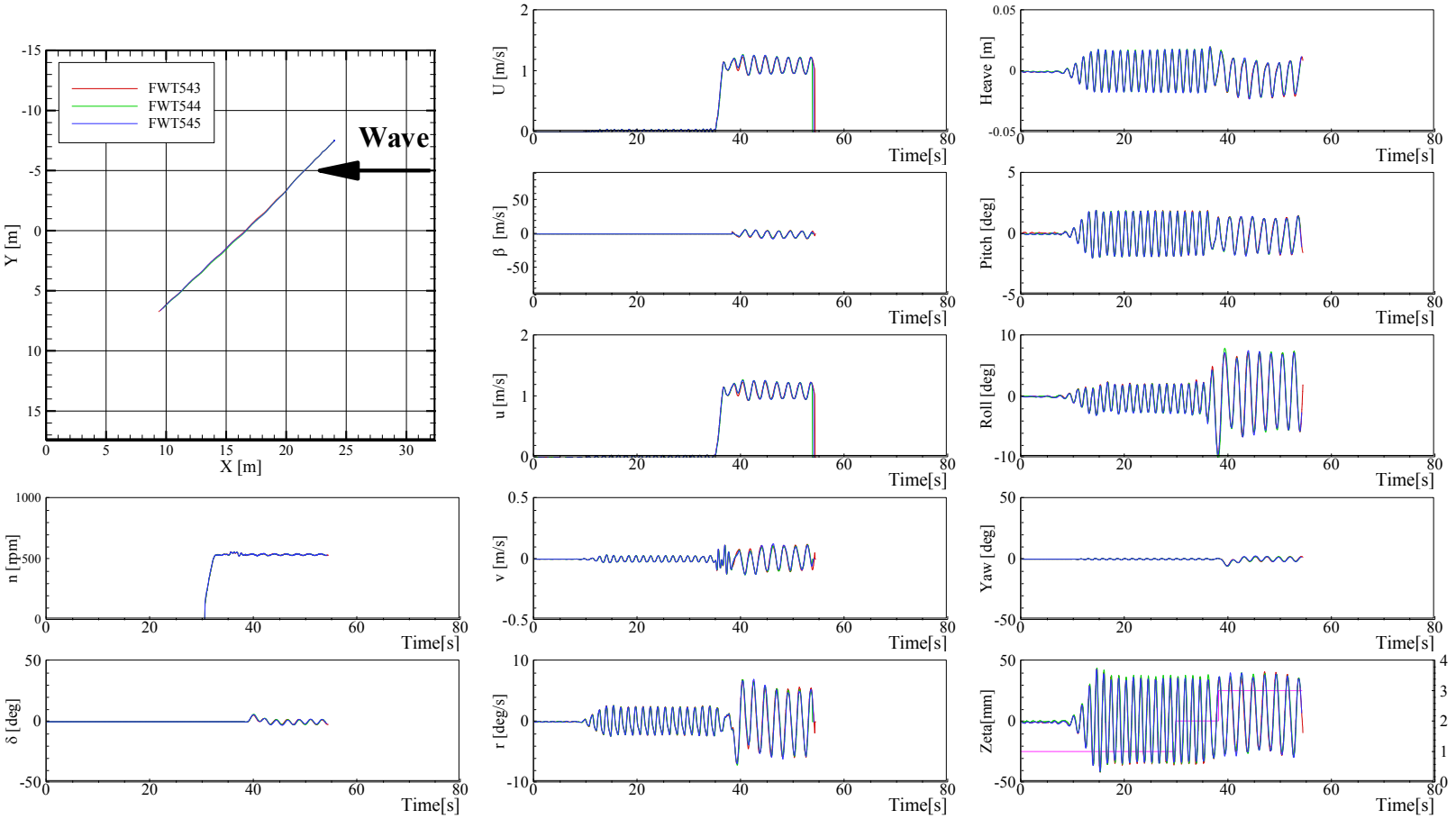

Figure C-3 Trajectories and time histories of course keeping at Fr = 0.2, λ/L = 1.0, H/λ = 0.02, and heading angle = -135°

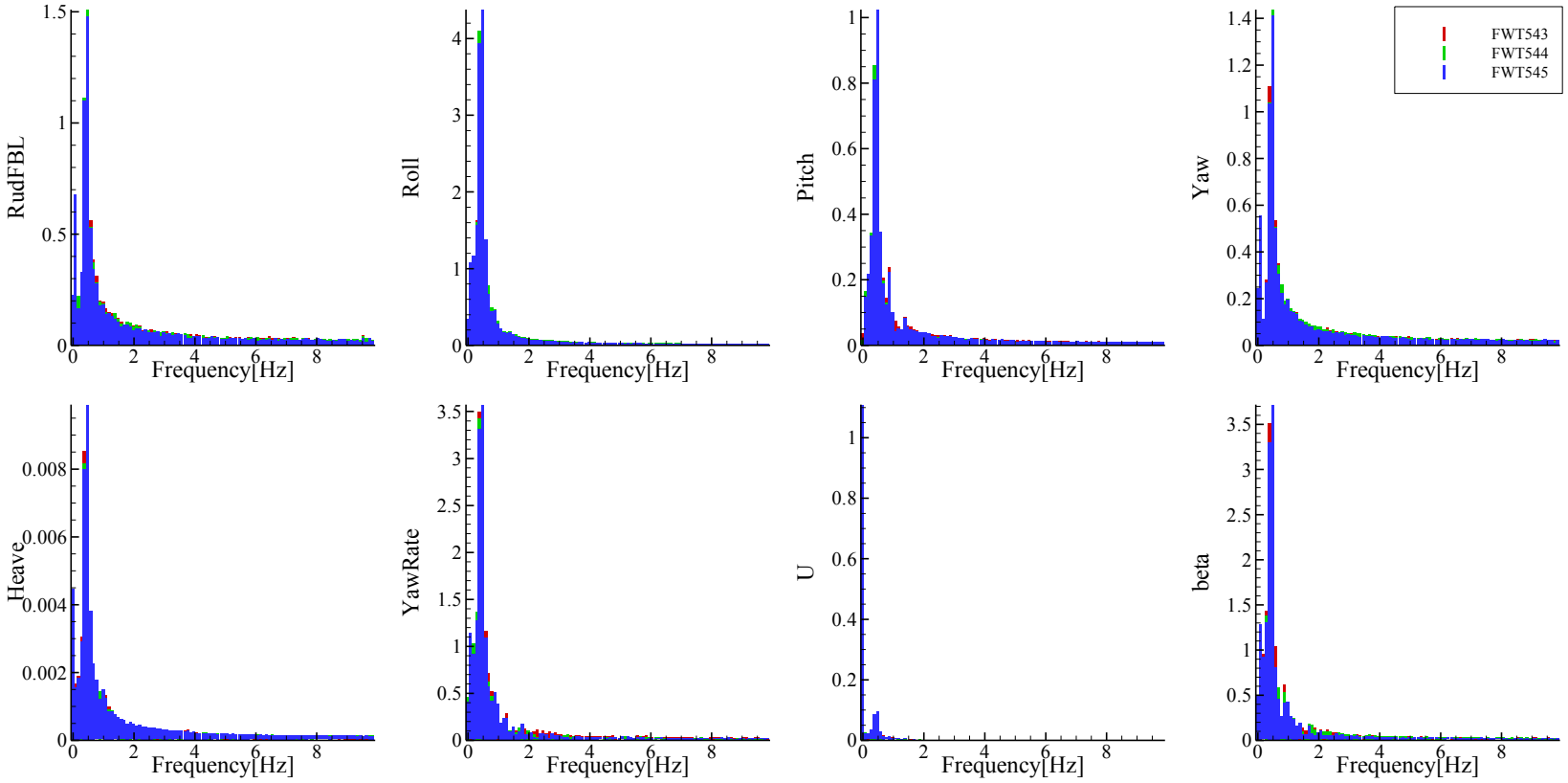

Figure C-4 FFT analysis of time histories of course keeping at Fr = 0.2, λ/L = 1.0, H/λ = 0.02, and heading angle = -135°

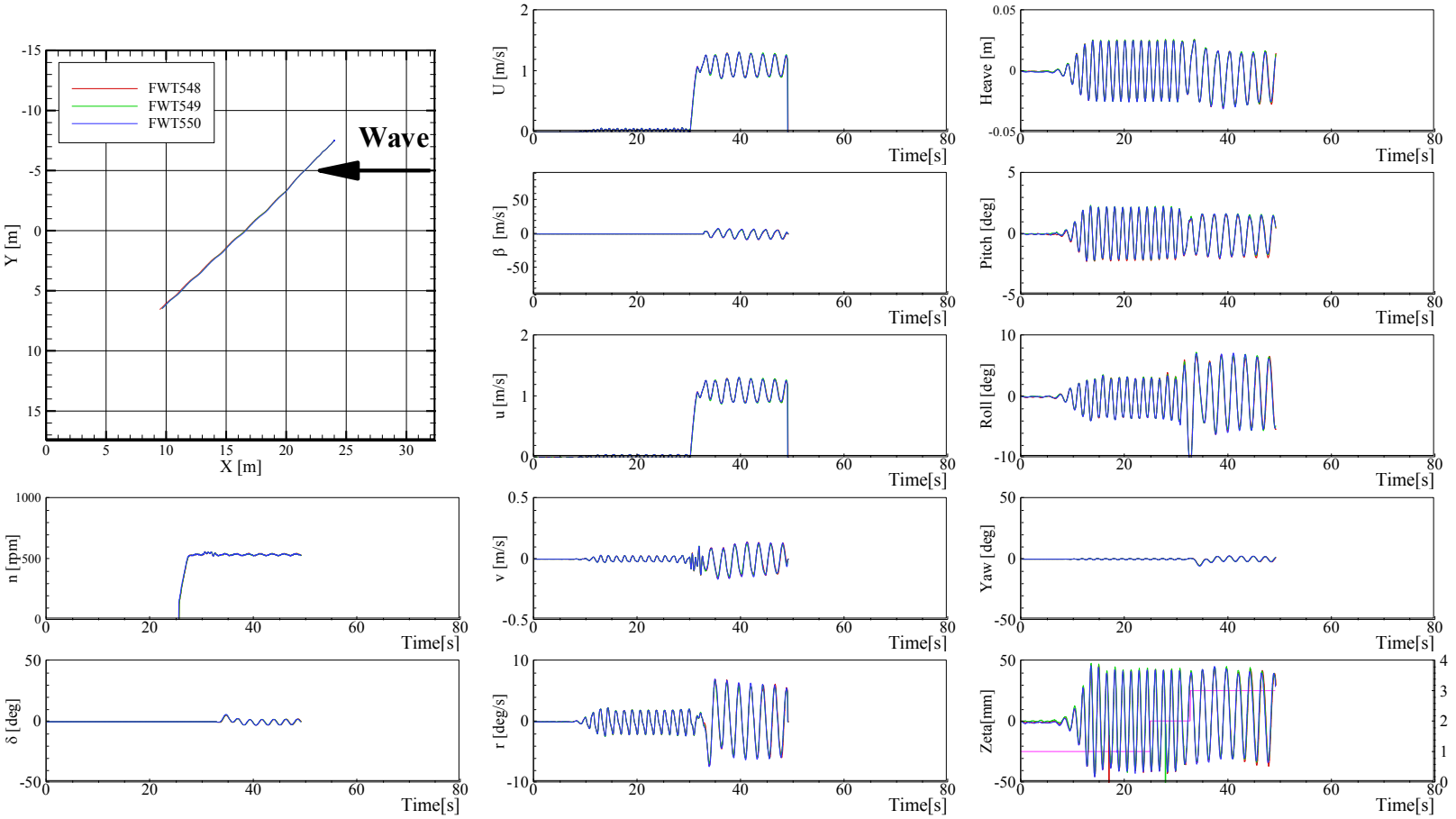

Figure C-5 Trajectories and time histories of course keeping at Fr = 0.2, λ/L = 1.2, H/λ = 0.02, and heading angle = -135°

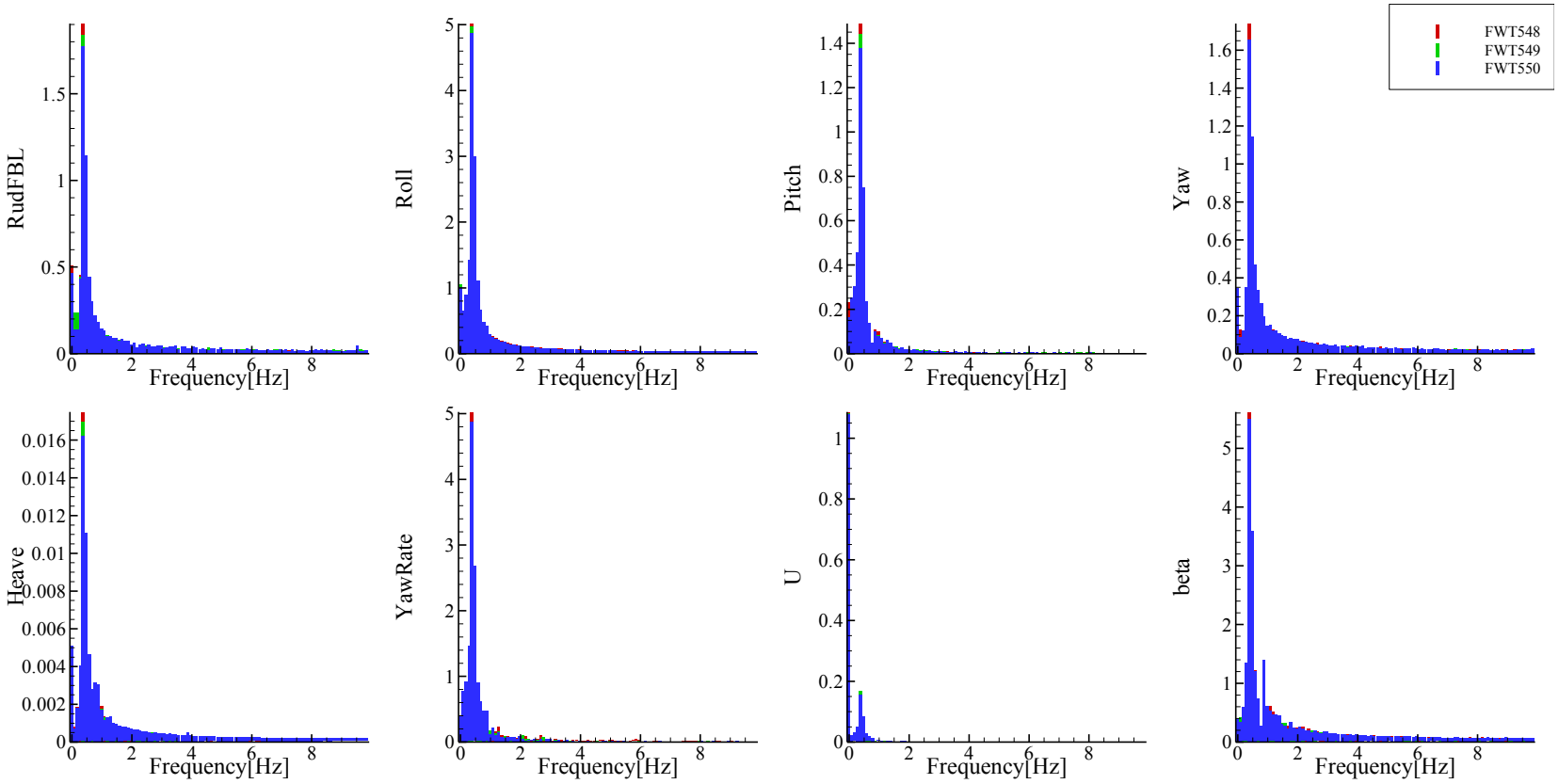

Figure C-6 FFT analysis of time histories of course keeping at Fr = 0.2, λ/L = 1.2, H/λ = 0.02, and heading angle = -135°

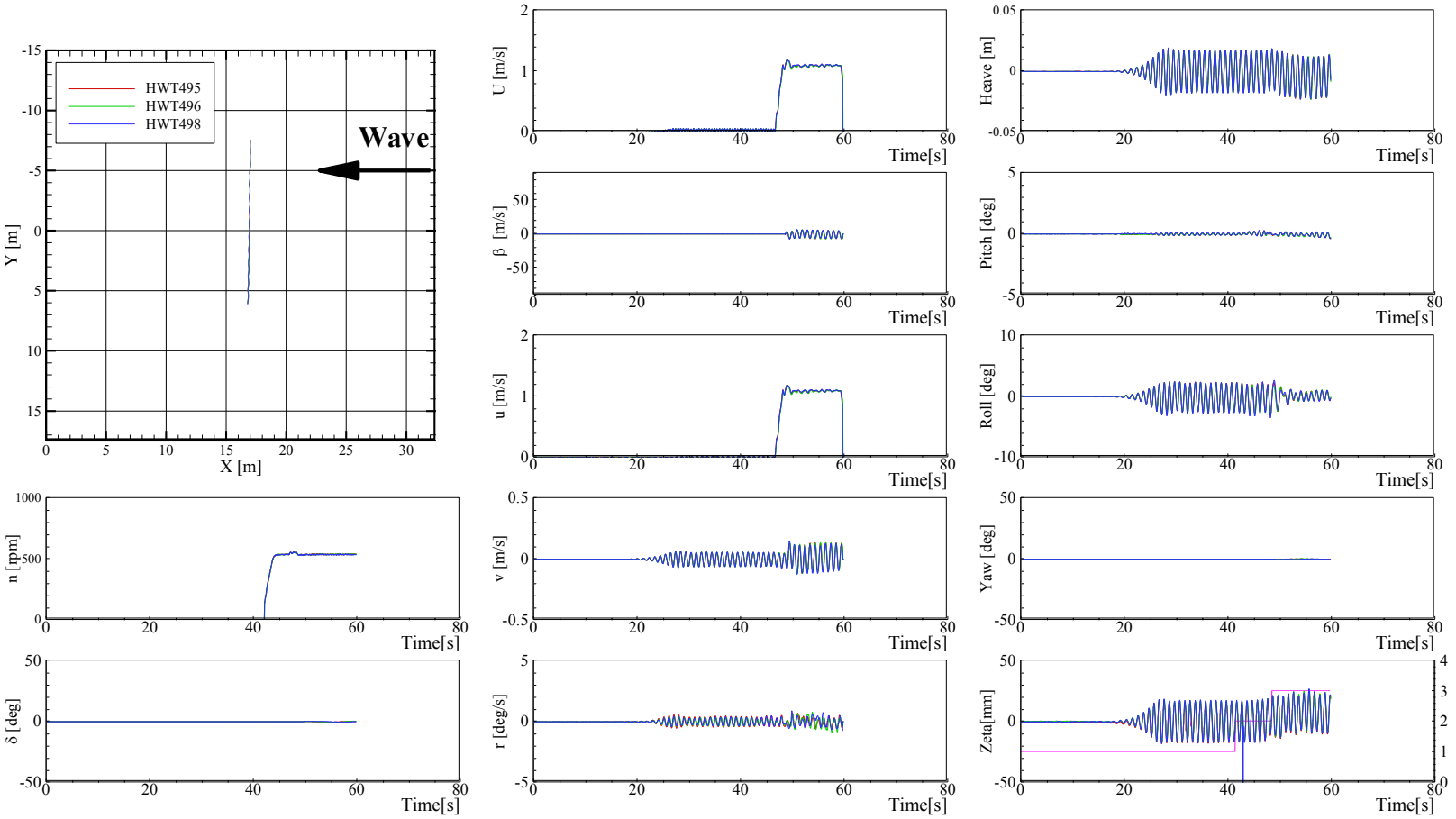

Figure C-7 Trajectories and time histories of course keeping at Fr = 0.2, λ/L = 0.5, H/λ = 0.02, and heading angle = -90°

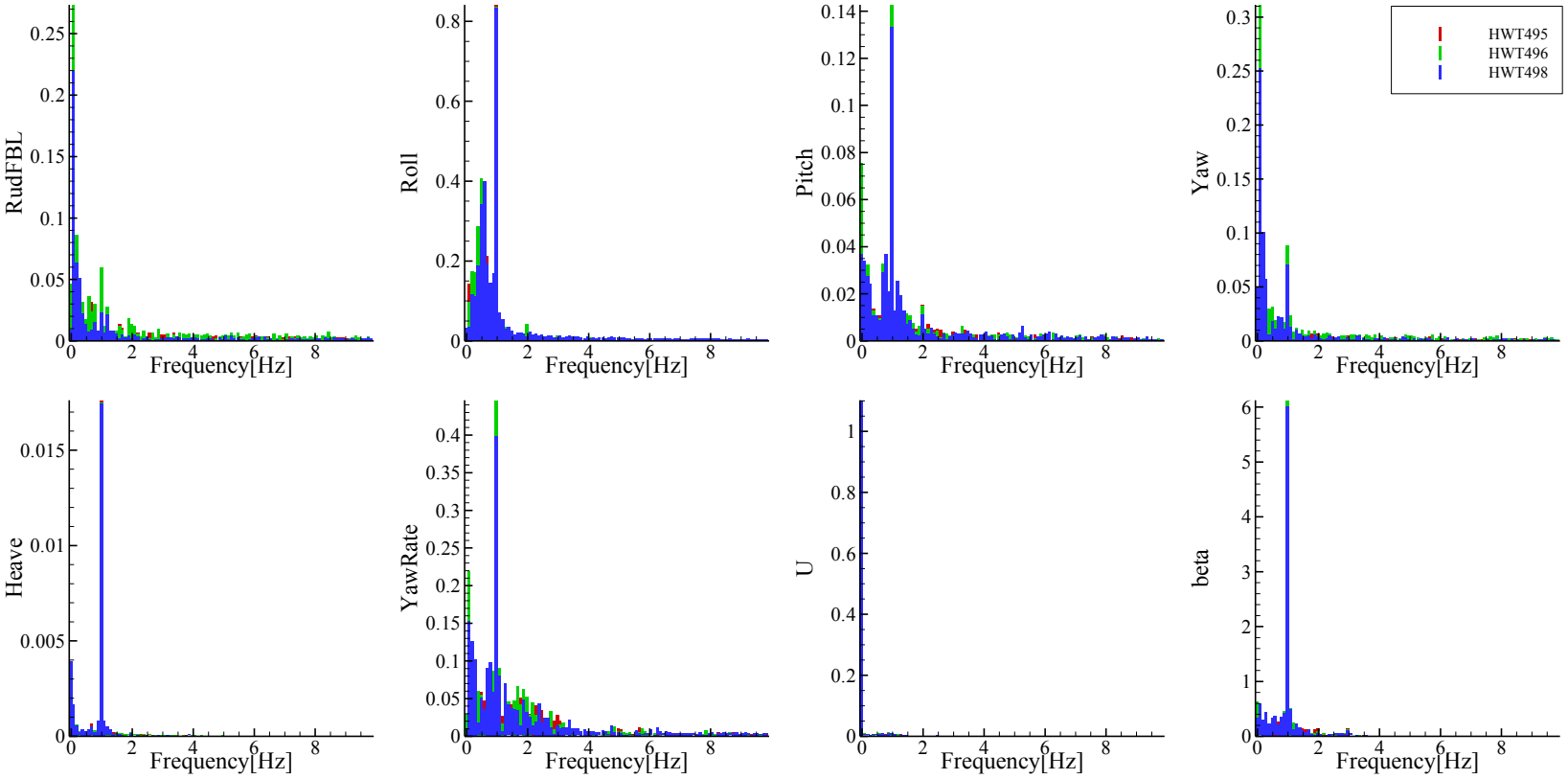

Figure C-8 FFT analysis of time histories of course keeping at Fr = 0.2, λ/L = 0.5, H/λ = 0.02, and heading angle = -90°

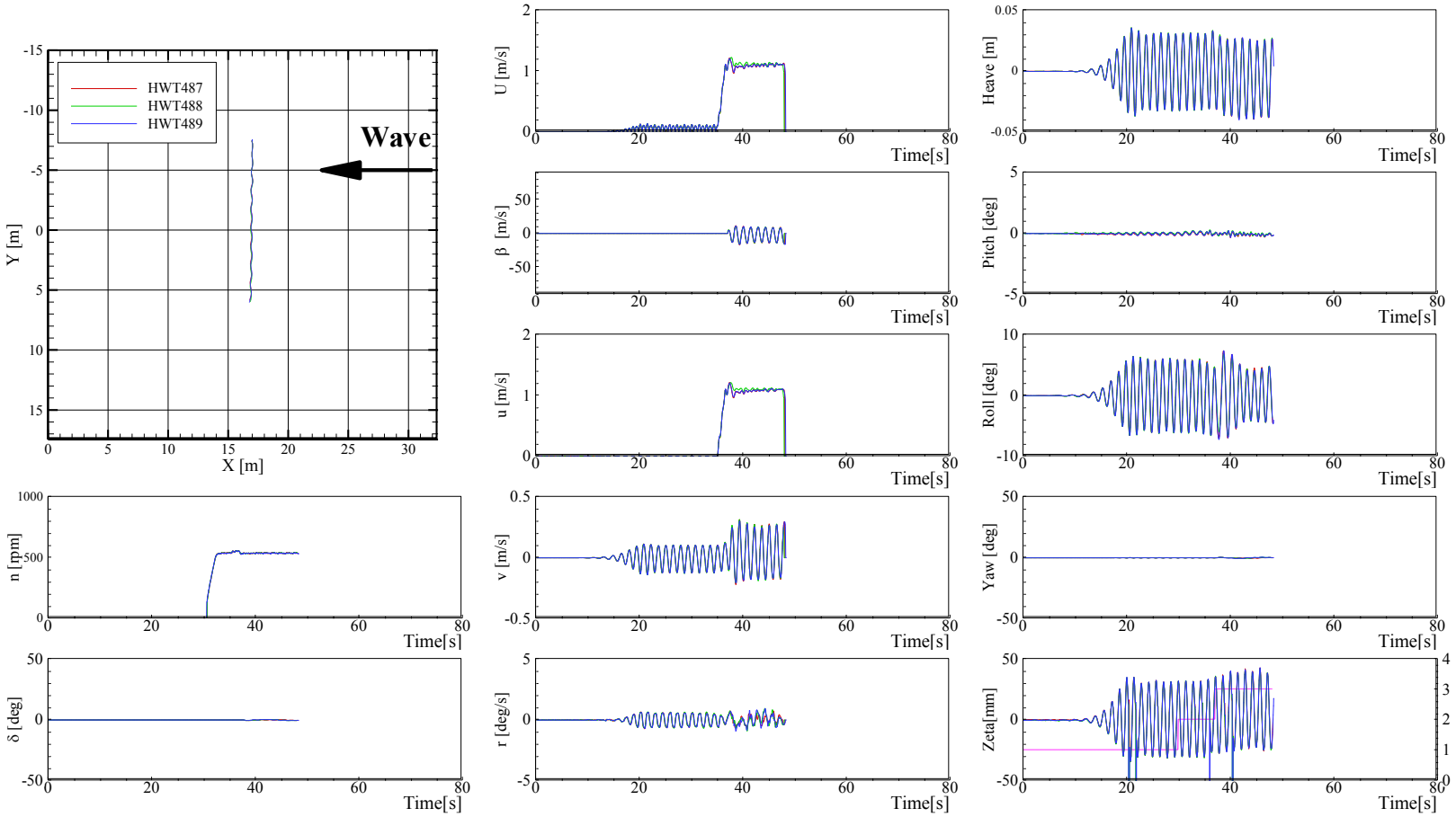

Figure C-9 Trajectories and time histories of course keeping at Fr = 0.2, λ/L = 1.0, H/λ = 0.02, and heading angle = -90°

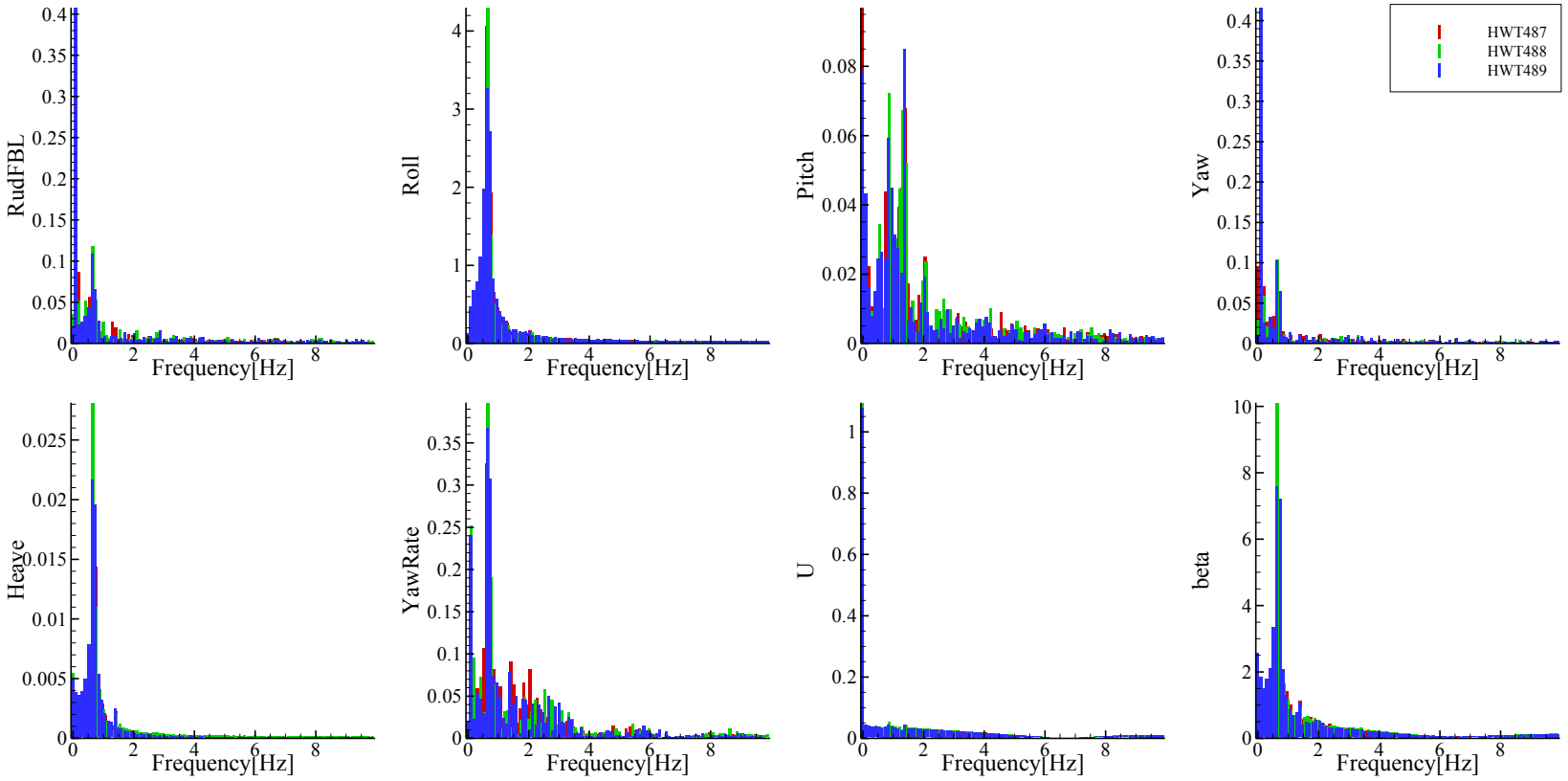

Figure C-10 FFT analysis of time histories of course keeping at Fr = 0.2, λ/L = 1.0, H/λ = 0.02, and heading angle = -90°

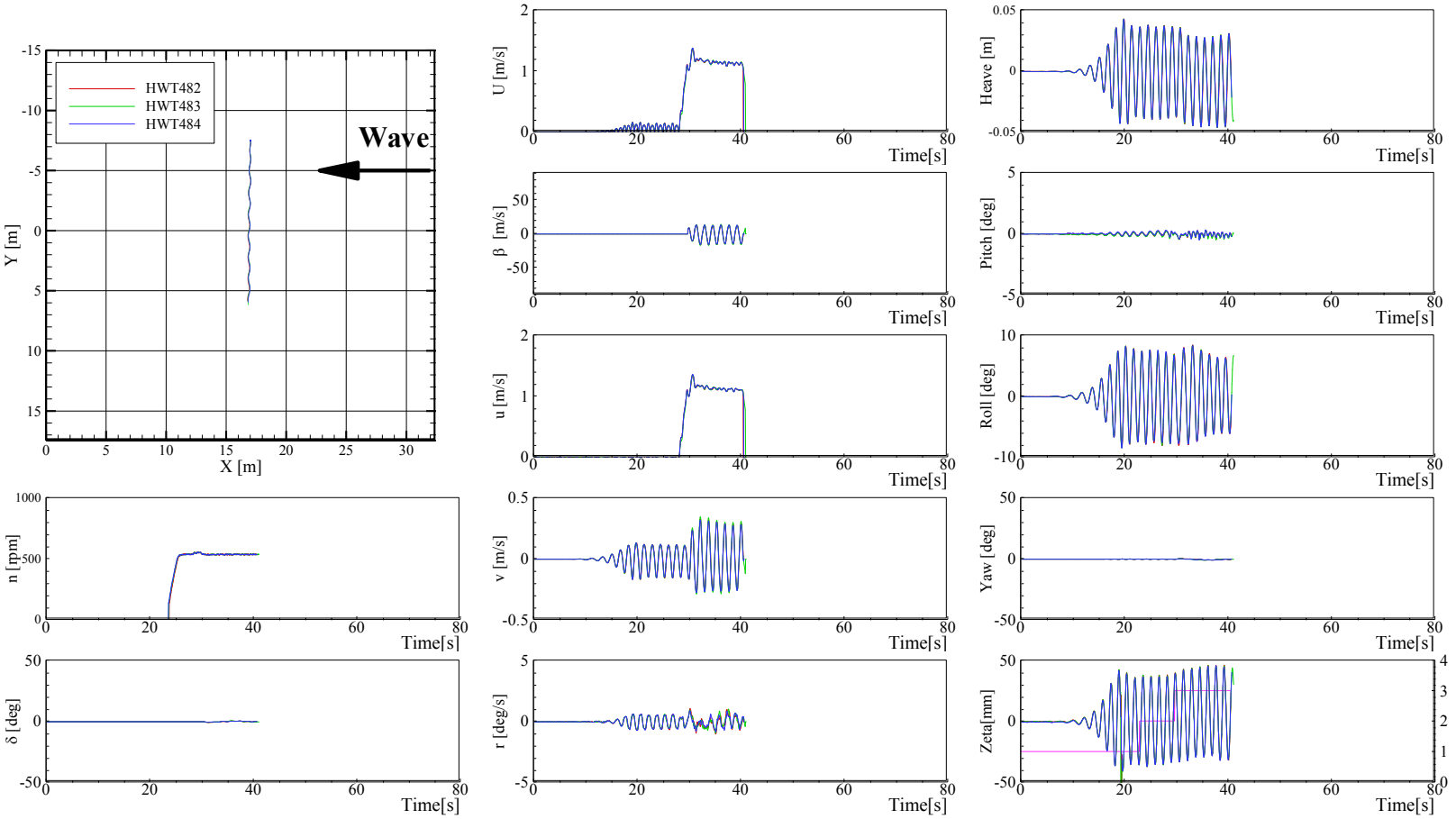

Figure C-11 Trajectories and time histories of course keeping at Fr = 0.2, λ/L = 1.2, H/λ = 0.02, and heading angle = -90°

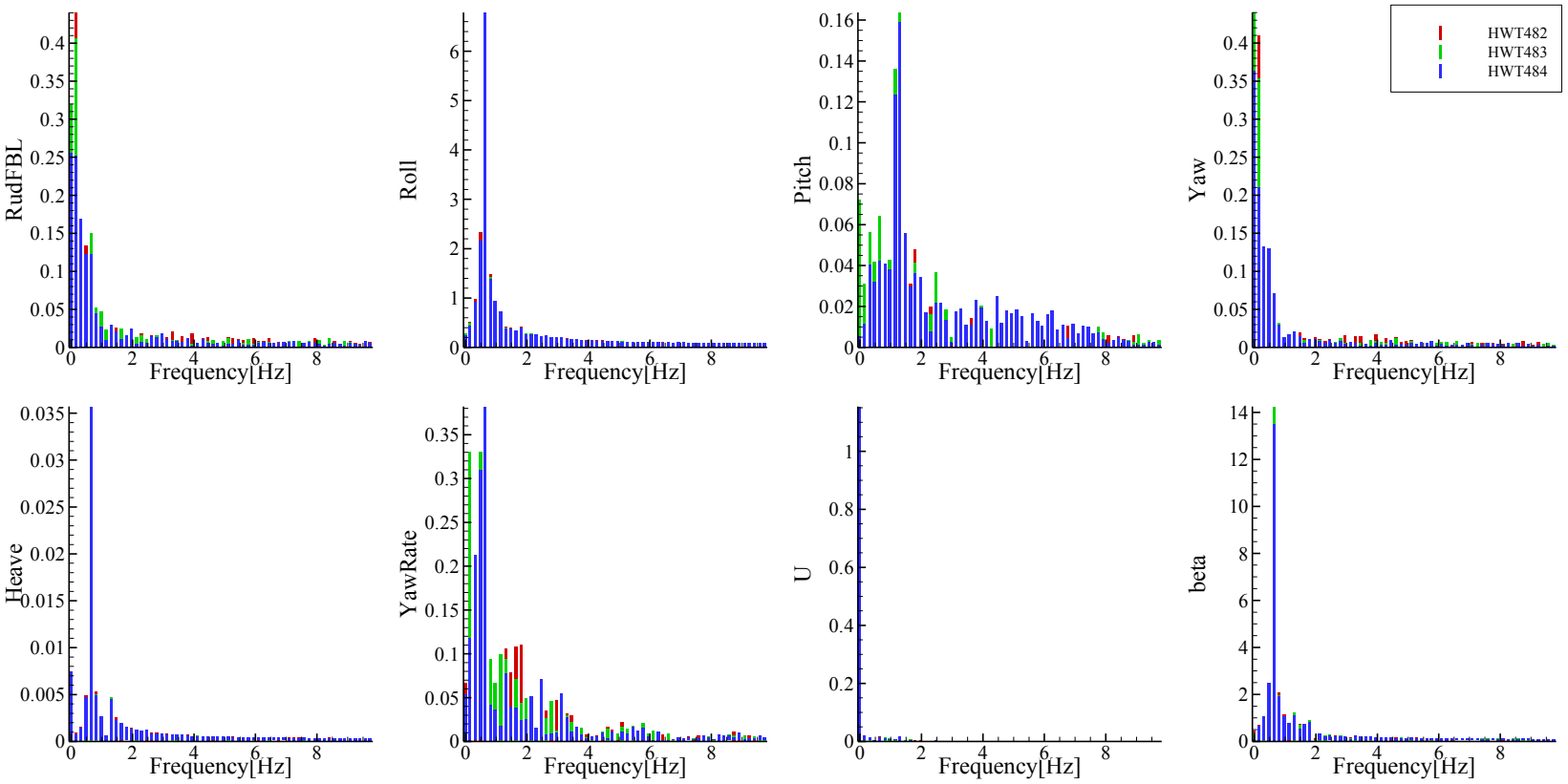

Figure C-12 FFT analysis of time histories of course keeping at Fr = 0.2, λ/L = 1.2, H/λ = 0.02, and heading angle = -90°

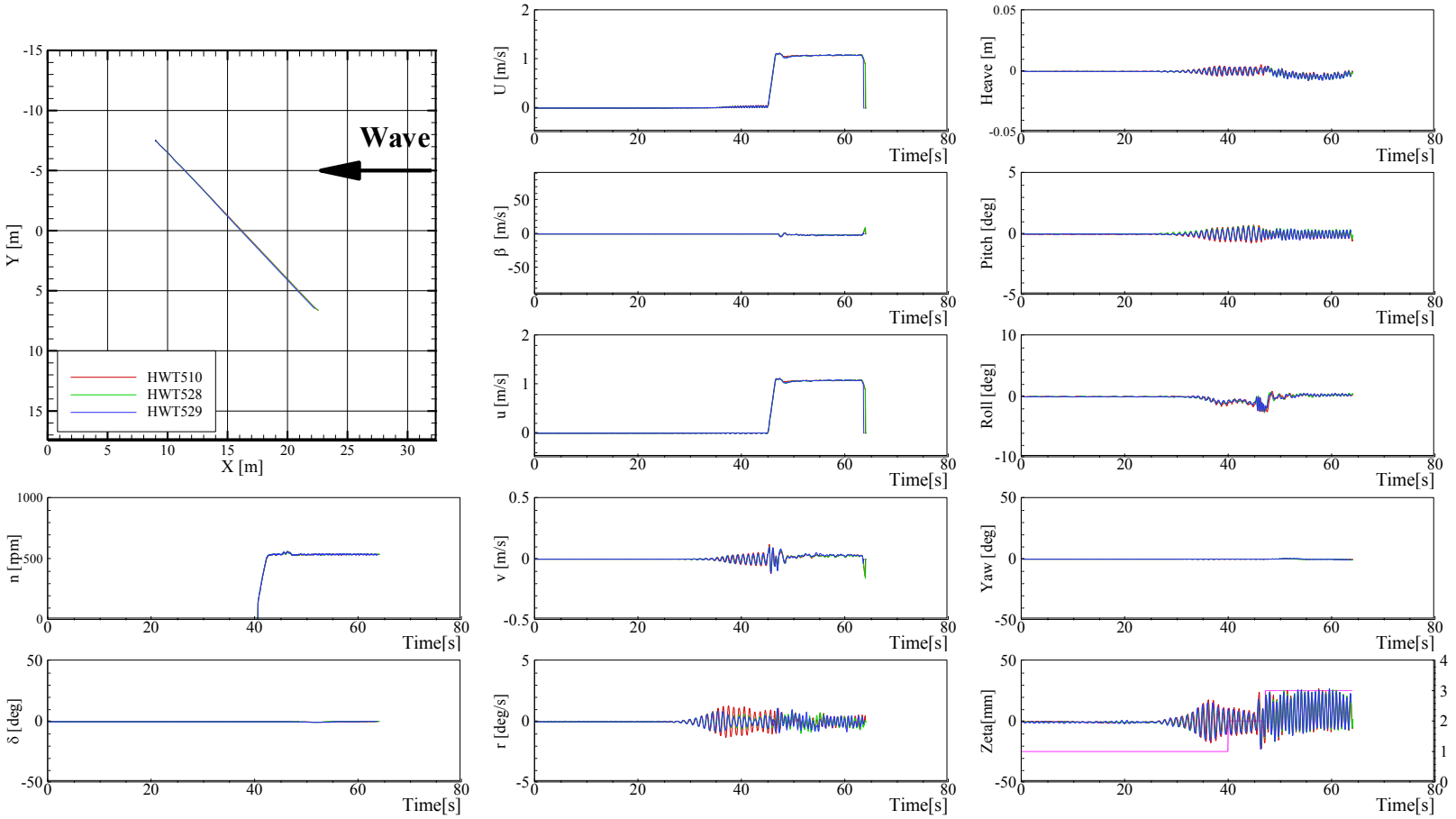

Figure C-13 Trajectories and time histories of course keeping at Fr = 0.2, λ/L = 0.5, H/λ = 0.02, and heading angle = -45°

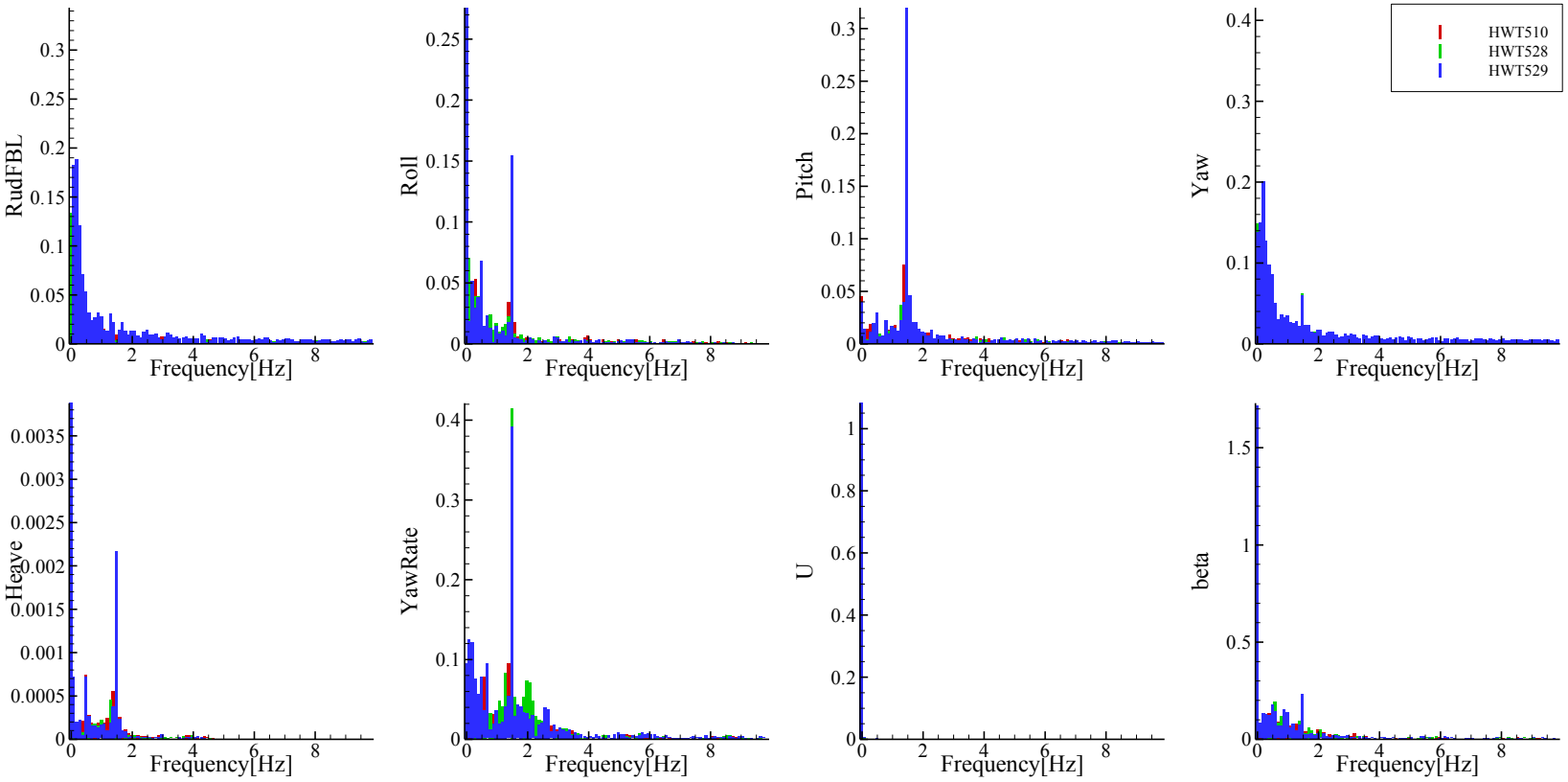

Figure C-14 FFT analysis of time histories of course keeping at Fr = 0.2, λ/L = 0.5, H/λ = 0.02, and heading angle = -45°

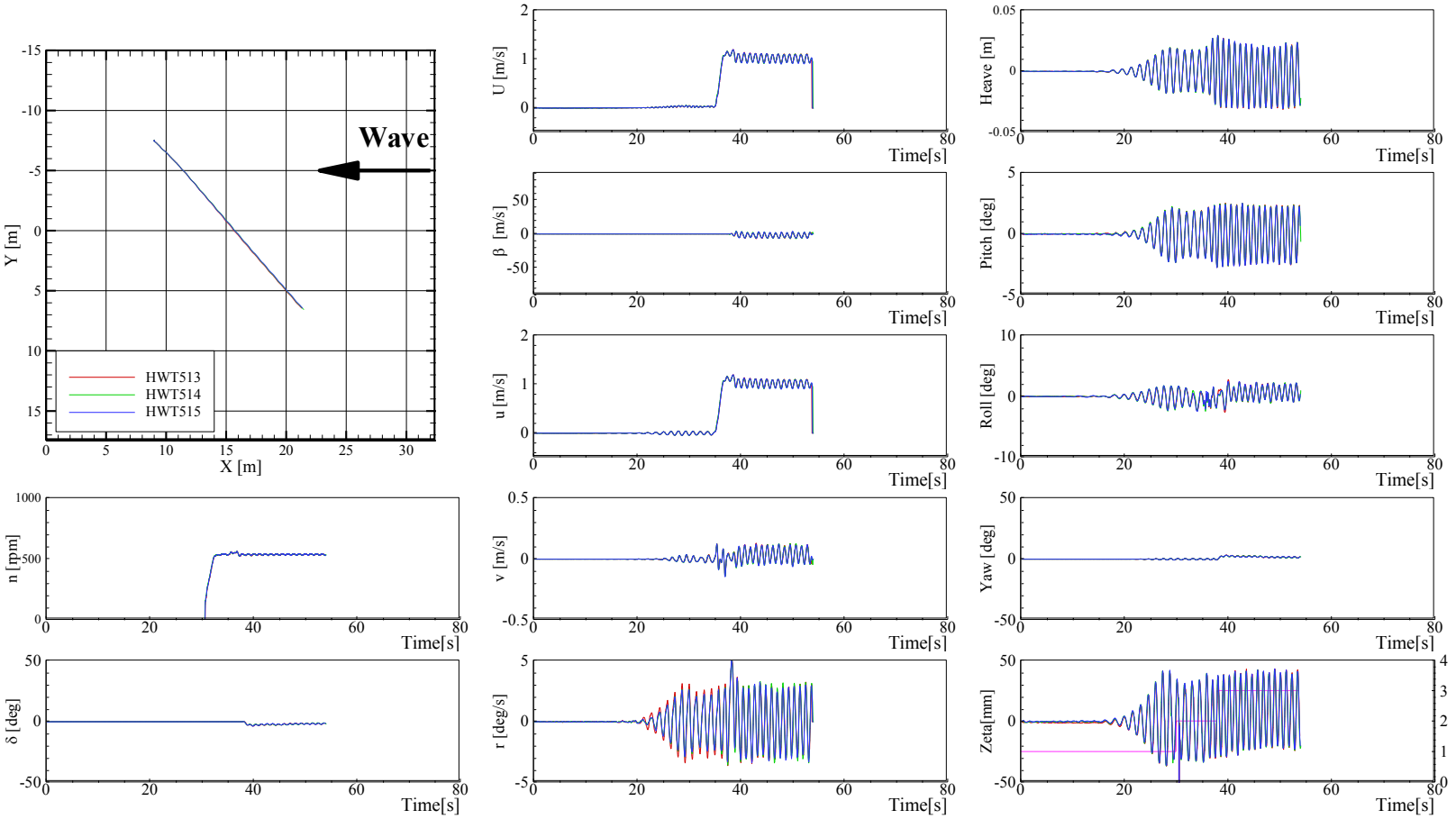

Figure C-15 Trajectories and time histories of course keeping at Fr = 0.2, λ/L = 1.0, H/λ = 0.02, and heading angle = -45°

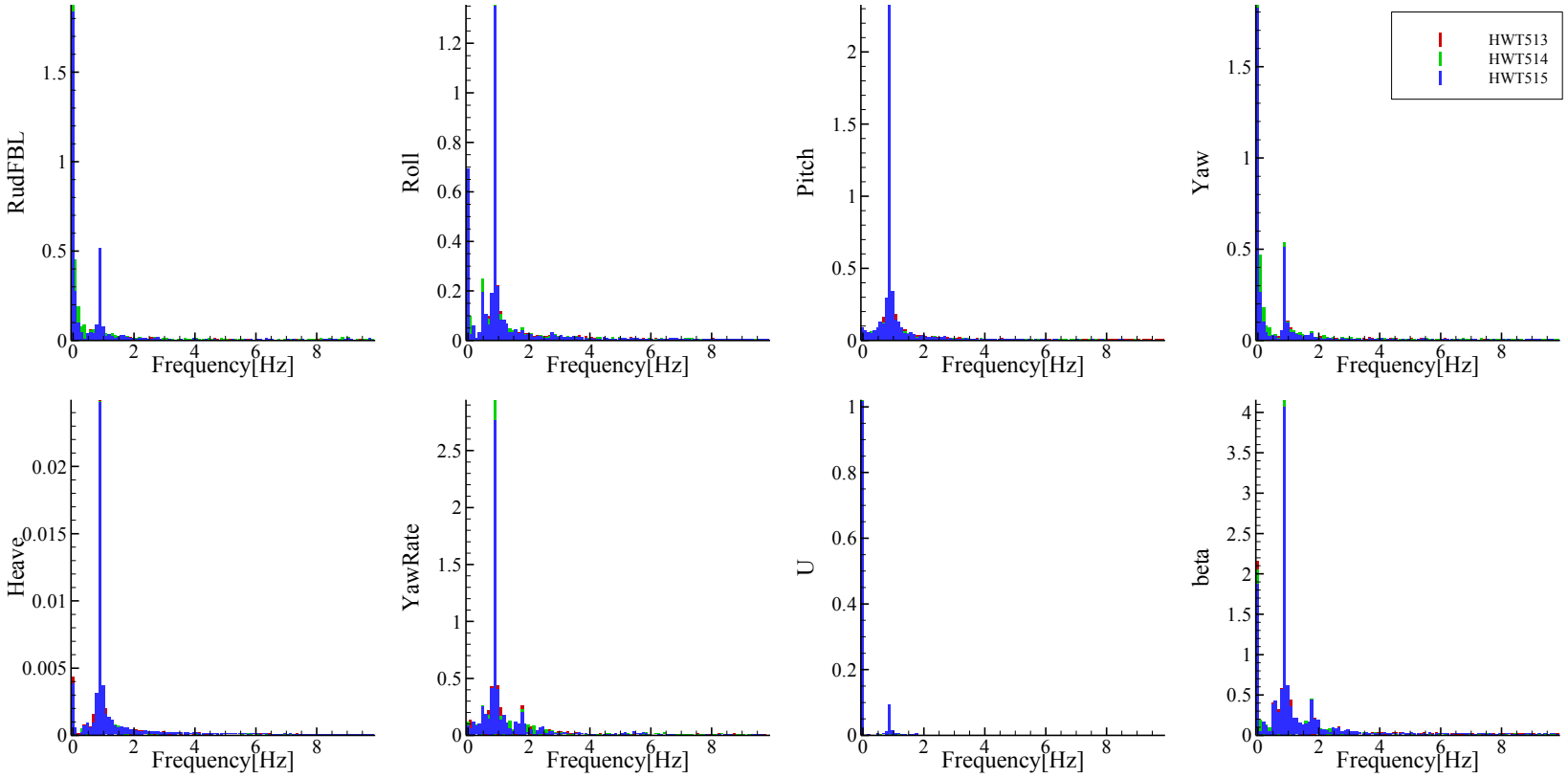

Figure C-16 FFT analysis of time histories of course keeping at Fr = 0.2, λ/L = 1.0, H/λ = 0.02, and heading angle = -45°

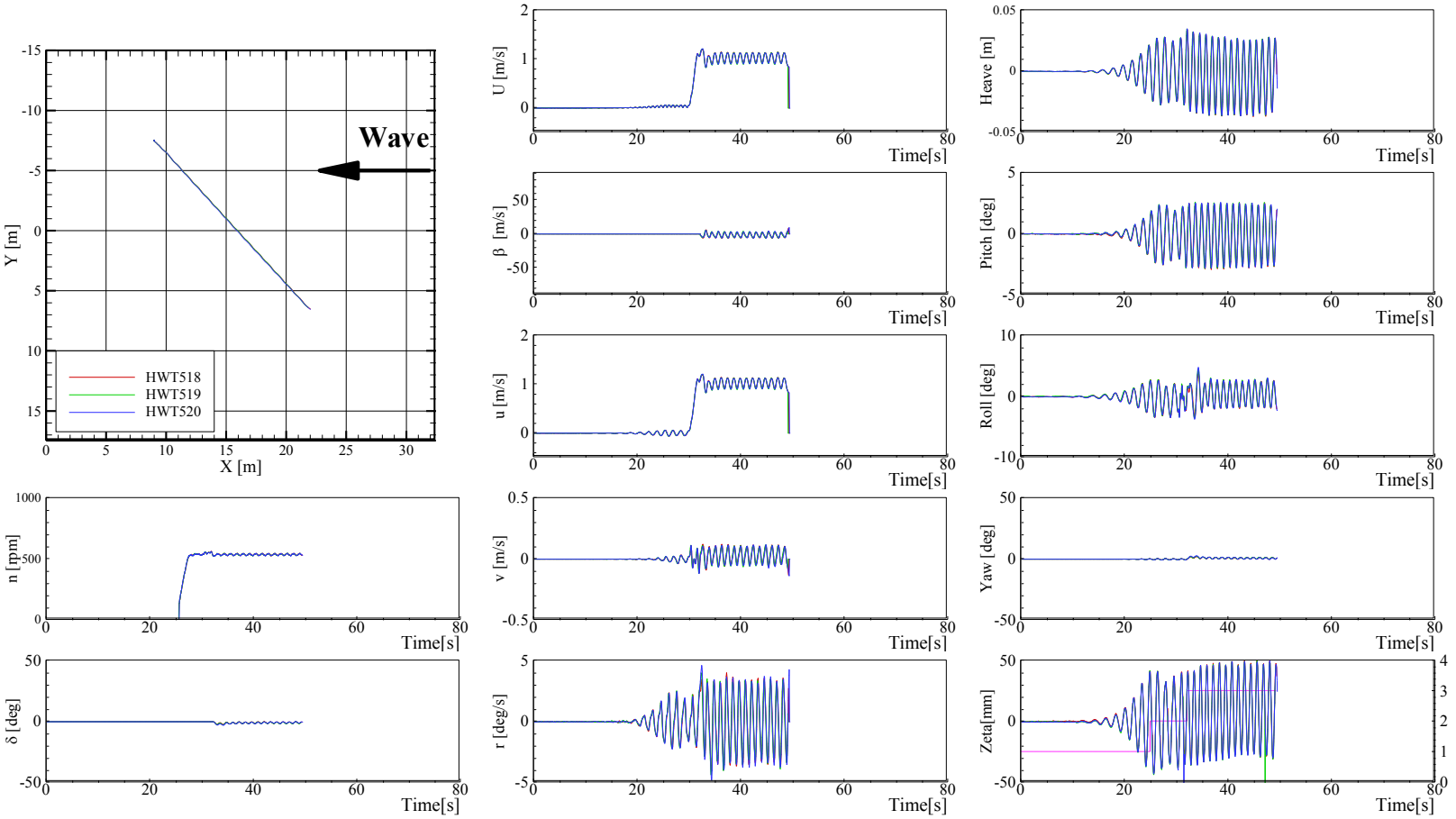

Figure C-17 Trajectories and time histories of course keeping at Fr = 0.2, λ/L = 1.2, H/λ = 0.02, and heading angle = -45°

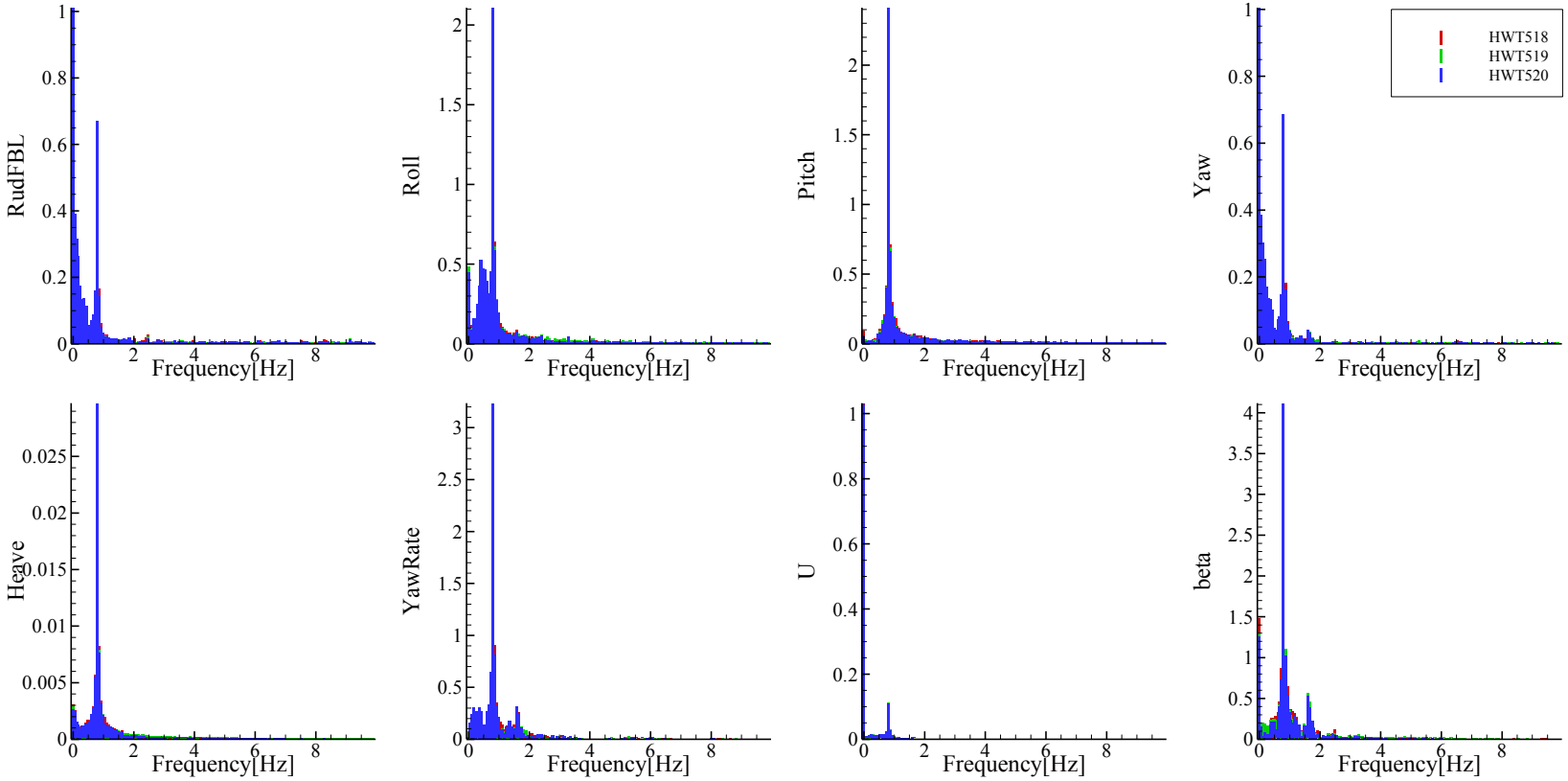

Figure C-18 FFT analysis of time histories of course keeping at Fr = 0.2, λ/L = 1.2, H/λ = 0.02, and heading angle = -45°

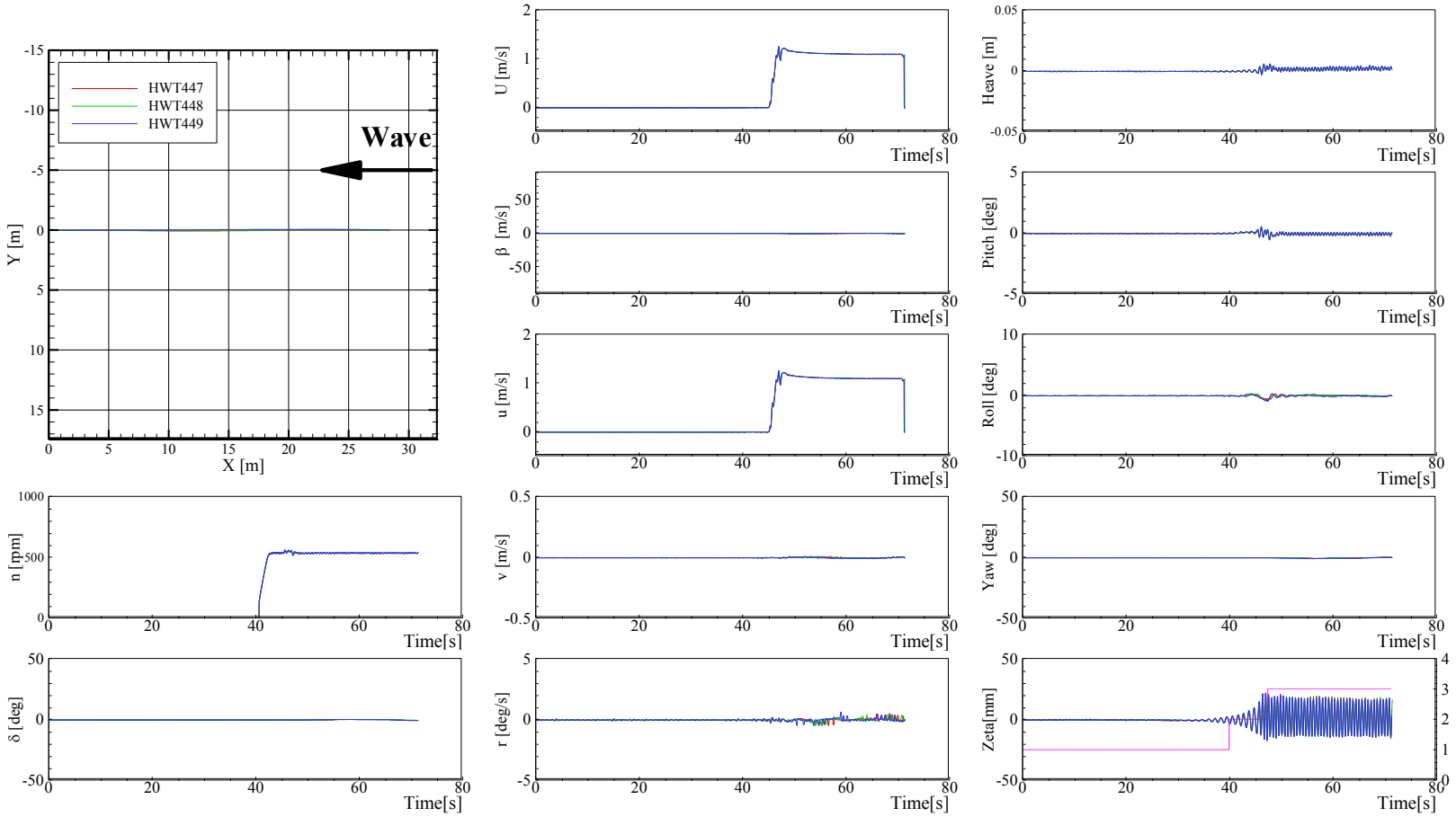

Figure C-19 Trajectories and time histories of course keeping at Fr = 0.2, λ/L = 0.5, H/λ = 0.02, and heading angle = 0°

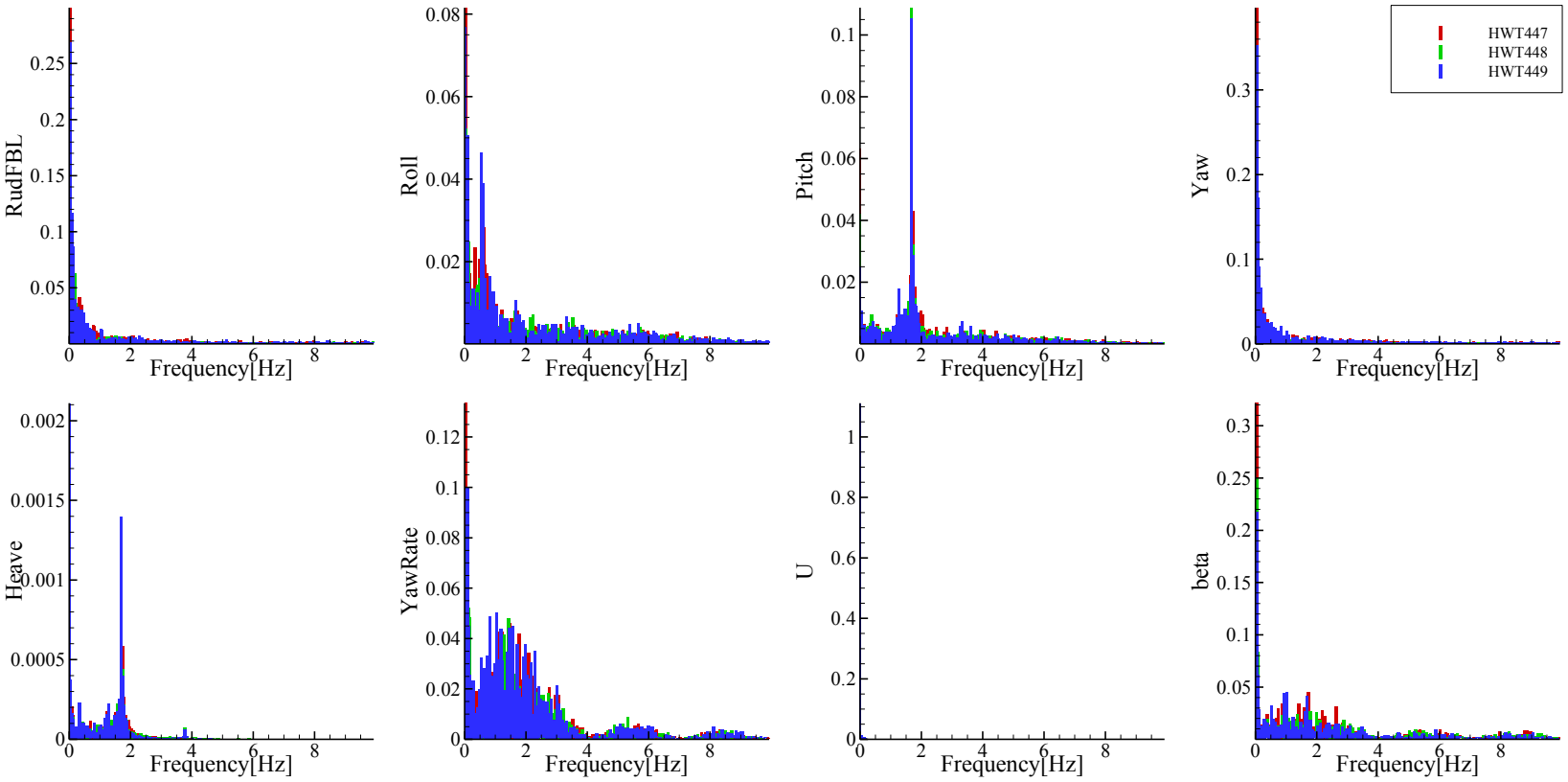

Figure C- 20 FFT analysis of time histories of course keeping at Fr = 0.2, λ/L = 0.5, H/λ = 0.02, and heading angle = 0°

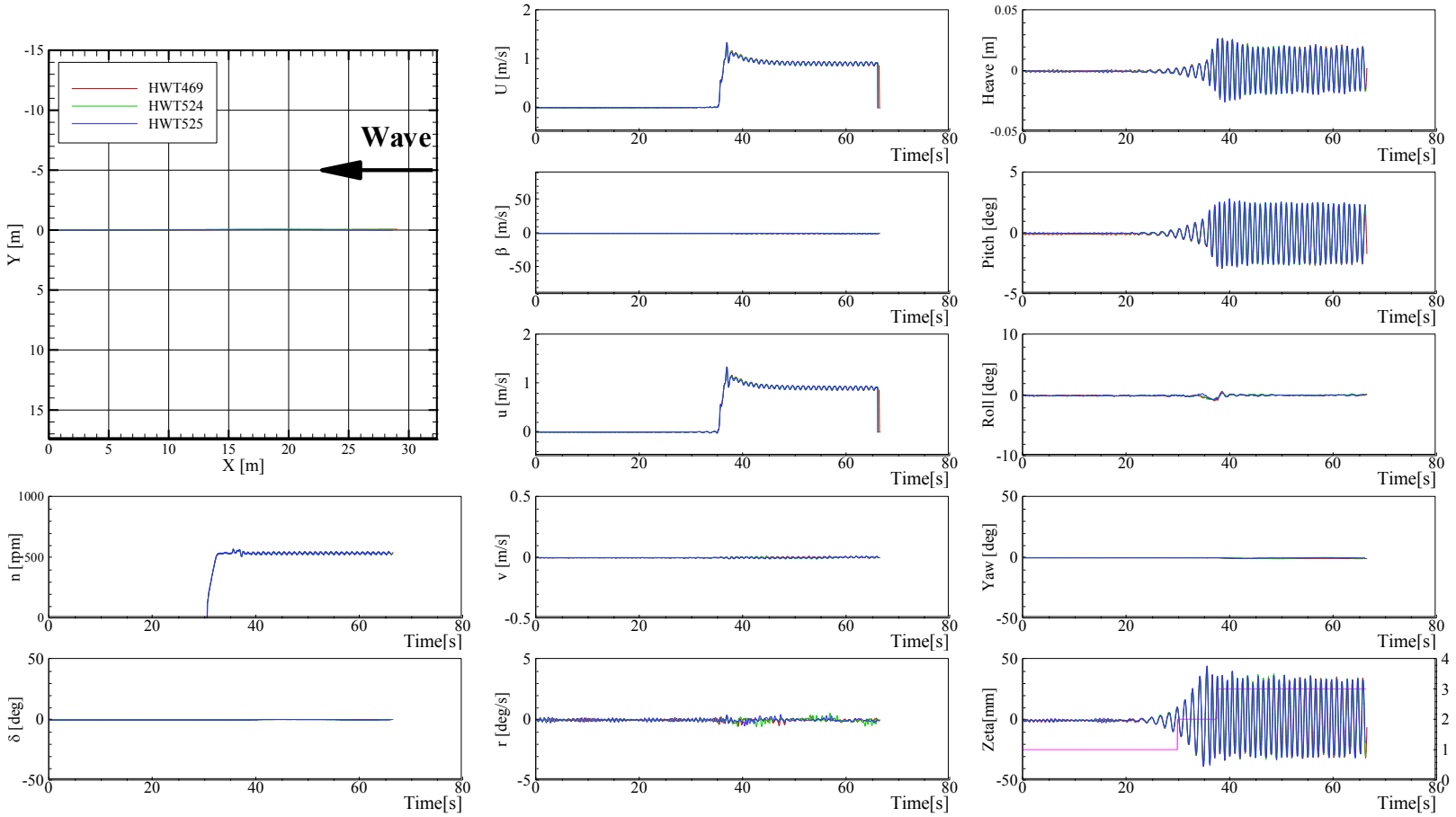

Figure C-21 Trajectories and time histories of course keeping at Fr = 0.2, λ/L = 1.0, H/λ = 0.02, and heading angle = 0°

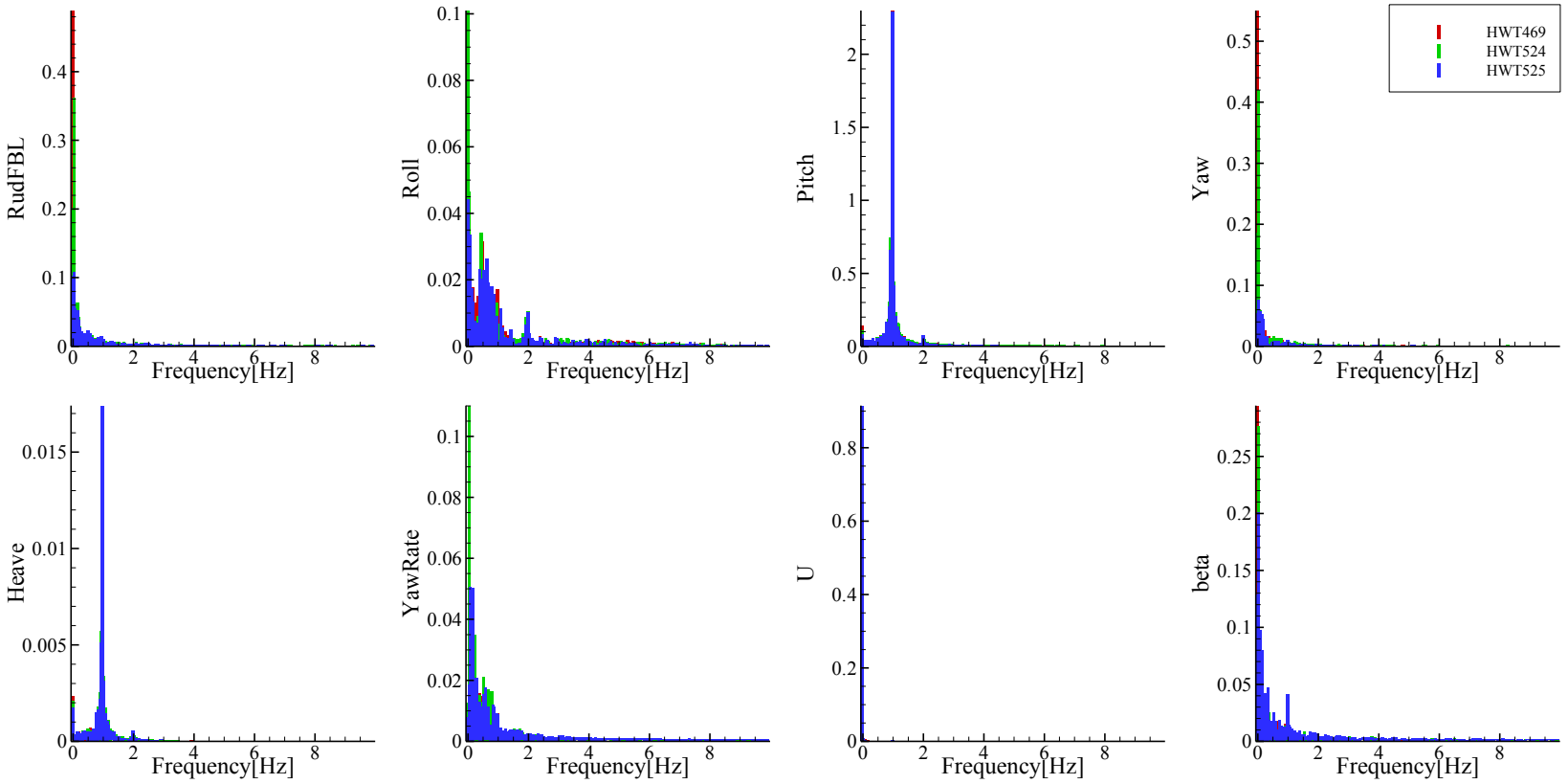

Figure C-22 FFT analysis of time histories of course keeping at Fr = 0.2, λ/L = 1.0, H/λ = 0.02, and heading angle = 0°

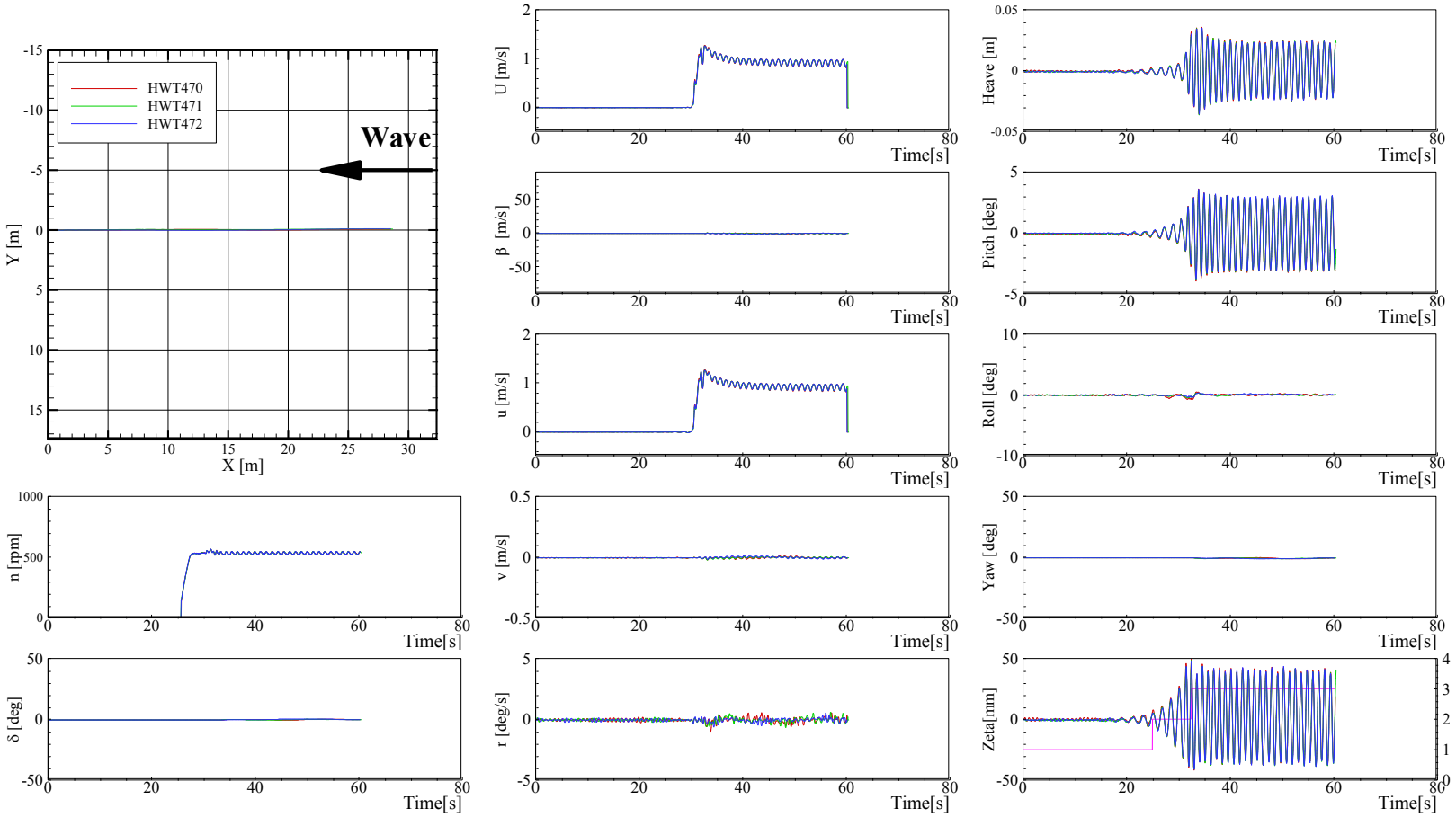

Figure C-23 Trajectories and time histories of course keeping at Fr = 0.2, λ/L = 1.2, H/λ = 0.02, and heading angle = 0°

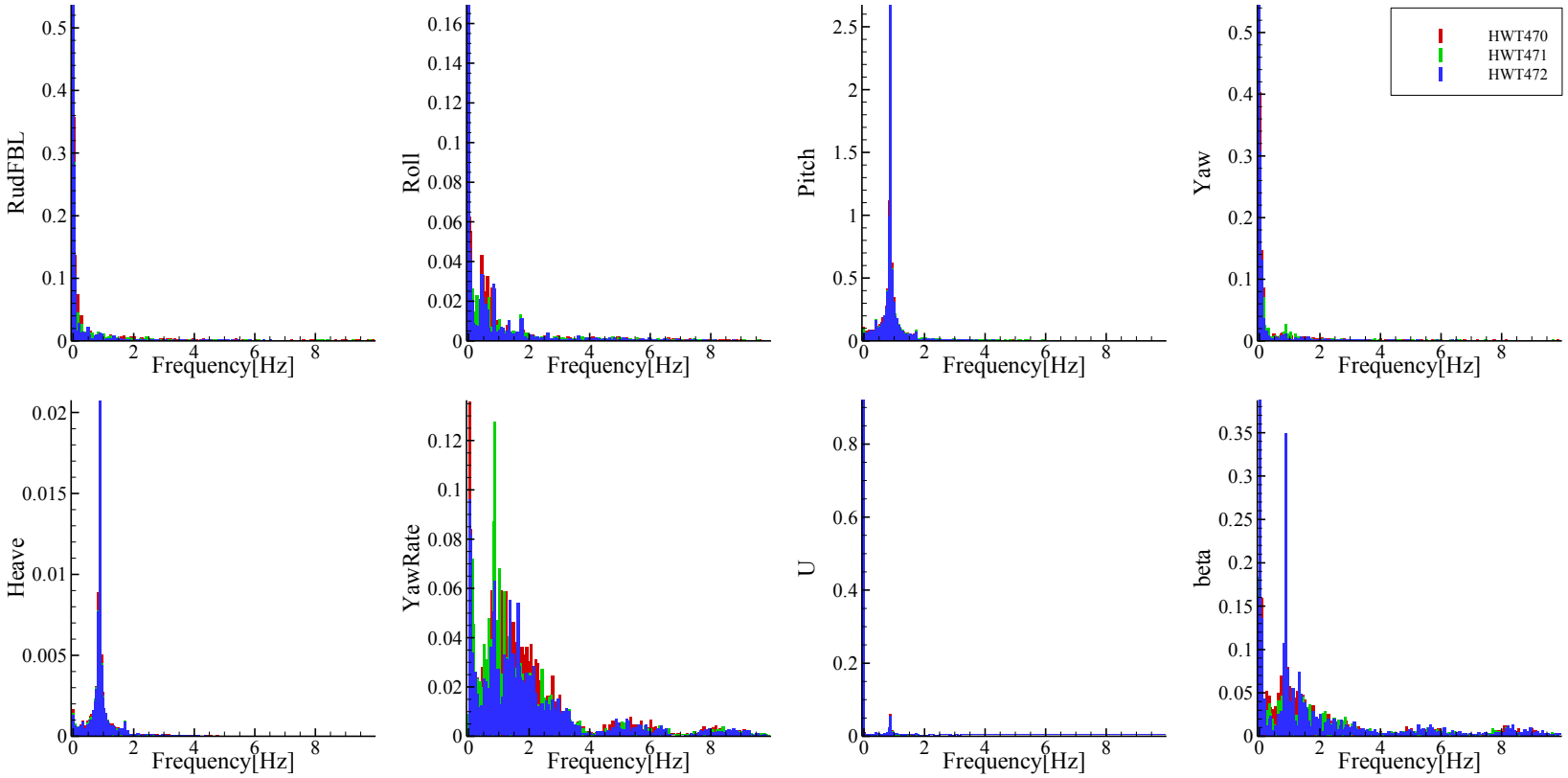

Figure C-24 FFT analysis of time histories of course keeping at Fr = 0.2, λ/L = 1.2, H/λ = 0.02, and heading angle = 0°

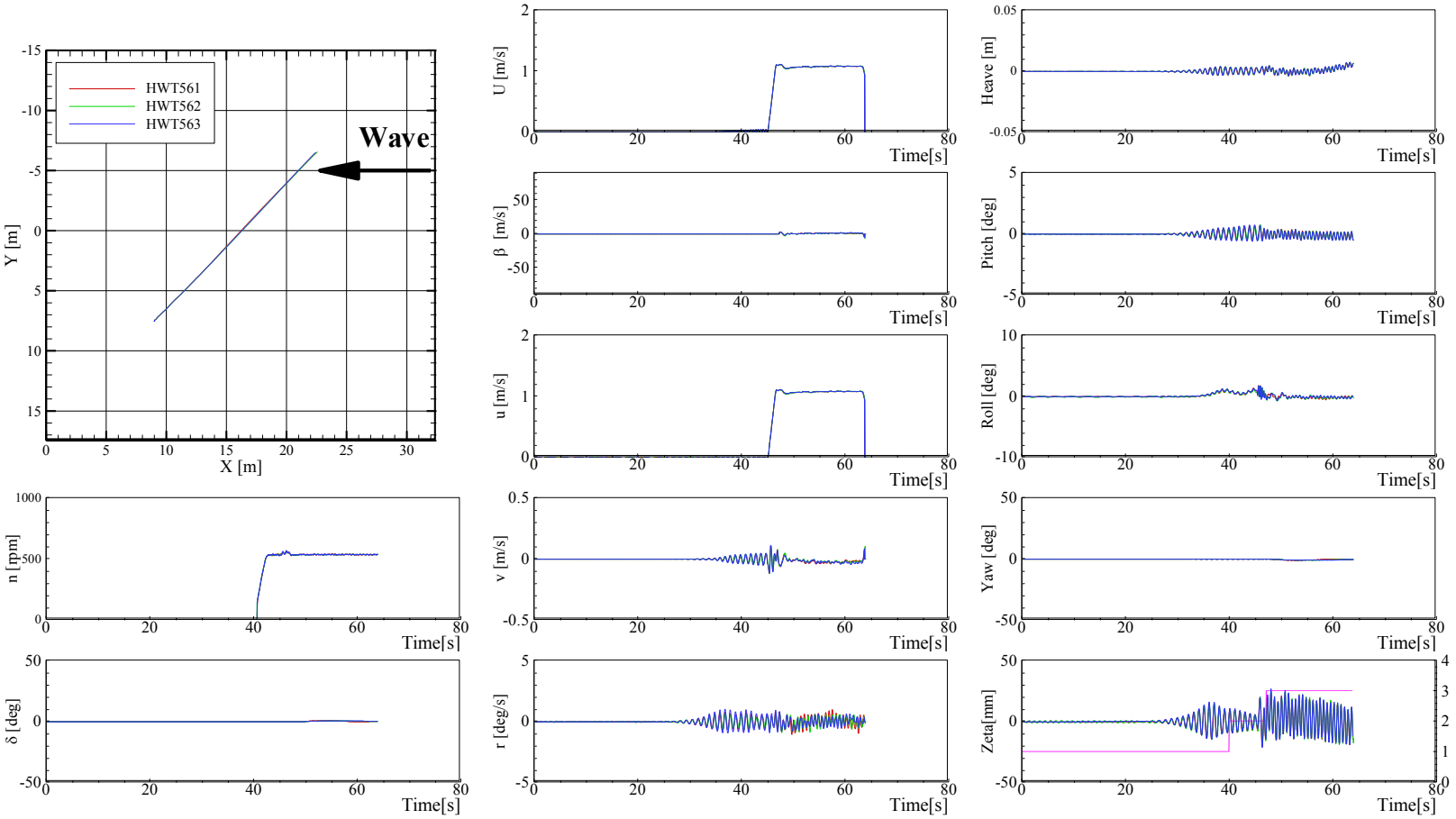

Figure C-25 Trajectories and time histories of course keeping at Fr = 0.2, λ/L = 0.5, H/λ = 0.02, and heading angle = 45°

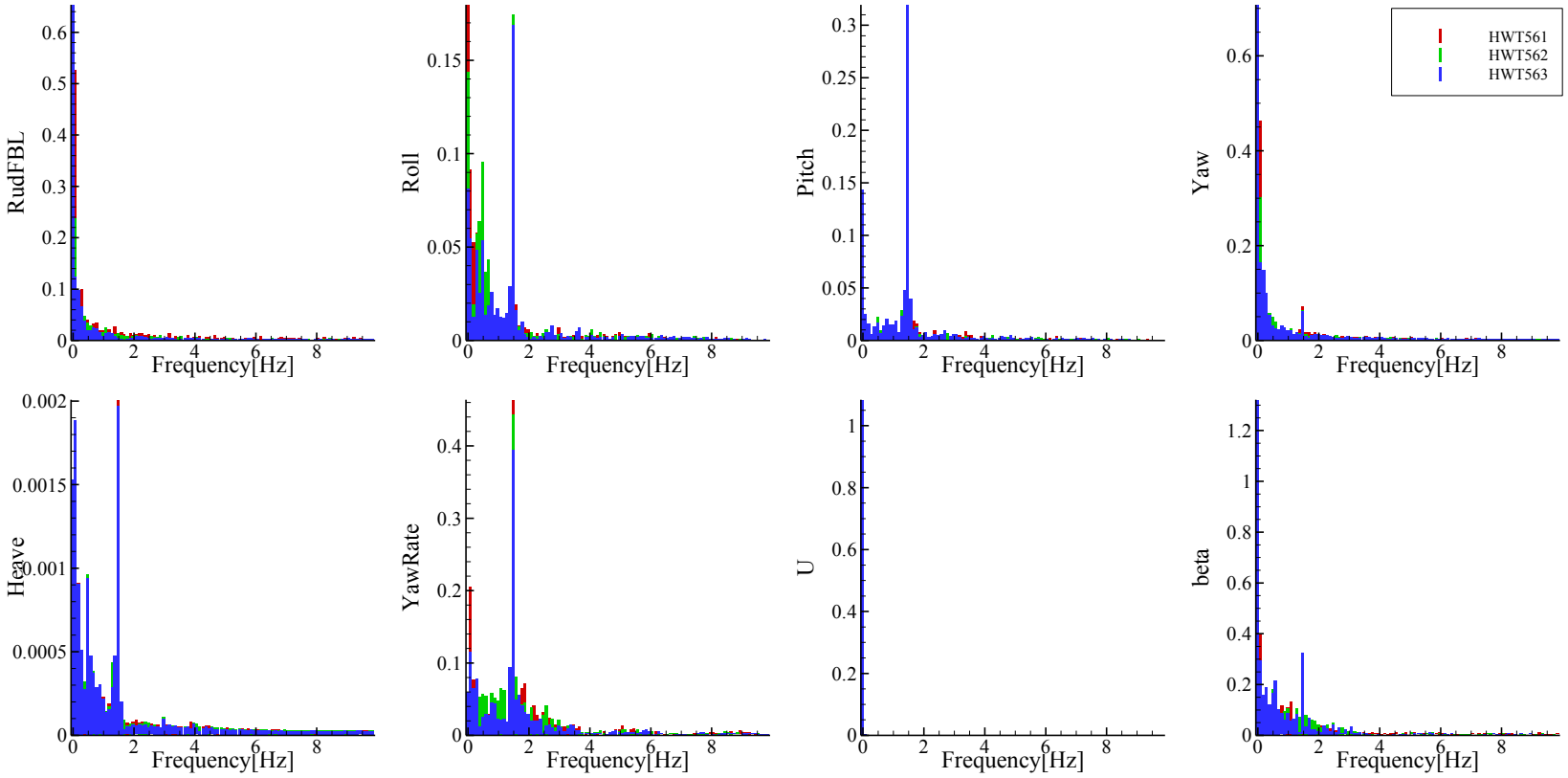

Figure C-26 FFT analysis of time histories of course keeping at Fr = 0.2, λ/L = 0.5, H/λ = 0.02, and heading angle = 45°

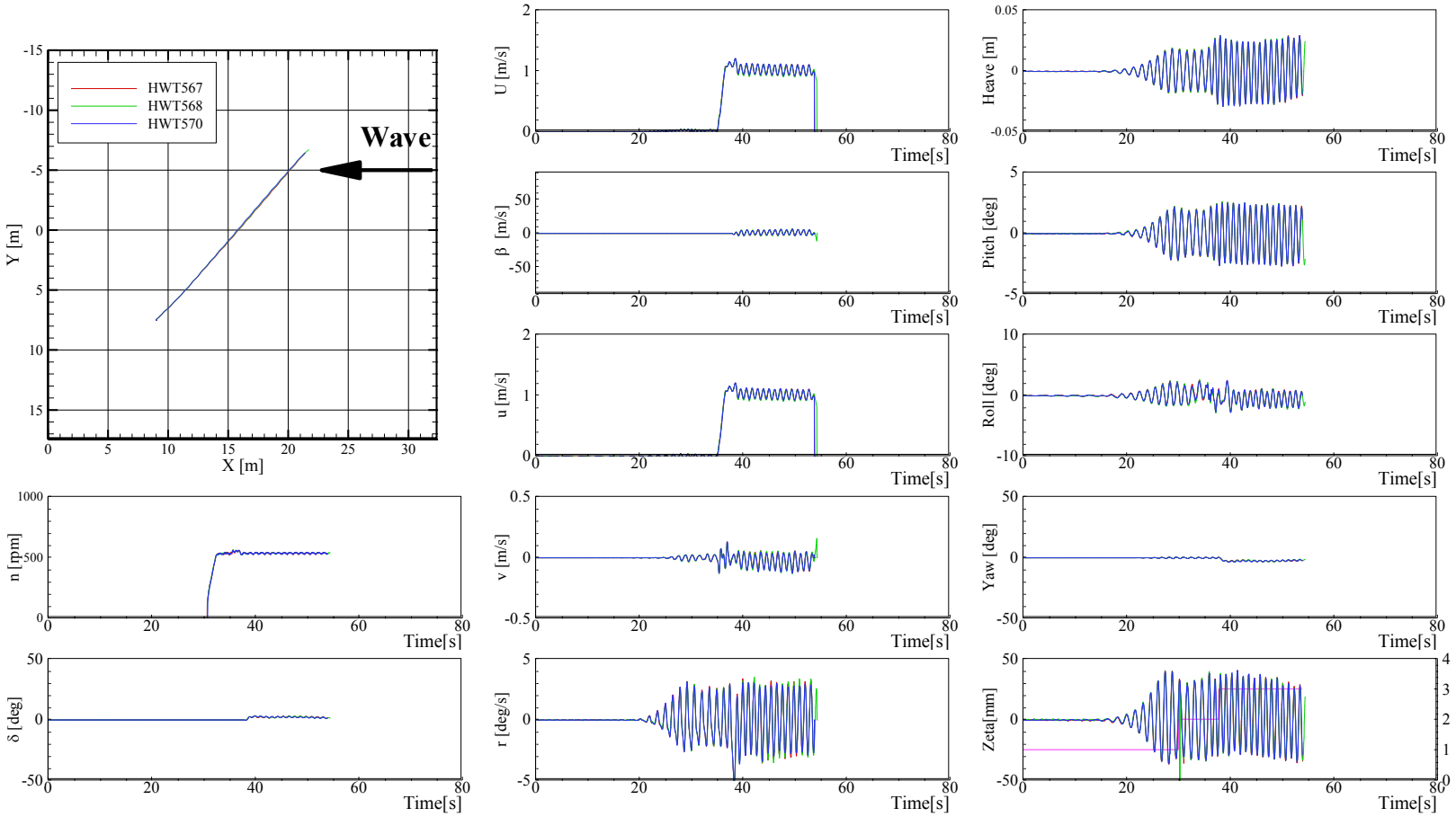

Figure C-27 Trajectories and time histories of course keeping at Fr = 0.2, λ/L = 1.0, H/λ = 0.02, and heading angle = 45°

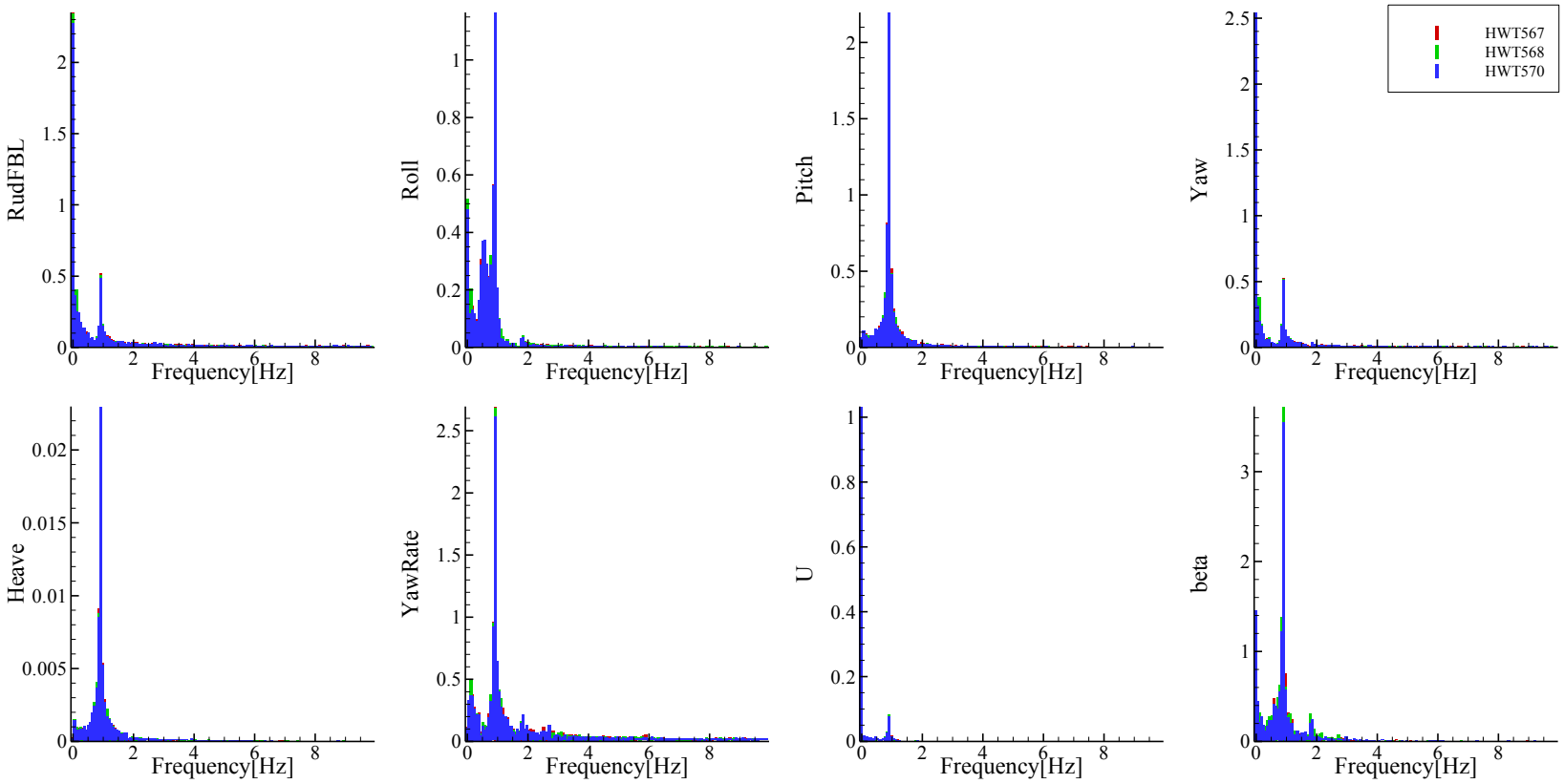

Figure C-28 FFT analysis of time histories of course keeping at Fr = 0.2, λ/L = 1.0, H/λ = 0.02, and heading angle = 45°

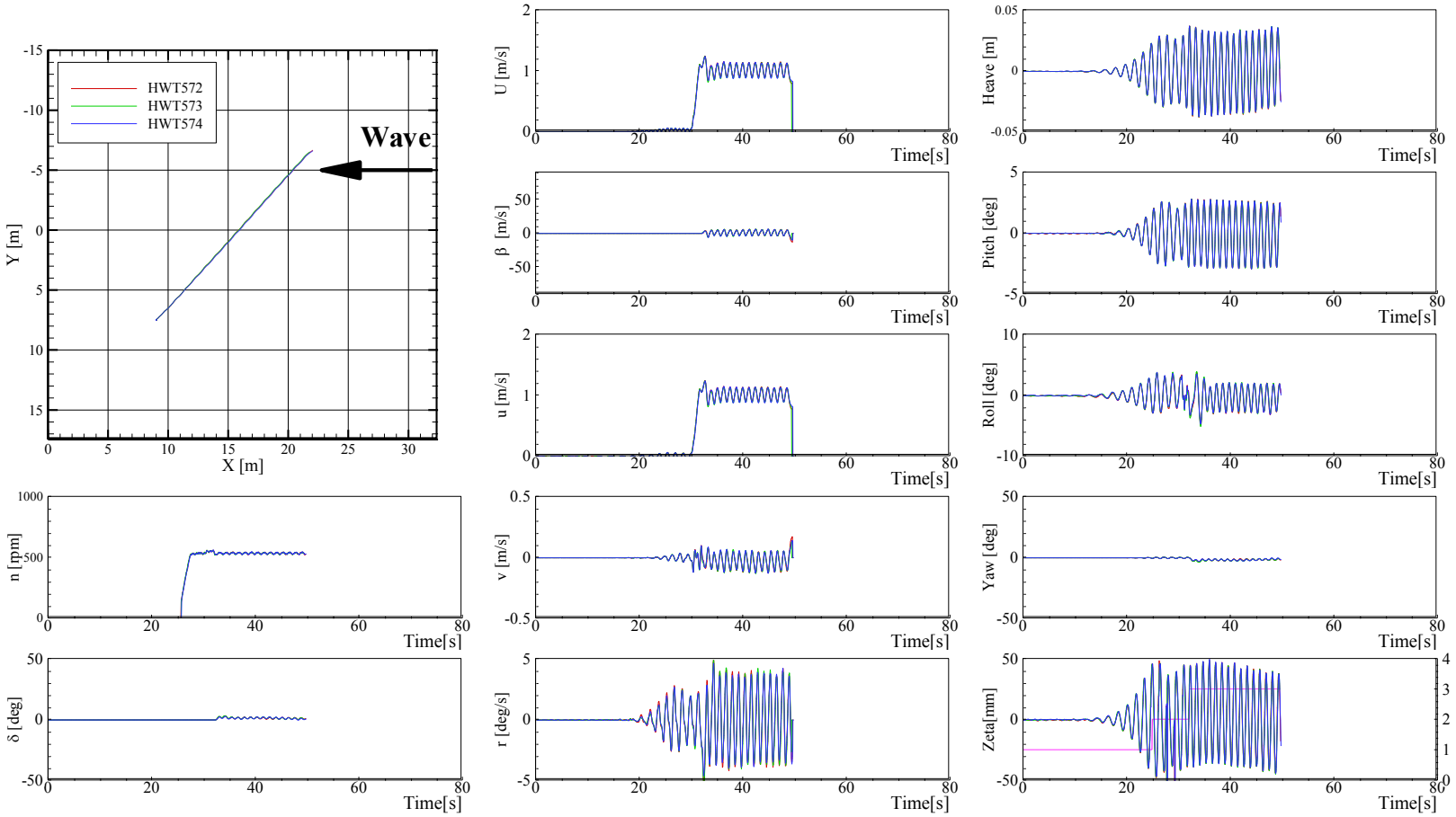

Figure C-29 Trajectories and time histories of course keeping at Fr = 0.2, λ/L = 1.2, H/λ = 0.02, and heading angle = 45°

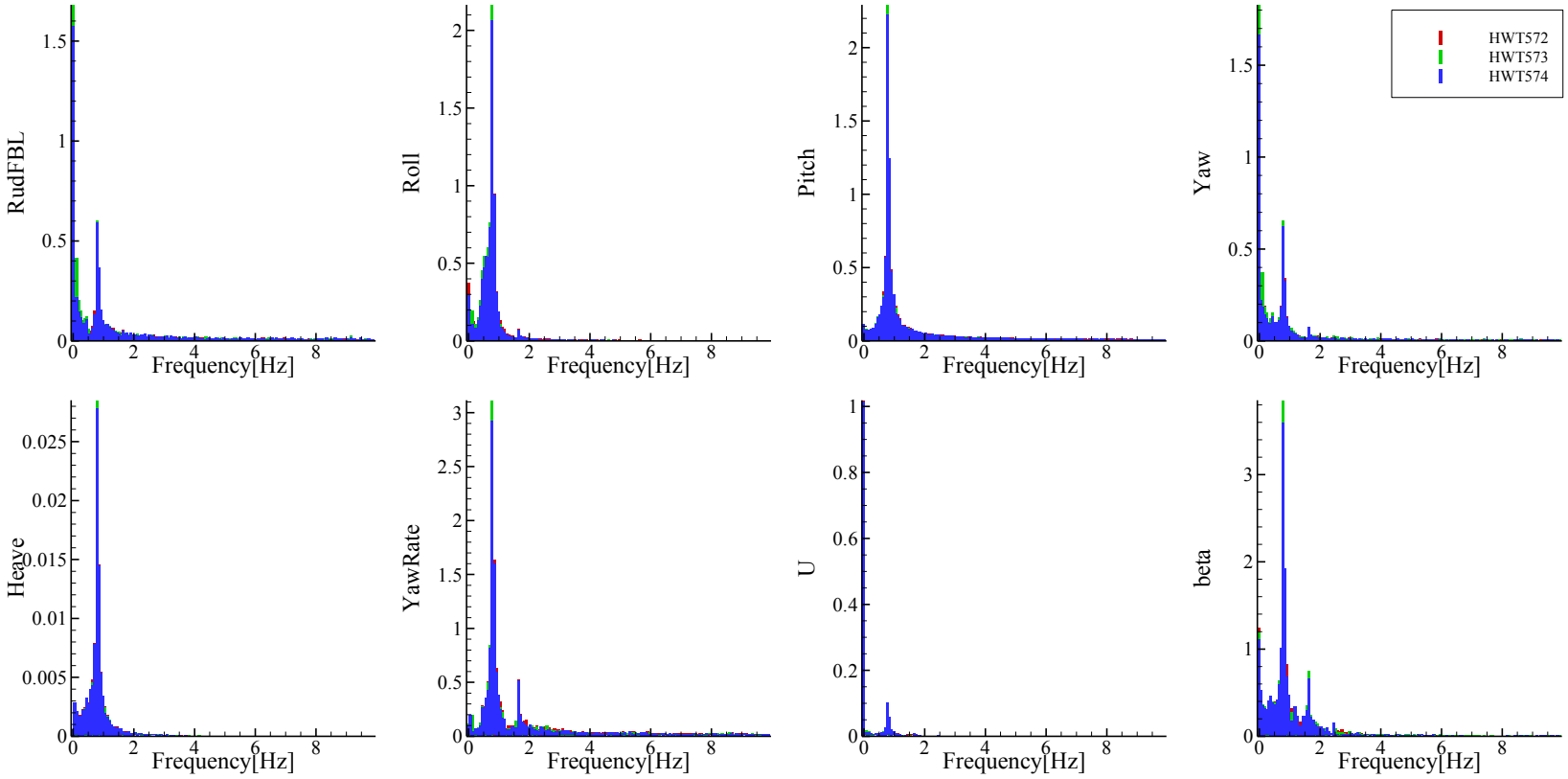

Figure C- 30 FFT analysis of time histories of course keeping at Fr = 0.2, λ/L = 1.2, H/λ = 0.02, and heading angle = 45°

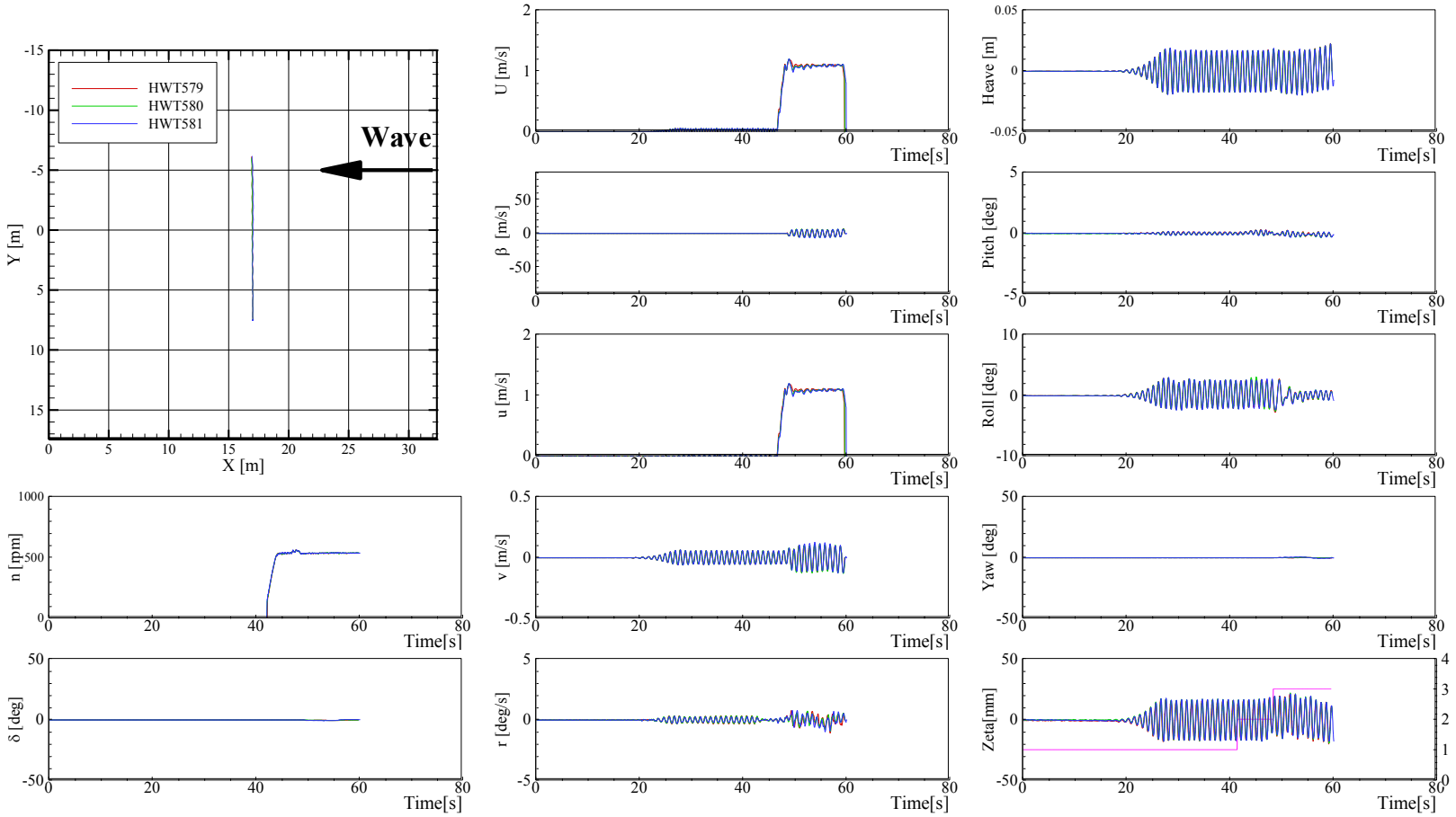

Figure C-31 Trajectories and time histories of course keeping at Fr = 0.2, λ/L = 0.5, H/λ = 0.02, and heading angle = 90°

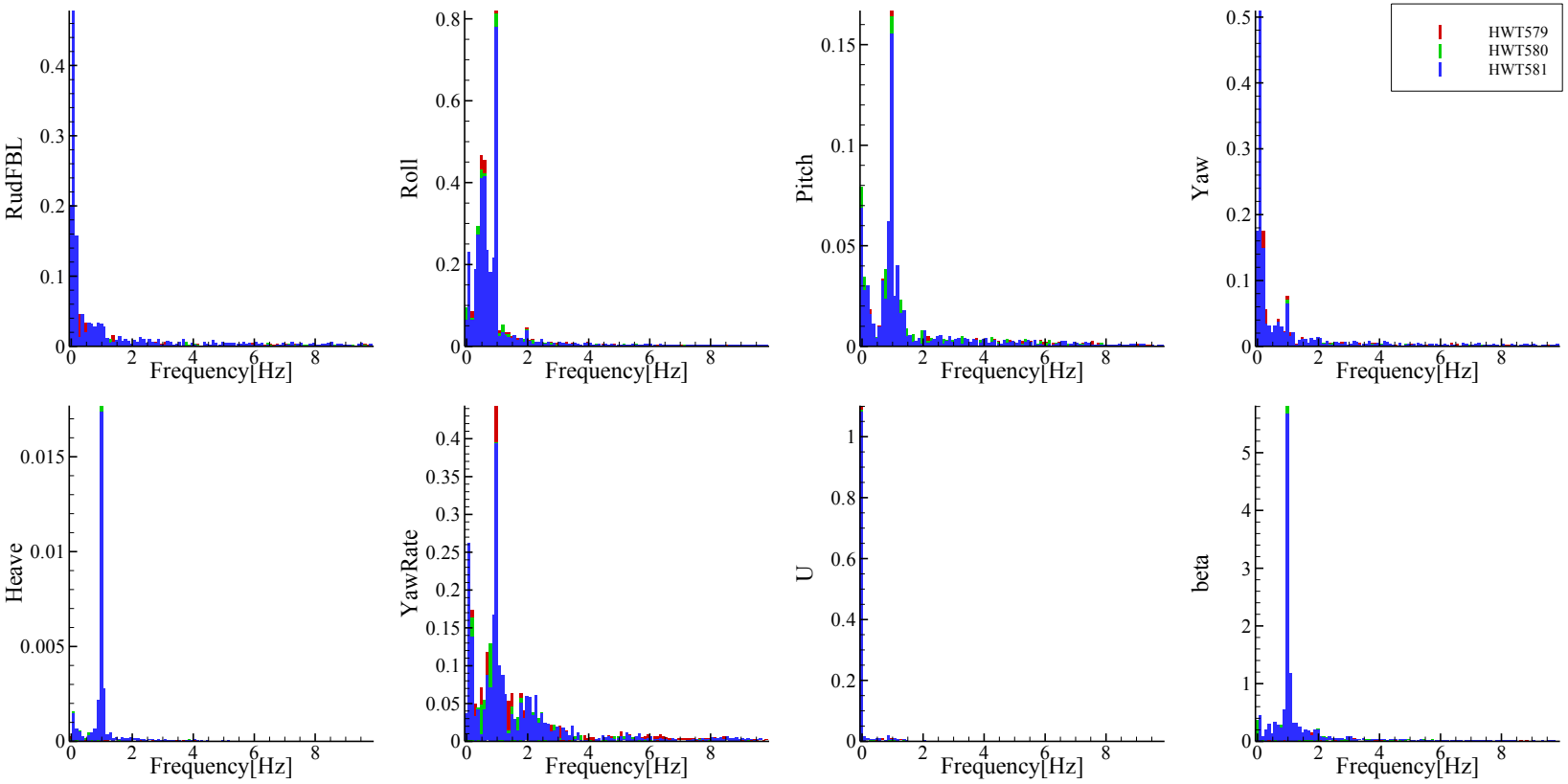

Figure C-32 FFT analysis of time histories of course keeping at Fr = 0.2, λ/L = 0.5, H/λ = 0.02, and heading angle = 90°

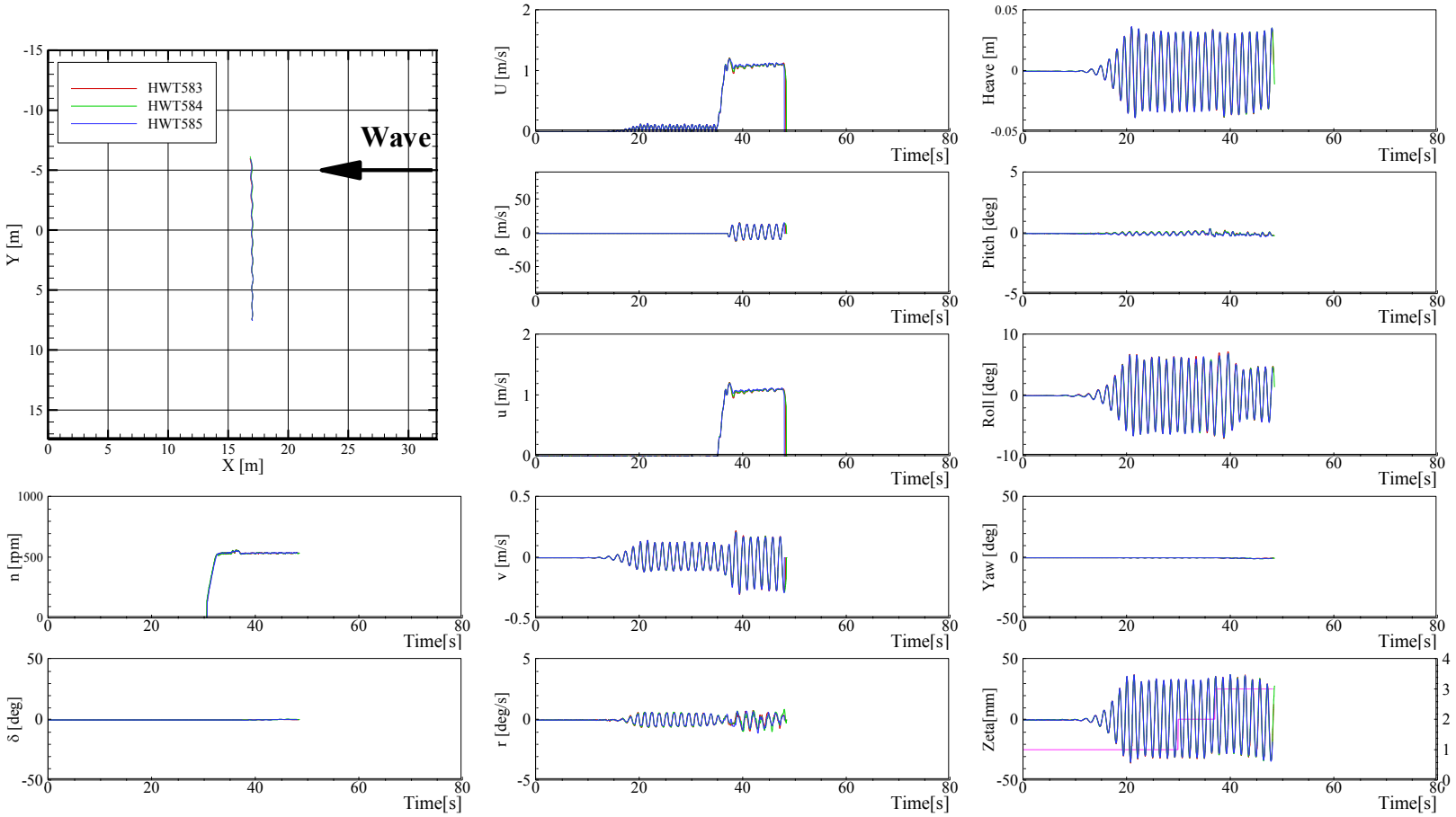

Figure C-33 Trajectories and time histories of course keeping at Fr = 0.2, λ/L = 1.0, H/λ = 0.02, and heading angle = 90°

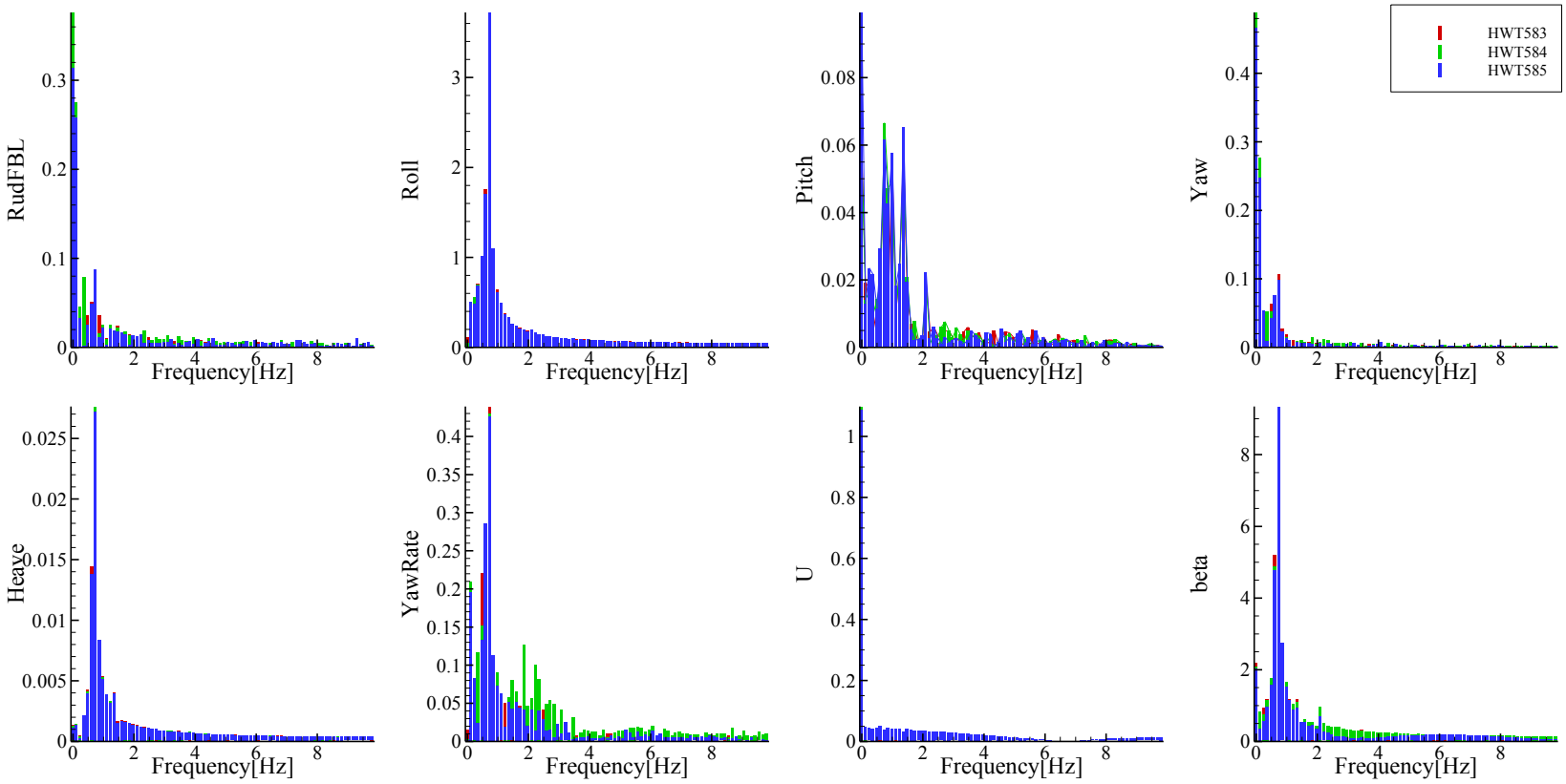

Figure C-34 FFT analysis of time histories of course keeping at Fr = 0.2, λ/L = 1.0, H/λ = 0.02, and heading angle = 90°

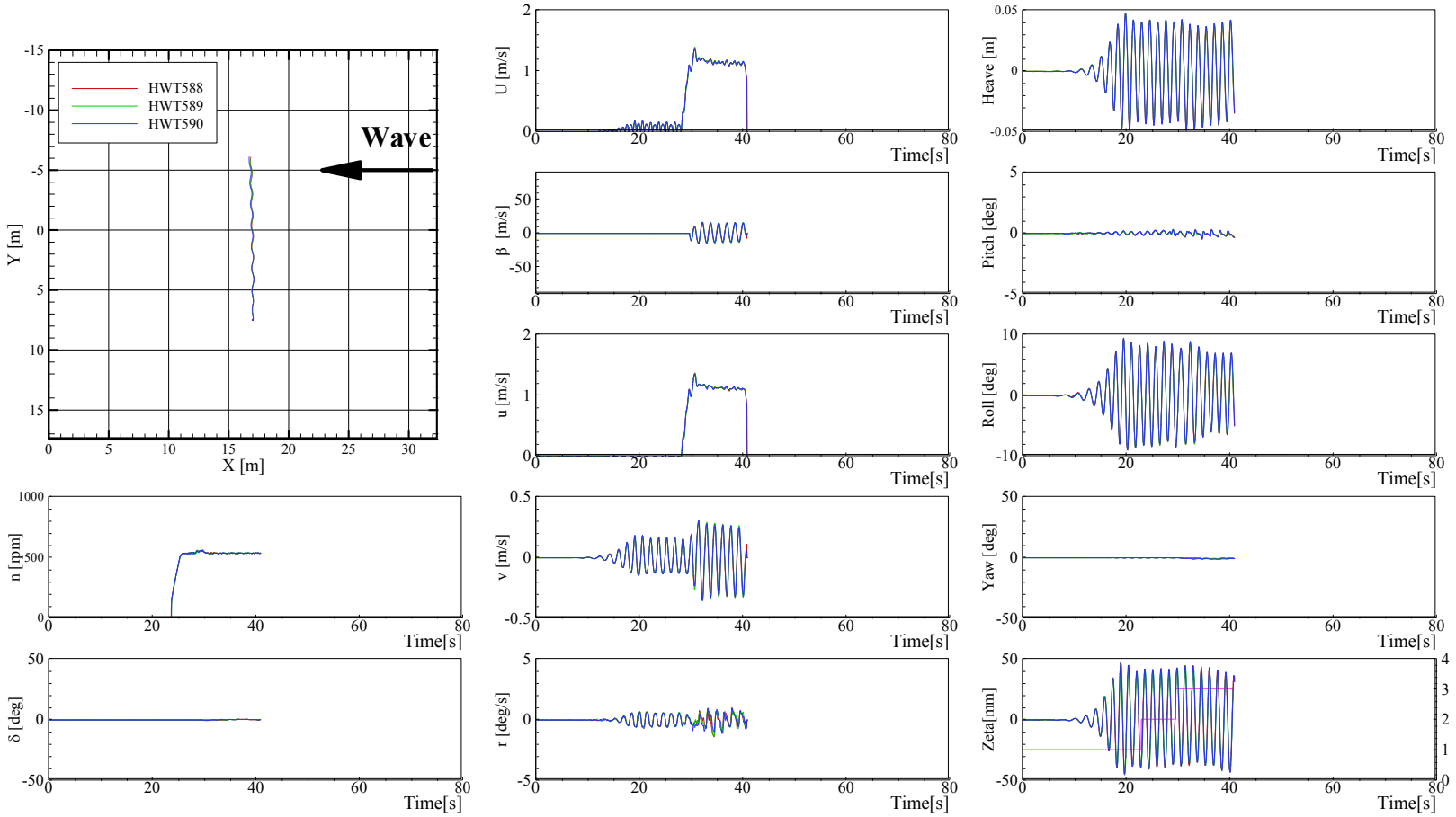

Figure C-35 Trajectories and time histories of course keeping at Fr = 0.2, λ/L = 1.2, H/λ = 0.02, and heading angle = 90°

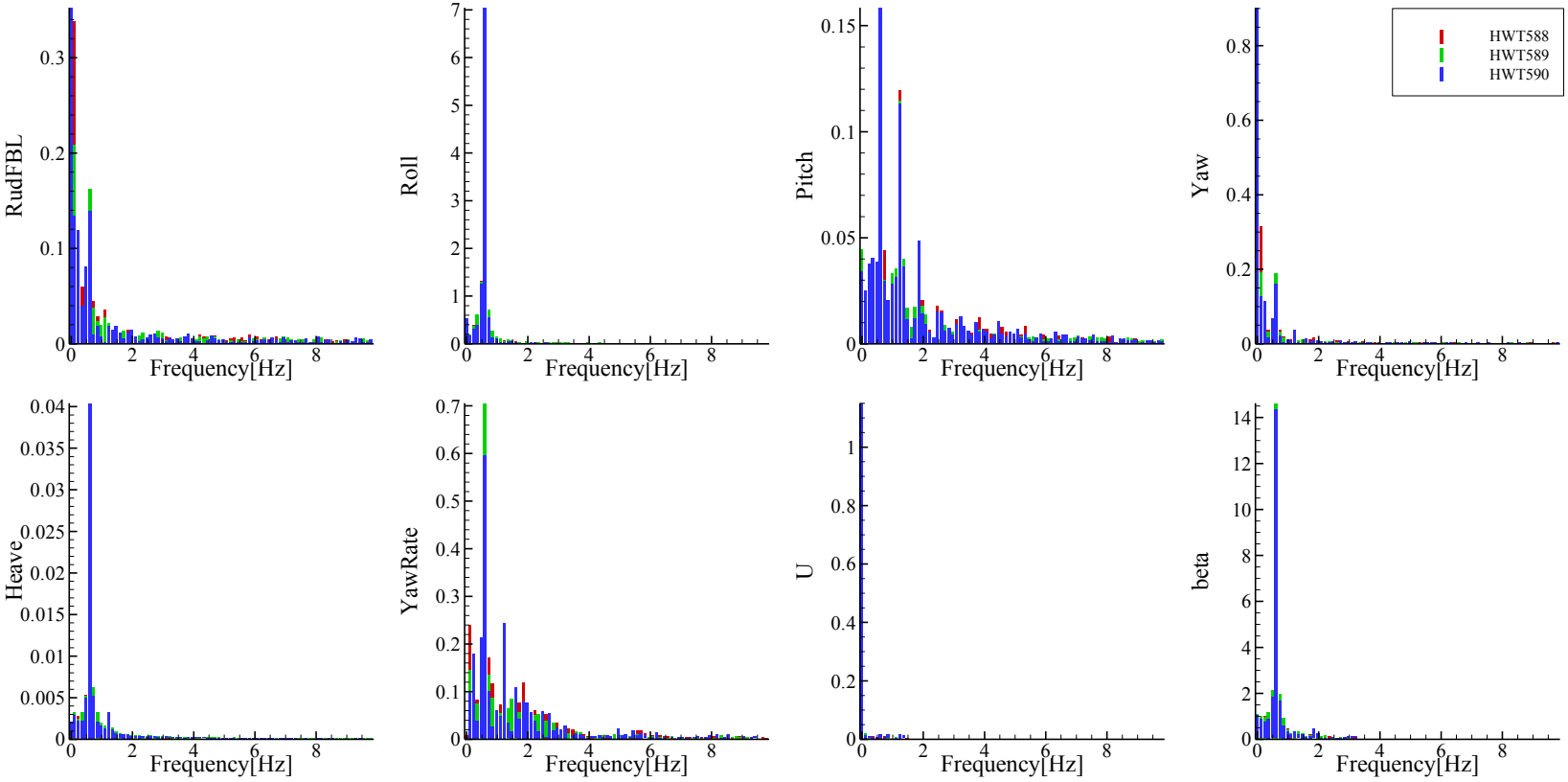

Figure C-36 FFT analysis of time histories of course keeping at Fr = 0.2, λ/L = 1.2, H/λ = 0.02, and heading angle = 90°

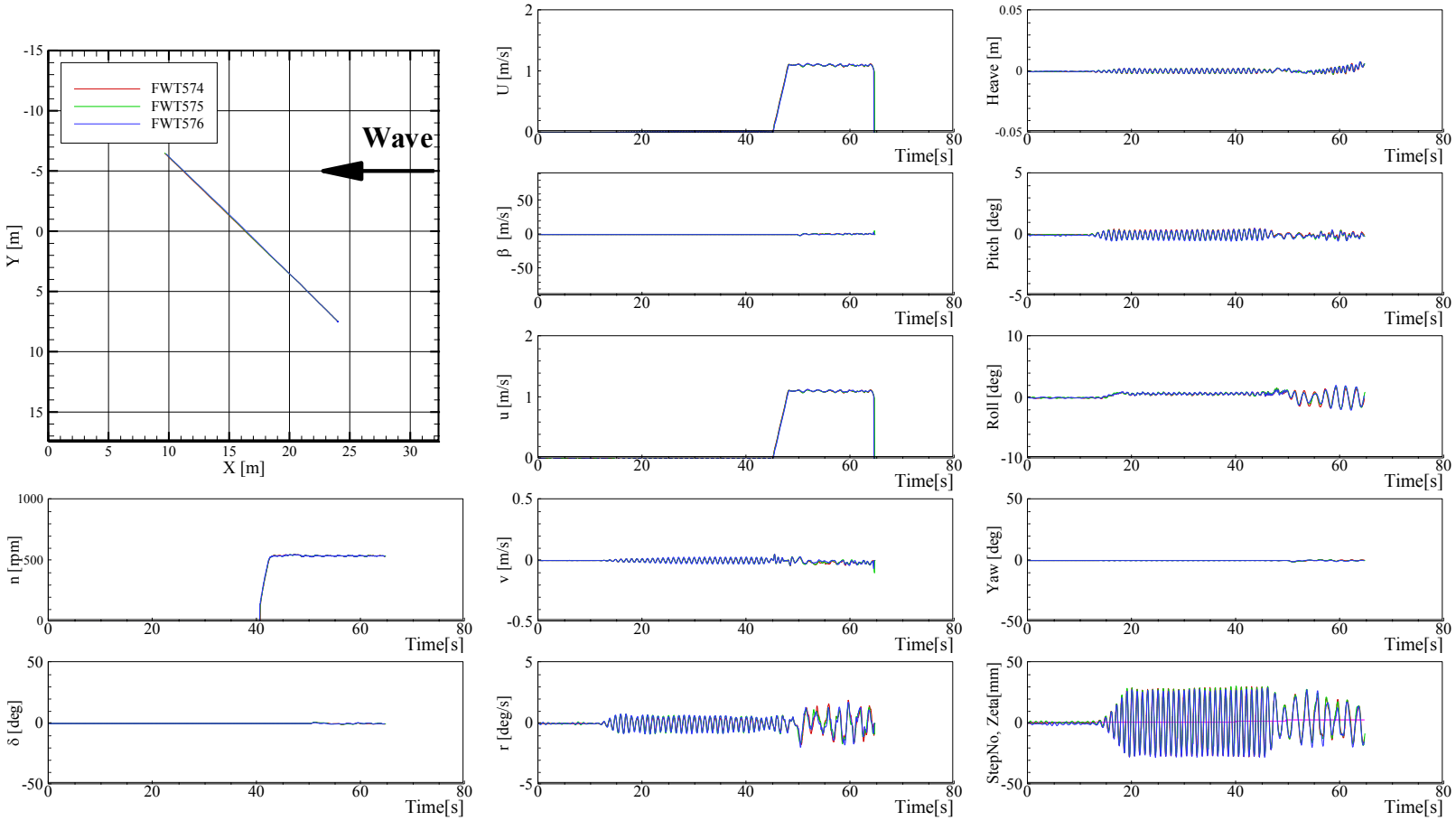

Figure C-37 Trajectories and time histories of course keeping at Fr = 0.2, λ/L = 0.5, H/λ = 0.02, and heading angle = 135°

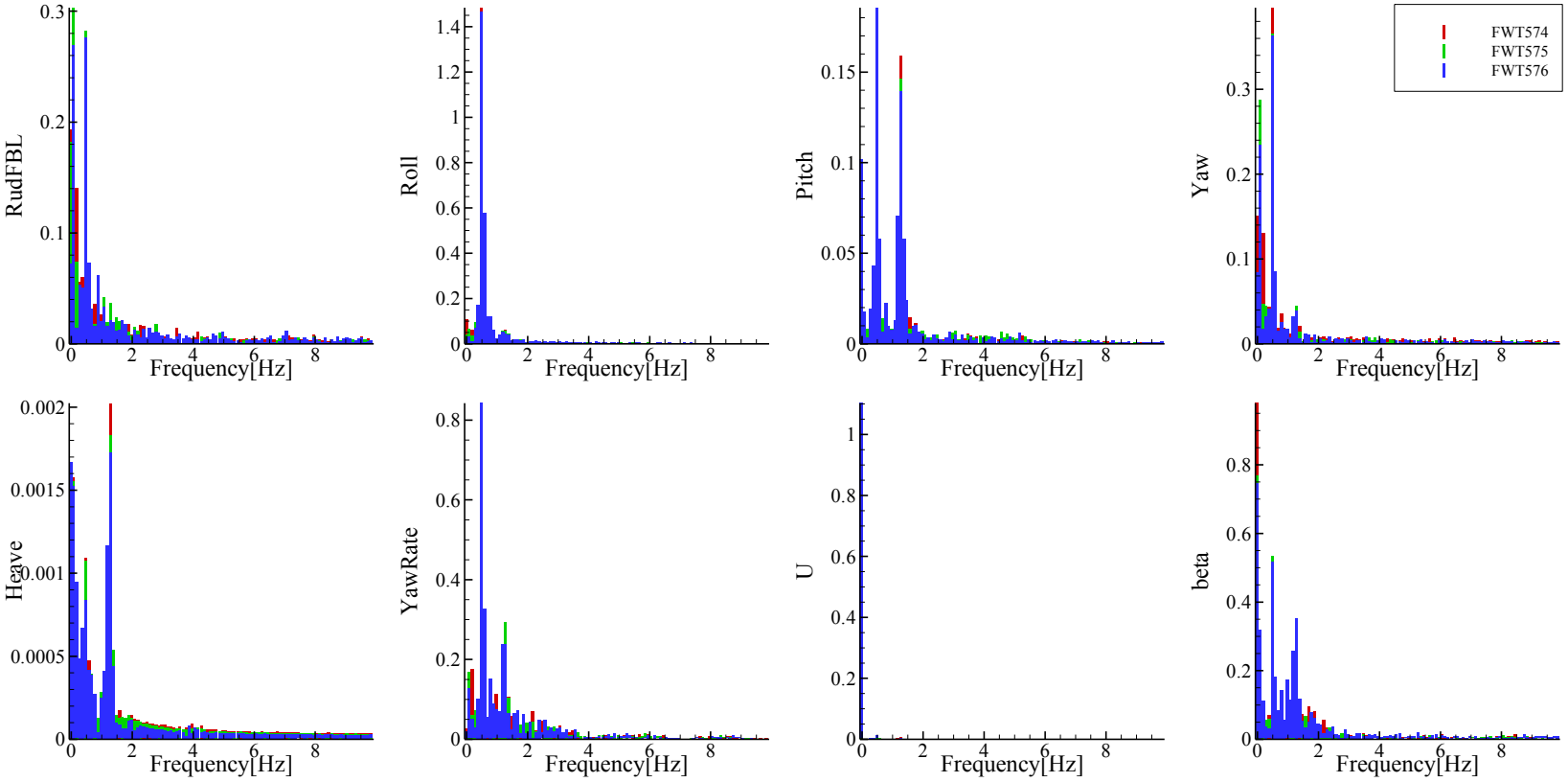

Figure C-38 FFT analysis of time histories of course keeping at Fr = 0.2, λ/L = 0.5, H/λ = 0.02, and heading angle = 135°

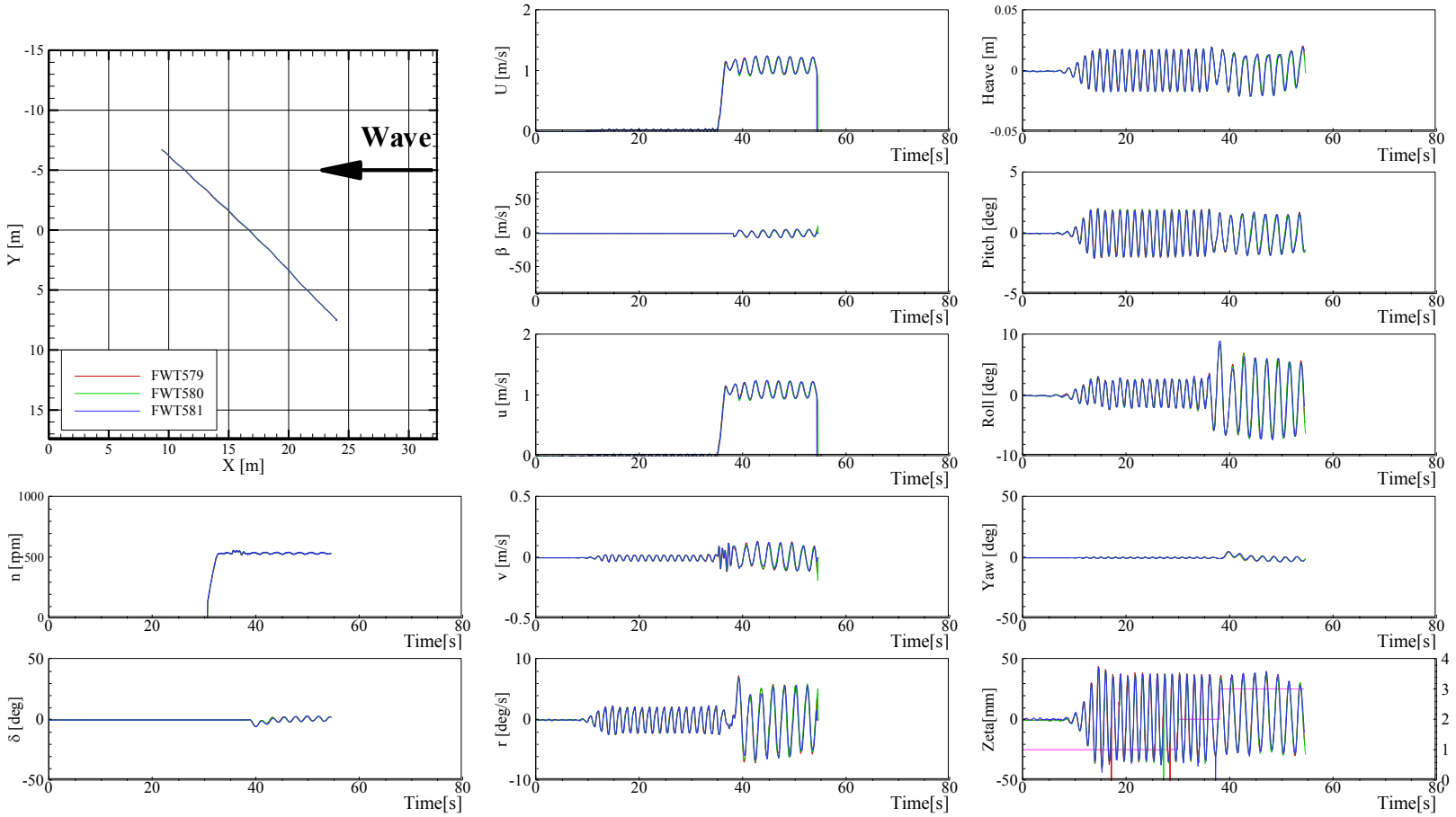

Figure C-39 Trajectories and time histories of course keeping at Fr = 0.2, λ/L = 1.0, H/λ = 0.02, and heading angle = 135°

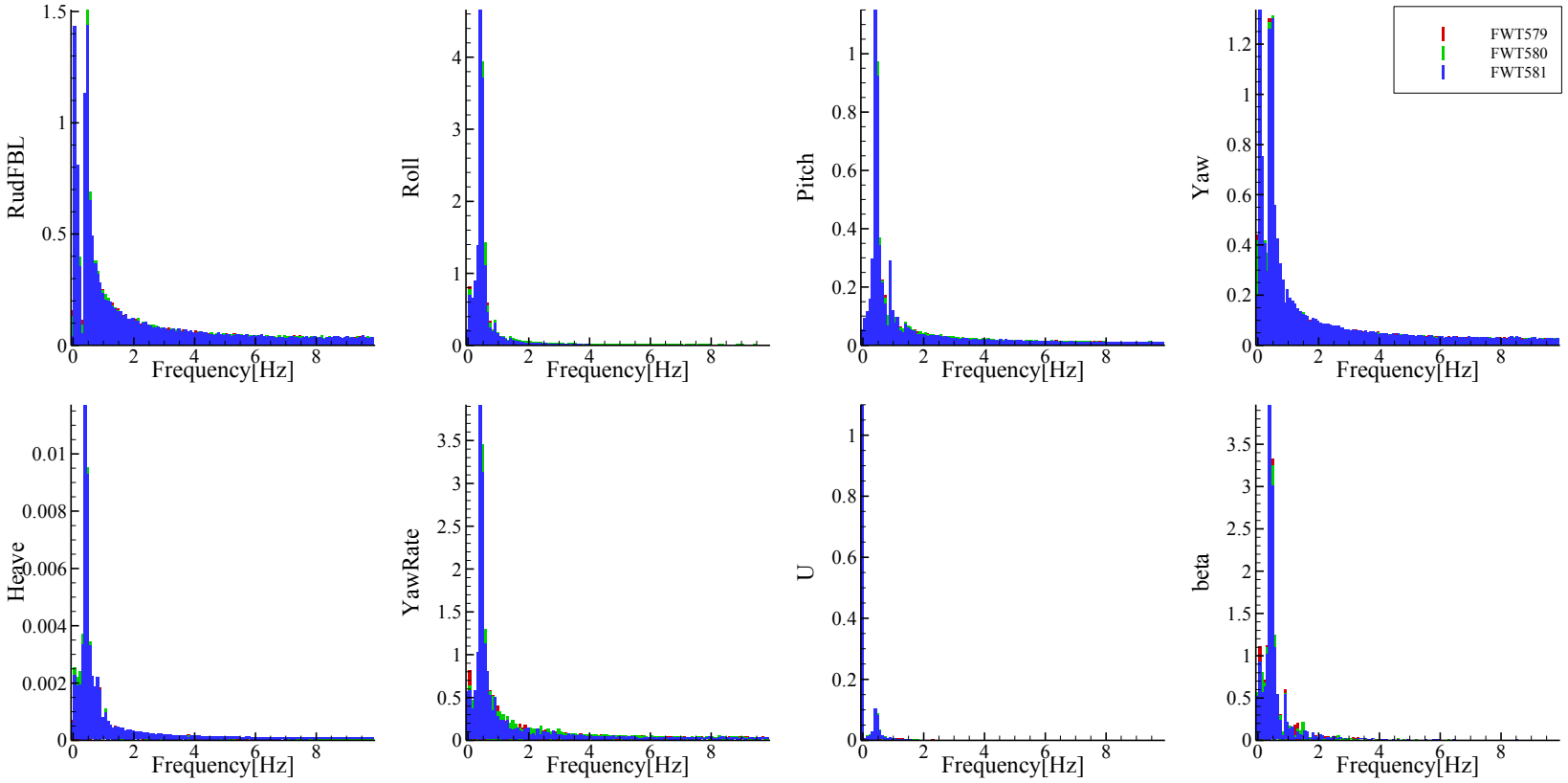

Figure C-40 FFT analysis of time histories of course keeping at Fr = 0.2, λ/L = 1.0, H/λ = 0.02, and heading angle = 135°

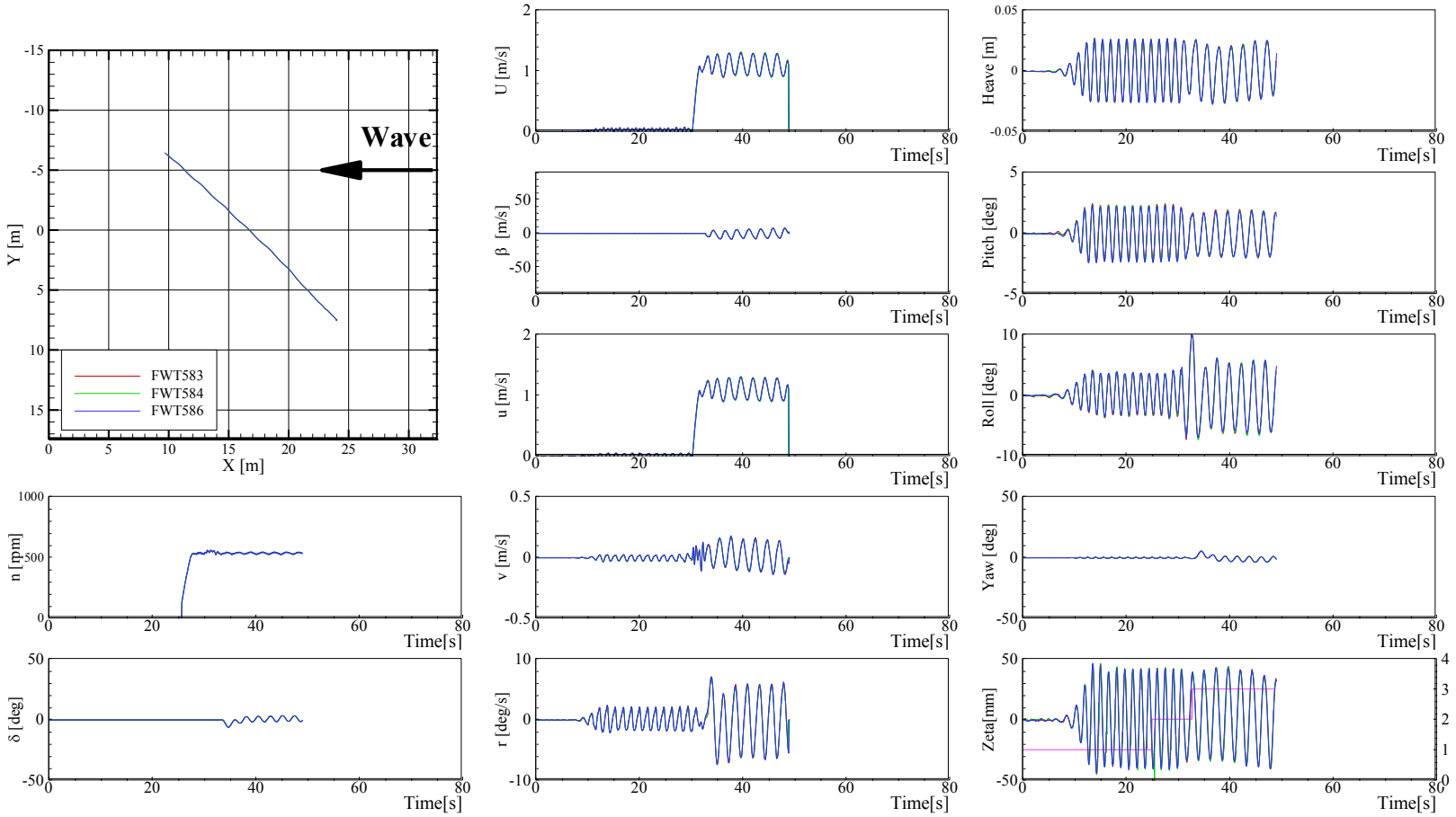

Figure C-41 Trajectories and time histories of course keeping at Fr = 0.2, λ/L = 1.2, H/λ = 0.02, and heading angle = 135°

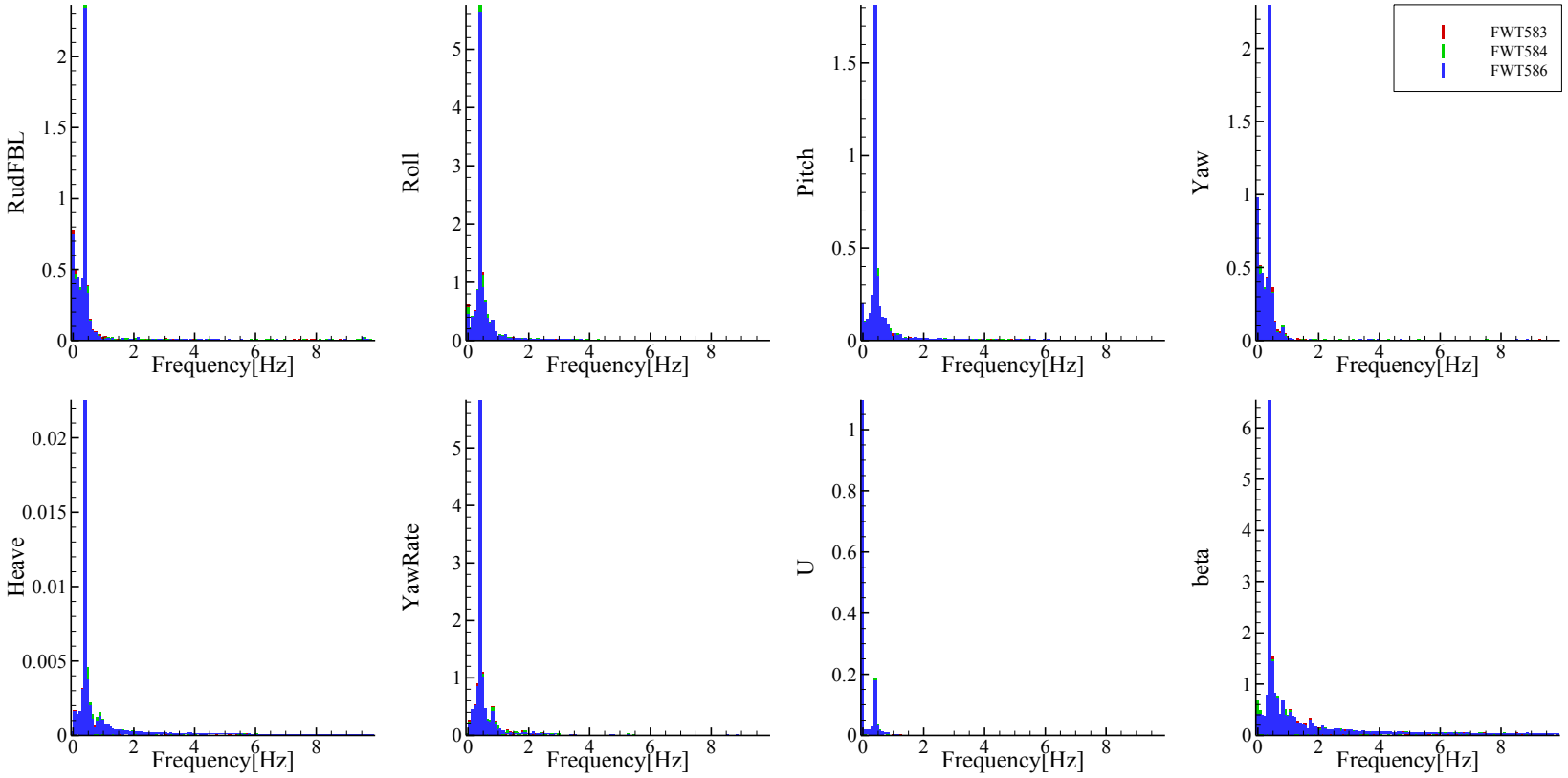

Figure C-42 FFT analysis of time histories of course keeping at Fr = 0.2, λ/L = 1.2, H/λ = 0.02, and heading angle = 135°

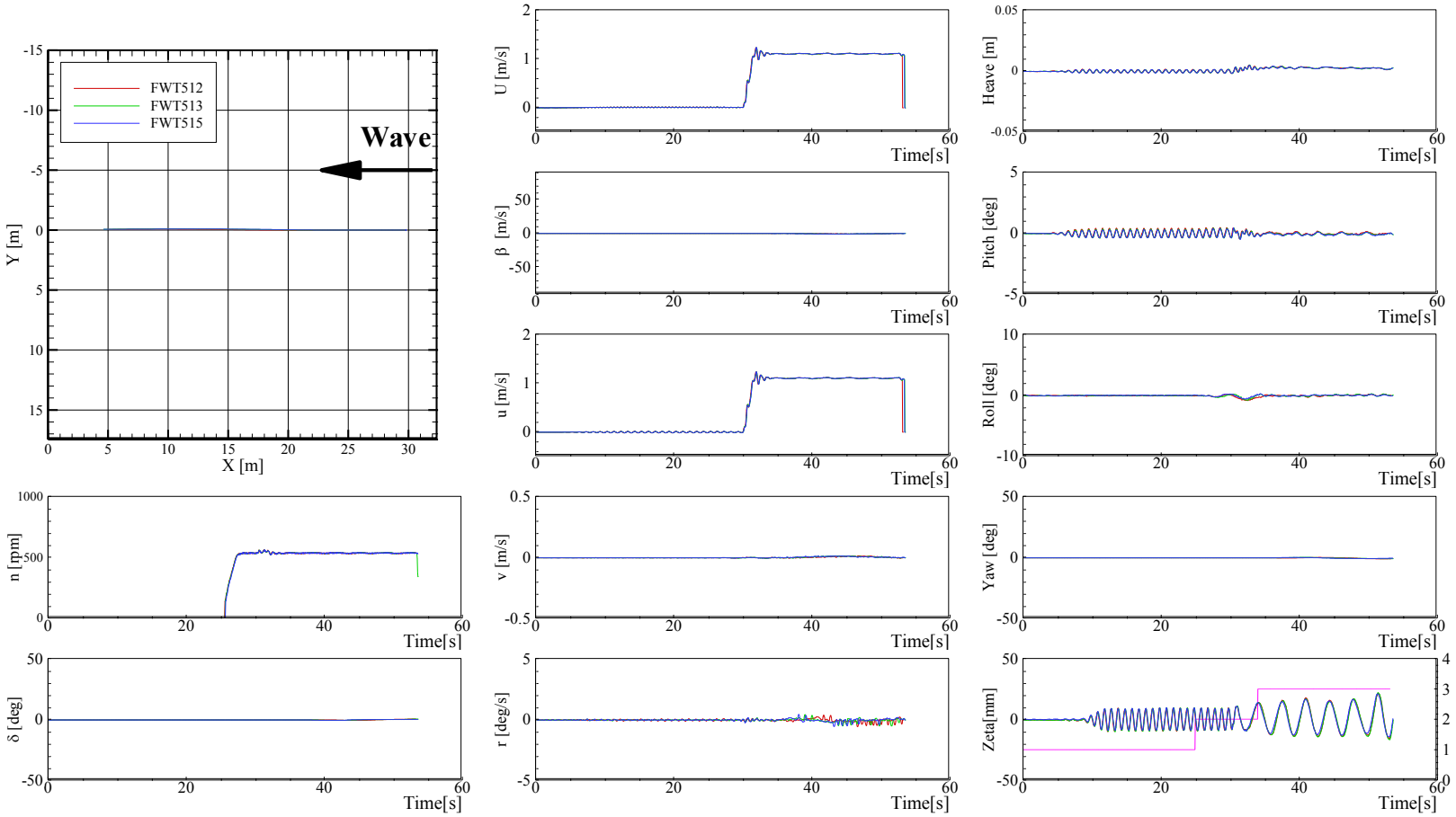

Figure C-43 Trajectories and time histories of course keeping at Fr = 0.2, λ/L = 0.5, H/λ = 0.02, and heading angle = 180°

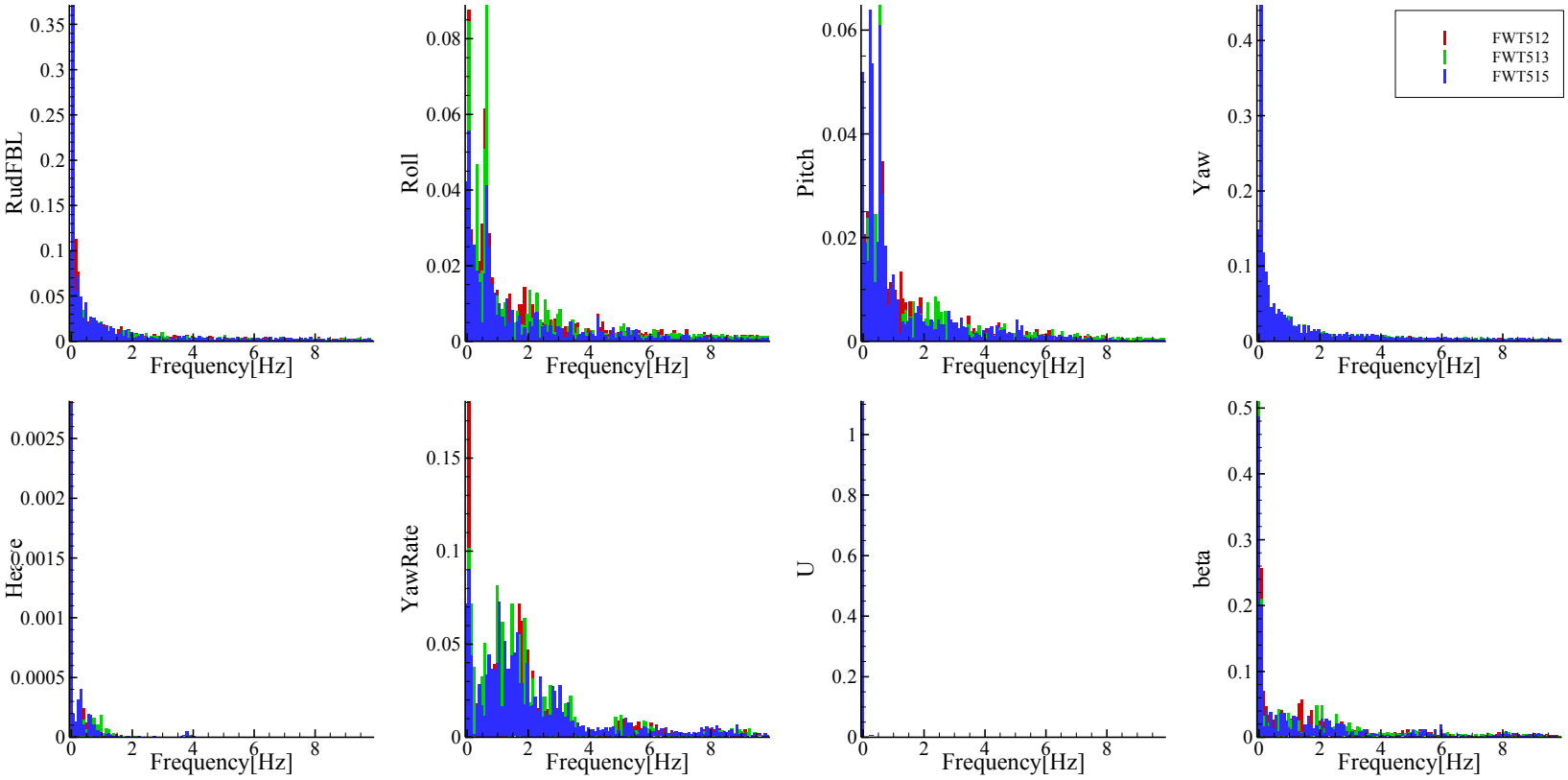

Figure C-44 FFT analysis of time histories of course keeping at Fr = 0.2, λ/L = 0.5, H/λ = 0.02, and heading angle = 180°

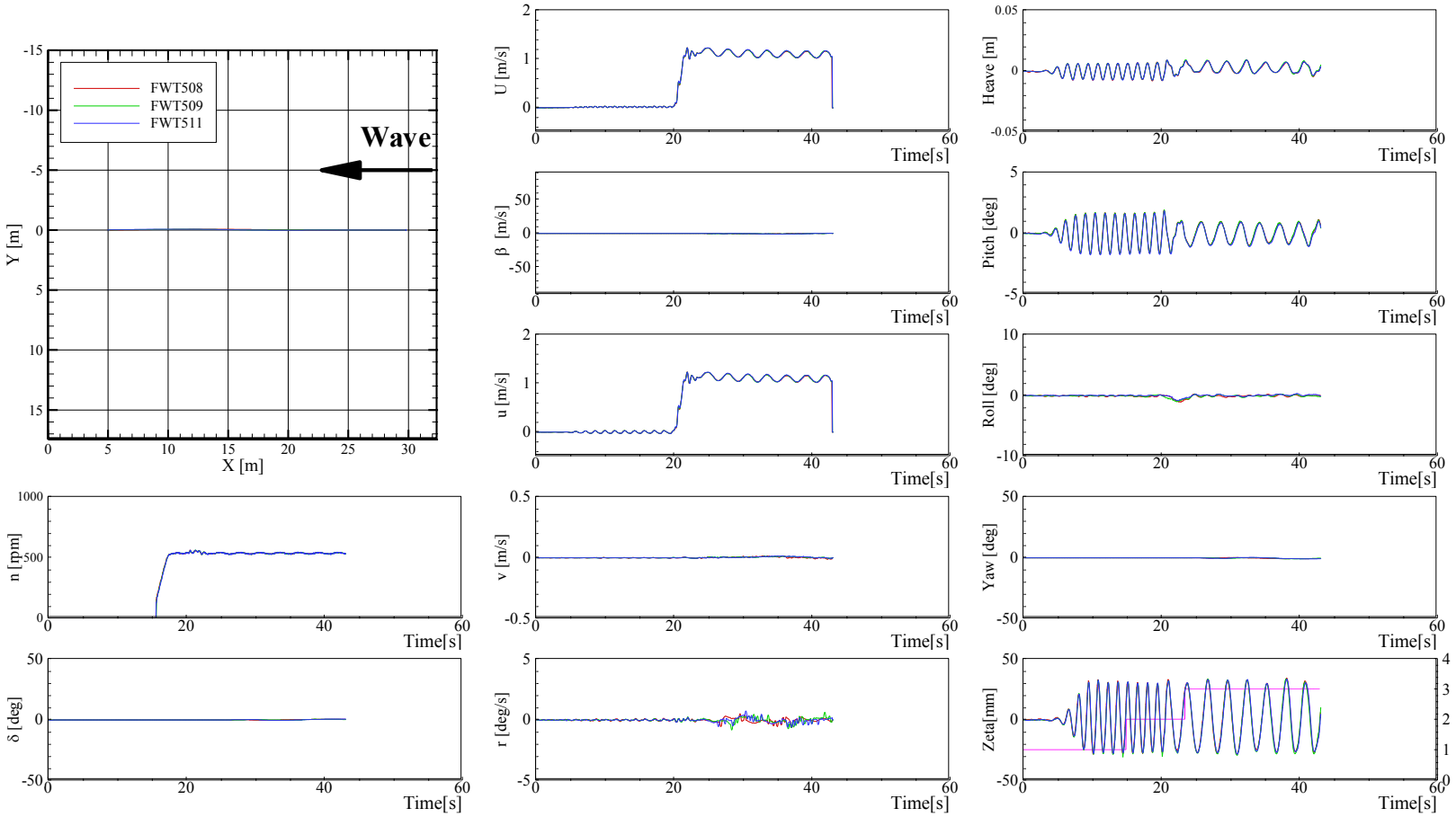

Figure C-45 Trajectories and time histories of course keeping at Fr = 0.2, λ/L = 1.0, H/λ = 0.02, and heading angle = 180°

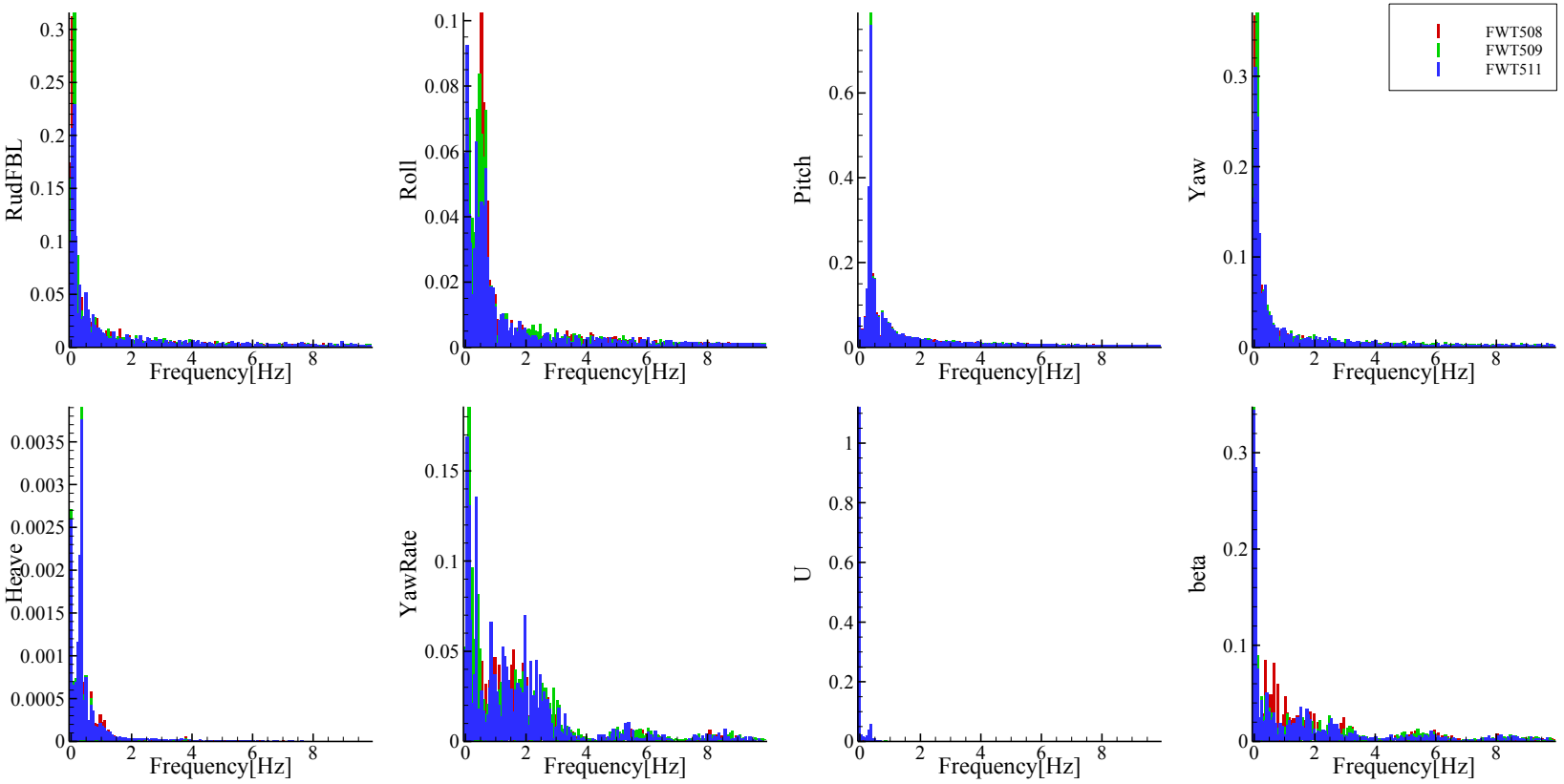

Figure C-46 FFT analysis of time histories of course keeping at Fr = 0.2, λ/L = 1.0, H/λ = 0.02, and heading angle = 180°

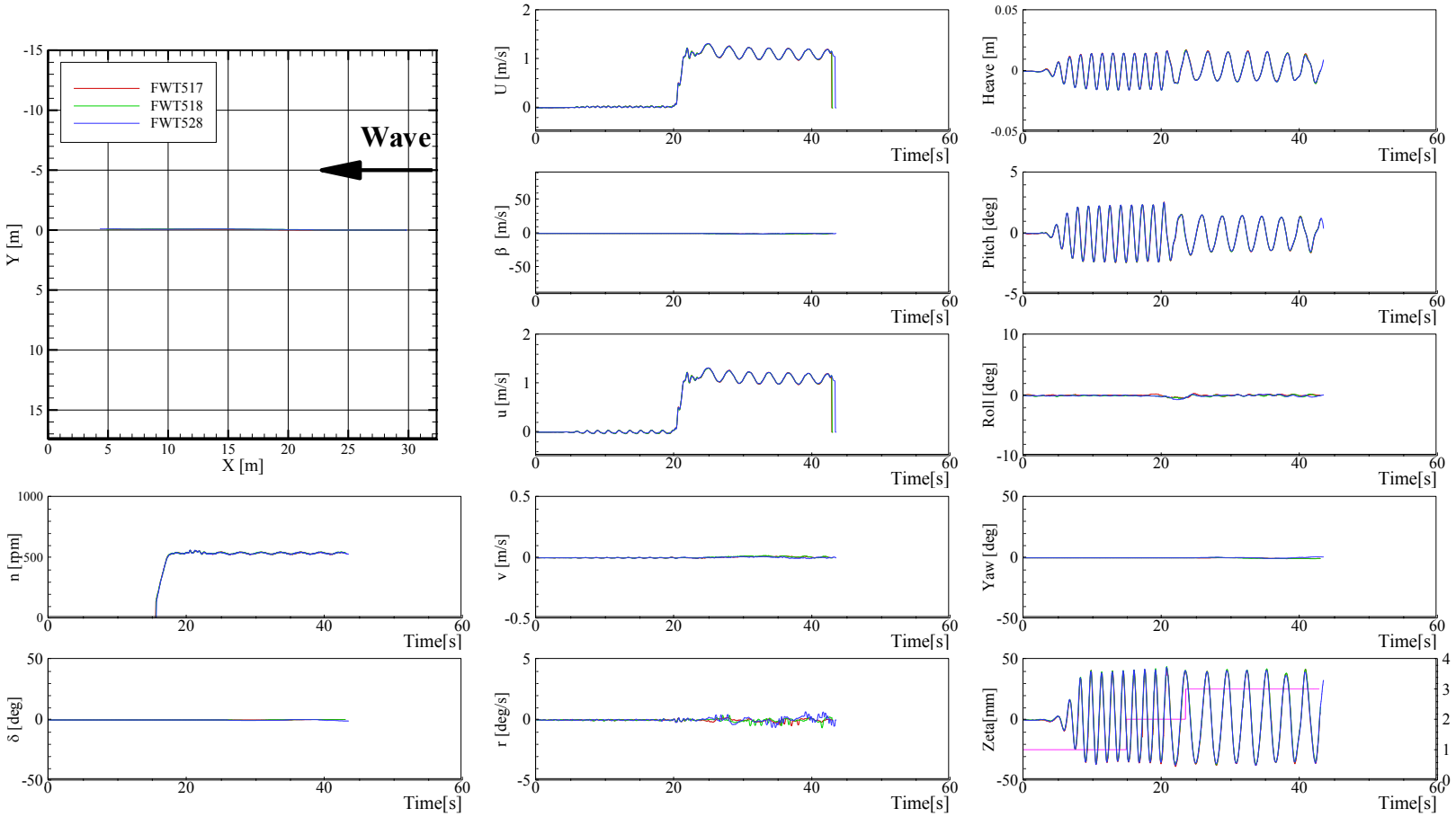

Figure C-47 Trajectories and time histories of course keeping at Fr = 0.2, λ/L = 1.2, H/λ = 0.02, and heading angle = 180°

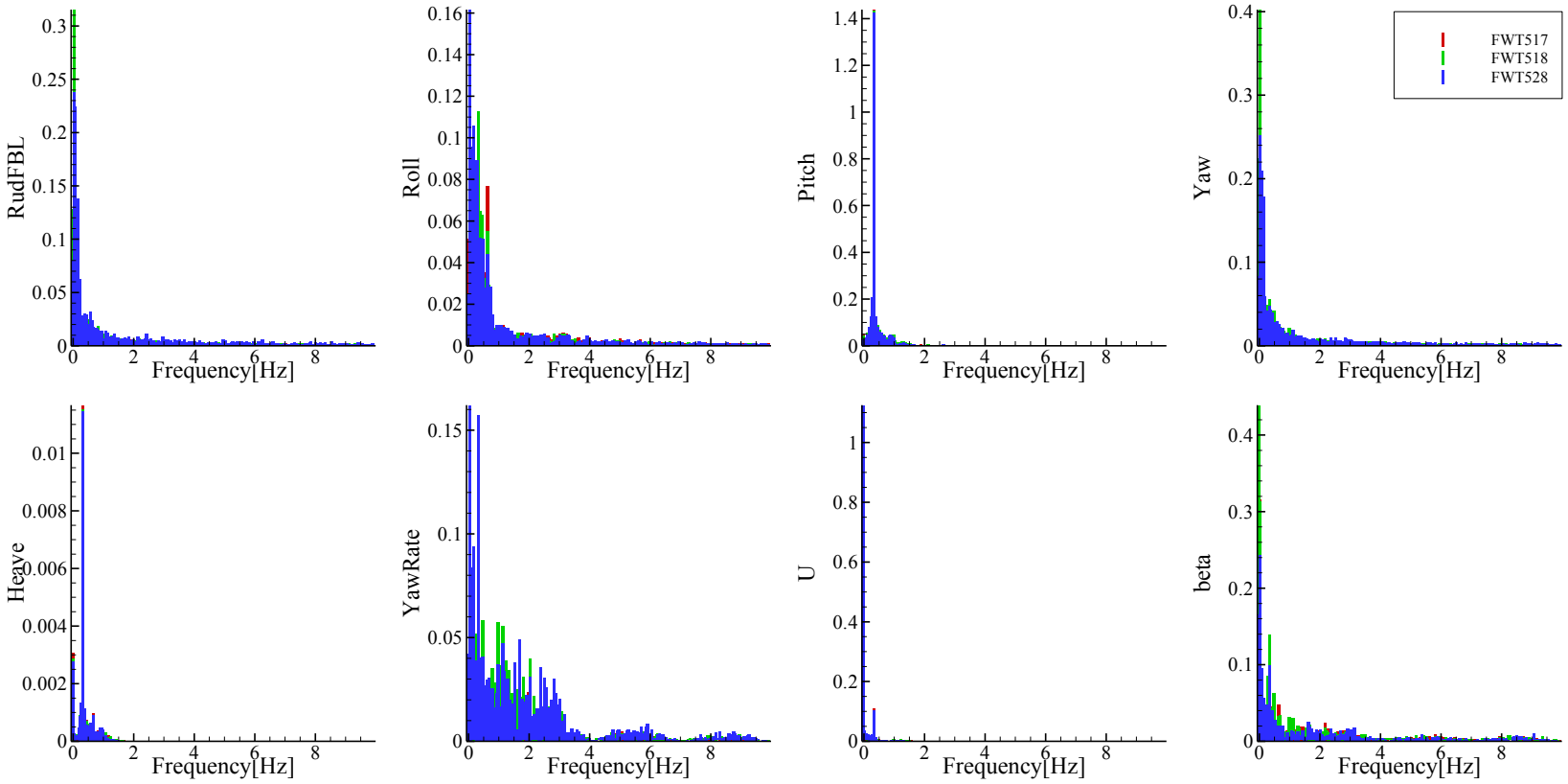

Figure C-48 FFT analysis of time histories of course keeping at Fr = 0.2, λ/L = 1.2, H/λ = 0.02, and heading angle = 180°

APPENDIX D TRAJECTORIES AND TIME HISTORIES RESULTS OF ZIGZAG TESTS IN CALM WATER

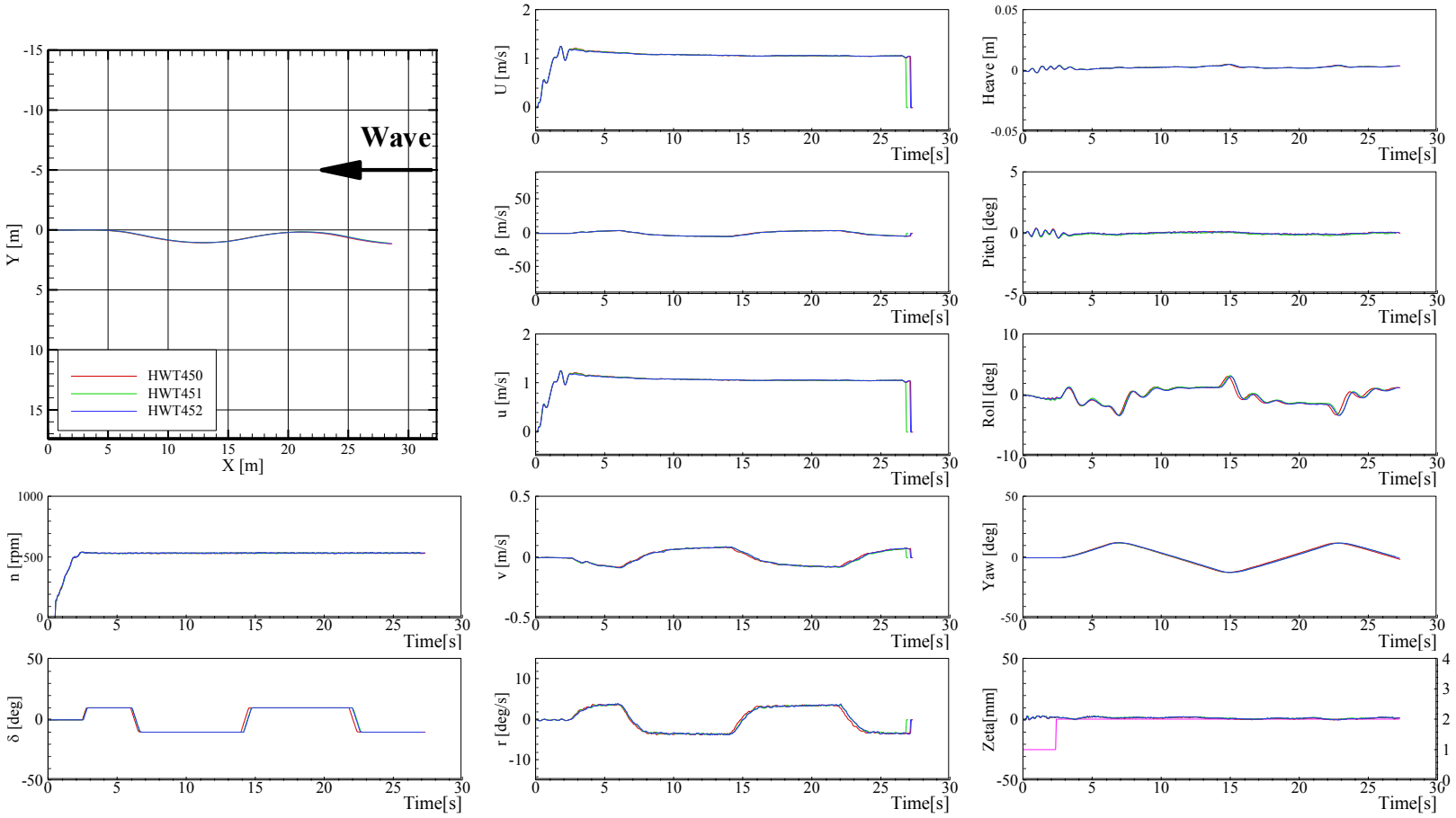

Figure D-1 Trajectories and time histories of zigzag 10°/10° in calm water at Fr = 0.2, and heading angle = 0°

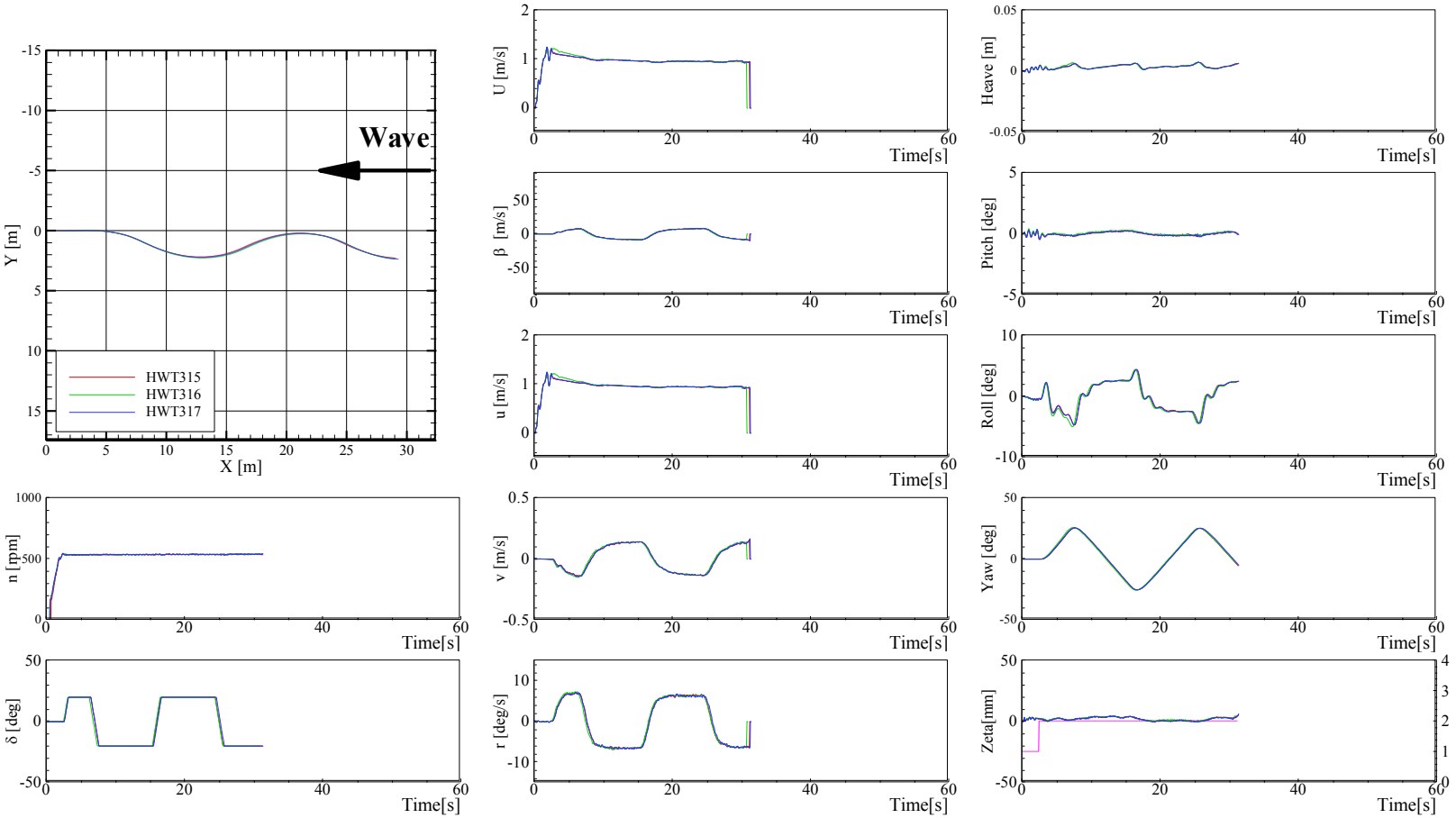

Figure D-2 Trajectories and time histories of zigzag 20°/20° in calm water at Fr = 0.2, and heading angle = 0°

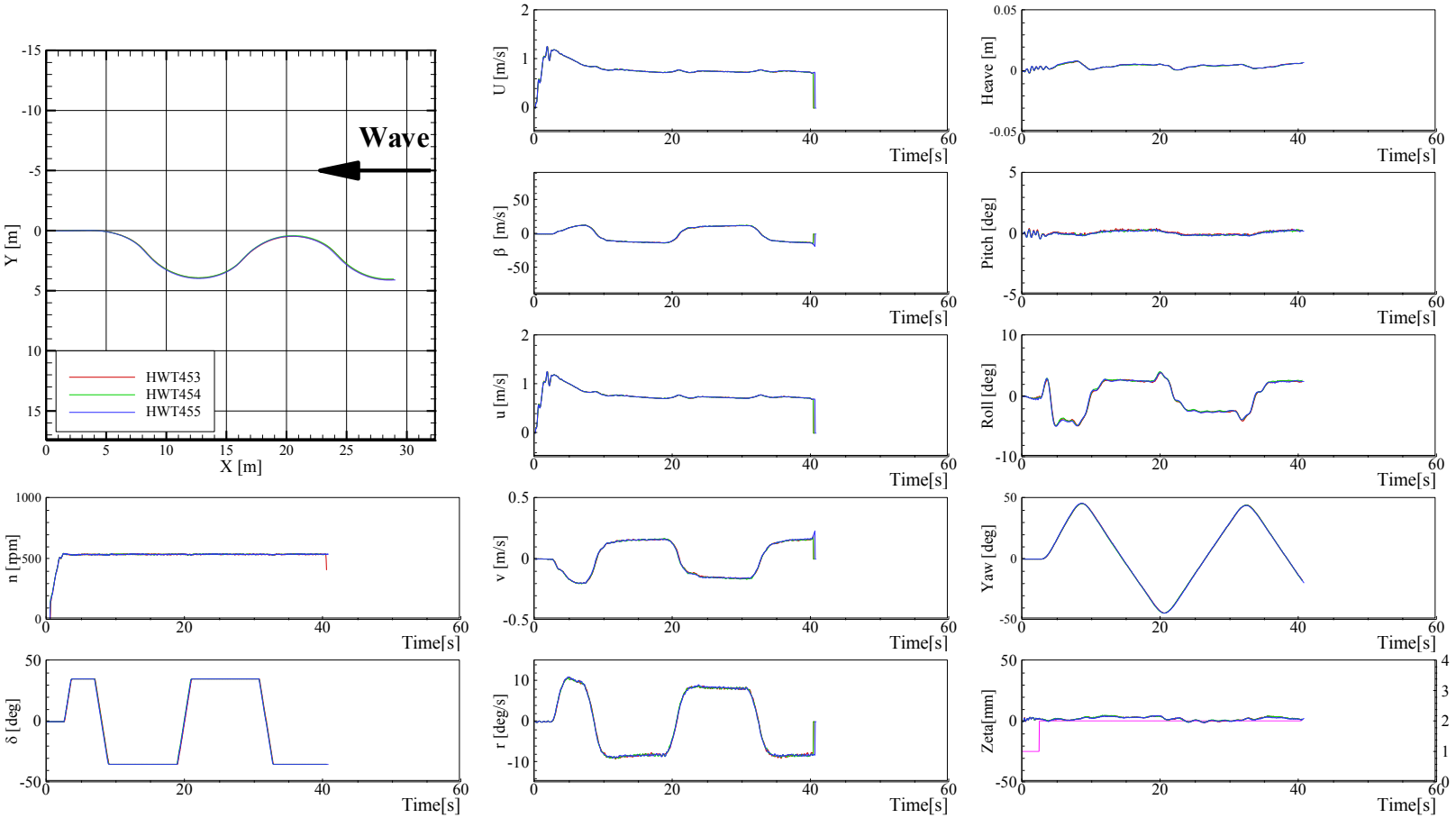

Figure D-3 Trajectories and time histories of zigzag 35°/35° in calm water at Fr = 0.2, and heading angle = 0°

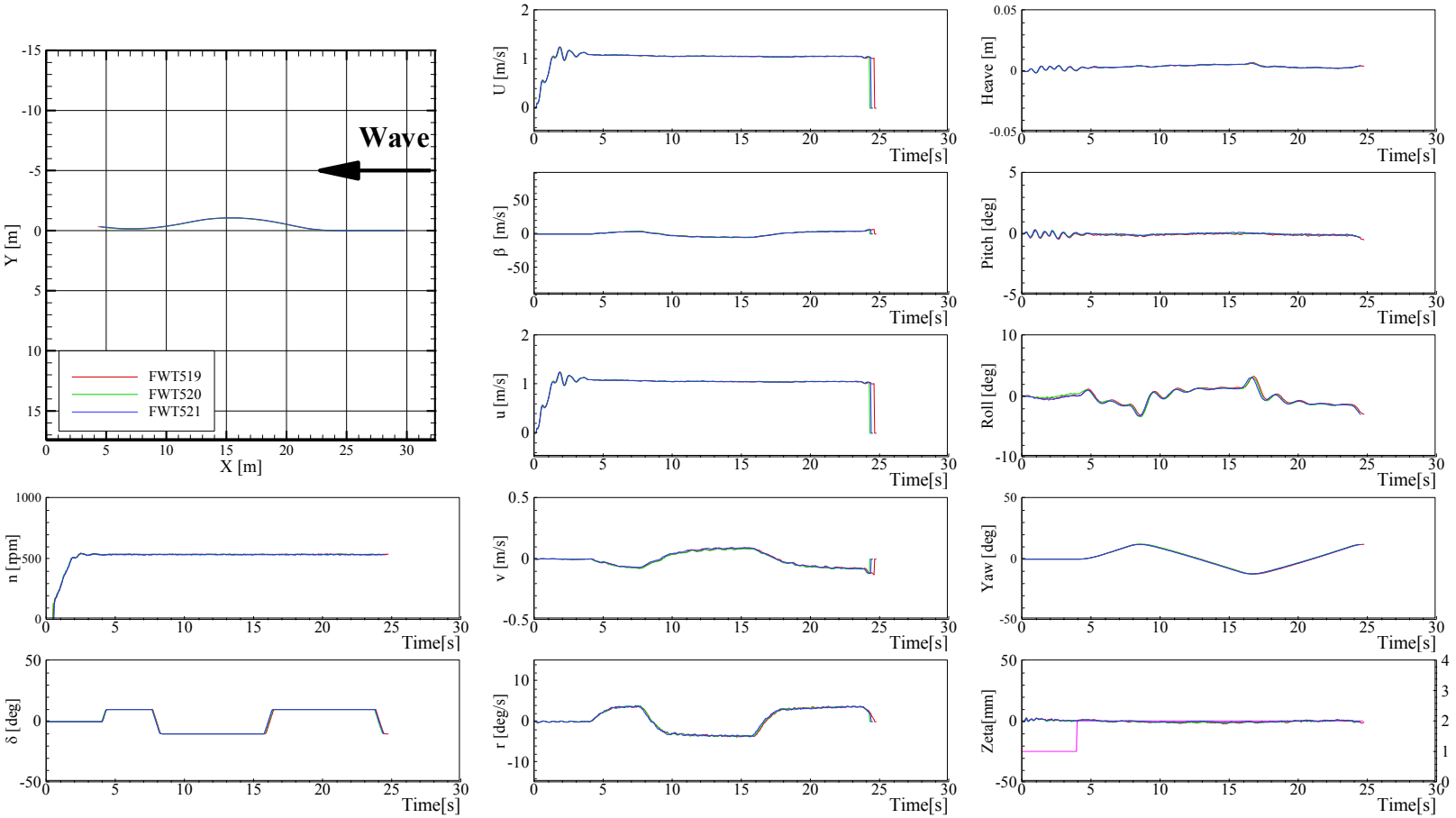

Figure D-4 Trajectories and time histories of zigzag 10°/10° in calm water at Fr = 0.2, and heading angle = 180°

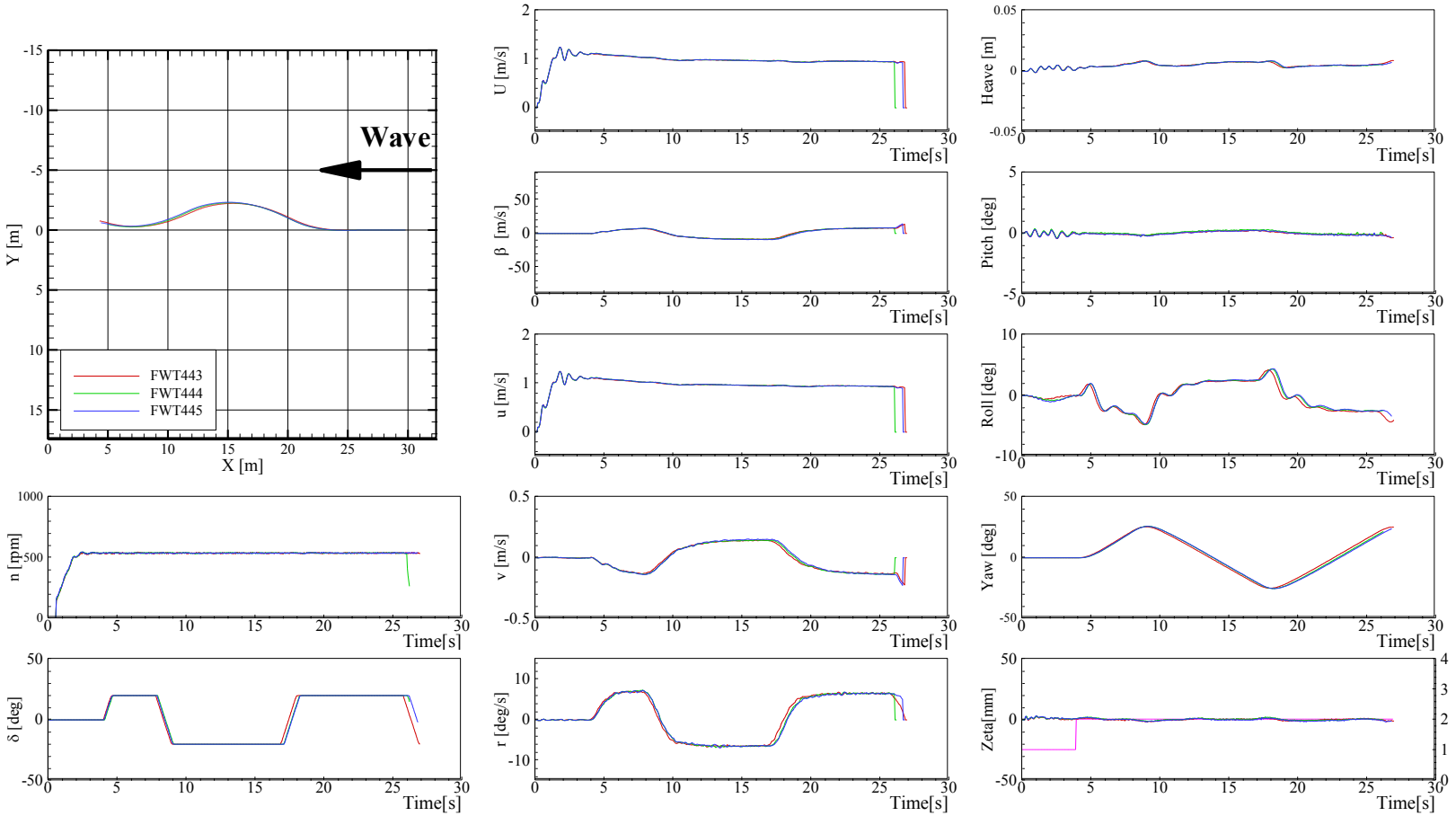

Figure D- 5 Trajectories and time histories of zigzag 20°/20° in calm water at Fr = 0.2, and heading angle = 180°

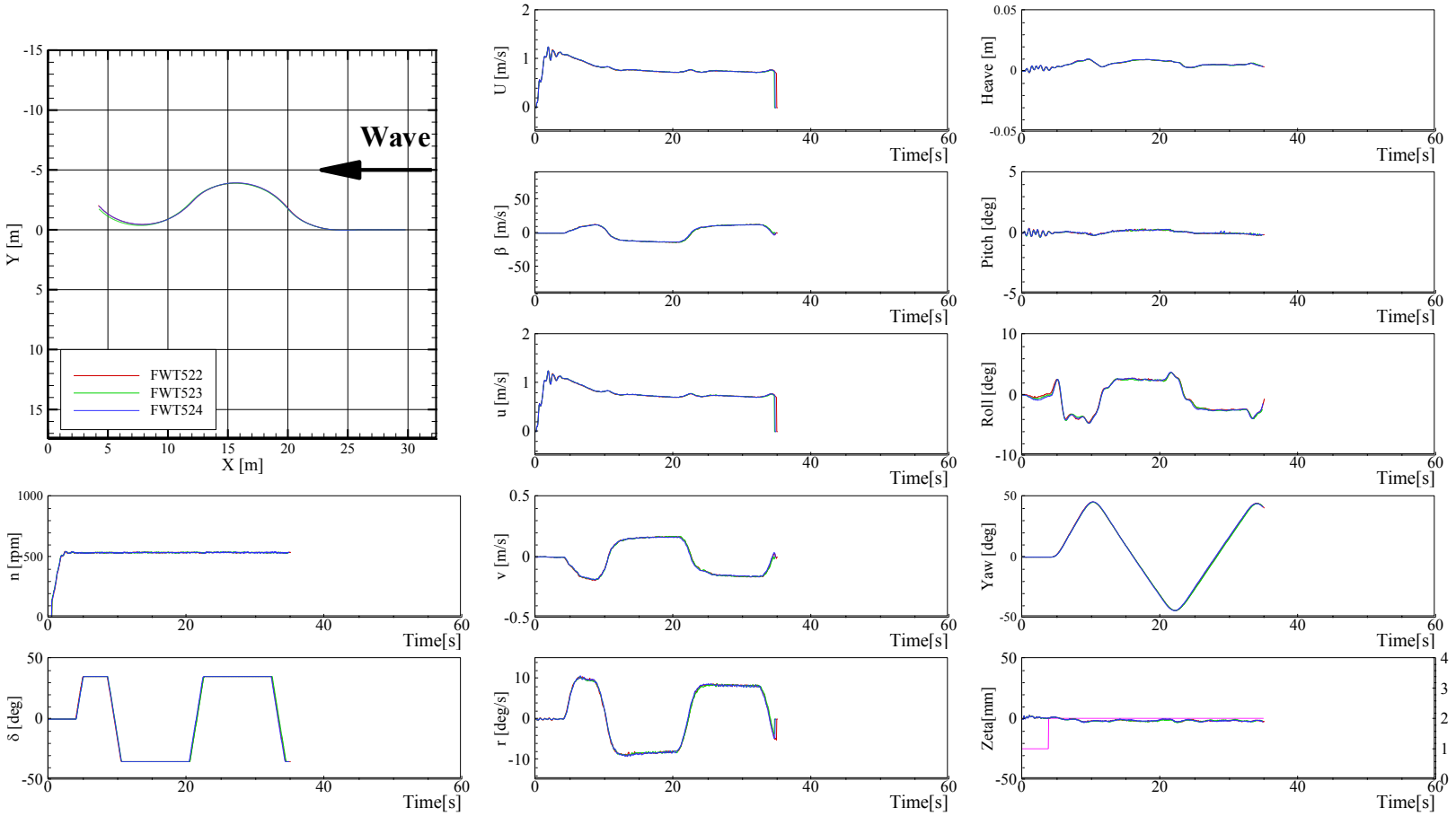

Figure D-6 Trajectories and time histories of zigzag 35°/35° in calm water at Fr = 0.2, and heading angle = 180°

APPENDIX E TRAJECTORIES AND TIME HISTORIES RESULTS OF ZIGZAG TESTS IN WAVES

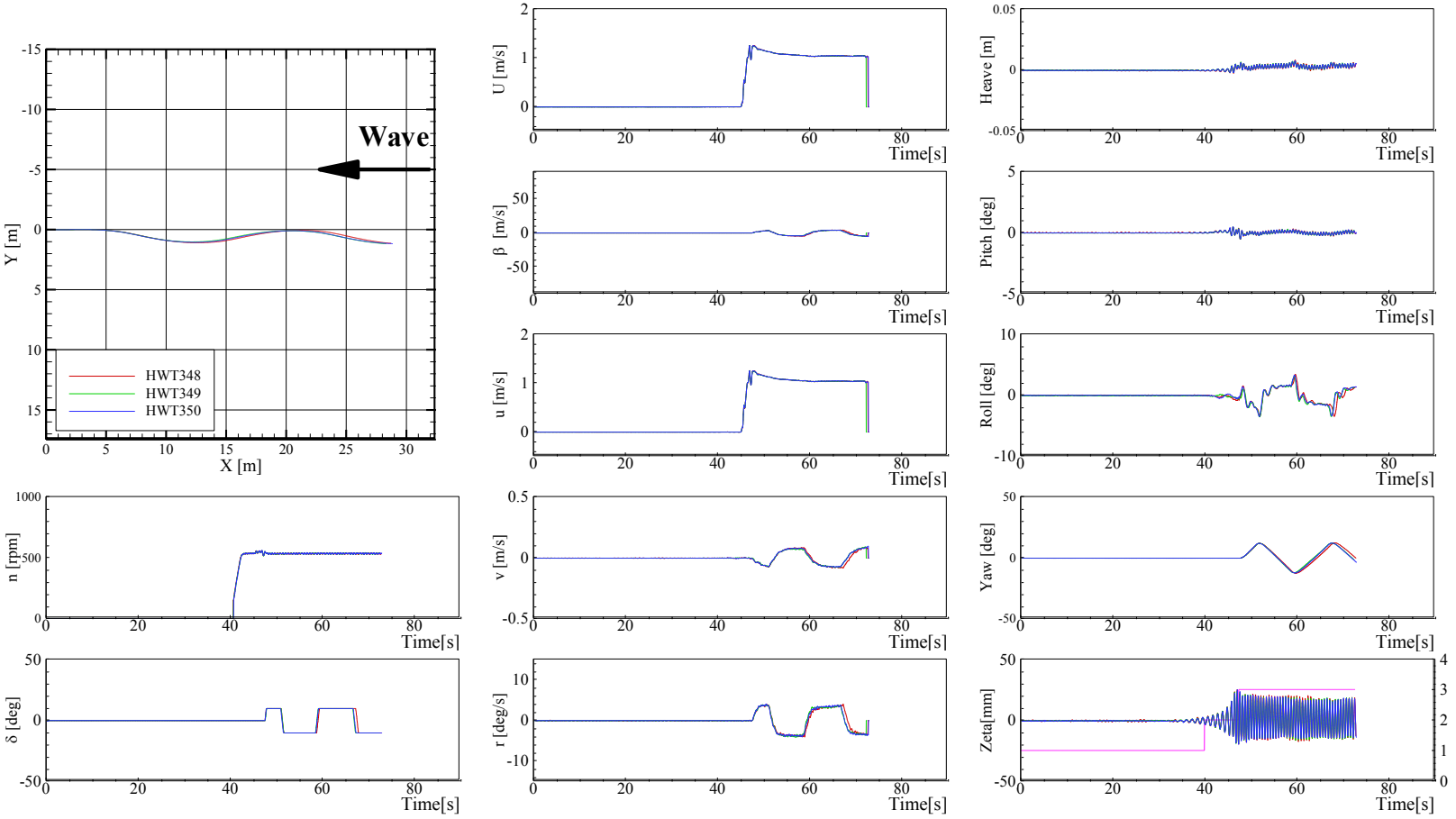

Figure E-1 Trajectories and time histories of zigzag 10°/10° in head waves at Fr = 0.2, λ/L = 0.5, and H/λ = 0.02

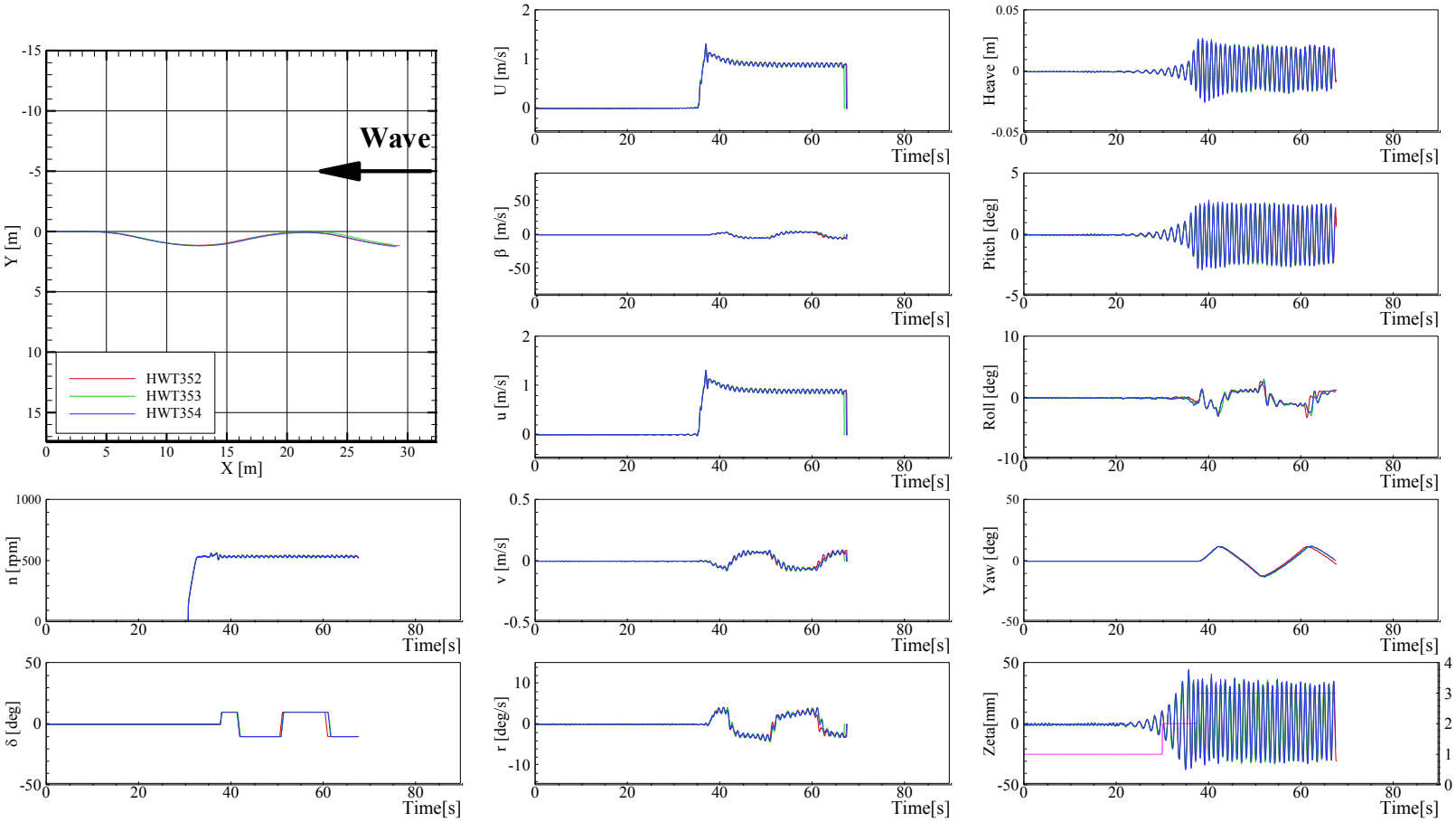

Figure E-2 Trajectories and time histories of zigzag 10°/10° in head waves at Fr = 0.2, λ/L = 1.0, and H/λ = 0.02

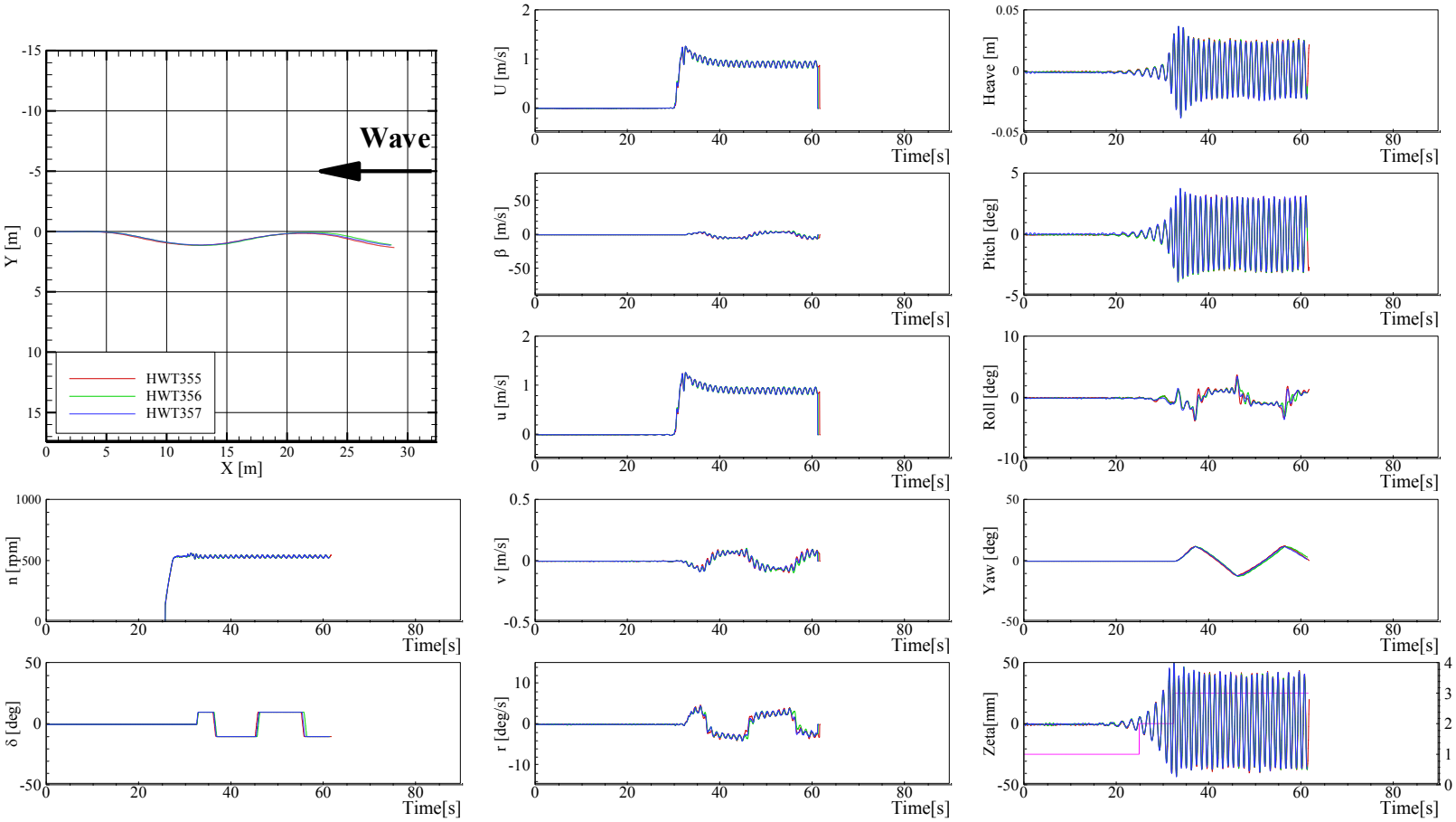

Figure E-3 Trajectories and time histories of zigzag 10°/10° in head waves at Fr = 0.2, λ/L = 1.2, and H/λ = 0.02

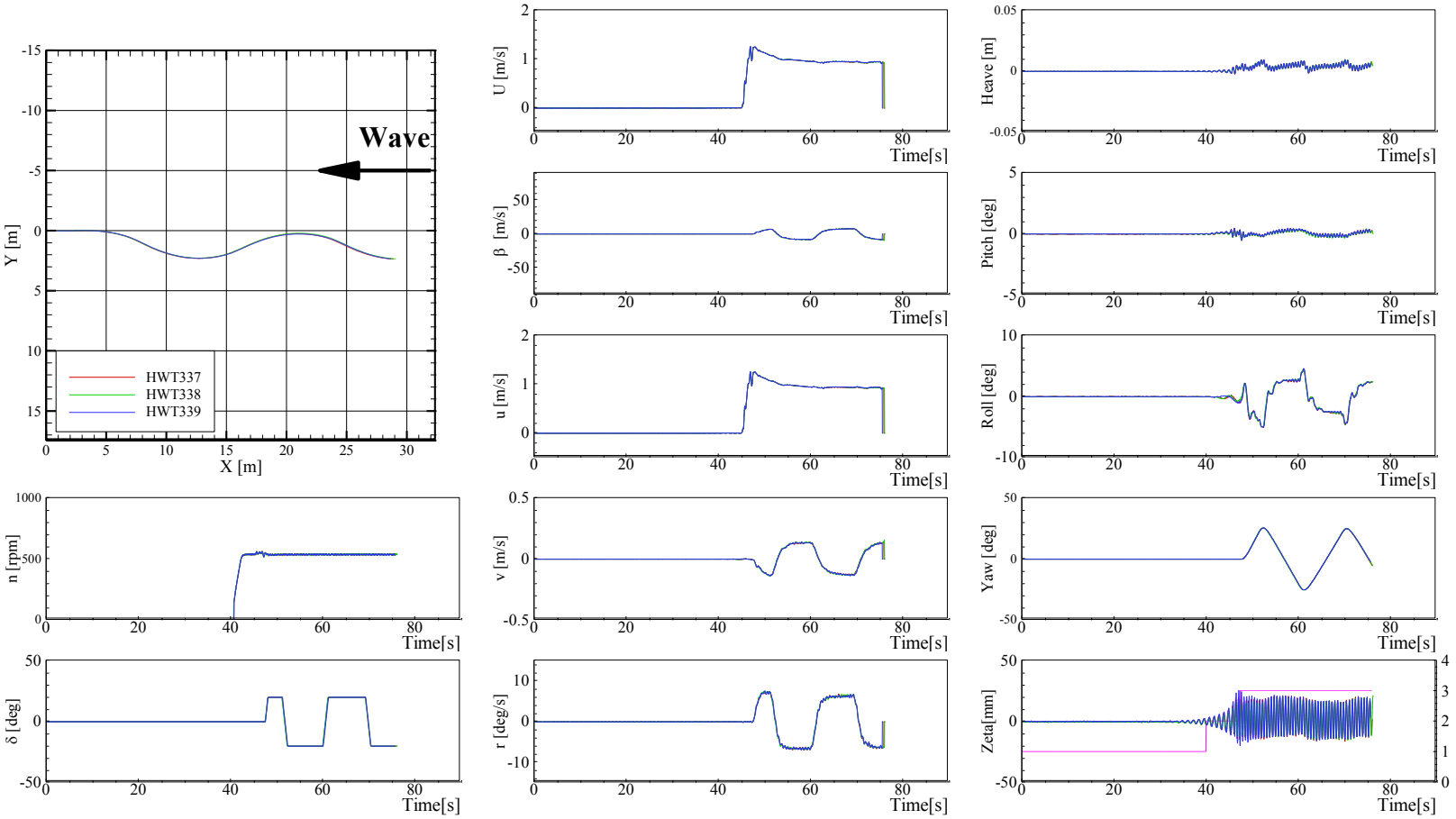

Figure E-4 Trajectories and time histories of zigzag 20°/20° in head waves at Fr = 0.2, λ/L = 0.5, and H/λ = 0.02

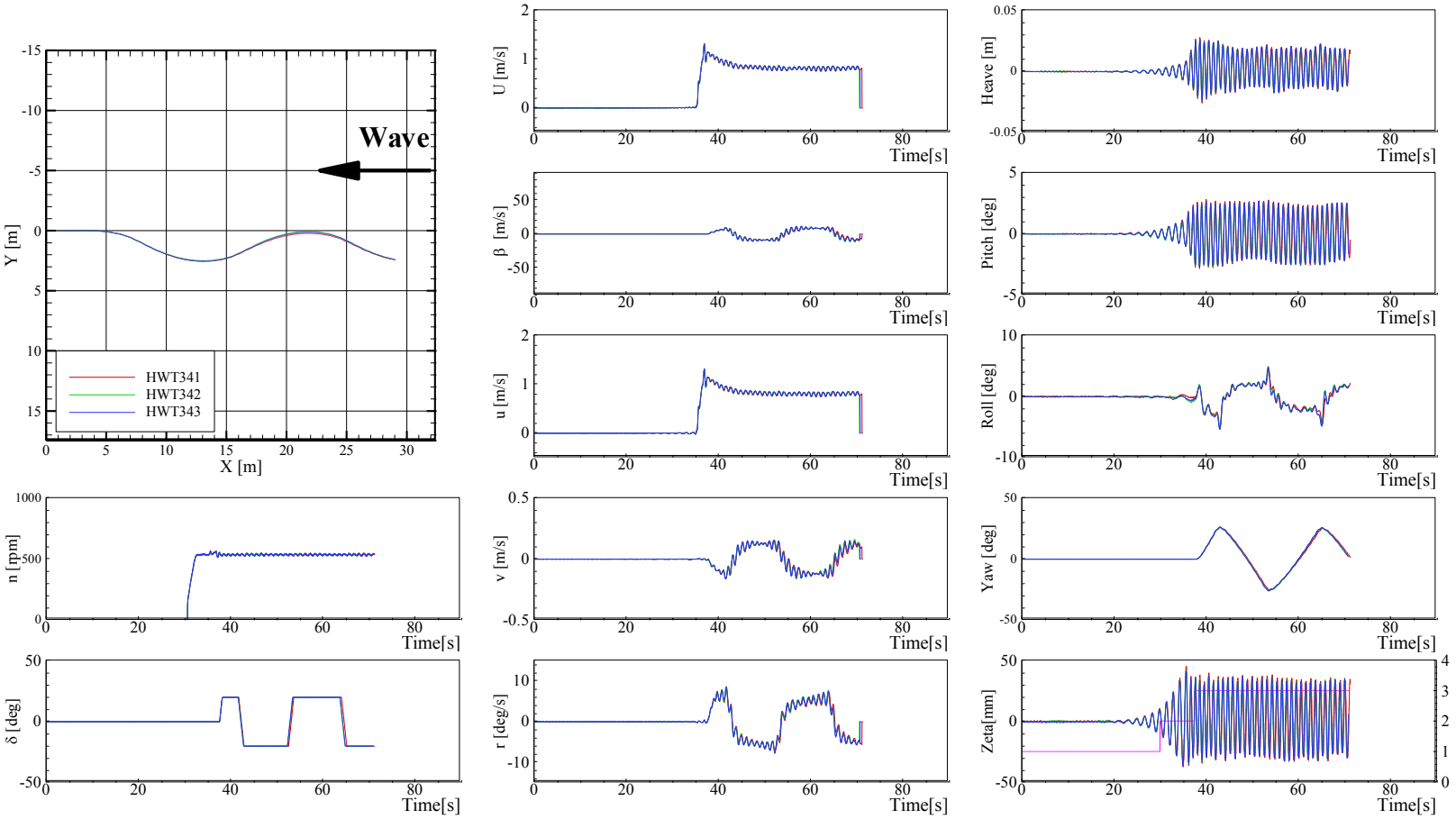

Figure E-5 Trajectories and time histories of zigzag 20°/20° in head waves at Fr = 0.2, λ/L = 1.0, and H/λ = 0.02

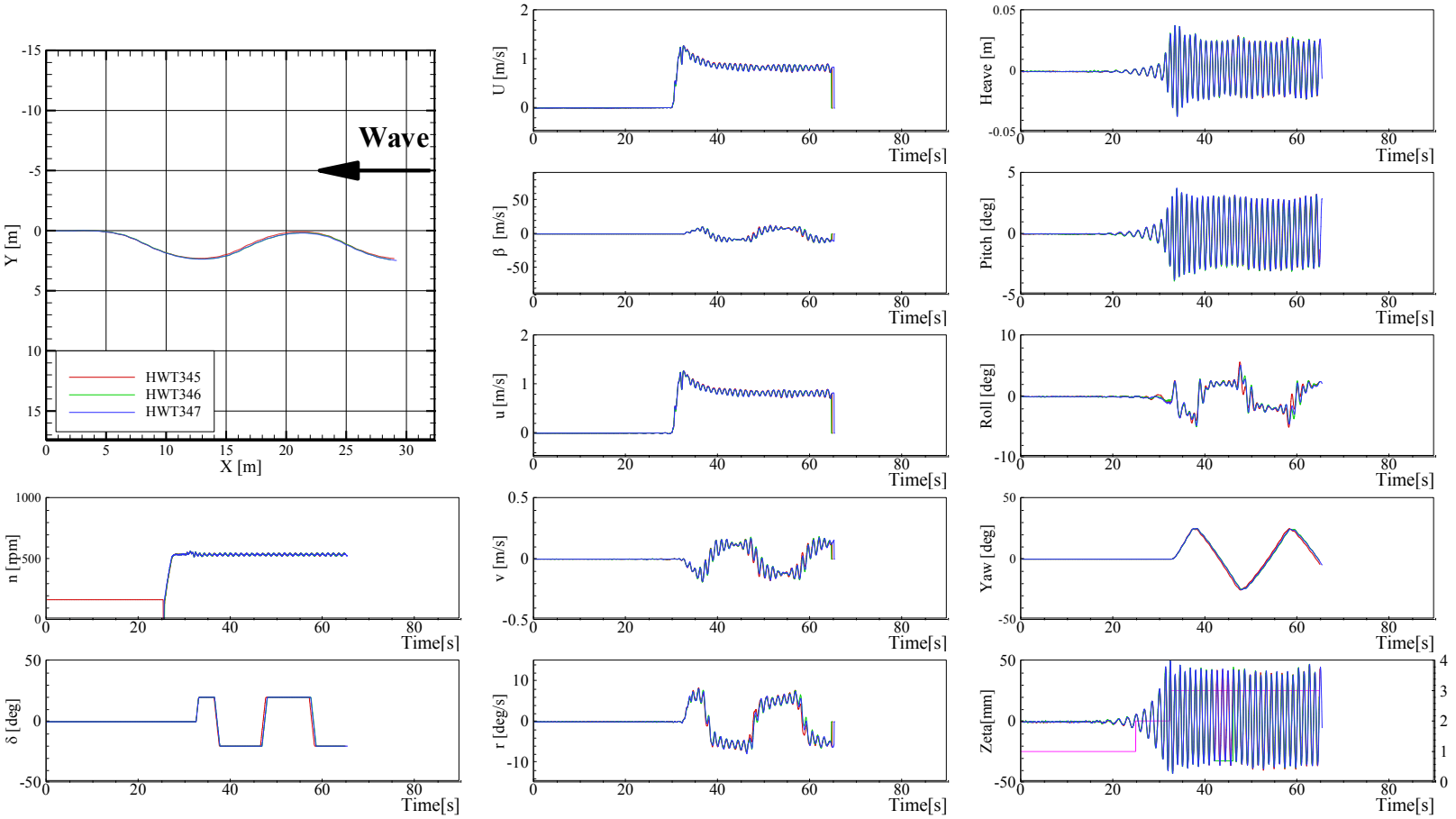

Figure E-6 Trajectories and time histories of zigzag 20°/20° in head waves at Fr = 0.2, λ/L = 1.2, and H/λ = 0.02

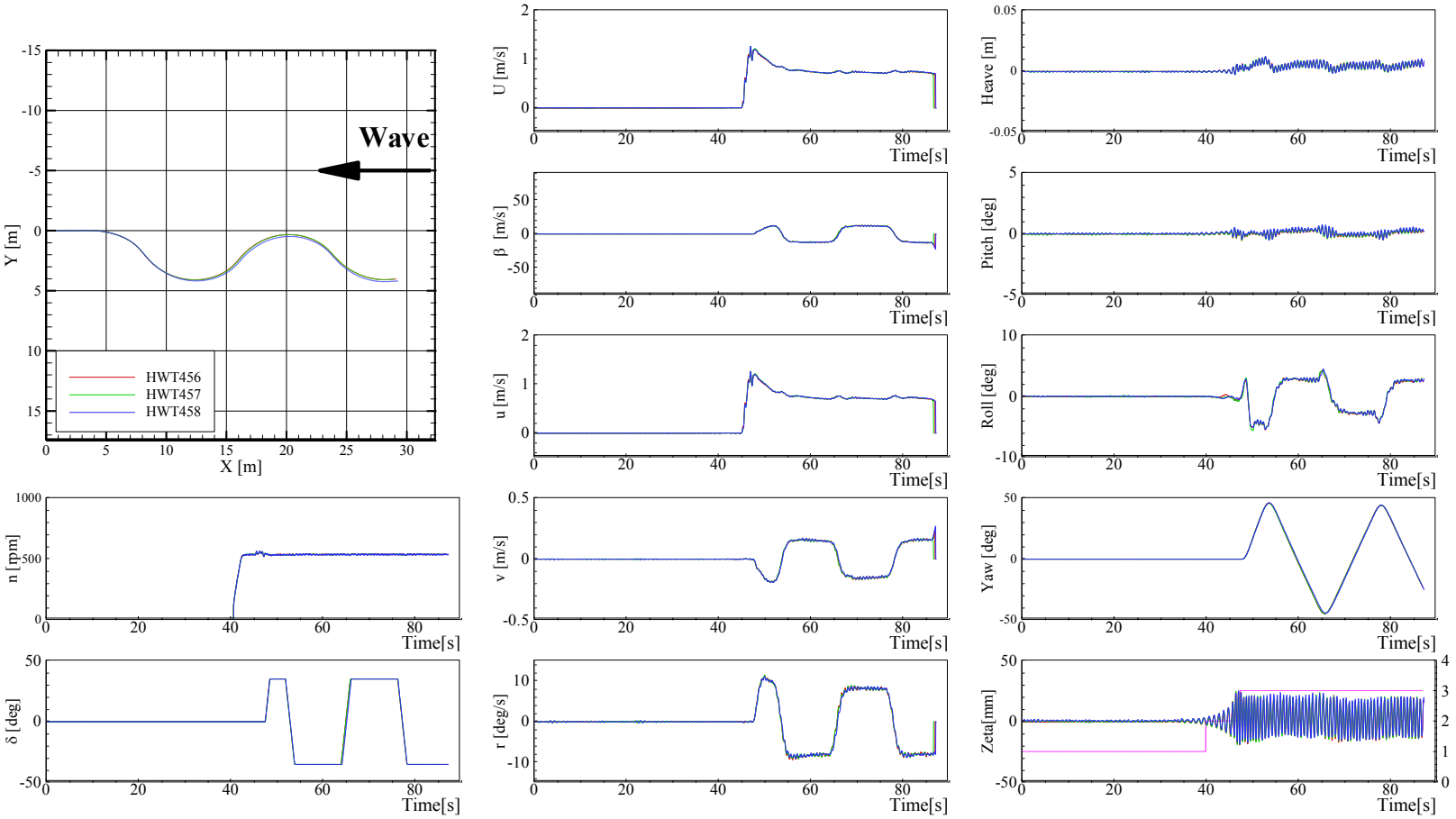

Figure E-7 Trajectories and time histories of zigzag 35°/35° in head waves at Fr = 0.2, λ/L = 0.5, and H/λ = 0.02

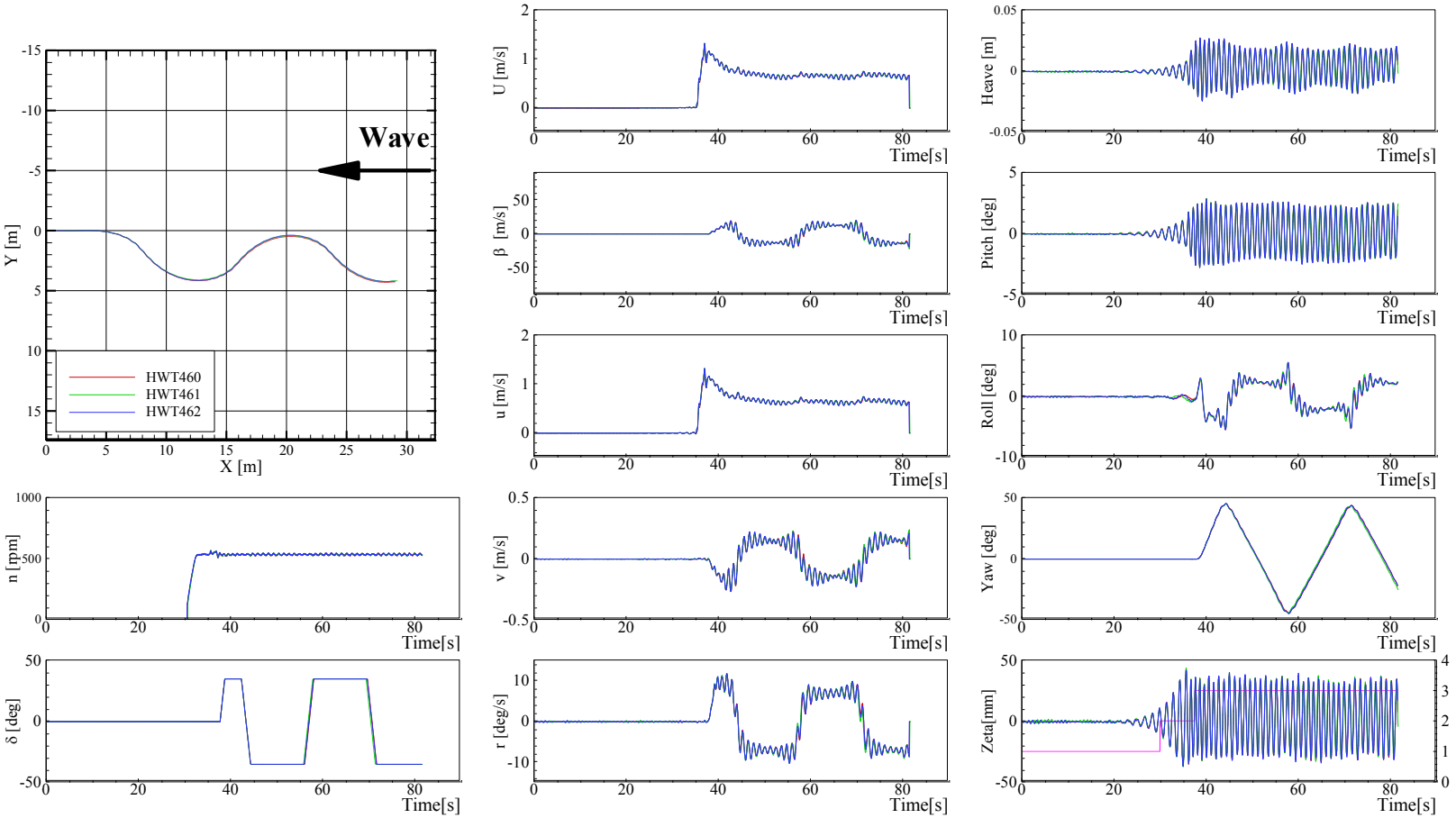

Figure E-8 Trajectories and time histories of zigzag 35°/35° in head waves at Fr = 0.2, λ/L = 1.0, and H/λ = 0.02

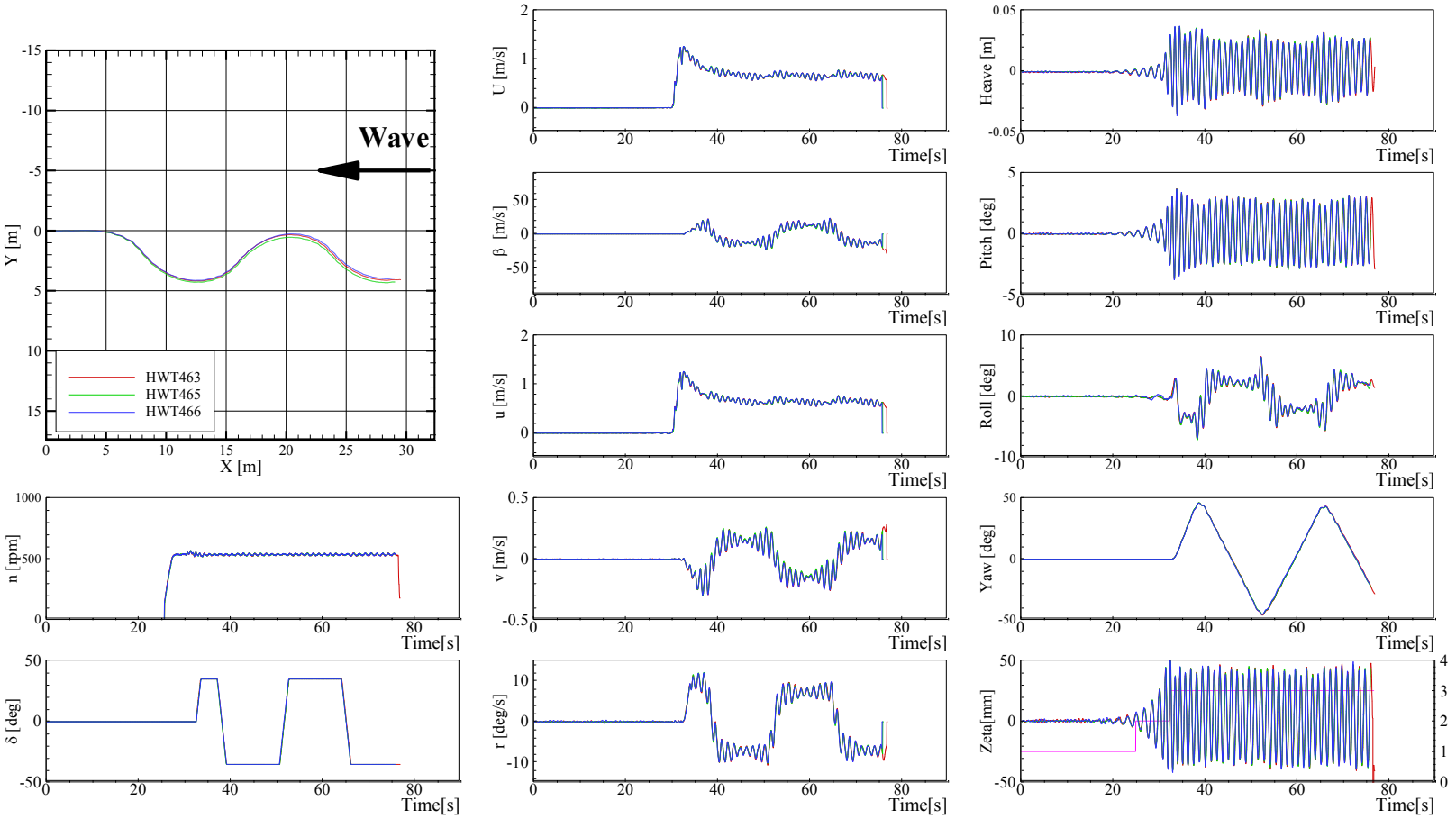

Figure E-9 Trajectories and time histories of zigzag 35°/35° in head waves at Fr = 0.2, λ/L = 1.2, and H/λ = 0.02

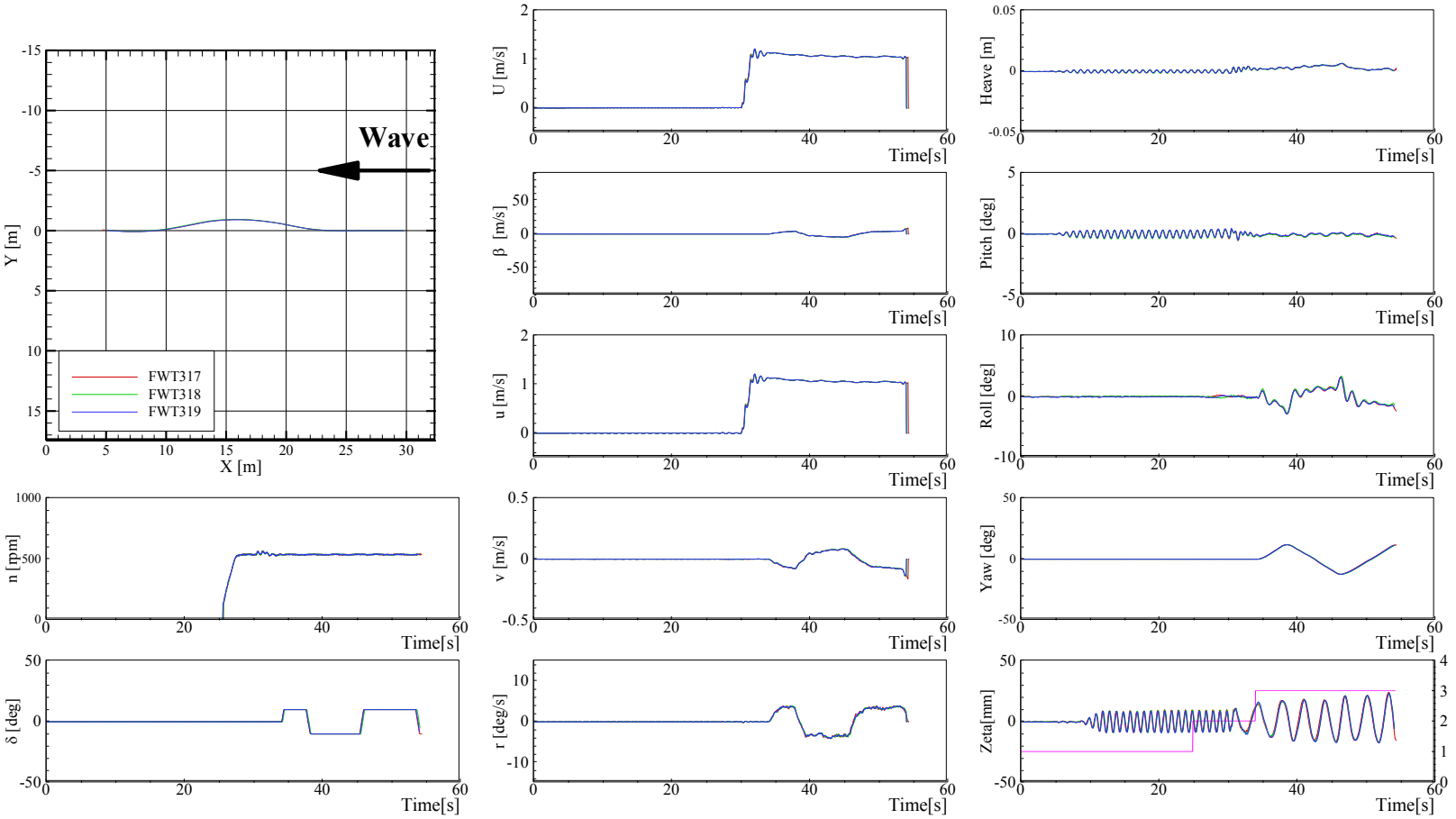

Figure E-10 Trajectories and time histories of zigzag 10°/10° in following waves at Fr = 0.2, λ/L = 0.5, and H/λ = 0.02

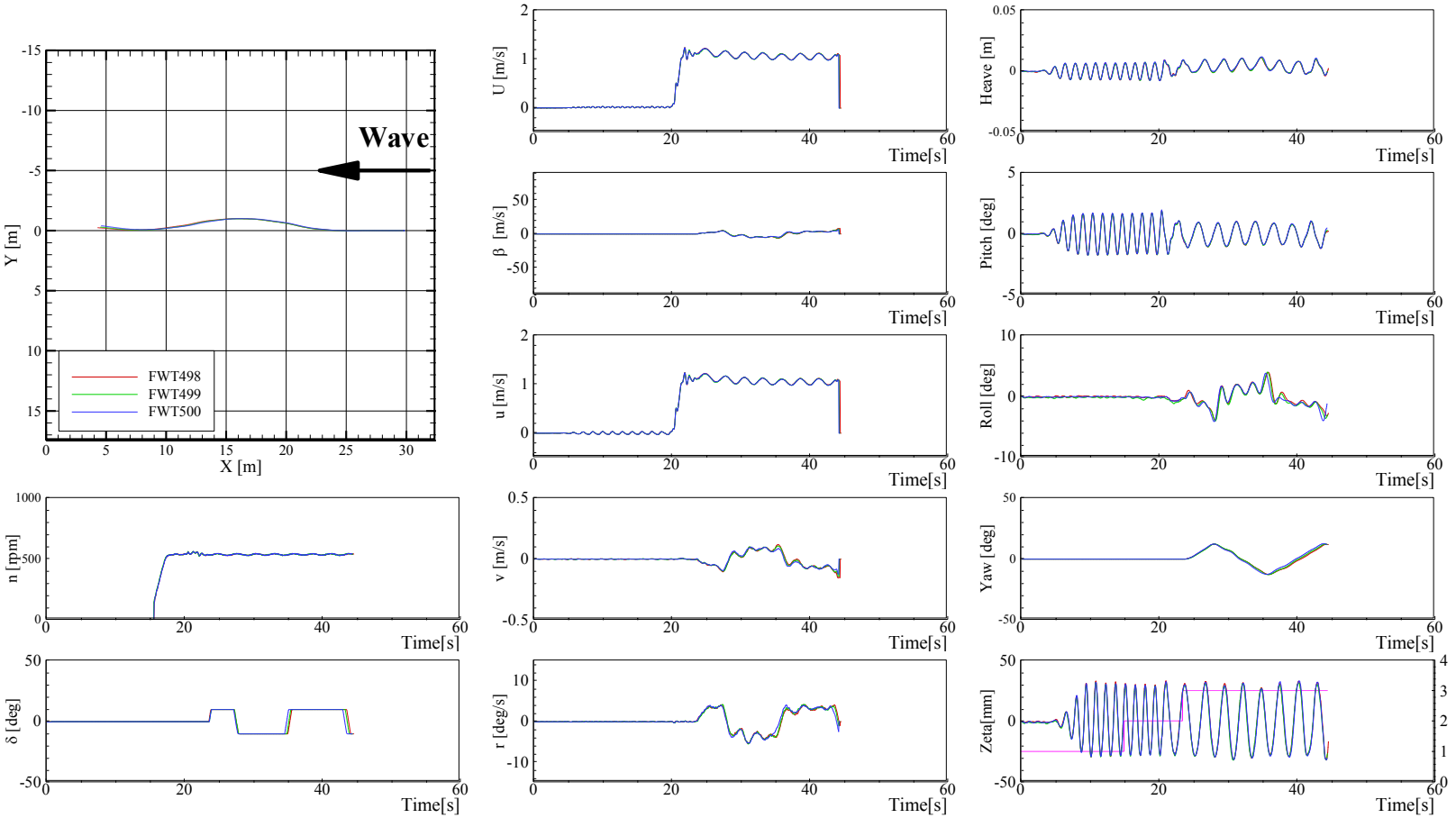

Figure E-11 Trajectories and time histories of zigzag 10°/10° in following waves at Fr = 0.2, λ/L = 1.0 and H/λ = 0.02

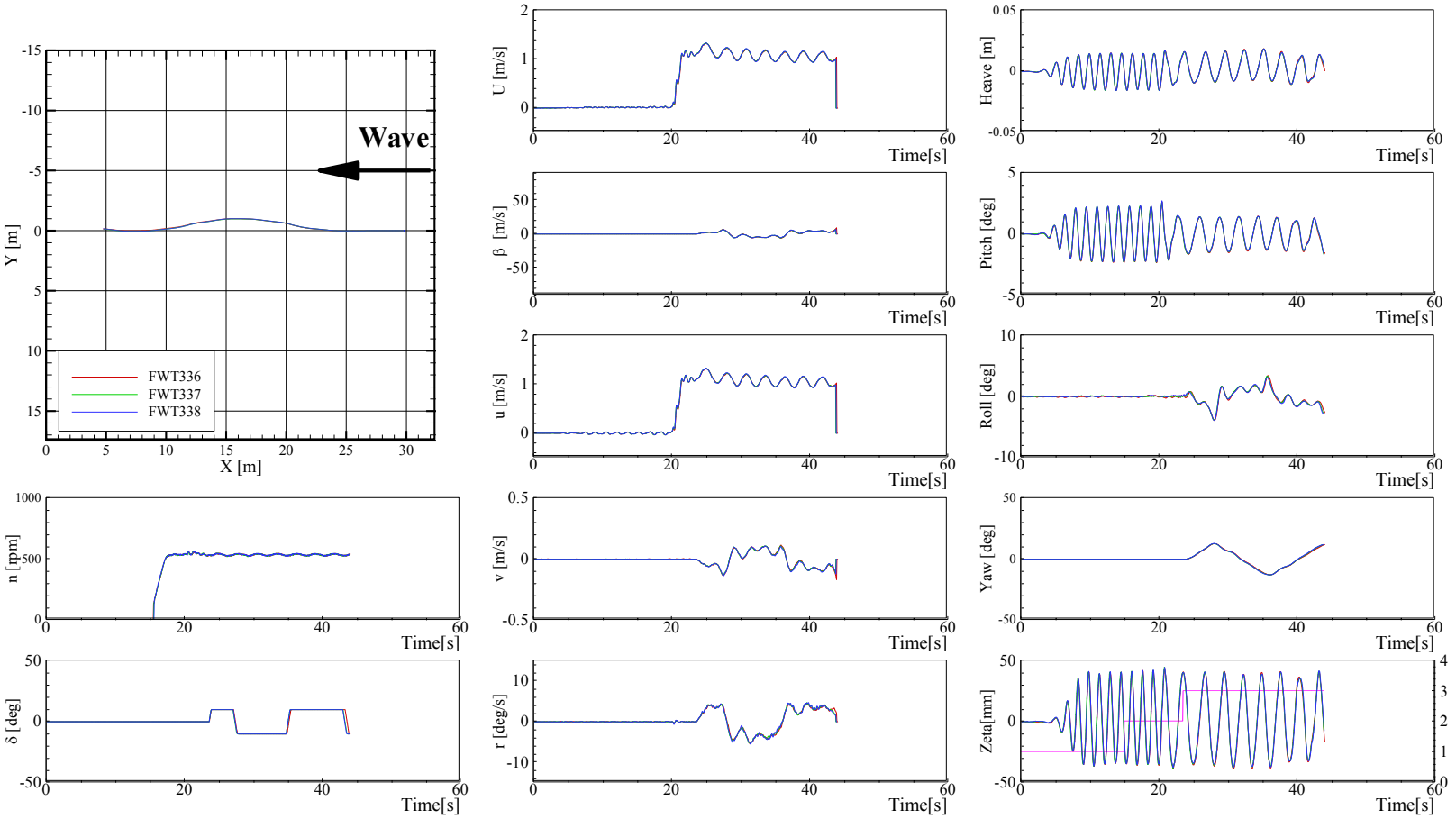

Figure E-12 Trajectories and time histories of zigzag 10°/10° in following waves at Fr = 0.2, λ/L = 1.2, and H/λ = 0.02

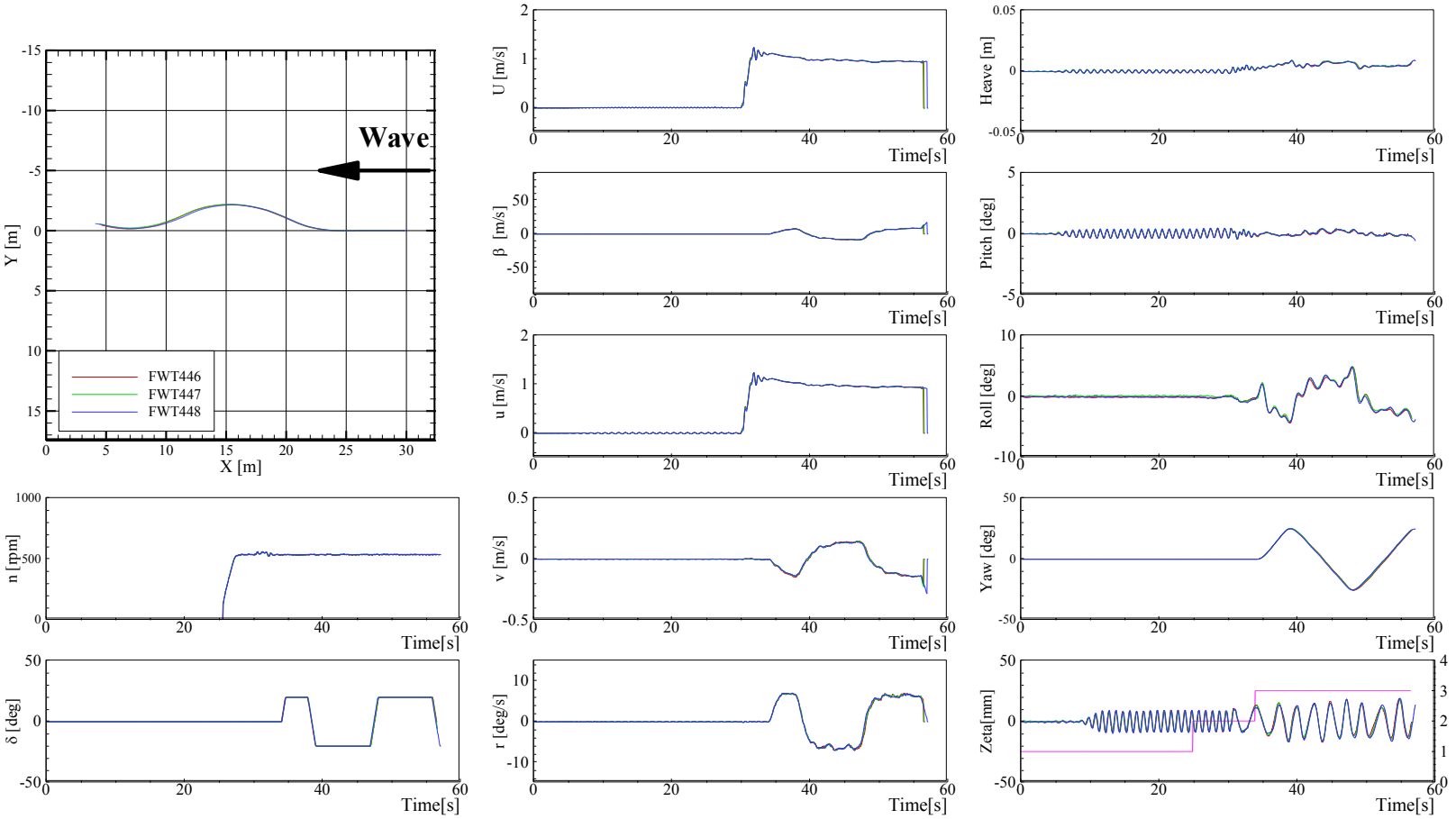

Figure E-13 Trajectories and time histories of zigzag 20°/20° in following waves at Fr = 0.2, λ/L = 0.5, and H/λ = 0.02

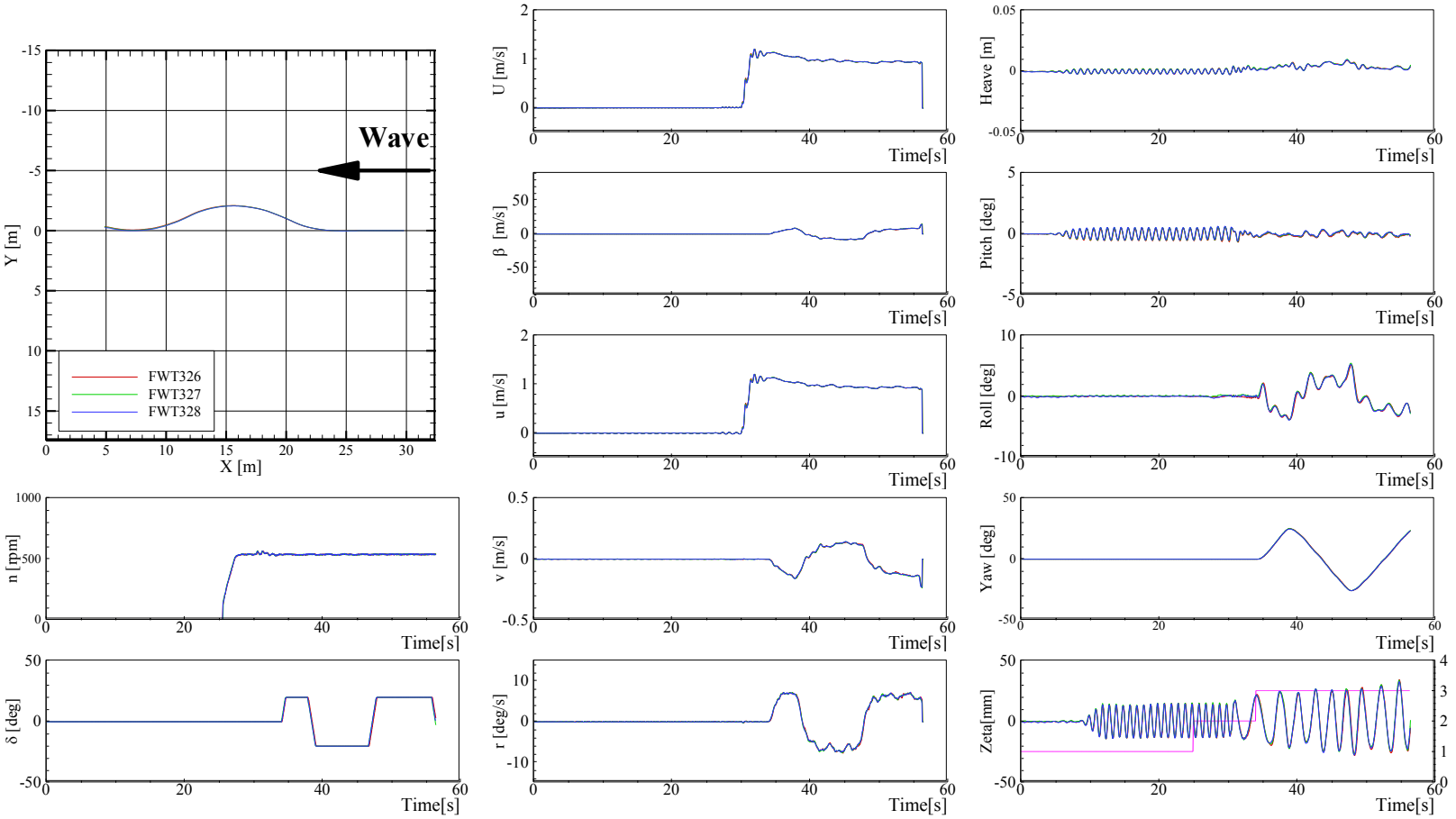

Figure E-14 Trajectories and time histories of zigzag 20°/20° in following waves at Fr = 0.2, λ/L = 0.5, and H/λ = 0.03

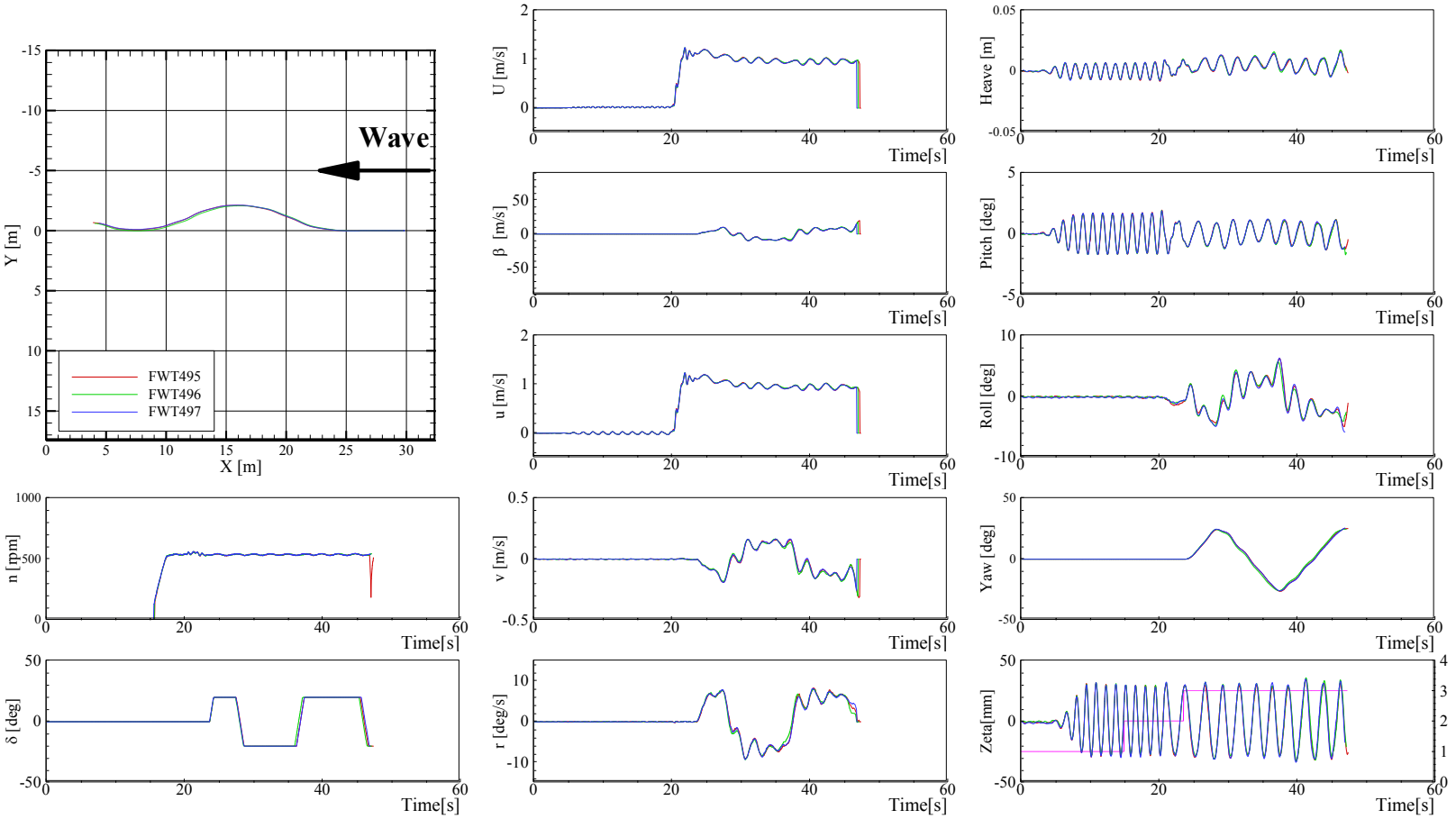

Figure E-15 Trajectories and time histories of zigzag 20°/20° in following waves at Fr = 0.2, λ/L = 1.0, and H/λ = 0.02

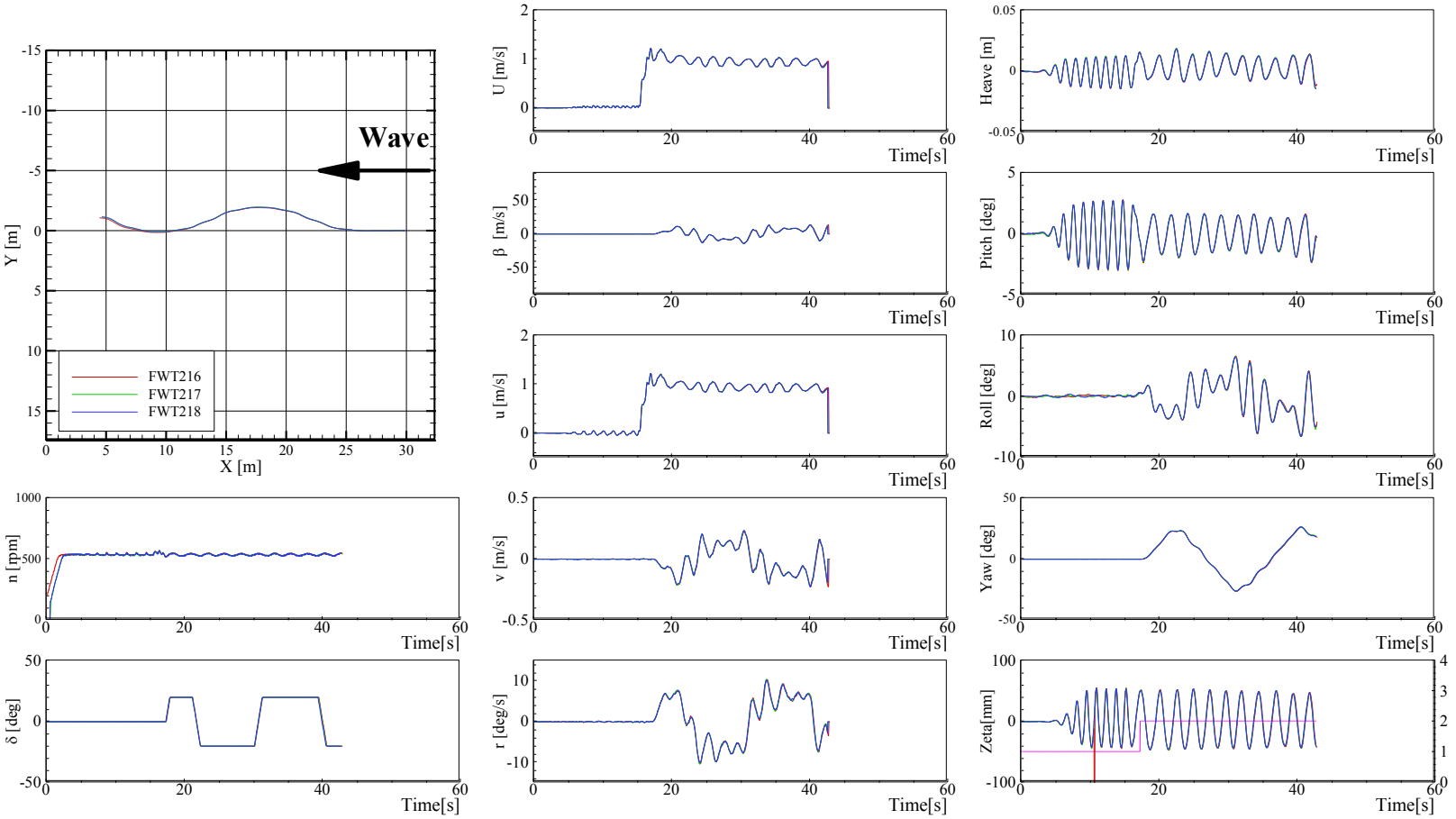

Figure E-16 Trajectories and time histories of zigzag 20°/20° in following waves at Fr = 0.2, λ/L = 1.0, and H/λ = 0.03

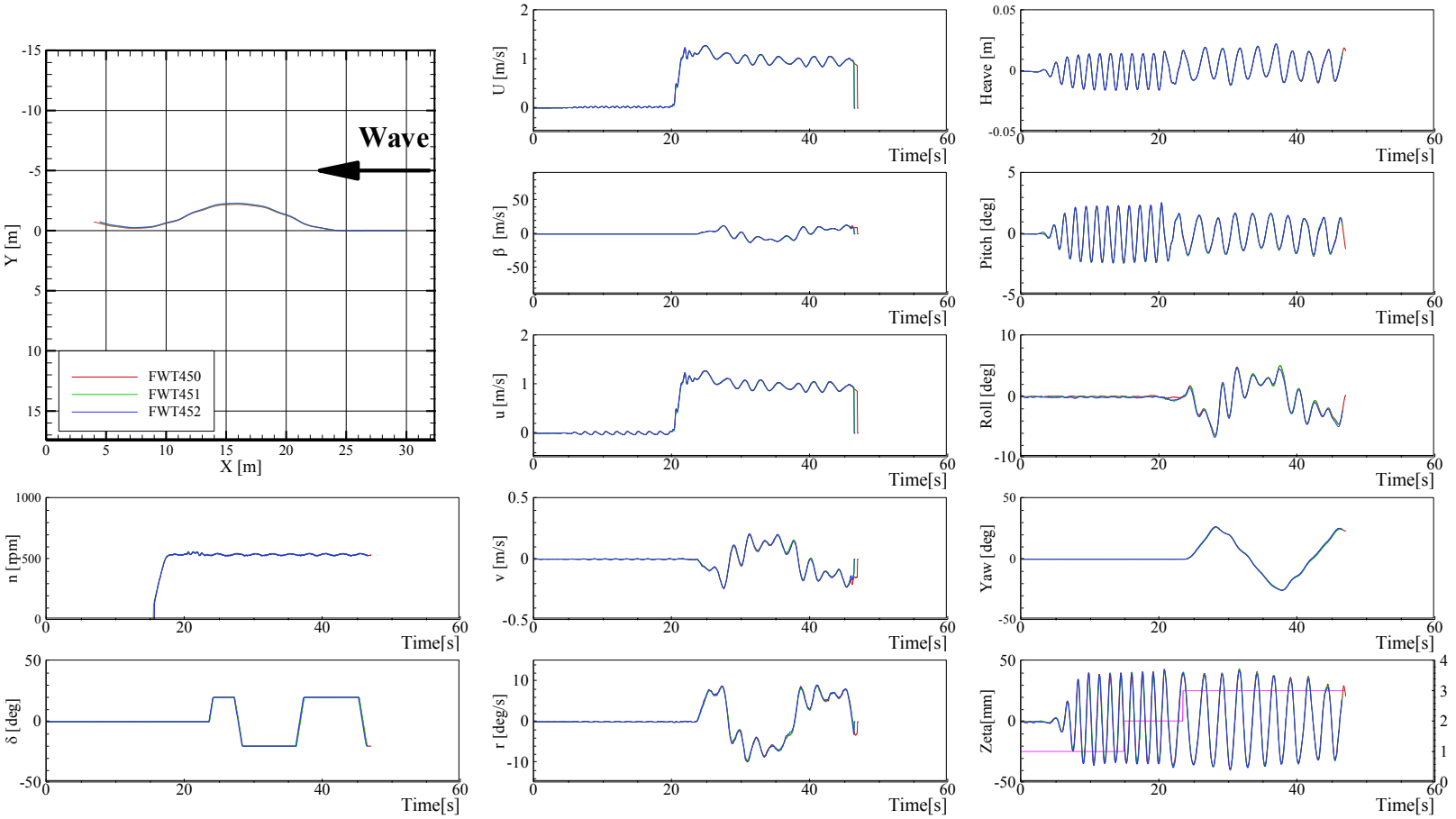

Figure E-17 Trajectories and time histories of zigzag 20°/20° in following waves at Fr = 0.2, λ/L = 1.2, and H/λ = 0.02

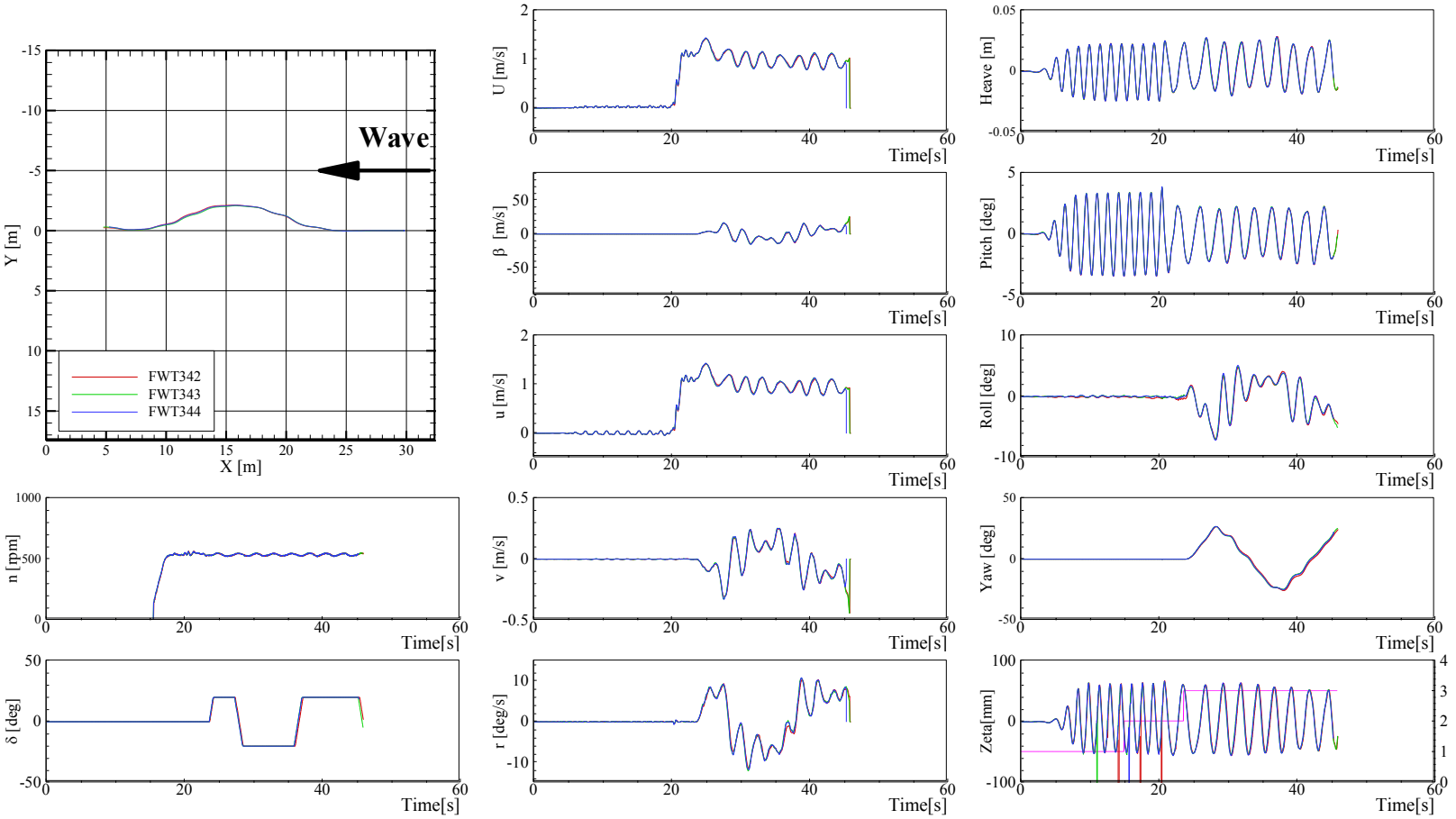

Figure E-18 Trajectories and time histories of zigzag 20°/20° in following waves at Fr = 0.2, λ/L = 1.2, and H/λ = 0.03

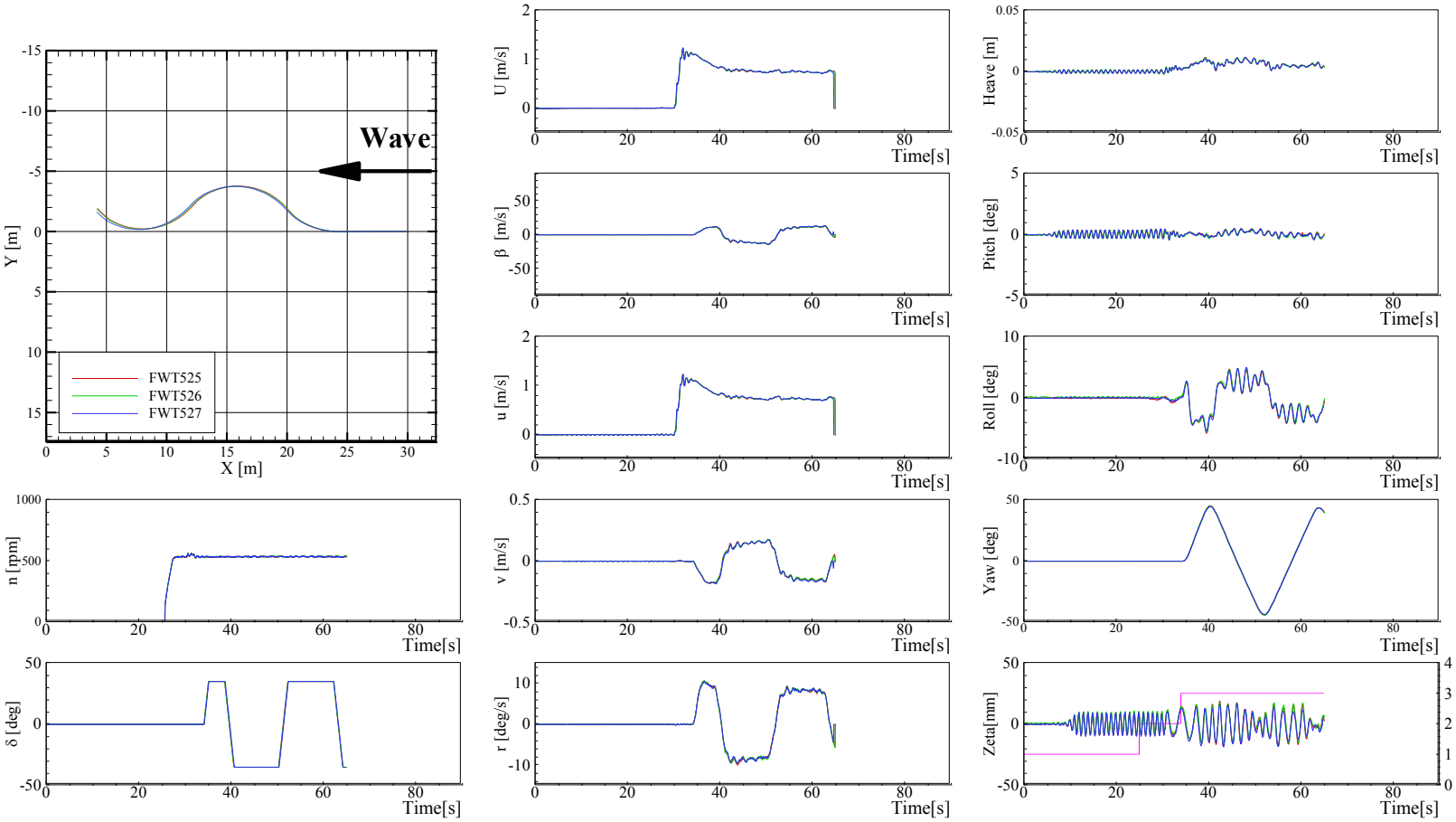

Figure E-19 Trajectories and time histories of zigzag 35°/35° in following waves at Fr = 0.2, λ/L = 0.5, and H/λ = 0.02

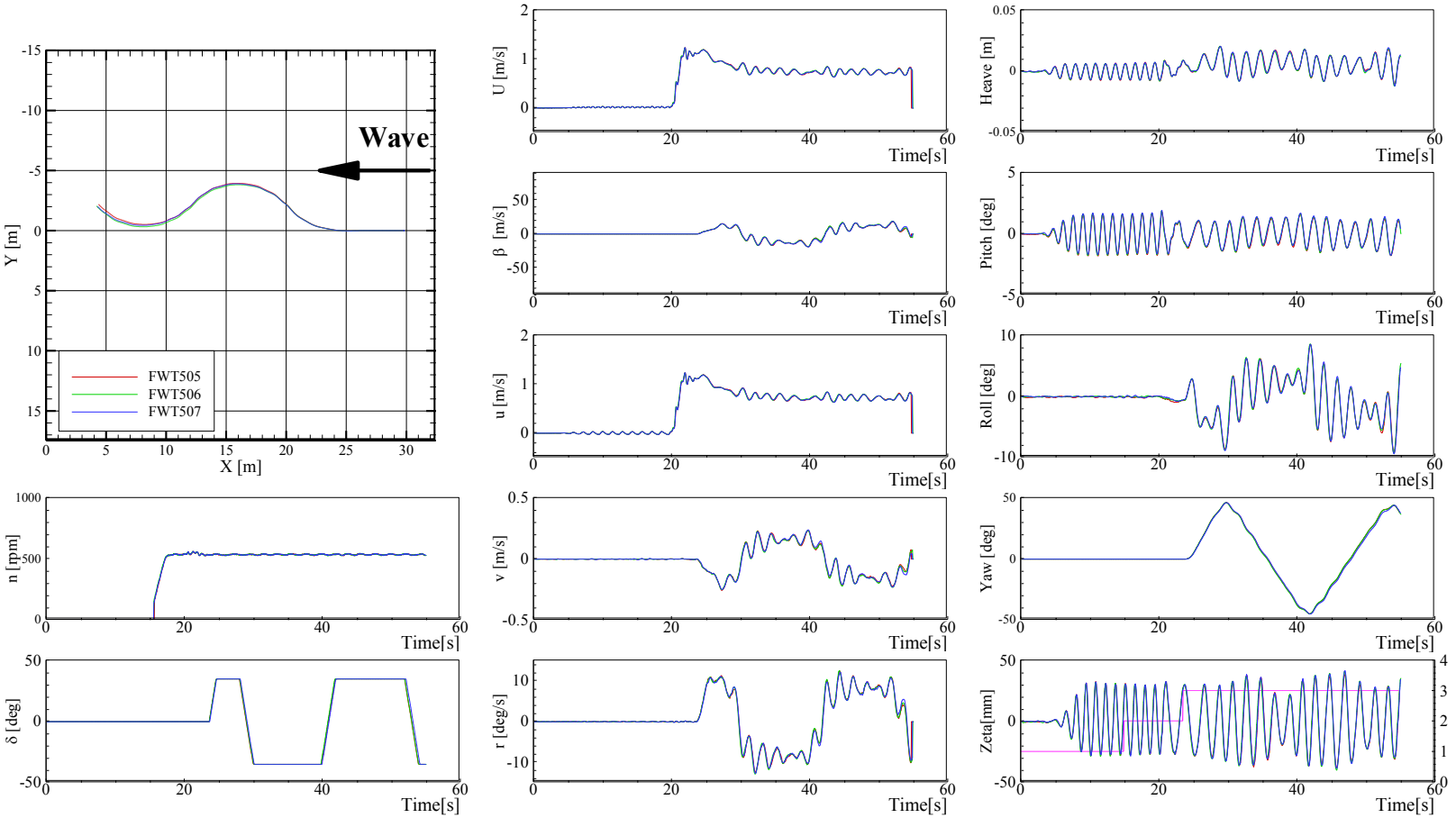

Figure E-20 Trajectories and time histories of zigzag 35°/35° in following waves at Fr = 0.2, λ/L = 1.0, and H/λ = 0.02

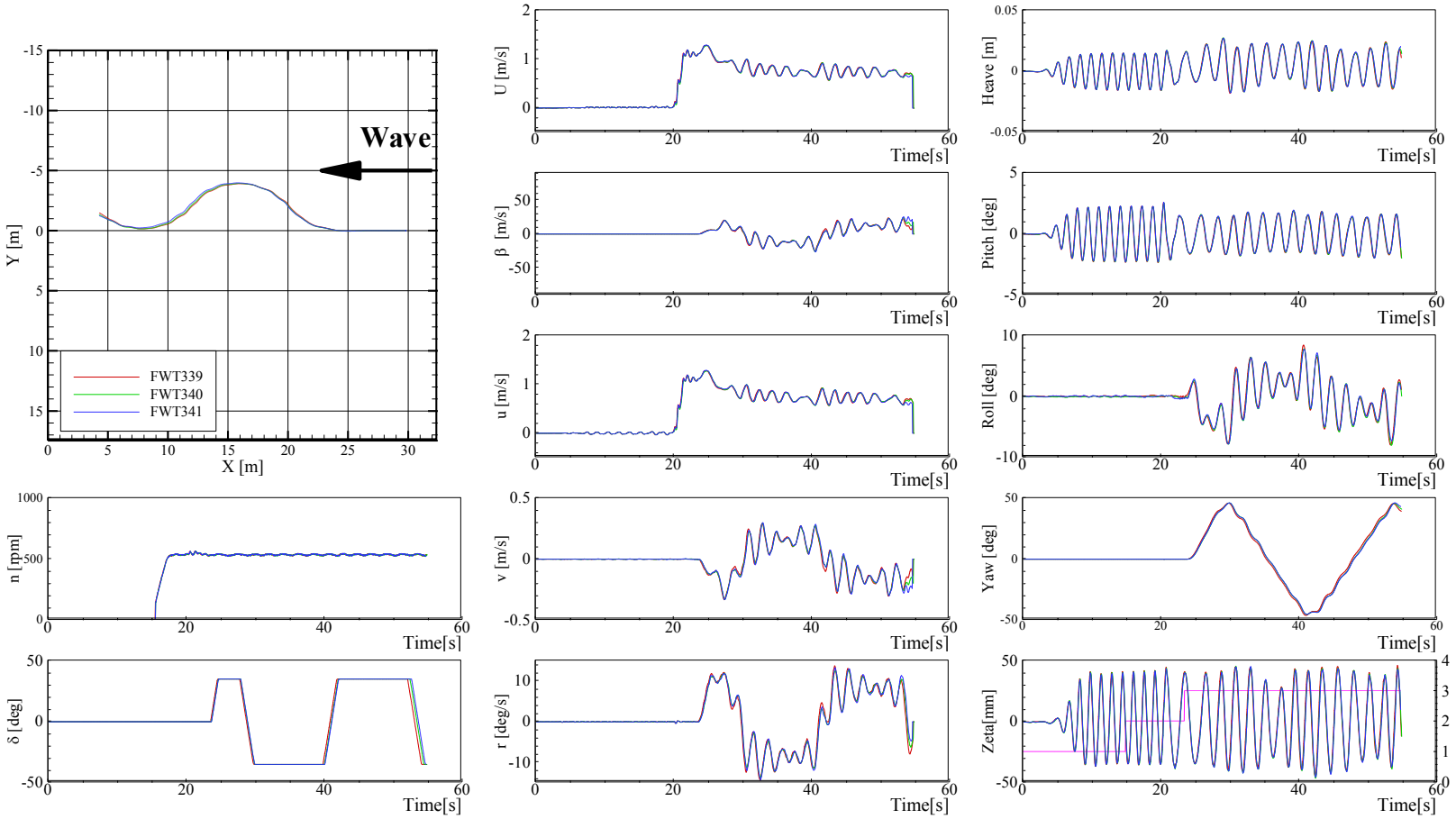

Figure E- 21 Trajectories and time histories of zigzag 35°/35° in following waves at Fr = 0.2, λ/L = 1.2, and H/λ = 0.02

APPENDIX F TRAJECTORIES AND TIME HISTORIES RESULTS OF TURNING TESTS IN CALM WATER

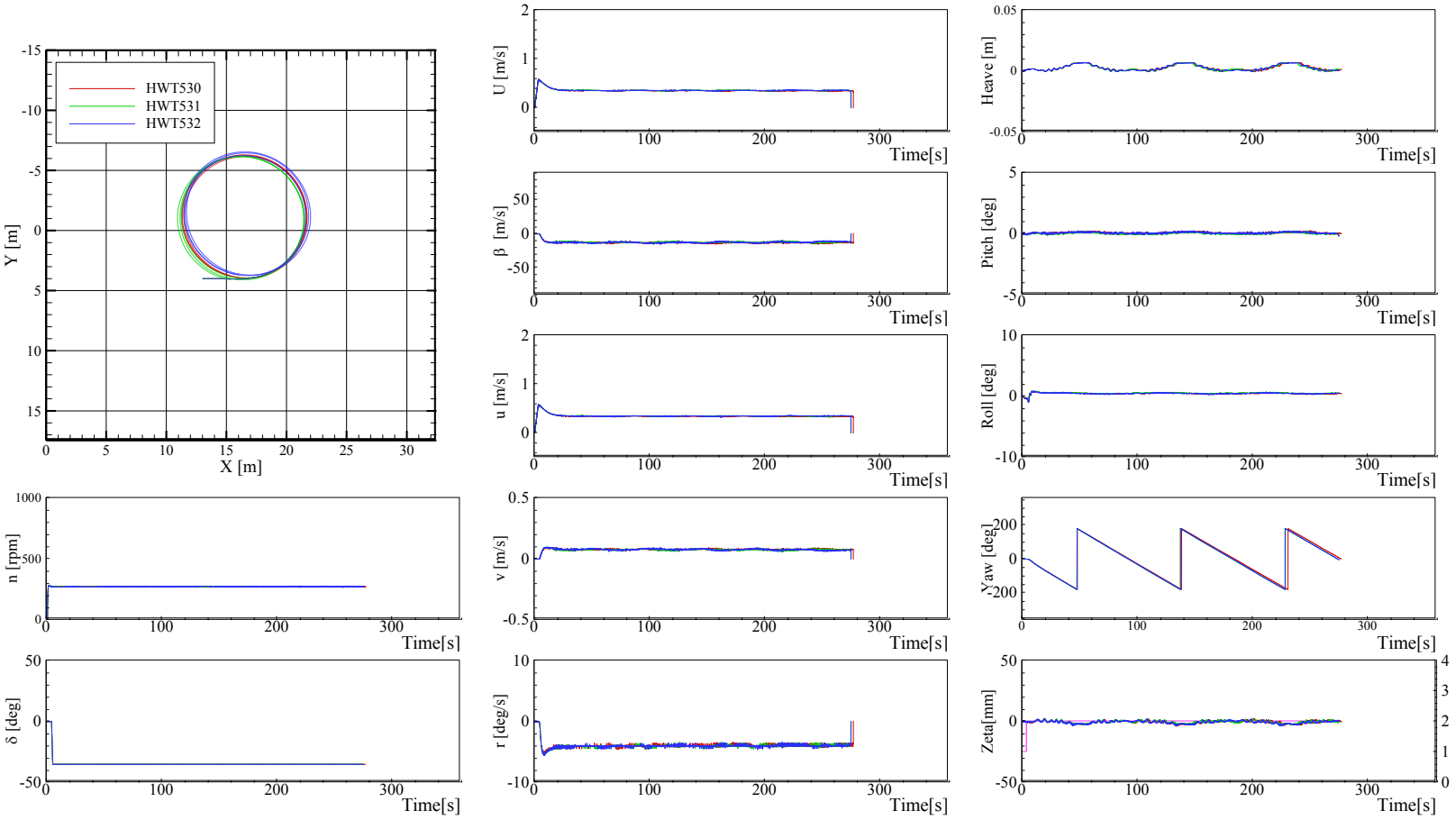

Figure F-1 Trajectories and time histories of turning in calm water at Fr = 0.1, δ = -35°, and heading angle = 0°

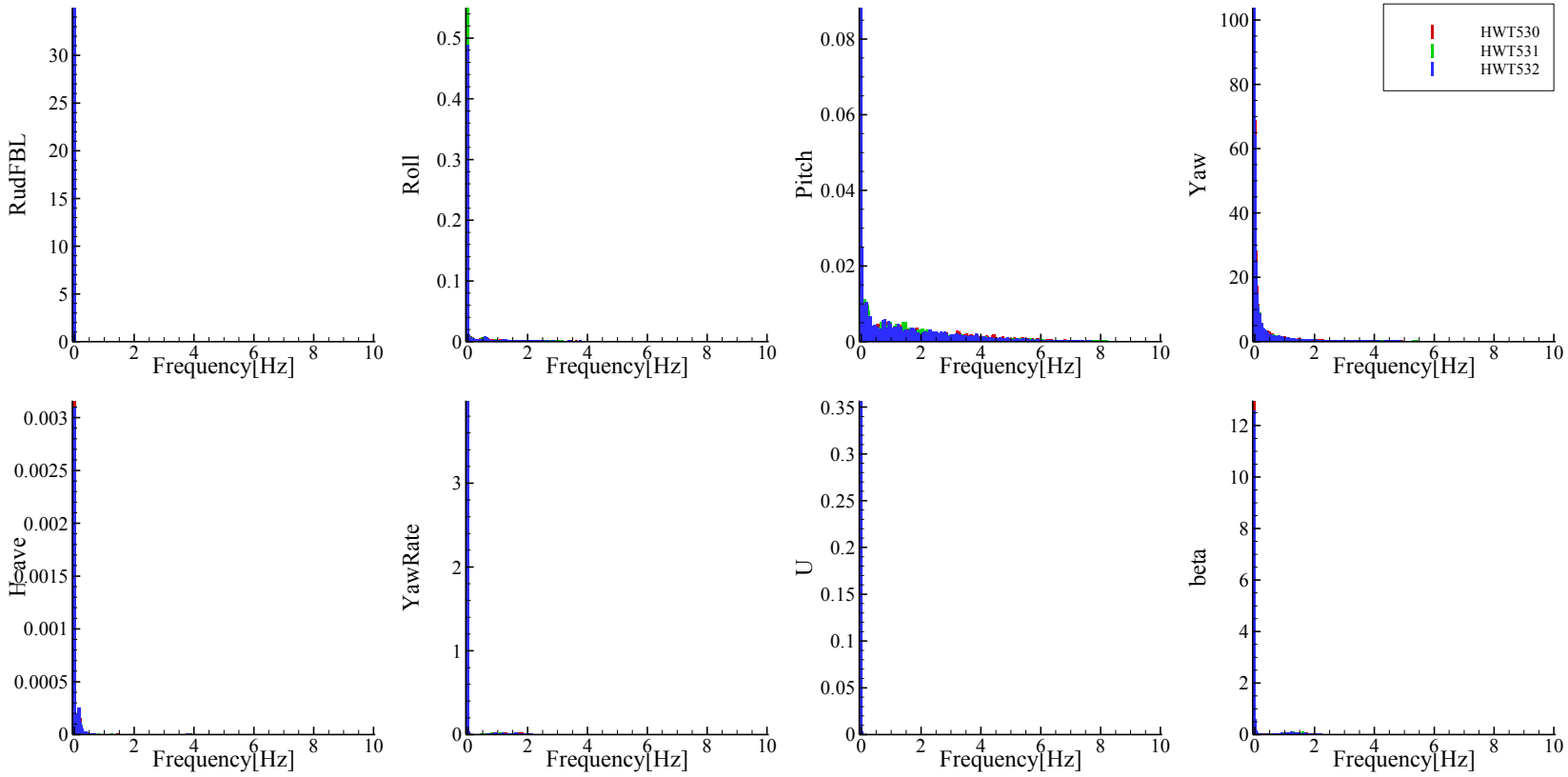

Figure F-2 FFT analysis of time histories of turning in calm water at Fr = 0.1, δ = -35°, and heading angle = 0°

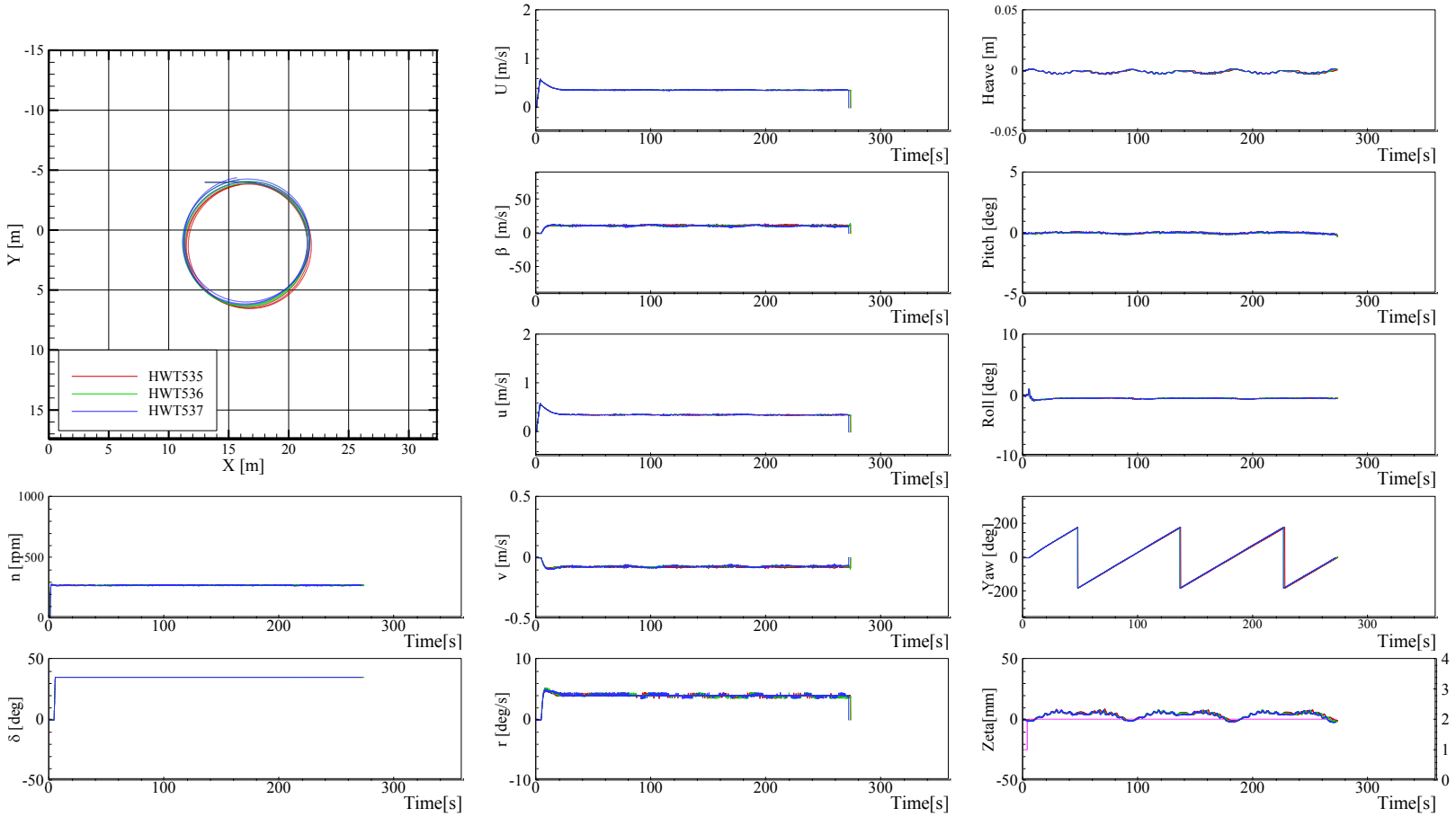

Figure F-3 Trajectories and time histories of turning in calm water at Fr = 0.1, δ = 35°, and heading angle = 0°

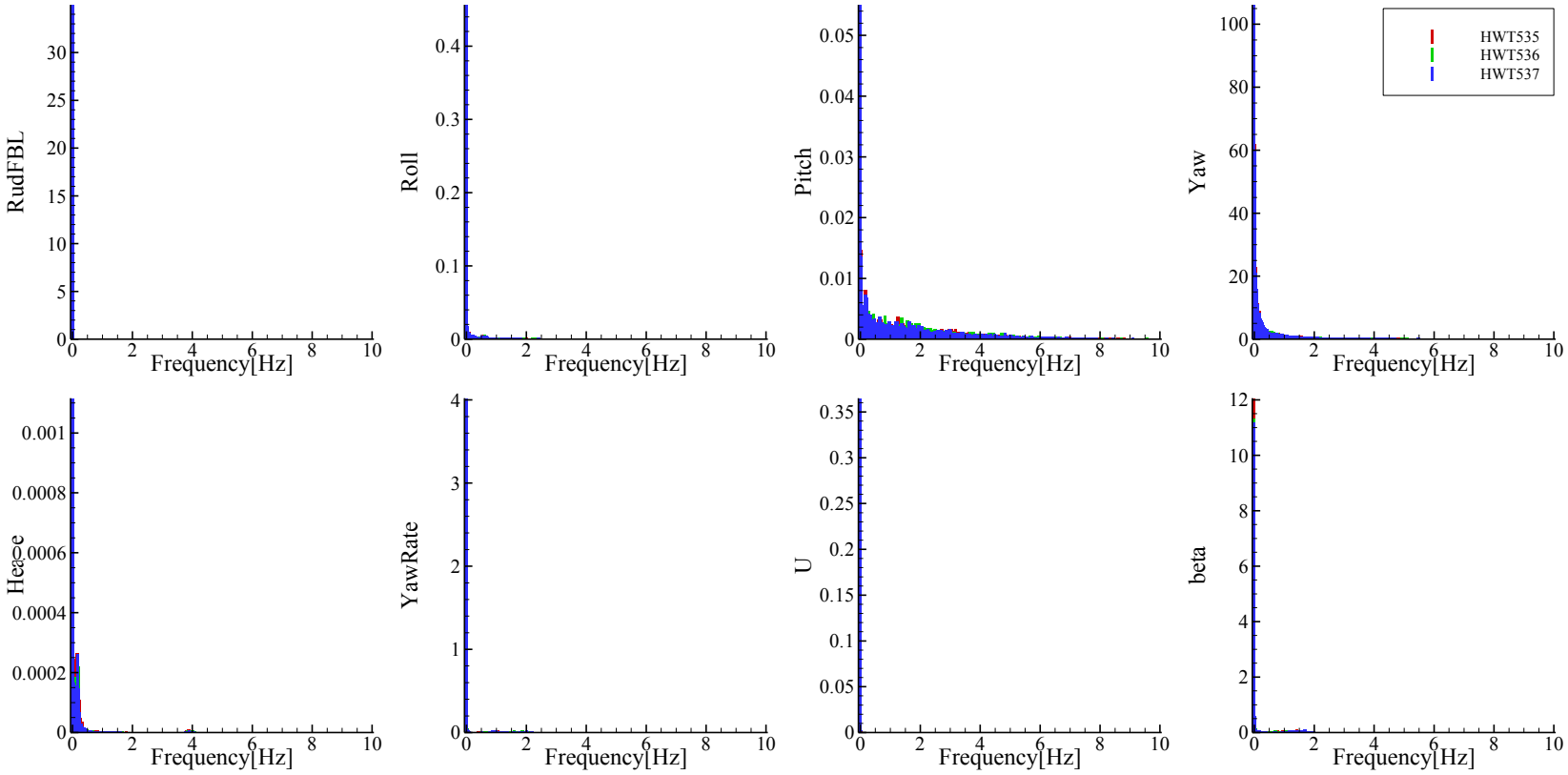

Figure F-4 FFT analysis of time histories of turning in calm water at Fr = 0.1, δ = 35°, and heading angle = 0°

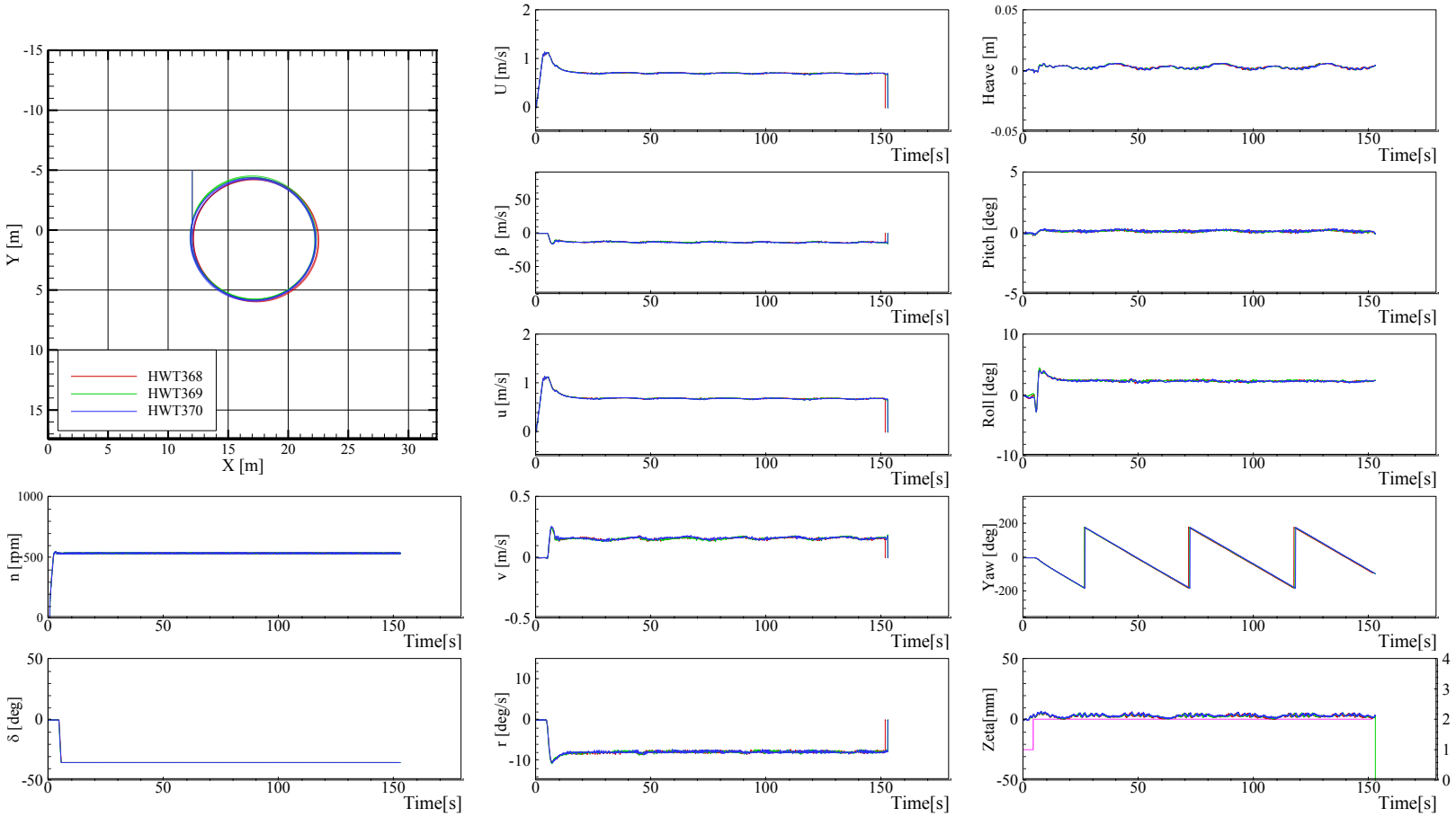

Figure F-5 Trajectories and time histories of turning in calm water at Fr = 0.2, δ = -35°, and heading angle = -90°

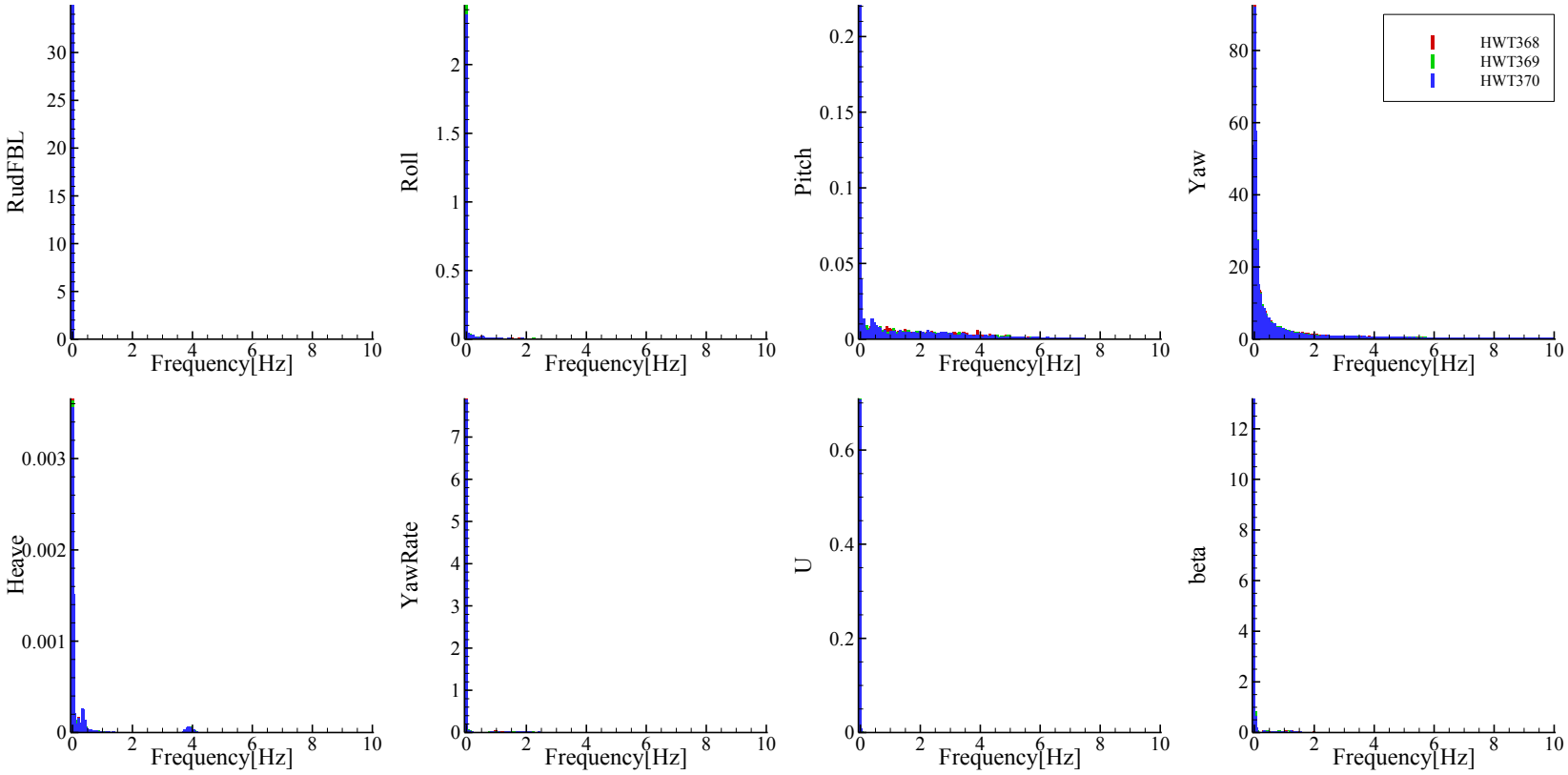

Figure F-6 FFT analysis of time histories of turning in calm water at Fr = 0.2, δ = -35°, and heading angle = -90°

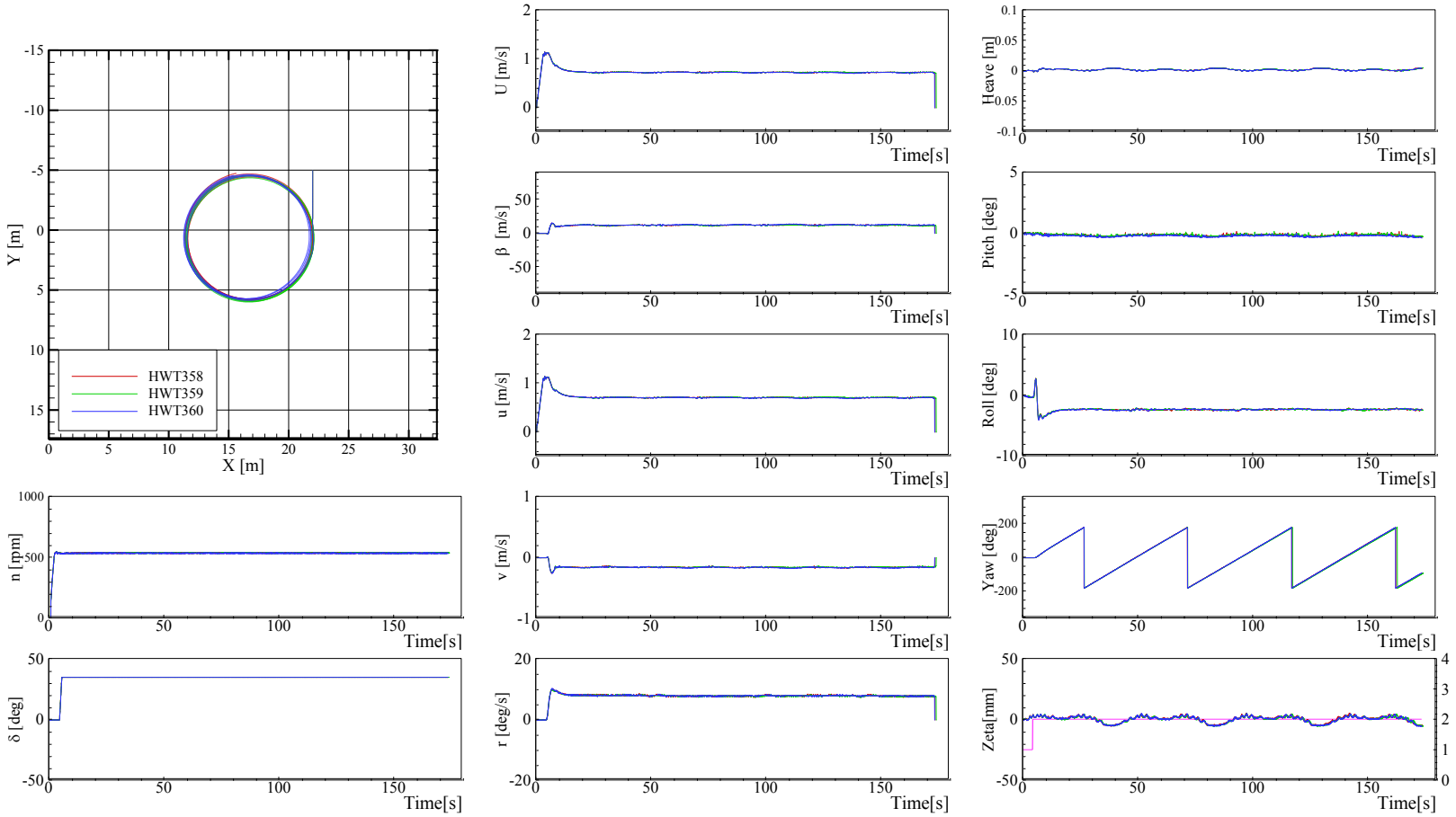

Figure F-7 Trajectories and time histories of turning in calm water at Fr = 0.2, δ = 35°, and heading angle = -90°

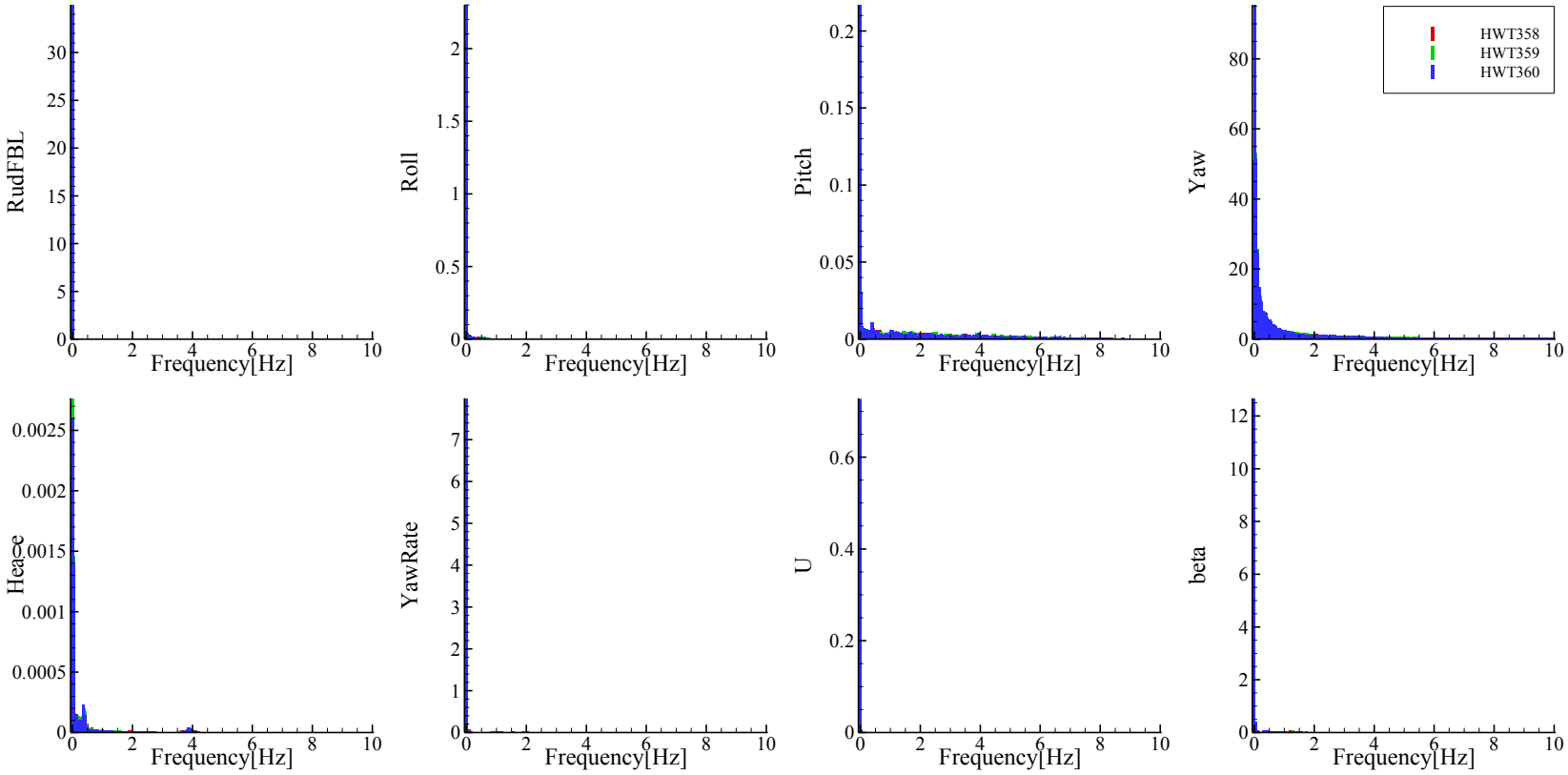

Figure F-8 FFT analysis of time histories of turning in calm water at Fr = 0.2, δ = 35°, and heading angle = -90°

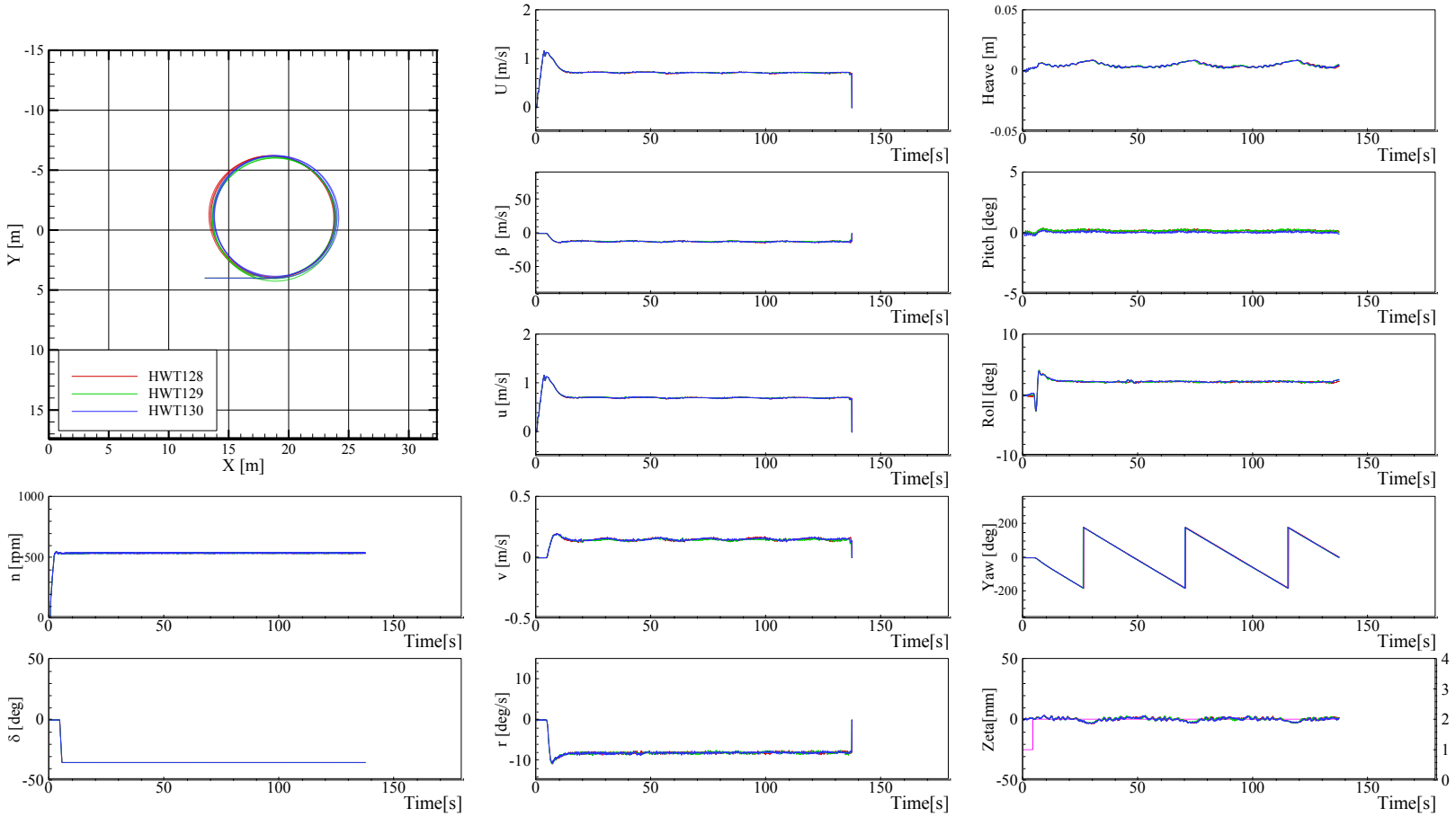

Figure F-9 Trajectories and time histories of turning in calm water at Fr = 0.2, δ = -35°, and heading angle = 0°

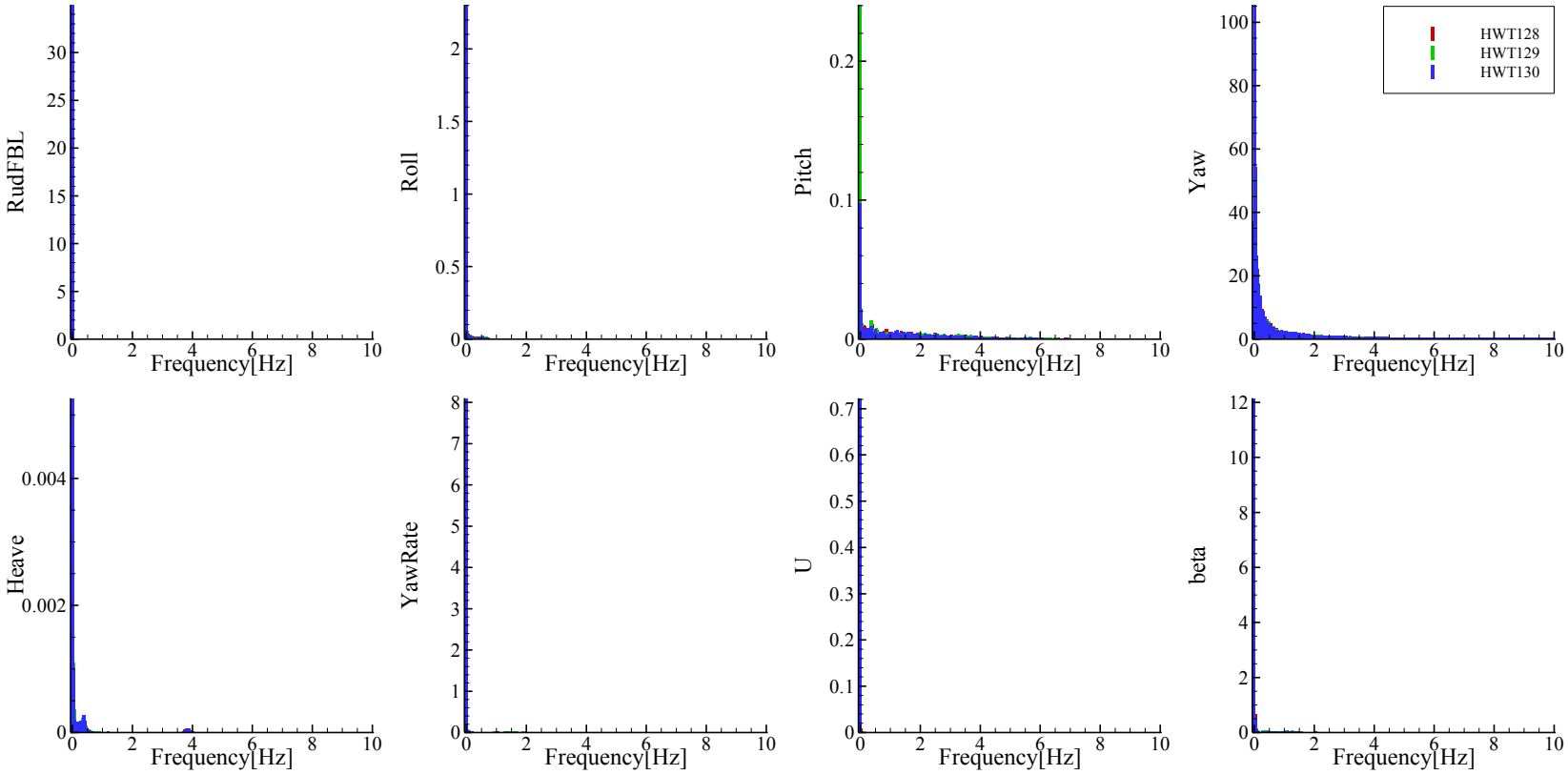

Figure F-10 FFT analysis of time histories of turning in calm water at Fr = 0.2, δ = -35°, and heading angle = 0°

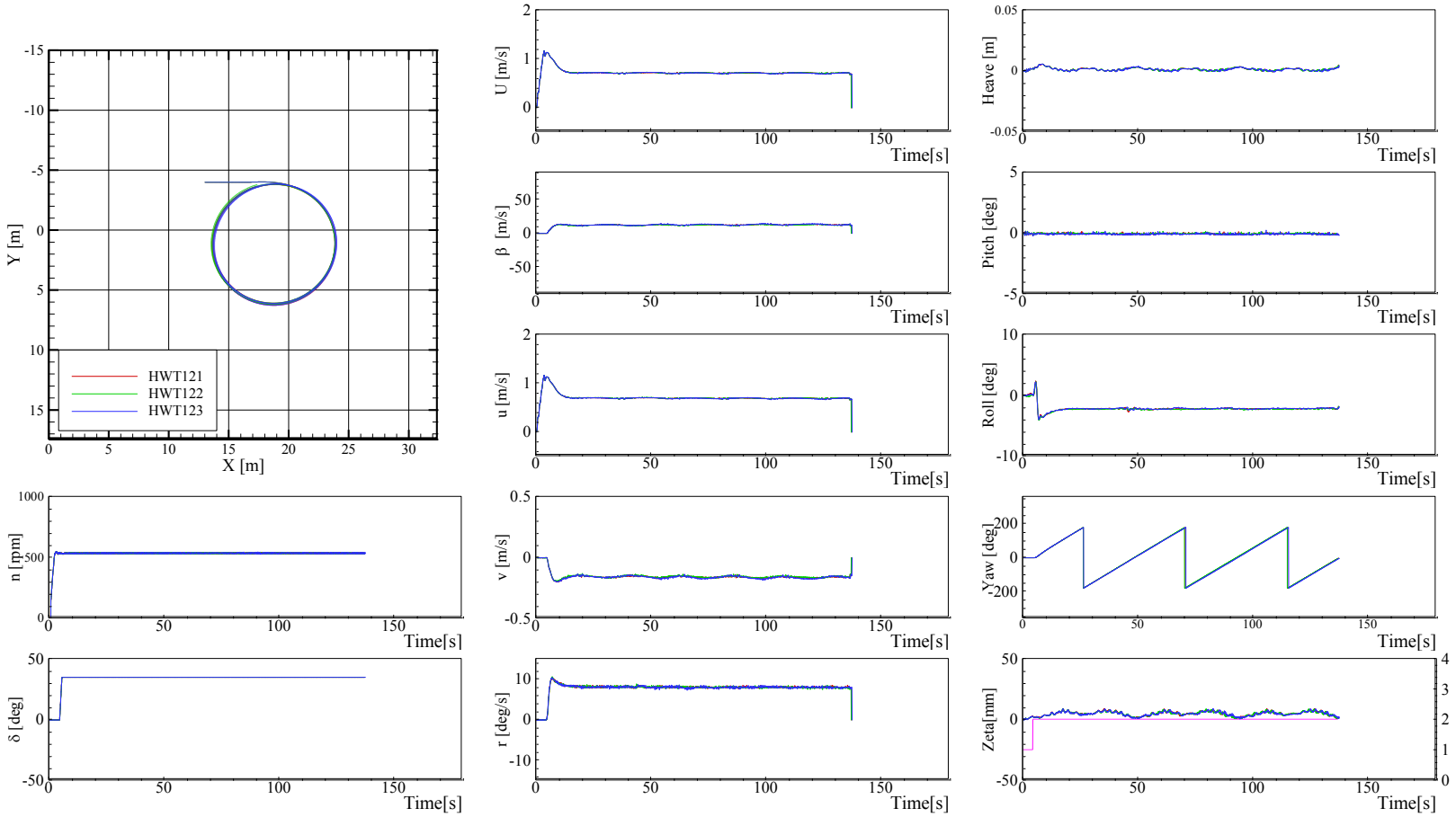

Figure F-11 Trajectories and time histories of turning in calm water at Fr = 0.2, δ = 35°, and heading angle = 0°

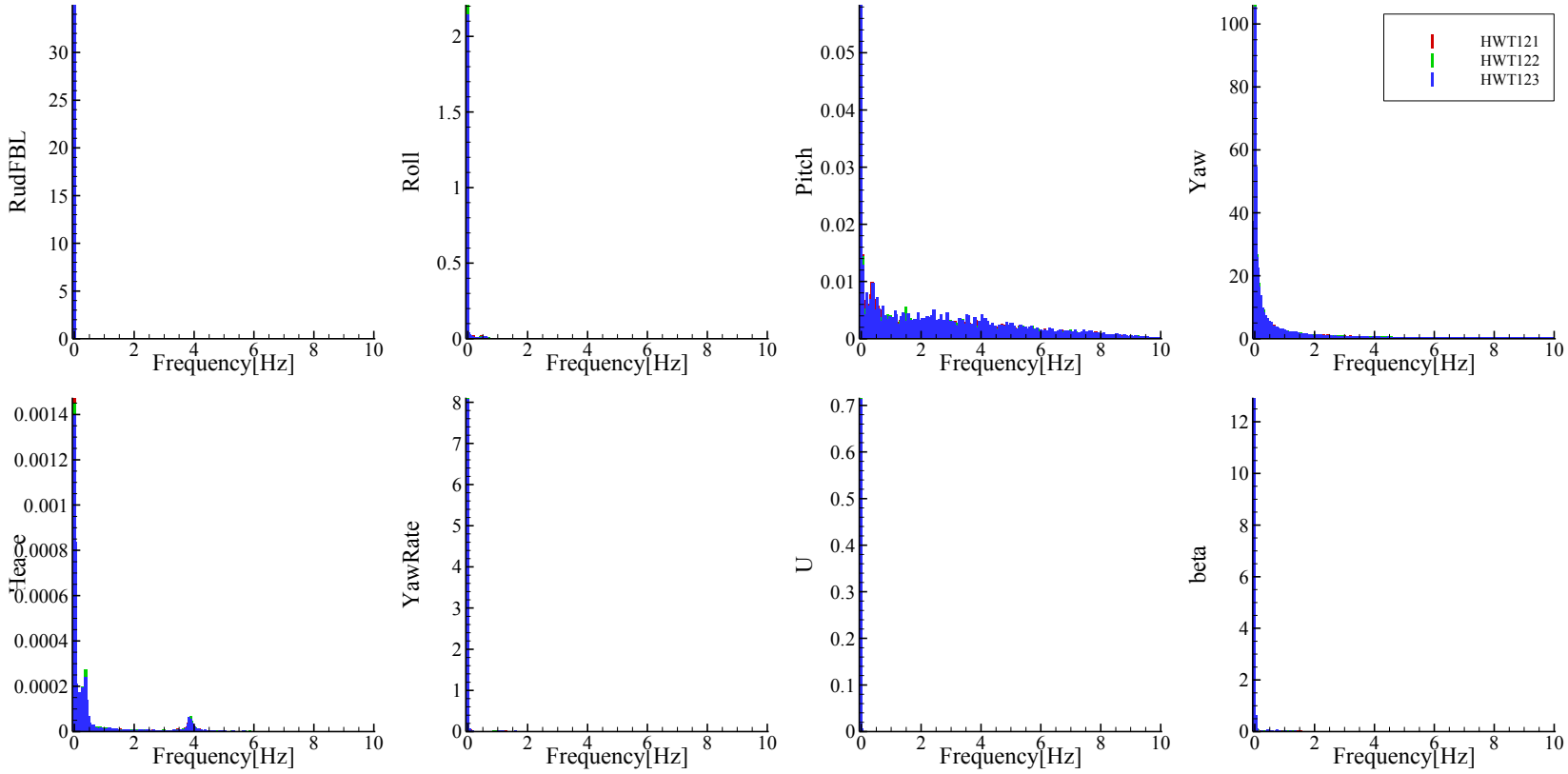

Figure F-12 FFT analysis of time histories of turning in calm water at Fr = 0.2, δ = 35°, and heading angle = 0°

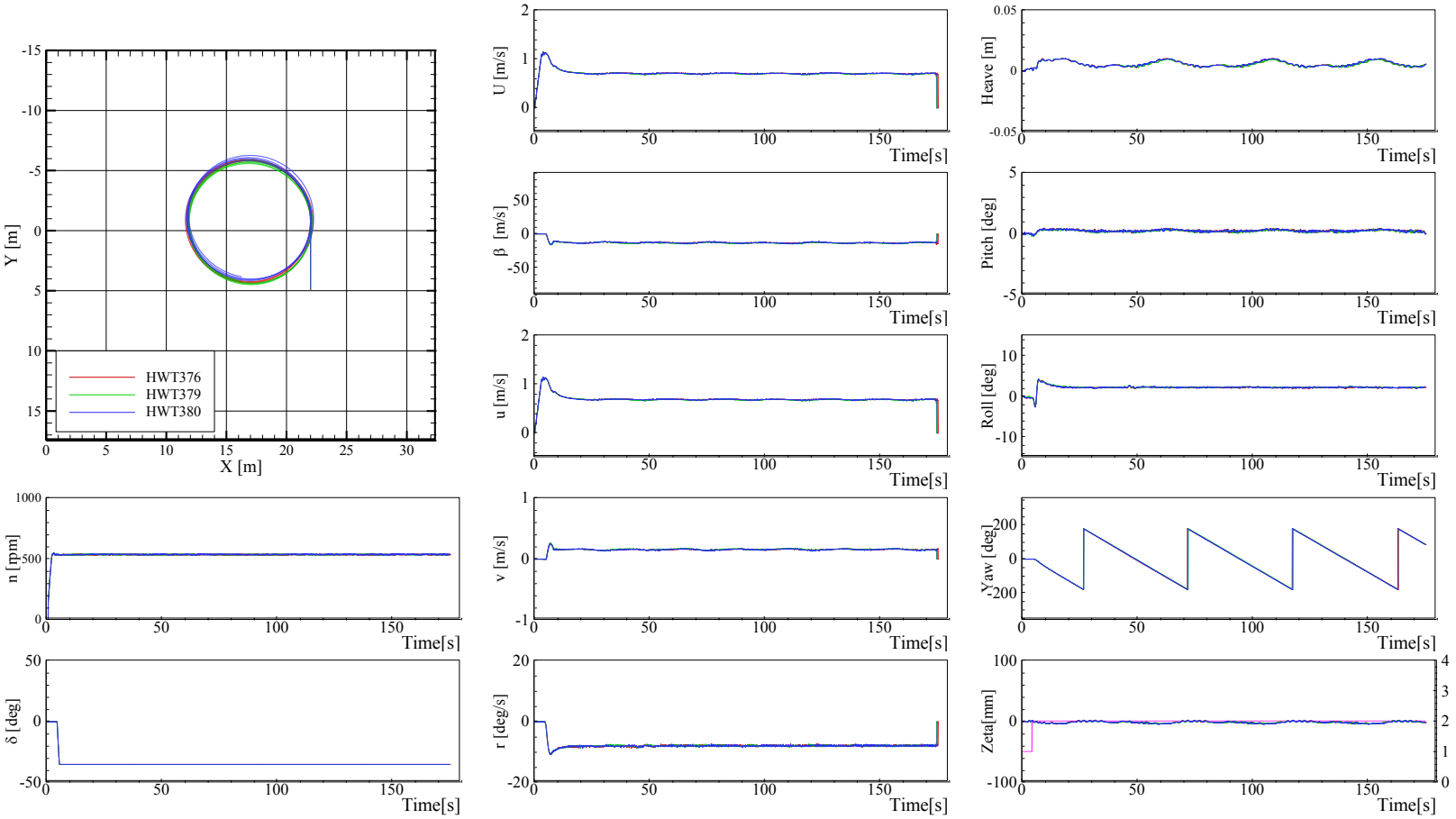

Figure F-13 Trajectories and time histories of turning in calm water at Fr = 0.2, δ = -35°, and heading angle = 90°

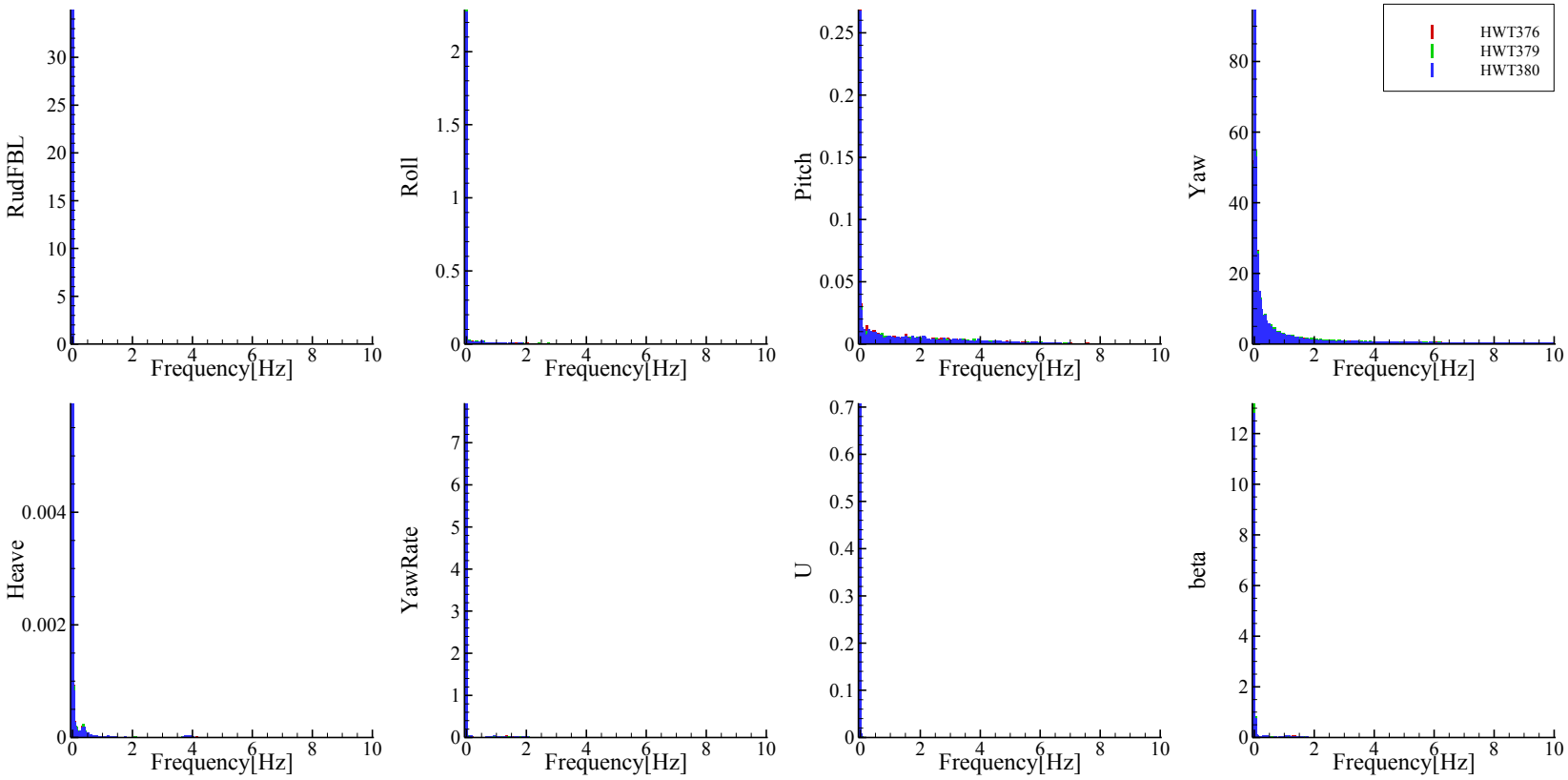

Figure F-14 FFT analysis of time histories of turning in calm water at Fr = 0.2, δ = -35°, and heading angle = 90°

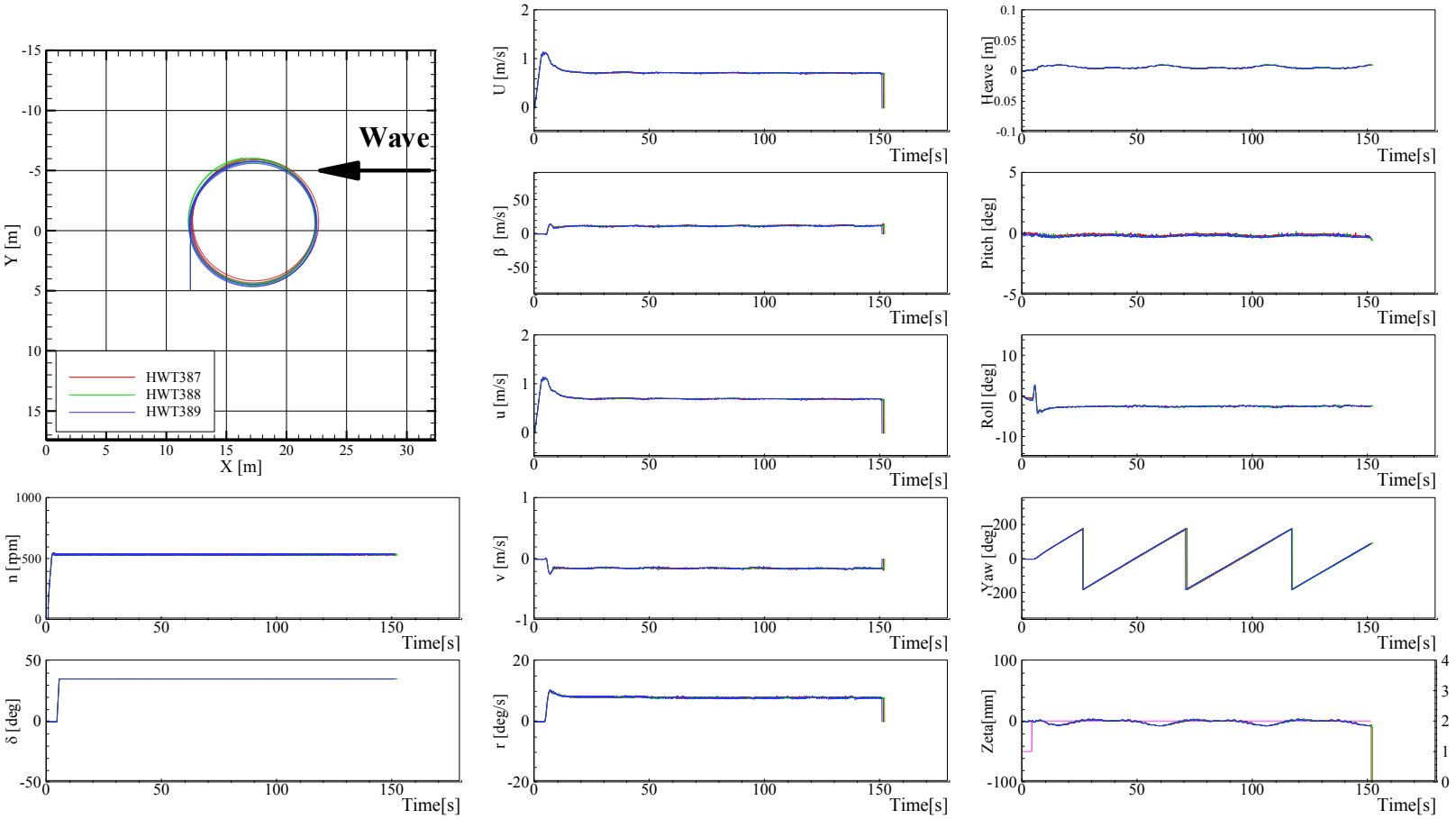

Figure F-15 Trajectories and time histories of turning in calm water at Fr = 0.2, δ = 35°, and heading angle = 90°

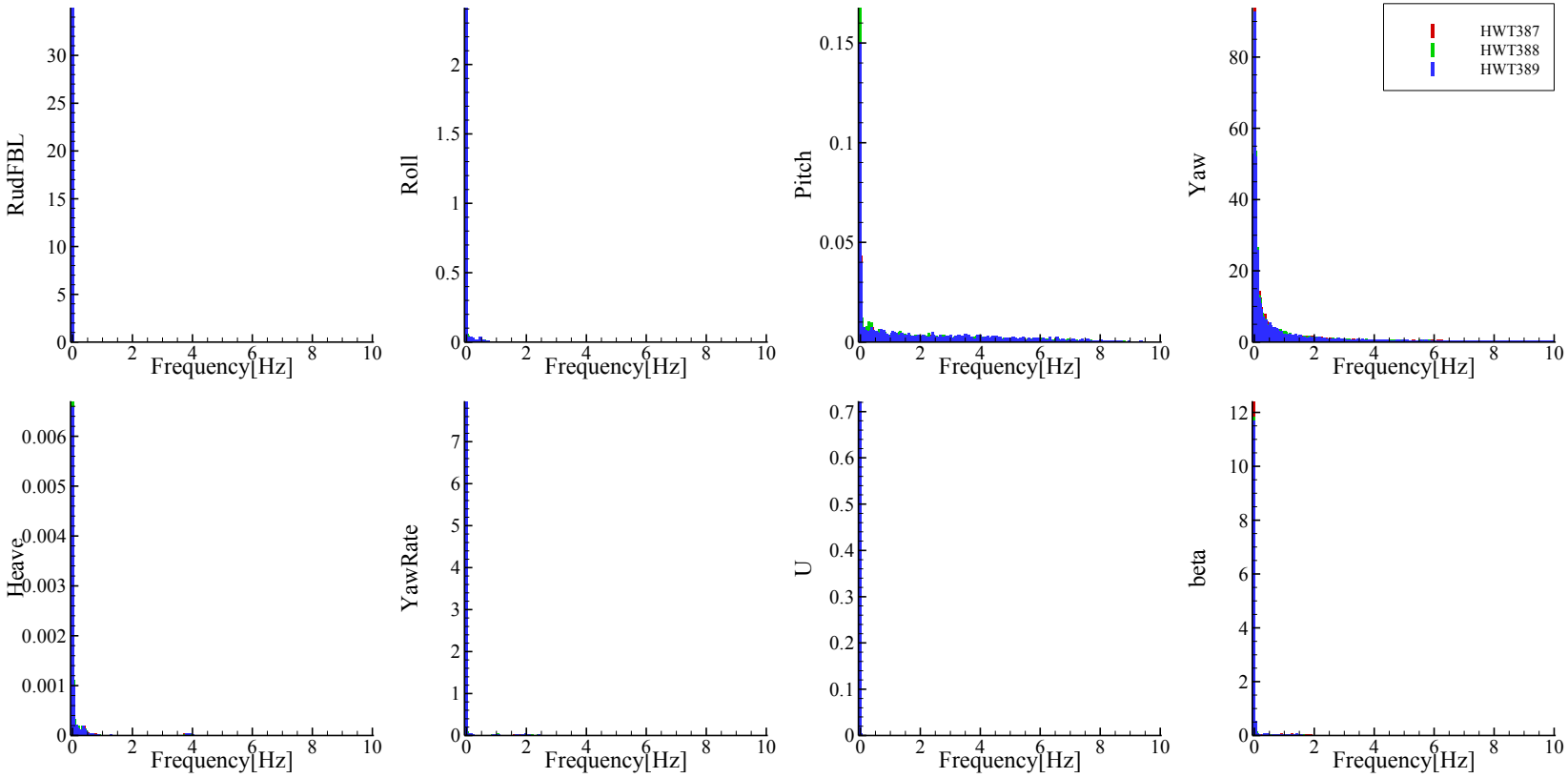

Figure F-16 FFT analysis of time histories of turning in calm water at Fr = 0.2, δ = 35°, and heading angle = 90°

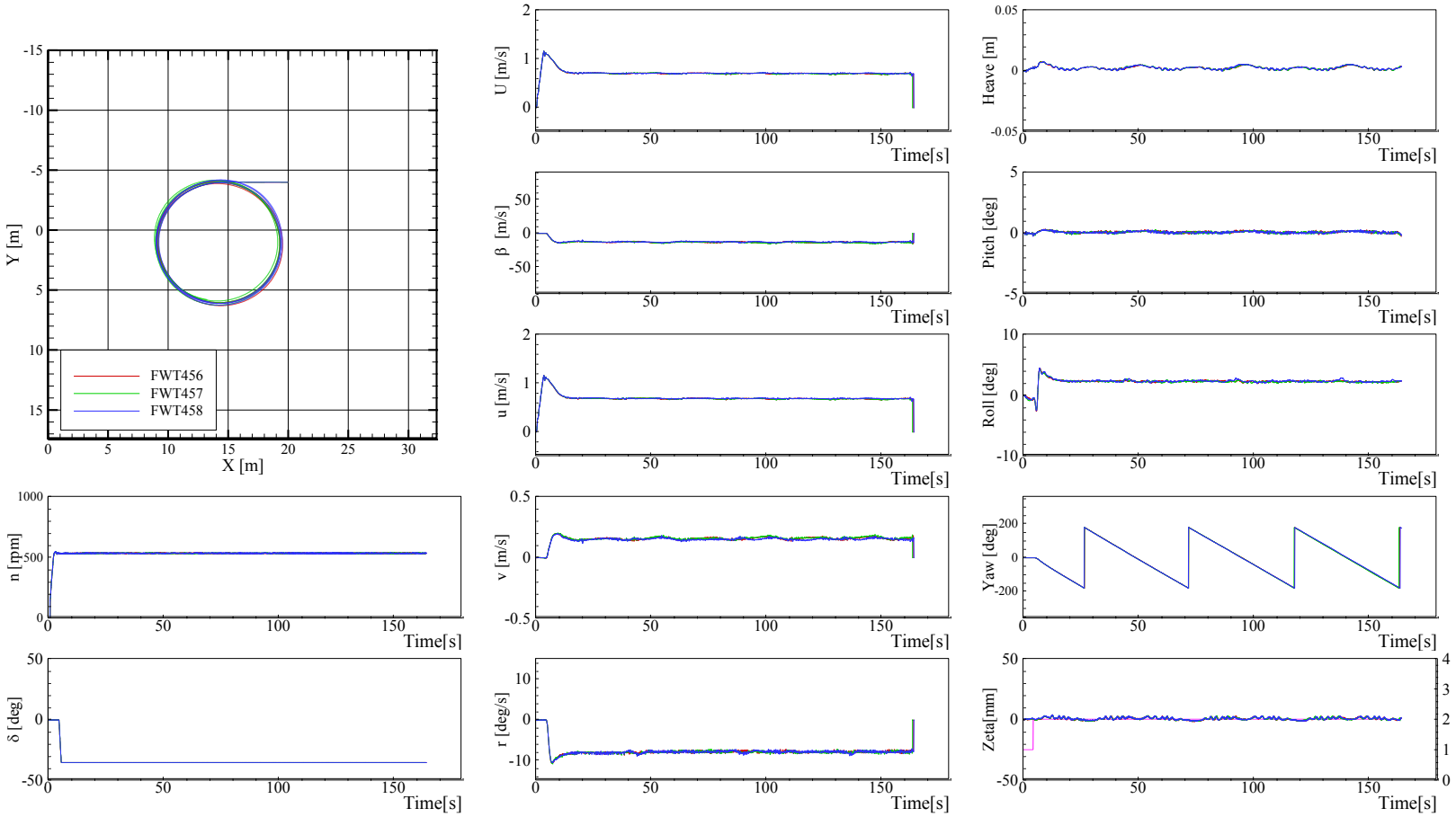

Figure F-17 Trajectories and time histories of turning in calm water at Fr = 0.2, δ = -35°, and heading angle = 180°

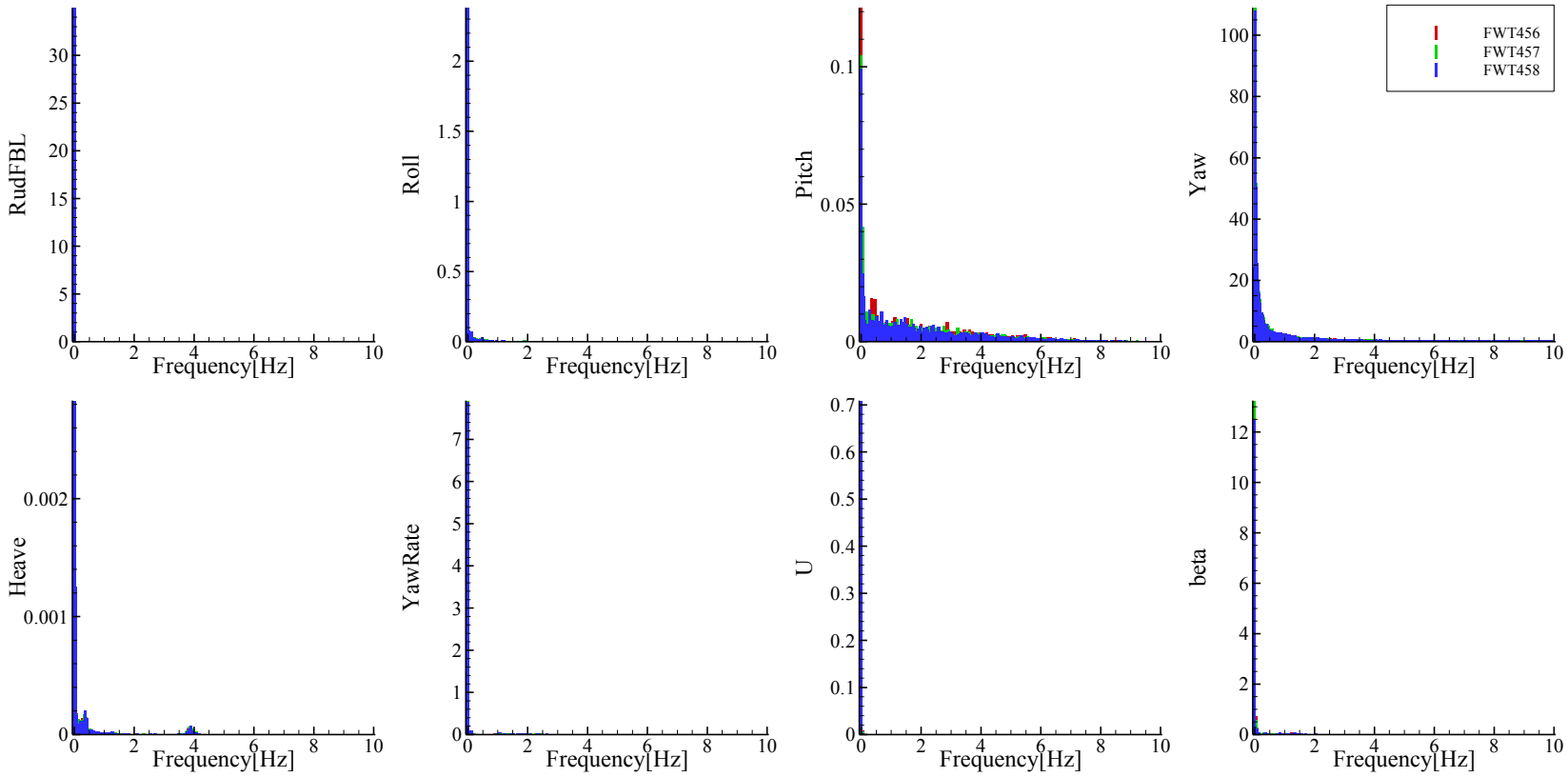

Figure F-18 FFT analysis of time histories of turning in calm water at Fr = 0.2, δ = -35°, and heading angle = 180°

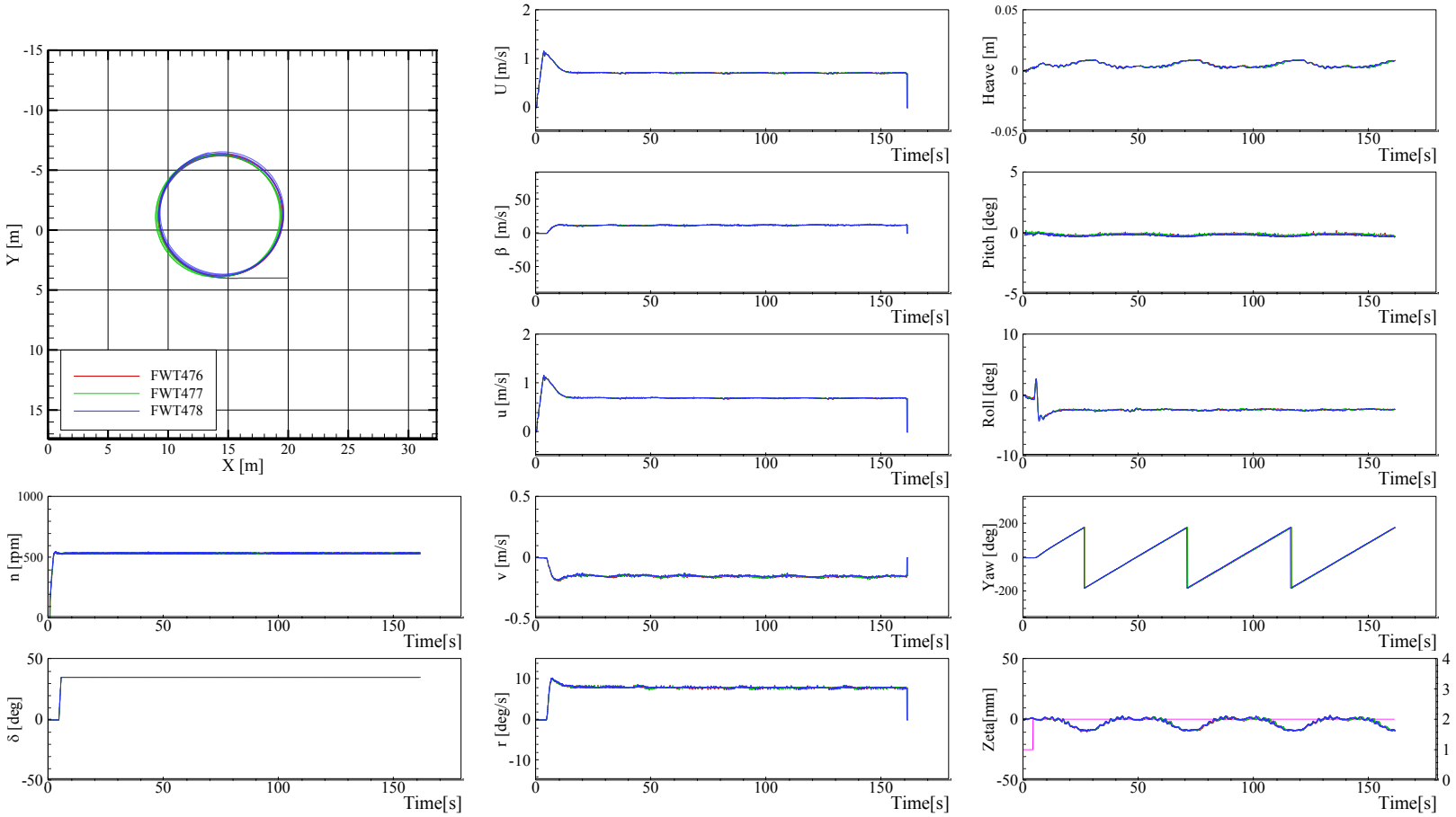

Figure F-19 Trajectories and time histories of turning in calm water at Fr = 0.2, δ = 35°, and heading angle = 180°

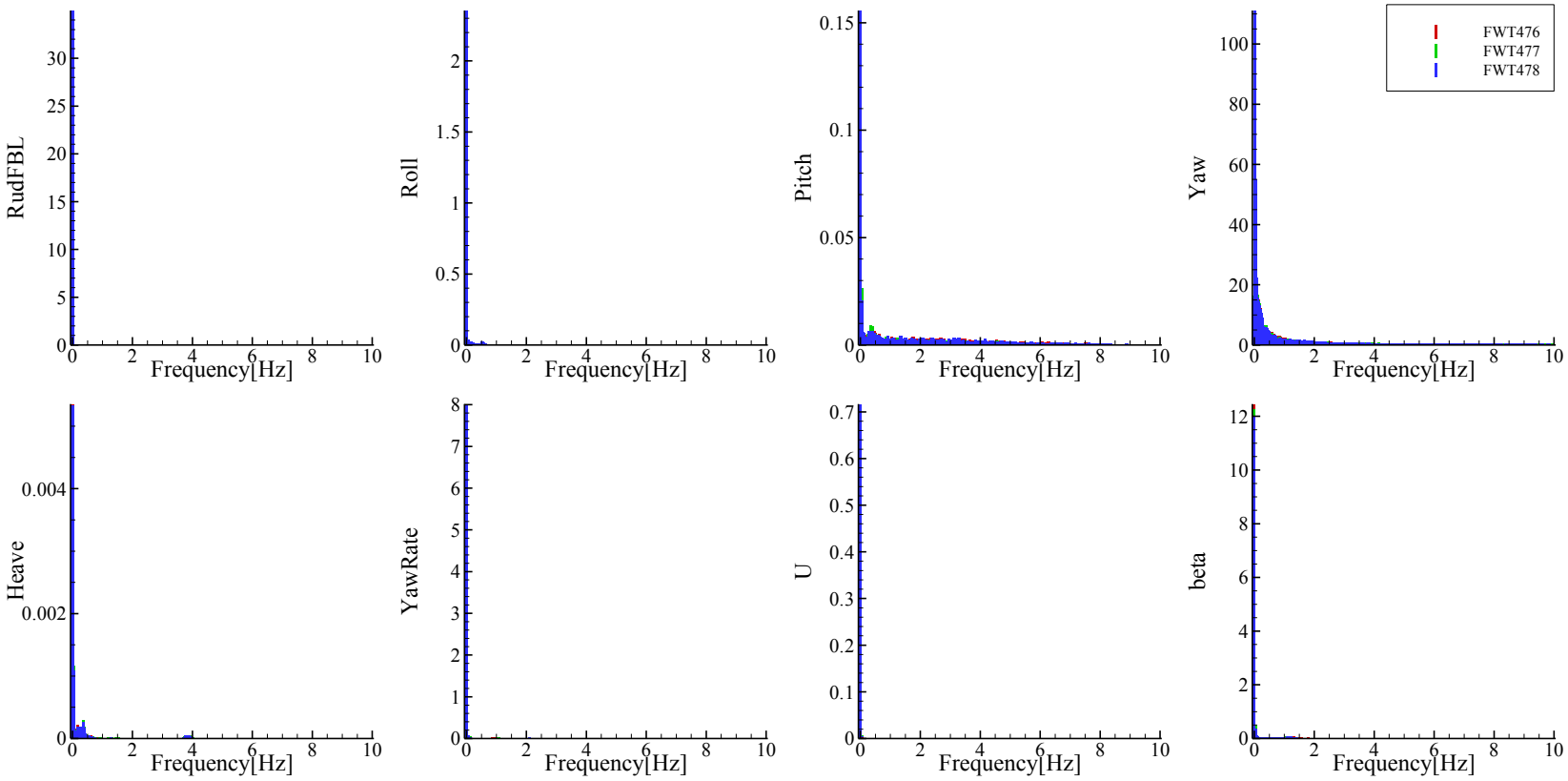

Figure F-20 FFT analysis of time histories of turning in calm water at Fr = 0.2, δ = 35°, and heading angle = 180°

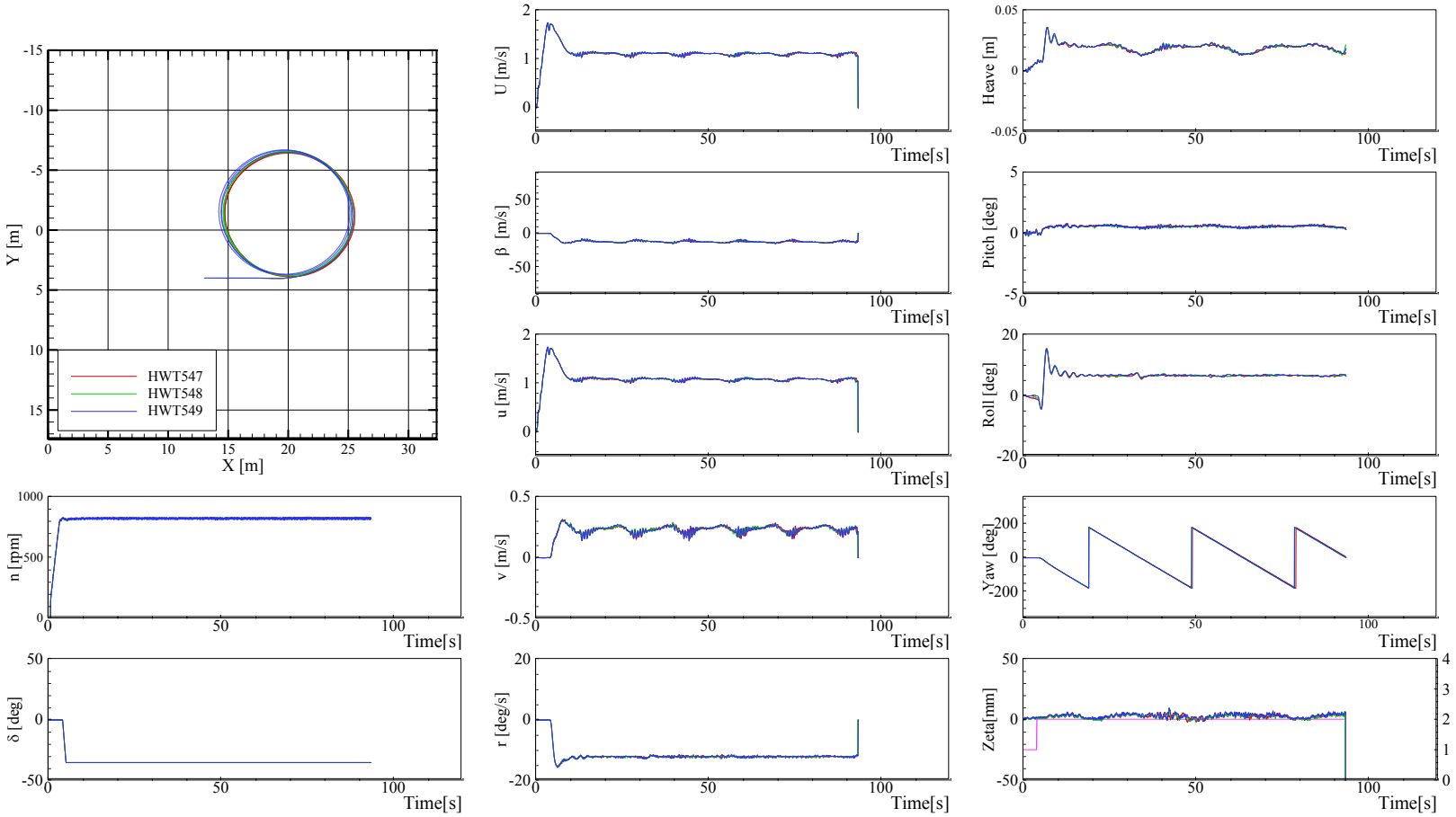

Figure F-21 Trajectories and time histories of turning in calm water at Fr = 0.3, δ = -35°, and heading angle = 0°

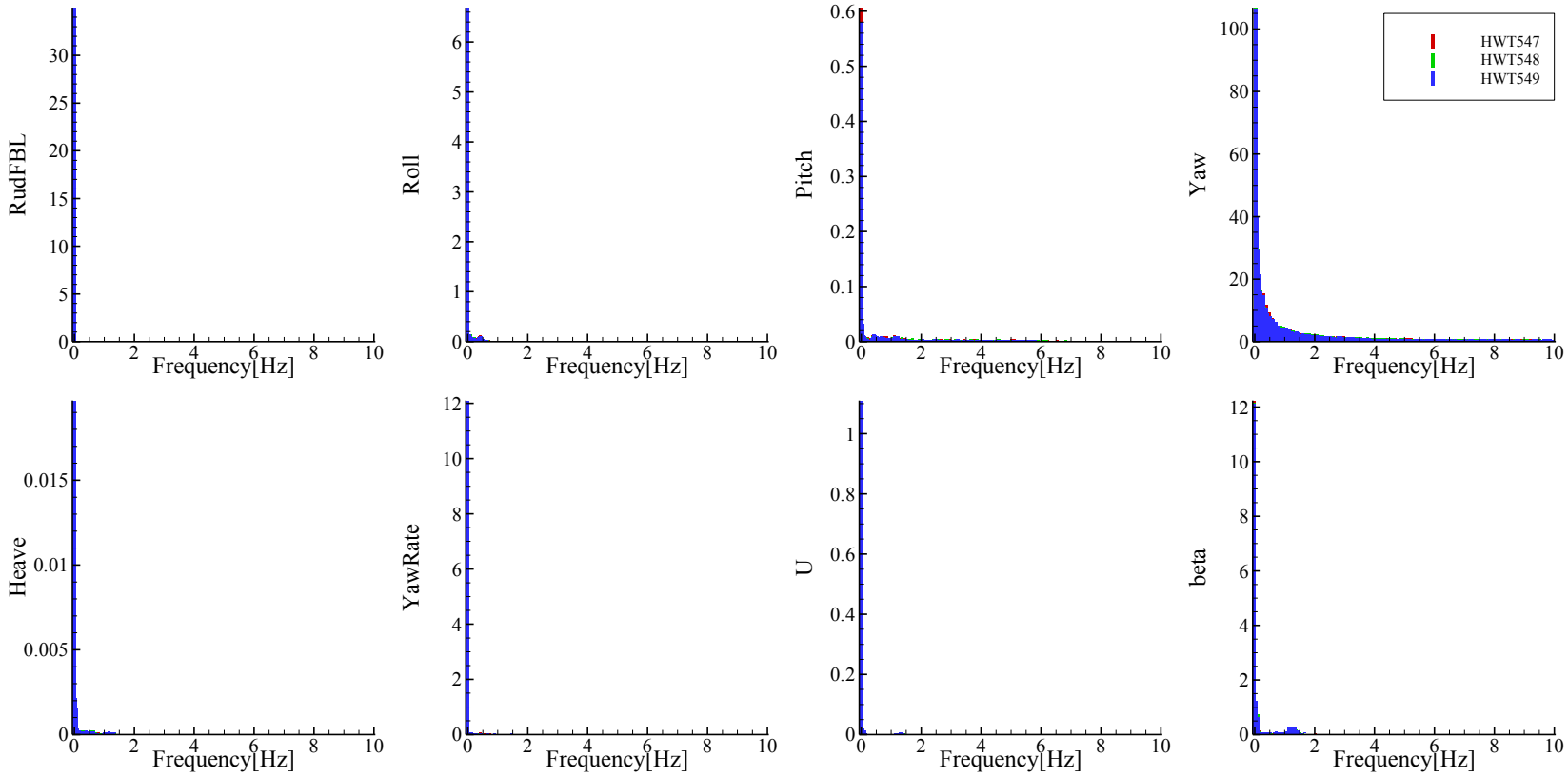

Figure F-22 FFT analysis of time histories of turning in calm water at Fr = 0.3, δ = -35°, and heading angle = 0°

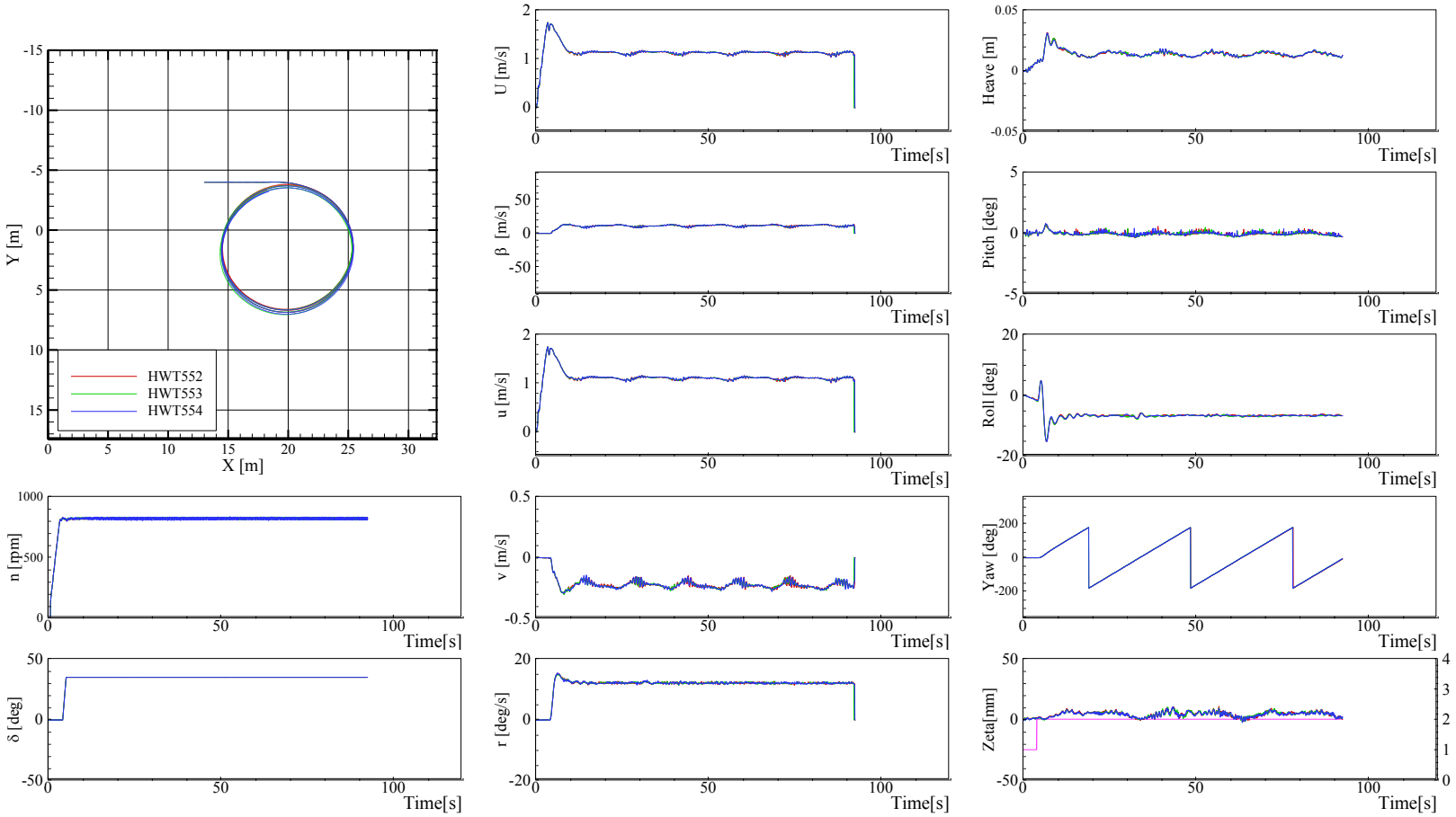

Figure F-23 Trajectories and time histories of turning in calm water at Fr = 0.3, δ = 35°, and heading angle = 0°

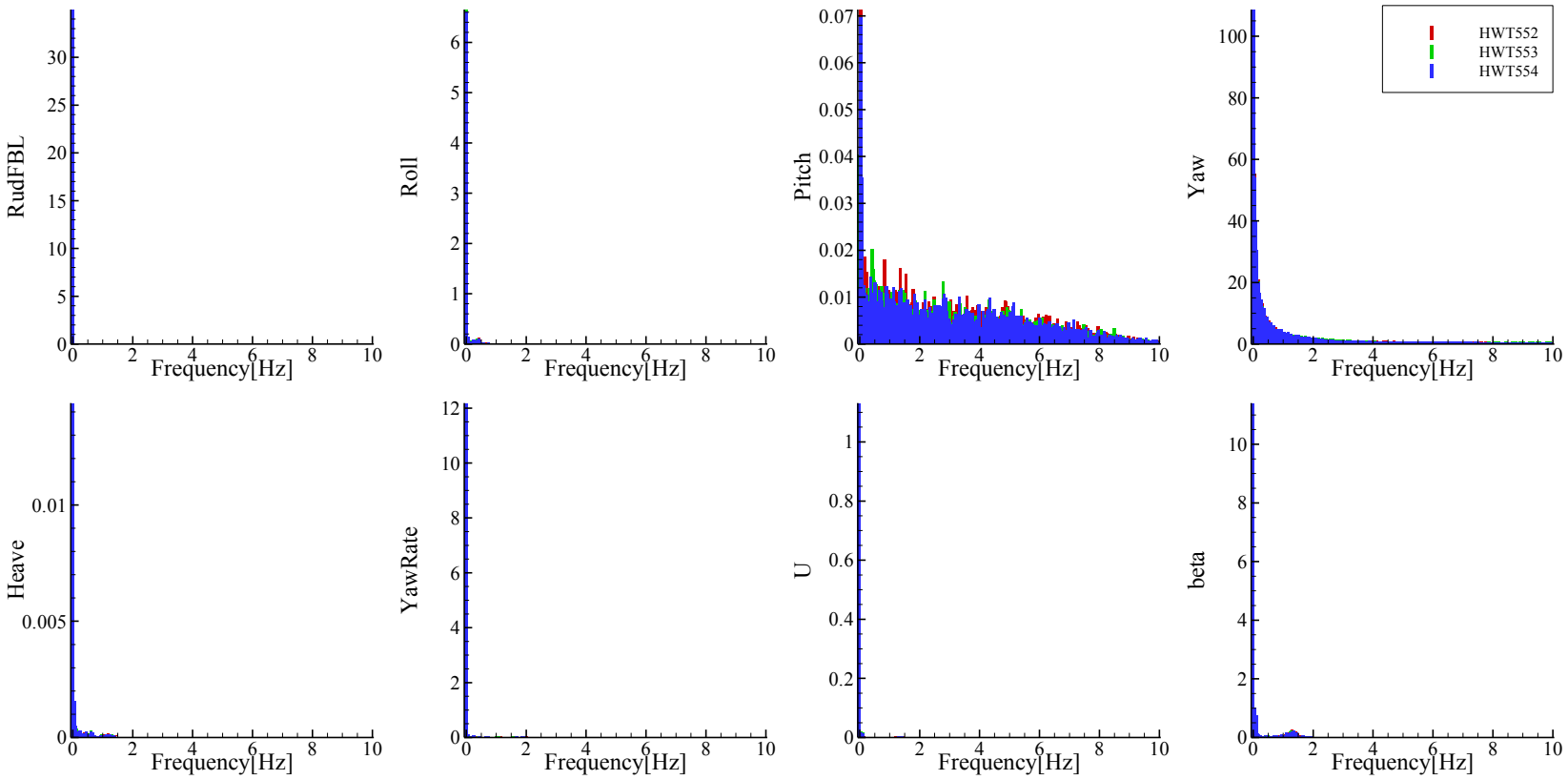

Figure F-24 FFT analysis of time histories of turning in calm water at Fr = 0.3, δ = 35°, and heading angle = 0°

APPENDIX G TRAJECTORIES AND TIME HISTORIES RESULTS OF TURNING TESTS IN WAVES

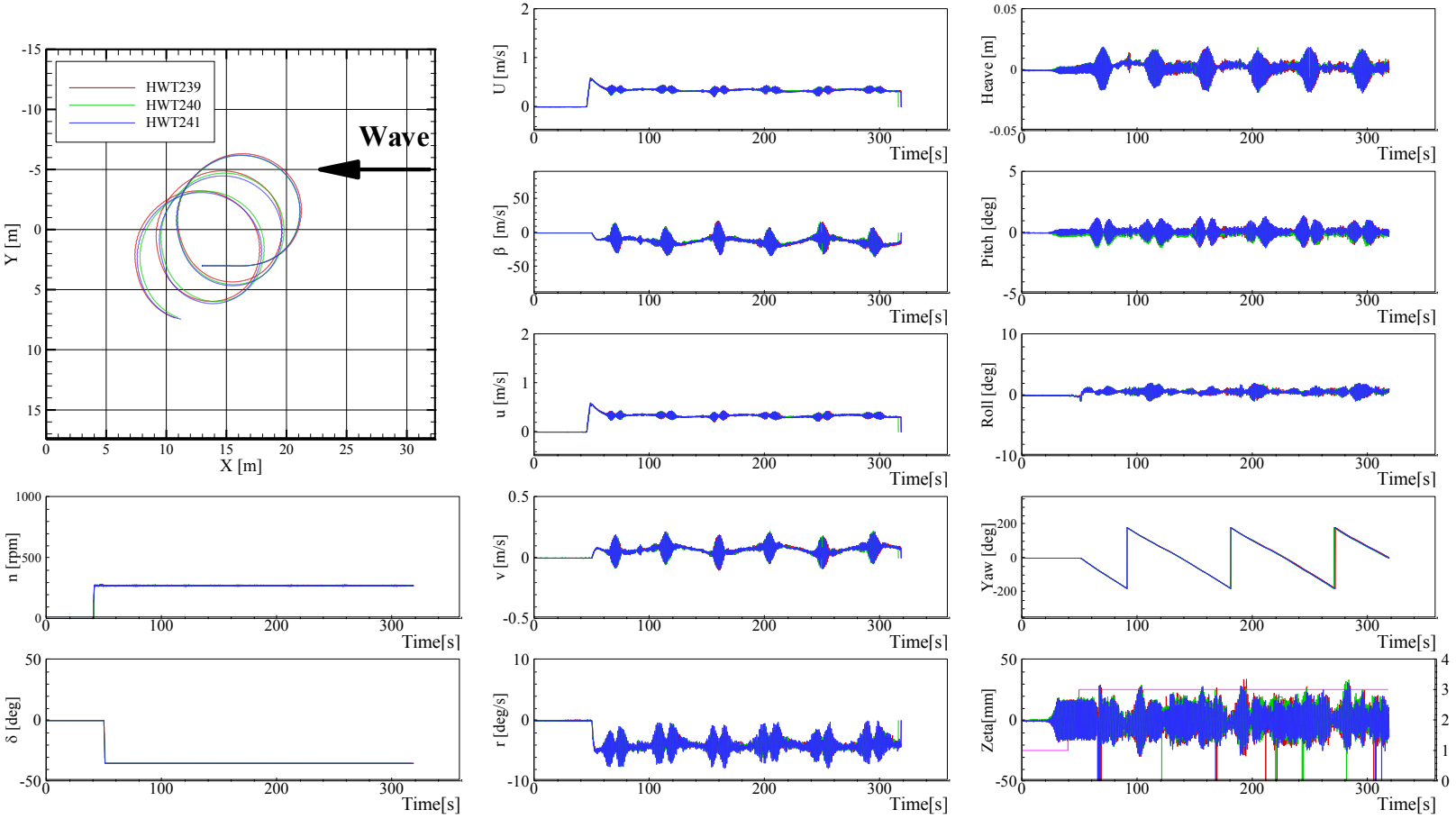

Figure G-1 Trajectories and time histories of turning in waves at Fr = 0.1, λ/L = 0.5, H/λ = 0.02, δ = -35, and χ = 0°

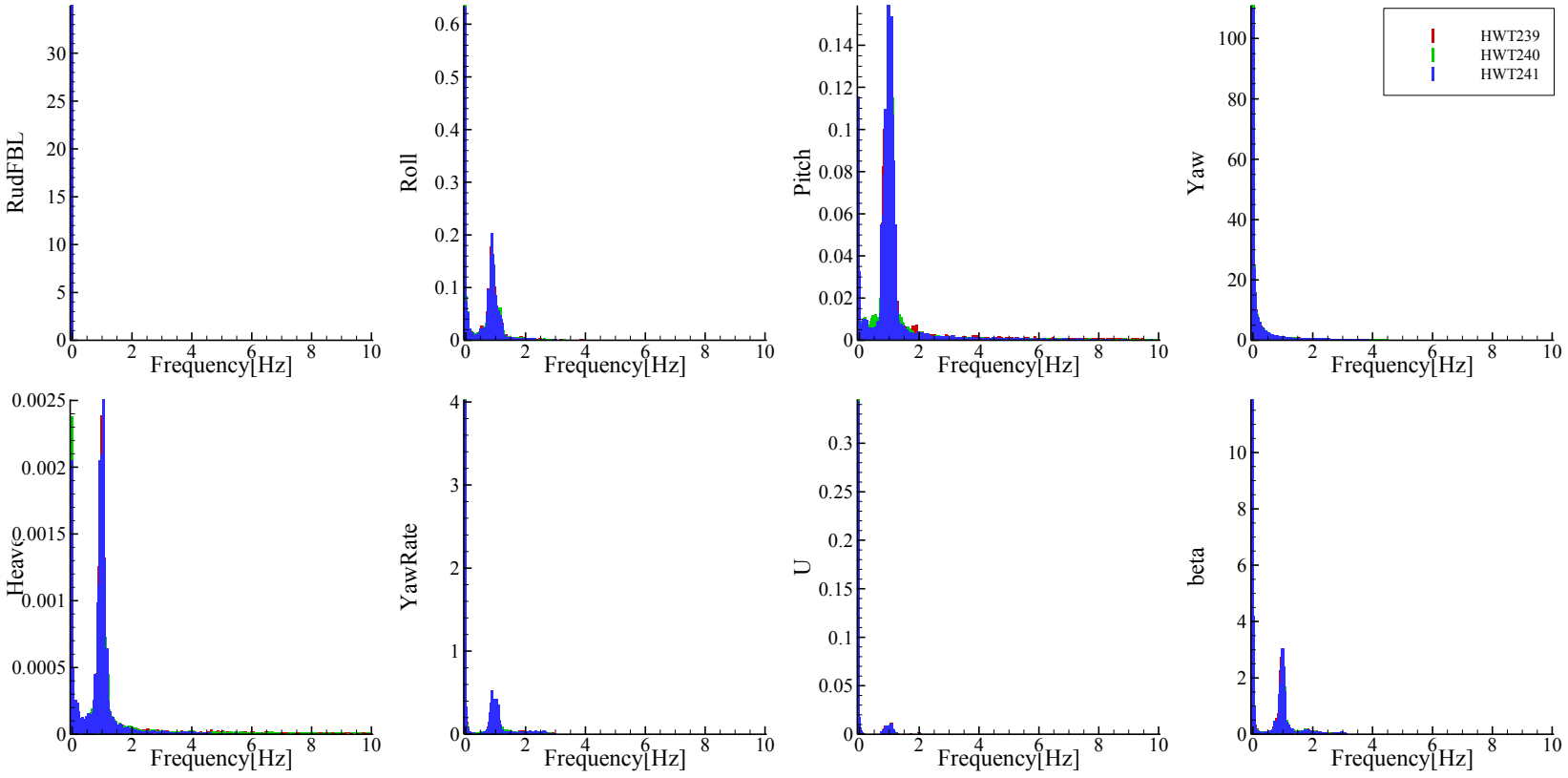

Figure G-2 FFT analysis of time histories of turning in waves at Fr = 0.1, λ/L = 0.5, H/λ = 0.02, δ = -35, and χ = 0°

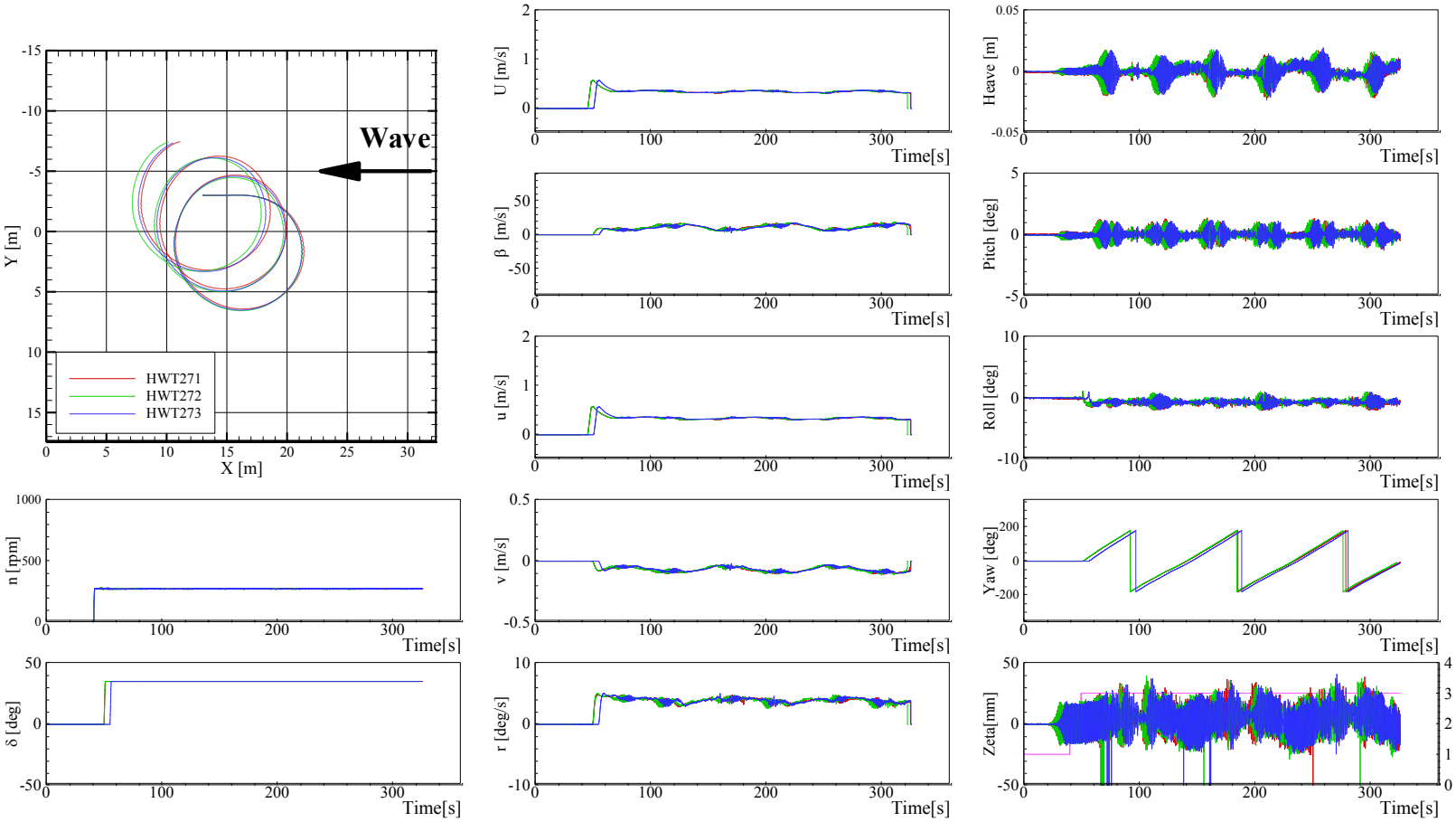

Figure G-3 Trajectories and time histories of turning in waves at Fr = 0.1, λ/L = 0.5, H/λ = 0.02, δ = 35, and χ = 0°

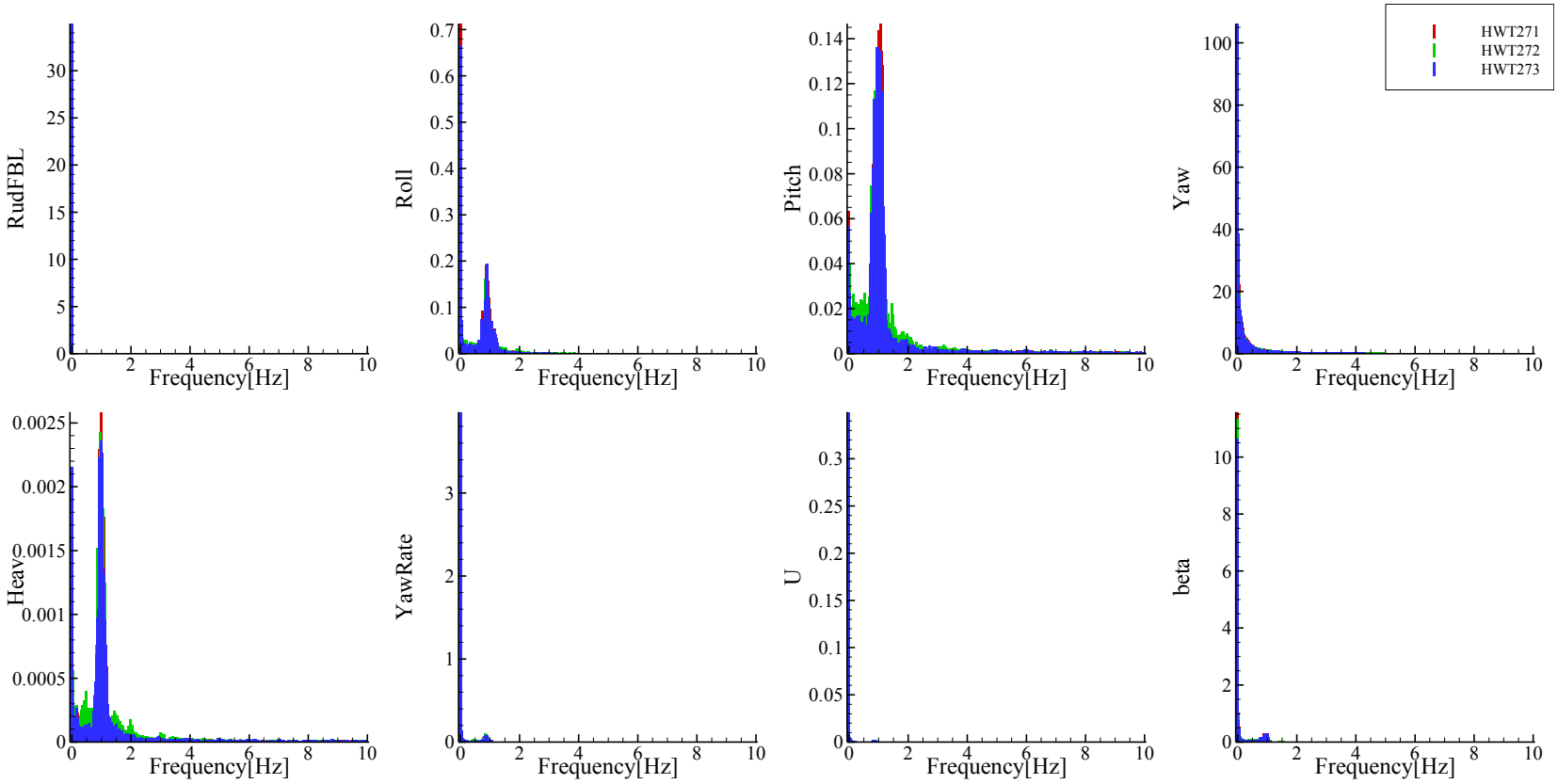

Figure G-4 FFT analysis of time histories of turning in waves at Fr = 0.1, λ/L = 0.5, H/λ = 0.02, δ = 35, and χ = 0°

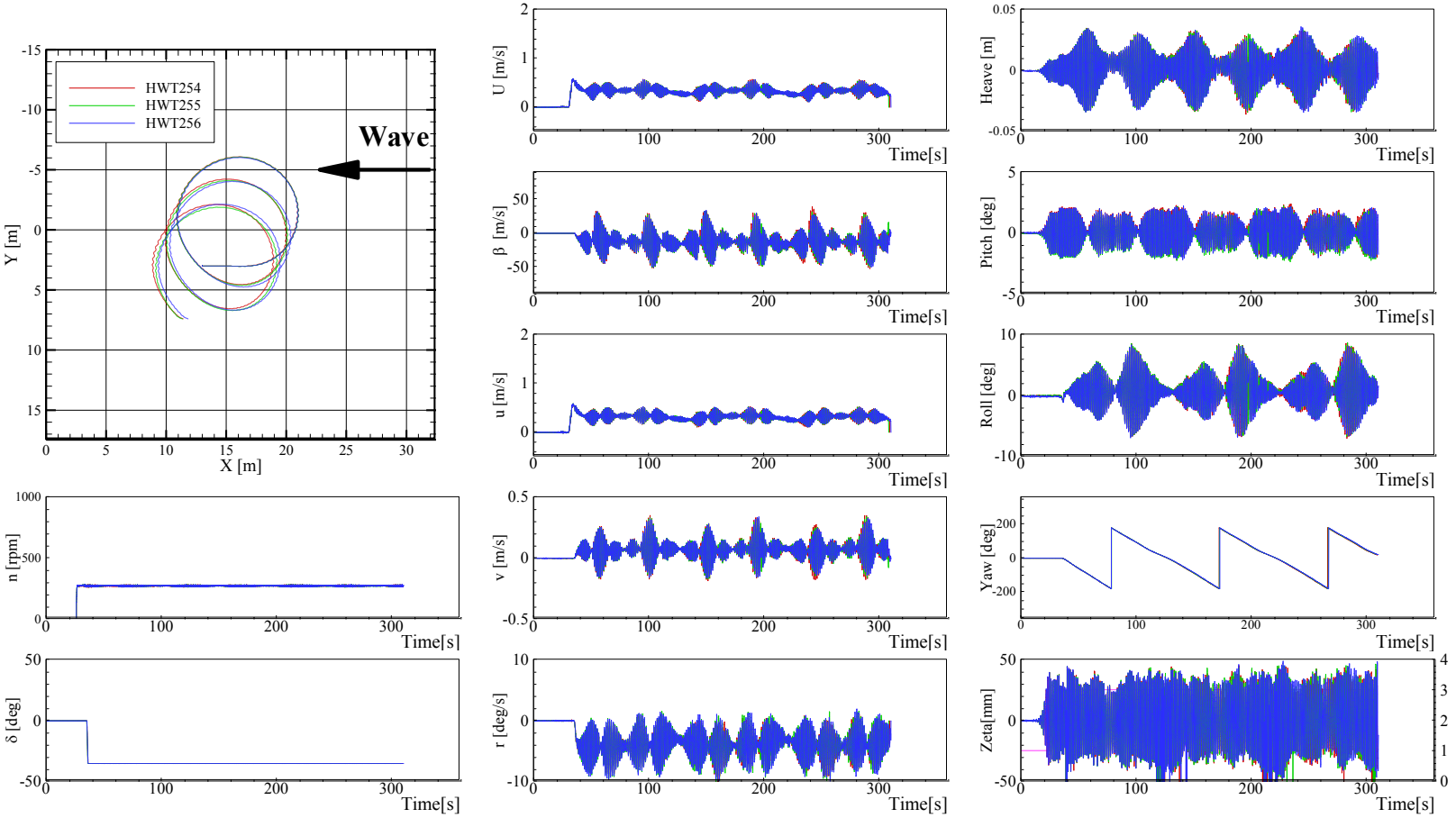

Figure G-5 Trajectories and time histories of turning in waves at Fr = 0.1, λ/L = 1.0, H/λ = 0.02, δ = -35, and χ = 0°

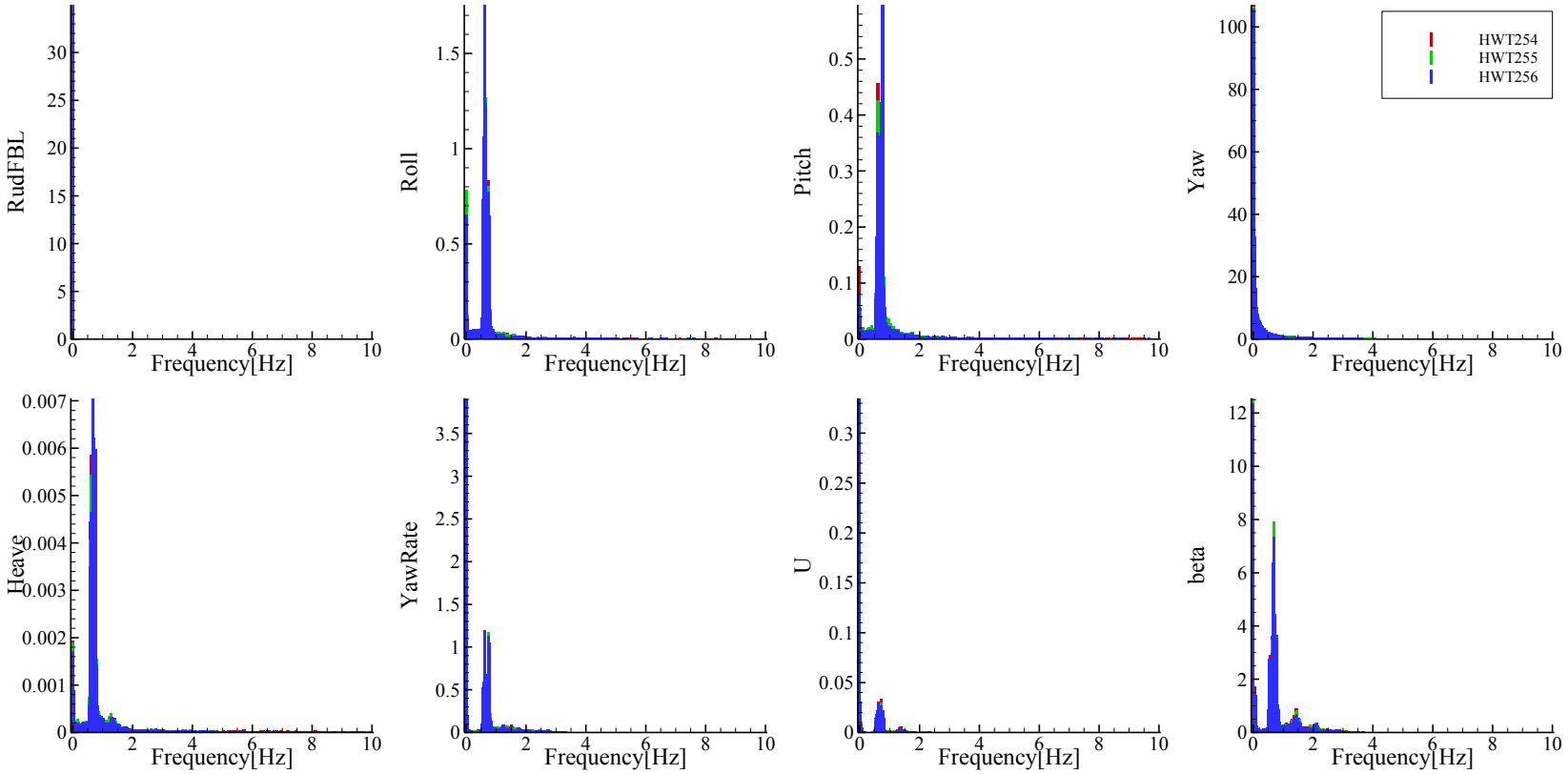

Figure G-6 FFT analysis of time histories of turning in waves at Fr = 0.1, λ/L = 1.0, H/λ = 0.02, δ = -35, and χ = 0°

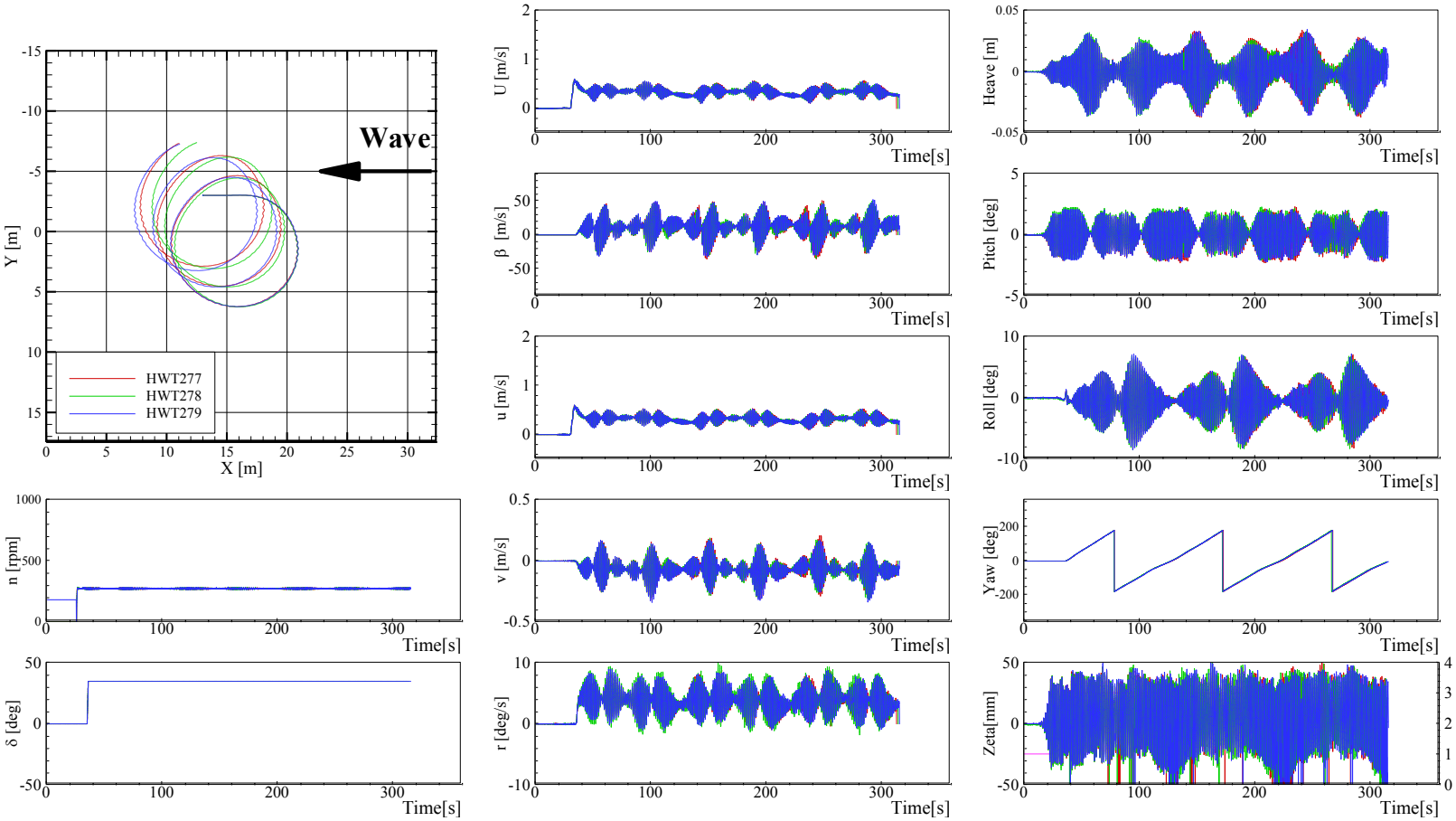

Figure G-7 Trajectories and time histories of turning in waves at Fr = 0.1, λ/L = 1.0, H/λ = 0.02, δ = 35, and χ = 0°

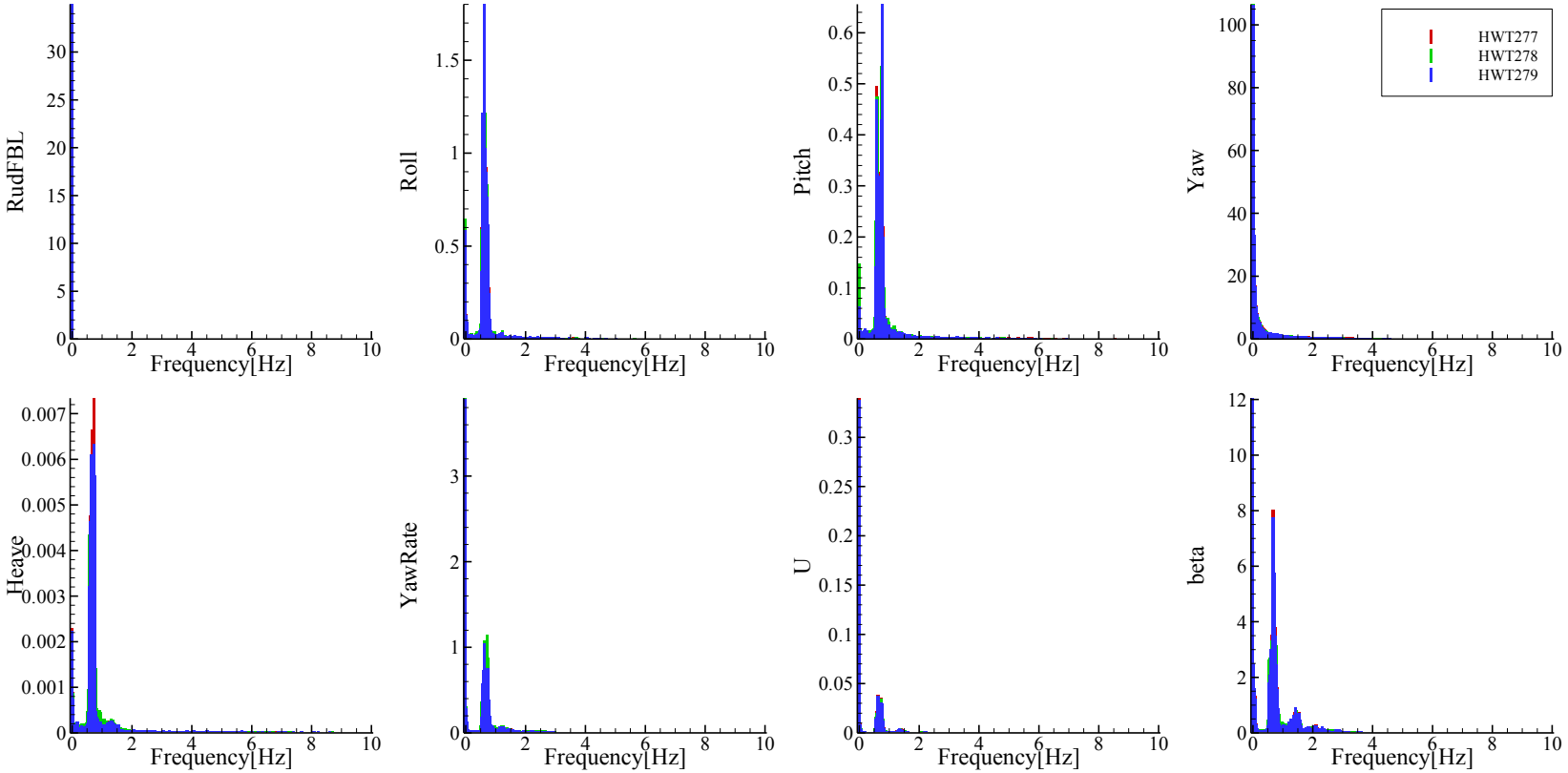

Figure G-8 FFT analysis of time histories of turning in waves at Fr = 0.1, λ/L = 1.0, H/λ = 0.02, δ = 35, and χ = 0°

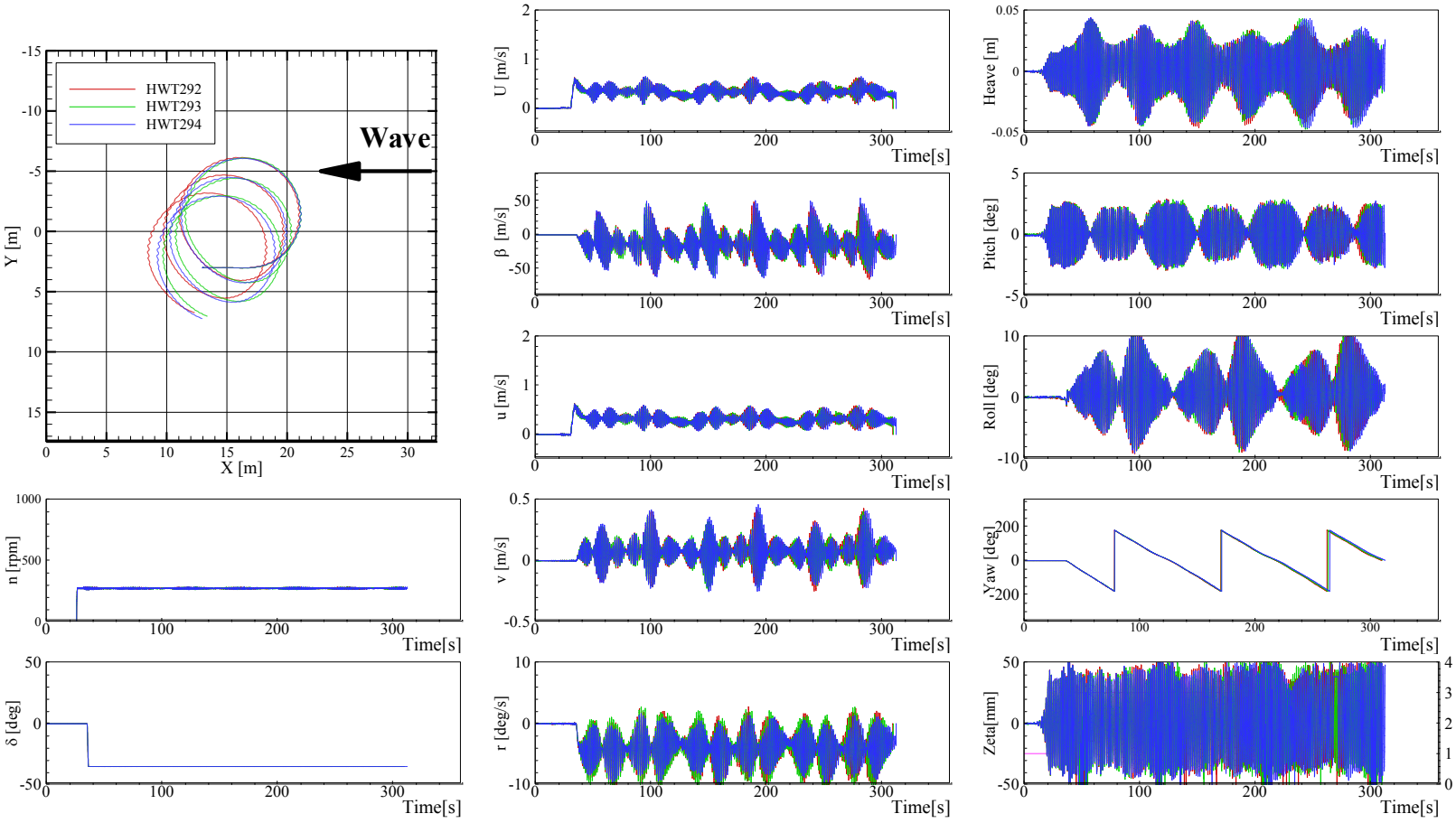

Figure G-9 Trajectories and time histories of turning in waves at Fr = 0.1, λ/L = 1.2, H/λ = 0.02, δ = -35, and χ = 0°

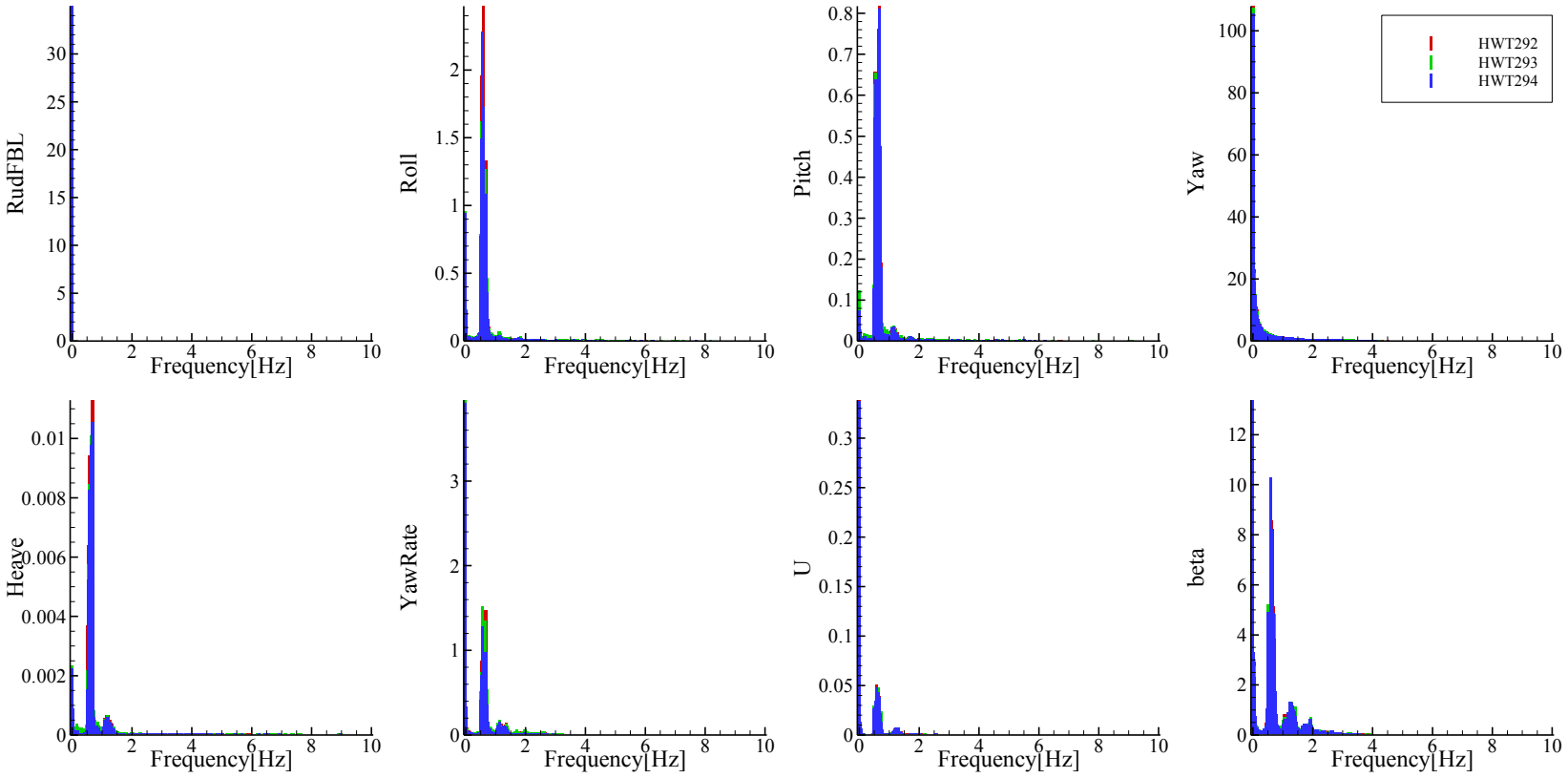

Figure G-10 FFT analysis of time histories of turning in waves at Fr = 0.1, λ/L = 1.2, H/λ = 0.02, δ = -35, and χ = 0°

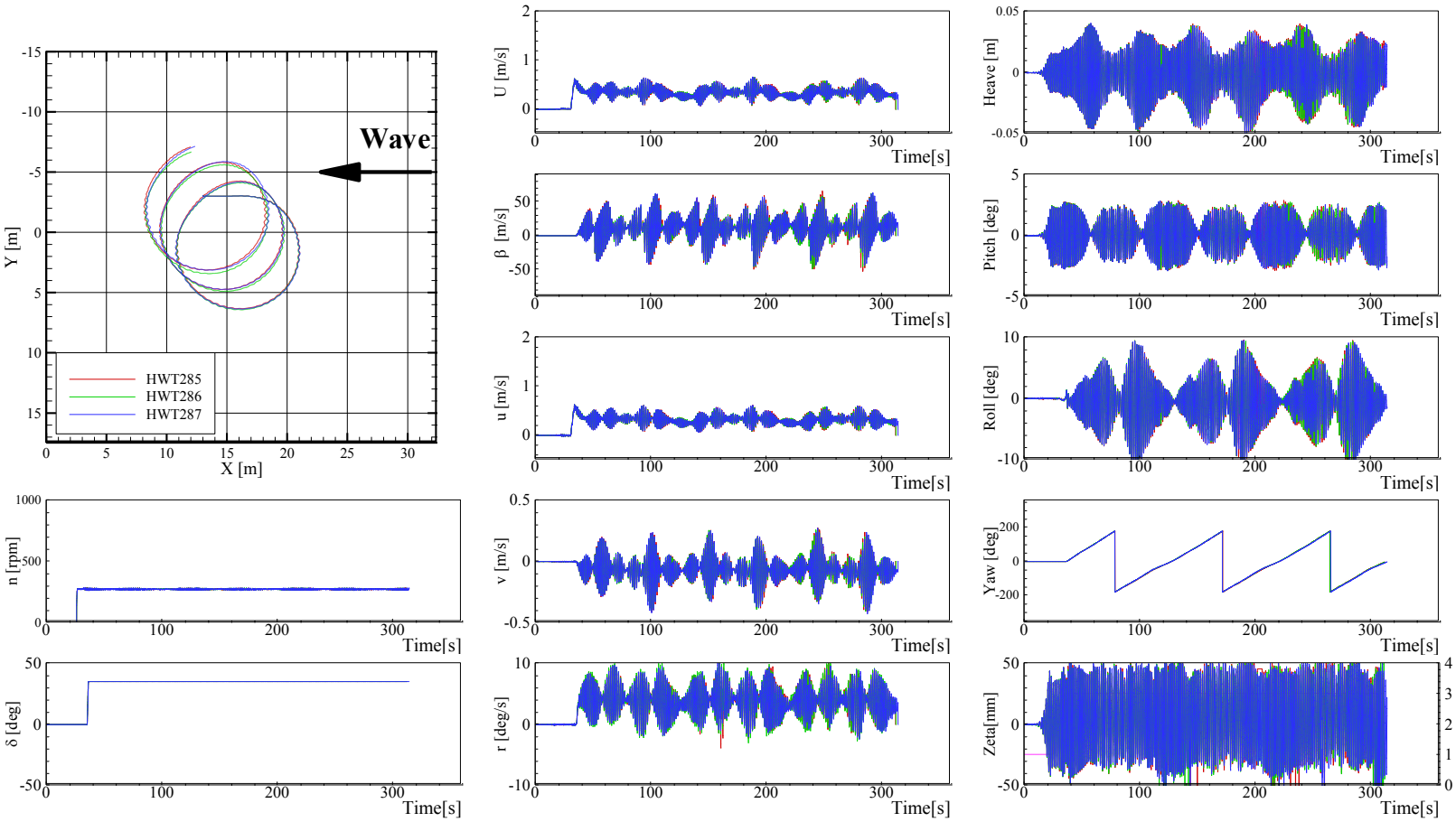

Figure G-11 Trajectories and time histories of turning in waves at Fr = 0.1, λ/L = 1.2, H/λ = 0.02, δ = 35, and χ = 0°

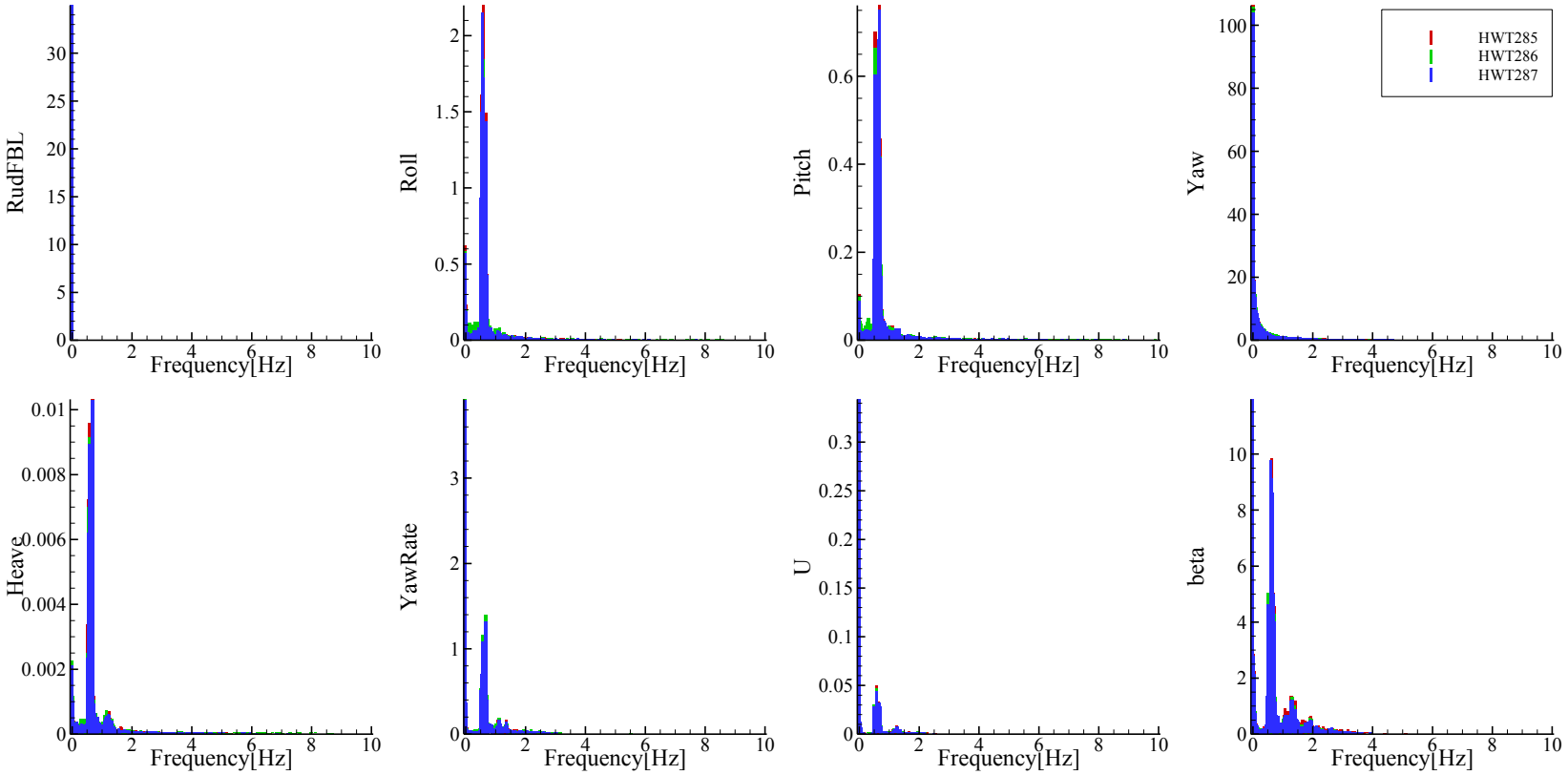

Figure G-12 FFT analysis of time histories of turning in waves at Fr = 0.1, λ/L = 1.2, H/λ = 0.02, δ = 35, and χ = 0°

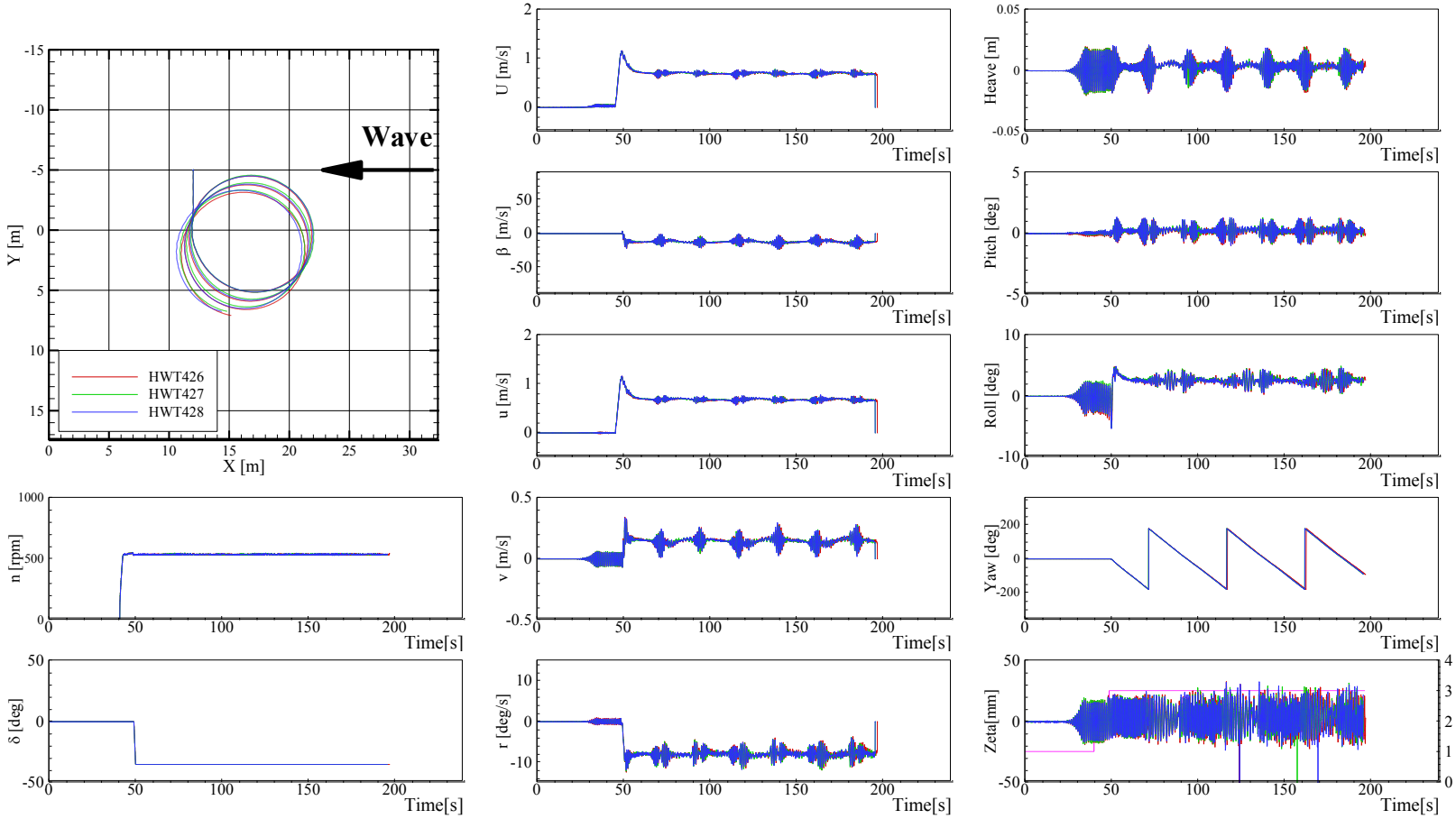

Figure G-13 Trajectories and time histories of turning in waves at Fr = 0.2, λ/L = 0.5, H/λ = 0.02, δ = -35, and χ = -90°

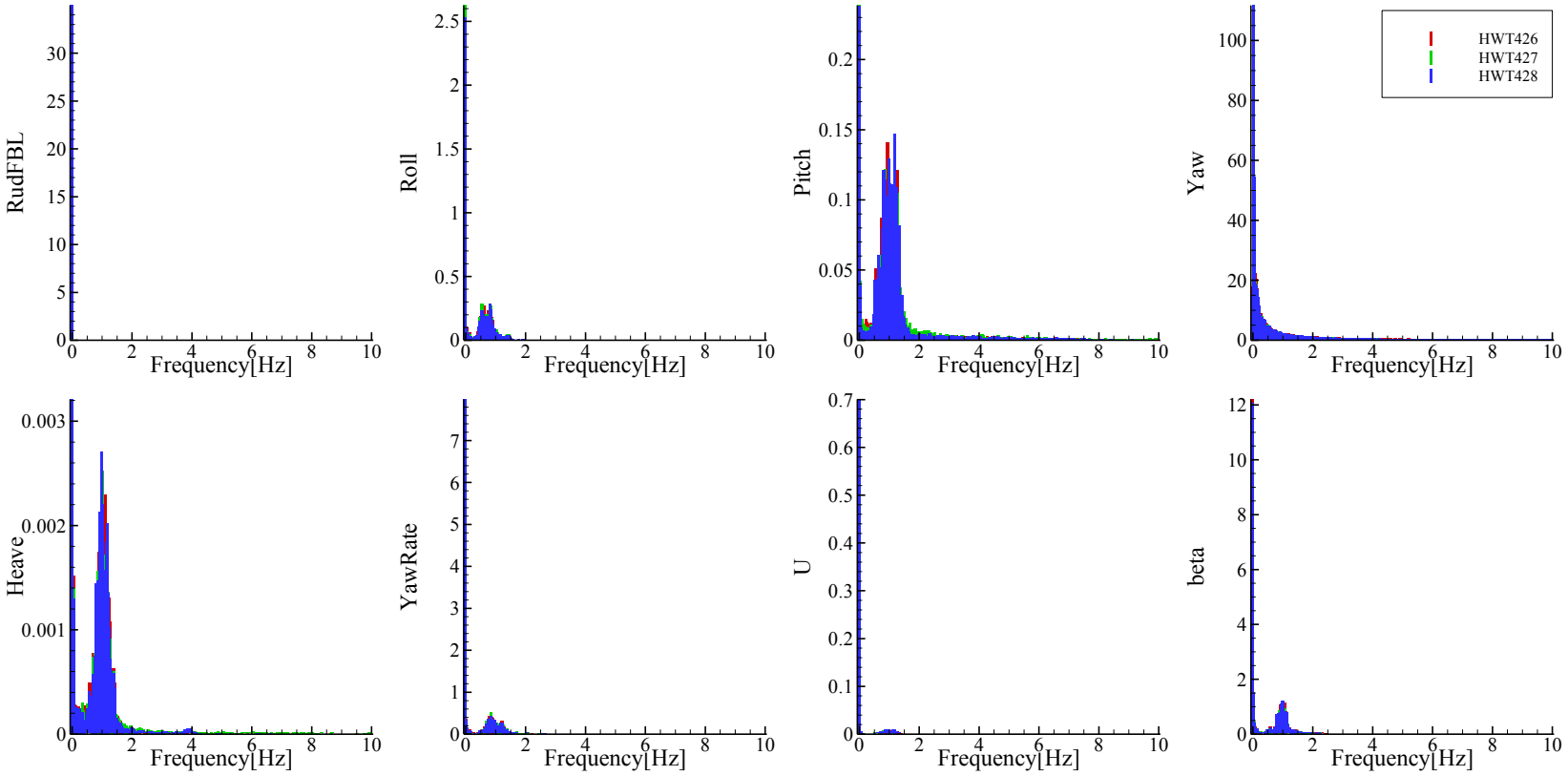

Figure G-14 FFT analysis of time histories of turning in waves at Fr = 0.2, λ/L = 0.5, H/λ = 0.02, δ = -35, and χ = -90°

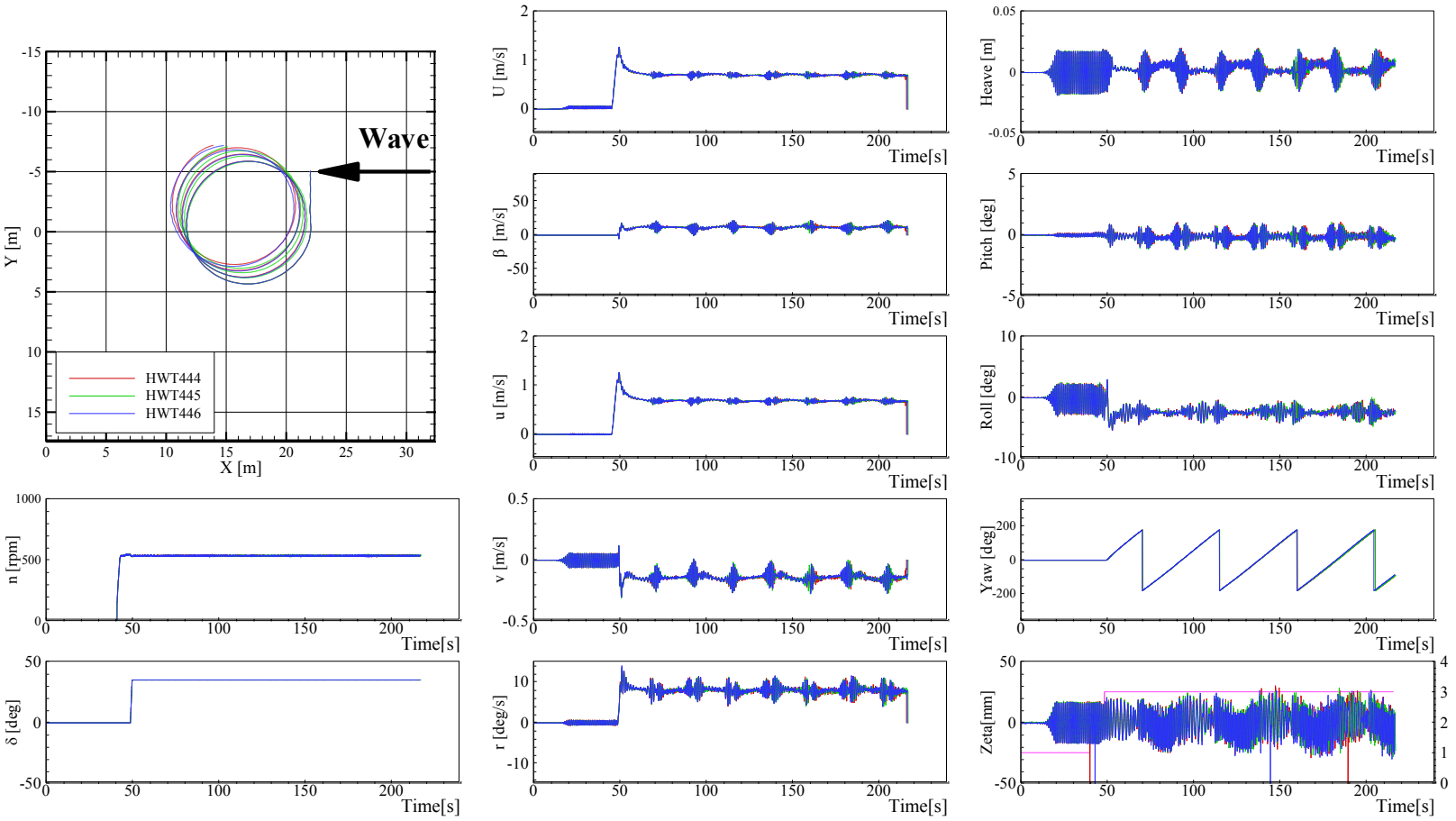

Figure G-15 Trajectories and time histories of turning in waves at Fr = 0.2, λ/L = 0.5, H/λ = 0.02, δ = 35, and χ = -90°

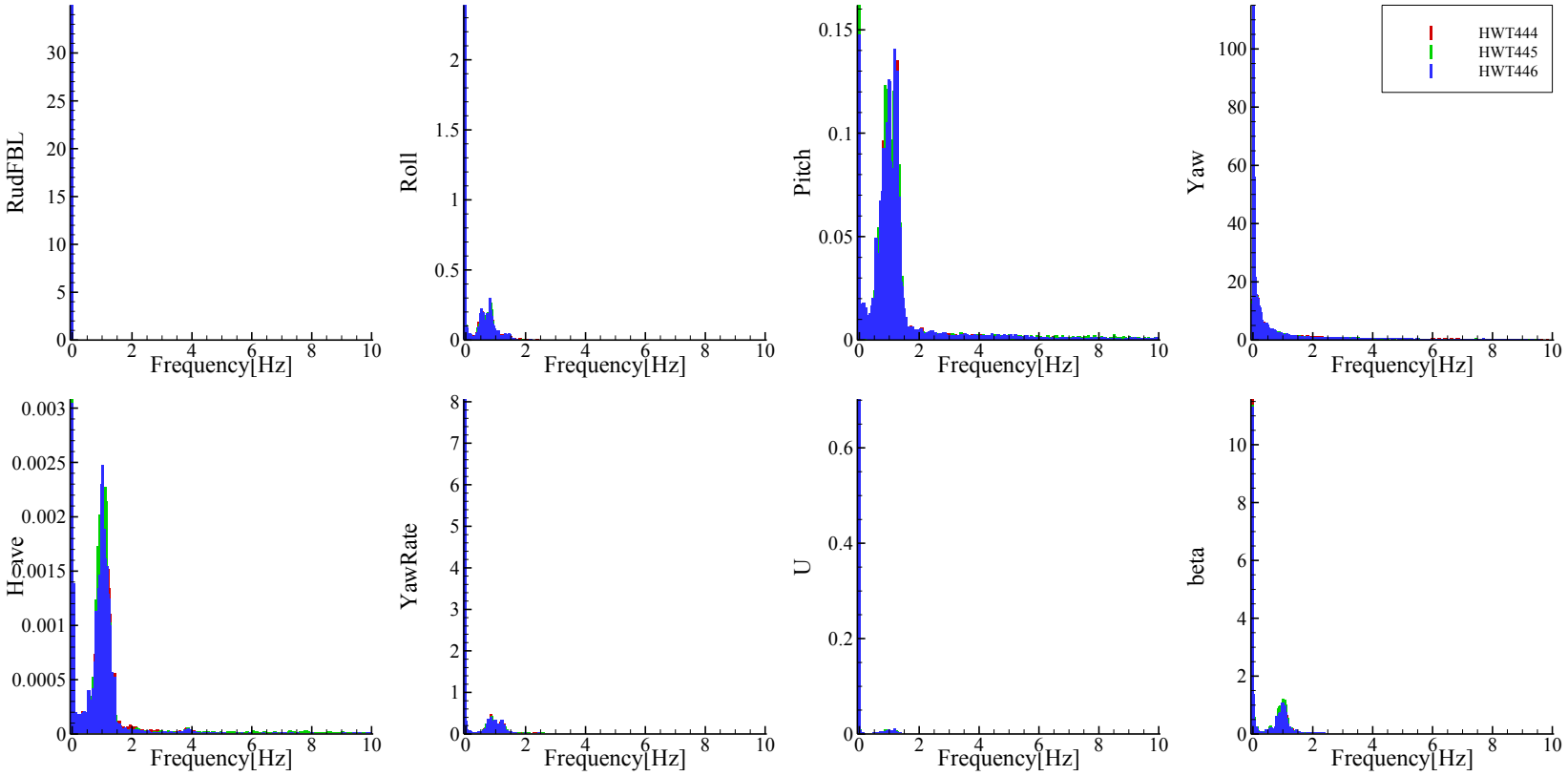

Figure G-16 FFT analysis of time histories of turning in waves at Fr = 0.2, λ/L = 0.5, H/λ = 0.02, δ = 35, and χ = -90°

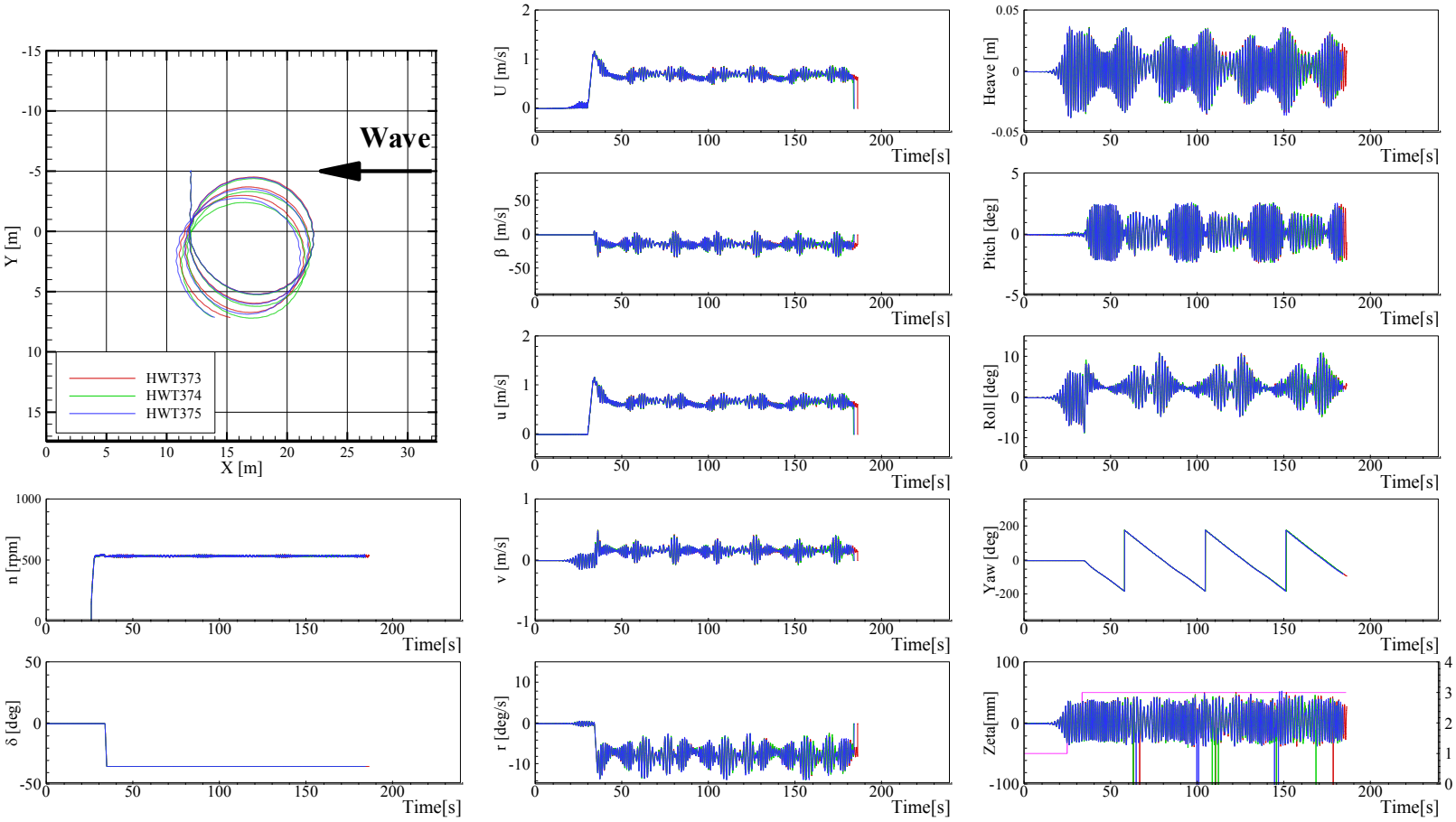

Figure G-17 Trajectories and time histories of turning in waves at Fr = 0.2, λ/L = 1.0, H/λ = 0.02, δ = -35, and χ = -90°

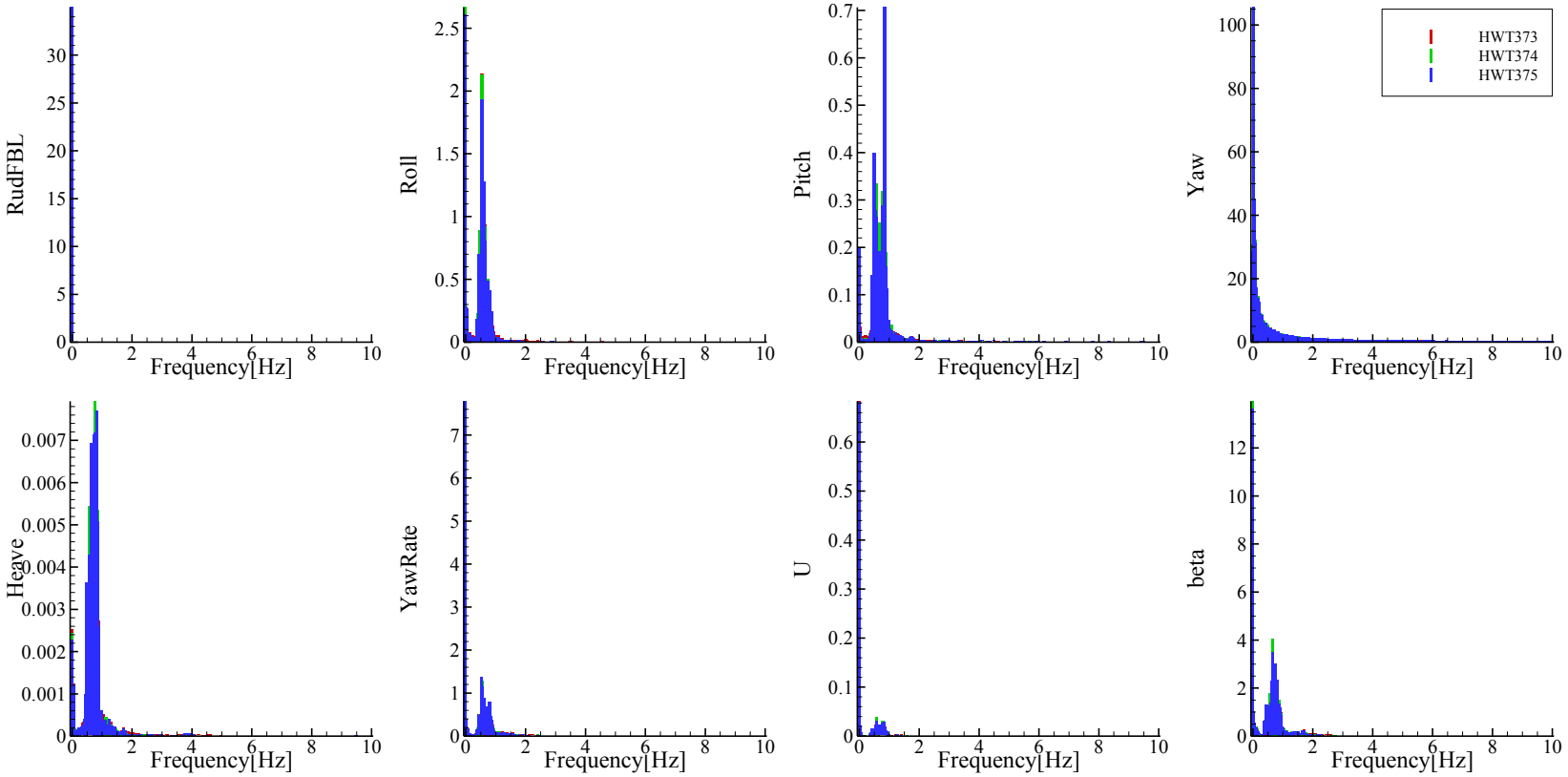

Figure G-18 FFT analysis of time histories of turning in waves at Fr = 0.2, λ/L = 1.0, H/λ = 0.02, δ = -35, and χ = -90°

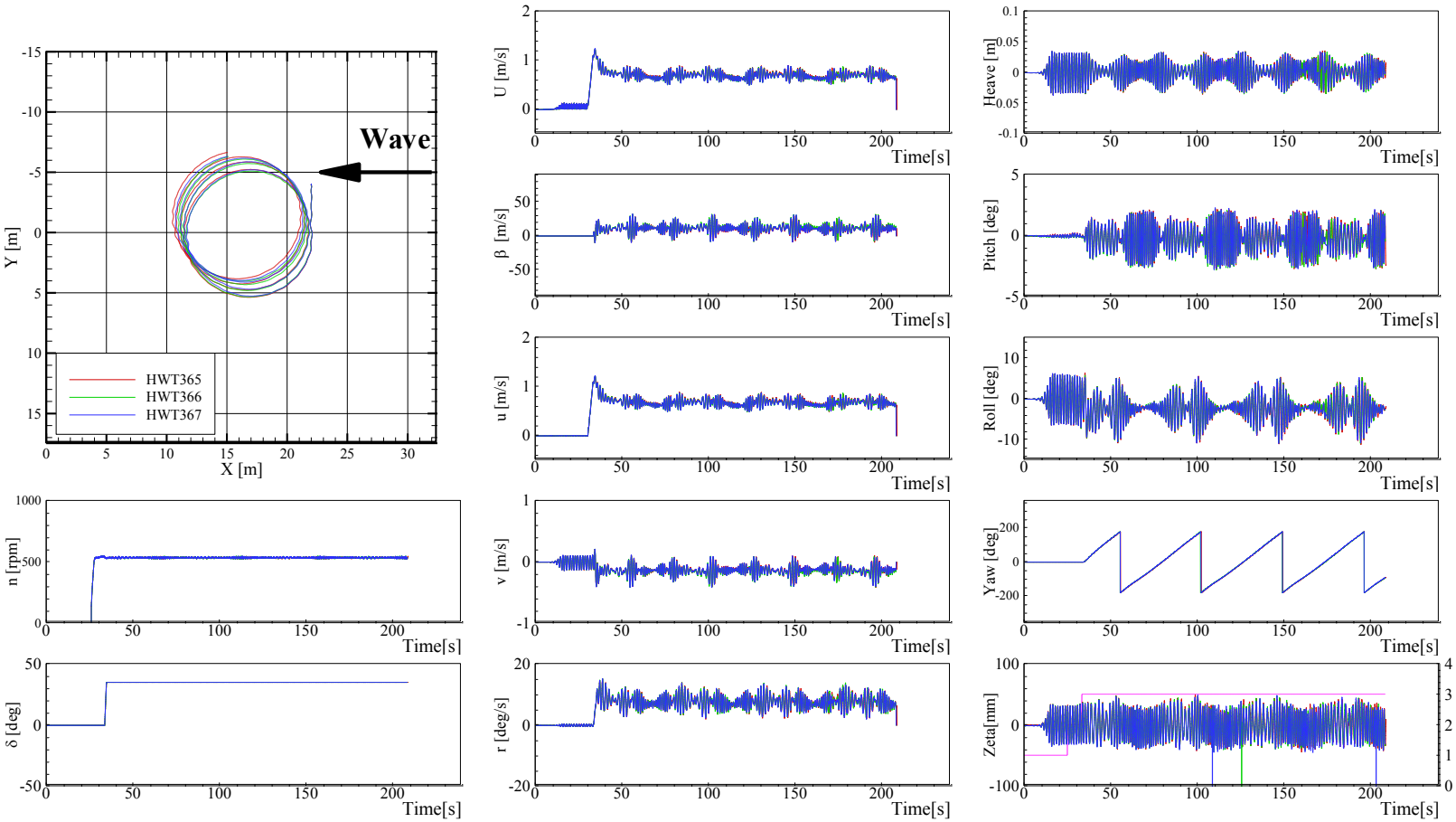

Figure G-19 Trajectories and time histories of turning in waves at Fr = 0.2, λ/L = 1.0, H/λ = 0.02, δ = 35, and χ = -90°

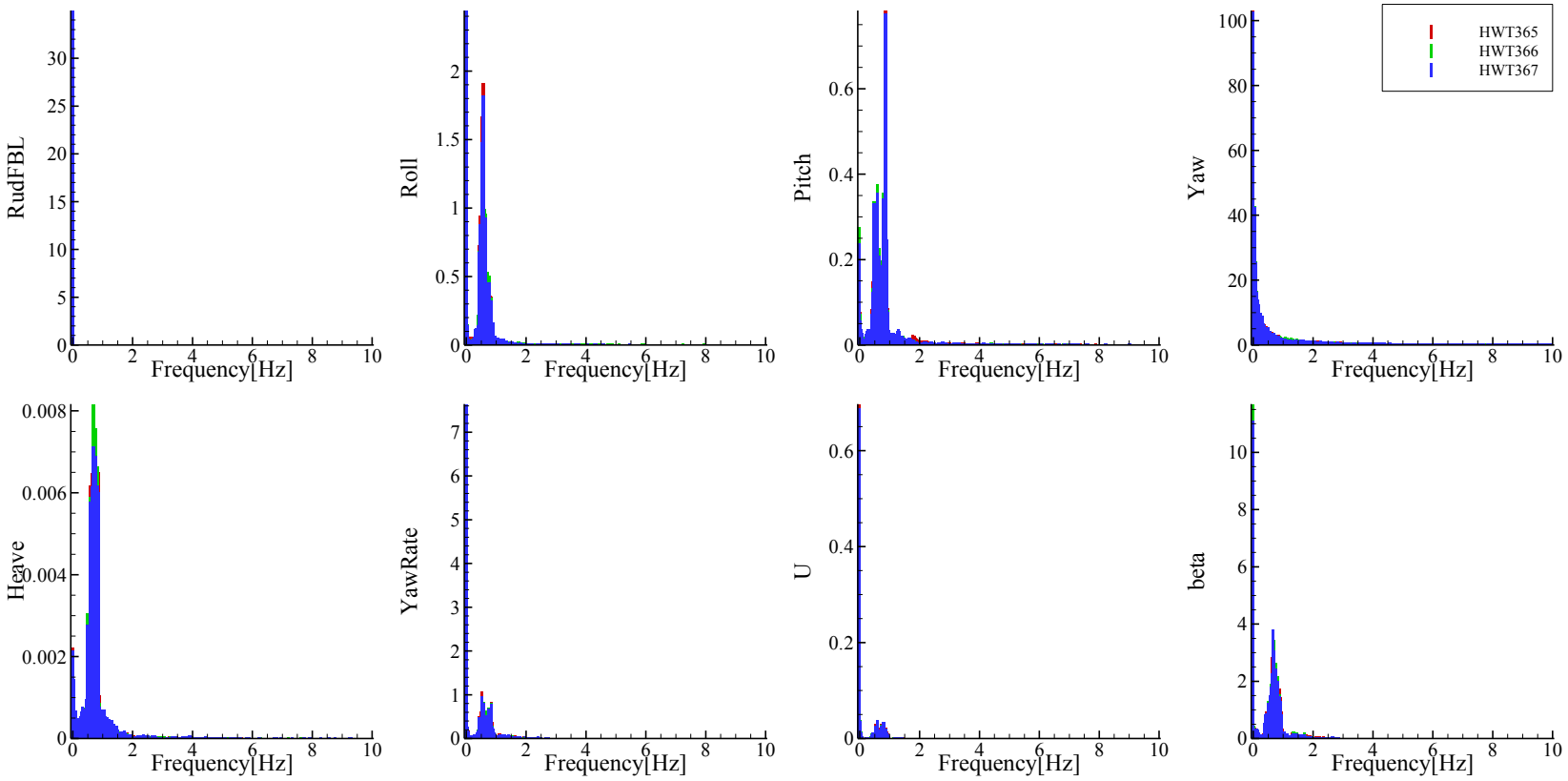

Figure G-20 FFT analysis of time histories of turning in waves at Fr = 0.2, λ/L = 1.0, H/λ = 0.02, δ = 35, and χ = -90°

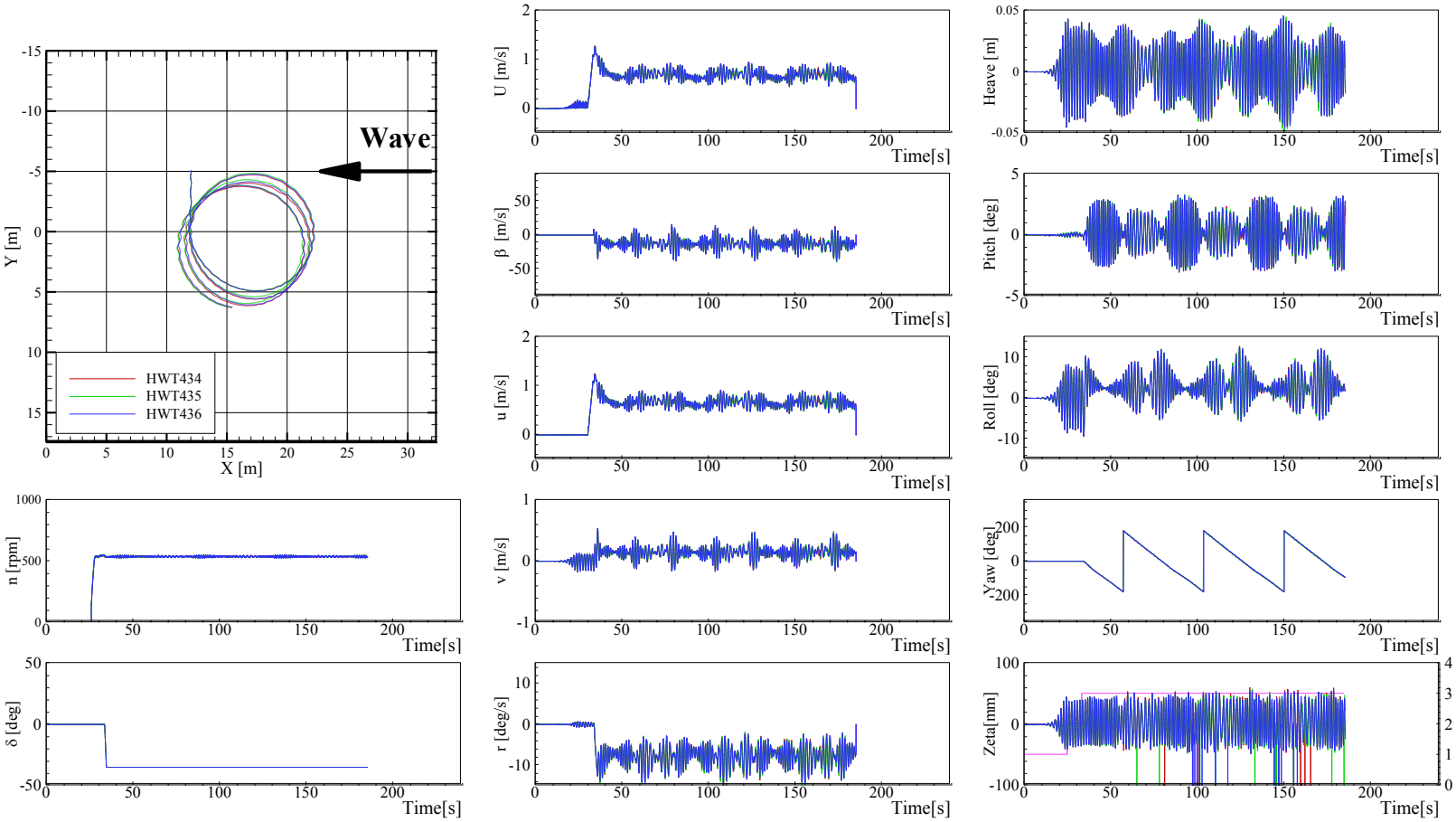

Figure G-21 Trajectories and time histories of turning in waves at Fr = 0.2, λ/L = 1.2, H/λ = 0.02, δ = -35, and χ = -90°

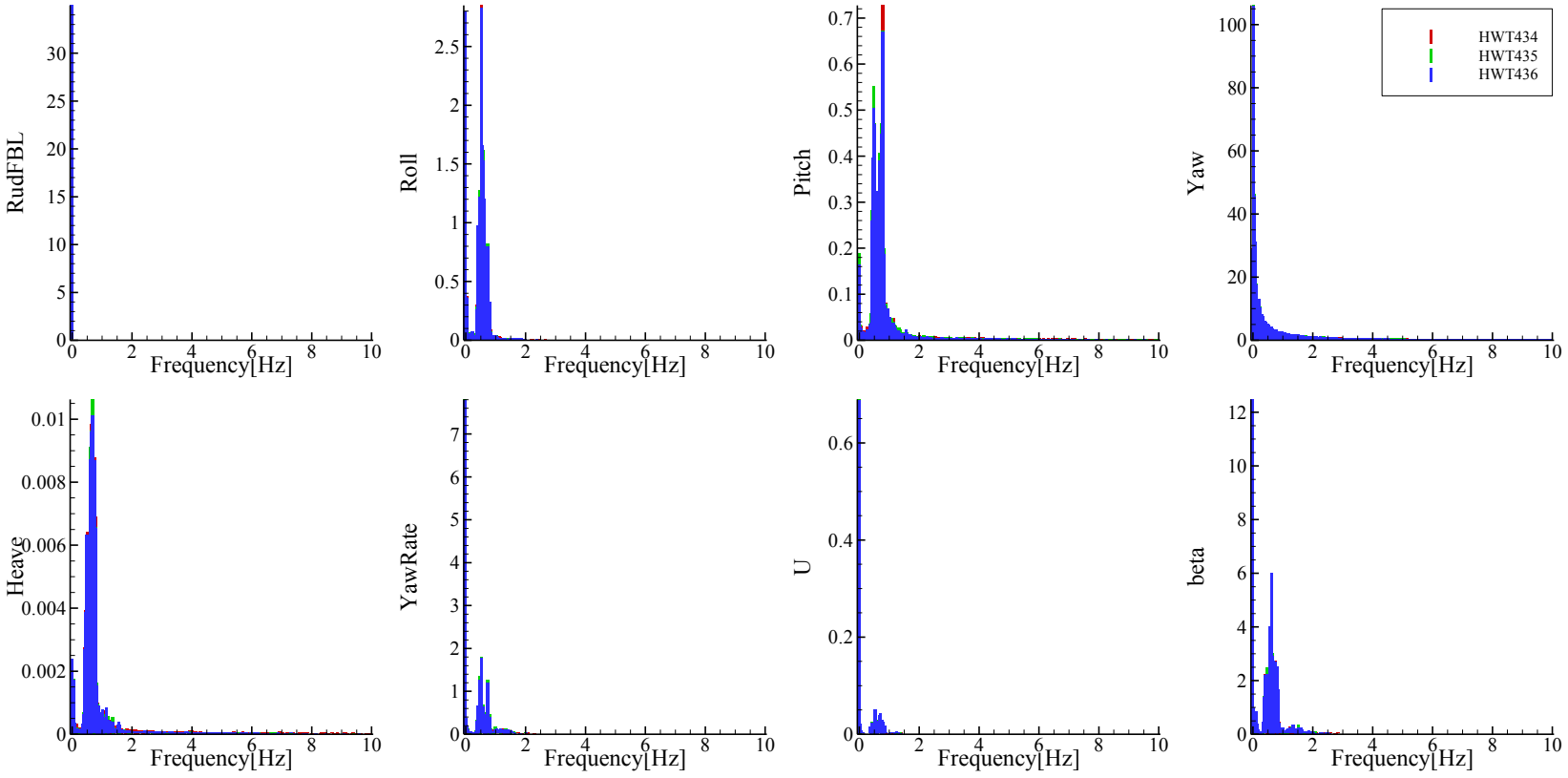

Figure G-22 FFT analysis of time histories of turning in waves at Fr = 0.2, λ/L = 1.2, H/λ = 0.02, δ = -35, and χ = -90°

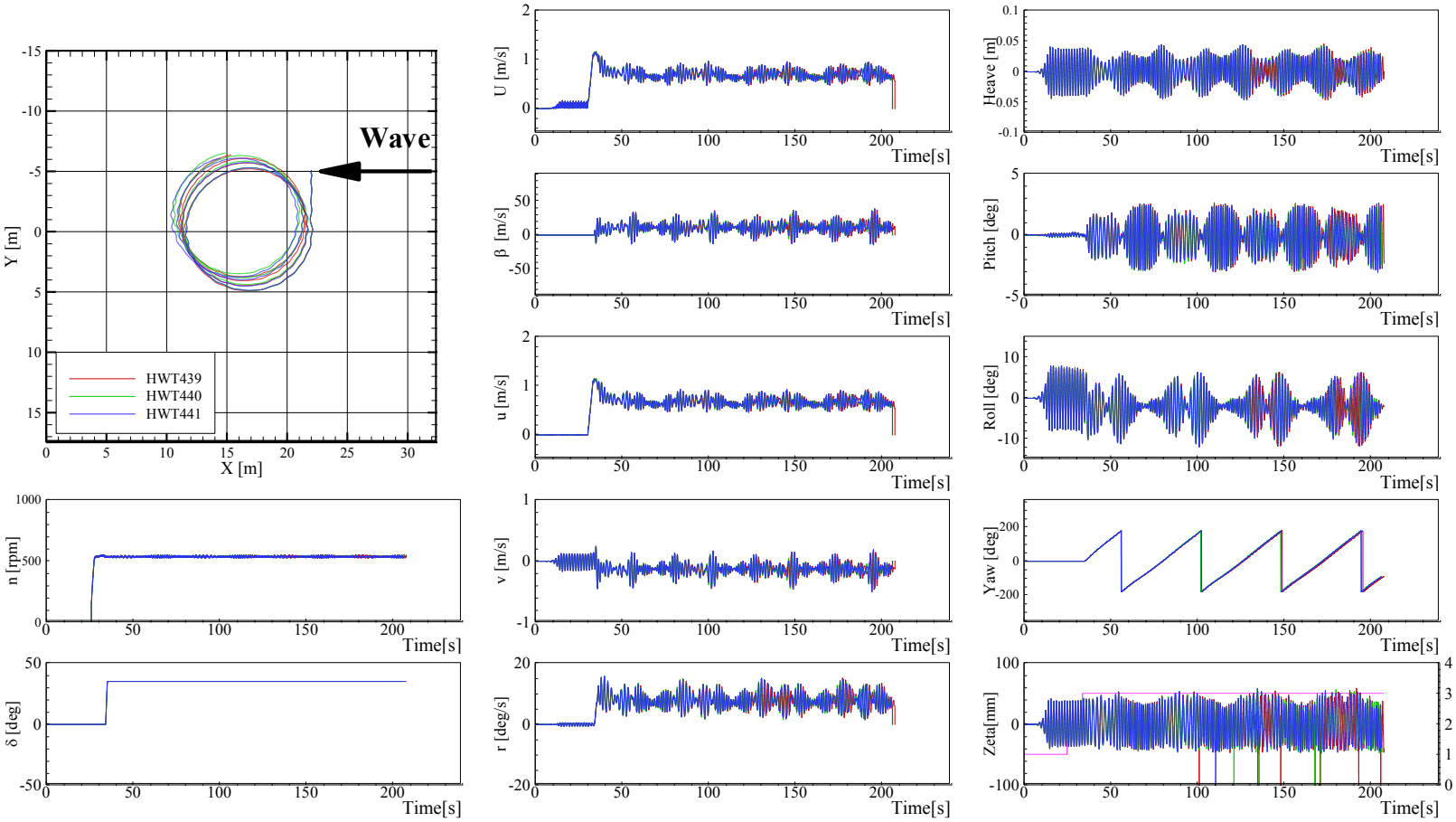

Figure G-23 Trajectories and time histories of turning in waves at Fr = 0.2, λ/L = 1.2, H/λ = 0.02, δ = 35, and χ = -90°

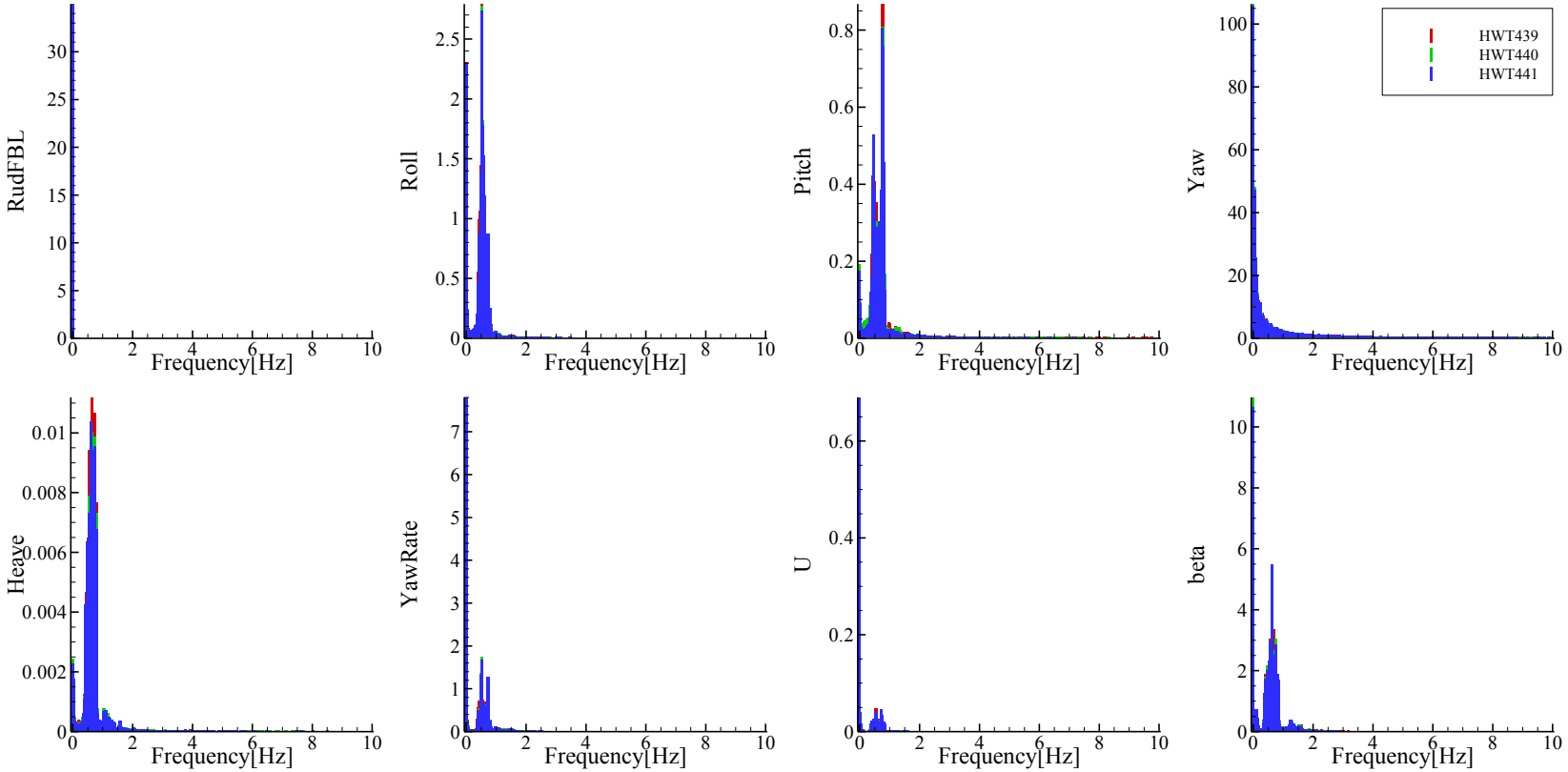

Figure G-24 FFT analysis of time histories of turning in waves at Fr = 0.2, λ/L = 1.2, H/λ = 0.02, δ = 35, and χ = -90°

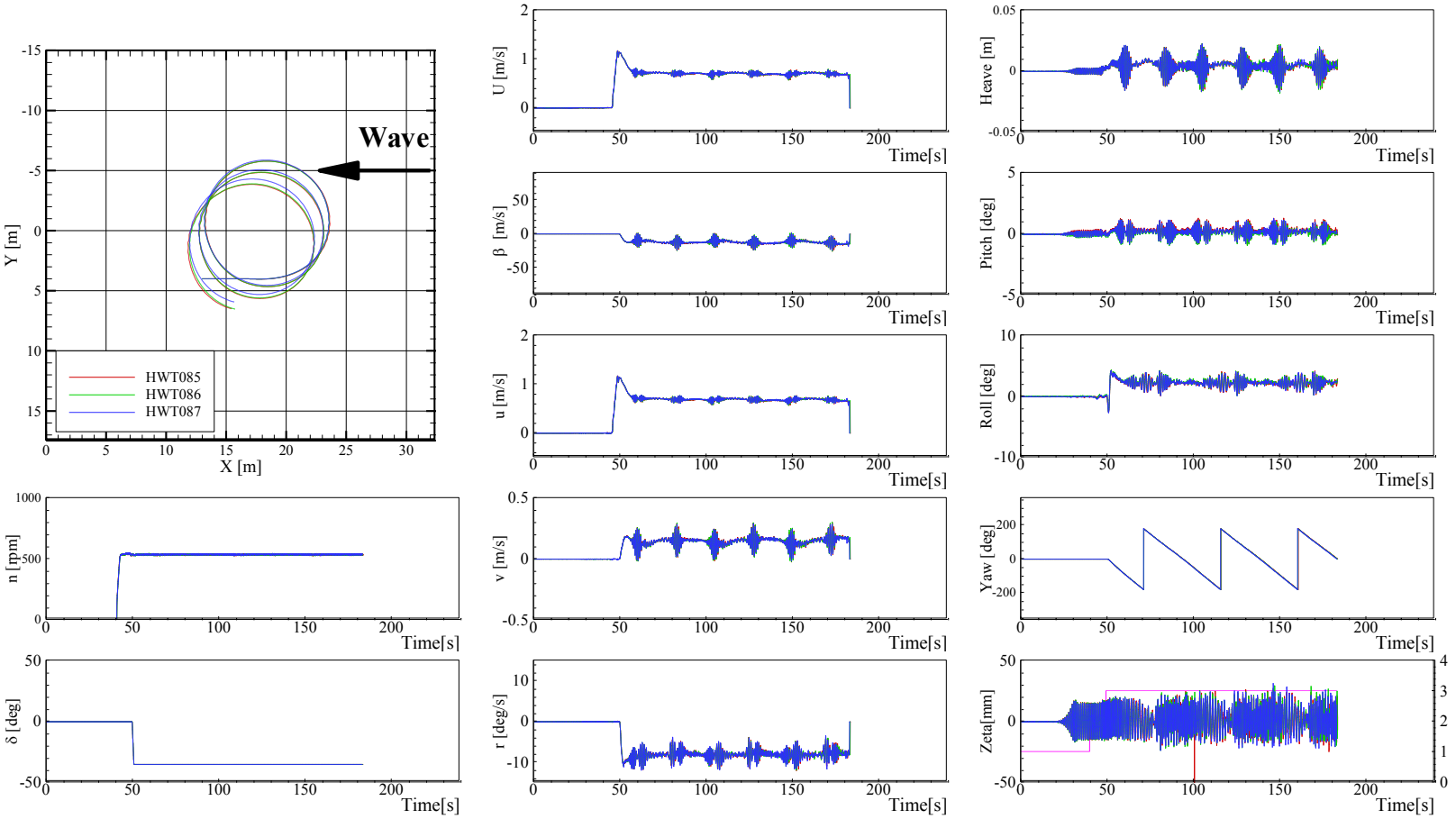

Figure G-25 Trajectories and time histories of turning in waves at Fr = 0.2, λ/L = 0.5, H/λ = 0.02, δ = -35, and χ = 0°

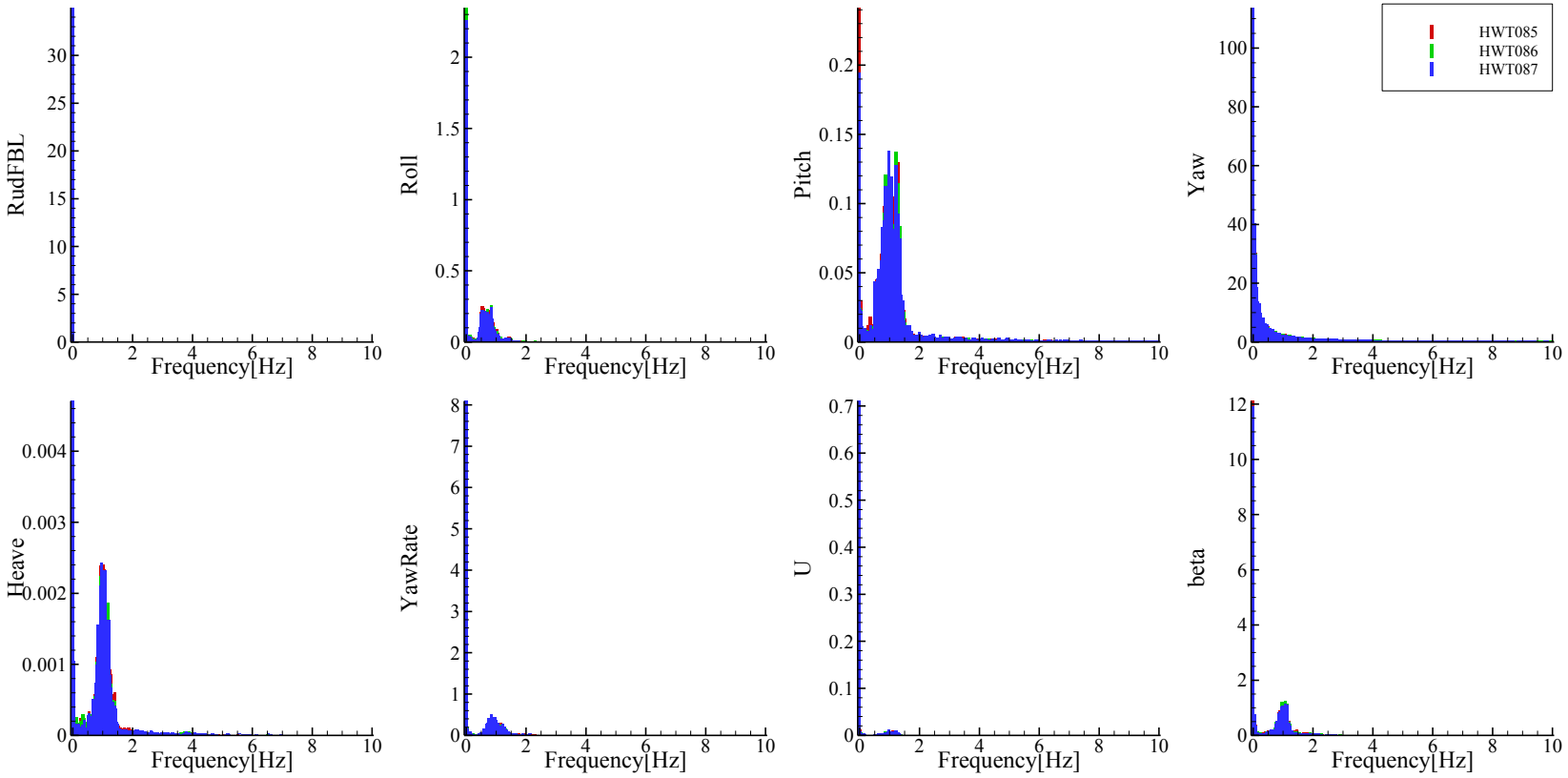

Figure G-26 FFT analysis of time histories of turning in waves at Fr = 0.2, λ/L = 0.5, H/λ = 0.02, δ = -35, and χ = 0°

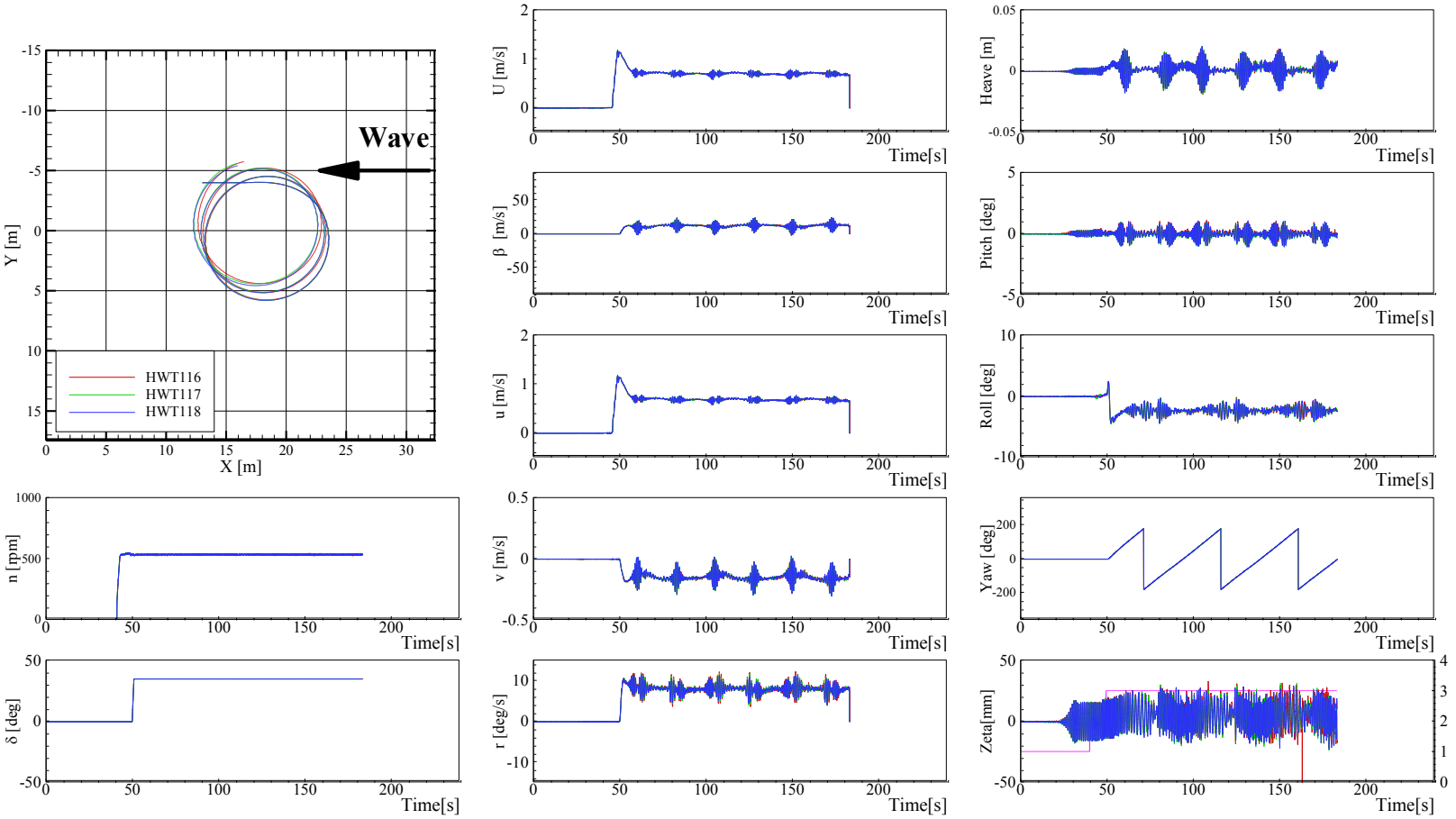

Figure G-27 Trajectories and time histories of turning in waves at Fr = 0.2, λ/L = 0.5, H/λ = 0.02, δ = 35, and χ = 0°

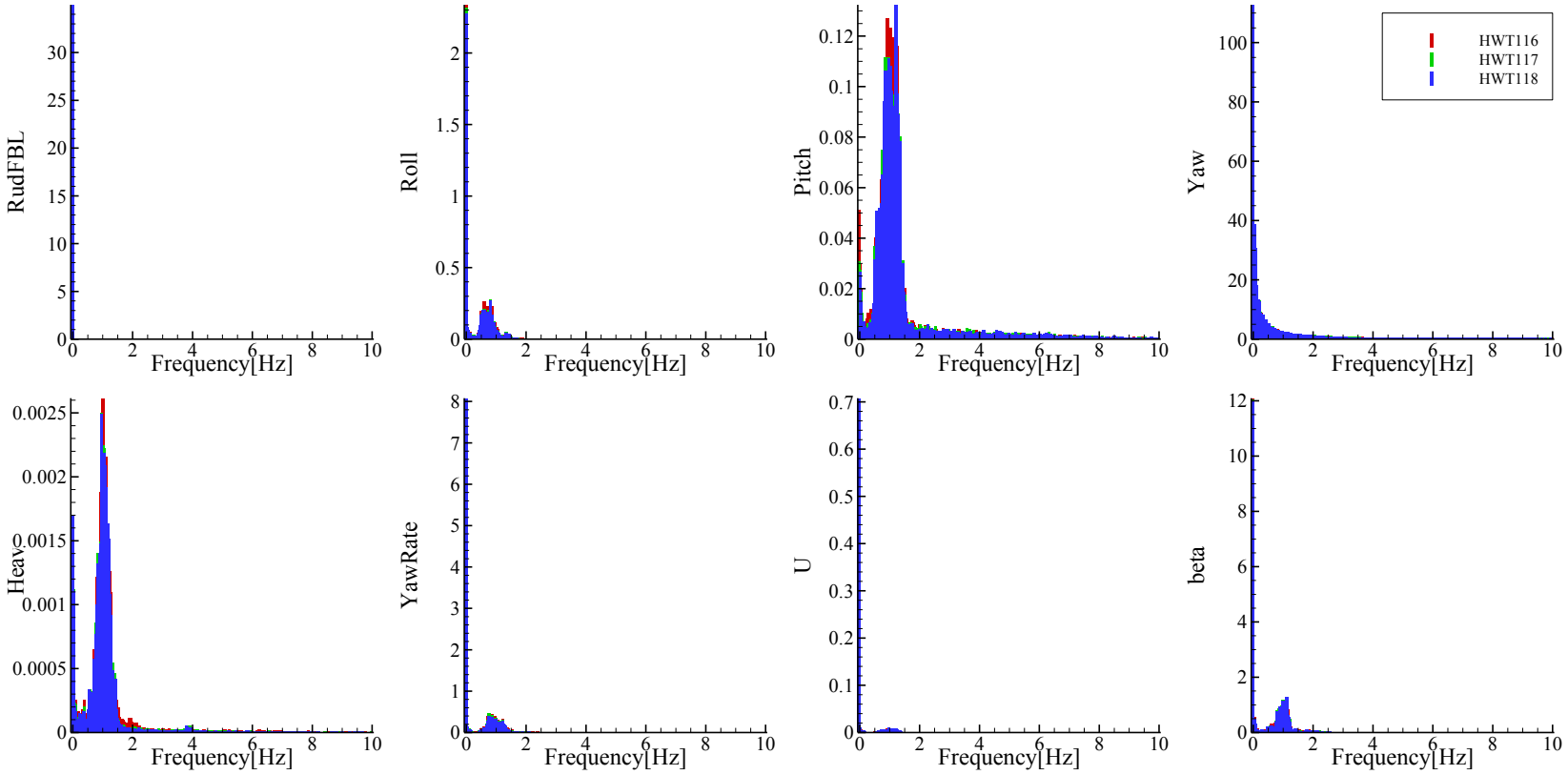

Figure G-28 FFT analysis of time histories of turning in waves at Fr = 0.2, λ/L = 0.5, H/λ = 0.02, δ = 35, and χ = 0°

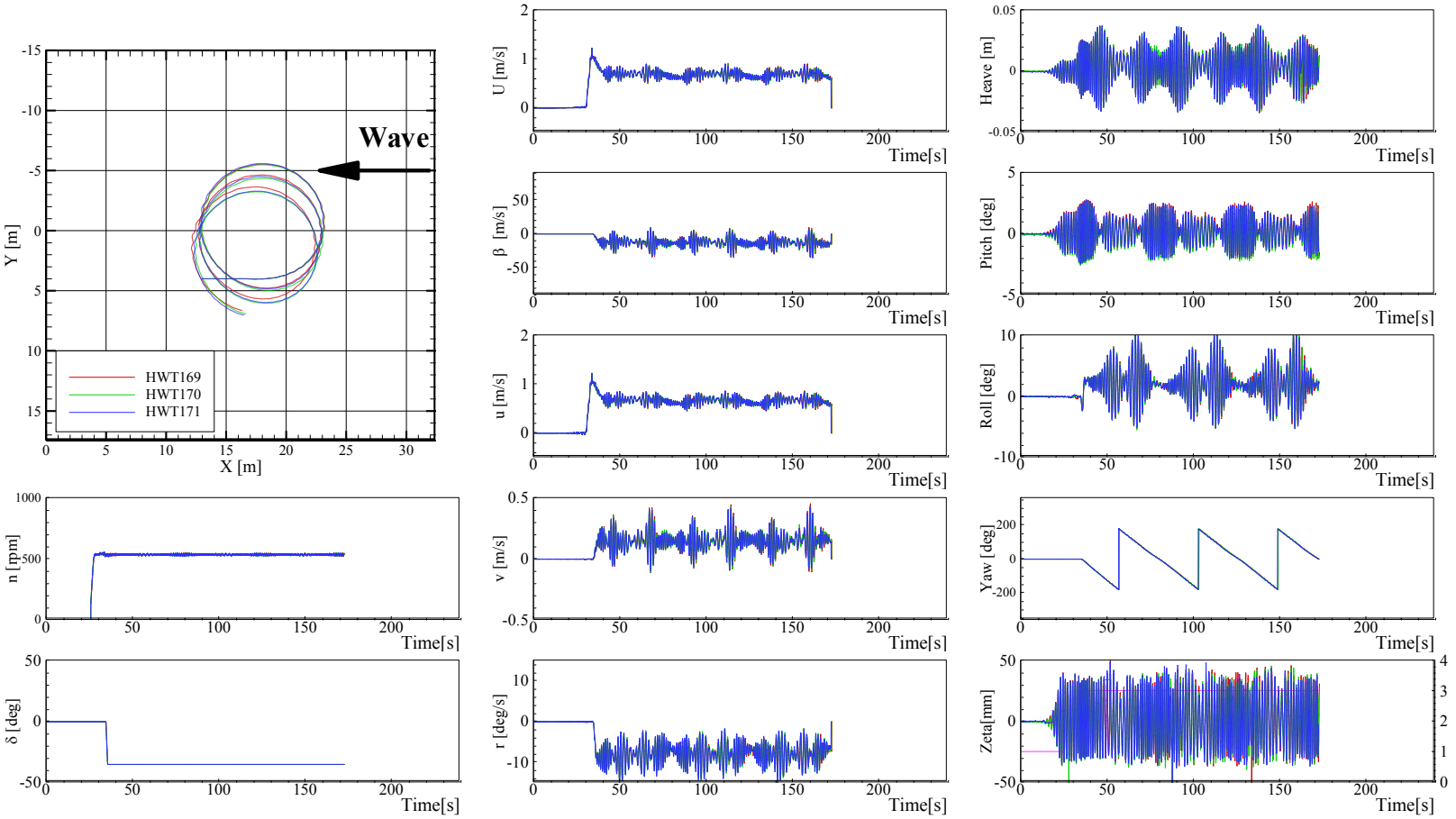

Figure G-29 Trajectories and time histories of turning in waves at Fr = 0.2, λ/L = 1.0, H/λ = 0.02, δ = -35, and χ = 0°

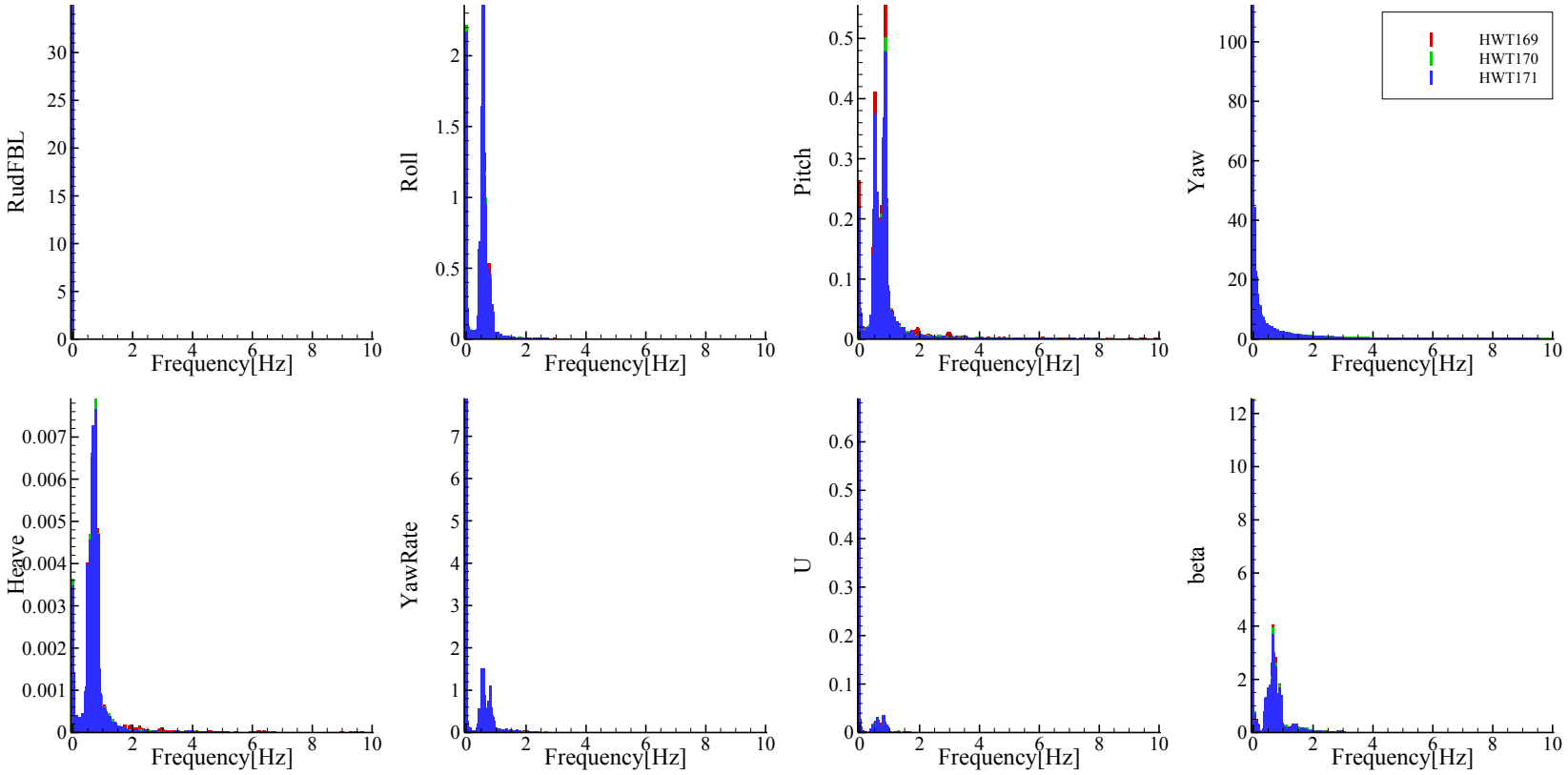

Figure G-30 FFT analysis of time histories of turning in waves at Fr = 0.2, λ/L = 1.0, H/λ = 0.02, δ = -35, and χ = 0°

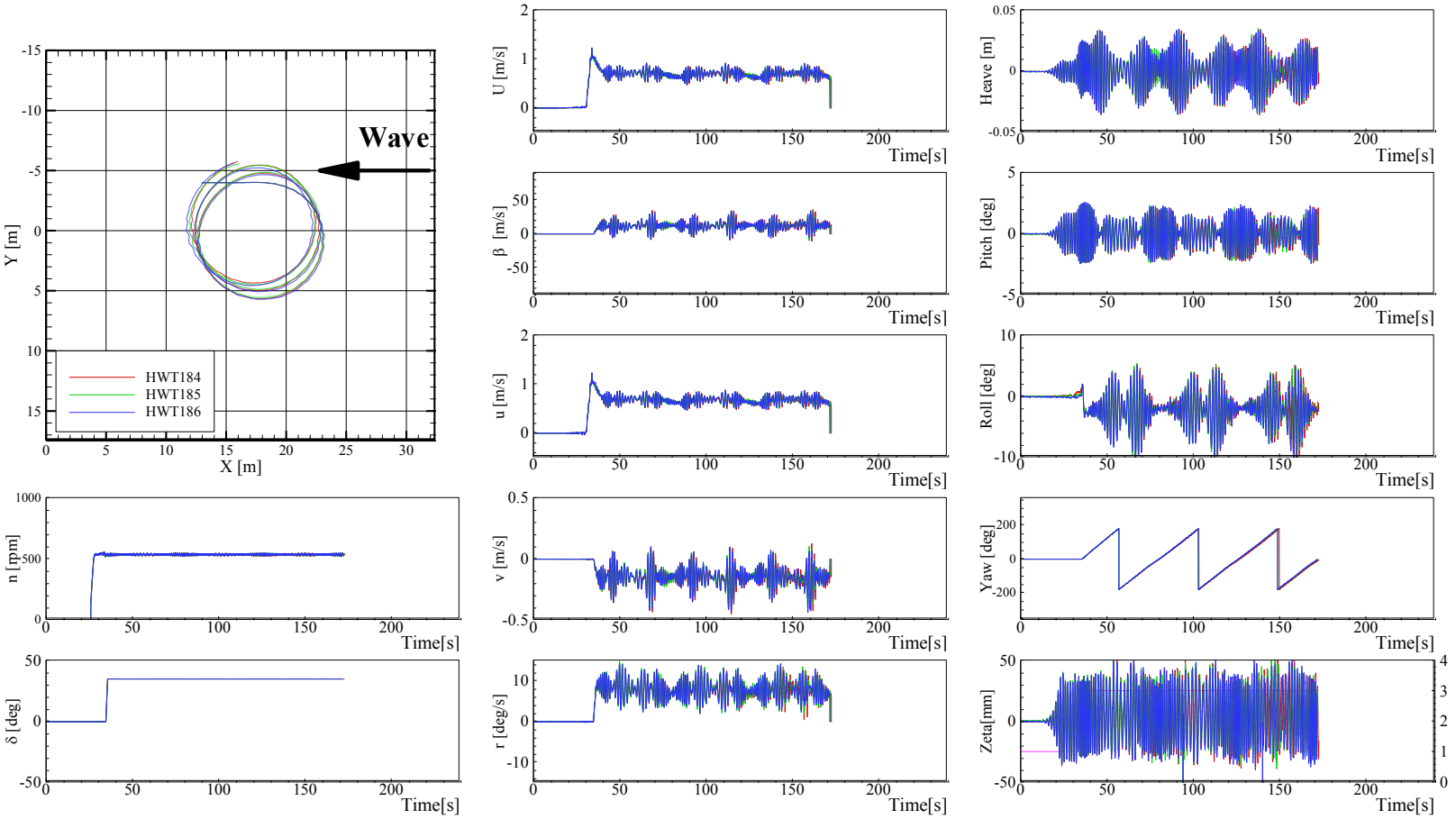

Figure G-31 Trajectories and time histories of turning in waves at Fr = 0.2, λ/L = 1.0, H/λ = 0.02, δ = 35, and χ = 0°

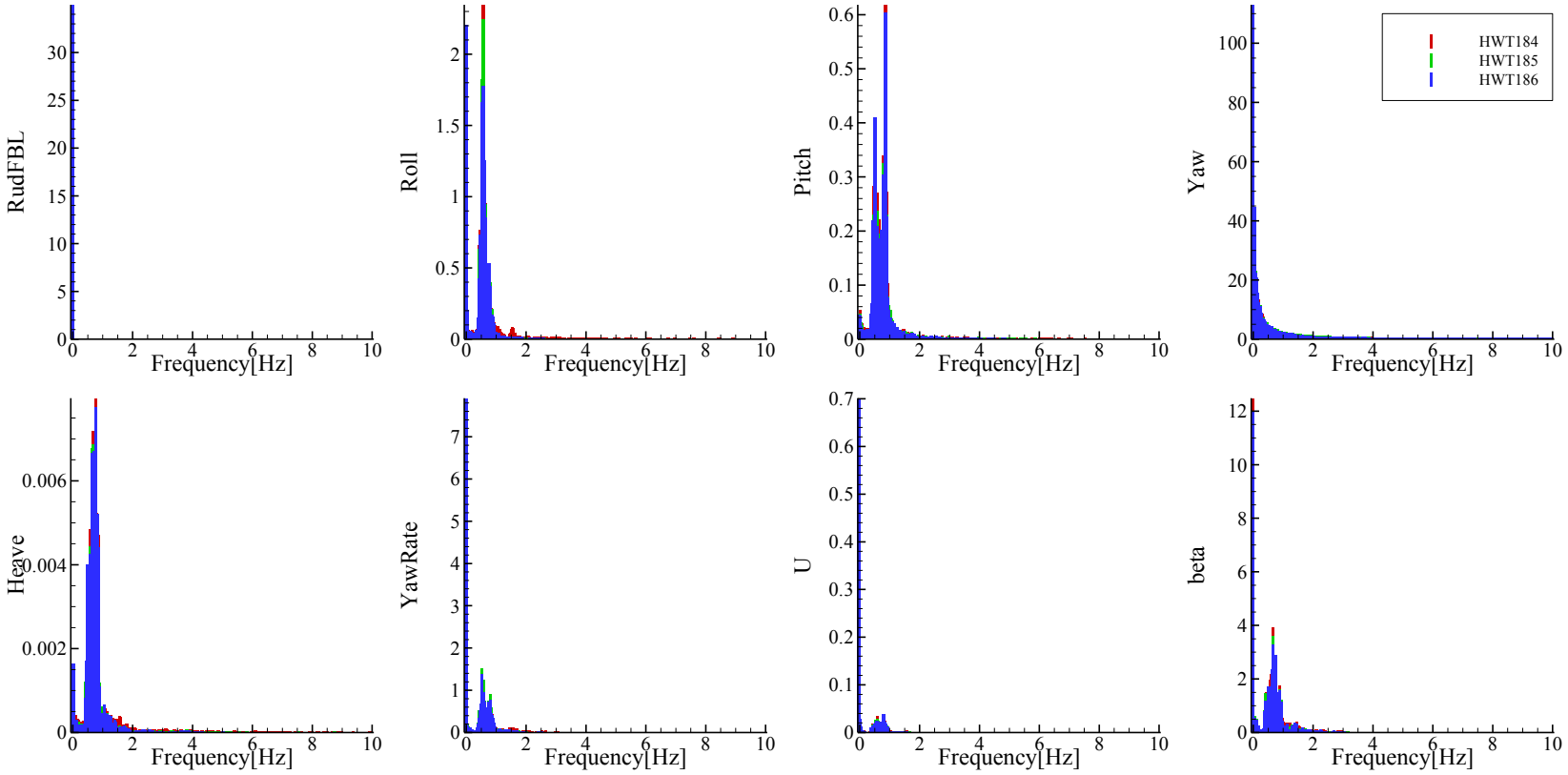

Figure G-32 FFT analysis of time histories of turning in waves at Fr = 0.2, λ/L = 1.0, H/λ = 0.02, δ = 35, and χ = 0°

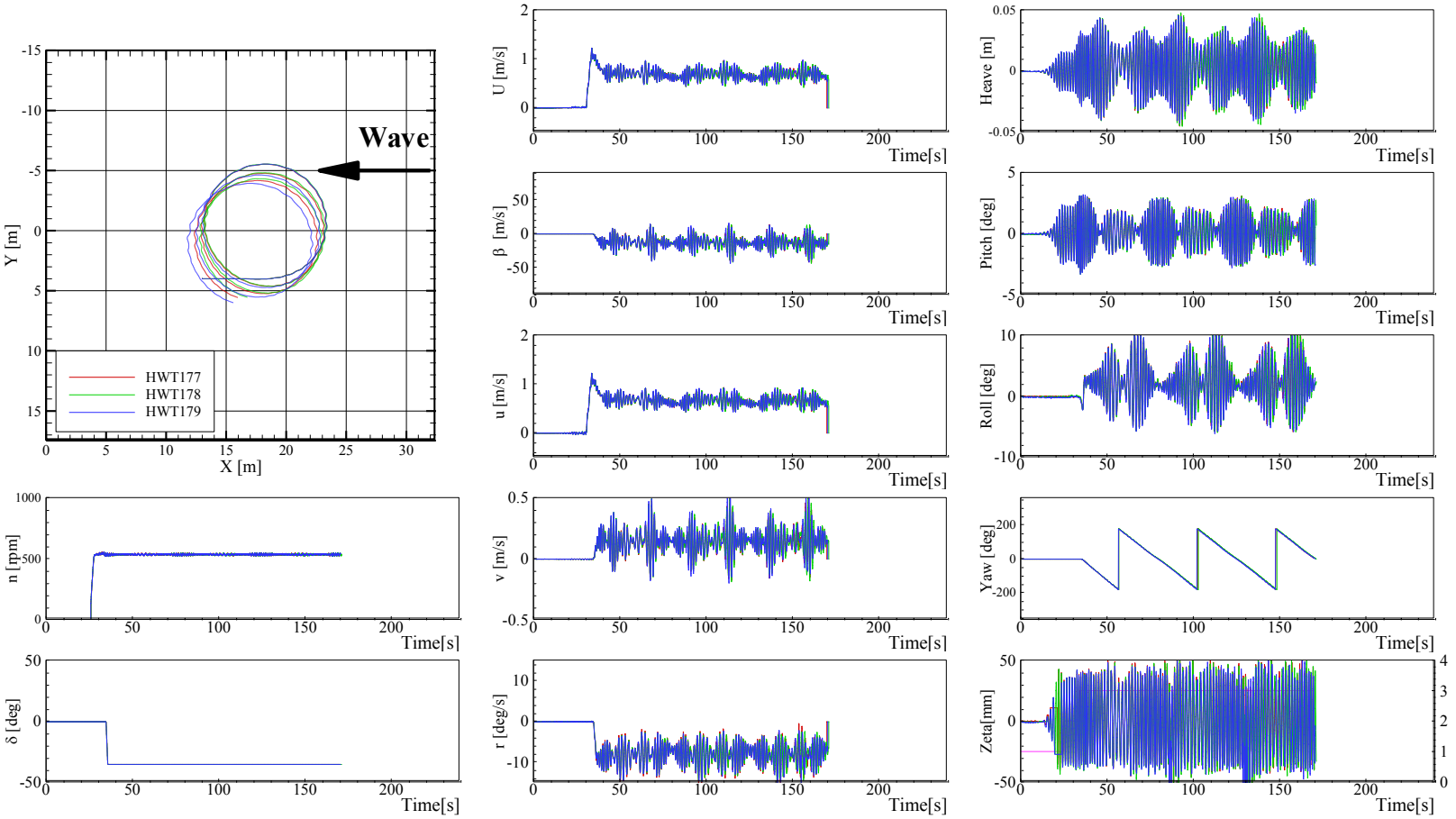

Figure G- 33 Trajectories and time histories of turning in waves at Fr = 0.2, λ/L = 1.2, H/λ = 0.02, δ = -35, and χ = 0°

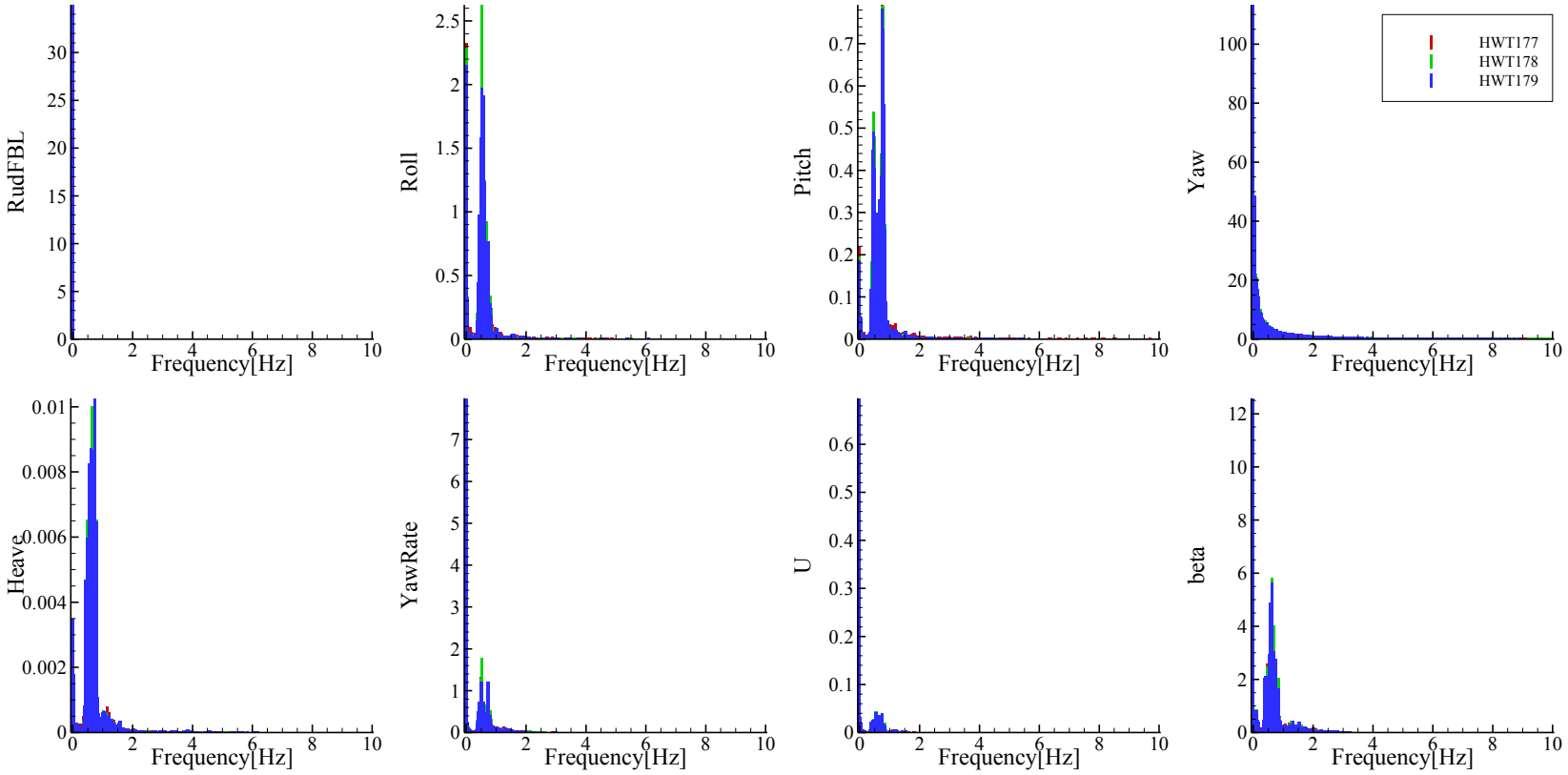

Figure G-34 FFT analysis of time histories of turning in waves at Fr = 0.2, λ/L = 1.2, H/λ = 0.02, δ = -35, and χ = 0°

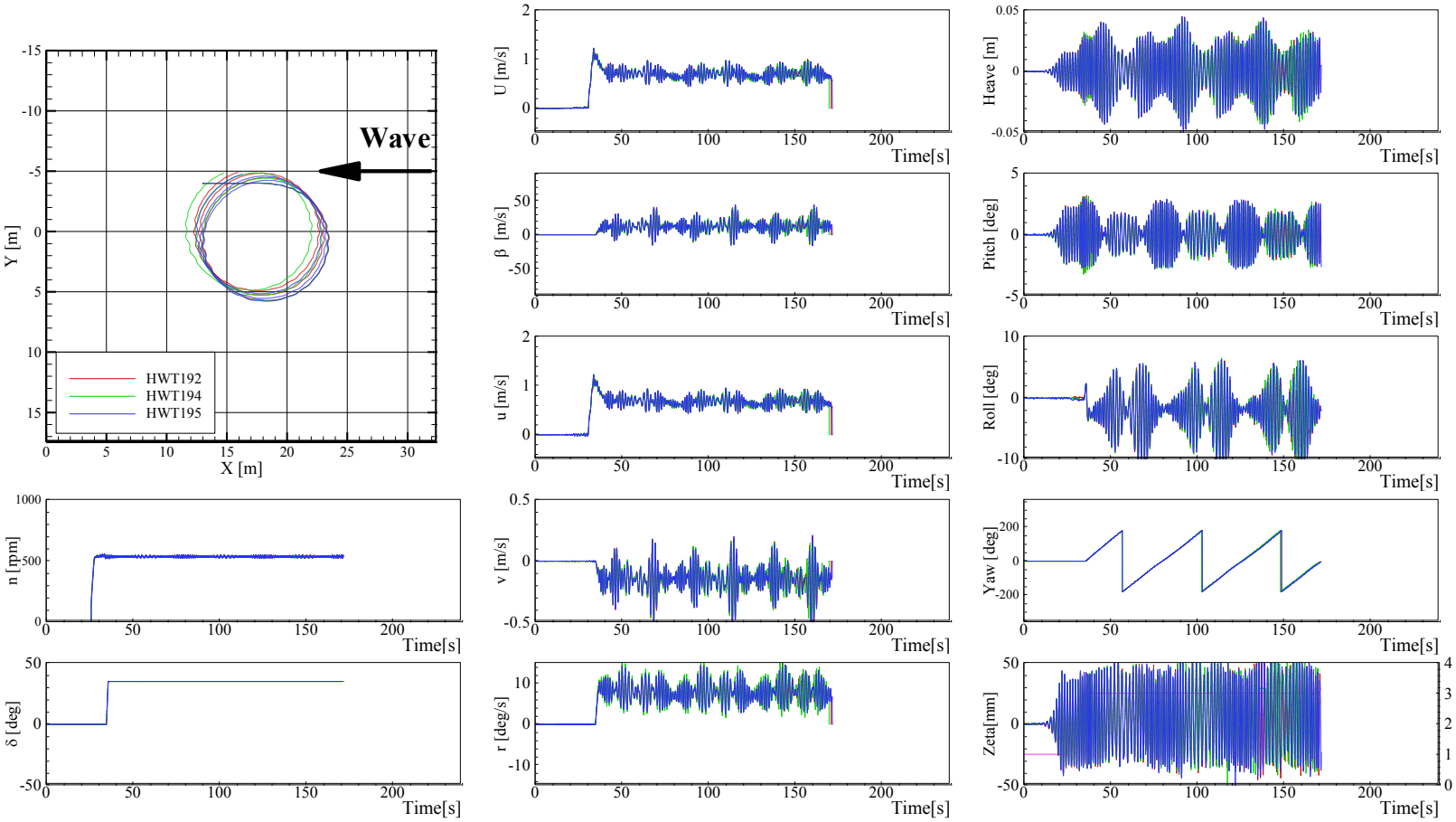

Figure G-35 Trajectories and time histories of turning in waves at Fr = 0.2, λ/L = 1.2, H/λ = 0.02, δ = 35, and χ = 0°

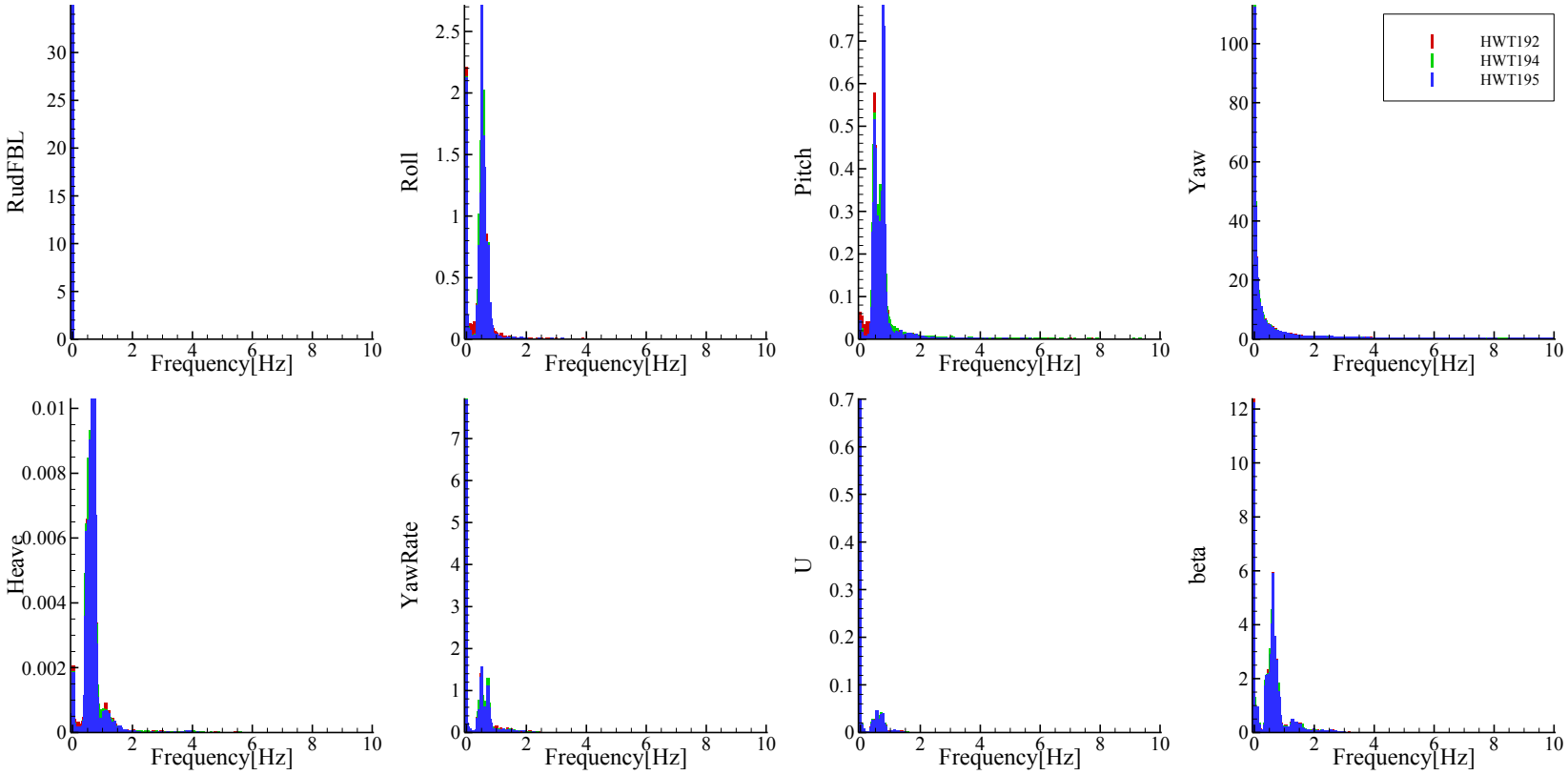

Figure G-36 FFT analysis of time histories of turning in waves at Fr = 0.2, λ/L = 1.2, H/λ = 0.02, δ = 35, and χ = 0°

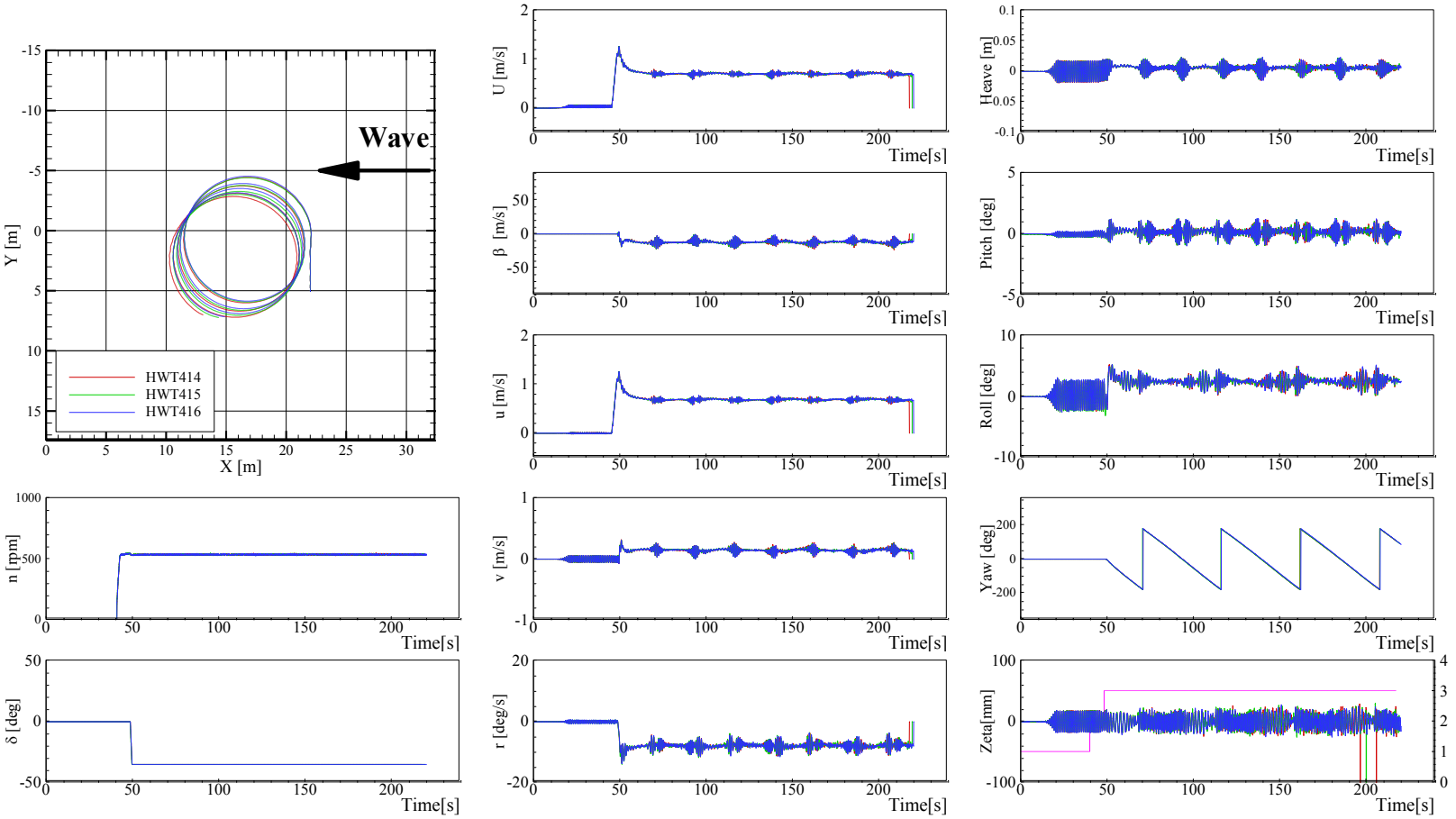

Figure G-37 Trajectories and time histories of turning in waves at Fr = 0.2, λ/L = 0.5, H/λ = 0.02, δ = -35, and χ = 90°

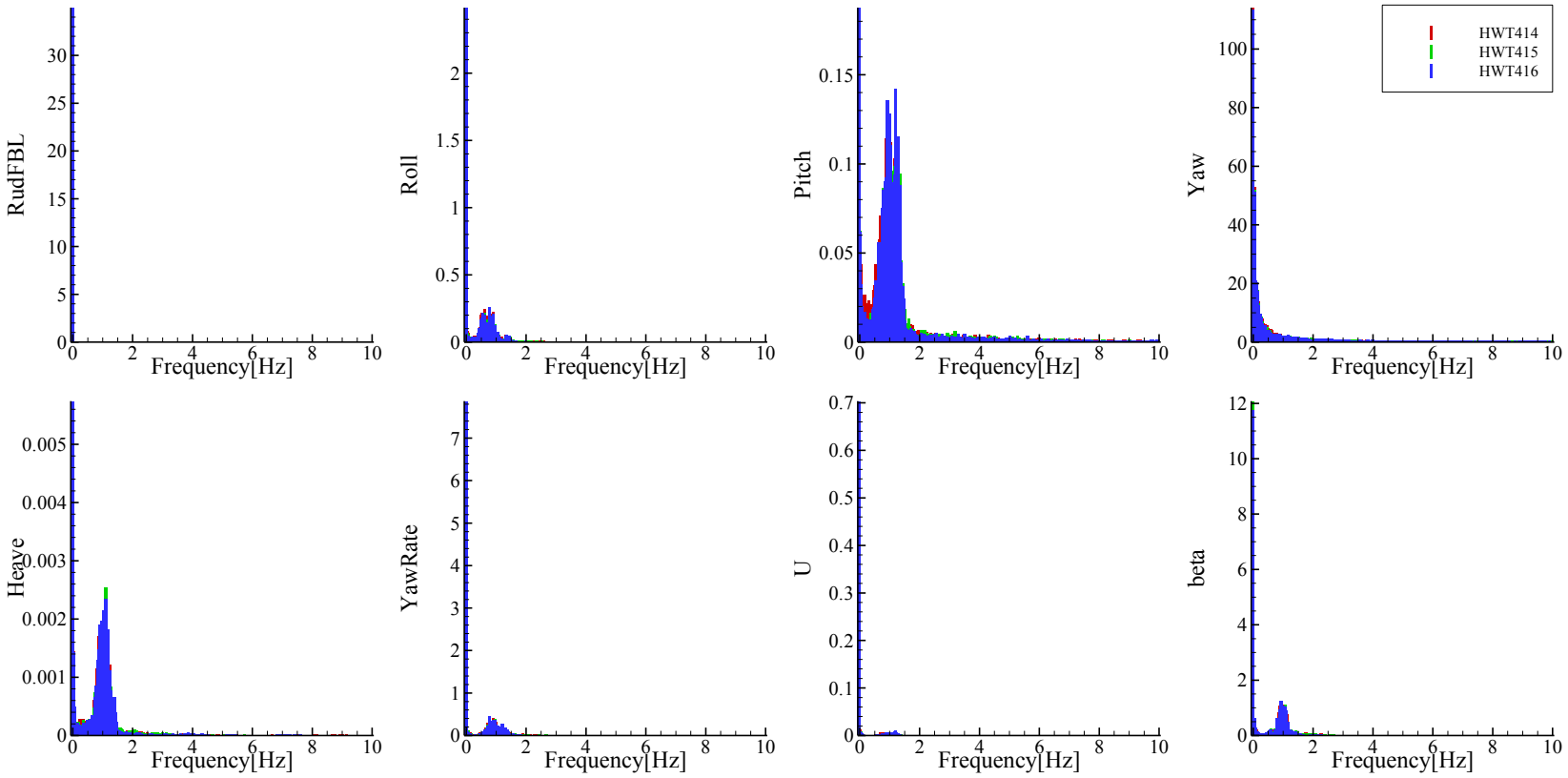

Figure G-38 FFT analysis of time histories of turning in waves at Fr = 0.2, λ/L = 0.5, H/λ = 0.02, δ = -35, and χ = 90°

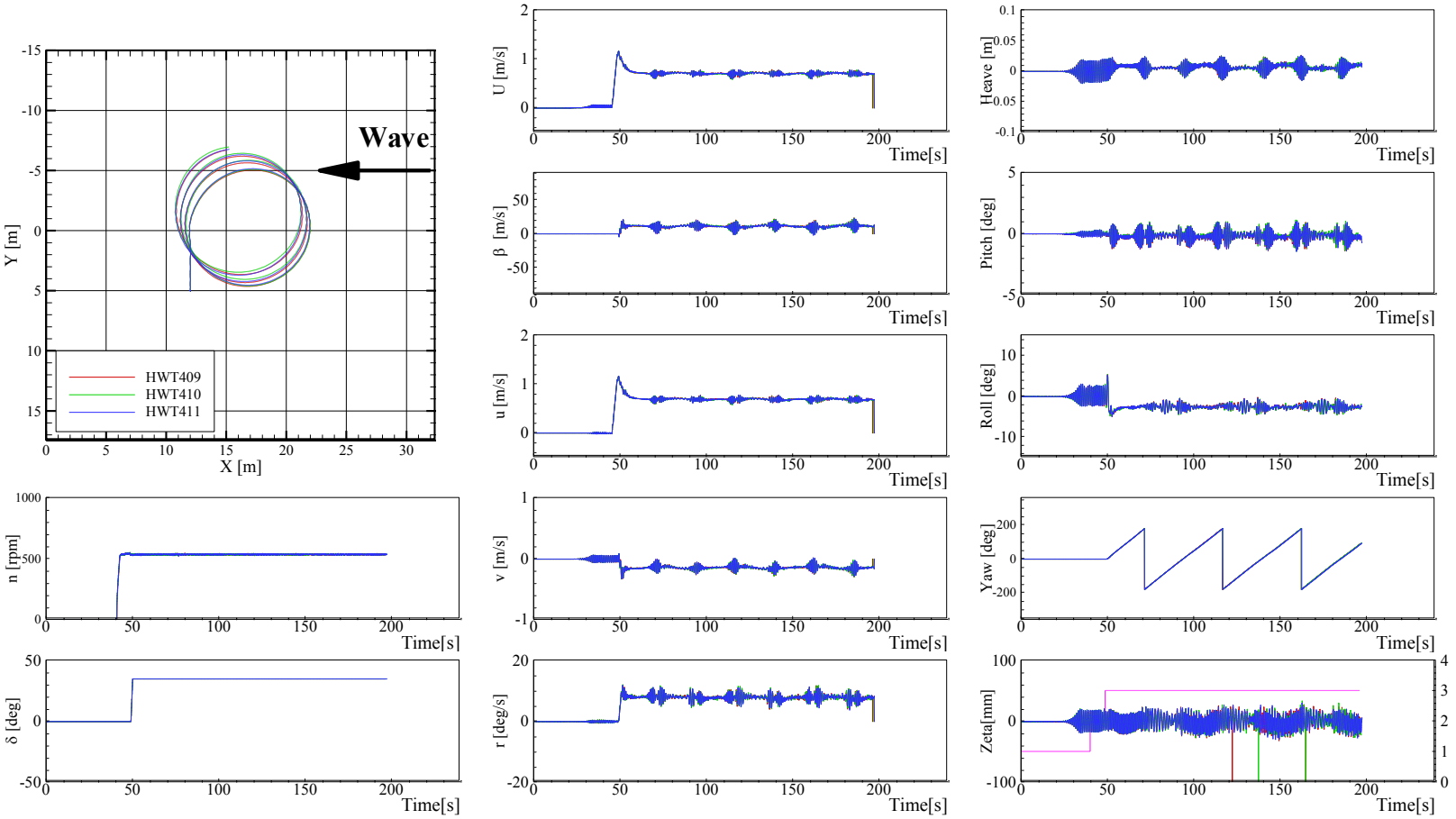

Figure G-39 Trajectories and time histories of turning in waves at Fr = 0.2, λ/L = 0.5, H/λ = 0.02, δ = 35, and χ = 90°

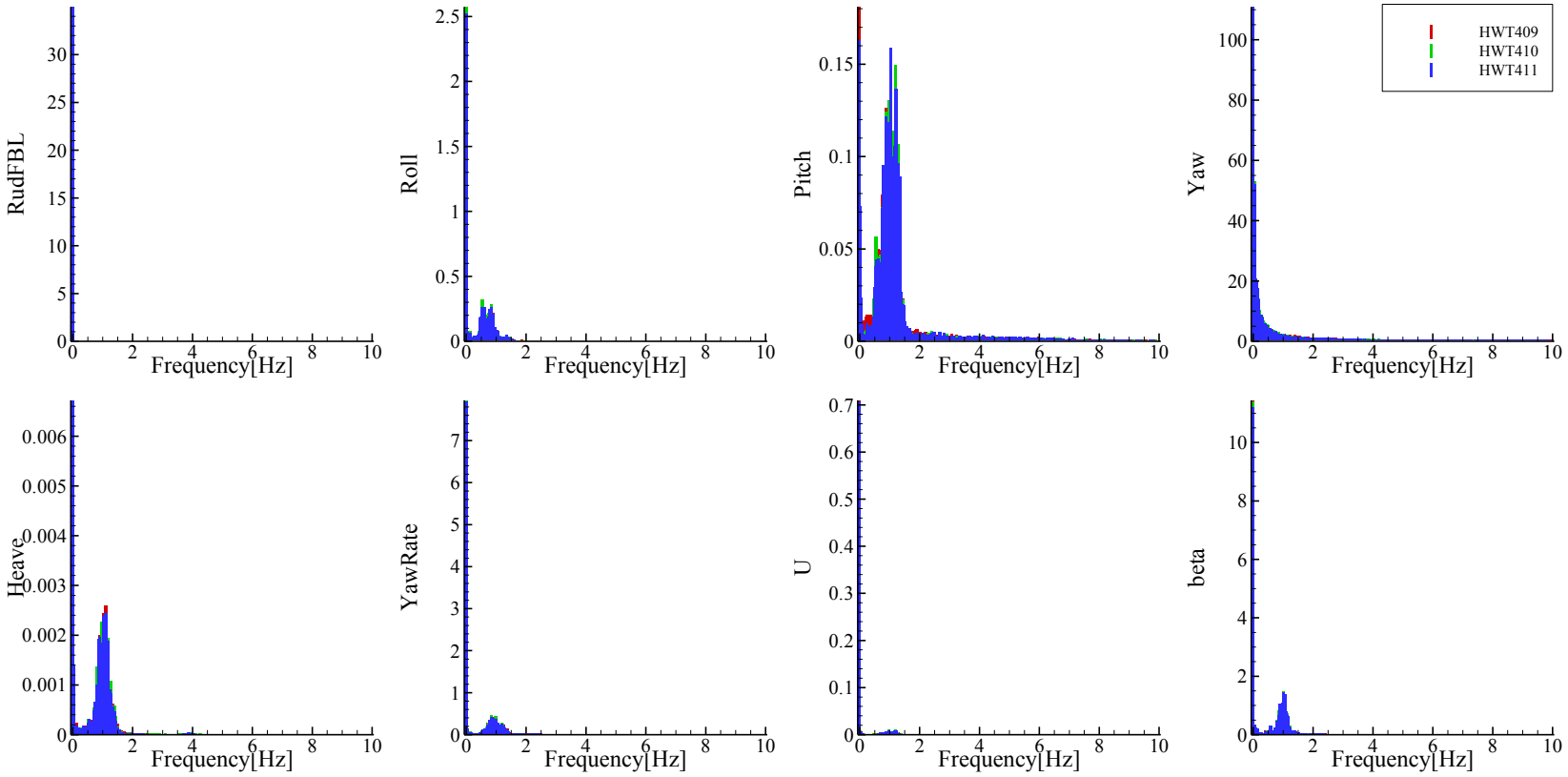

Figure G-40 FFT analysis of time histories of turning in waves at Fr = 0.2, λ/L = 0.5, H/λ = 0.02, δ = 35, and χ = 90°

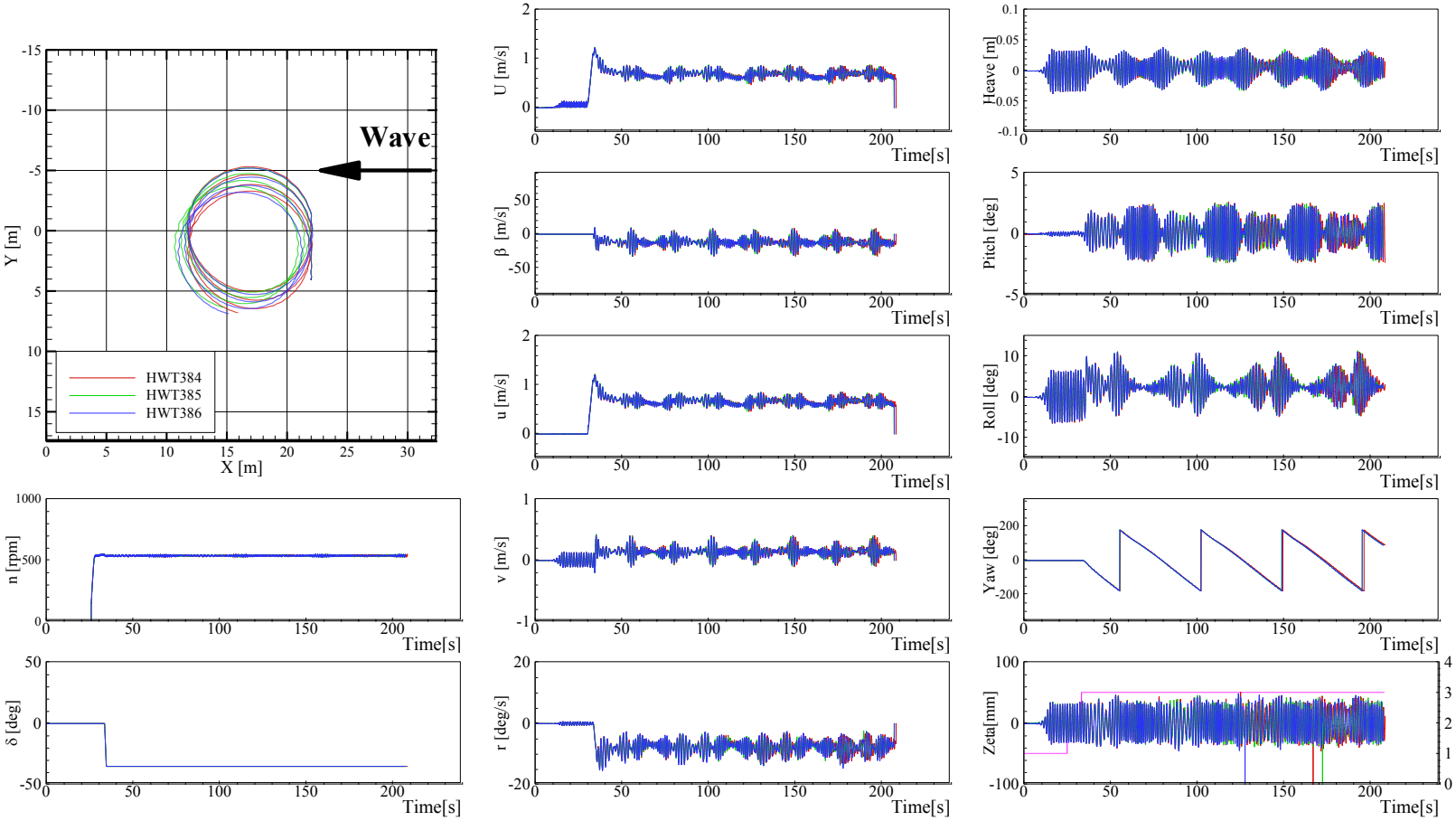

Figure G-41 Trajectories and time histories of turning in waves at Fr = 0.2, λ/L = 1.0, H/λ = 0.02, δ = -35, and χ = 90°

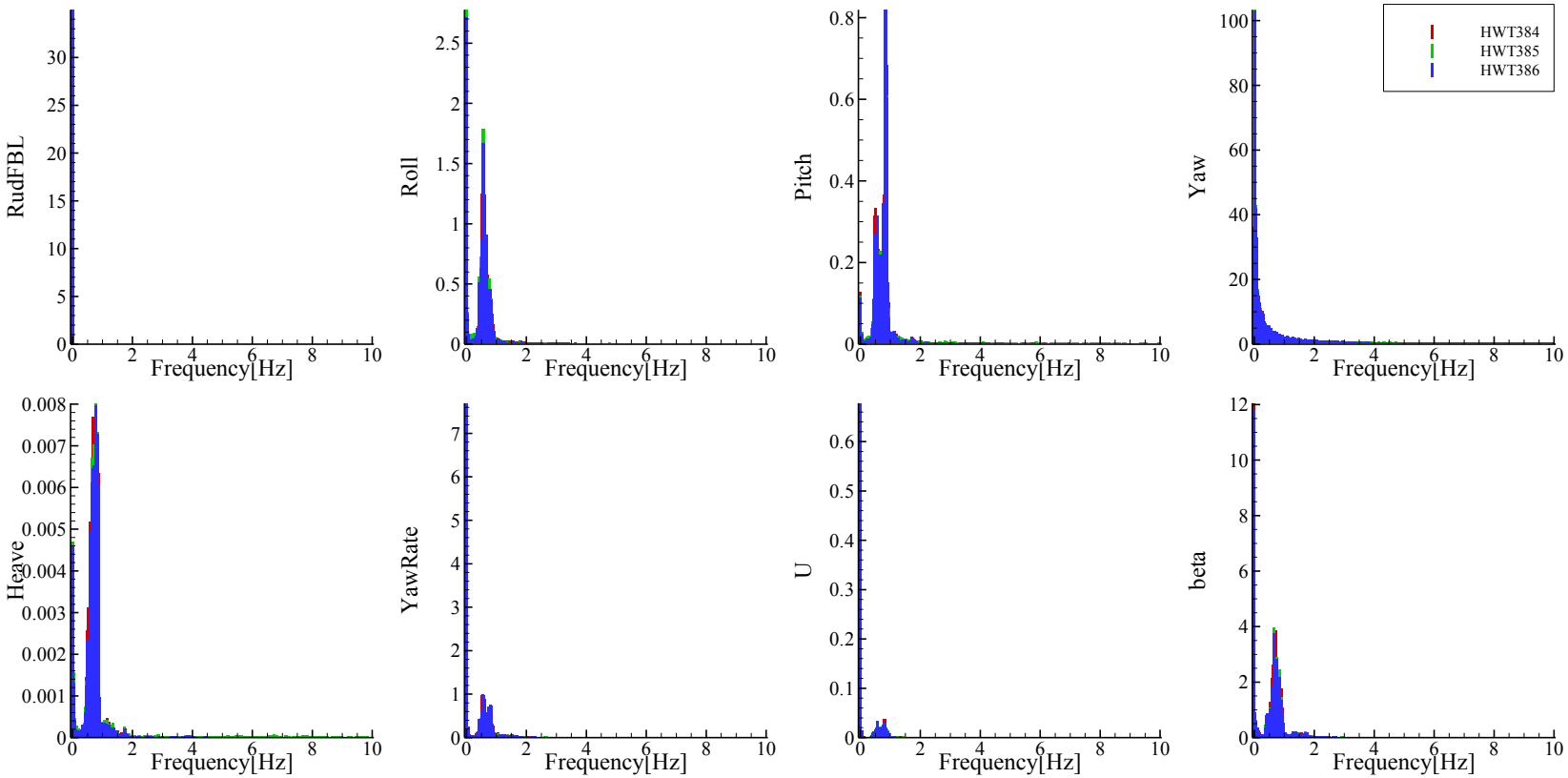

Figure G-42 FFT analysis of time histories of turning in waves at Fr = 0.2, λ/L = 1.0, H/λ = 0.02, δ = -35, and χ = 90°

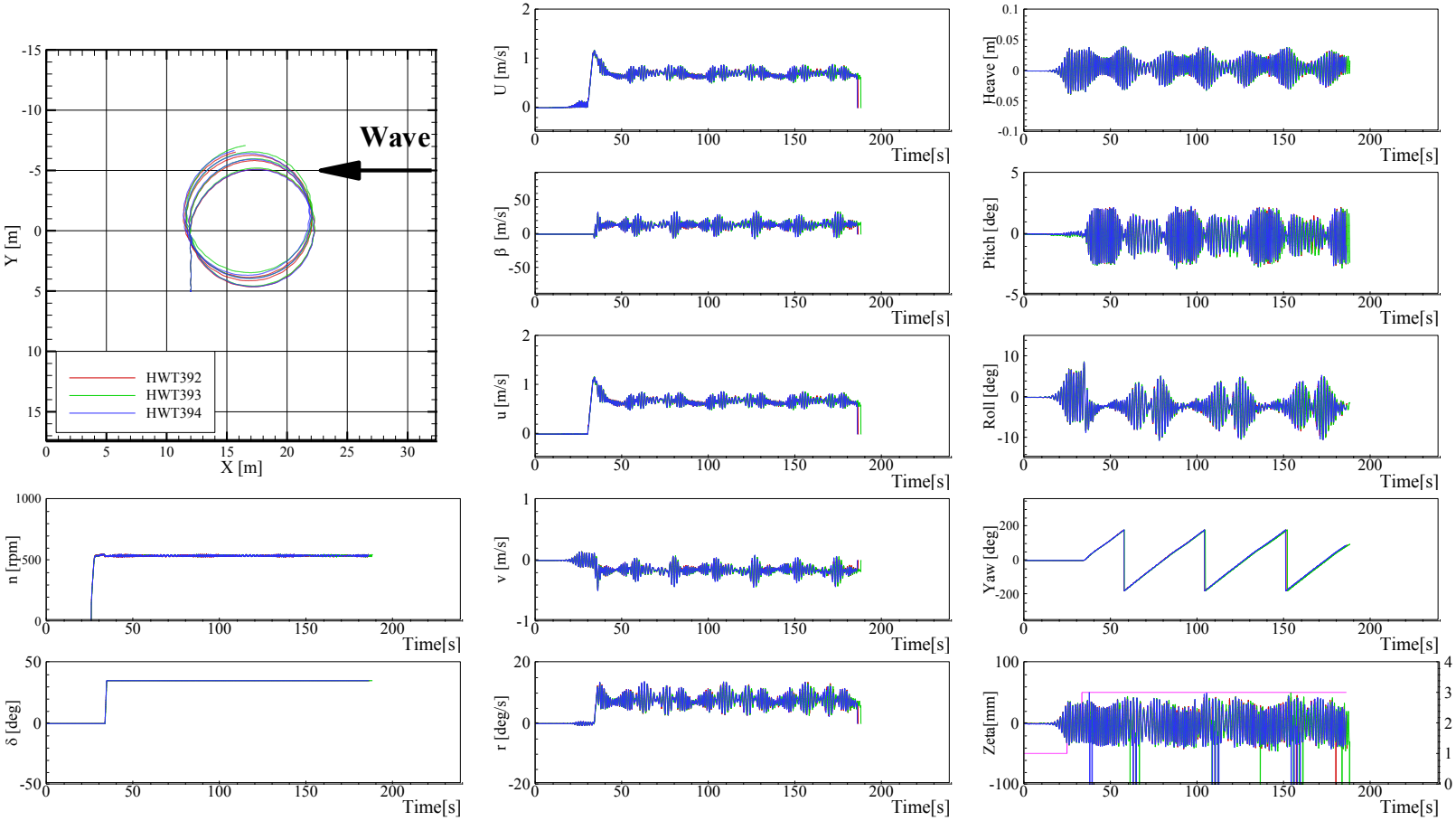

Figure G-43 Trajectories and time histories of turning in waves at Fr = 0.2, λ/L = 1.0, H/λ = 0.02, δ = 35, and χ = 90°

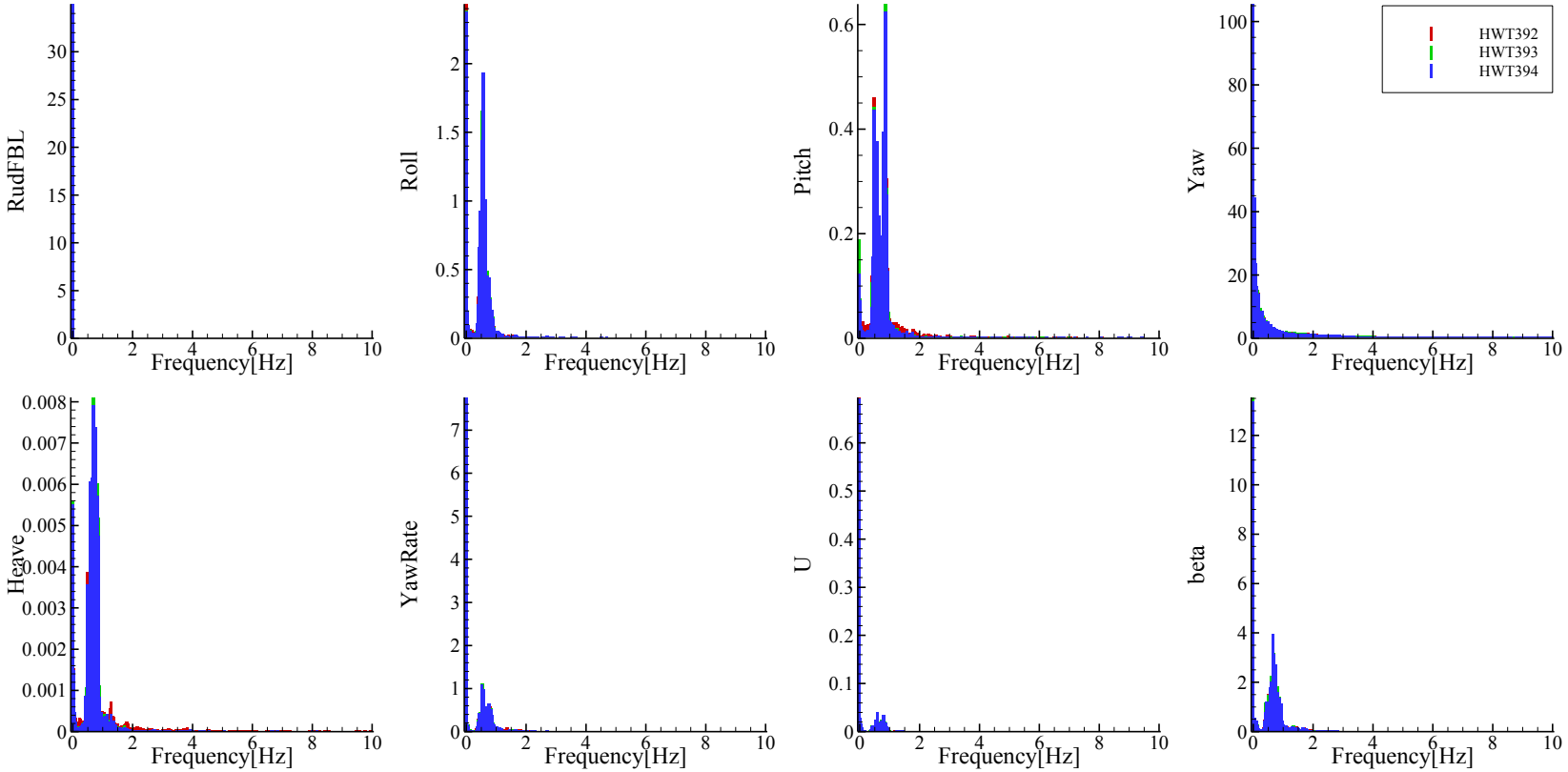

Figure G-44 FFT analysis of time histories of turning in waves at Fr = 0.2, λ/L = 1.0, H/λ = 0.02, δ = 35, and χ = 90°

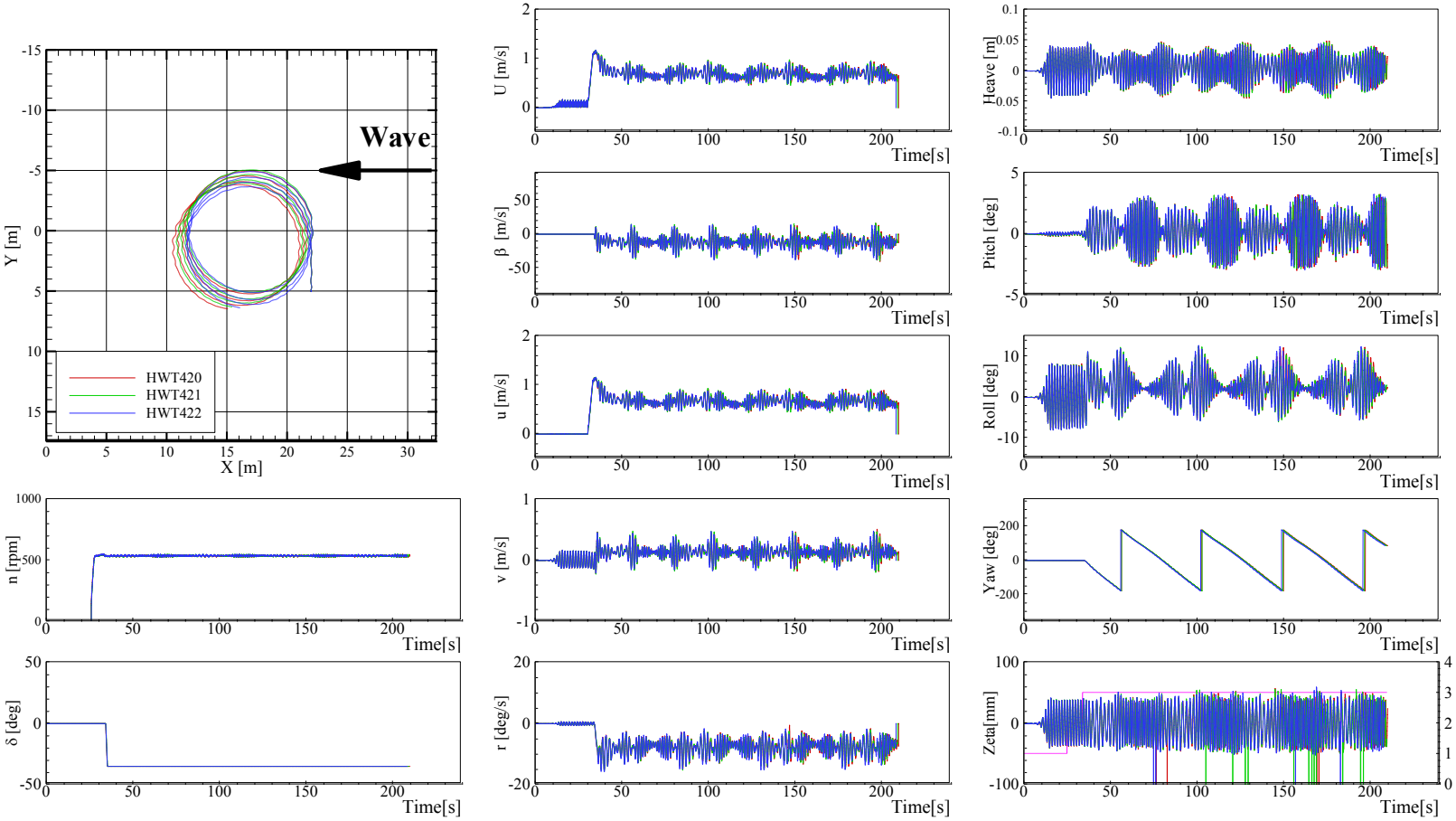

Figure G-45 Trajectories and time histories of turning in waves at Fr = 0.2, λ/L = 1.2, H/λ = 0.02, δ = -35, and χ = 90°

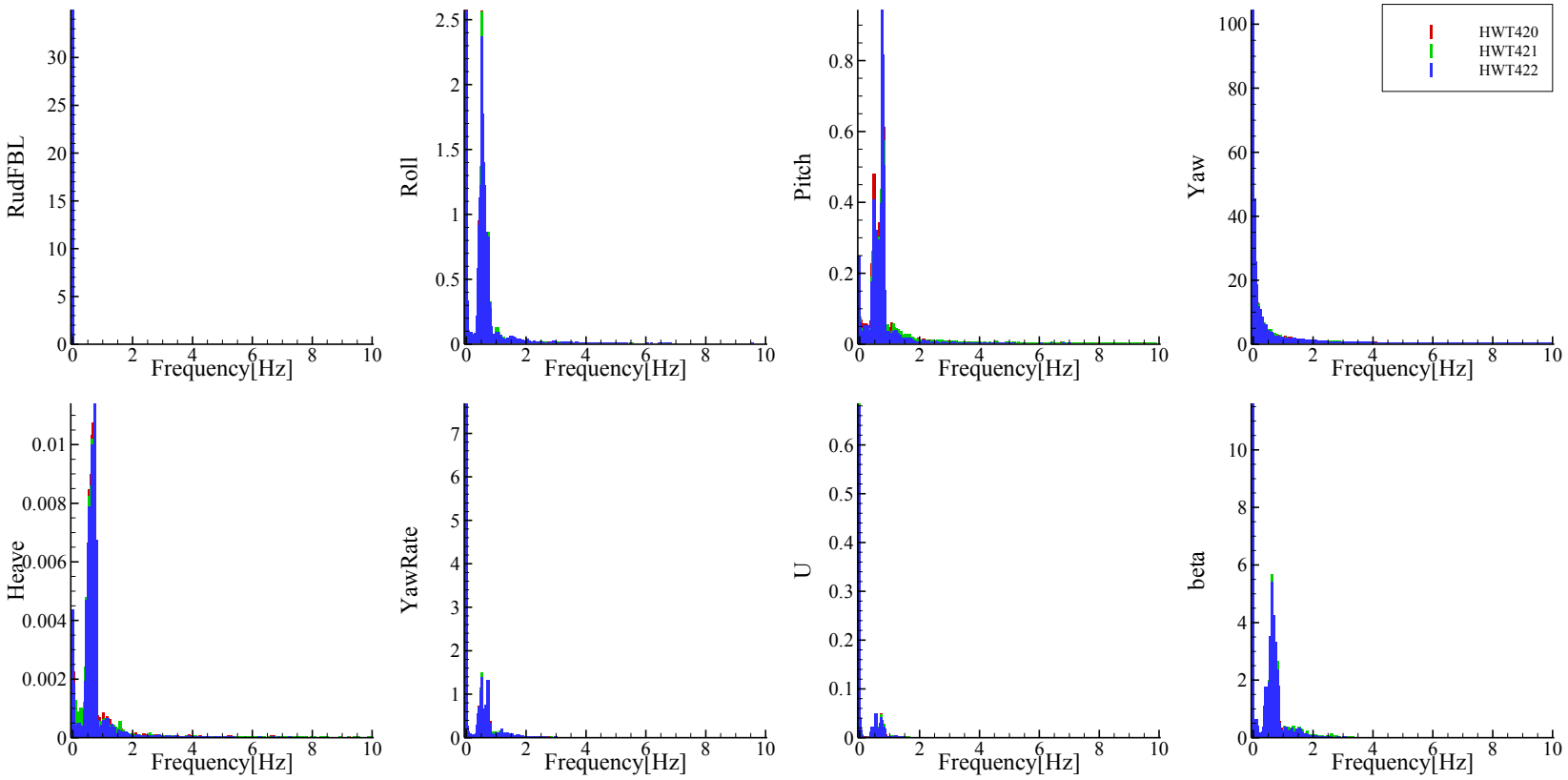

Figure G-46 FFT analysis of time histories of turning in waves at Fr = 0.2, λ/L = 1.2, H/λ = 0.02, δ = -35, and χ = 90°

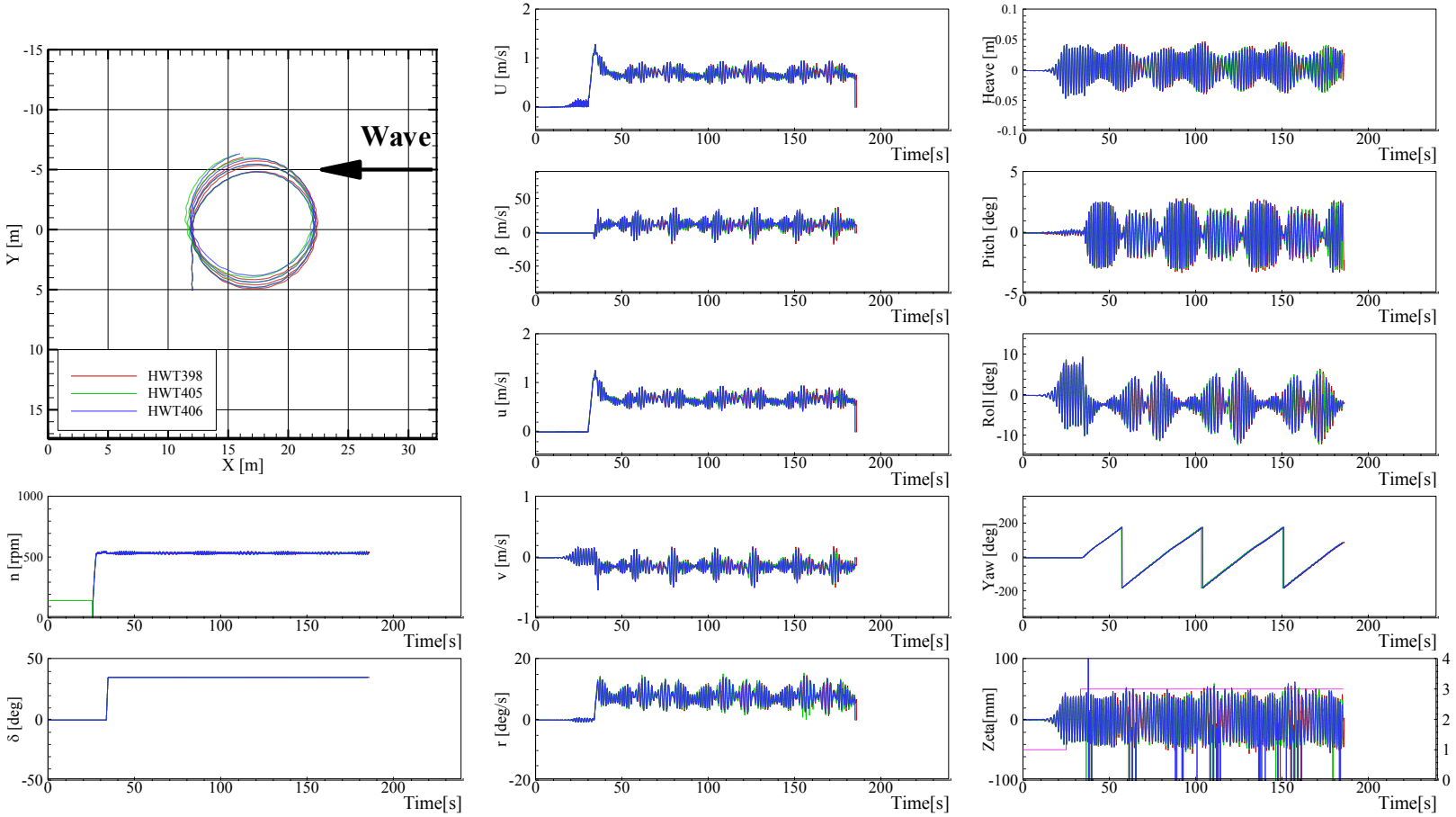

Figure G-47 Trajectories and time histories of turning in waves at Fr = 0.2, λ/L = 1.2, H/λ = 0.02, δ = 35, and χ = 90°

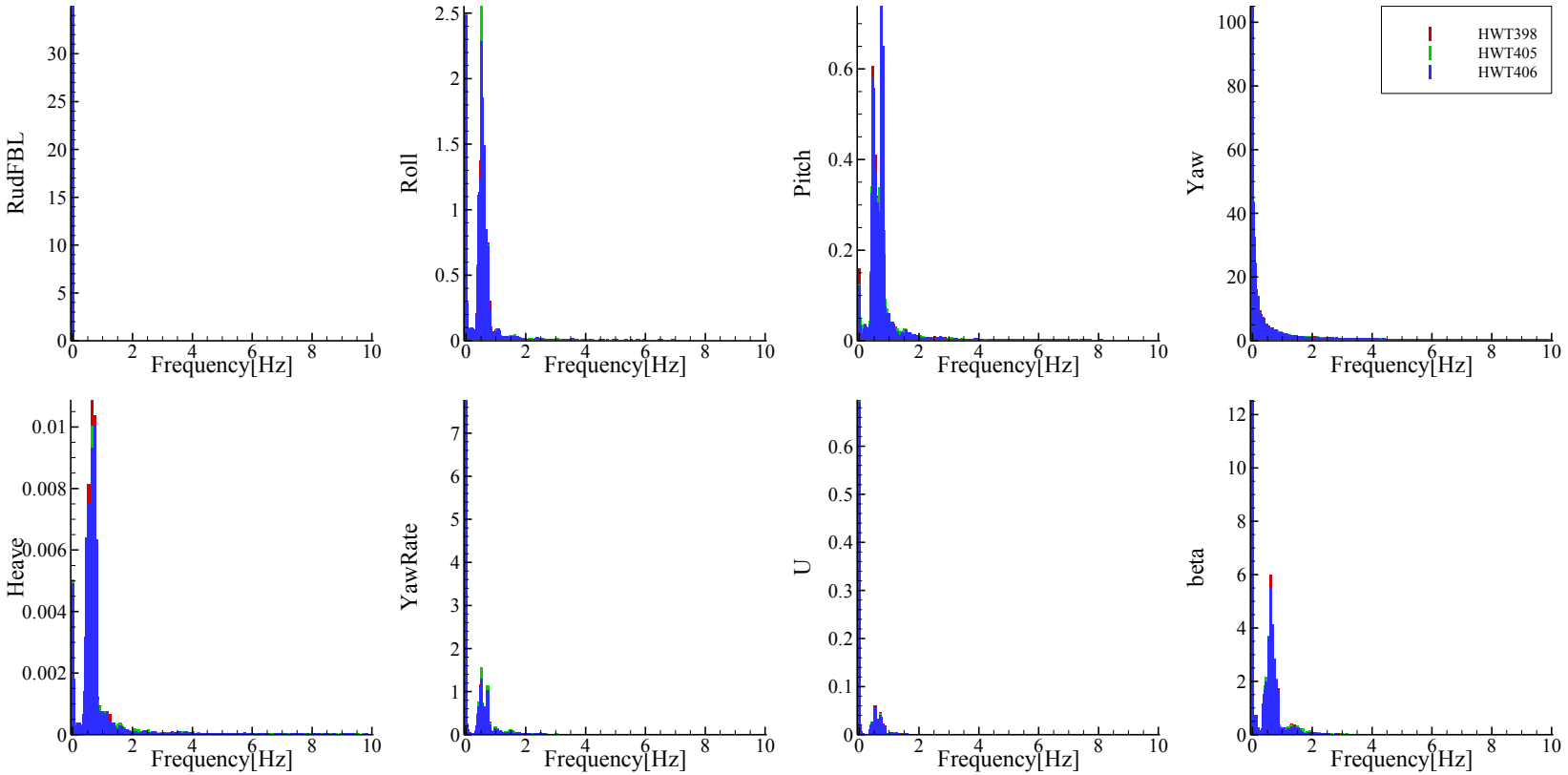

Figure G-48 FFT analysis of time histories of turning in waves at Fr = 0.2, λ/L = 1.2, H/λ = 0.02, δ = 35, and χ = 90°

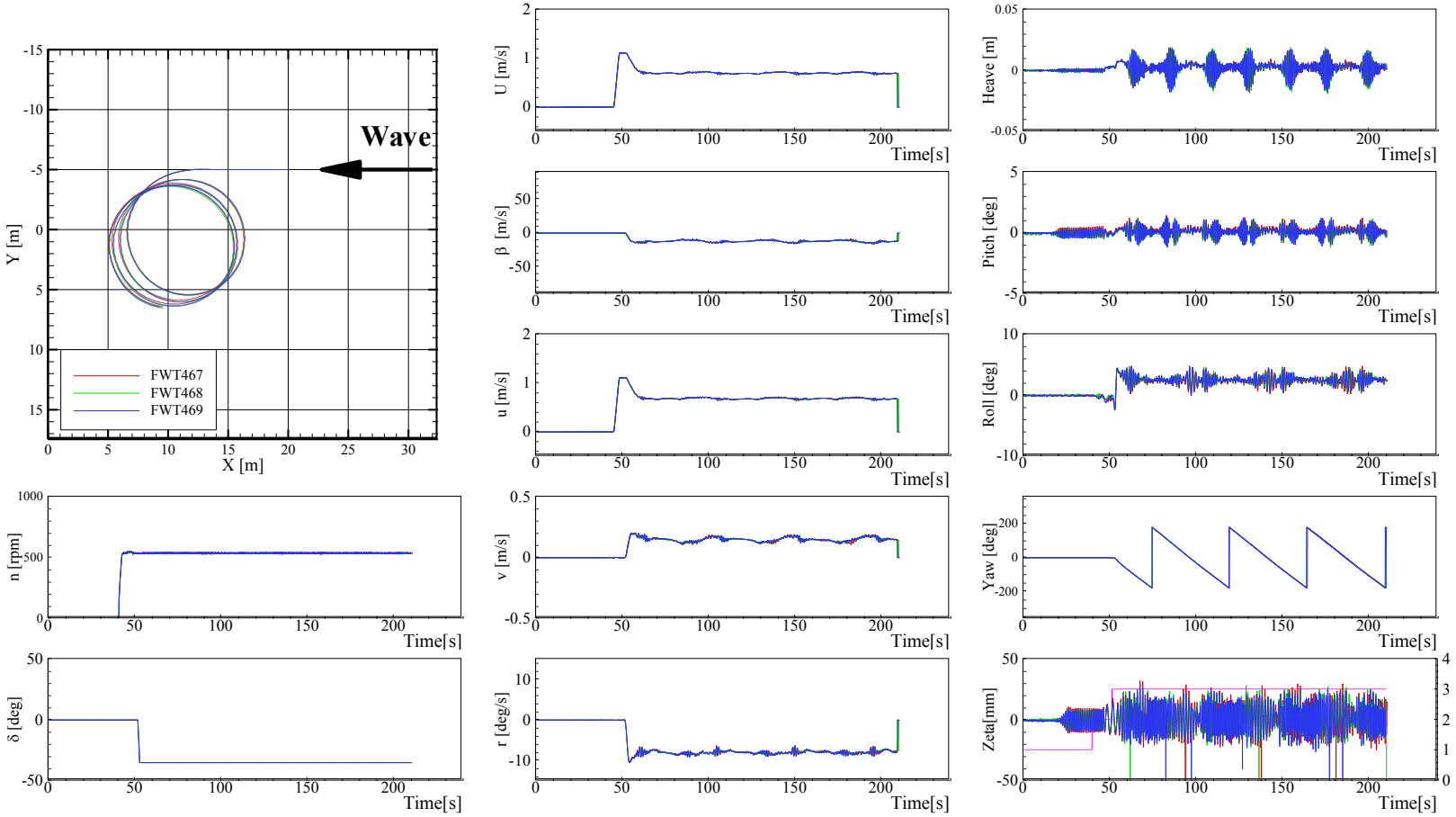

Figure G-49 Trajectories and time histories of turning in waves at Fr = 0.2, λ/L = 0.5, H/λ = 0.02, δ = -35, and χ = 180°

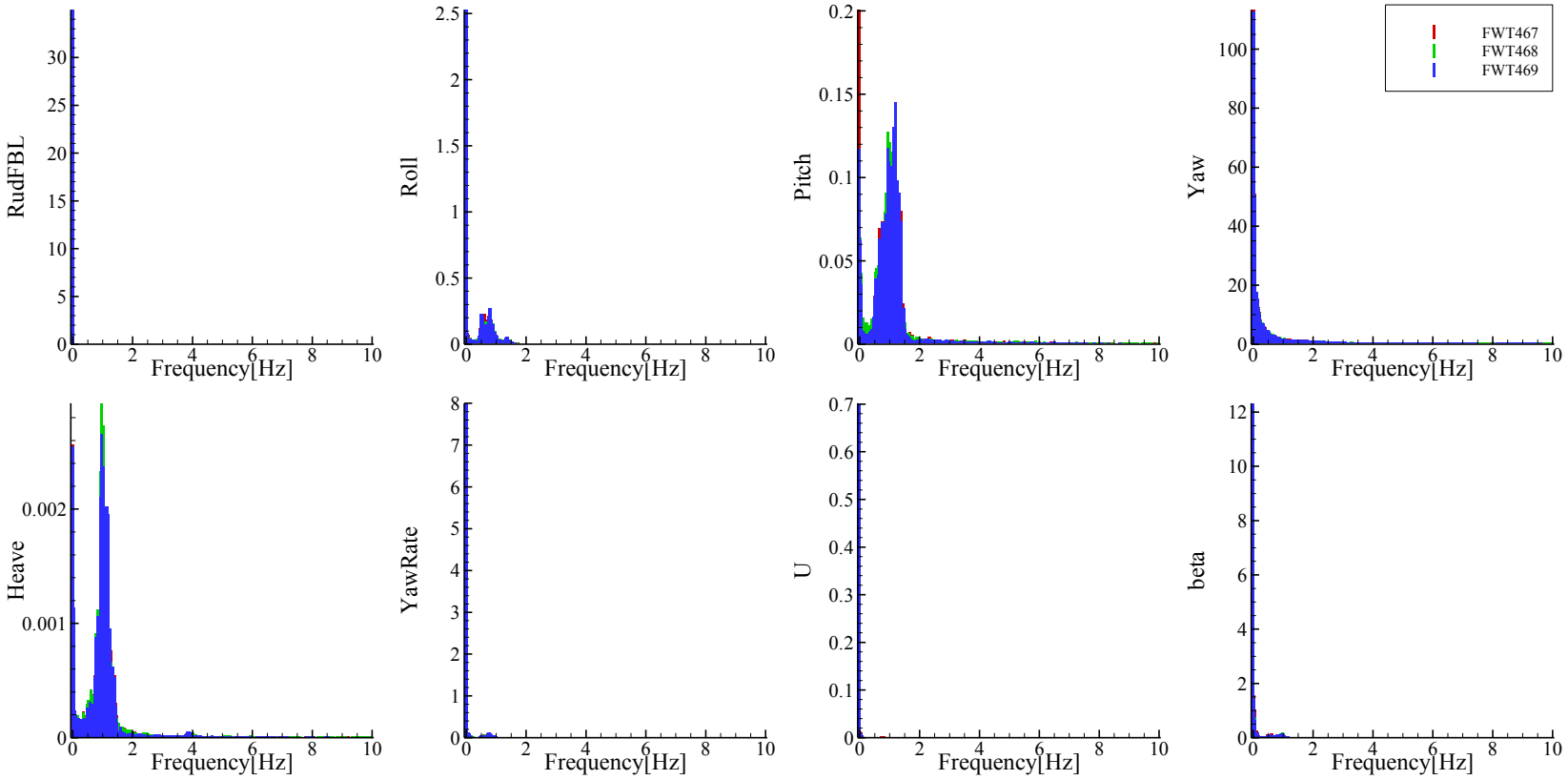

Figure G-50 FFT analysis of time histories of turning in waves at Fr = 0.2, λ/L = 0.5, H/λ = 0.02, δ = -35, and χ = 180°

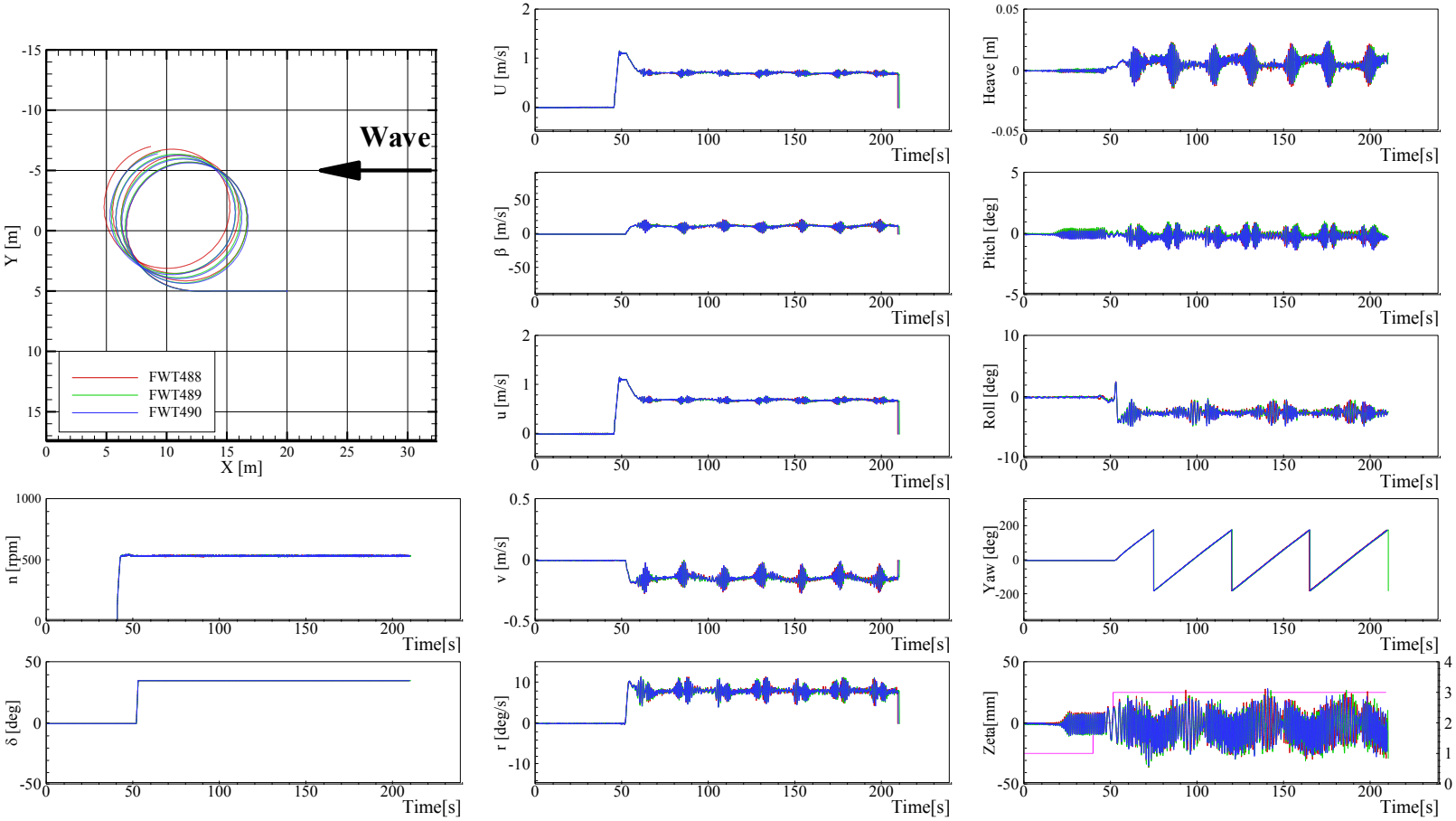

Figure G-51 Trajectories and time histories of turning in waves at Fr = 0.2, λ/L = 0.5, H/λ = 0.02, δ = 35, and χ = 180°

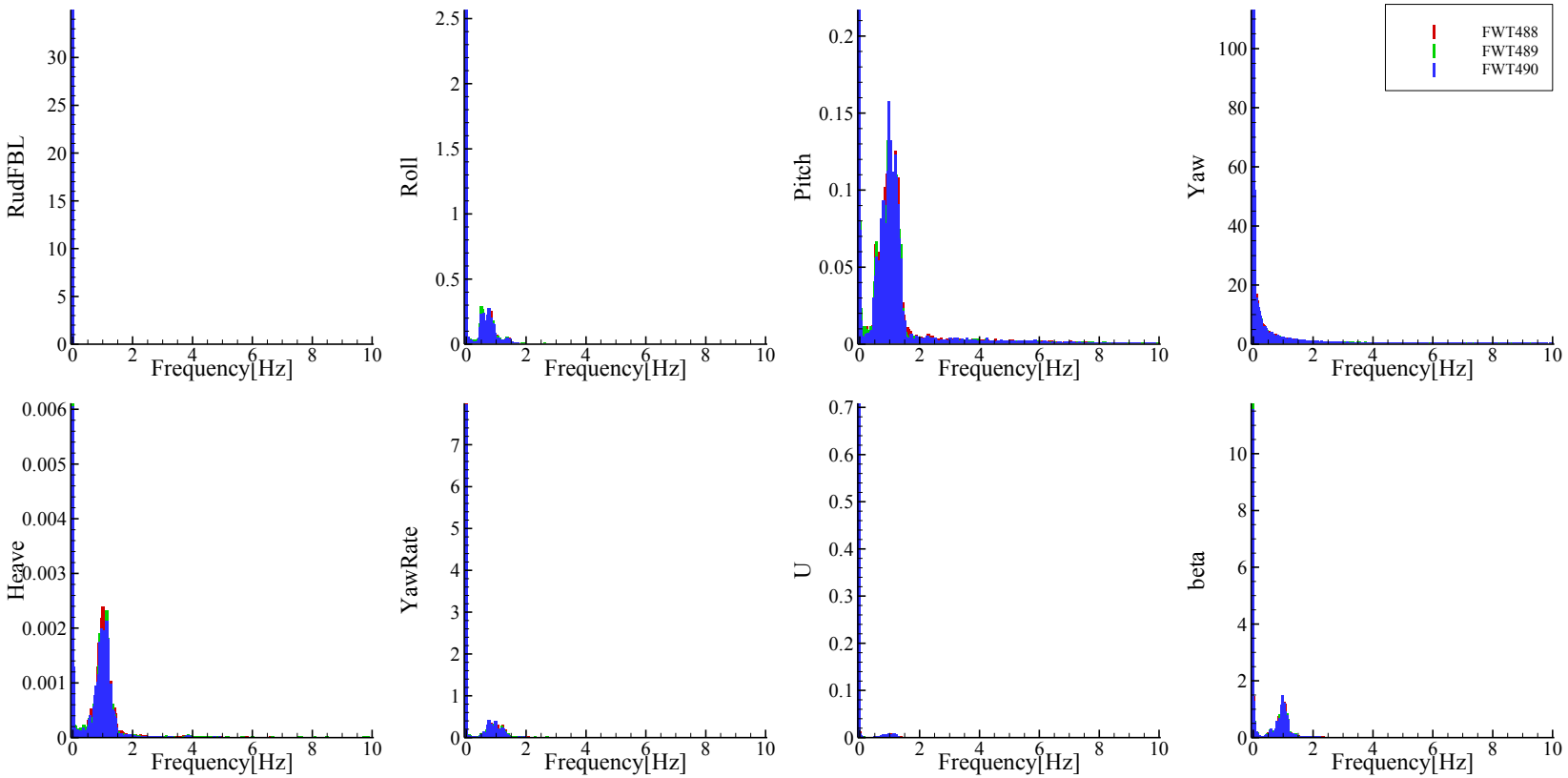

Figure G-52 FFT analysis of time histories of turning in waves at Fr = 0.2, λ/L = 0.5, H/λ = 0.02, δ = 35, and χ = 180°

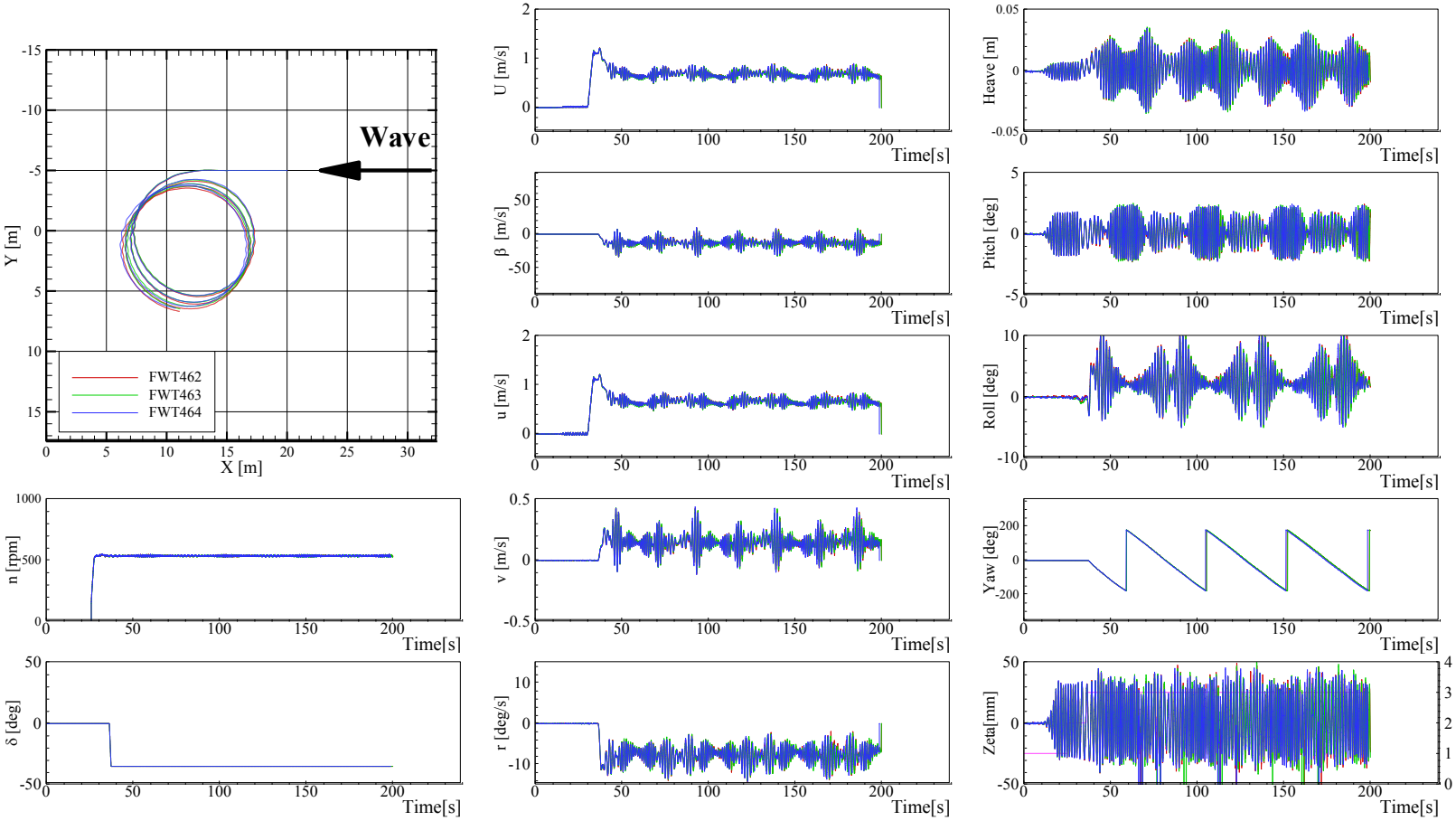

Figure G-53 Trajectories and time histories of turning in waves at Fr = 0.2, λ/L = 1.0, H/λ = 0.02, δ = -35, and χ = 180°

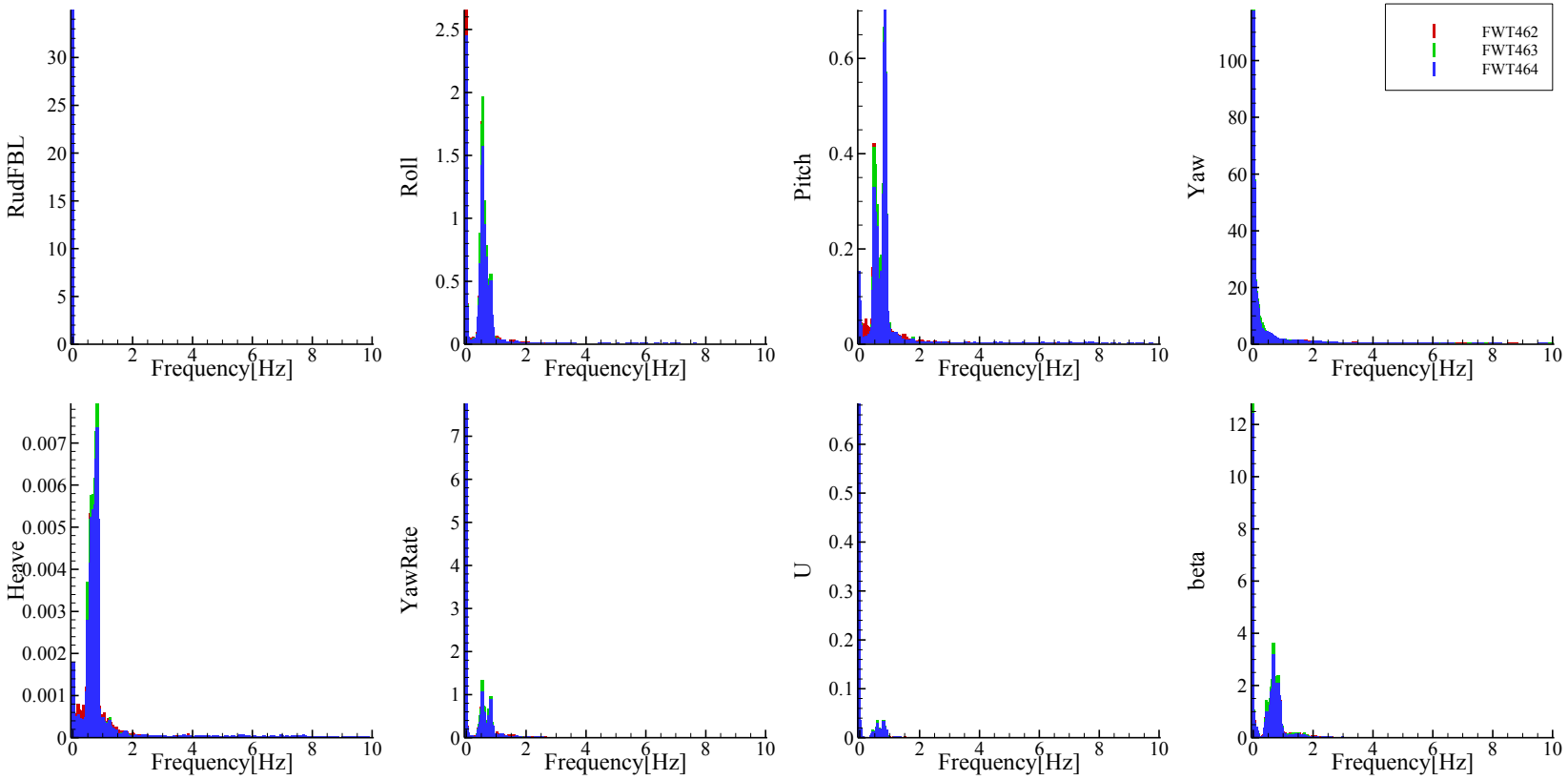

Figure G-54 FFT analysis of time histories of turning in waves at Fr = 0.2, λ/L = 1.0, H/λ = 0.02, δ = -35, and χ = 180°

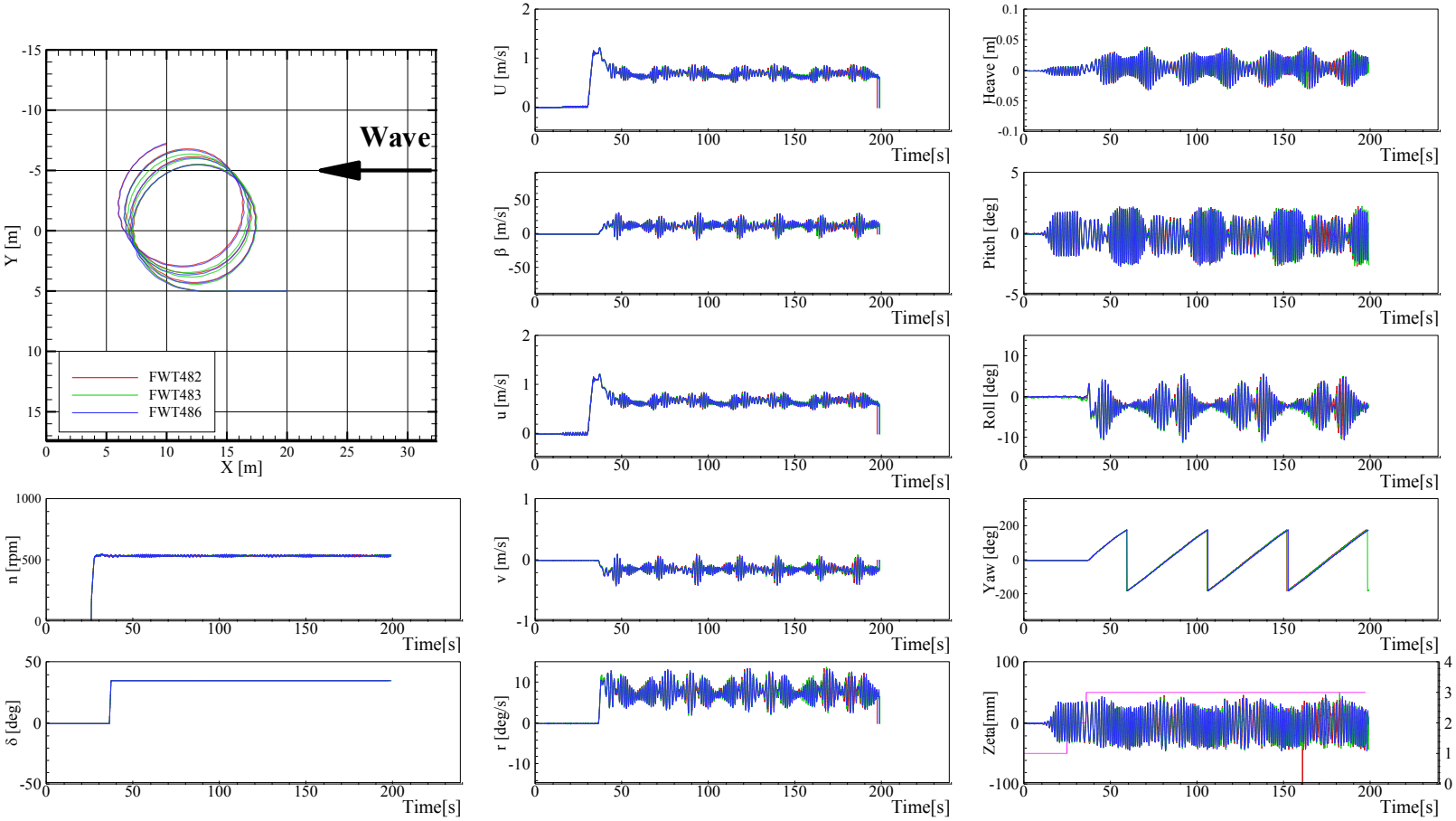

Figure G-55 Trajectories and time histories of turning in waves at Fr = 0.2, λ/L = 1.0, H/λ = 0.02, δ = 35, and χ = 180°

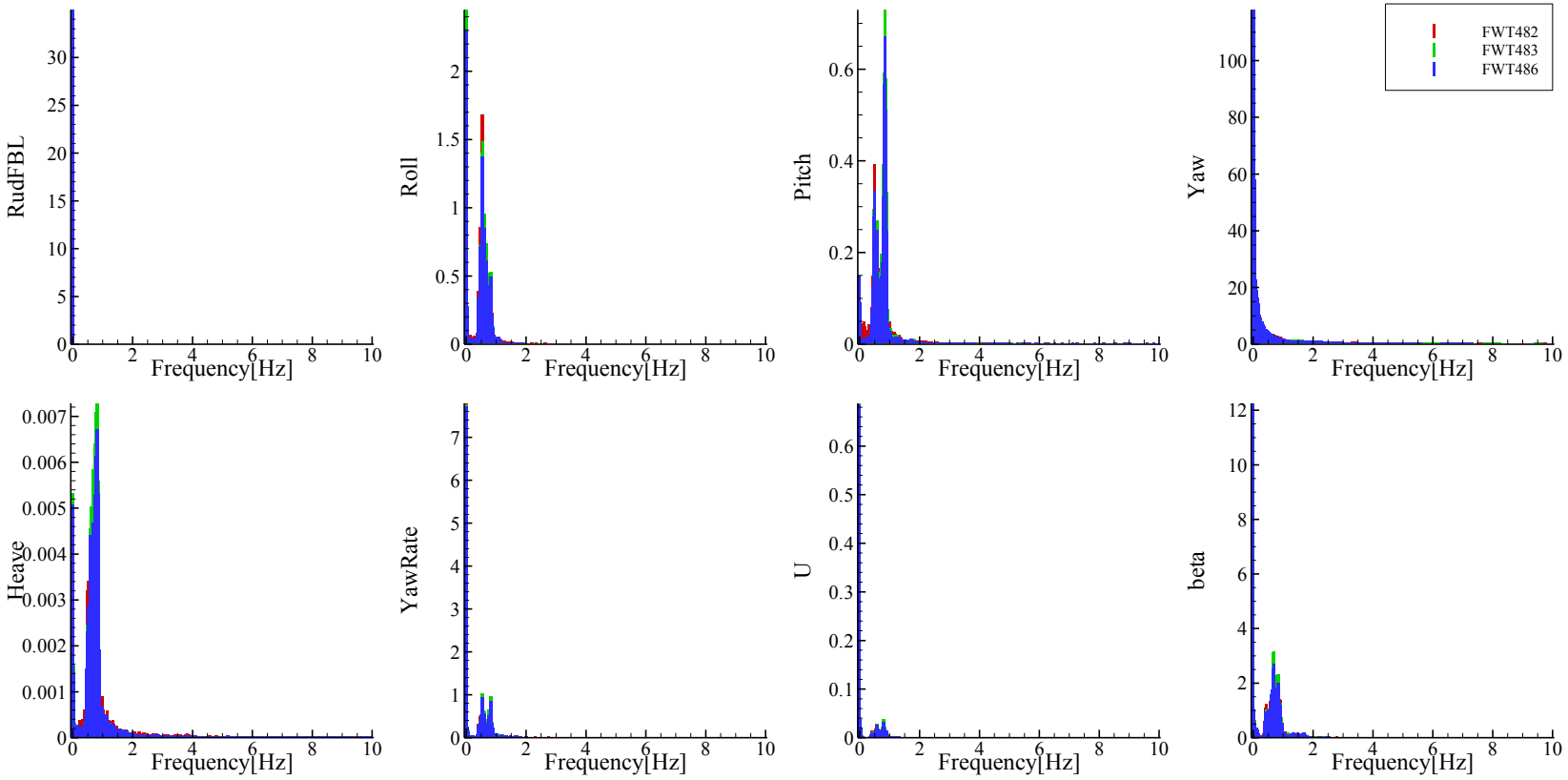

Figure G-56 FFT analysis of time histories of turning in waves at Fr = 0.2, λ/L = 1.0, H/λ = 0.02, δ = 35, and χ = 180°

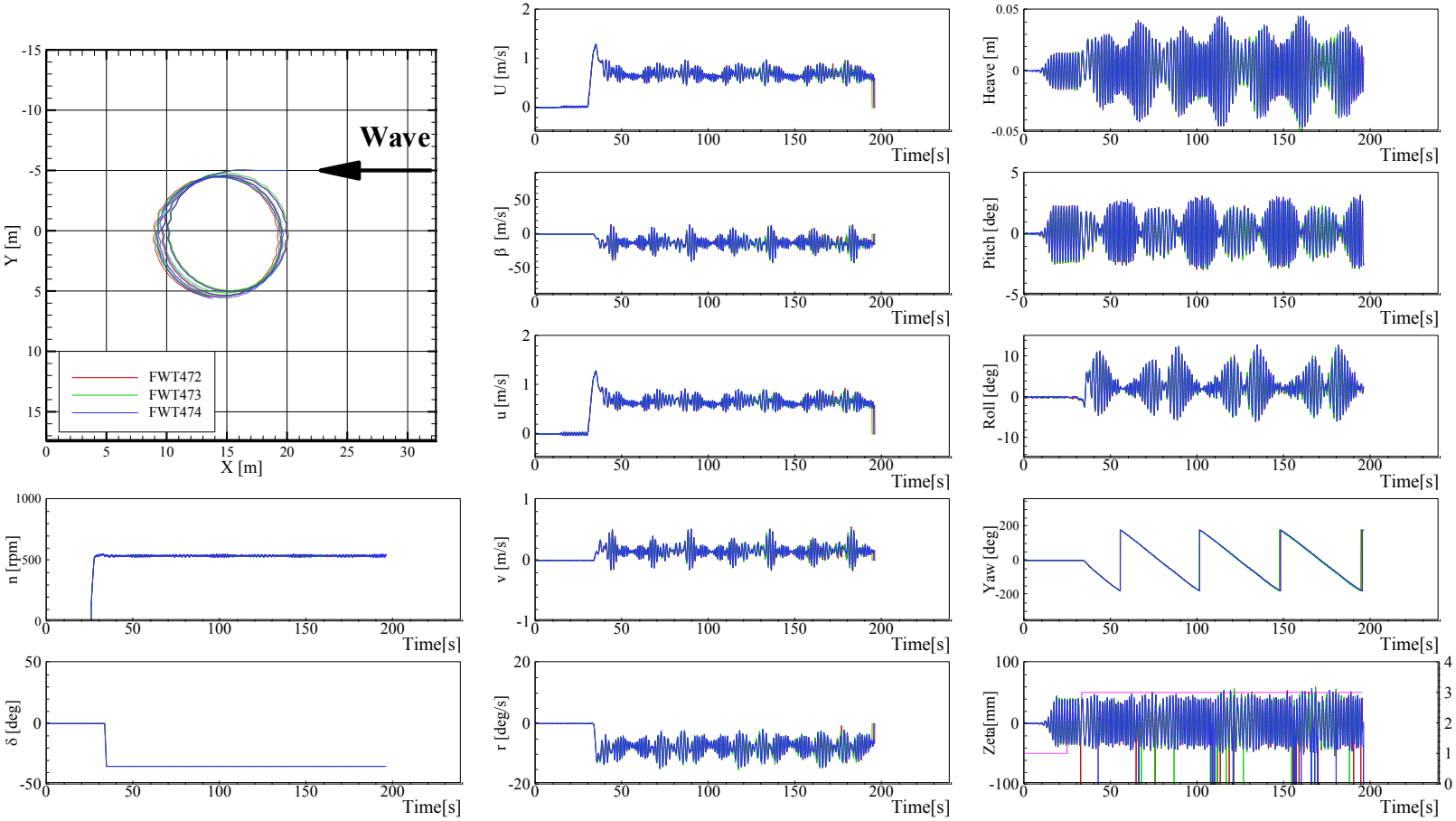

Figure G-57 Trajectories and time histories of turning in waves at Fr = 0.2, λ/L = 1.2, H/λ = 0.02, δ = -35, and χ = 180°

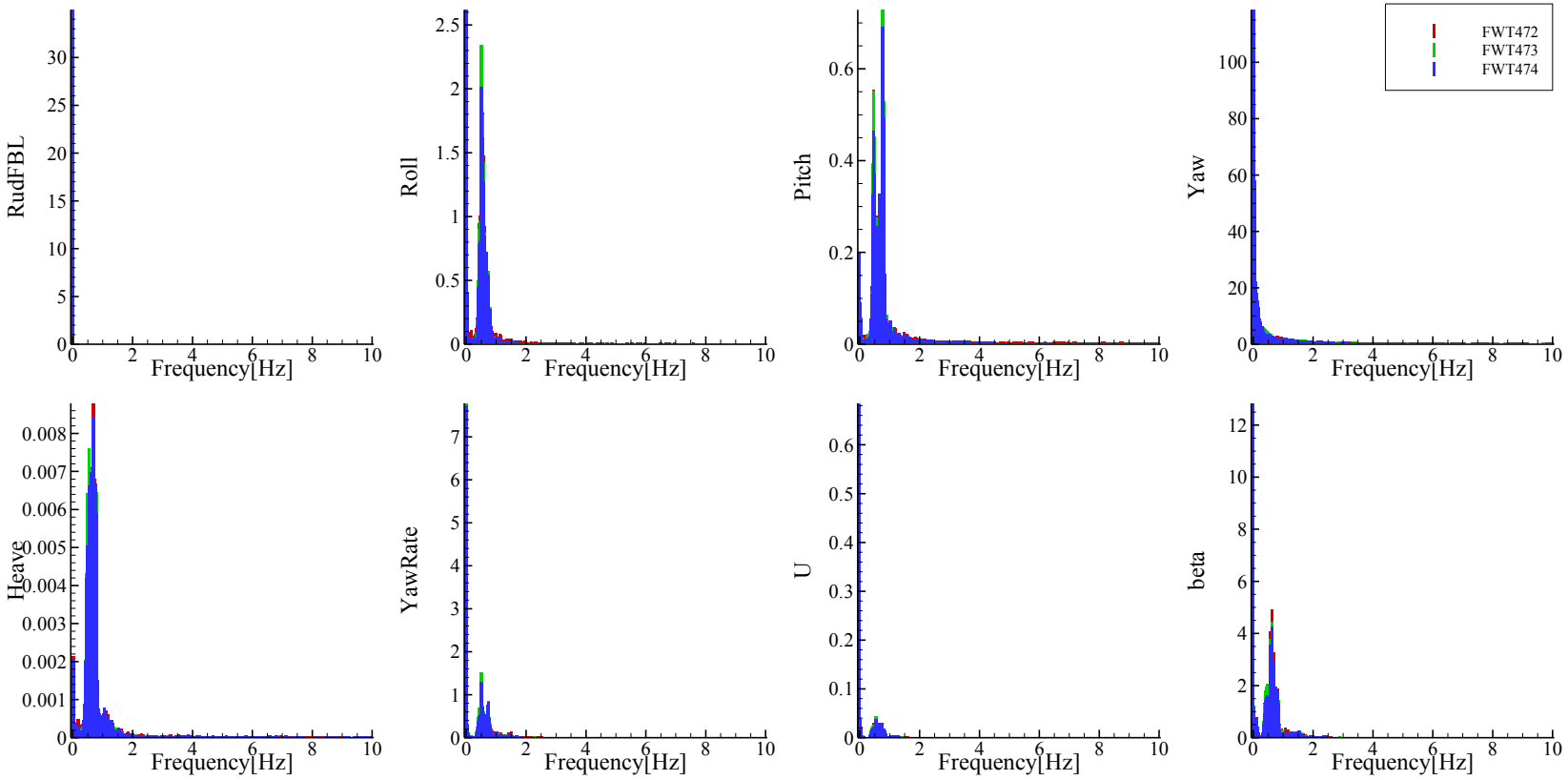

Figure G-58 FFT analysis of time histories of turning in waves at Fr = 0.2, λ/L = 1.2, H/λ = 0.02, δ = -35, and χ = 180°

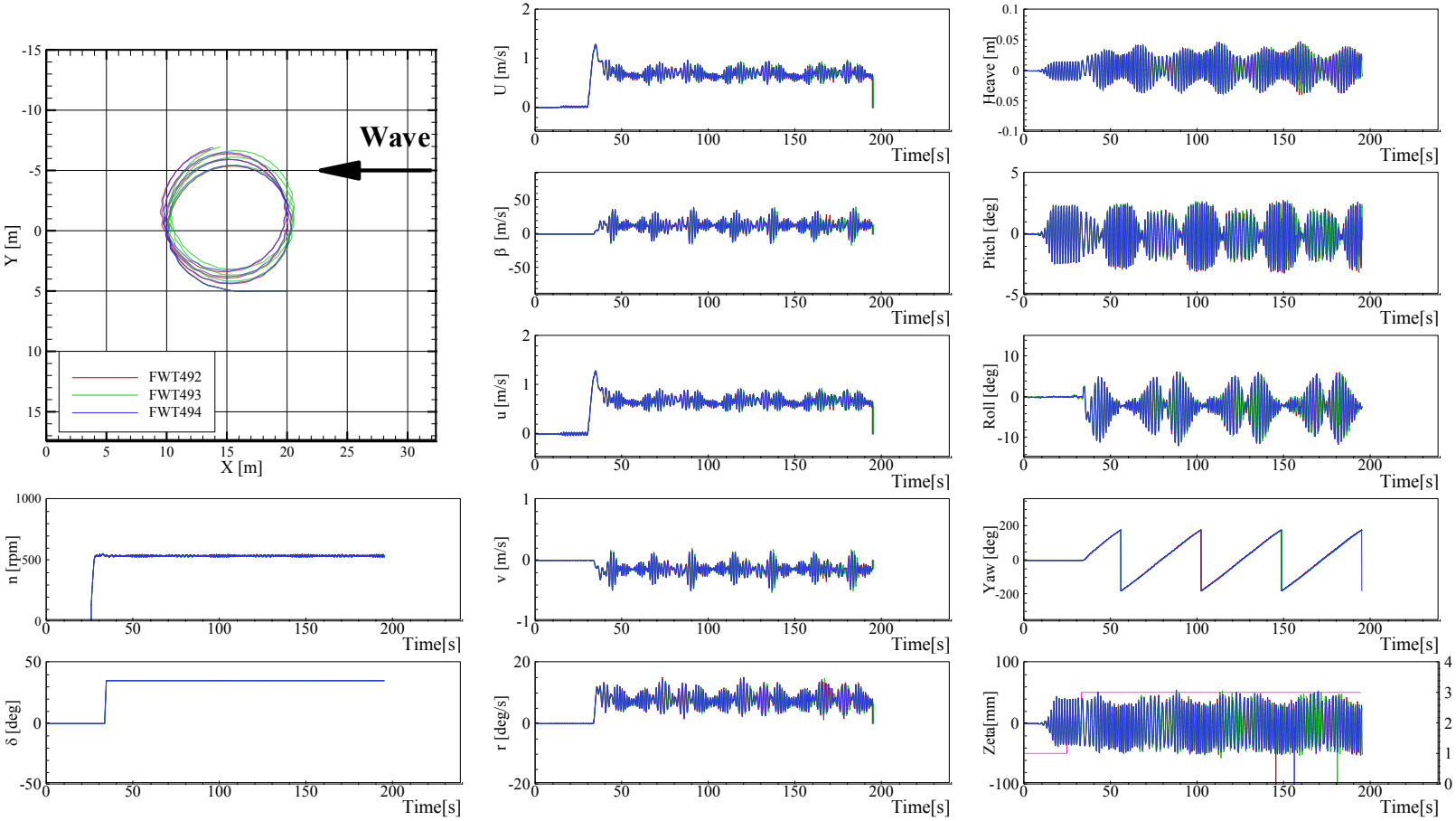

Figure G-59 Trajectories and time histories of turning in waves at Fr = 0.2, λ/L = 1.2, H/λ = 0.02, δ = 35, and χ = 180°

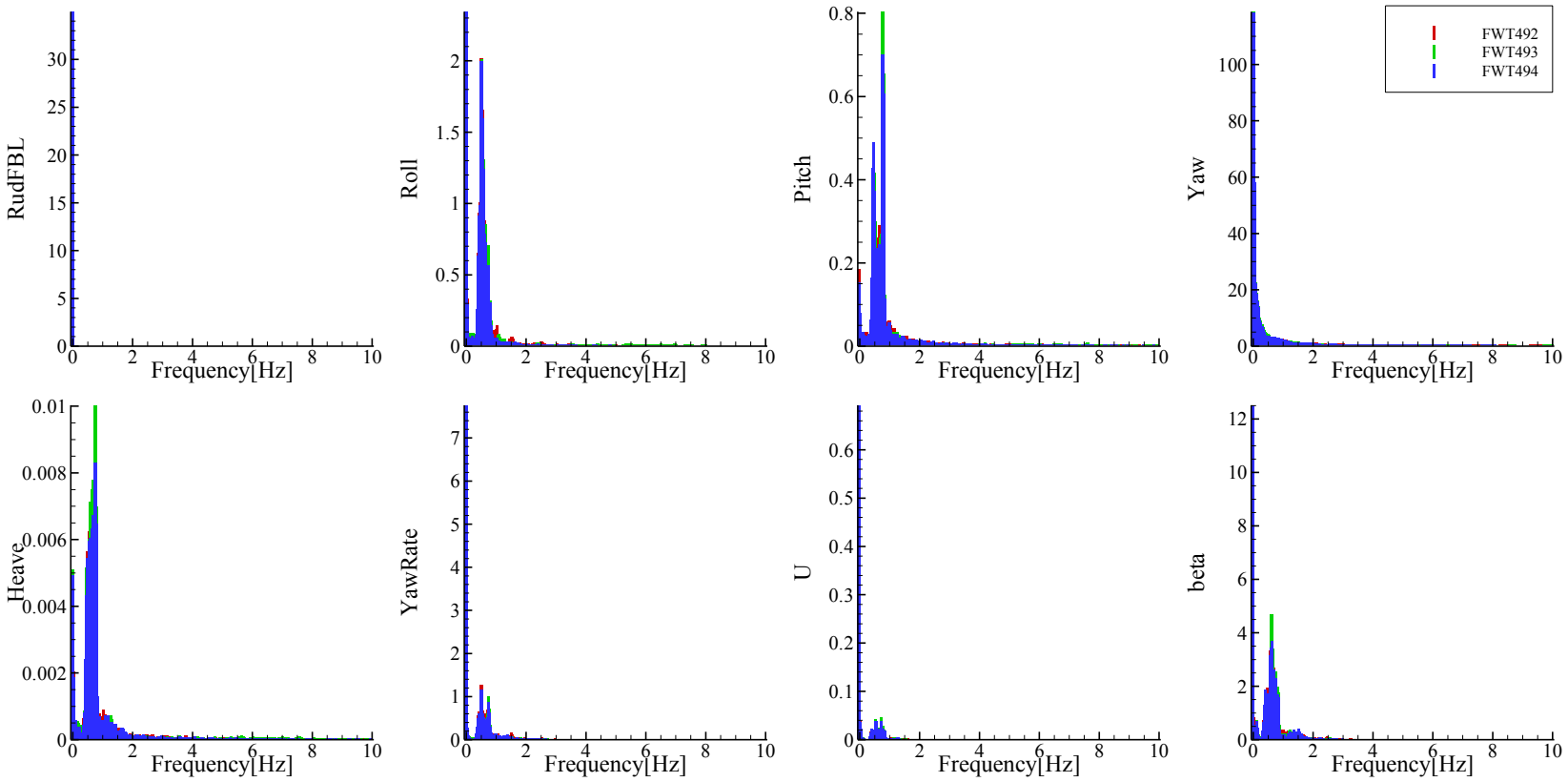

Figure G-60 FFT analysis of time histories of turning in waves at Fr = 0.2, λ/L = 1.2, H/λ = 0.02, δ = 35, and χ = 180°

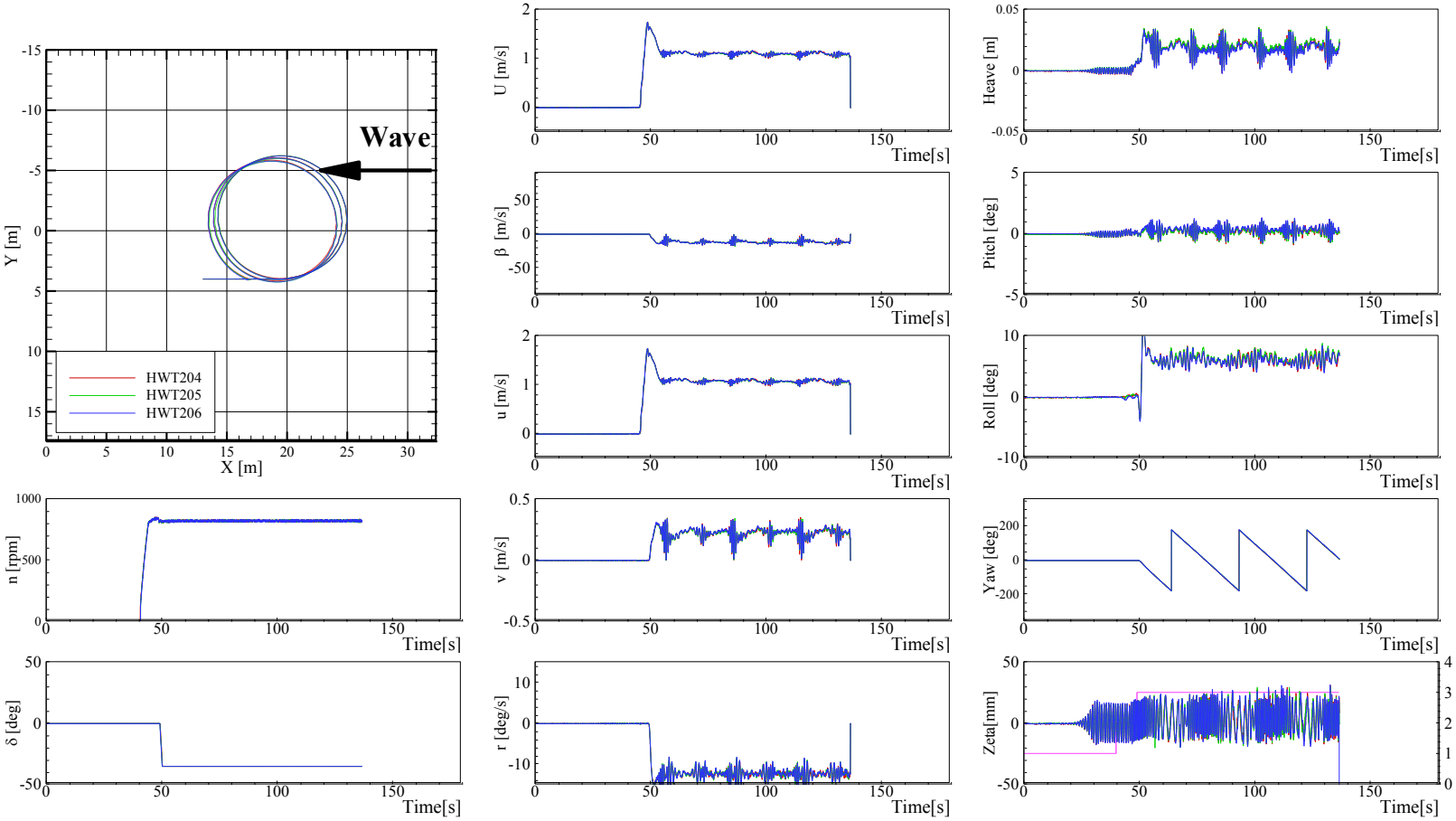

Figure G-61 Trajectories and time histories of turning in waves at Fr = 0.3, λ/L = 0.5, H/λ = 0.02, δ = -35, and χ = 0°

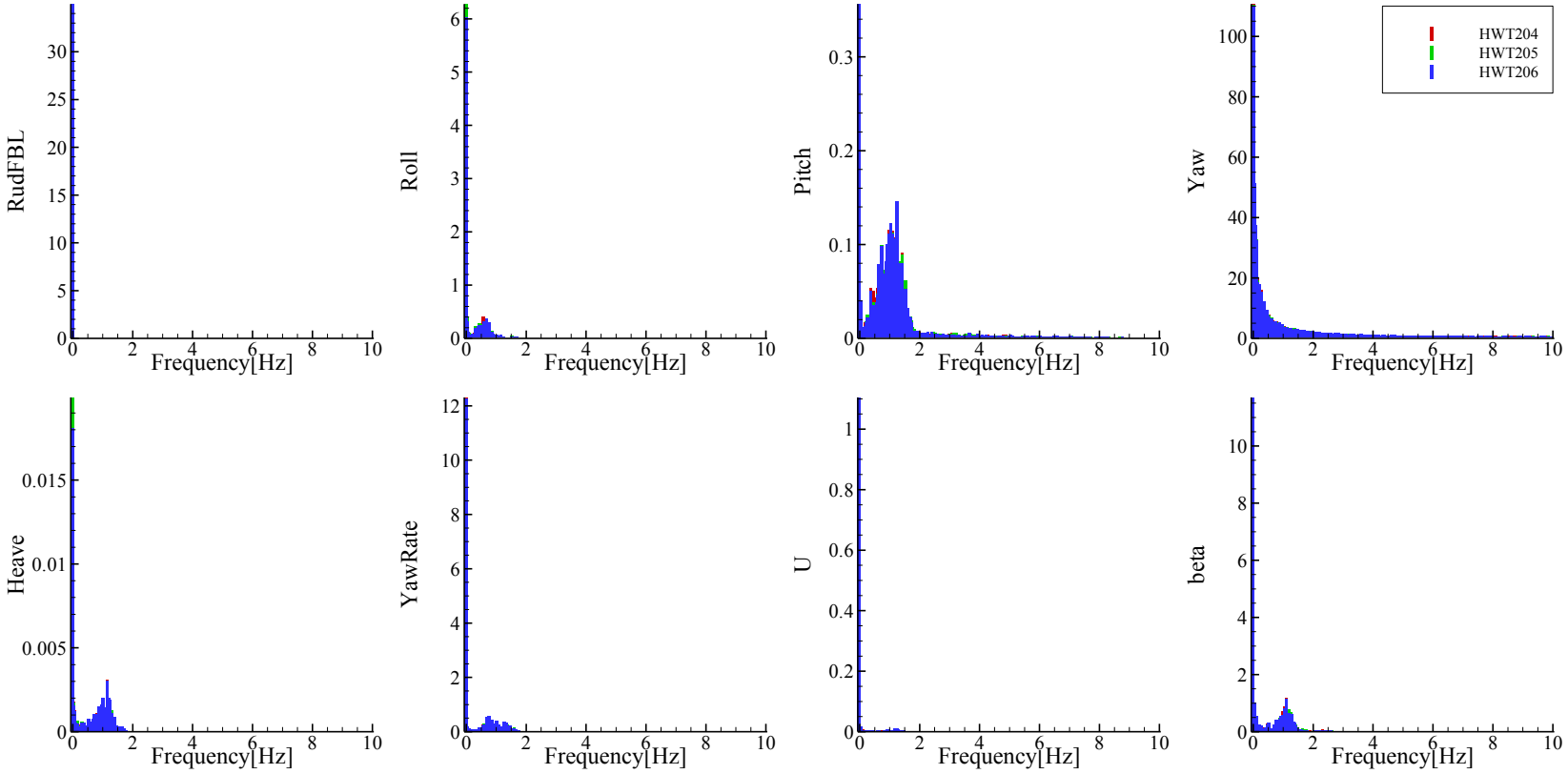

Figure G-62 FFT analysis of time histories of turning in waves at Fr = 0.3, λ/L = 0.5, H/λ = 0.02, δ = -35, and χ = 0°

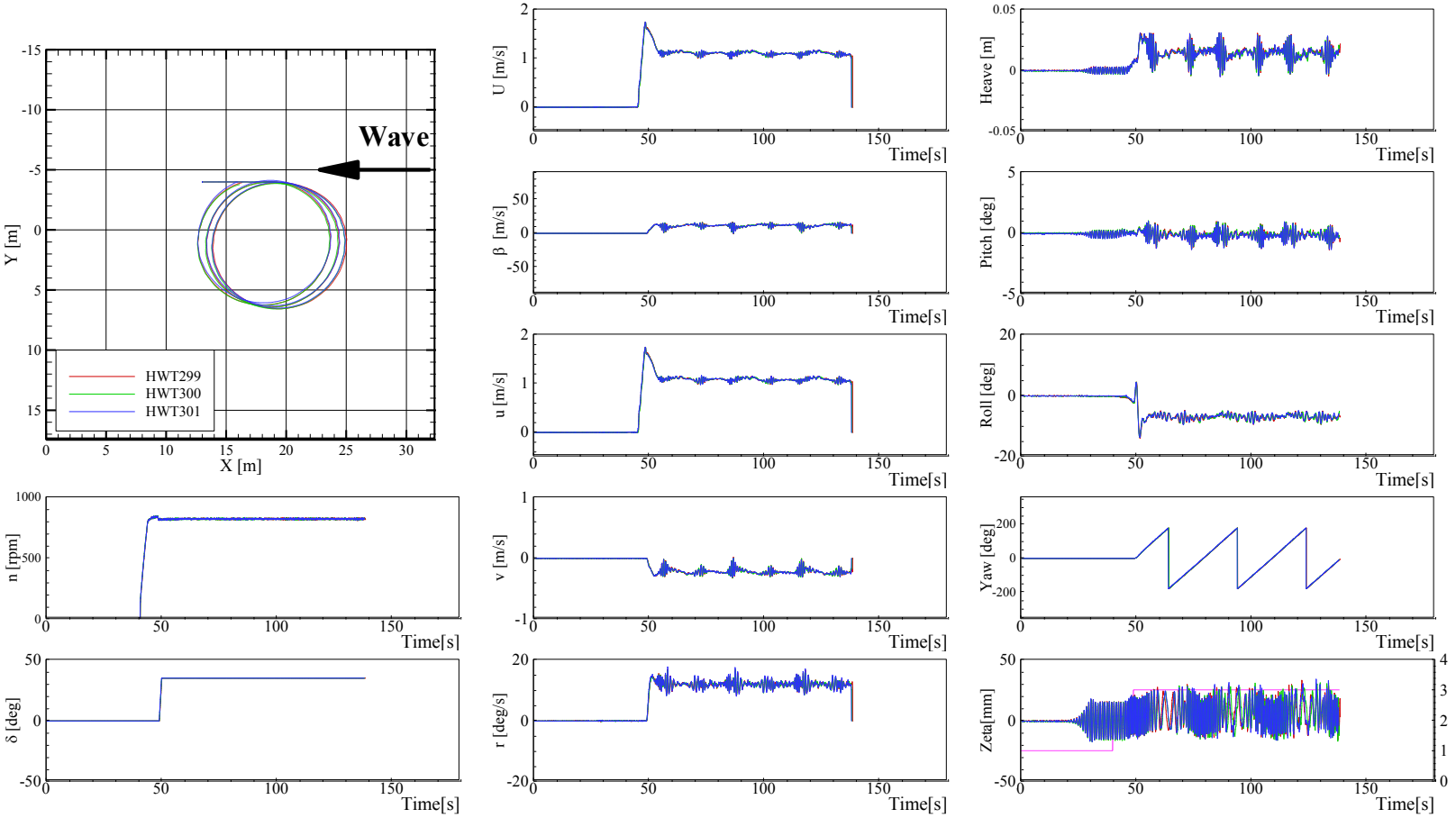

Figure G-63 Trajectories and time histories of turning in waves at Fr = 0.3, λ/L = 0.5, H/λ = 0.02, δ = 35, and χ = 0°

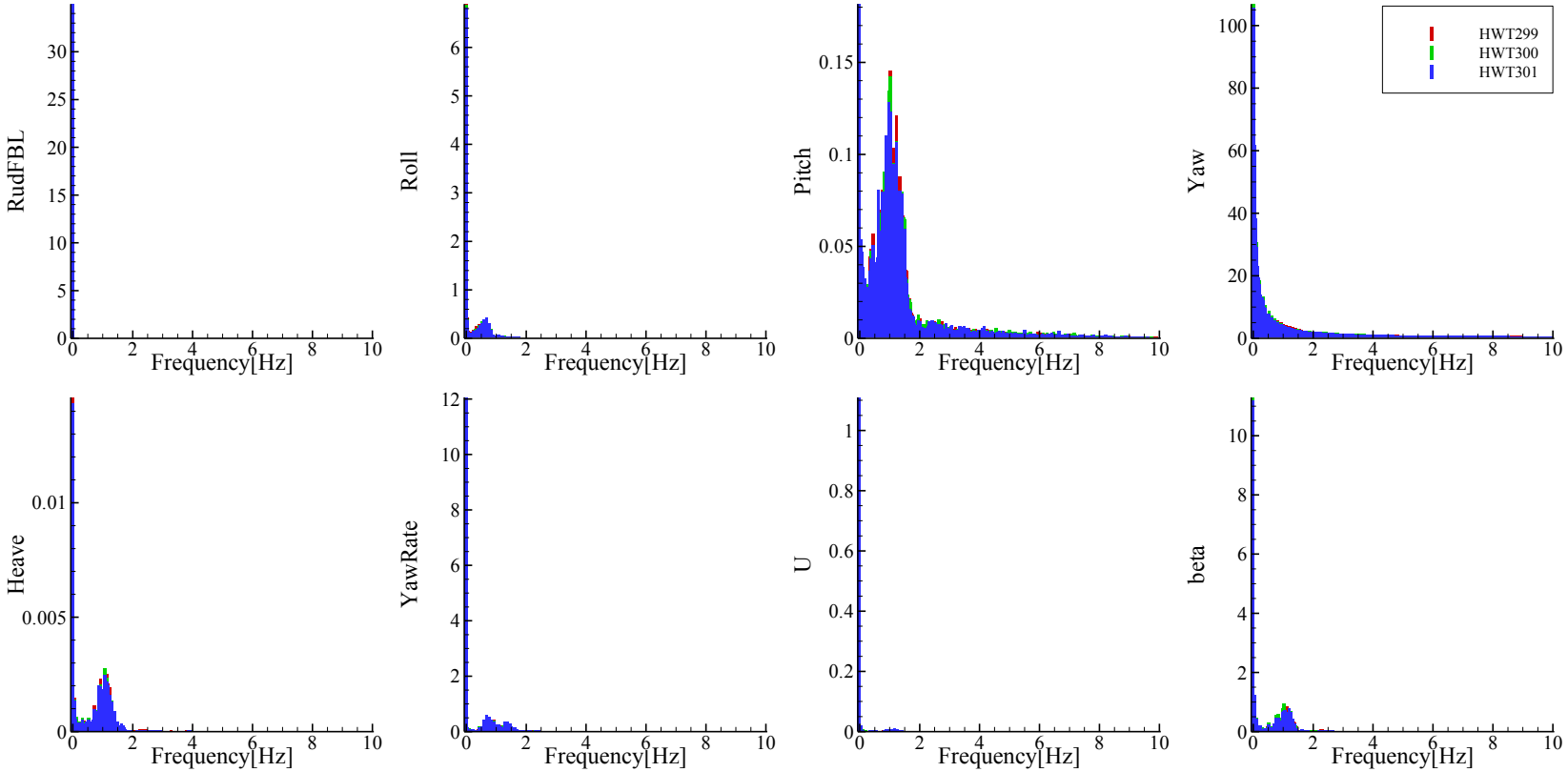

Figure G-64 FFT analysis of time histories of turning in waves at Fr = 0.3, λ/L = 0.5, H/λ = 0.02, δ = 35, and χ = 0°

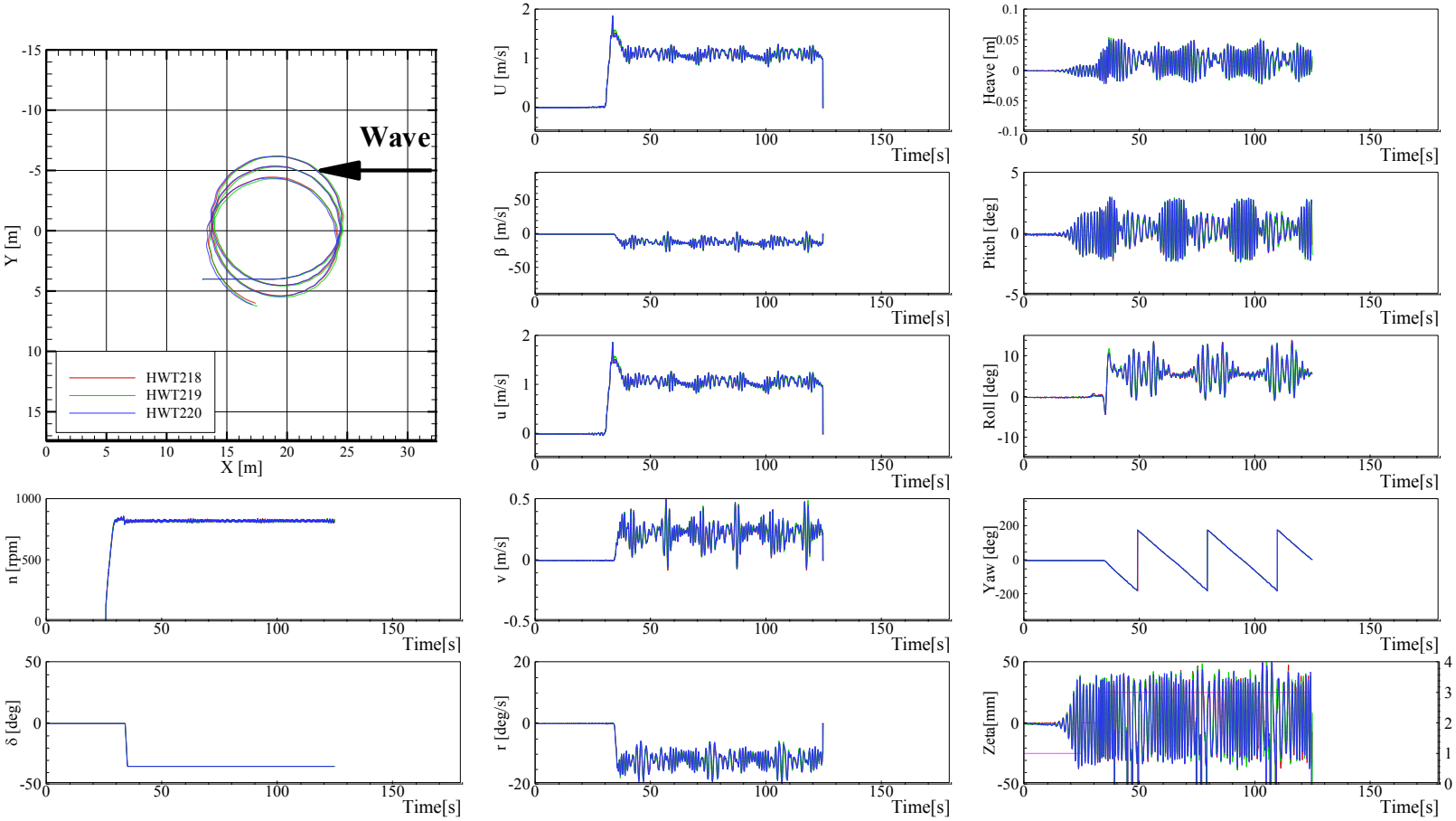

Figure G-65 Trajectories and time histories of turning in waves at Fr = 0.3, λ/L = 1.0, H/λ = 0.02, δ = -35, and χ = 0°

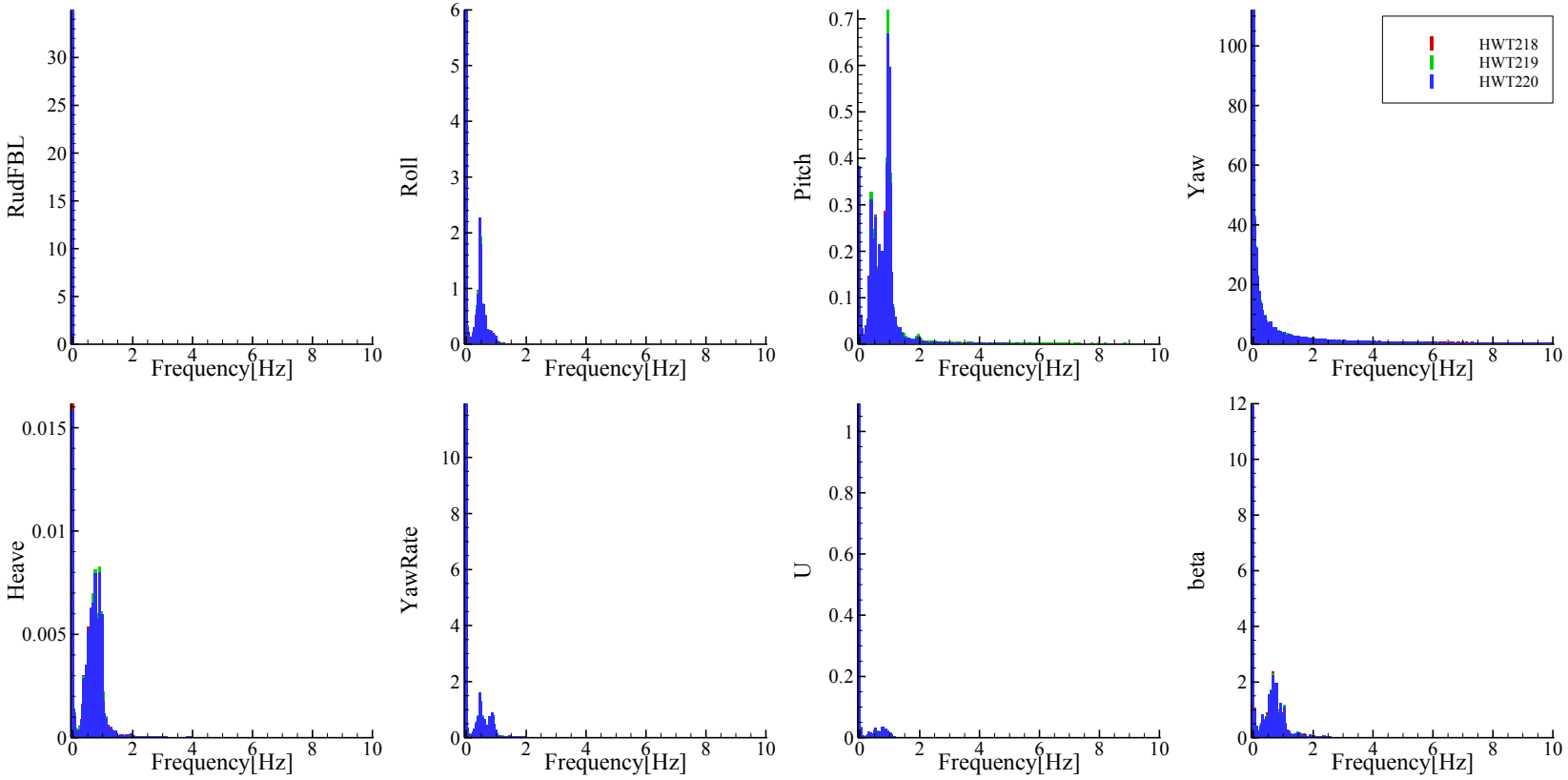

Figure G-66 FFT analysis of time histories of turning in waves at Fr = 0.3, λ/L = 1.0, H/λ = 0.02, δ = -35, and χ = 0°

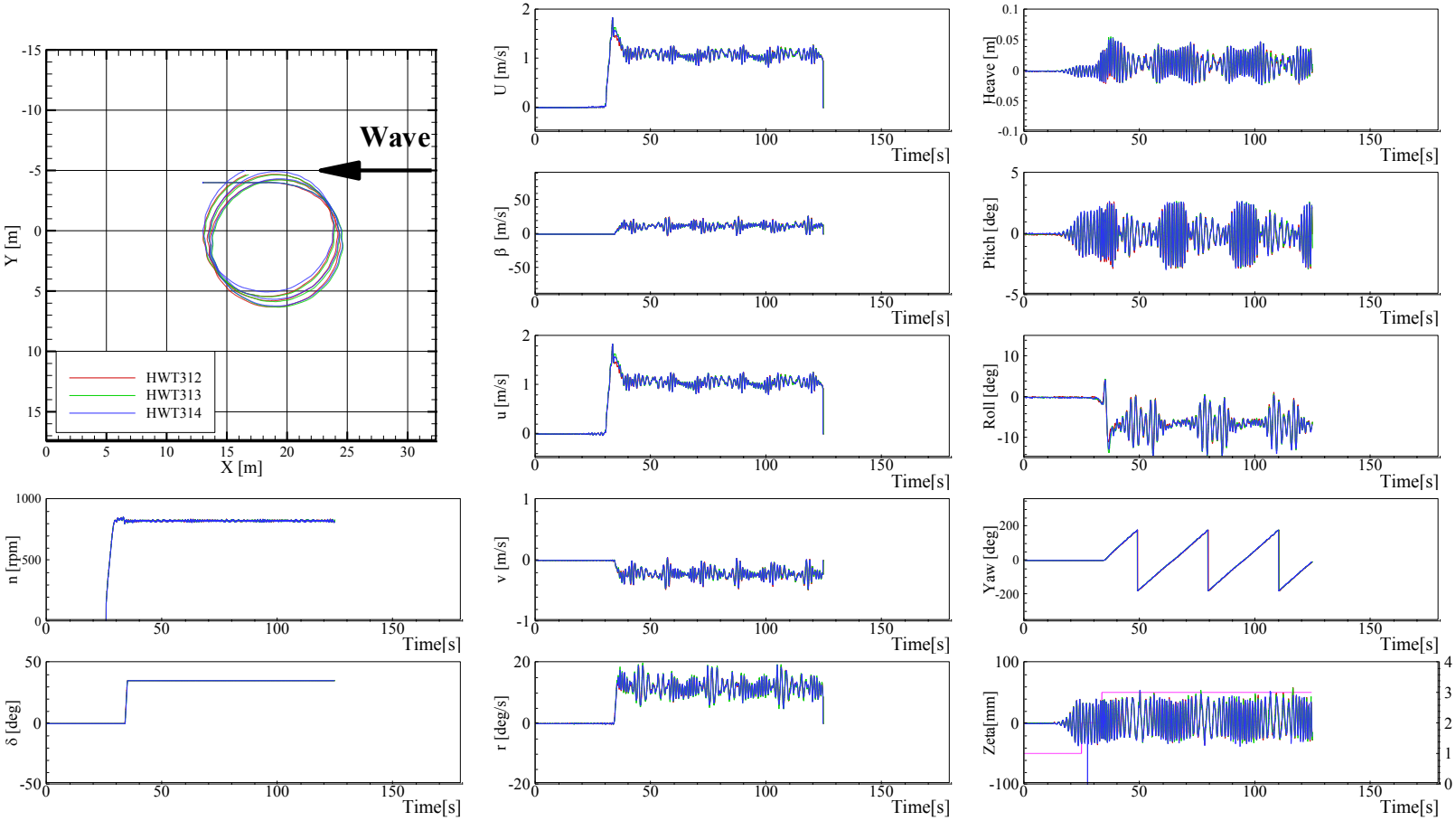

Figure G-67 Trajectories and time histories of turning in waves at Fr = 0.3, λ/L = 1.0, H/λ = 0.02, δ = 35, and χ = 0°

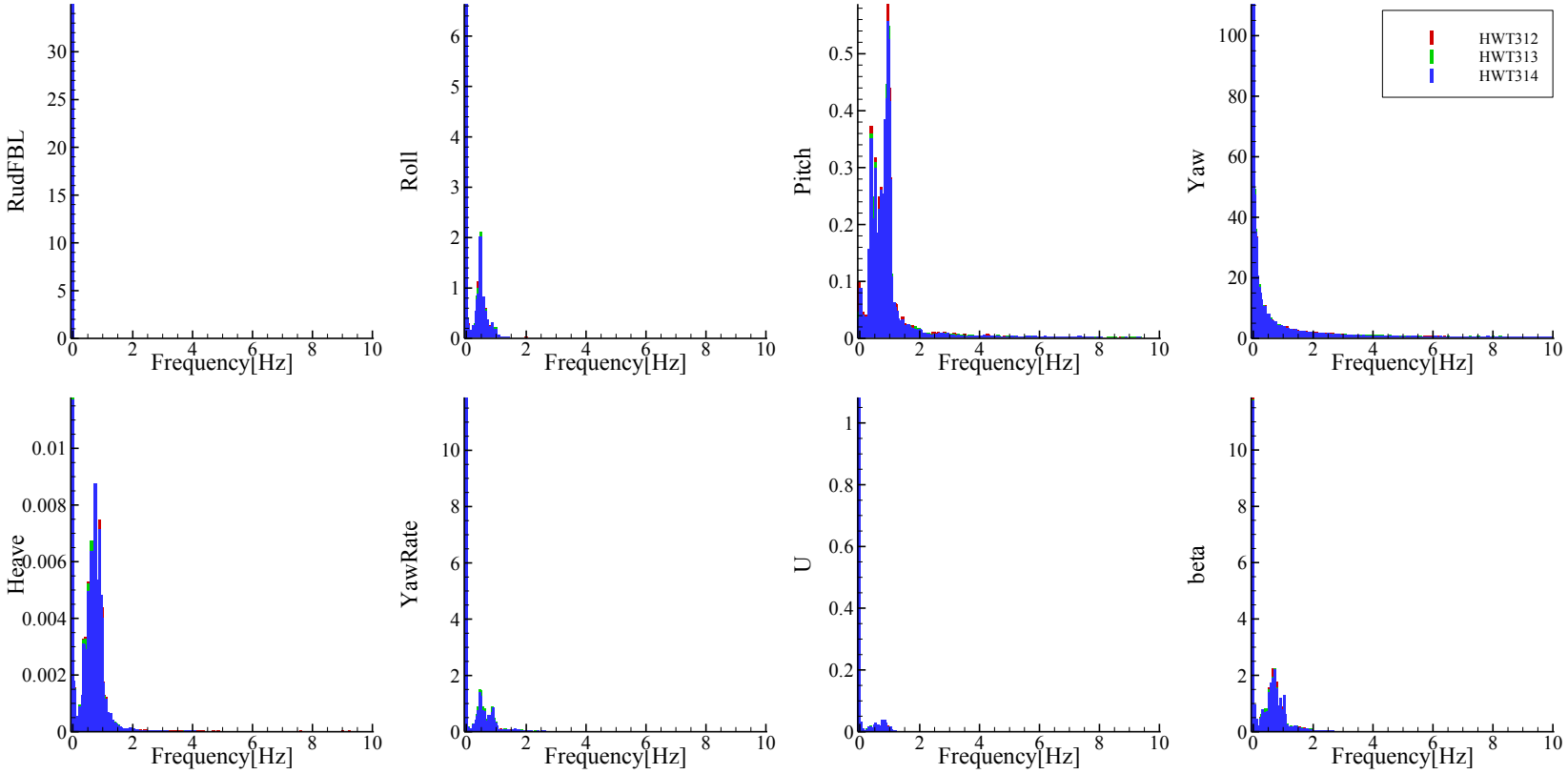

Figure G-68 FFT analysis of time histories of turning in waves at Fr = 0.3, λ/L = 1.0, H/λ = 0.02, δ = 35, and χ = 0°

APPENDIX H IMO MANEUVERABILITY CRITERIA

Table H- 1 IMO Maneuverability Criteria (MSC137 (76), 2002)

Ability	Criteria
Turning ability	The advance (A_D) should not exceed 4.5 ship lengths (L) and the tactical diameter (T_D) should not exceed 5.0L in the turning circle maneuver.
Initial turning ability	With the application of 10° rudder angle to port/starboard; the ship should not have travelled more than 2.5L by the time the heading has changed by 10° from the original heading
Yaw-checking and course-keeping abilities	1) 10°/10° zigzag test The value of the 1st overshoot angle should not exceed: < 10° (L/U < 10 s) < (5 + 1/2(L/U)) ° (10 s < L/U <30 s) < 20° (30 s < L/U) The value of the 2nd overshoot angle should not exceed: < 25° (L/U <10 s) < 40° (30 s < L/U) < (17.5 + 0.75(L/V))°, (10 s < L/U <30 s) 2) 20°/20° zigzag test The value of the 1st overshoot angle should not exceed: < 25° L and U are expressed in m and m/s, respectively.
Stopping ability	The track reach in the full astern stopping test should not exceed 15L. However, this value may be modified by the Administration where ships of large displacement make this criterion impracticable, but should in no case exceed 20L.